Copy #7

NASA CR-72601
UARL H910666-16

71-18030

KINETIC PERFORMANCE HANDBOOK

by

L.S. BENDER, V.J. SARLI, and W.G. BURWELL

United Aircraft Research Laboratories

UNITED AIRCRAFT CORPORATION

EAST HARTFORD, CONNECTICUT

prepared for

NATIONAL AERONAUTICS AND SPACE ADMINISTRATION

SEPTEMBER 15, 1970

CONTRACT NAS3-11225

NASA Lewis Research Center

Cleveland, Ohio Advanced Rocket Technology Branch

P. N. Herr, Project Manager

NOTICE

This report was prepared as an account of Government sponsored work. Neither the United States, nor the National Aeronautics and Space Administration (NASA) nor any person acting on behalf of NASA:

A.) Makes any warranty or representation, expressed or implied, with respect to the accuracy, completeness, or usefulness of the information contained in this report, or that the use of any information, apparatus, method, or process disclosed in this report may not infringe privately owned rights; or

B.) Assumes any liabilities with respect to the use of, or for damages resulting from the use of any information, apparatus, method or process disclosed in this report.

As used above, "person acting on behalf of NASA" includes any employee or contractor of NASA, or employee of such contractor, to the extent that such employee or contractor of NASA, or employee of such contractor prepares, disseminates, or provides access to, any information pursuant to his employment of contract with NASA, or his employment with such contractor.

Requests for copies of this report should be referred to:

National Aeronautics and Space Administration
Office of Scientific and Technical Information
Attention: AFSS-A
Washington, D. C. 20546

FOREWORD

This Handbook was prepared by the United Aircraft Research Laboratories for the National Aeronautics and Space Administration under Contract NAS 3-11225 initiated June 6, 1968.

Included among those who cooperated in performance of the work under Contract NAS 3-11225 were Dr. V. J. Sarli, Program Manager; Dr. W. G. Burwell, Chief, Kinetics and Thermal Sciences Section; Dr. A. S. Kesten, Mr. L. S. Bender and Mr. R. Roback of the UARL and Mr. T. F. Zupnik and Mr. L. Aceto, Scientific Staff of Pratt & Whitney Aircraft Division of United Aircraft Corporation.

This work was conducted under program management of the NASA Lewis Research Center, Cleveland, Ohio, and the Project Manager was Mr. P. N. Herr. Operational critique and format suggestion of Kinetic Handbook by Mr. C. A. Aukerman of NASA Lewis is also acknowledged.

This document is unclassified in its entirety.

KINETIC PERFORMANCE HANDBOOK

by

L. S. Bender, V. J. Sarli, and W. G. Burwell

ABSTRACT

Presented in this handbook, prepared by the United Aircraft Research Laboratories under Contract NAS 3-11225, are self-consistent kinetic performance and aerodynamic degradation charts to permit rapid evaluation of the deliverable performance for five liquid propellant combinations, H_2-F_2, H_2-O_2, Aerozine 50-N_2O_4, CH_4-Flox (82.6% F_2), and B_2H_6-OF_2 over wide ranges of operating conditions and for different nozzle geometries and engine sizes. The conditions generally encompass a range of oxidizer/fuel ratios surrounding the anticipated optimum mixture ratio, and include combustion chamber pressures from 100 to 1000 psia (50 to 500 psia for B_2H_6-OF_2). Charts are presented for both conical and bell nozzle contours for values of nozzle exit area ratio between 20 and 100 and for nominal thrust levels between 100 and 1,000,000 pounds. Also included is sufficient information for the user of this handbook to estimate the effect on kinetic performance loss of variations in reaction rate constants relative to those used in the handbook. The procedures and reaction rate constants employed herein are consistent with those recommended by the ICRPG Performance Standarization Working Group.

NASA CR-72601

KINETIC PERFORMANCE HANDBOOK

Contract NAS 3-11225

TABLE OF CONTENTS

	Page
FOREWORD	i
ABSTRACT	ii
INTRODUCTION	1
OUTLINE OF PERFORMANCE PREDICTION METHOD	3
The Performance Mode	3
The Contour Selection Mode	4
DESCRIPTION OF TECHNIQUES	7
Kinetic Losses	7
Description of Bray Sudden Freezing Criterion	7
Modified Bray Criterion for Multireaction Systems	8
Method of Calculation of Freezing Point	10
Reaction Rate Data	14
Equilibrium & Frozen Performance	18
Partial-Equilibrium Performance	18
Aerodynamic Losses	19
Flow Divergence Loss	19
Boundary Layer Loss	20
Transonic Loss	20
Performance Estimation for Gaseous Propellants	21
INDEX TO FIGURES AND TABLES	27
SAMPLE CALCULATIONS	29
LIST OF SYMBOLS	41
REFERENCES	43
APPENDIX I (Distribution List)	I-1

INTRODUCTION

Extensive effort has been expended in recent years to assess "real gas" flow properties in subsonic-supersonic expansion nozzles. A particularly large amount of work has been performed with the objective of establishing chemical nonequilibrium flow effects in such nozzles, a prerequisite to predicting, correlating or extrapolating the performance of high-energy chemical rocket engines. To a large extent, most of the early work was concerned with defining simplified analytical procedures for assessing the point and ultimate extent of departure from chemical equilibrium in the gas flow through typical convergent-divergent nozzles (e.g., Refs. 1, 2, 3, 4 and 5). A few investigators (Refs. 6, 7, 8, 9 and 10) addressed themselves to the problem of constructing, by exact numerical means, the entire set of flow properties within one-dimensional nozzles although few results were obtained.

Most recently, much more sophisticated numerical procedures have become available (e.g., Refs. 11 and 12) and much work of both an experimental and analytical nature has been reported on the evaluation of nonequilibrium flow effects in a variety of engine/nozzle configurations (e.g., Refs. 13, 14, 15, 16 and 17). Indeed, exact numerical procedures are now available (Refs. 11, 12, 18 and 19) which solve simultaneously the chemical kinetic and gas dynamic equations pertinent to two-dimensional and axisymmetric flow fields, such as those encountered in the supersonic portions of typical expansion nozzles. In combination with these kinetic procedures, additional computational schemes have become available for treating the turbulent boundary layer (e.g. Ref. 20) and for handling the transonic flow problem (Ref. 21). It has thus proved feasible within the last few years to undertake detailed analysis and correlation of actual rocket engine test data and to predict "a priori" the delivered performance of propellant systems and engine configurations of future interest for space application (Ref. 22, 23, 24, 25, 26 and 27). The performance data which have been analyzed and correlated by this contractor are reported in Refs. 27, 28, 29, 30, 31 and 32. Generally, correlation of performance data has been achieved for the five propellant combinations presented in this handbook. Selected H_2-F_2 data available at low pressure and high area ratio (Ref. 32) did not correlate well with the large mass of data reported in Ref. 27, 28, and 29; the measured performance reported in Ref. 32 is higher than predicted delivered performance for similar operating conditions and nozzle geometries.

Use of computational procedures such as those described above is not entirely straightforward, however, for several reasons. First, each procedure makes use of selective input data, restrictive assumptions and/or optional subroutines which result in significant variations in computed performance results; second, the performance losses predicted by procedures which individually handle such phenomena as nonequilibrium nozzle flow, viscous drag, and exit flow divergence

are not necessarily additive losses; and third, most procedures are lengthy and all require access to high-speed digital computation equipment. In order to develop effective methods to accommodate these problems, work has been performed by this Contractor (Ref. 25) and by the Performance Standarization Working Group of the Interagency Chemical Rocket Propulsion Group (ICRPG) (Ref. 33) which has resulted in defining "recommended" computer codes and both simplified and standard methodologies for predicting and correlating liquid rocket propellant engine performance. Remaining has been a more exact specification of the interaction between the combustor and nozzle components and development of an approximate method for estimating rapidly, without digital computation equipment, the deliverable performance of propellant combinations of current interest. It is for this latter purpose that the charts assembled herein have been prepared.

Specifically, a procedure of verified accuracy has been developed which presumes the various component losses in an expansion nozzle can be deducted from the theoretical one-dimensional, shifting-equilibrium performance of the nozzle, neglecting any coupling effects which may actually occur in the flow system. Using this procedure a series of performance estimation graphs has been prepared for five propellant combinations typical of current earth-storable, space-storable and cryogenic systems (viz. aerozine 50-N_2O_4, CH_4-O_2 (17.4%)-F_2(82.6%), B_2H_6-OF_2, H_2-O_2 and H_2-F_2). Included are kinetic performance and aerodynamic degradation charts which are sufficiently general to permit user-supplied nozzle contour data to be employed to estimate the nonequilibrium performance of virtually any nozzle. Additionally, sufficient information is provided to enable estimation of the effect on kinetic performance loss of variations in reaction rate constants relative to the values used in the handbook.

Every attempt has been made to maintain performance prediction accuracy within $\pm 1\%$ of the performance predicted by the full-kinetic axisymmetric machine program (TDK) recommended by the ICRPG (Ref. 33).

OUTLINE OF PERFORMANCE PREDICTION METHOD

Work previously reported by the United Aircraft Research Laboratories (Refs. 22-25) has shown that reliable prediction of deliverable rocket engine performance can be made provided that accurate and complete kinetic data are available to assess nonequilibrium flow effects in high area ratio nozzles and that appropriate accounting can be made of influences imposed by inefficient combustion and nozzle aerodynamics. This work combined with additional efforts reported in Refs. 16, 17 and 34 suggest that simplified procedures may be employed to approximate the nonequilibrium flow effects for common high-energy liquid rocket propellants and, further, that aerodynamic performance losses due to viscous drag and nozzle exit flow divergence are additive with nonequilibrium losses when the appropriate optional gas model is employed to evaluate the aerodynamic losses. Thus, exclusive of combustor-induced losses such as incomplete reaction or flow striation, all major sources of nozzle performance degradation can be treated separately. It is this fact which serves as the basis for the method described herein to estimate deliverable engine performance.

In outline form, the prediction method involves a sequence of steps, each undertaken to evaluate one of the component performance losses relative to the theoretical, one-dimensional thermochemical performance of the propellant combination under consideration. Charts are provided to permit interpolation of each component loss over wide ranges of operating conditions and for different nozzle geometries and engine sizes. The charts have been compiled recognizing two primary modes of utilization: a "performance" mode and a "contour selection" mode. Under the performance mode, the desired objective is to predict the net deliverable performance of a given propellant combination for a specified set of operating conditions within a prescribed engine/nozzle configuration. Under the contour selection mode (not necessarily an optimum contour) on the other hand, the desired objective is to arrive at a nozzle size or configuration which will produce a specified level of performance for a given propellant combination under a prescribed set of operation conditions. The logic for each mode is given below.

The Performance Mode

Specified under the performance mode are the following:

1. The propellant combination

2. Engine operating conditions (including O/F ratio and combustion chamber pressure, P_c)

3. The nozzle configuration and size (including throat radius, r_t; radius ratio, r_c/r_t; exit area ratio, (A/A_{min}) exit; and nozzle contour -- i.e. conical nozzle with prescribed expansion angle, bell nozzle with prescribed truncation, or other generalized type with area ratio gradient, $\frac{d\left(A/A_{min}\right)}{dx}$, specified as a function of local nozzle area ratio).

To be determined from the appropriate performance charts and tables are:

1. The theoretical, one-dimensional, shifting-equilibrium and frozen-flow performance ($I_{sp_{vac}}$).

2. The freezing-point location, denoting the location beyond which recombination reactions are no longer possible kinetically.

3. The one-dimensional, partial-equilibrium performance (determined by the freezing-point location), from which the kinetic loss can be inferred.

4. Aerodynamic losses, including

   a. The divergence loss

   b. The viscous drag loss

   c. The transonic-flow loss (assumed to be 0.5% of the shifting-equilibrium performance for most common nozzle configurations)

5. The net deliverable specific impulse performance, which is equal to the partial equilibrium performance (from 3 above) minus the divergence, drag and transonic aerodynamic losses (from 4 above).

6. The net deliverable thrust (from 5 above and tabulated equilibrium throat mass flow rates).

The Contour Selection Mode

Specified under the Contour Selection mode are the following:

1. The propellant combination and operating conditions.

2. The desired thrust level

3. The general nozzle configuration (conical or bell nozzle) and overall expansion area ratio, $(A/A_{min})_{exit}$.

4. Geometrical constraints (r_c/r_t and expansion half-angle, θ, for conical nozzles; design area ratio -- i.e. the area ratio at which the exit flow becomes parallel -- for bell nozzles).

To be determined from the appropriate performance charts are:

1. The theoretical, one-dimensional, shifting-equilibrium and frozen-flow performance ($I_{sp_{vac}}$).

2. The shifting-equilibrium specific mass flow rate, $\dot{w}/A$, through the nozzle throat.

3. The nominal size, r_t, of the nozzle throat (from the specified thrust level and the specific mass flow rate, from 2 above).

4. The freezing point location, denoting the location beyond which recombination reactions are no longer possible kinetically.

5. The one-dimensional, partial-equilibrium performance (determined by the freezing point location), from which the kinetic loss can be inferred.

6. Aerodynamic losses including

   a. The divergence loss

   b. The viscous drag loss

   c. The transonic-flow loss (assumed to be 0.5% of the shifting-equilibrium performance for most common nozzle configurations)

7. The net deliverable specific impulse performance, which is equal to the partial-equilibrium performance (from 5 above) minus the divergence, drag and transonic aerodynamic losses (from 6 above).

8. The net deliverable thrust (from 7 above and the equilibrium throat mass flow rate from 2 above).

As the net nozzle thrust is necessarily less than the specified nominal thrust, it is required that an adjustment be made to the nozzle throat size (calculated in 3 above) and the series of calculations from 4 through 8 repeated. The number of iterations necessary to achieve the desired net thrust may, of

course, be reduced initially by increasing nozzle throat size slightly over the value calculated in step (3).

Many variations, too numerous to specify, are possible on the above procedures when specific effects of various parameters, such as r_c/r_t for conical nozzles or design area ratio for bell nozzles, are to be studied. To permit such studies, the charts have been compiled with as much generality as possible, and full exploitation of the data contained herein is left to the user.

DESCRIPTION OF TECHNIQUES

In order to establish a more complete understanding and insight into the application and manipulation of the charts displayed in the various sections of this handbook, as well as to achieve a better realization of the limitations of the methods employed to calculate the various flow losses, a description of each of the component loss mechanisms is presented below.

Kinetic Losses

Kinetic losses are evaluated herein using the modified Bray criterion for multireaction systems (Ref. 17). In order to fully utilize the data presented in this handbook, a thorough understanding of this criterion is essential, although straightforward calculation of nonequilibrium performance for typical conical and bell nozzles does not require such familiarity.

Description of Bray Sudden-Freezing Criterion

The Bray criterion is an approximate procedure for predicting the point in a reacting nozzle flow where a reaction has departed significantly from equilibrium. This is accomplished by determining the point at which the forward rate of reaction becomes of the same order as the rate required to maintain equilibrium. This concept is illustrated by considering a nozzle expansion in which an arbitrary three-body recombination reaction takes place,

$$2J + M \underset{k_b}{\overset{k_f}{\rightleftharpoons}} J_2 + M \tag{1}$$

where the change of J_2 concentration with time at constant density is found from phenomenological kinetics (Ref. 30),

$$\left(\frac{\partial [J_2]}{\partial t}\right)_\rho = k_f [J_2] [M] \left\{\frac{[J]^2}{[J_2]} - \frac{[J]_{eq}^2}{[J_2]_{eq}}\right\} \equiv a\{y - y_{eq}\} \tag{2}$$

In Eq. (2) the bracket, $[\ ]$, indicates the actual instantaneous concentration of the indicated species, k_f, denotes the forward rate constant, and the sub-script "eq" denotes the instantaneous equilibrium values. For near-equilibrium flow, it is clear that $Y - Y_{eq} \ll Y_{eq}$, so that

$$\left(\frac{\partial [J_2]}{\partial t}\right)_\rho << a y_{eq} \tag{3}$$

while for near-frozen flow $Y_{eq} \ll Y$, so that

$$\left(\frac{\partial [J_2]}{\partial t}\right)_\rho \simeq a y \quad >> a y_{eq} \tag{4}$$

Therefore, from Eqs. (3) and (4) it can be deduced that an approximate criterion for the freezing point of the reaction can be defined according to

$$\left(\frac{\partial [J_2]}{\partial t}\right)_\rho \simeq a y_{eq} \equiv (r_f)_{eq} \tag{5}$$

as previously stated, where the forward reaction rate expression, r_f, is evaluated with very little loss in accuracy using equilibrium quantities up to the freezing point.

The Bray criterion has been used successfully to analyze flows in which only one reaction is energetically and kinetically important. However, this method of solution considering only a single reaction may be valid only for a relatively few complex chemical systems.

For the expansion of products of combustion in a nozzle, several reactions must be considered if an effective point of chemical freezing is to be found. Extension of Bray's one-reaction criterion to multireaction one-equilibrium nozzle flows is not necessarily straightforward, unless one reaction out of the many taking place has tied up most of the energy in the combustion process, or unless all energetic reactions tend to leave equilibrium at nearly the same location in the nozzle. When this is not the case, the simple freezing criterion can at best bracket the actual nozzle flow parameters (by assuming that the fastest and slowest of the many reactions control).

Modified Bray Criterion for Multireaction Systems

The concept of a composite freezing point is based on the assumption that an important rate-controlling species exists whose net rate of formation or depletion becomes very small as the reactions in which it participates become very slow, and that once this species has frozen at some point in the nozzle (which will be referred to as the "composite-reaction freezing point"), all remaining species can no longer react. The problem of finding a composite-reaction freezing point reduces to determining the kinetically, and thermodynamically, important species and reactions which must be studied. The importance of many of the existing species can be evaluated on the basis of (1) their relative equilibrium composition values, a mole fraction of 0.005 being a practical lower limit, (2) the energy release of the chemical reactions in which they participate, and (3) their role in effecting the chain-breaking steps in the overall reaction mechanism.

The reaction rate that is necessary to keep an important species in equilibrium can easily be found knowing the equilibrium composition history as calculated using the conservation equations, state relations, and the pertinent Guldberg-Waage laws of mass action (Refs. 31 and 32). The required time rate of

change of the concentration for component i due to reaction only, i.e., excluding expansion effects, is

$$\left(\frac{\partial [M_i]}{\partial t} \right)_{\rho, eq} = \left[\rho V \frac{d(X_i/\bar{W})}{dX} \right]_{eq} \tag{6}$$

where $[M_i] = \rho x_i/\bar{W}$, x_i is the mole fraction of species i, and $\bar{W}$ is the mean molecular weight, $\sum_{i=1}^{n} x_i W_i$. While equilibrium machine solutions employ the local flow area to minimum flow area ratio (i.e., A/A_{min}) as an independent variable, the axial distance, X, is a more convenient variable since

$$\left(\frac{\partial [M_i]}{\partial t} \right)_{\rho, eq} = \left[\rho V \frac{d(X_i/\bar{W})}{d(A/A_{MIN})} \right]_{eq} \frac{d(A/A_{MIN})}{dX} \tag{7}$$

becomes indeterminate at the minimum area (i.e., at $A = A_{min}$). Evaluation of Eq. (6) can proceed once the equilibrium properties and a nozzle geometry have been specified. Use of the equilibrium values for computing the required gradients will be accurate up to the point where the first important reaction freezes; but, since the species under consideration will usually appear in this reaction, this does not represent a severe limitation on the method when one reaction is controlling or all reactions freeze at the same location.

In complete analogy with the simple one-reaction Bray criterion, it is necessary when treating a multireaction system to compare the required reaction rate, Eq. (6), with the total forward rate of reaction written in terms of all reactions that make substantial contributions to the overall rate of production or depletion of species. The forward reaction rate equation for the net rate of production of species M_i is

$$\left(\frac{\partial [M_i]}{\partial t} \right)_{\rho} = \sum_{j=i}^{N} (\alpha''_{ij} - \alpha'_{ij}) \left\{ k'_{fj} \prod_{k=1}^{n} [M_k]^{\alpha'_{kj}} \right\} \tag{8}$$

where N is the total number of reactions, n the total number of species, k_{fj} the forward rate constant for the jth reaction, and α'_{ij} and α''_{ij} the stoichiometric coefficients of the ith species in the jth reaction for the reactants and products, respectively, when the jth reaction taking place in the exothermic direction is written as (Ref. 30)

$$\sum_{i=1}^{n} \alpha'_{ij} M_i \underset{k_{D_j}}{\overset{k_{f_j}}{\rightleftharpoons}} \sum_{i=1}^{n} \alpha''_{ij} M_i \tag{9}$$

When a single rate-controlling reaction exists, for example, the oxygen recombination reaction in the expansion of air up to 6000 K, Eq. (8) takes the simple form

$$\left(\frac{\partial [M_i]}{\partial t}\right)_\rho = (\alpha''_{ij} - \alpha'_{ij}) k_{f_j} \prod_{k=1}^{n} [M_k]^{\alpha'_{kj}} \qquad j = j_o \tag{10}$$

where M_i refers to the species in the jth reaction which, in addition to being thermodynamically important, has a large variation in composition through the nozzle to ensure accurate differentiation of the composition with respect to axial distance in Eq. (6). An effective freezing point for a multireaction nozzle flow can then be defined from Eqs. (6) and (8) as

$$\left(\frac{\partial [M_i]}{\partial t}\right)_\rho = \left[\rho V \frac{d(X_i/\bar{W})}{dX}\right]_{eq} = \sum_{j=1}^{n} (\alpha''_{ij} - \alpha'_{ij}) \left\{k_{f_j} \prod_{k=1}^{n} [M_k]^{\alpha'_{kj}}\right\} \tag{11}$$

In the situation described above where one dominant reaction exists, the right-hand side of Eq. (11) is replaced by Eq. (10) so that this freezing criterion reduces essentially to the simple Bray criterion. In any event, it is clear that there can be as many freezing points as radicals or atoms to which Eq. (11) is applied, but these points usually remain in close proximity to one another in practice, depending on the choice of reactions employed in the forward reaction rate equation.

The most successful results from this composite reaction effective freezing point analysis are achieved when only three-body reactions are considered in evaluating the right side of Eq. (11), since bimolecular reactions in which one or more new radicals are formed for every radical consumed add very little energy to the flow after the three-body reactions have frozen..

Graphical solutions to Eq. (11) are easily carried out for arbitrary flow systems, once the important reactions and species have been ascertained, by performing graphical differentiation of the equilibrium concentration profiles as a function of axial distance for a preselected nozzle geometry, $X = X(A/A_{min})$. Then, for a given set of forward rate constants and with all the equilibrium properties known as a function of area ratio, the left side of Eq. (11) can be plotted against the right side over the range of area ratios. The point of crossing indicates where significant freezing has occurred, and is thus termed the freezing point.

Method of Calculation of Freezing Point

As was defined in Eq. (11), the location of the freezing point is determined to be that position within a nozzle where the equilibrium composition gradient and the kinetic composition gradient become equal. Although the kinetic composition

gradient is independent of the nozzle area ratio gradient, the equilibrium composition gradient is proportional to the nozzle area ratio gradient $d(A/A_{min})/dx$ for a prescribed value of area ratio, A/A_{min}. Specifically, from Eq. (7)

$$\left(\frac{d\left[M_i\right]}{dt}\right)_{EQUIL} = \left\{\frac{d\left[M_i\right]}{d\left(A/A_{min}\right)} V\right\}_{EQUIL} \left\{\frac{d\left(A/A_{min}\right)}{dx}\right\} \tag{12}$$

or alternatively,

$$\left(\frac{d\left[M_i\right]}{dt}\right)_{EQUIL} = \left\{\frac{d\left[M_i\right]}{d\left(A/A_{min}\right)} V\right\}_{EQUIL} \left\{\frac{1}{r_t} \quad \frac{d\left(A/A_{min}\right)}{d\left(x/r_t\right)}\right\} \tag{13}$$

Therefore, for a selected propellant system, O/F ratio, and chamber pressure, the term

$$\left\{\frac{d\left[M_i\right]}{d\left(A/A_{min}\right)} \quad V\right\}_{EQUIL}$$

is independent of nozzle geometry. All of the geometric constraints particular to a given nozzle are in the second term of Eqs. (12) and (13).

Use has been made of this fact in preparing generalized charts to permit determinations to be made of freezing points for each of the five propellant combinations under consideration. In particular, both kinetic and "normalized" equilibrium gradients have been established as functions of local nozzle area ratio and plotted for several combustion chamber pressures and O/F ratios. Two normalized gradients are used; one which basically shows the dependence of the term

$$\left\{\frac{d\left[M_i\right]}{d\left(A/A_{min}\right)} \quad V\right\}_{EQUIL}$$

on (A/A_{min}) by assuming

$$\frac{d\left(A/A_{min}\right)}{dx} = 1\ Ft^{-1}$$

and the second which shows the gradient for a 15 deg conical nozzle with $r_c/r_t = 1$, $r_t = 1.0$ Ft. (0.3048m). The latter gradient provides a practical reference from which freezing points can easily be obtained for scaled 15 deg conical nozzles simply by multiplying the gradient displayed by the factor $\frac{1}{r_t}$. This former

gradient is the more general one and can be used to represent any given nozzle simply by multiplying the gradient displayed by the factor

$$\frac{d\ (A/A_{min})}{dx} = \frac{1}{r_t} \left\{\frac{d\ (A/A_{min})}{d\ (x/r_t)}\right\}$$

Curves displaying the differential gradient, $\frac{d(A/A_{min})}{d\ (x/r_t)}$, are provided for representative nozzle configurations in Figs. ND-1 through ND-4. Gradients are presented for conical nozzles of half angle from 5 to 30 deg and values of r_c/r_t up to 10 in Fig. ND-1. Similarly, gradients for bell (perfect) nozzles are shown in Figs. ND-2 to ND-4. The gradient curves (Figs. ND-2 to ND-4) as well as corresponding nozzle profiles (Figs. ND-5 to ND-9) are presented for families of perfect nozzles with design area ratios of from 100 to 1000, an $r_c/r_t = 1$ and for 3 values of specific heat ratio, 1.25, 1.30 and 1.35. The data displayed allow the user to select a bell nozzle subject to any truncation criterion of his own choosing. The user is reminded that the equilibrium gradient to be employed to determine freezing point location is a function of throat radius and it is not the non-dimensional gradients which are illustrated in Figs. ND-1 through ND-4.

As was indicated previously, the kinetic gradients displayed in the charts presented herein are independent of the nozzle area ratio gradients. However, the kinetic gradients are functions of the local equilibrium flow properties and compositions within the nozzle and the kinetic rate constants. For a simple recombination reaction such as that given by Eq. (1), the appropriate kinetic gradient from Eq. (5) is

$$\left(\frac{\partial[M_i]}{\partial t}\right)_{\rho,KIN} = \left\{k_f\ [M_i]^2\ [M]\right\} \tag{14}$$

For the more general case involving multiple reactions as given by Eq. (9), the appropriate kinetic gradient is

$$\left(\frac{\partial\ [M]}{\partial t}\right)_{\rho,KIN} = \sum_{j=1}^{n} (\alpha''_{ij} - \alpha'_{ij}) \left\{k_{f_j} \prod_{k=1}^{n} [M_k]^{\alpha'_{kj}}\right\}_{EQUIL} \tag{15}$$

where the term on the right-hand side of Eq. 15 is called the "composite" kinetic gradient.

In both Eqs. (14) and (15), one recognizes that the kinetic gradient for each reaction is scaled directly by the rate constant, k_f, for that reaction. Thus, it becomes a relatively straightforward process to use the gradient charts provided herein to evaluate the sensitivity of the partial-equilibrium performance

to variations or changes in rate constants relative to those already employed. In the most simple case, the user may choose to work with the composite kinetic gradient only. Typically, in this instance, the kinetic gradient is scaled by a factor which is assumed to apply to the reaction rates for each individual reaction comprising the composite. In the more general case, however, factors can be applied to each individual reaction and a new composite gradient computed. To affect such changes the ratio of desired reaction rate to the rate used in the handbook can be determined from the reaction rate tables supplied herein for the specific propellant, and the individual kinetic gradient curves then scaled by these factors. The new composite kinetic gradient must be established by summing the contributions of the several reactions and the new freezing point then established.

Graphical solution of Eq. (11) to establish the freezing point results in defining an area ratio within the nozzle beyond which the energetic three-body recombination reactions cease to be important. The assumption is that no further chemical reaction takes place downstream of the freezing area ratio. This assumption may be validated by comparing performance results obtained on this basis with results of exact numerical calculations using a one-dimensional full-kinetic machine program such as those described in Refs. 12 and 33. In effect, such comparisons calibrate the sudden-freezing criterion. For example, it was found in Refs. 22 and 25 that the effective freezing point for the H_2-F_2 propellant combination occurred at an area ratio where the composite kinetic gradient was equal to two times the equilibrium gradient. This delayed freezing apparently accounts for some continued energy release in the flow beyond the simple freezing point, which energy may be attributed to relatively fast two-body reactions (e.g., $H_2 + F \longrightarrow HF + H$, in this particular case). This delayed freezing may be accommodated by use of a transition factor in the sudden-freezing analysis which numerically equals the ratio of the composite-kinetic gradient to the equilibrium gradient required to achieve correlation between full-kinetic and sudden-freezing performance results. For the charts appearing in this handbook the following transition factors were employed.

Propellant Combination	Transition Factor
Aerozine 50-N_2O_4	1
CH_4-Flox	2
H_2-O_2	1
H_2-F_2	2
B_2H_6-OF_2	2

Recent evidence (Ref. 26) indicates that a transition factor of 2 may be more appropriate for the CH_4-Flox and B_2H_6-OF_2 propellant combinations, and the user of this handbook is advised to adopt such a factor if the greatest precision is desired. The transition factors for the Aerozine 50-N_2O_4 and H_2-O_2 propellant combinations have been verified in Ref. 13.

A tabulation indicating the location in this handbook where the kinetic and equilibrium charts can be found appears in the "Index to Figures and Tables". In this index, figures are numbered with prefix letters or roman numerals to refer to each specific section or propellant. For example, Fig. I-13 to I-30 provide the desired gradients for the H_2-F_2 combination; Fig. II-13 to II-30 provide those for the H_2-O_2 combination; Figs. III-13 to III-30 provide for the CH_4-Flox combination; Figs. IV-13 to IV-30 for the Aerozine 50-N_2O_4 combination, Figs. V-9 to V-24 for the B_2H_6-OF_2 combination.

Reaction Rate Data

Of the five propellant combinations considered during the course of this analysis, viz. H_2-O_2, H_2-F_2, A50-N_2O_4, CH_4-Flox (82.6% F_2), and B_2H_6-OF_2 the CH_4-Flox and B_2H_6-OF_2 are the most complex. The CH_4-Flox propellant combination involves at least twelve (12) gaseous species which can be related by twenty-three (23) reactions when all third bodies are considered as equally efficient (Ref. 38). The number of reactions is substantially higher if particular third-body efficiencies must be identified for the propellant combinations and also if condensed species, e.g. carbon were considered. The reaction mechanisms which describe the recombination process of the other propellants are subsets of the CH_4-Flox system, since the combustion species that are present for the H_2-O_2, H_2-F_2 and A50-N_2O_4 (N_2 excepted) are common to the species generated in CH_4-Flox combustion. The exception, nitrogen, which is present in A50-N_2O_4, and possible nitrogen containing species are not involved in significant recombination reactions; however, the nitrogen and its compounds may be significant as third bodies.

The reactions contributing significantly to the recovery of energy during recombination processes are usually limited to three-body reactions. Many other reactions, such as bimolecular reactions, occur in the full mechanism, but they can usually be neglected as secondary in establishing the nonequilibrium performance of the propellant combinations (Refs. 16, 22, 38 and 39). Although the bimolecular reactions are important to the production of selected species for the three-body energetic reactions, their influence on propulsion performance is felt indirectly and only as long as the conditions are present in the nozzle for the three-body recombination reactions to occur at the minimum critical rate (freezing point) (Ref. 16). With the view of reducing the mechanisms to a tolerable number of reactions that can be treated utilizing the modified freezing-point analysis only significant three-body reactions can be considered for the complex combination of species possible for the CH_4 fuel when combined with F_2-O_2

bearing oxidizers and the other fuel-oxidizer combinations. The mechanisms, therefore, have been limited to the principal recombination reactions:

$$H + H + M \longrightarrow H_2 + M$$

$$H + F + M \longrightarrow HF + M$$

$$H + OH + M \longrightarrow H_2O + M$$

where M represents significant third bodies unique to the propellant combination. The selection of the particular three-body reactions has been based in part on analysis performed to correlate space-storable engine test data (Ref. 26). Also studies to establish the sensitivity of performance to reactions and rates include the recent investigations by the ICRPG (Ref. 38) and NASA (Ref. 39). The studies corroborated the conclusions presented earlier in Refs. 13, 16 and 22.

The B_2H_6-OF_2 propellant combination involves at least sixteen (16) gaseous species and as many as fifty (50) reactions when all third bodies are considered as equally efficient (Ref. 38). As in the CH_4-Flox combination the number of reactions is substantially higher if particular third-body efficiencies must be identified. Analagous to CH_4-Flox the important reactions are limited to the three body recombination reactions listed on page 19 with appropriate consideration given to 3rd bodies unique to the B_2H_6-OF_2 propellant combination namely, BF and BOF. The third body efficiencies for BF and BOF were estimated during a separate phase of the contract involving analysis and correlation of B_2H_6-OF_2 performance test data (Ref. 26). The other third bodies, namely H_2, H, HF, and H_2O are common to the propellant combinations.

The recombination mechanism for each propellant combination has not been simplified to the point that only general third bodies, M, are considered. However, the number of individual third bodies have been reduced to include only those of prime importance. It was assumed that the mole fraction concentration of a species must be at least 10^{-4} to be potentially important as a third body for the three-body recombination reactions. Species whose mole fraction concentrations are less than 10^{-4} are considered only if they are prime reactants or products in the mechanism, e.g., OH in the water recombination reaction.

This compromise approach between general and individual third bodies allows maximum flexibility in the kinetic performance charts so that individual reference reaction rates used in this investigation can be changed when better data become available or can be changed to reflect differences in rates as reported in the literature. This is in contrast to the rates listed in the ICRPG compilation presented in Ref. 38, for which only a general third-body effect can be assessed.

The table below summarizes the reaction rate constants and the third-body efficiencies which can be combined to establish the reaction mechanism and rates appropriate for each of the propellant combinations, viz. H_2-O_2, H_2-F_2, A50-N_2O_4, CH_4-Flox and B_2H_6-OF_2.

Summary of Elementary Reactions and Reaction Rate Constants

Reaction	Forward Rate: lbs-moles, ft^{-3}, sec, ^oR
1 $H + H + Ar \rightleftharpoons H_2 + Ar$	$k_f = 4.62 \times 10^{14} T^{-1}$
2 $H + F + Ar \rightleftharpoons HF + Ar$	$k_f = 1.155 \times 10^{15} T^{-1}$
3 $H + OH + Ar \rightleftharpoons H_2O + Ar$	$k_f = 7.85 \times 10^{15} T^{-1}$

Third-Body Efficiencies Relative to Argon

	Reaction		
Third Body	1	2	3
H	20	1	3
H_2	2.5	2.5	3
HF	2.5	2.5	3
CO_2	2	2	10
CO	2	2	3
H_2O	2.5	2.5	20
N_2	2.0	--	3
BOF	2.0	2.0	10
BF	2	2	3

The H_2-O_2 propellant combination mechanism includes reactions (1) and (3) with third bodies H, H_2 and H_2O (a total of six reactions). The H_2-F_2 propellant combination mechanism includes reactions (1) and (2) with third bodies H, H_2 and HF (a total of six reactions).

The A50-N_2O_4 propellant combination mechanism includes reactions (1) and (2) with third bodies H, H_2, H_2O, CO_2, CO and N_2 (a total of 12 reactions).

The CH_4-Flox propellant combination mechanism includes reactions (1), (2) and (3) with third bodies H, H_2, HF, CO_2, CO and H_2O (a total of 18 reactions).

The B_2H_6-OF_2 propellant combination mechanism includes reactions (1), (2) and (3) with third bodies H, H_2, HF, H_2O, BOF, and BF (a total of 18 reactions).

Individual tables of the reactions and rate constants have been expanded for each propellant combination from the above summary and are included separately in the handbook compilation (c.f. Index to Figures and Tables).

The rate constants for the H_2-F_2 system are consistent with the literature data and have been selected by UARL as being representative of the most reliable data available at this time (Refs. 40 and 41).

The rate constants for the H_2-O_2 recombination reactions are also consistent with the literature data. The hydrogen recombination reaction:

$$H + H + M \rightleftharpoons H_2 + M$$

with H and H_2 as third bodies is common to both the H_2-F_2 and H_2-O_2 propellant combination. The rate constant for the water recombination reaction with argon as a third body:

$$H + OH + M \rightleftharpoons H_2O + M$$

has been established from analysis of the experiments of Schott and Bird (Ref. 42) along with the dependent hydrogen recombination rate for:

$$H + H + M \rightleftharpoons H_2 + M$$

as established in Ref. 40 (see e.g. Ref. 43). The effect of H_2O as the third body on the H_2O recombination is about 20 times that of argon as established by comparison of the rate with argon (Ref. 43) and experimentally measured values in flame studies for which H_2O was the significant third body (Refs. 44 and 45).

The third-body efficiencies for H, H_2, HF, CO_2, CO, H_2O, and N_2, BOF, and BF relative to argon for reactions not cited in literature have been estimated and, therefore, are not based on experimental verification. For example, the third-body efficiencies of CO_2, CO, H_2O and N_2 for reaction (1) of the above table are estimated to be near that reported for H_2. The order and relative third-body efficiencies estimated for reaction (3) above are generally consistent with the values recommended in Ref. 46.

Equilibrium & Frozen Performance

The calculation of the equilibrium, frozen, and partial-equilibrium flow properties and performance was performed with the machine program described in Refs. (36 and 37) using latest JANAF thermochemical data (Ref. 47). The Ref. 37 computer program has been found to give results identical to those from the ICRPG reference one-dimensional equilibrium (ODE) program (Ref. 33).

Estimates of the maximum performance that can be obtained from a specific propellant system can be obtained from the equilibrium performance curves presented for each of the propellant systems considered. An estimate of the maximum possible kinetic performance loss can similarly be obtained by comparing the frozen-flow performance with the equilibrium performance for a particular propellant combination; the difference is the maximum kinetic loss.

The maximum thrust available from a particular propellant system with a nozzle of specified exit area ratio and throat radius is obtained from the equilibrium vacuum specific impulse and the appropriate equilibrium mass flow rate tabulated in this handbook (i.e. from Tables I-2, II-2, III-2, IV-2, and V-2). The maximum thrust, T_{max}, is then evaluated by:

$$T_{max} = \pi r_t^2 \left(\frac{\dot{W}}{A}\right)_{equilibrium} \left(I_{SP_{vac}}\right)_{equilibrium} \qquad (16)$$

Additionally, the effective frozen specific heat ratio for a particular propellant and O/F ratio is given in these tables for use with the bell nozzle design curves and divergence loss curves which require specification of specific heat ratio.

Partial-Equilibrium Performance

The procedures outlined in a preceding section of this handbook are utilized to obtain the freezing-point location for a given propellant system in a nozzle of specified geometry under a fixed set of assumed operating conditions. In order to use the freezing-point location to establish the corresponding nonequilibrium (i. e., partial-equilibrium) performance, it is necessary to perform thermochemical calculations which assume that shifting-equilibrium expansion occurs up to the freezing-point location, and that frozen-flow expansion occurs downstream of the freezing-point location. A large number of such calculations have been performed using the Ref. 37 (see also Ref. 33) computer program for each propellant combination considered herein for broad ranges of O/F ratio, combustion chamber pressure and nozzle exit area ratio. The results of these calculations appear in graphical form to show the effect of freezing area ratio on partial-equilibrium specific impulse performance. These graphs are indexed in the "Index to Figures and Tables". Partial-equilibrium performance results for H_2-F_2, H_2-O_2, CH_4-Flox, A50-N_2O_4 and B_2H_6-OF_2, appear in Figs. I-31 to -48, II-31 to -48, IV-31 to -48, and V-25 to V-40, respectively. Entering the appropriate curve with a freezing area ratio

and the nozzle exit area ratio, partial equilibrium specific impulse is obtained. It is to be emphasized that the specific impulse so defined must be reduced by the aerodynamic losses (to be described subsequently) in order to obtain the net deliverable performance.

Aerodynamic Losses

The primary aerodynamic losses which are encountered in expanding flows through convergent-divergent nozzles are three-fold: losses due to viscous dissipation along the nozzle walls, losses due to exit flow divergence and losses due to the nonuniform nature of the flow in the transonic region of the nozzle.

Flow Divergence Loss

The divergence losses presented in this handbook have been calculated by comparing analytical one-dimensional and axisymmetric thrust coefficients for the nozzle types, propellant combinations and conditions considered in this handbook. The computer programs used for these calculations include the two-dimensional equilibrium program (TDE) recommended by the ICRPG (Ref. 33) and developed by the United Aircraft Corporation (Ref. 48) and the one-dimensional equilibrium program described in Ref. 36.

Divergence losses are presented for families of perfect nozzles as a function of amount of nozzle truncation (percentage of the design area ratio) for three values of specific heat ratio (Figs. AL-1, -2 and -3).

For conical nozzles, the divergence loss can be estimated for the larger exit area ratio nozzles -- e.g. (A/A_{min}) exit = 20, as

$$D.L. = \left(\frac{1-\cos\theta}{2}\right) \left(I_{sp_{vac}}\right)_{frozen} \qquad (17)$$

where θ is the half-angle of the conical nozzle. Estimation of divergence loss using this expression is found to be within $\frac{1}{4}\%$ for exit area ratios greater than 20; extension to lower values of area ratio may induce slightly greater divergence losses. Divergence loss is noted to be independent of nozzle scale.

Additionally, divergence losses are presented (Fig. AL-4 and AL-5) for the 15 deg conical and 70% bell nozzles at a series of pressure and thrust levels to allow immediate estimation of divergence loss for these commonly used nozzles. The 70% bell nozzles, as used here, refer to a truncated perfect nozzle 70% of the length of a 15 deg conical nozzle of the same exit area ratio. Thus, for a fixed specific heat ratio, a unique design area ratio is also implied when a 70% bell is discussed. The non-dimensional length of a 70% bell nozzle of specified exit area ratio is given by the equation:

$$\frac{X_e}{r_t} = 0.70\left(\sqrt{\frac{A_e}{A_t}} - 1\right) \Big/ \tan 15^\circ$$

or

$$\frac{X_e}{r_t} = 0.70\left(\frac{\sqrt{\frac{A_e}{A_t}} - 1}{0.26795}\right); \quad \frac{r_e}{r_t} = \sqrt{\frac{A_e}{A_t}} \tag{18}$$

The factor 0.70 would be changed, of course, for the appropriate value for some other truncation criterion, say to (.60) for a 60% bell, etc.

The calculated coordinates of the exit point of a bell nozzle ($\frac{x_e}{r_t}$, $\frac{r_e}{r_t}$) are then plotted on the appropriate Figure: ND-5, -6, or -7 and the nozzle contour required of the design area ratio selected, usually by interpolation. Nozzle area ratio gradients are presented for most of these nozzles in Figure ND-2, -3 and -4 and the appropriate nozzle area ratio gradient obtained for a particular nozzle by interpolation. For these later results divergence losses were evaluated using a chemically-frozen gas model and the corresponding option in the axisymmetric-flow machine program (Ref. 48). Experience has shown the effects of flow divergence and nozzle curvature can be accurately estimated by this flow model (Ref. 25).

Boundary Layer Loss

Frictional boundary layer losses have been evaluated for 15 deg conical and 70% bell nozzles with the modified Bartz boundary layer procedures (Ref. 20) using the ICRPG reference turbulent boundary layer (TBL) computer program (Refs. 33 and 49). In using this program a frozen, axisymmetrical-flow gas model was assumed together with the adiabatic wall temperature option. Use of this gas model and wall temperature option has been shown to provide results consistent with results of rocket engine data correlations (Ref. 25).

Results obtained over wide ranges of conditions are presented in Figs. AL-6 to AL-13. A sufficient number of pressure levels and thrust levels have been examined to allow interpolation of drag loss over the range of pressure and thrust values listed for each propellant in the figures. In contrast to divergence loss, boundary layer loss is known to be a function of nozzle scale. No effect of wall heat transfer has been included in the handbook. The user is referred to Ref. 33 for a more comprehensive treatment of the boundary layer loss mechanism.

Transonic Loss

The flow characteristics in a sonic throat are such that the sonic line is more nearly parabolic than linear and that its position relative to the minimum cross-section is dependent upon the geometric parameters of the throat. It is evident that mass flow calculations based on the assumption of uniform axial flow across the minimum section will be somewhat in error.

The transonic loss accounts for nonuniform transonic flow and for frictional drag loss in the subsonic portion of the nozzle. For throat curvature to throat radius ratios, r_c/r_t, greater than 2 the procedures developed by Hall (Ref. 50) could be utilized. However, the use of such simplified procedures are not applicable for small values of throat approach (subsonic) r_c/r_t (e.g. $r_c/r_t = 1$). For such configurations the transonic solution developed at UAC (Ref. 21) is more applicable and was utilized in order to obtain a corrected mass flow rate, and impulse performance. On the basis of a large number of such calculations it has been found that the transonic loss amounts to a maximum of approximately 0.5% of the shifting equilibrium performance for reasonably configured nozzles (viz. $r_c/r_t > 0.5$). Because of the very small magnitude of this loss, no charts have been prepared to permit its interpolation, and it is recommended that the user assign a conservative value of 0.5% for all nozzles, propellant combinations and conditions considered herein.

Performance Estimation for Gaseous Propellants

Tables and figures presented herein apply to liquid oxidizer-liquid fuel systems. Performance estimates for other than these liquid oxidizer-liquid fuel systems are determinable in the form of ΔI_{sp} values to be used as corrections to the liquid-liquid estimates. A general equation, applicable to gaseous oxidizer-liquid fuel, liquid oxidizer-gaseous fuel and gaseous oxidizer-gaseous fuel systems is presented.

Sufficient data are included in Table 1 to allow calculations of ΔI_{sp} for the various propellants in their commonly used states. In a typical application, for example, cryogenic propellants are injected at their respective boiling points, hence specific heat data for the liquid phase of these components is not presented. In the A50-N_2O_4 system, on the other hand, Aerozine 50 is commonly injected at a "standard" temperature of 77°F (25°C) and as the boiling point of Aerozine 50 is considerably above this value, it is assumed that only liquid phase injection is of interest. Data for N_2O_4 is included for both liquid and gaseous phase since the boiling point of this component is 70°F, and the options of injection of the liquid at a temperature other than the boiling point or of gaseous injection are available to the user.

An average specific heat has been presented for the propellants in Table 1; no great effect on ΔI_{sp} was found to occur as a result of this approximation and it does afford considerable simplification in the calculation of ΔI_{sp}.

The performance of a system with one or both components in a gaseous state may be estimated from the approximate equation:

$$I_{sp}{}_{\substack{g\cdot\ell \\ \ell\cdot g \\ \ell\cdot\ell}} = \sqrt{\frac{2J}{g}\cdot\overline{\Delta H} + I_{sp_{\ell\ell}}^{2}} \qquad (19)$$

where $I_{sp_{\ell\ell}}$ = Equilibrium vacuum specific impulse of the liquid-liquid systems;

$J = 778 \frac{ft \cdot lb}{BTU}$; g = gravitational constant (32.174 ft/sec^2) (in metric units,

$J/g = 1 \frac{N\ sec^2}{kg\text{-}m}$

and

$$\overline{\Delta H} = \frac{\Delta H_{FUEL} + (O/F)\ (\Delta H_{OXIDIZER})}{1 + O/F} \tag{20}$$

where: ΔH_{FUEL} = (Enthalpy of fuel at desired state) - (Enthalpy of liquid fuel at its boiling point)

$\Delta H_{oxidizer}$ = (Enthalpy of oxidizer at desired state) - (Enthalpy of liquid oxidizer at its b.p.)

O/F = oxidizer-fuel weight ratio

Since ΔI_{sp} corrections are necessarily small relative to the total equilibrium performance value, calculations may be simplified by retaining only the first term of a Maclaurin series expansion of the full equation for approximate performance gain:

Defining:

$$\Delta I_{sp} = I_{sp}{}_{\substack{g\cdot\ell \\ \ell\cdot g \\ g\cdot g}} - I_{sp_{\ell\ell}} \tag{21}$$

one obtains:

$$\Delta I_{sp} = (1/2^*)\left(\frac{2J}{g}\overline{\Delta H}\right)\left(\frac{1}{I_{sp_{\ell\ell}}}\right) \tag{22}$$

which can then be applied as a correction to the liquid-liquid performance obtained from the tables and figures presented in this handbook.

Values of the heat of vaporization for each fuel and oxidizer used in the handbook are presented in Table 1 and are for the particular component in the gaseous state at its boiling point. Values of average specific heat are also presented to allow calculation of sensible enthalpy change of the propellant component if it is desired to inject the component into the combustion chamber at some temperature T other than its boiling point:

$$\Delta H_j = \int_{T_{injection}}^{T_{B.P.j}} C_{p_j}{}_{liquid}\ dT + H_{vap_j} + \int_{T_{B.P.j}}^{T} C_{p_j}{}_{gas}\ dT \tag{23}$$

where j = FUEL or OXIDIZER

or, in terms of the average specific heat, C_{p_j}:

$$\Delta H_j = \overline{c_{pj}}_{liquid} (T_{BP_j} - T_{inject}) + H_{vap_j} + \overline{c_{pj}}_{gas} (T_j - T_{BP_j}) \qquad (24)$$

where ΔH_{VAP_j}; T_{BP_j} and C_{p_j} are obtained from Table 1.

The resulting ΔH_j is then used in Eq. 20 to find the mean $\overline{\Delta H}$ to use in Eq. 22 to establish the performance change due to the altered component.

As an example, choose a $H_2(\ell)$-$O_2(g)$ system operating at an O/F = 6 with the gaseous oxidizer injected at 100°F above its boiling point.

From Eq. (24)

$$\Delta H \text{ oxidizer} = 91.69 \text{ BTU/lb} + 100 \times \overline{C_p} = 104 \text{ BTU/lb}$$

$$\Delta H_{fuel} = 0$$

From Eq. (22)

$$\Delta I_{sp} = \tfrac{1}{2} \cdot \frac{\left(\frac{2J}{g}\right)\left(\overline{\Delta H}\right)}{I_{sp_{\ell\ell}}} = \tfrac{1}{2}\left(\frac{48.362(104)}{I_{sp_{\ell\ell}}}\right)$$

$I_{sp_{\ell\ell}}$ is then selected from the appropriate figure at the specified chamber pressure and nozzle exit area ratio, for example, from figure II-1,

$$@ \text{ 100 psia, } (A/A_{min})_{exit} = 100,$$

$$I_{sp_{\ell\ell}} = 465.2 \text{ sec } (4559.0 \text{ N·sec/kg})$$

$$\Delta I_{sp} = 5.4 \text{ sec } (52.9 \text{ N·sec/kg})$$

Net performance for the $H_2(\ell)$-$O_2(g)$ is then:

$$I_{sp_{\ell g}} = I_{sp_{\ell\ell}} + \Delta I_{sp} = 465.2 + 5.4 = 470.6 \text{ sec } (4611.9 \text{ N·sec/kg})$$

Table 1

Thermodynamic Properties for Performance Estimation of Gaseous Propellants

Component	$\Delta H_{vaporization}$ Btu/lb	$\Delta H_{vaporization}$ Kcal/mole	$T_{boiling}$ °F	$T_{boiling}$ °C	$\overline{C}_p$ Btu/lb·°R or $\frac{Kcal}{Kg.°C}$
O_2	91.7	1.63	-297.4	-183.0	0.22
H_2	191.8	0.2148	-423.2	-252.9	3.50
F_2	73.9	1.56	-306.7	-188.1	0.19
CH_4	219.4	1.96	-242.5	-152.5	0.52
Flox	77.0	1.572	-305.0	-187.3	0.18
N_2O_4	178.2*	9.11	70.0	21.15	0.37** 0.65
A50	425.8*	9.54	190.0	87.8	0.70**
OF_2	88.67	2.66	-229.5	-145.3	0.17
B_2H_6	221.2	3.41	-134.5	- 92.5	0.36

* at 77°F (25°C)
** Liquid

Summary of Relevant Equations for Performance Calculations

$$T_{max} = \pi \; r_t^2 \left(\frac{\dot{W}}{A}\right)_{equilibrium} \quad \left(I_{sp_{vac}}\right)_{equilibrium} \tag{16}$$

$$\text{Conical nozzle divergence loss} = \left(\frac{1-\cos\theta}{2}\right) \left(I_{sp_{vac}}\right)_{frozen} \tag{17}$$

$$\frac{X_e}{r_t} = 0.70\left(\sqrt{\frac{A_e}{A_t}} - 1\right)\left(\frac{1}{0.26795}\right)$$

$$\frac{r_e}{r_t} = \sqrt{\frac{A_e}{A_t}} \tag{18}$$

$$I_{sp}\begin{matrix} g\cdot\ell \\ \ell\cdot g \\ g\cdot g \end{matrix} = \sqrt{\frac{2J}{g}\cdot\overline{\Delta H} + I_{sp_{\ell\ell}}^2} \tag{19}$$

$$\overline{\Delta H} = \frac{\Delta H_{Fuel} + O/F\left(\Delta H_{oxidizer}\right)}{1 + O/F} \tag{20}$$

$$\Delta I_{sp} = I_{sp}\begin{matrix} g\cdot\ell \\ \ell\cdot g \\ g\cdot g \end{matrix} - I_{sp_{\ell\ell}} \tag{21}$$

$$I_{sp} = \frac{1}{2}\left(\frac{2J}{g}\,\overline{\Delta H}\right)\frac{1}{I_{sp_{\ell\cdot\ell}}} \tag{22}$$

$$\Delta H_j = \int_{T_{inject}}^{T_{bpj}} C_{pj_{liquid}}\,dT + H_{vap_j} + \int_{T_{bpj}}^{T_j} C_{pj_{gas}}\,dT \tag{23}$$

$$\Delta H_j = \overline{C_{pj}}_{liquid}\left(T_{BP_j} - T_{inject}\right) + H_{vap_j} + \overline{C_{pj}}_{gas}\left(T_j - T_{BP_j}\right) \tag{24}$$

$$\text{Transonic Loss} = 0.005\left(I_{sp_{vac}}\right)_{equilibrium} \tag{25}$$

$$\left(I_{sp_{vac}}\right)_{net} = \left(I_{sp_{vac}}\right)_{\substack{partial \\ equilibrium}} - \sum \left(\Delta I_{sp}\right)_{\substack{aerodynamic \\ loss}} \tag{26}$$

$$T_{net} = \left(I_{sp_{vac}}\right)_{net} * \left(\frac{\dot{W}}{A}\right)_{equilibrium} * \pi r_t^2 \tag{27}$$

$$r_{t_{net}} = \left[\frac{T}{\left(\frac{\dot{W}}{A}\right)_{equilibrium} * \pi * \left(I_{sp_{vac}}\right)_{equilibrium}}\right]^{1/2} \tag{28}$$

$$r_{t_{net}} = \left[\frac{T}{\left(\frac{\dot{W}}{A}\right)_{equilibrium} * \pi * \left(I_{sp_{vac}}\right)_{net}}\right]^{1/2} \tag{29}$$

INDEX TO FIGURES AND TABLES

	Figures and Tables
I. Geometrical Considerations	
1. Conical Nozzle Area Ratio Gradients	ND-1
2. Bell Nozzle Area Ratio Gradients	ND-2 to ND-4
3. Bell Nozzle Contours	ND-5 to ND-7
II. Gross Performance Estimation	
Hydrogen-Fluorine System	
1. Reaction Rate Table	Table I-1
2. Nozzle Throat Flow Properties	Table I-2
3. Equilibrium and Frozen Flow Performance	I-1 to I-12
4. Equilibrium and Kinetic Gradients	I-13 to I-30
5. Partial Equilibrium Performance	I-31 to I-48
Hydrogen-Oxygen System	
1. Reaction Rate Table	Table II-1
2. Nozzle Throat Flow Properties	Table II-2
3. Equilibrium and Frozen Flow Performance	II-1 to II-12
4. Equilibrium and Kinetic Gradients	II-13 to II-30
5. Partial Equilibrium Performance	II-31 to II-48
Methane-Flox System	
1. Reaction Rate Table	Table III-1
2. Nozzle Throat Flow Properties	Table III-2
3. Equilibrium and Frozen Flow Performance	III-1 to III-12
4. Equilibrium and Kinetic Gradients	III-13 to III-30
5. Partial Equilibrium Performance	III-31 to III-48
Aerozine 50-N_2O_4 System	
1. Reaction Rate Table	Table IV-1
2. Nozzle Throat Flow Properties	Table IV-2
3. Equilibrium and Frozen Flow Performance	IV-1 to IV-12
4. Equilibrium and Kinetic Gradients	IV-13 to IV-30
5. Partial Equilibrium Performance	IV-31 to IV-48
Diborane - OF_2 System	
1. Reaction Rate Table	Table V-1
2. Nozzle Throat Flow Properties	Table V-2
3. Equilibrium and Frozen Flow Performance	V-1 to V-8
4. Equilibrium and Kinetic Gradients	V-9 to V-24
5. Partial Equilibrium Performance	V-25 to V-40

		Figures and Tables
III.	Aerodynamic Losses	
	1. Divergence Loss for General Perfect Nozzles	AL-1 to AL-3
	2. Divergence Loss for 15 deg Conical Nozzles	AL-4
	3. Divergence Loss for 70% Bell Nozzles	AL-5
	4. Viscous Drag for 15 deg Conical Nozzles	AL-6 to AL-8
	5. Viscous Drag for 70% Bell Nozzles	AL-9 to AL-13

SAMPLE CALCULATIONS

Examples of the calculation procedure are presented to enable the user to familiarize himself with the mechanics of estimation of nozzle performance.

Example 1. Performance Estimation Of Specified Conical Nozzle

Using the handbook in the performance mode, estimate the net performance of the following 15 deg conical nozzle operating as specified:

(1) Nozzle: 15 deg conical

$r_t = 0.3333$ ft (0.1016 m)

$(A/A_{min})_{exit} = 100$

(2) Propellant and Conditions: $H_2(\ell)$-$F_2(\ell)$

O/F = 12

$P_c = 100$ psia (6.895×10^5 N/m^2)

Quantities to be determined are:

(1) Equilibrium performance (Fig. I-1); frozen performance (Fig. I-2); and maximum thrust (Eq. 16) and Table I-2
(2) Freezing point (Fig. I-14); partial-equilibrium performance (Fig. I-32)
(3) Aerodynamic losses: Flow divergence loss (Eq. 17); drag loss (Fig. AL-6) and transonic loss ($\frac{1}{2}$% of equilibrium performance) (Eq. 25)
(4) Net performance (partial-equilbrium I_{sp}- Σ (aerodynamic losses)) (Eq. 26).

Actual determination of values for the above quantities proceeds as follows:

(1) For this H_2-F_2 system operating at 100 psia and an O/F = 12, and a nozzle of $(A/A_{min})_{exit} = 100$, the equilibrium performance is 488 sec ($4782 \frac{N \cdot sec}{kg}$) obtained from Fig. I-1. Frozen performance is likewise obtained from Fig. I-2 for this system and is found to be 415.5 sec ($4072 \frac{N \cdot sec}{kg}$). The partial equilibrium performance must lie between these two values. The maximum thrust obtainable with this nozzle can be found by using the equilibrium mass flow rate in Table I-2, the equilibrium vacuum specific impulse and the nozzle throat radius in Eq. 16:

$$T_{max} = \pi r_t^2 * \frac{\dot{W}}{A} * (I_{sp_{vac}})_{eq}$$

or

$$T_{max} = 3.1416\ (0.3333)^2\ (58.3)\ (488)$$

or

$$T_{max} = 9931\ \text{lb}\ (4.417 \times 10^4 \text{N})$$

(2) In Fig. I-14, dividing the equilibrium gradient for the 15 deg conical nozzle with r_t = 1.0 ft (0.3048 m) by the specified throat radius r_t = 0.3333 ft (0.1016 m) gives the new equilibrium curve for the smaller nozzle. The intersection of this new equilibrium curve with the composite kinetic curve establishes the freezing point which is found to occur at (A/A_{min}) = 2.10.

An alternative procedure to establish the freezing point location is to utilize the second equilibrium gradient curve presented in Fig. I-14 along with the appropriate data from Fig. ND-1.

For several values of area ratio, values of area ratio gradient are picked from Fig. ND-1. The selected points are given in columns 1 and 2 in table below. These area ratio gradient values are then divided by the throat radius of the desired nozzle and are tabulated in column 3 of the table. From Fig. I-14 one obtains the kinetic gradient for a nozzle of unity area ratio gradient for each previously selected value of area ratio (col. 1) and these are given in column 4. The net equilibrium H-atom gradient is then calculated by the following equation and listed in column 5,

$$\left.\frac{\partial [H]}{\partial t}\right|_{eq} = \frac{1}{r_t} \left\{ \frac{d\left(A/A_{MIN}\right)}{d\left(X/r_t\right)} \right\} \left(\frac{\partial H}{\partial t}\right)_{eq}; \left[\frac{d\left(A/A_{MIN}\right)}{dX} = 1\right]$$

or

$$\left.\frac{\partial H}{\partial t}\right|_{eq} = (\text{Column 3}) * (\text{Column 4})$$

and is calculated for each value of A/A_{min} in column 1.

This resulting data is then plotted on Fig. I-14 (an overlay should be used) and the intersection of the resulting curve with the "composite kinetic (transition factor = 2)" curve in this figure establishes the freezing point.

1	2	3	4	5
A/A_{MIN}	$\left(\frac{d(A/A_{MIN})}{d(X/r_t)}\right)$	$\frac{1}{r_t}\left(\frac{d(A/A_{MIN})}{d(X/r_t)}\right)$	$\left(\frac{\partial[H]}{\partial t}\right)_{eq.,\left[\frac{d\,A/A_{MIN}}{dX}\right]=1}$	$\left(\frac{\partial H}{\partial t}\right)_{eq}$
1.02	0.18	0.54	0.90	0.486
1.05	0.40	1.20	0.60	0.720
*1.08	0.555	1.665	0.50	0.833
1.20	0.585	1.755	0.30	0.526
1.50	0.660	1.980	0.13	0.257
2.00	0.760	2.280	0.075	0.171
2.50	0.85	2.55	0.047	0.120

This procedure is necessary when other than 15 deg conical nozzles are examined. The values of area ratio gradient may be obtained for conical nozzles of various r_c/r_t and half angle specification from Fig. ND-1, and perfect nozzles of specified design area ratios from Figs. ND-2, -3, -4. For the conical nozzle-circular arc combinations shown in Fig. ND-1, the area ratio gradient is obtained by following the desired r_c/r_t curve from the throat to the intersection of this curve with the conical section curve of the specified half-angle and then following this curve. The intersection of the two curves represents the point at which the circular-arc and conical section are tangent and the contour is conical downstream of this point. Using either procedure, once the freezing point is established, the partial equilibrium performance is then obtained from Fig. I-32. For this case with $(A/A_{min})_{fr} = 2.10$, the nonequilibrium performance is 461.7 sec $(4525 \frac{N.sec}{kg})$.

(3) For a 15 deg conical nozzle, divergence loss is calculated from Eq. 17 (or found from Fig. AL-4).

$$D.L. = \frac{1-\cos\theta}{2} (I_{sp_{vac}})_{frozen}$$

$$= \frac{1-0.96593}{2} * 415.5$$

$$D.L. = 7.1 \text{ sec } (69 \frac{N\cdot sec}{kg})$$

By interpolation, the drag loss is estimated from Fig. AL-6 as (1.2%)* $(I_{sp_{vac}})_{frozen}$ (Fig. I-2) = 1.2% * 415.5 = 5.0 sec $(48.9 \frac{N\cdot sec}{kg})$ for this nozzle. Transonic loss is $\frac{1}{2}\%$ * $(I_{sp_{vac}})_{equilibrium}$

*Tangent point and transition from circular-arc throat to conical skirt

(Fig. I-1) and is 2.4 sec ($23.9 \frac{N \cdot sec}{kg}$).

(4) Net performance is then the partial equilibrium performance (Fig. I-32) less the component losses (Eq. 26):

$$(I_{sp_{vac}})_{net} = (I_{sp_{vac}})_{partial\text{-}eq.} - \Sigma (\Delta I_{sp})_{aerodynamic\ loss}$$

$$= 461.7-(7.1 + 5 + 2.4)$$

thus

$$(I_{sp_{vac}})_{net} = 447.2 \text{ sec} \quad (4383 \frac{N \cdot sec}{kg})$$

(5) Net thrust is the net vacuum specific impulse times the equilibrium mass flow at the throat (Table II) (Eq. 10)

$$T_{net} = (I_{sp_{vac}})_{net} * (\frac{\dot{W}}{A})_{eq} * A_t$$

$$T_{net} = 447.2 \text{ sec} * 58.3 \frac{lb}{sec} * \pi * (3333)^2 = 9101/lb \ (4.048 \times 10^4 N)$$

Performance results and the appropriate figures and equations are summarized below:*

Equilibrium Performance	488 sec ($4782 \frac{N \cdot sec}{kg}$)	Figure I-1
Frozen Performance	415.5 sec ($4072 \frac{N \cdot sec}{kg}$)	Figure I-2
Freezing Area Ratio	2.10	Figure I-14
Kinetic Performance	461.7 sec ($4525 \frac{N \cdot sec}{kg}$)	Figure I-32
Equilibrium Mass Flow	58.3 lb/sec/ft^2 ($284.7 \frac{kg}{sec^2 m^2}$)	Table I-2
Maximum Thrust Possible	9931 lb ($4.417 \times 10^4 \frac{N \cdot sec}{kg}$)	Equation 16
Aerodynamic Drag	5.0 sec ($48.9 \frac{N \cdot sec}{kg}$)	Figure AL-6
Divergence Loss	7.1 sec ($69 \frac{N \cdot sec}{kg}$)	Equation 17
Transonic Loss	2.4 sec ($23.9 \frac{N \cdot sec}{kg}$)	Equation 25
Net Delivered Performance	447.2 sec ($4383 \frac{N \cdot sec}{kg}$)	Equation 26
Net Delivered Thrust	9101 lb ($4.048 \times 10^4 \frac{N \cdot sec}{kg}$)	Equation 27

*A summary of relevant equations may be found on p. 24.

Example 2. Performance Estimation Of Specified Bell Nozzle

Using the handbook in the performance mode, estimate the net performance of the following bell nozzle operating as specified:

(1) Nozzle: Bell, $(A/A_{min})_{design} = 300$

$r_c/r_t = 1.0$

$r_t = 0.3333$ ft. (0.1016m)

$(A/A_{min})_{exit} = 100$

(2) Propellant and Conditions: $H_2(\ell)$-$F_2(\ell)$

$O/F = 12$

$P_c = 100$ psia (6.895×10^5 N/m^2)

Quantities to be determined are:

(1) Equilibrium performance (Fig. I-1), frozen performance (Fig. I-2) and maximum thrust (Eq. 16) and Table I-2.
(2) Freezing point (Fig. I-14), partial equilibrium performance (Fig. I-32).
(3) Aerodynamic losses: Flow divergence loss (Fig. AL-3), drag loss (Fig. AL-8) and transonic loss ($\frac{1}{2}\%$ of equilibrium performance) (Eq. 25).
(4) Net Performance (partial equilibrium I_{sp} - Σ(aerodynamic losses)) (Eq. 26).

Determination of values for the above quantities proceeds as follows:

(1) For this H_2-F_2 system operating at 100 psia and an O/F = 12 and a nozzle of $(A/A_{min})_{exit} = 100$, the equilibrium performance is 488 sec ($4782 \frac{N \cdot sec}{kg}$) obtained from Fig. I-1. Frozen performance is obtained from Fig. I-2 for this system and is found to be 415.5 sec ($4072 \frac{N \cdot sec}{kg}$).

The partial equilibrium performance must lie between these two values. The maximum thrust obtainable with this nozzle can be found by using the equilibrium mass flow rate in Table II, the equilibrium vacuum specific impulse and the nozzle throat radius in Eq. 16:

$$T_{max} = \pi * r_t^2 * \frac{\dot{W}}{A} * (I_{sp_{vac}})_{eq}$$

or

$$T_{max} = 3.1416\ (0.3333)^2 * (58.3) * (488)$$

or

$$T_{max} = 9931\ \text{lb}\ (4.417 \times 10^4 \text{N})$$

(2) The appropriate specific heat ratio is found from Table I-2 to be 1.34, thus, the perfect nozzle contour from Fig. ND-7 ($\gamma = 1.35$) and the corresponding nozzle gradient from Fig. ND-4 ($\gamma = 1.35$) are utilized. Interpolation between the values of area ratio gradient for $\gamma = 1.30$ (Fig. ND-3) and $\gamma = 1.35$ (Fig. ND-4) has been avoided since the actual specific heat ratio and the Fig. ND-4 value differ by a small amount for the sake of clarity in this example.

In order to establish the freezing point, the alternative procedure described in step (2), example 1 must be followed. The area ratio gradient values obtained from Fig. ND-4, the normalized equilibrium gradient from Fig. I-14 and the calculated equilibrium gradient shown below:

A/A_{MIN}	$\left(\frac{d(A/A_{MIN})}{d(X/r_t)}\right)$	$\frac{1}{r_t}\left(\frac{d(A/A_{MIN})}{d(X/r_t)}\right)$	$\left(\frac{\partial[H]}{\partial t}\right)_{eq;\left[\frac{d(A/A_{MIN})}{dX}\right]=1}$	$\left(\frac{\partial H}{\partial t}\right)_{eq}$
1.2	1.07	3.21	0.30	.963
1.4	1.32	3.96	0.17	.673
1.6	1.44	4.32	0.12	.518
1.8	1.55	4.65	0.091	.423
2.0	1.65	4.95	0.075	.371
2.5	1.84	5.52	0.047	.259

where $$\left.\frac{\partial H}{\partial t}\right|_{eq} = \frac{1}{r_t}\left\{\frac{d(A/A_{MIN})}{d(X/r_t)}\right\}\left(\frac{\partial H}{\partial t}\right)_{eq;\left[\frac{d(A/A_{MIN})}{dX}=1\right]}$$

The values of equilibrium gradient tabulated above are then plotted on Fig. I-14 and the intersection of the equilibrium and composite kinetic curve employing a transition factor of 2 curves establishes the freezing point at $(A/A_{min}) = 1.75$.

The partial equilibrium performance is then obtained from Fig. I-32. For the present example and the freezing area ratio of 1.75, the

partial equilibrium performance is 457 sec ($4479 \frac{N \cdot sec}{kg}$).

(3) By interpolation from Fig. AL-3, the divergence loss is found to be 1.3% times $(I_{sp_{vac}})_{frozen}$ (Fig. I-2):

$$D.L. = .013 \cdot 415.5$$

$$D.L. = 5.4 \text{ sec } (52.9 \frac{N \cdot sec}{kg})$$

Interpolation on Fig. AL-8 gives an estimate of drag loss for this nozzle as 1% * $(I_{sp_{vac}})_{frozen}$ (Fig. I-2) = .01 * 415.5 = 4.2 sec ($41 \frac{N \cdot sec}{kg}$). As the 70% bell nozzles had about the same truncation fraction as the present example, the 70% bell curves are used for drag loss estimation without appreciable error. Transonic loss is

$\frac{1}{2}\%$ $(I_{sp_{vac}})_{eq}$ (Fig. I-1) = .005 * 488 = 2.4 sec ($23.5 \frac{N \cdot sec}{kg}$).

(4) Net performance is then the partial equilibrium performance less the component losses (Eq. 26)

$$(I_{sp_{vac}})_{net} = (I_{sp_{vac}})_{partial\ eq.} - \Sigma (\Delta I_{sp})_{aerodynamic\ loss}$$

$$= 457 - (5.4 + 4.2 + 2.4)$$

$$(I_{sp_{vac}})_{net} = 455 \text{ sec } (4361 \frac{N \cdot sec}{kg})$$

Performance results and the appropriate figures and equations are summarized below:

Equilibrium Performance	488 sec ($4782 \frac{N \cdot sec}{kg}$)	Figure I-1
Frozen Performance	415.5 sec ($4072 \frac{N \cdot sec}{kg}$)	Figure I-2
Freezing Area Ratio	1.75	Figure I-14
Kinetic Performance	457 sec ($4479 \frac{N \cdot sec}{kg}$)	Figure I-32
Equilibrium Mass Flow	$58.3 \frac{lbm}{sec\ ft^2}$ ($284.7 \frac{kg}{sec\ m^2}$)	Table I-2
Maximum Possible Thrust	9931 lb (4.417×10^4N)	Equation 16
Aerodynamic Drag	4.2 sec ($41 \frac{N \cdot sec}{kg}$)	Figure AL-8
Divergence Loss	5.4 sec ($52.9 \frac{N \cdot sec}{kg}$)	Figure AL-3

Transonic Loss	2.4 sec (23.5 $\frac{N.sec}{kg}$)	Equation 25
Net Delivered Performance	445 sec (4361 $\frac{N.sec}{kg}$)	Equation 26
Net Delivered Thrust	9056.16 (4.028×10^4N)	Equation 27

Example 3. Selection of Conical Nozzle of Specified Thrust

Using the contour selection mode, size a 15 deg conical nozzle of specified exit area ratio and throat radius ratio to deliver 1000 lb (4448N) thrust utilizing the specified propellant and operating conditions.

(1) Nozzle: 15° conical

$(A/A_{min})_{exit} = 60$

$r_c/r_t = 1.0$

Deliver 1000 lb (4448N) net thrust

(2) Propellant and Conditions: $H_2(\ell)$-$O_2(\ell)$

$O/F = 6$

$P_c = 200$ psia (1.379×10^6 N/m^2)

In order to establish the required nozzle throat radius the following quantities must be determined:

(1) Equilibrium performance (Fig. II-3) and frozen performance (Fig. II-4).
(2) Equilibrium mass flow at the throat (Table II-2) and the approximate throat size:

$$r_t = \left(\frac{T}{\frac{\dot{W}}{A} \cdot \pi \cdot (I_{sp_{vac}})_{eq.}} \right)^{\frac{1}{2}} \qquad \text{(Eq. 28)}$$

(3) Freezing point (Fig. II-17) and nonequilibrium performance (Fig. II-35).
(4) Aerodynamic Losses: Flow divergence loss (Eq. 17), drag loss (Fig. AL-7) and transonic loss ($\frac{1}{2}$% of equilibrium performance) (Eq. 25).
(5) Since the nozzle throat size required to deliver a specified thrust is dependent on the aerodynamic and kinetic losses which themselves are functions of nozzle throat size, the exact nozzle radius must be established through an iterative process.

Evaluation of the above quantities follows:

(1) For an H_2-O_2 propellant at an O/F = 6 and P_c = 200 psia and a nozzle of exit area ratio 60, the equilibrium performance from (Fig. II-3) is found to be 457.5 sec ($4484 \frac{N \cdot sec}{kg}$). Similarly, the frozen performance from Fig. II-4 is 425 sec ($4165 \frac{N \cdot sec}{kg}$).

(2) Equilibrium mass flow at the throat is found from Table II-2 to be 124.2 lb/sec/ft^2 ($606.5 \frac{kg}{sec\ m^2}$) the approximate throat radius is then (Eq. 21)

$$r_t = \left(\frac{T}{\frac{\dot{W}}{A} \cdot \pi \cdot (I_{sp_{vac}})_{eq.}} \right)^{\frac{1}{2}}$$

$$r_t = \left(\frac{1000}{(124.2)(3.1416)(457.5)} \right)^{\frac{1}{2}}$$

$$r_t = 0.075 \text{ ft } (0.0229m)$$

(3) Once the throat radius has been calculated the freezing point may be established. In Fig. II-17, the equilibrium gradient for the 15 deg conical nozzle with r_t = 1.0 ft (0.3048m) is dividied by the throat radius determined above, r_t = 0.075 ft (0.0229m). This new equilibrium curve is then plotted on Fig. II-17 and its intersection with the composite kinetic curve establishes the freezing point which is found to occur at (A/A_{min}) = 1.24. The nonequilibrium performance is then obtained from Fig. II-35 and is 441 sec ($4322 \frac{N \cdot sec}{kg}$).

(4) For a 15 deg conical nozzle divergence loss is calculated from Eq. 17:

$$\text{D. L.} = \frac{1-\cos\theta}{2} (I_{sp_{vac}})_{frozen} \text{ (Fig. II-4)}$$

$$= \left(\frac{1-0.96593}{2}\right) * 425$$

$$\text{D. L.} = 7.2 \text{ sec } (71.0 \frac{N \cdot sec}{kg})$$

Drag loss is obtained by interpolation from Fig. AL-7 and is

$1.4\%* (I_{sp_{vac}})_{frozen}$ (Fig. II-4) = (0.014)(425) = 6.0 sec ($58.3 \frac{N \cdot sec}{kg}$).

Transonic loss is 0.005 * $(I_{sp_{vac}})_{eq}$. (Fig. II-3) = (0.005) (457.5) = 2.3 sec (22.4 $\frac{N \cdot sec}{kg}$).

(5) Net performance is then the partial-equilibrium performance less the component losses (Eq. 26)

$$(I_{sp_{vac}})_{net} = (I_{sp_{vac}})_{partial\ eq.} - \Sigma(\Delta I_{sp})_{\substack{aerodynamic \\ loss}}$$

$$= 441 - (7.2 + 6.0 + 2.3)$$

Thus

$$(I_{sp_{vac}})_{net} = 425.5 \text{ sec } (4170 \frac{N \cdot sec}{kg})$$

The delivered thrust is thus, from Eq. 20,

$$T_{net} = (I_{sp_{vac}})_{net} (\frac{\dot{W}}{A})_{eq} \pi r_t^2$$

$$= (425.5)(124.2)(3.1416)(0.075)^2$$

$$= 933.9 \text{ lbs } (4154N)$$

As this delivered thrust is less than the specified thrust, throat radius should be increased slightly and the calculation repeated for this increased nozzle size and iteration continued until the required delivered thrust is obtained. A good approximation to the required throat radius may be obtained by using the calculated delivered specific impulse instead of the equilibrium value initially used in the radius equation (Eq. 22):

$$r_t = \left(\frac{T}{\frac{\dot{W}}{A} \pi (I_{sp_{vac}})_{net}} \right)^{\frac{1}{2}}$$

For the present example, this becomes

$$r_t = \left(\frac{1000}{(124.2)(3.1416)(425.5)} \right)^{\frac{1}{2}}$$

$$r_t = 0.0776 \text{ ft } (0.0237m)$$

and is accepted as a final value for r_t since no discernible change in partial equilibrium performance or in the aerodynamic losses was found.

Performance results and the appropriate figures and equations are summarized below for the first iteration.

Equilibrium Performance	457.5 sec (4490 $\frac{N \cdot sec}{kg}$)	Figure II-3
Frozen Performance	425 sec (4160 $\frac{N \cdot sec}{kg}$)	Figure II-4
Freezing Area Ratio	1.24	Figure II-17
Kinetic Performance	439 sec (4303 $\frac{N \cdot sec}{kg}$)	Figure II-35
Equilibrium Mass Flow	124.2 $\frac{lbm}{sec\ ft^2}$ (606.5 $\frac{kg}{sec\ m^2}$)	Table II-2
Aerodynamic Drag	6.0 sec (58.3 $\frac{N \cdot sec}{kg}$)	Figure AL-7
Divergence Loss	7.2 sec (71.0 $\frac{N \cdot sec}{kg}$)	Equation 17
Transonic Loss	2.3 sec (22.4 $\frac{N \cdot sec}{kg}$)	Equation 25
Net Delivered Performance	423.5 sec (4150 $\frac{N \cdot sec}{kg}$)	Equation 26
Net Delivered Thrust	929.5 lbs (4134N)	Equation 27

Example 4. Establishing The Effect Of Reaction Rate Change

Utilizing the handbook in the performance mode, establish the effect on kinetic performance of a 4 fold increase in the reaction rate constants for the specified propellant, operating conditions and nozzle:

(1) Nozzle: 15 deg cone

$(A/A_{min})_{exit} = 100$

$r_t = 1.0$ ft (0.3048m)

$r_c/r_t = 1$

(2) Propellant and Conditions: $H_2(\ell)$-$F_2(\ell)$

O/F = 8

$P_c = 100$ psia (6.895×10^5 N/m^2)

(3) Reaction Rates: Reaction rates uniformly adjusted to 4 times the reference rates used for the handbook preparation (Table I-1).

Quantities to be determined:

(1) Freezing point (Fig. I-13) with standard rates (Table I-1) and corresponding nonequilibrium performance (Fig. I-31).
(2) Freezing point (Fig. I-13) with new reaction rates (each rate in Table I-1 times 4) and corresponding nonequilibrium performance (Fig. I-31).
(3) Net Performance change due to reaction rate increase.

Calculations of the above quantities follows:

(1) The equilibrium gradient curve for the 15 deg conical nozzle, r_t = 1 ft (0.3048m) is shown in Fig. I-13. The freezing point located at the intersection of the composite kinetic and equilibrium curves is at A/A_{min} = 1.90. The corresponding partial equilibrium performance is then, from Fig. I-31, 471 sec

($4616 \frac{N \cdot sec}{kg}$).

(2) Since all the component reactions have been multiplied by a factor of 4, the sum of the component reactions has also multiplied by 4 and the composite kinetic curve is increased by this factor, and replotted on Fig. I-13, establishing the new freezing point at A/A_{min} = 2.5. The corresponding nonequilibrium performance is seen from Fig. I-31 to be 476 sec ($4665 \frac{N \cdot sec}{kg}$).

(3) A performance gain of 5 sec ($49 \frac{N \cdot sec}{kg}$) is thus realized by an increase in the reaction rates of a factor of 4.

Performance results and the appropriate figures and equations are summarized below:

Original Freezing-Area Ratio	1.90	Figure I-13
Kinetic Performance	471 sec ($4616 \frac{N \cdot sec}{kg}$)	Figure I-31
Revised Freezing-Area Ratio	2.5	Figure I-13
Revised Kinetic Performance	476 sec ($4665 \frac{N \cdot sec}{kg}$)	Figure I-31
Net Performance Change	+5 sec ($+49 \frac{N \cdot sec}{kg}$)	

LIST OF SYMBOLS

a	Forward rate parameter (see Eq. 2)
A	Area
A_{min}	Minimum area
$I_{sp_{vac}}$	Vacuum Specific Impulse
J	General Molecular Species (see Eq. 1)
k_f	Reaction rate constant in forward direction
k_b	Reaction rate constant in backward direction
M	General molecular species or general third body
O/F	Oxidizer-fuel ratio
P_c	Chamber pressure
r	Radius
r_c	Throat radius of curvature
r_t	Throat radius
t	Time
T	Thrust
V	Velocity in axial direction
W	Molecular weight
$\overline{W}$	Mean molecular weight
$\dot{W}/A$	Specific mass flow rate
x	Axial distance
x_i	Mole fraction
y	Concentration ratio defined by Eq. (2)

α'_{ij}, α''_{ij}	Stoichiometric coefficients of the th species in the jth reaction for the reactants and products
γ	Specific heat ratio
θ	Conical (divergence) half-angle
ρ	Density

Subscripts

eq	Equilibrium conditions evaluated on the basis of infinite reaction rates.
fr	Frozen condition or freezing area ratio
kin	Conditions evaluated on the basis of finite reaction rates
*	Sonic conditions
i, k	Refers to species i or k
j	Refers to reaction j

REFERENCES

1. Penner, S. S.: Introduction to the Study of Chemical Reactions in Flow Systems. Butterworths Scientific Publications, London, 1955.

2. Bray, K. N. C.: Journal of Fluid Mechanics, Vol. 6, No. 1, 1959.

3. Heims, S. P.: Effect of Oxygen Recombination on One-Dimensional Flow at High Mach Numbers. NACA TN 4144, January 1958.

4. Boyer, D. W., A. Q. Eschenroeder and A. L. Russo: Approximate Solutions for Nonequilibrium Airflow in Hypersonic Nozzles. Cornell Aeronautical Laboratories, Inc., Report No. A. D.-1345-W3, August 1960.

5. Wegener, P. P.: Experiments in the Departure from Chemical Equilibrium on a Supersonic Flow. ARS Journal, Vol. 30, No. 4, April 1960, p. 322.

6. Emanuel, G. and W. G. Vincenti: Method for Calculation of the One-Dimensional Nonequilibrium Flow of a General Air Mixture Through a Hypersonic Nozzle. AEDC TDR 62-131, 1962.

7. Sarli, V. J., A. W. Blackman and R. F. Buswell: Kinetics of Hydrogen Air Flows, II. Calculations of Nozzle Flows for Ramjets. Ninth International Symposium on Combustion, Academic Press, New York, 1963.

8. Eschenroeder, A. W. and J. A. Lordi: Catalysis of Recombination in Nonequilibrium Flows, Ninth Symposium (International) on Combustion, Academic Press, New York, 1963, pp. 741-756.

9. Westenberg, A. A. and S. Favin: Complex Chemical Kinetics in Supersonic Nozzle Flow. Ninth Symposium (International) on Combustion, Academic Press, New York, 1963, pp. 741-756.

10. Pergament, Harold S.: A Theoretical Analysis of Nonequilibrium Hydrogen-Air Reactions in Flow Systems. AIAA Hypersonic Ramjet Conference, April 23-25, 1963, AIAA Preprint 63113.

11. Sarli, V. J.: Investigation of Nonequilibrium Flow Effects in High Expansion Nozzles, Final Report under Contract NASw-366. United Aircraft Corporation Research Laboratories Report B910056-12, September 20, 1963.

12. Zupnik, T. F., E. N. Nilson and V. J. Sarli: Investigation of Nonequilibrium Flow Effects in High Expansion Ratio Nozzles, Computer Program Manual, NASA Contract No. NAS3-2572, Report No. NASA CR-54042, September 15, 1964. United Aircraft Corporation Research Laboratories Report C910096-11.

REFERENCES (cont'd)

13. Sarli, V. J., W. G. Burwell and T. F. Zupnik: Investigation of Nonequilibrium Flow Effects in High Expansion Ratio Nozzles. Final Report Contract NAS3-2572, NASA CR-54221, December 1964.

14. Burwell, W. G., V. J. Sarli and T. F. Zupnik: Analytically Determined Nonequilibrium Mixture Properties in High Expansion Ratio Nozzles. Presented at 3rd Conference on the Performance of High Temperature Systems, Pasadena, California, December 7-9, 1964.

15 Burwell, W. G., V. J. Sarli and T. F. Zupnik: Kinetically Limited Performance of the H_2-F_2 Propellant System. Presented at AIChE Meeting, San Francisco, May 16-19, 1965. Also available in AIChE Symposium Series - Aerospace, V. 62, 1966.

16. Burwell, W. G., V. J. Sarli and T. F. Zupnik: Applicability of Sudden-Freezing Criteria in Analysis of Chemically-Complex Rocket Nozzle Expansions. Presented at 7th AGARD Colloquium on Recent Advances in Aerothermochemistry, Oslo, Norway, May 16-20, 1966. Also available as United Aircraft Corporation Research Laboratories Report UAR-E72, May 1966.

17. Sarli, V. J., W. G. Burwell, R. Hofland, Jr. and T. F. Zupnik: Evaluation of the Bray Sudden-Freezing Criterion for Predicting Nonequilibrium Performance in Multireaction Rocket Nozzle Expansions. Presented at the AIAA Propulsion Joint Specialist Conference, Colorado Springs, Colorado, June 14-18, 1965. AIAA Paper No. 65-554.

18. User's Manual for Chemical Kinetic Analysis (Deck 2). PWA-2888, Supplement 2, prepared under Air Force Contract No. AF 33(615)-3128, July 1966.

19. Axisymmetric Reacting Gas Nonequilibrium Performance Program. TRW Systems Report No. 02874-6004-R000, prepared under NASA Contract NAS 9-4358, March 8, 1967.

20. Elliot, D. G., D. R. Bartz and S. Silver: Calculation of Turbulent Boundary Layer Growth and Heat Transfer in Axisymmetric Nozzles. Jet Propulsion Laboratories Report TR No. 32-387, February 1963.

21. User's Manual for Chemical Kinetic Analysis (Deck 4). PWA-2888, Supplement 2, prepared under Air Force Contract No. AF 33(615)-3128, July 1966.

22. Sarli, V. J., W. G. Burwell and T. F. Zupnik: Investigation of Nonequilibrium Flow Effects in Hydrogen-Fluorine Rocket Nozzles. NASA Report CR-72162. Contract NASw-1293. First Annual Technical Report, September 1966.

REFERENCES (cont'd)

23. Sarli, V. J., W. G. Burwell and T. F. Zupnik: Correlation of Theoretical and Experimental Engine Performance Data of Hydrogen-Fluorine Rockets (U). United Aircraft Research Laboratories Report UAR-E142, presented at AIAA 2nd Propulsion Joint Specialist Conference, Colorado Springs, Colorado, June 13-17, 1966.

24. Bailey, T. E., W. G. Burwell and V. J. Sarli: Experimental and Analytical Investigation of Chemical Nonequilibrium Losses in Fluorine-Hydrogen Rocket Engines (U). 9th Liquid Propulsion Symposium, October 25-27, 1967 in St. Louis, Missouri.

25. Sarli, V. J., W. G. Burwell, L. S. Bender, T. F. Zupnik and L. D. Aceto: Investigation of Nonequilibrium Flow Effects in Hydrogen-Fluorine Rocket Nozzles (U), Second Annual Technical Report, Contract NASw-1293, NASA CR 72347, December 1967.

26. Sarli, V. J., L. S. Bender, L. D. Aceto and W. G. Burwell: Kinetic Flow Performance in Nozzles, Contract NAS 3-11225, NASA CR-72600, September 1969.

27. Fluorine-Hydrogen Performance Evaluation; Phase II: Space Storable Propellant Performance Demonstration, Contract NASw-1229, NASA CR-72542, Rocketdyne R-6636-3, April 1969.

28. Bailey, T. E. and W. R. Munk: Hydrogen-Fluorine Propulsion System. Contract No. NASw-754, Final Report P&WA FR-1585, 1966, NASA Report No. 72074.

29. Waldman, B. J. and E. B. Shuster: Fluorine-Hydrogen Performance Evaluation Phase I, Part II: Nozzle Performance Analysis and Demonstration. Contract No. NASw-1229, Final Report NAA Rocketdyne R-6636-2, April, 1967, NASA Report No. CR-72038.

30. Masters, A. I.: Investigation of Light Hydrocarbon Fuels with Fluorine-Oxygen Mixtures as Liquid Rocket Propellants, Final Report NASA CR-72147, September 1967.

31. Masters, A. I.: Investigation of Light Hydrocarbon Fuels with Fluorine-Oxygen Mixtures as Liquid Rocket Propellants,Final Report NASA CR-72425, November 1968.

32. Aukerman, C. A. and B. E. Church: Experimental Hydrogen-Fluorine Rocket Performance at Low Pressures and High Area Ratios (U). NASA TM X-724, September 1963.

33. Pieper, J. L.: ICRPG Liquid Propellant Thrust Chamber Performance Evaluation Manual Central Propulsion Information Agency No. 178, September 1968.

34. Sarli, V. J., L. S. Bender and W. G. Burwell: Optimization of Non-equilibrium Nozzle Performance for Selected System Considerations, AIAA Paper #69-472, Presented at AIAA 5th Propulsion Joint Specialists Conference, U. S. Air Force Academy, Colorado, June 9-13, 1969.

35. Penner, S. S.: Chemistry Problems in Jet Propulsion, Pergamon Press Book, The MacMillan Co., New York, 1957.

36. Brinkley S. R., Jr.: Calculation of Thermodynamic Properties of Multi-component Systems and Evaluation of Propellant Performance Parameters; Kinetics, Equilibria and Performance of High Temperature Systems. Proceedings of 1st Conference, Western States Section, Butterworths Scientific Publications, London, 1960.

37. McMahon, D. G. and R. Roback: Machine Computations of Chemical Equilibria in Reacting Systems; Kinetics, Equilibria and Performance of High Temperature Systems. Proceedings of 1st Conference, Western States Section, Butterworths Scientific Publications, London, 1960.

38. Cherry, S. S. and L. J. Van Nice: Screening of Reaction Rates, Phase II, Final Report, TRW Systems Group, Report No. 08832-6002-T000, Redondo Beach, California, December 6, 1967.

39. Bittker, D. A.: Nonequilibrium Calculations of Methane-Fluorine-Oxygen and Butene-1-Fluorine-Oxygen Rocket Performance, NASA TN D-4991, January 1969.

40. Jacobs, T. A., R. R. Giedt and N. Cohen: J. Chem. Phys., 47, 54 (1967).

41. Jacobs, T. A., R. R. Giedt and N. Cohen: J. Chem. Phys., 43, 3688 (1965).

42. Schott, G. L. and P. F. Bird: J. Chem. Phys., 41, 2869 (1964).

43. Bowman, C. T.: Application of Kinetics Calculations to the Interpretation of Shock Tube Data, Meeting of Combustion Institute, Western States Section, Berkeley, October 30, 1968.

44. Sudgen, T. M. and E. M. Bulewicz: Trans. Far. Soc., 54, 1855 (1968).

45. McAndrew, R. and R. Wheeler, J. Phys. Chem., 66, 229 (1962).

REFERENECES (cont'd)

46. Baulch, D. L., D. D. Drysdale, and A. C. Lloyd: Critical Evaluation of Rate Data for Homogeneous, Gas-Phase Reactions of Interest in High-Temperature Systems, December 1968, School of Chemistry, The University, Leeds 2, England.

47. D. R. Stull, et al: JANAF Thermochemical Tables. Thermal Research Lab., Dow Chemical Co., Midland, Michigan; supplementary tables included through June 1968.

48. Aceto, L. and Zupnik, T. F.: Two-Dimensional Equilibrium Nozzle Analysis Computer Program-TDE, prepared for the ICRPG Performance Standarization Working Group, July 1968, AD 842700.

49. Weingold, H. D., and Zupnik, T. F.: Turbulent Boundary Layer Nozzle Analysis Computer Program-TBL, prepared for the ICRPG Performance Standarization Working Group, July 1968, AD 841202.

50. Hall, I. M.: Transonic Flow in Two-Dimensional and Axially-Symmetric Nozzles, Quart. J. Mechanics and Applied Math, Vol. XV, Pt. 4, pp. 487-508 (1962).

APPENDIX I

DISTRIBUTION LIST FOR KINETIC PERFORMANCE HANDBOOK (NASA CR72601)

Addressee	Report Copies	Letter Only
National Aeronautics & Space Administration Lewis Research Center 21000 Brookpark Road Cleveland, Ohio 44135		
Attn: Contracting Officer MS 500-313	1	
Attn: Liquid Rocket Technology Branch MS 500-209	5	
Attn: Technical Report Control Office MS 5-5	1	
Attn: Technology Utilization Office MS 3-16	1	
Attn: AFSC Liaison Office 501-3	2	
Attn: Library	2	
Attn: Office of Reliability and Quality Assurance MS 500-111	1	
Attn: D. L. Nored, Chief, LRTB MS 500-209	1	
Attn: P. N. Herr, Project Manager MS 500-209	6	
Chief, Liquid Experimental Engineering, RPX Office of Advanced Research & Technology NASA Headquarters Washington, D. C. 20546	1	

Addressee	Report Copies	Letter Only
Chief, Liquid Propulsion Technology, RPL Office of Advanced Research & Technology NASA Headquarters Washington, D. C. 20546	1	
Director, Launch Vehicles & Propulsion, SV Office of Space Science & Applications NASA Headquarters Washington, D. C. 20546	1	
Director, Advanced Manned Missions, MT Office of Manned Space Flight NASA Headquarters Washington, D. C. 20546	1	
NASA Scientific & Technical Information Facility P. O. Box 33 College Park, Maryland 20740	6	
National Aeronautics and Space Administration Ames Research Center Moffett Field, California 94035		
Attn: Library	1	
Attn: Hans M. Mark Mission Analysis Division		1
National Aeronautics and Space Administration Goddard Space Flight Center Greenbelt, Maryland 20771		
Attn: Library	1	
Attn: Merland L. Moseson Code 620		1
National Aeronautics and Space Administration Langley Research Center Langley Station Hampton, Virginia 23365		
Attn: Library	1	
Attn: E. Cortwright Director		1

Addressee	Report Copies	Letter Only
National Aeronautics and Space Administration Manned Spacecraft Center Houston, Texas 77001		
Attn: Library	1	
Attn: J. G. Thibodaux, Jr. Chief, Propulsion & Power Division	1	
Attn: Ronald Kahl	1	
National Aeronautics and Space Administration George C. Marshall Space Flight Center Huntsville, Alabama 35812		
Attn: Library	1	
Attn: E. Jacobs	1	
Attn: Hans G. Paul	1	
Jet Propulsion Laboratory 4800 Oak Grove Drive Pasadena, California 91103		
Attn: Library	1	
Attn: Duane Dipprey		1
Attn: Walter Powell	1	
Defense Documentation Center Cameron Station Building 5 5010 Duke Street Alexandria, Virginia 22314		
Attn: TISIA	1	

Addressee	Report Copies	Letter Only
Arnold Engineering Development Center Air Force Systems Command Tullahoma, Tennessee 37389		
Attn: Library	1	
Attn: Dr. H. K. Doetsch		1
Aeronautical Systems Division Air Force Systems Command Wright-Patterson Air Force Base Dayton, Ohio		
Attn: Library	1	
Attn: D. L. Schmidt Code ARSCNC-2		1
Air Force Rocket Propulsion Laboratory (RPR) Edwards, California 93523		
Attn: Library	1	
Space & Missile Systems Organization Air Force Unit Post Office Los Angeles, California 90045		
Attn: Technical Data Center	1	
U. S. Army Missile Command Redstone Scientific Information Center Redstone Arsenal, Alabama 35808		
Attn: Document Section	1	
Attn: Dr. W. Wharton		1
Bureau of Naval Weapons Department of the Navy Washington, D. C.		
Attn: Library	1	
Attn: J. Kay Code RTMS-41		1

Addressee	Report Copies	Letter Only
Commander U. S. Naval Missile Center Point Mugu, California 93041		
Attn: Technical Library	1	
Commander U. S. Naval Weapons Center China Lake, California 93557		
Attn: Library	1	
Picatinny Arsenal Dover, New Jersey 07801		
Attn: Library	1	
Attn: I. Forsten		1
Air Force Aero Propulsion Laboratory Research & Technology Division Air Force Systems Command United States Air Force Wright-Patterson AFB, Ohio 45433		
Attn: APRP (Library)	1	
Attn: R. Quigley		1
Attn: C. M. Donaldson		1
Aerojet Liquid Rocket Company P. O. Box 13222 Sacramento, California 95813		
Attn: Technical Library 2484-2015A	1	
Attn: R. Stiff		1
Attn: D. L. Kors	1	

Addressee	Report Copies	Letter Only
Aeronutronic Division of Philco Ford Corp. Ford Road Newport Beach, California 92663		
Attn: Technical Information Department	1	
Attn: Dr. L. H. Linder		1
Aerospace Corporation 2400 E. El Segundo Blvd. Los Angeles, California 90045		
Attn: Library-Documents	1	
Attn: J. G. Wilder		1
Susquehanna Corporation Atlantic Research Division Shirley Highway & Edsall Road Alexandria, Virginia 22314		
Attn: Library	1	
Bell Aerosystems, Inc. Box 1 Buffalo, New York 14240		
Attn: Library	1	
Attn: T. Reinhardt	1	
Bellcomm 955 L'Enfant Plaza, S. W. Washington, D. C.		
Attn: Library	1	
Attn: H. S. London		1

Addressee	Report Copies	Letter Only
Boeing Company Space Division P. O. Box 868 Seattle, Washington 98124		
Attn: Library	1	
Attn: J. D. Alexander		1
Attn: C. F. Tiffany		1
Chemical Propulsion Information Agency Applied Physics Laboratory 8621 Georgia Avenue Silver Spring, Maryland 20910	1	
Attn: Tom Reedy	1	
Chrysler Corporation Missile Division P. O. Box 2628 Detroit, Michigan		
Attn: Library	1	
Attn: John Gates		1
Chrysler Corporation Space Division P. O. Box 29200 New Orleans, Louisiana 70129		
Attn: Librarian	1	
Fairchild Stratos Corporation Aircraft Missiles Division Hagerstown, Maryland		
Attn: Library	1	
General Dynamics/Convair P. O. Box 1128 San Diego, California 92112		
Attn: Library	1	
Attn: Frank Dore		1

Addressee	Report Copies	Letter Only
Missiles and Space Systems Center General Electric Company Valley Forge Space Technology Center P. O. Box 8555 Philadelphia, Pennsylvania 19101		
Attn: Library	1	
Attn: A. Cohen		1
General Electric Company Flight Propulsion Lab. Department Cincinnati, Ohio		
Attn: Library	1	
Attn: D. Suichu		1
Grumman Aircraft Engineering Corporation Bethpage, Long Island, New York		
Attn: Library	1	
Attn: Joseph Gavin		1
Ling-Temco-Vought Corporation P. O. Box 5907 Dallas, Texas 75222		
Attn: Library	1	
Lockheed Missiles and Space Company P. O. Box 504 Sunnyvale, California 94087		
Attn: Library	1	
Marquardt Corporation 16555 Saticoy Street Box 2013 - South Annex Van Nuys, California 91409	1	
Attn: T. Hudson		1

Addressee	Report Copies	Letter Only
Denver Division Martin-Marietta Corporation P. O. Box 179 Denver, Colorado 80201		
Attn: Library	1	
Attn: Dr. Morganthaler		1
Western Division McDonnell Douglas Astronautics 5301 Bolsa Avenue Huntington Beach, California 92647		
Attn: Library	1	
Attn: R. W. Hallet		1
McDonnell Douglas Aircraft Corporation P. O. Box 516 Lambert Field, Missouri 63166		
Attn: Library	1	
Attn: R. A. Herzmark		1
Rocketdyne Division North American Rockwell, Inc. 6633 Canoga Avenue Canoga Park, California 91304		
Attn: Library, Department 596-306	1	
Attn: S. F. Iacobellis	1	
Space & Information Systems Division North American Rockwell 12214 Lakewood Boulevard Downey, California		
Attn: Library	1	

Addressee	Report Copies	Letter Only
Northrop Space Laboratories 3401 West Broadway Hawthorne, California		
Attn: Library	1	
Attn: Dr. William Howard		1
Radio Corporation of America Astro-Electronics Products Princeton, New Jersey		
Attn: Library	1	
Rocket Research Corporation Willow Road at 116th Street Redmond, Washington 98053		
Attn: Library	1	
Attn: F. McCullough, Jr.		1
TRW Systems, Inc. 1 Space Park Redondo Beach, California 90278		
Attn: Tech. Lib. Doc. Acquisitions	1	
Attn: D. H. Lee		1
United Aircraft Corporation Pratt & Whitney Division Florida Research & Development Center P. O. Box 2691 West Palm Beach, Florida 33402		
Attn: Library	1	
Attn: Dr. Schmitke	1	

FIG. ND-1

COMPARISON OF NOZZLE AREA RATIO GRADIENTS FOR TYPICAL CIRCULAR ARC AND CONICAL CONTOURS

r_c/r_t = RADIUS OF CURVATURE / THROAT RADIUS FOR ARC CONTOUR

θ = HALF-ANGLE OF CONICAL CONTOUR

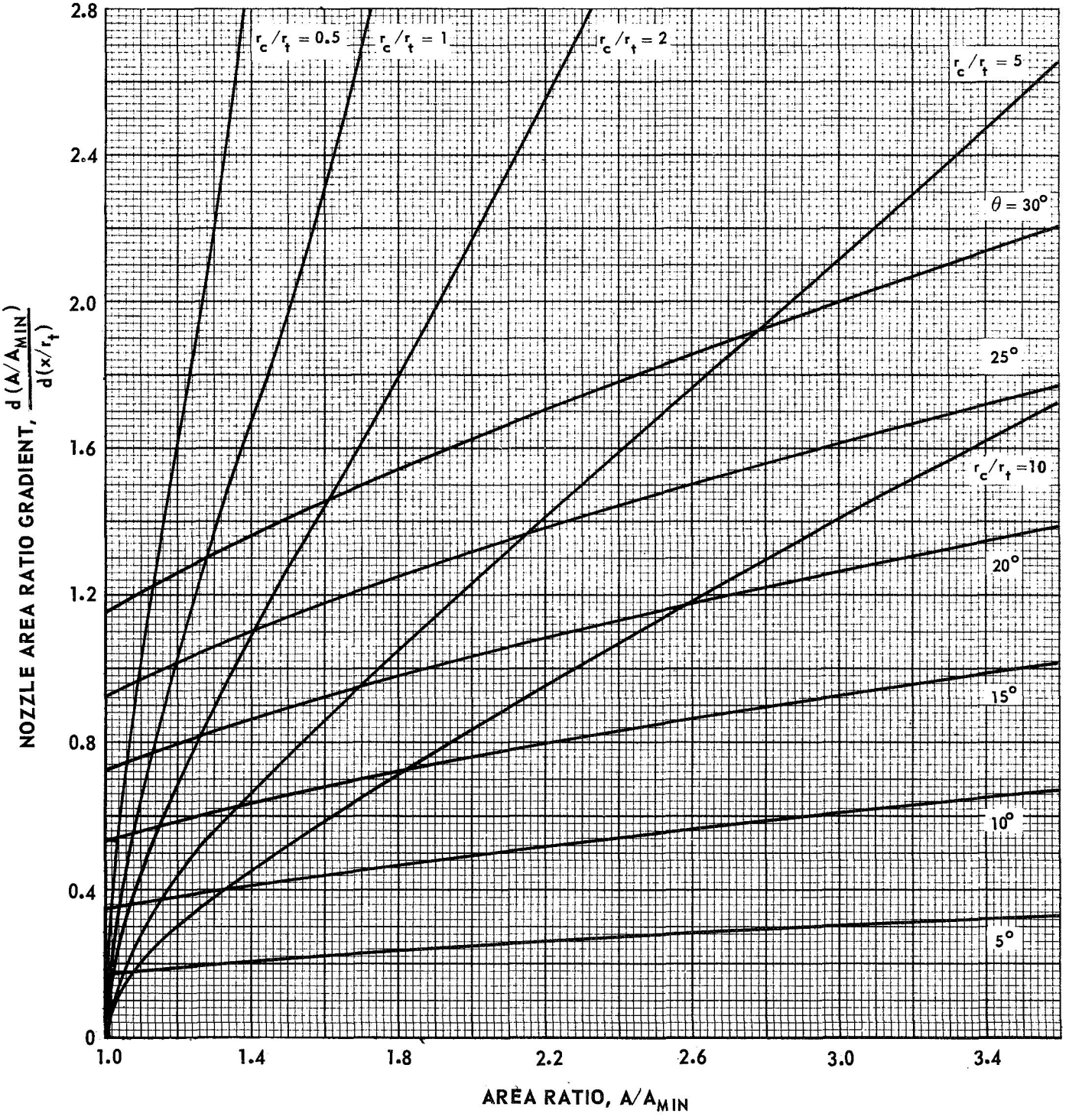

FIG. ND–2

NOZZLE AREA RATIO GRADIENTS OF SELECTED PERFECT NOZZLE CONTOURS

SPECIFIC HEAT RATIO = 1.25

$r_c / r_t = 1.0$

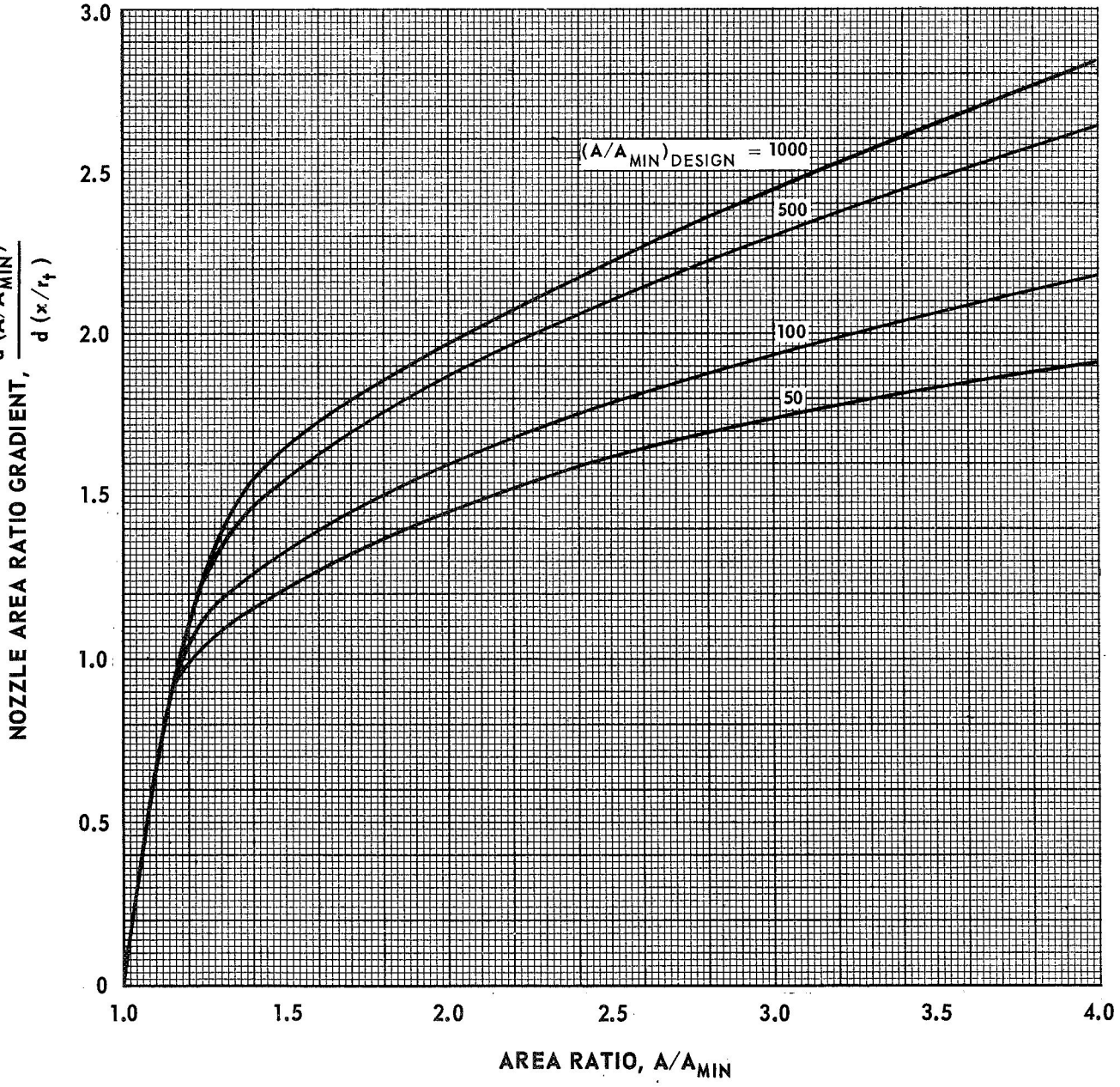

FIG. ND-3

NOZZLE AREA RATIO GRADIENTS OF SELECTED PERFECT NOZZLE CONTOURS

SPECIFIC HEAT RATIO = 1.30

$r_c / r_t = 1.0$

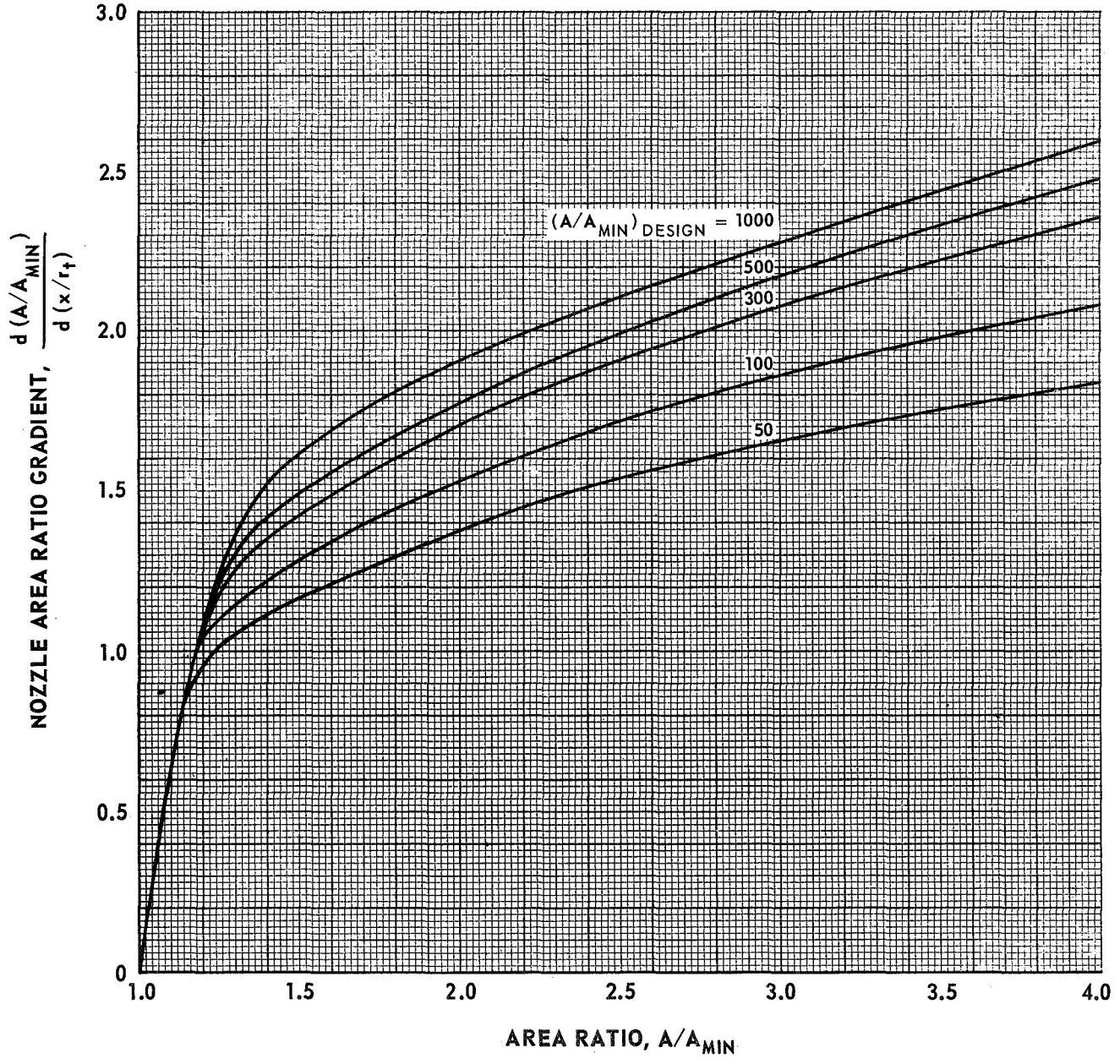

FIG. ND-4

NOZZLE AREA RATIO GRADIENTS OF SELECTED PERFECT NOZZLE CONTOURS

SPECIFIC HEAT RATIO = 1.35

$r_c/r_t = 1.0$

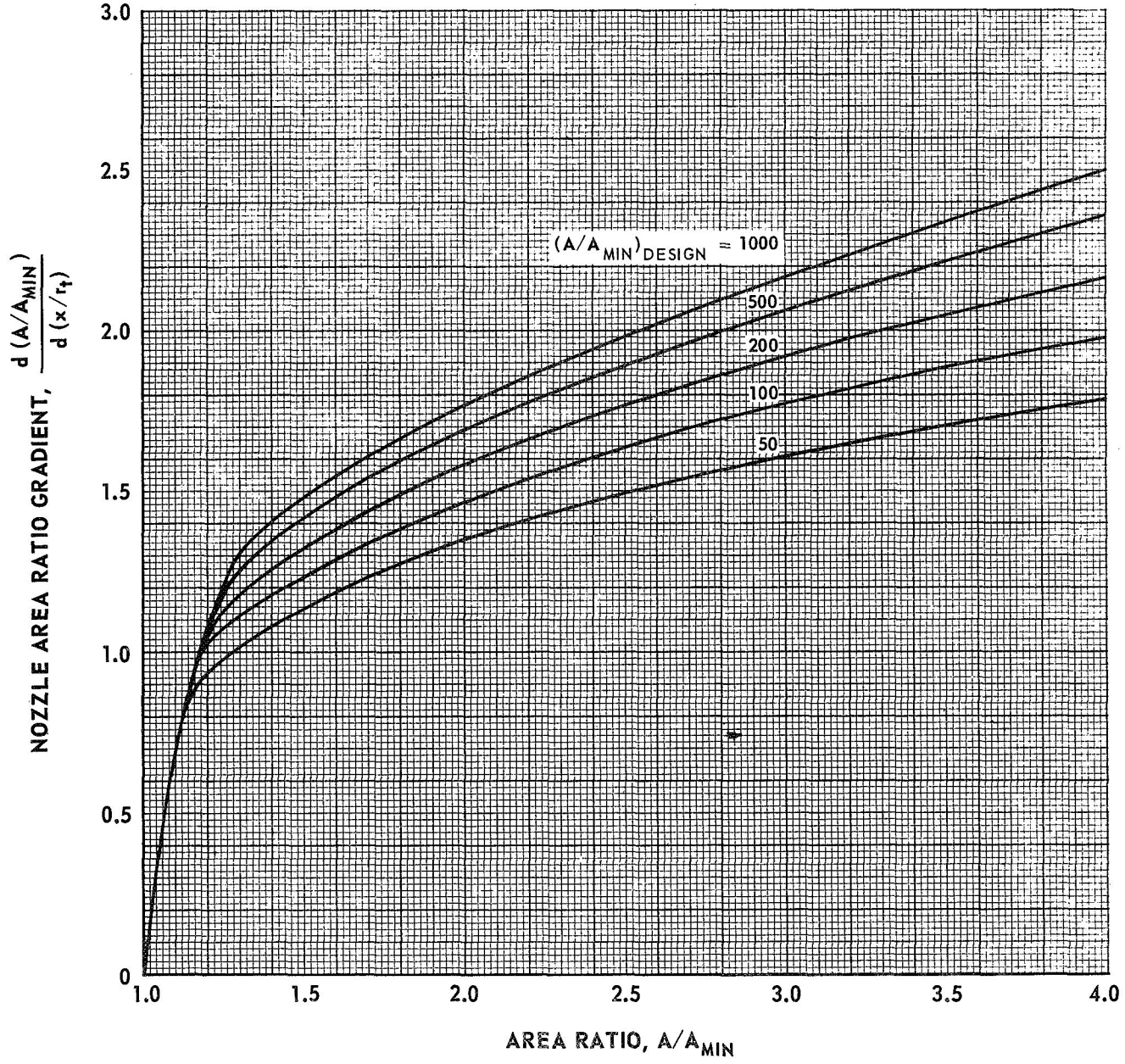

FIG. ND-5

AXISYMMETRIC PERFECT NOZZLE CONTOURS

SPECIFIC HEAT RATIO = 1.25

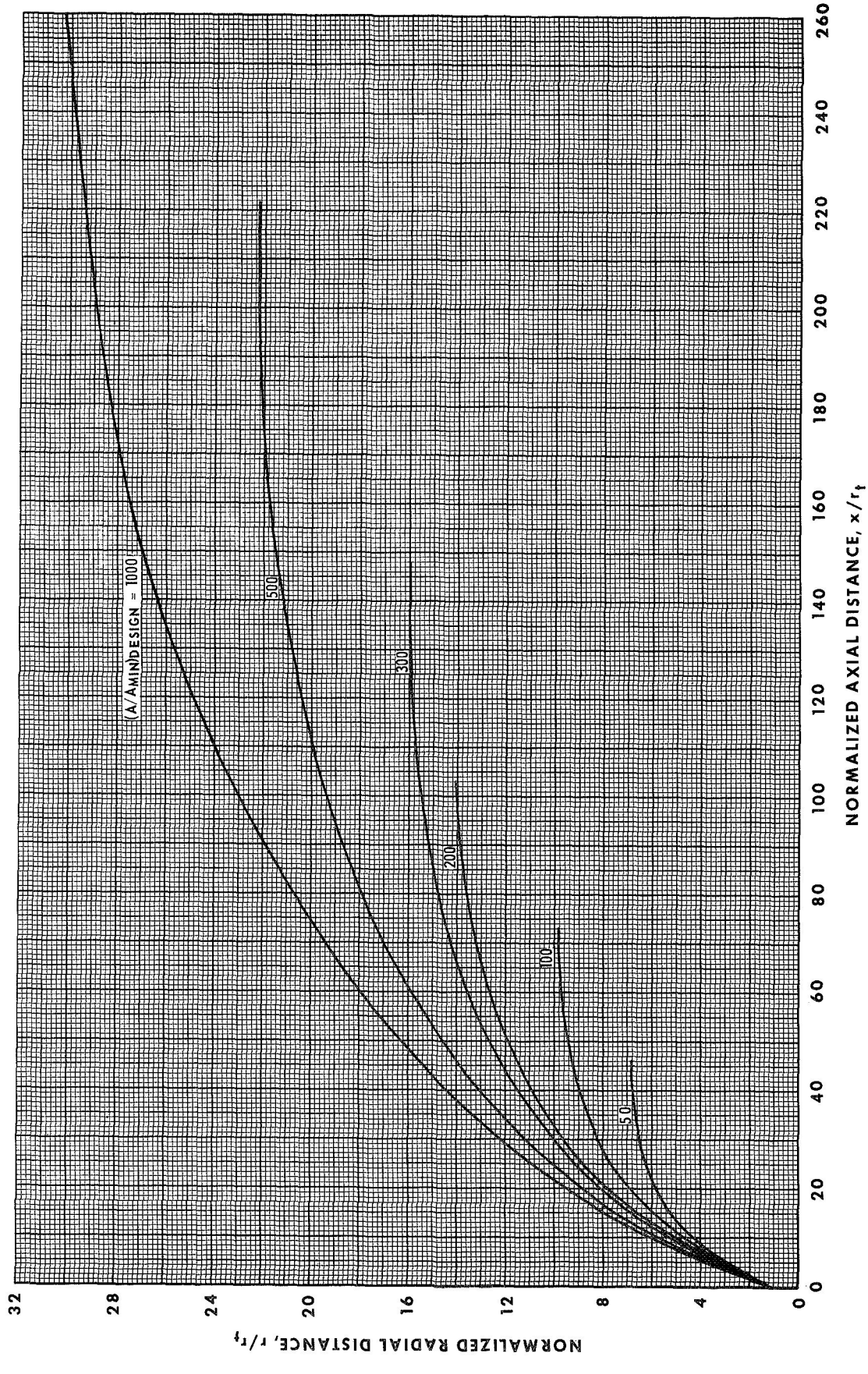

H910666-16

FIG. ND-6

AXISYMMETRIC PERFECT NOZZLE CONTOURS

SPECIFIC HEAT RATIO = 1.30

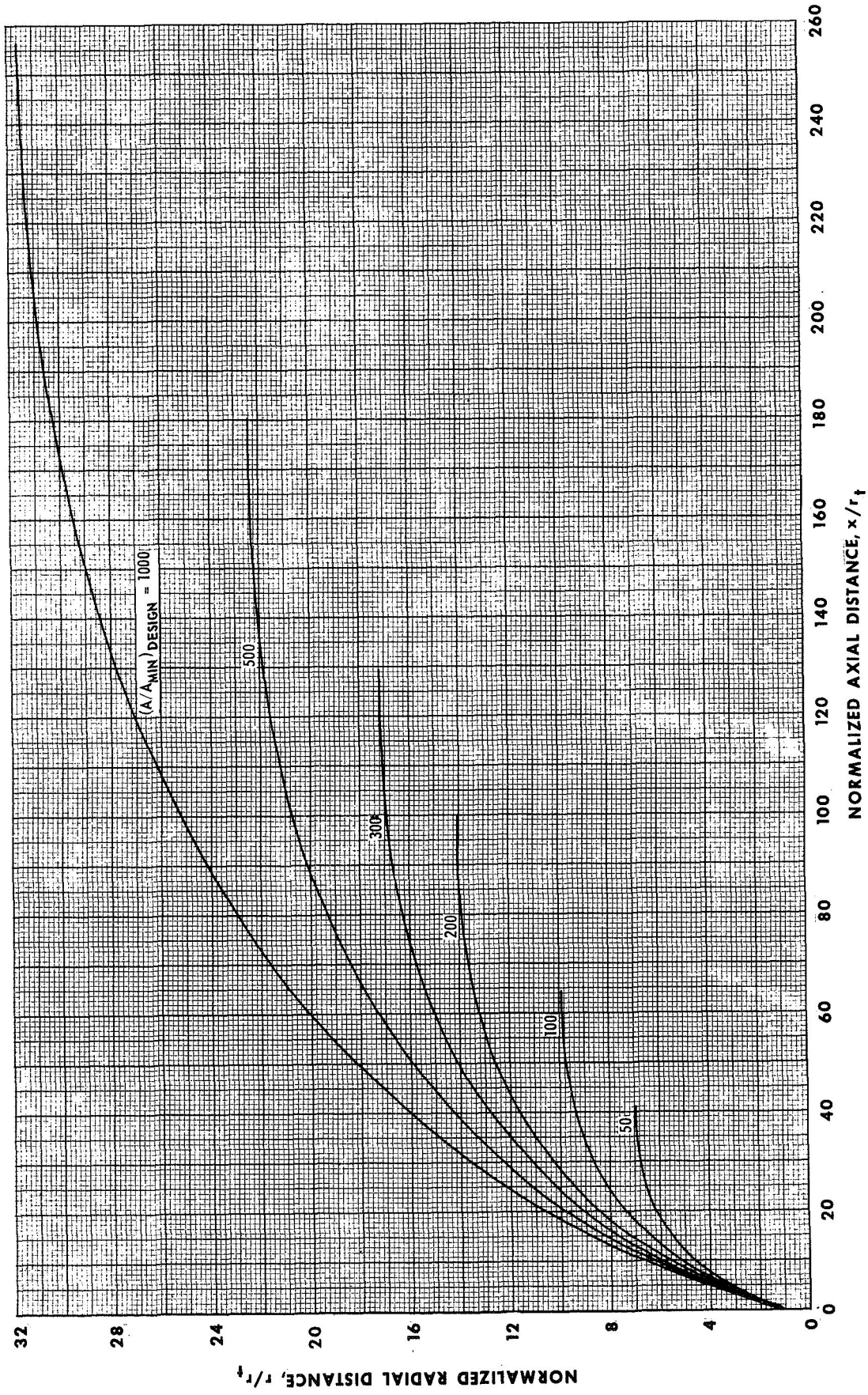

H910666-16

FIG. ND-7

AXISYMMETRIC PERFECT NOZZLE CONTOURS

SPECIFIC HEAT RATIO = 1.35

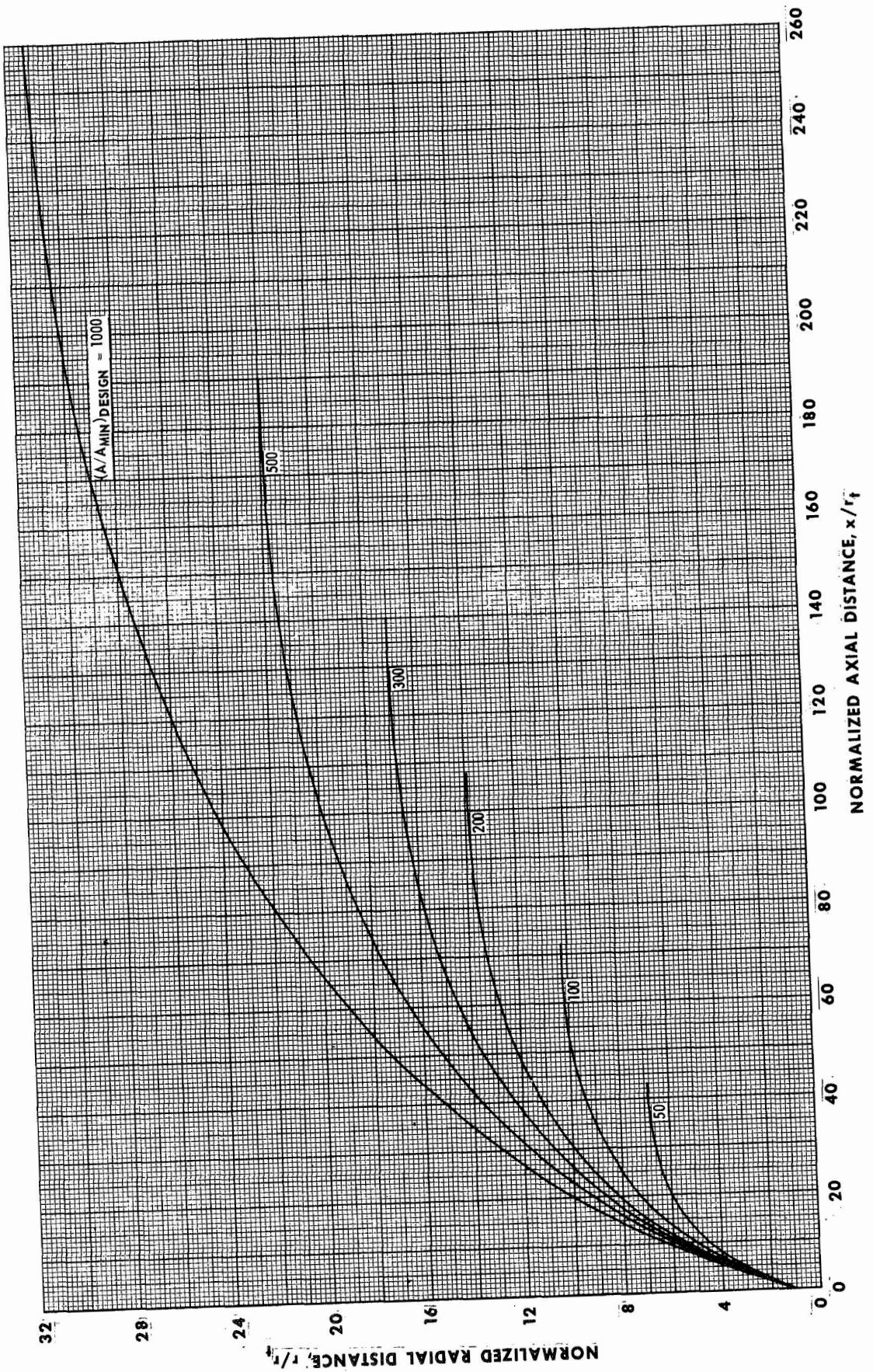

TABLE I-1
SUMMARY OF ELEMENTARY REACTIONS AND REACTION RATE CONSTANTS EMPLOYED IN $H_2 - F_2$ RECOMBINATION MECHANISM

	REACTION	FORWARD RATE
	$H + H + A \rightleftharpoons H_2 + A$	$K_f = 4.62 \times 10^{-14} T^{-1}$
	$H + F + A \rightleftharpoons HF + A$	$K_f = 1.155 \times 10^{15} T^{-1}$
1	$H + H + F \rightleftharpoons H_2 + F$	$K_f = 1\,(4.62 \times 10^{14} T^{-1})$
2	$H + F + F \rightleftharpoons HF + F$	$K_f = 1\,(1.155 \times 10^{15} T^{-1})$
3	$H + H + H \rightleftharpoons H_2 + H$	$K_f = 20\,(4.62 \times 10^{14} T^{-1})$
4	$H + F + H \rightleftharpoons HF + H$	$K_f = 1\,(1.155 \times 10^{15} T^{-1})$
5	$H + H + HF \rightleftharpoons H_2 + HF$	$K_f = 2.5\,(4.62 \times 10^{14} T^{-1})$
6	$H + F + HF \rightleftharpoons HF + HF$	$K_f = 2.5\,(1.155 \times 10^{15} T^{-1})$
7	$H + H + H_2 \rightleftharpoons H_2 + H_2$	$K_f = 2.5\,(4.62 \times 10^{14} T^{-1})$
8	$H + F + H_2 \rightleftharpoons HF + H_2$	$K_f = 2.5\,(1.155 \times 10^{15} T^{-1})$

NOTE: ALL RATES ARE EXPRESSED IN TERMS OF LB-MOLES, FT^3, SEC; AND T IS IN °R

TO CONVERT TO kg-MOLES, m^3, SEC, AND T IN °K; MULTIPLY ABOVE RATE BY 2.165×10^{-3}

TABLE I-2

EQUILIBRIUM AND FROZEN FLOW PROPERTIES AT NOZZLE THROAT

$H_2(\ell) - F_2(\ell)$

	P_c-psia	OXIDIZER - FUEL WEIGHT RATIO						
		4.0	6.0	8.0	10.0	12.0	14.0	16.0
Equilibrium	100	55.4	55.8	56.9	57.7	58.3	59.0	59.8
Mass	200	110.7	110.9	112.8	114.3	115.5	116.7	118.3
Flow -	300	165.9	165.9	168.4	170.6	172.3	174.0	176.3
W/A	500	276.4	275.5	279.0	282.4	285.1	287.9	291.5
Lbm	750	414.6	412.1	416.8	421.5	425.4	429.4	434.6
$\frac{\text{Lbm}}{\text{Ft}^2.\text{Sec}}$	1000	552.7	548.6	554.2	560.0	565.0	570.2	576.9
Frozen	100	56.4	57.8	59.3	60.3	61.3	62.2	63.3
Mass	200	112.4	114.5	117.1	119.1	120.9	122.7	124.8
Flow -	300	168.1	170.8	174.4	177.4	180.0	182.6	185.6
W/A	500	279.5	282.8	288.3	293.0	297.1	301.4	306.2
Lbm	750	418.5	422.3	429.8	436.4	442.3	448.5	455.6
$\frac{\text{Lbm}}{\text{Ft}^2.\text{Sec}}$	1000	557.6	561.2	570.5	579.0	586.6	594.7	603.9
Frozen	100	1.31	1.31	1.32	1.33	1.34	1.34	1.35
Specific	200	1.31	1.31	1.32	1.33	1.33	1.34	1.34
Heat	300	1.31	1.31	1.31	1.32	1.33	1.33	1.34
Ratio	500	1.31	1.30	1.31	1.32	1.33	1.33	1.34
γ FR	750	1.31	1.30	1.31	1.32	1.32	1.33	1.33
	1000	1.31	1.30	1.31	1.31	1.32	1.32	1.33

NOTE: P_c (psia) x $6.895 \times 10^3 = P_c$ (N/m^2)

Mass Flow $\left(\frac{\text{Lbm}}{\text{Ft}^2.\text{sec}}\right)$ x 4.883 = Mass Flow $\left(\frac{\text{kg}}{\text{m}^2\ \text{sec}}\right)$

FIG. I-1

VARIATION OF EQUILIBRIUM VACUUM SPECIFIC IMPULSE WITH AREA RATIO

H_2 (ℓ) – F_2 (ℓ)

P_C = 100 PSIA ($6.895 \times 10^5 N/m^2$)

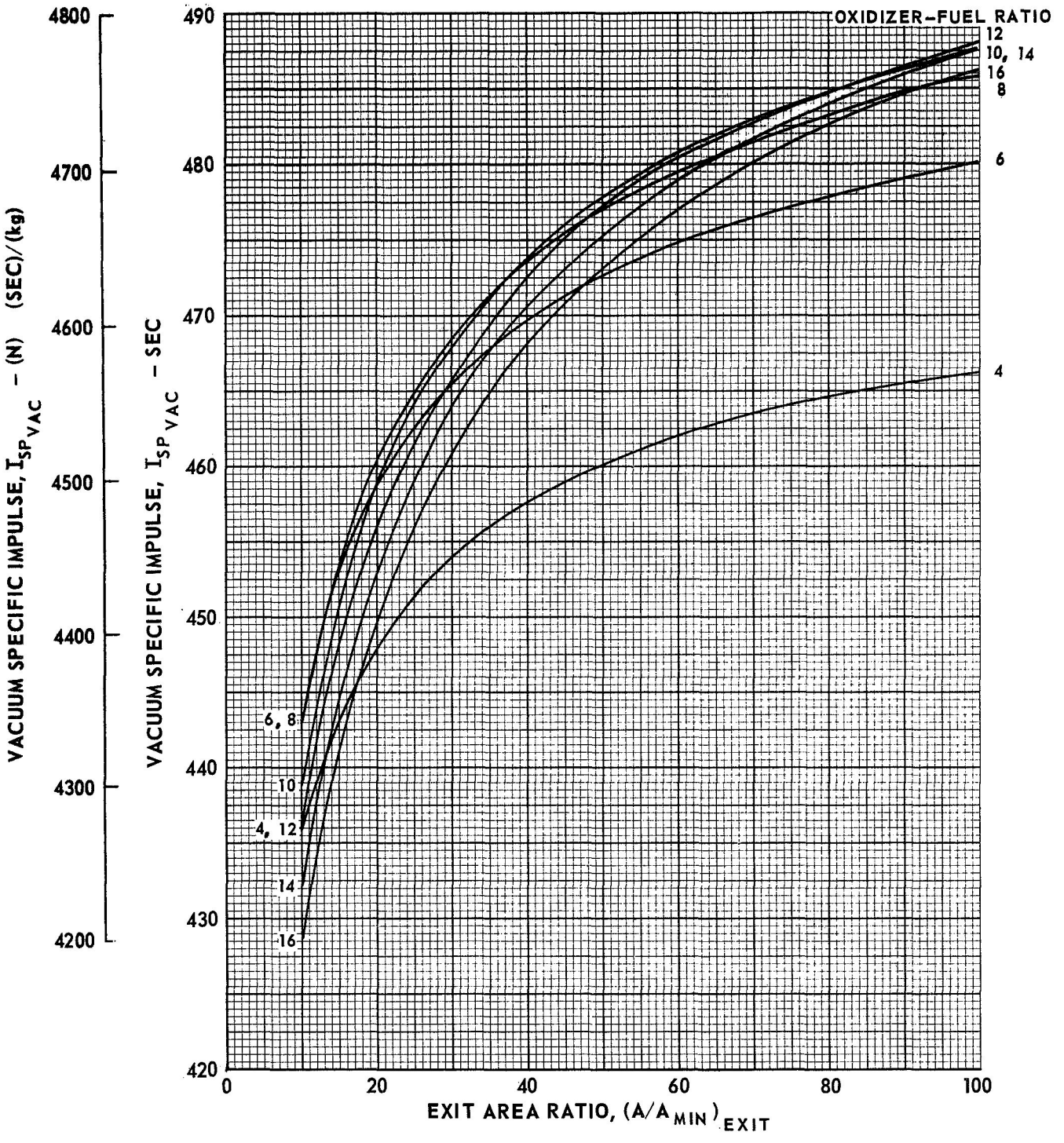

H910666-16

FIG. I-2

VARIATION OF FROZEN VACUUM SPECIFIC IMPULSE WITH AREA RATIO

H_2 (ℓ) - F_2 (ℓ)

P_C = 100 PSIA (6.895X10^{5}N/m^2)

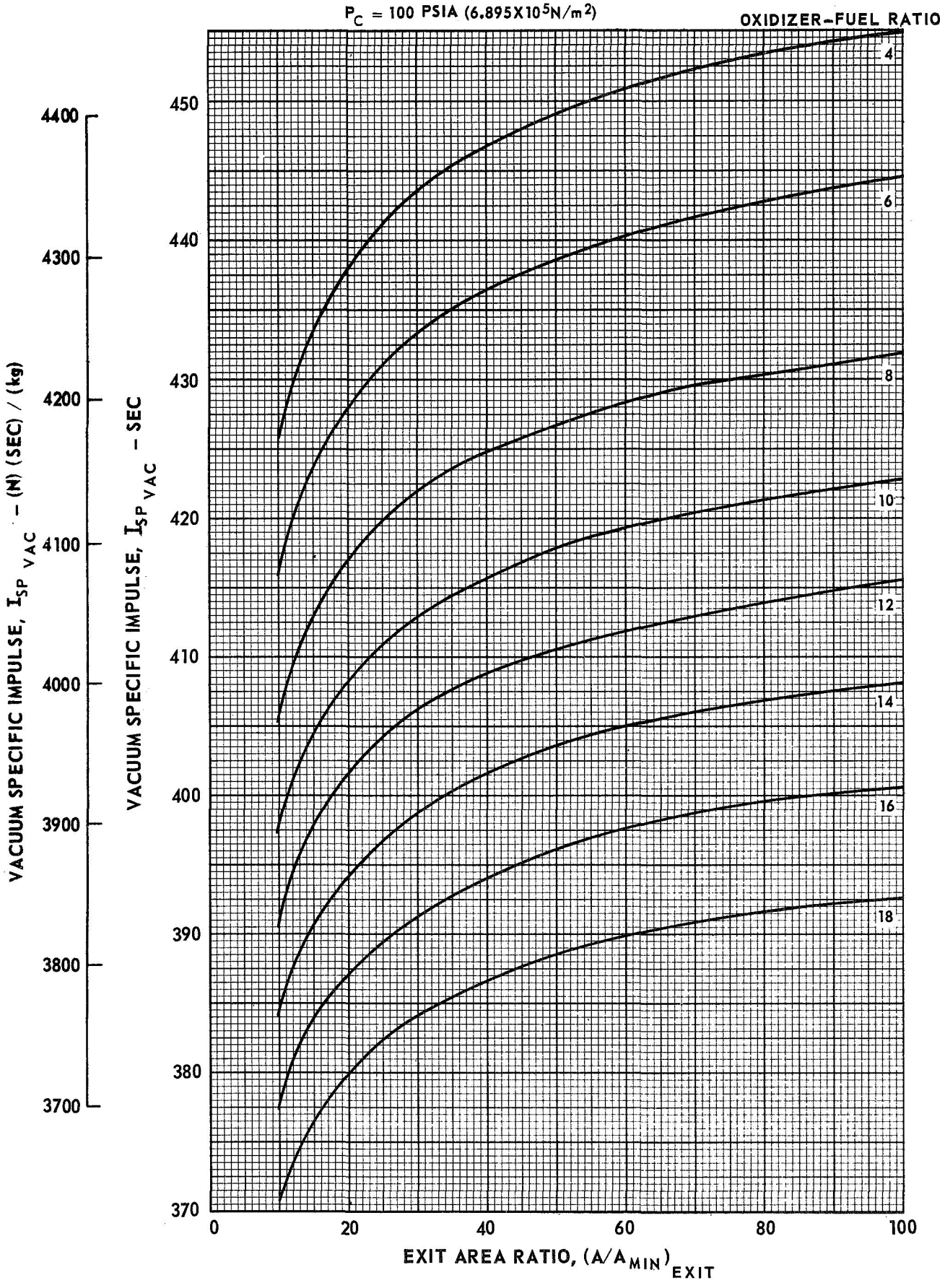

VARIATION OF EQUILIBRIUM VACUUM SPECIFIC IMPULSE WITH AREA RATIO

H_2 (ℓ) – F_2 (ℓ)

P_C = 200 PSIA (1.379X10^{6}N/m^2)

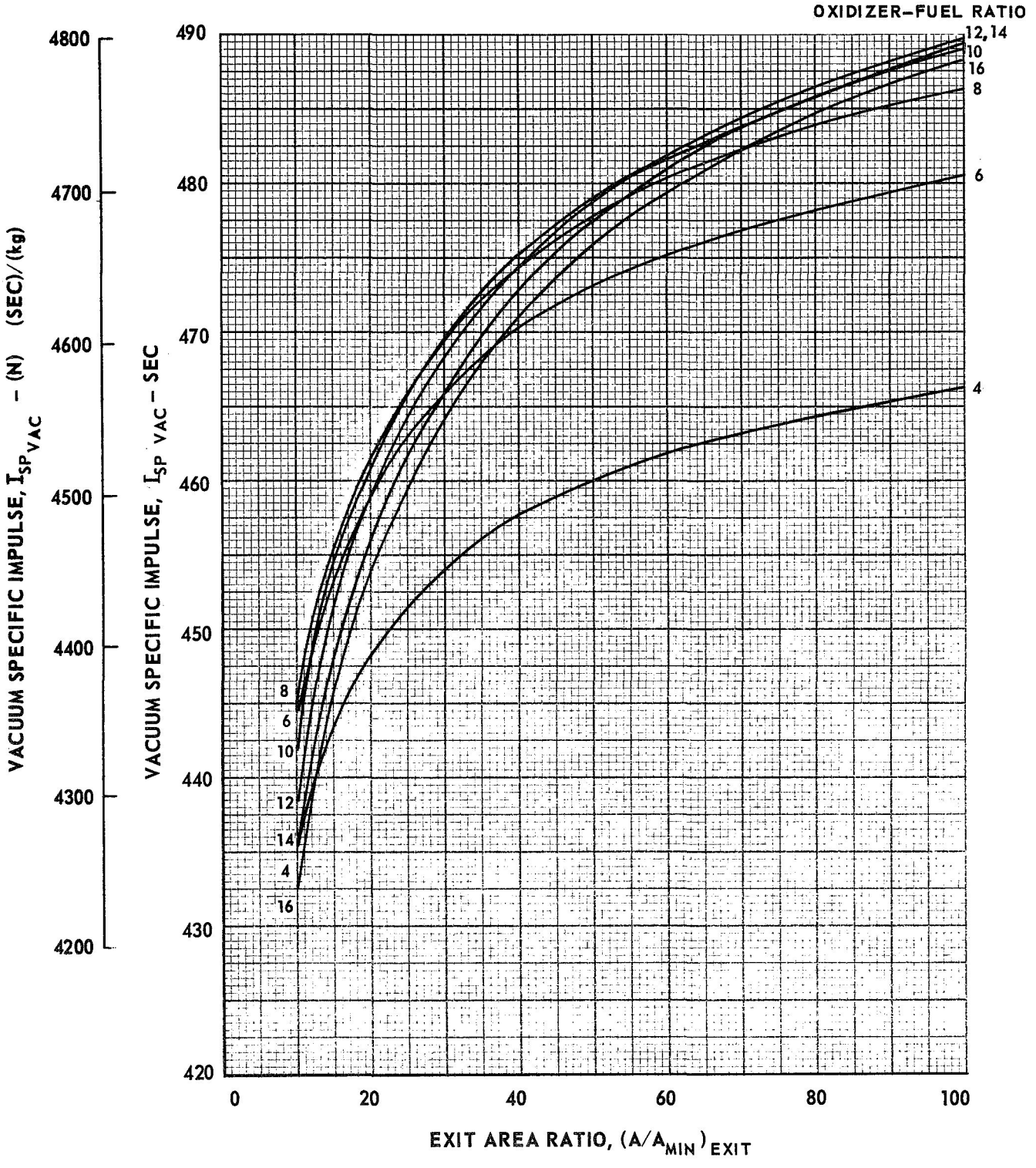

FIG. I-4

VARIATION OF FROZEN VACUUM SPECIFIC IMPULSE WITH AREA RATIO

H_2 (ℓ) – F_2 (ℓ)

P_C = 200 PSIA (1.379 X 10^6 N/m^2)

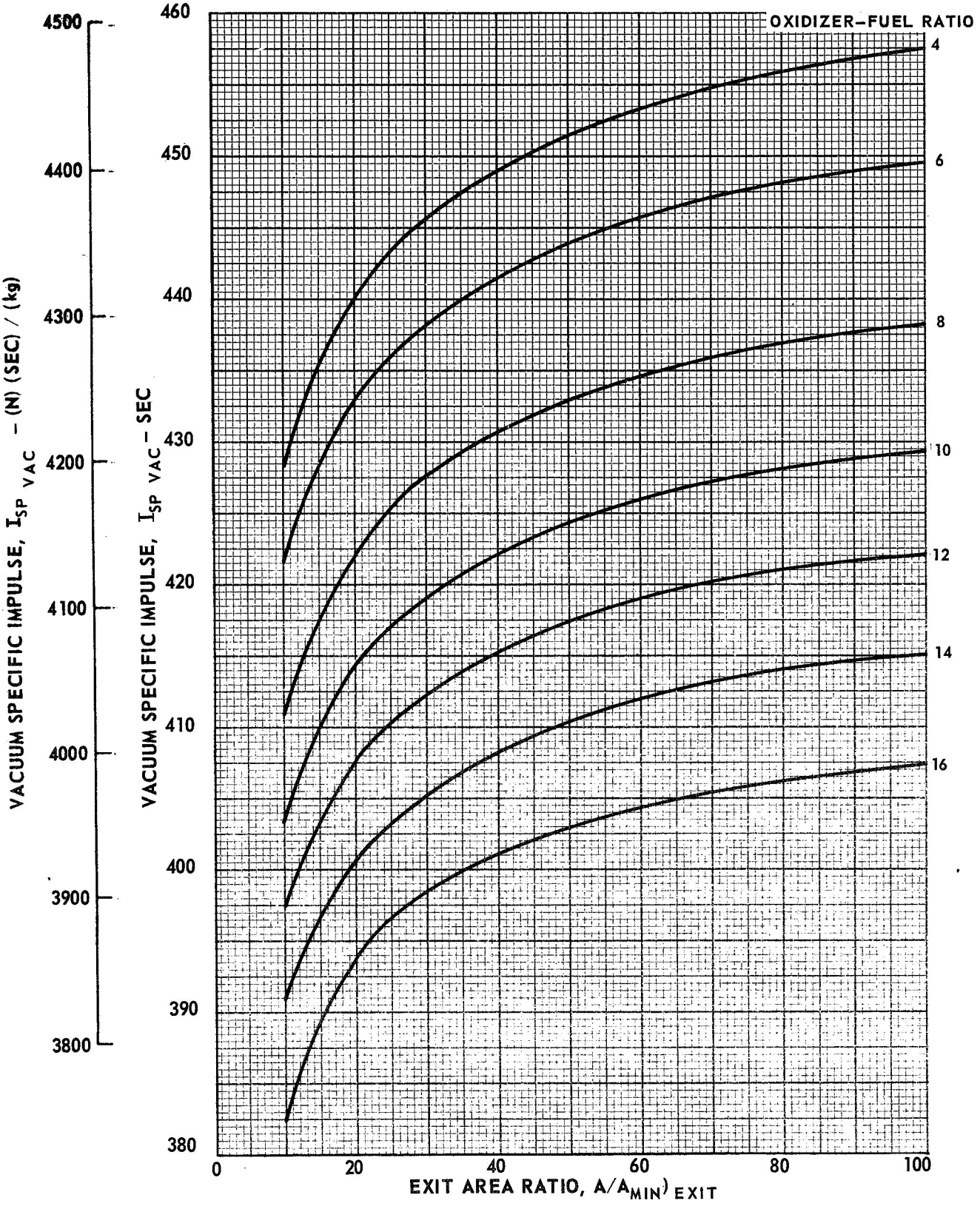

FIG. I-5

VARIATION OF EQUILIBRIUM VACUUM SPECIFIC IMPULSE WITH AREA RATIO

H_2 (ℓ) – F_2 (ℓ)

P_C = 300 PSIA (2.069 X 10^6 N/m^2)

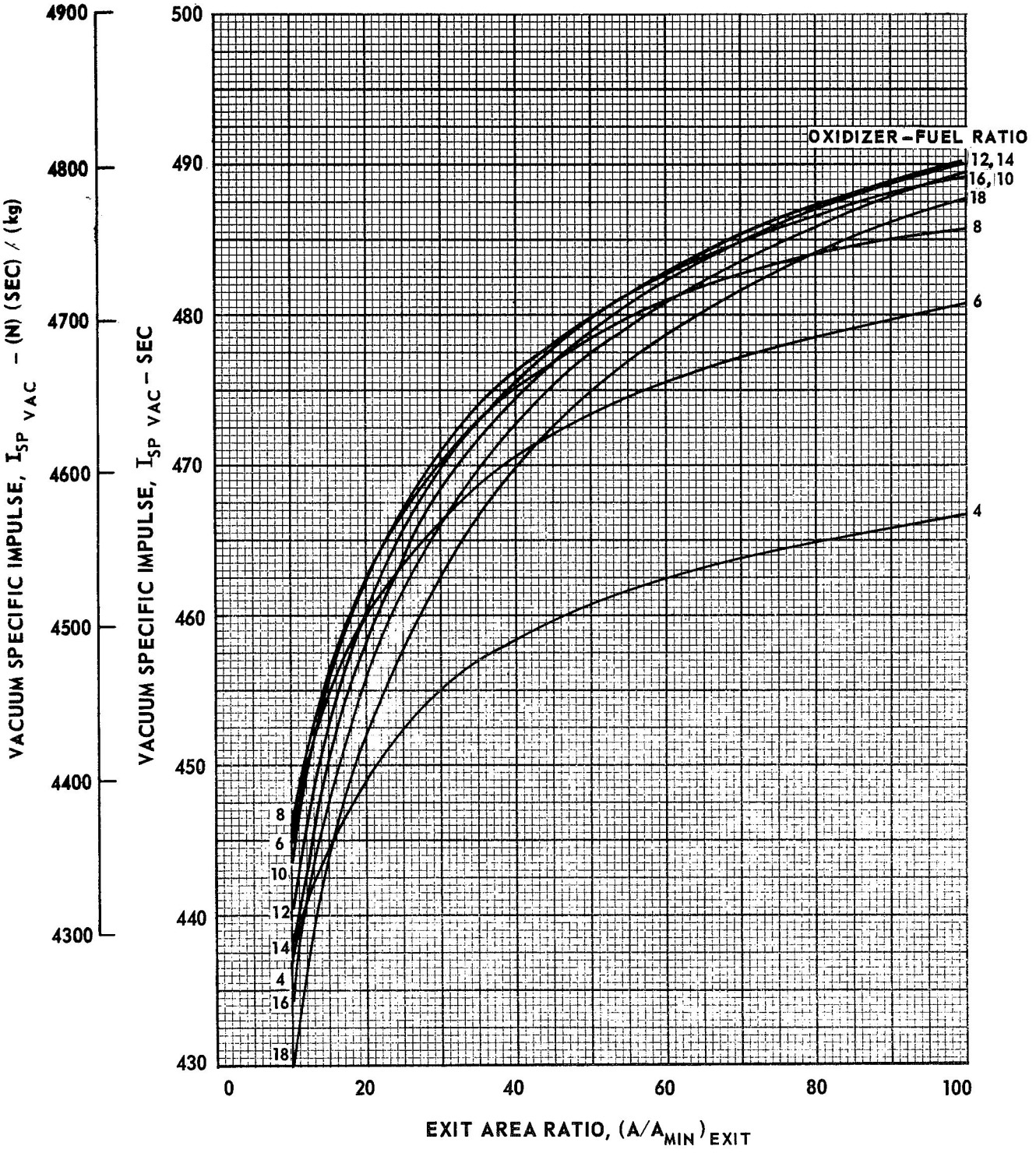

FIG. 1-6

VARIATION OF FROZEN VACUUM SPECIFIC IMPULSE WITH AREA RATIO

H_2 (ℓ) - F_2 (ℓ)

P_C = 300 PSIA (2.069 X 10^6 N/m^2)

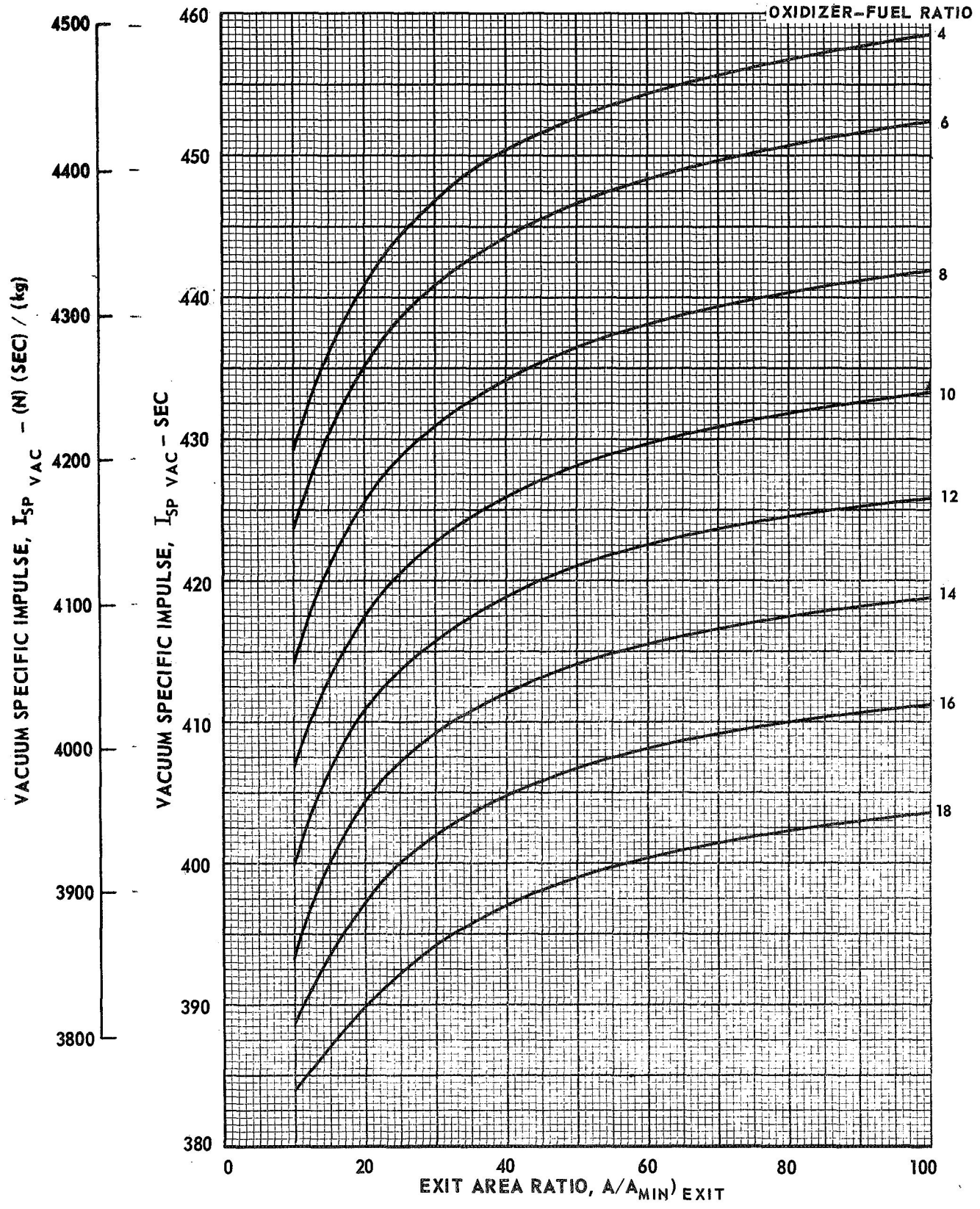

FIG. 1-7

VARIATION OF EQUILIBRIUM VACUUM SPECIFIC IMPULSE WITH AREA RATIO

H_2 (ℓ) – F_2 (ℓ)

P_C = 500 PSIA (3.448 X 10^6 N/m^2)

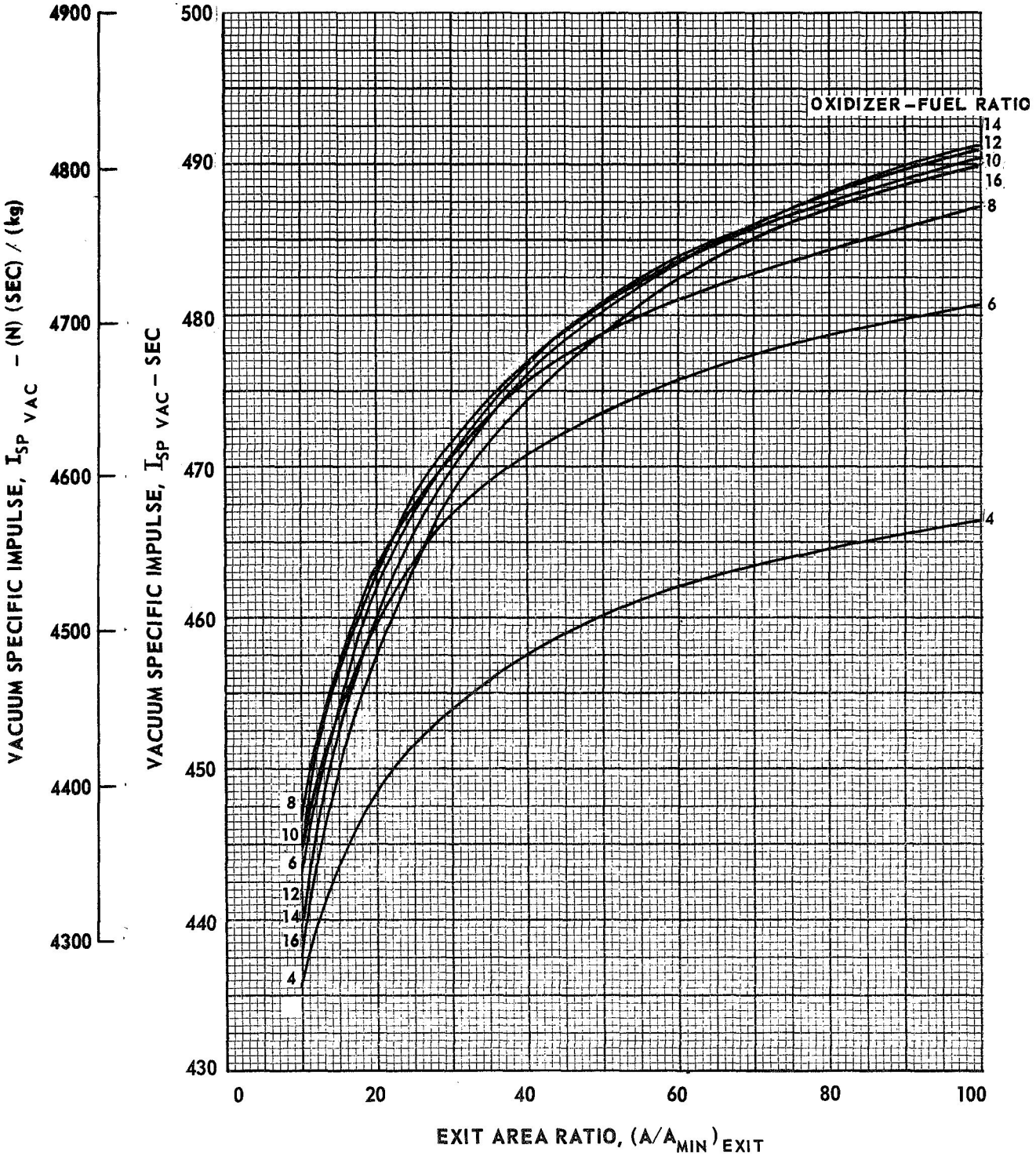

FIG. 1-8

VARIATION OF FROZEN VACUUM SPECIFIC IMPULSE WITH AREA RATIO

H_2 (ℓ) – F_2 (ℓ)

P_C = 500 PSIA (3.448 X 10^6 N/m^2)

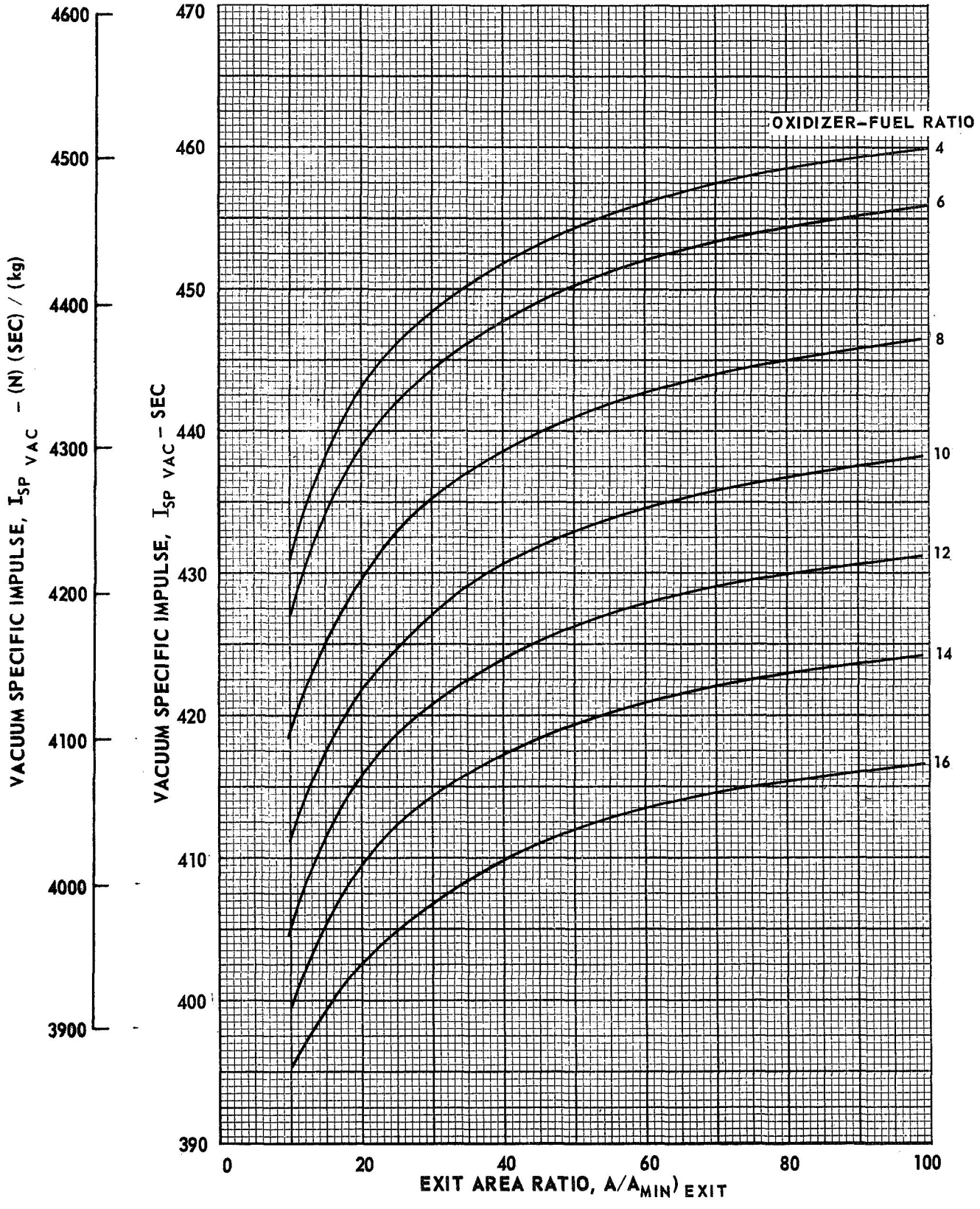

FIG. I-9

VARIATION OF EQUILIBRIUM VACUUM SPECIFIC IMPULSE WITH AREA RATIO

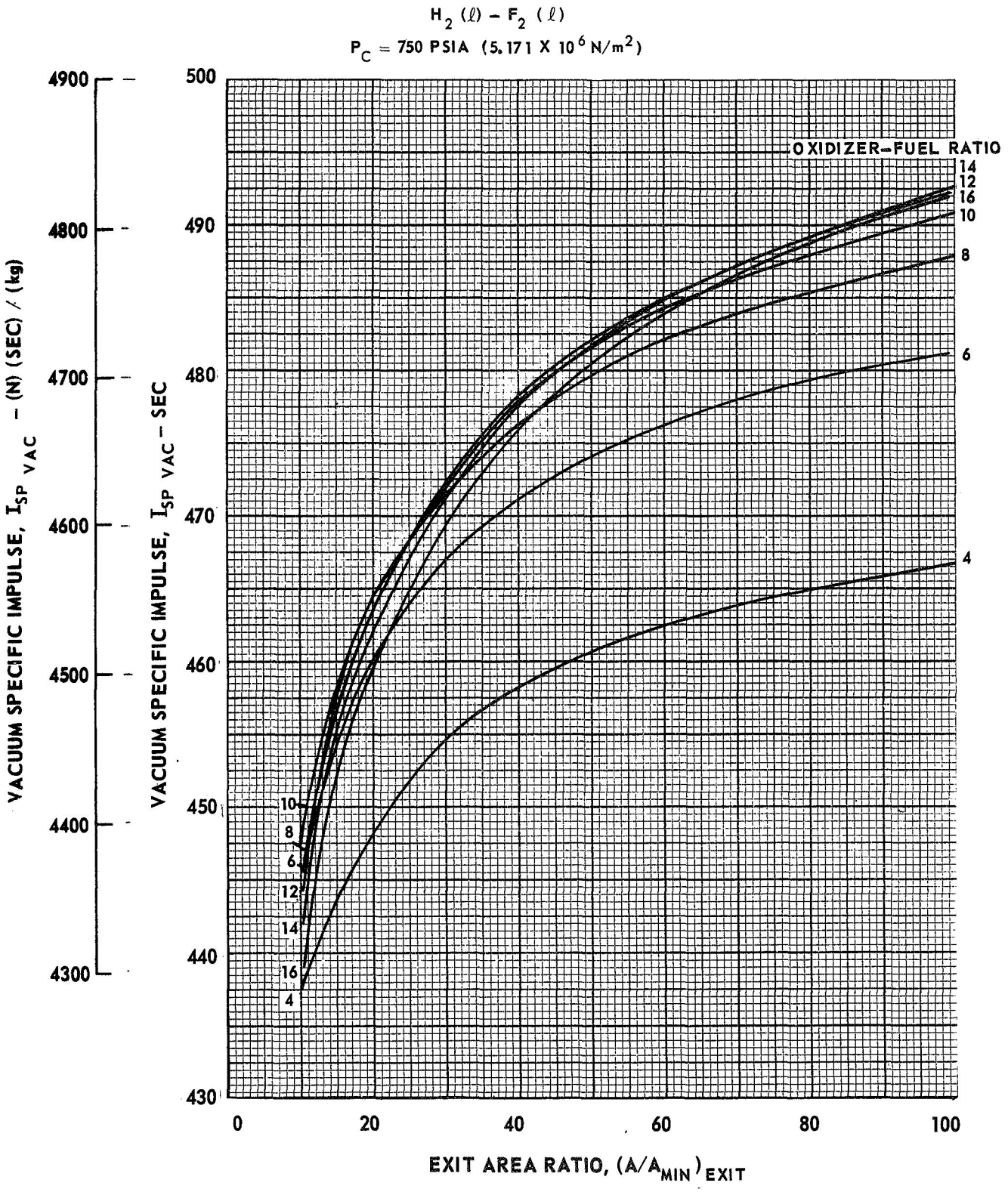

FIG. I-10

VARIATION OF FROZEN VACUUM SPECIFIC IMPULSE WITH AREA RATIO

H_2 (ℓ) - F_2 (ℓ)

P_C = 750 PSIA (5.171 X 10^6 N/m^2)

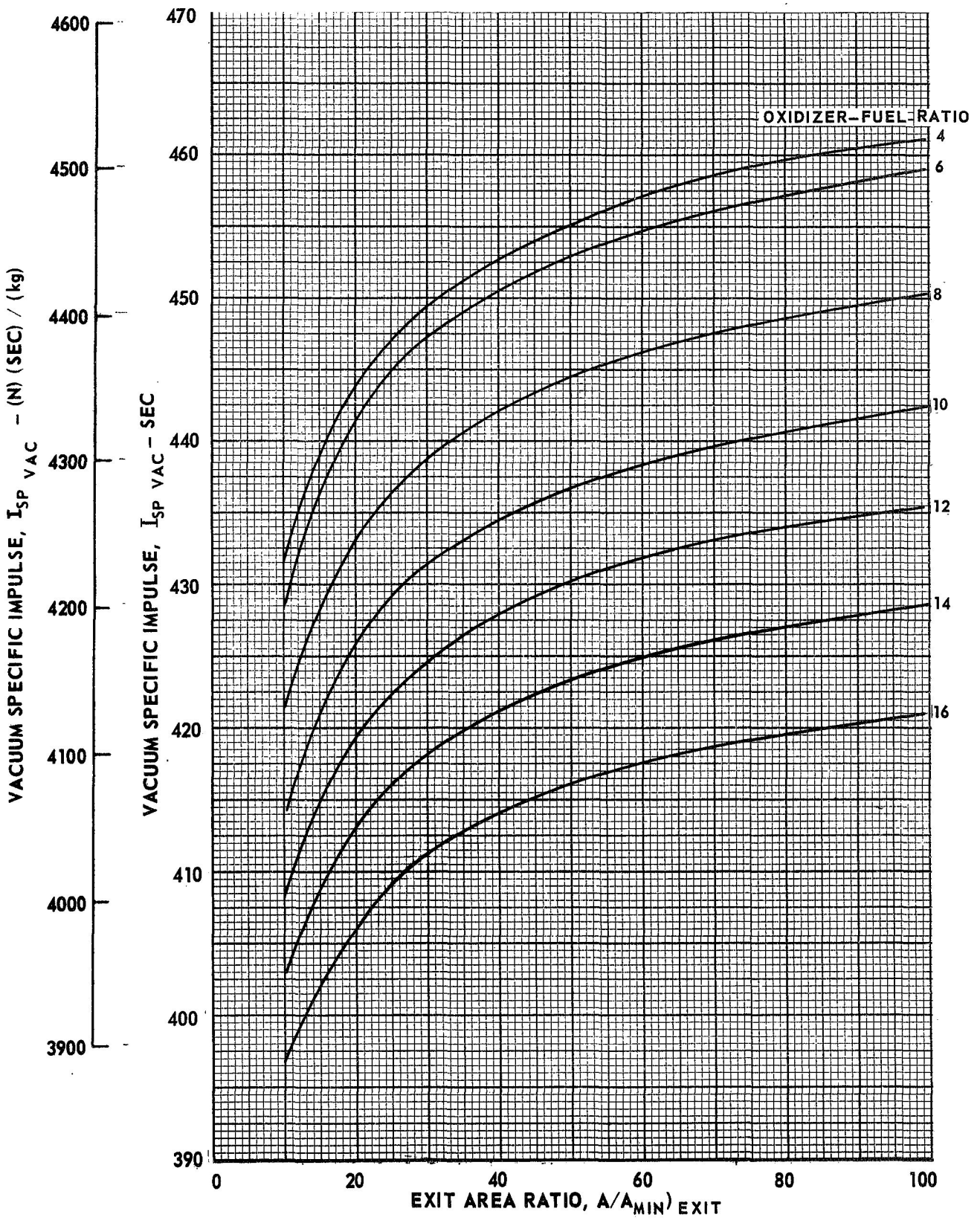

FIG. I-11

VARIATION OF EQUILIBRIUM VACUUM SPECIFIC IMPULSE WITH AREA RATIO

H_2 (ℓ) – F_2 (ℓ)

P_C = 1000 PSIA ($6.895 \times 10^6 N/m^2$)

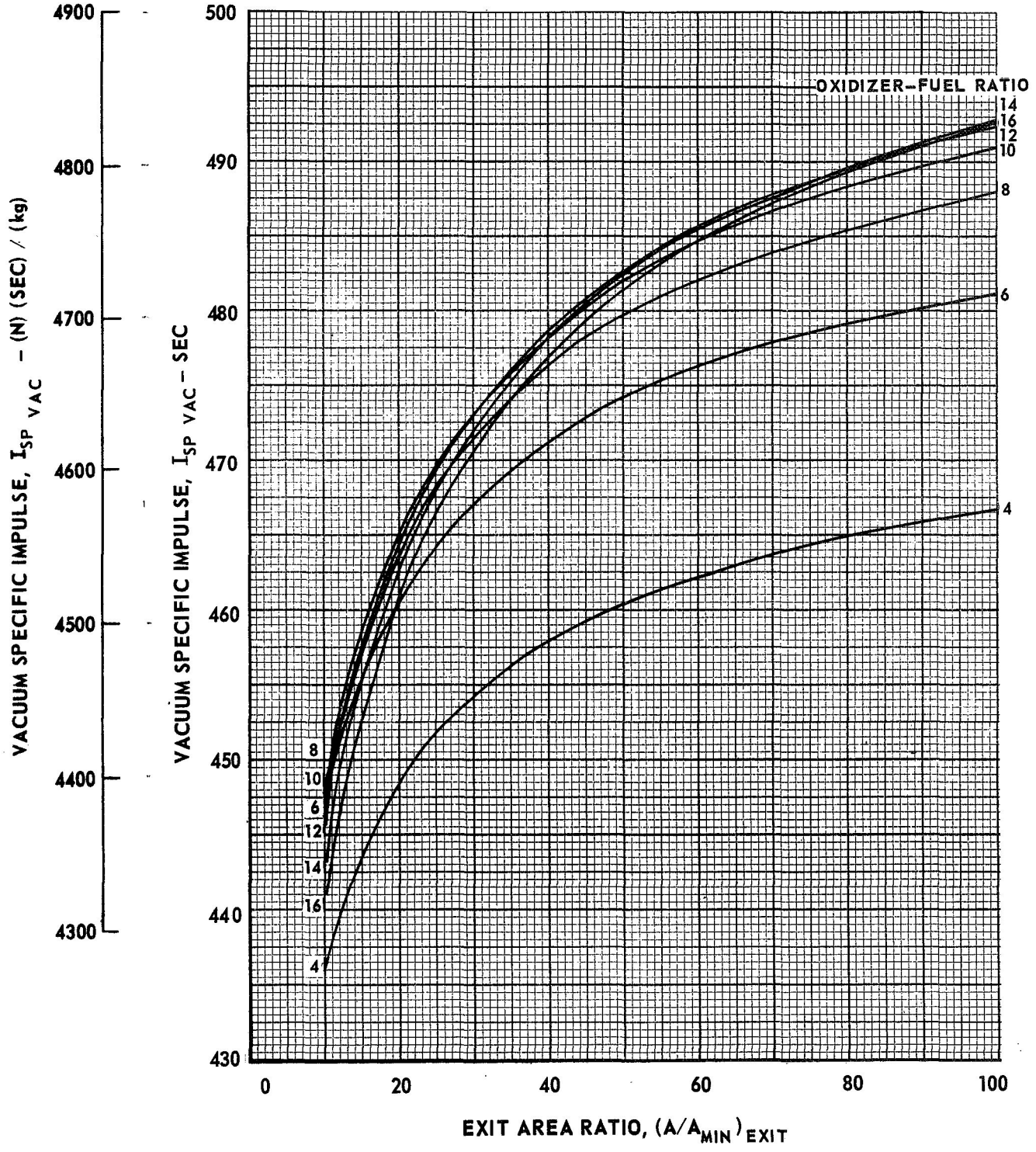

FIG. I-12

VARIATION OF FROZEN VACUUM SPECIFIC IMPULSE WITH AREA RATIO

H_2 (ℓ) – F_2 (ℓ)

P_C = 1000 PSIA (6.895X10^6 N/m^2)

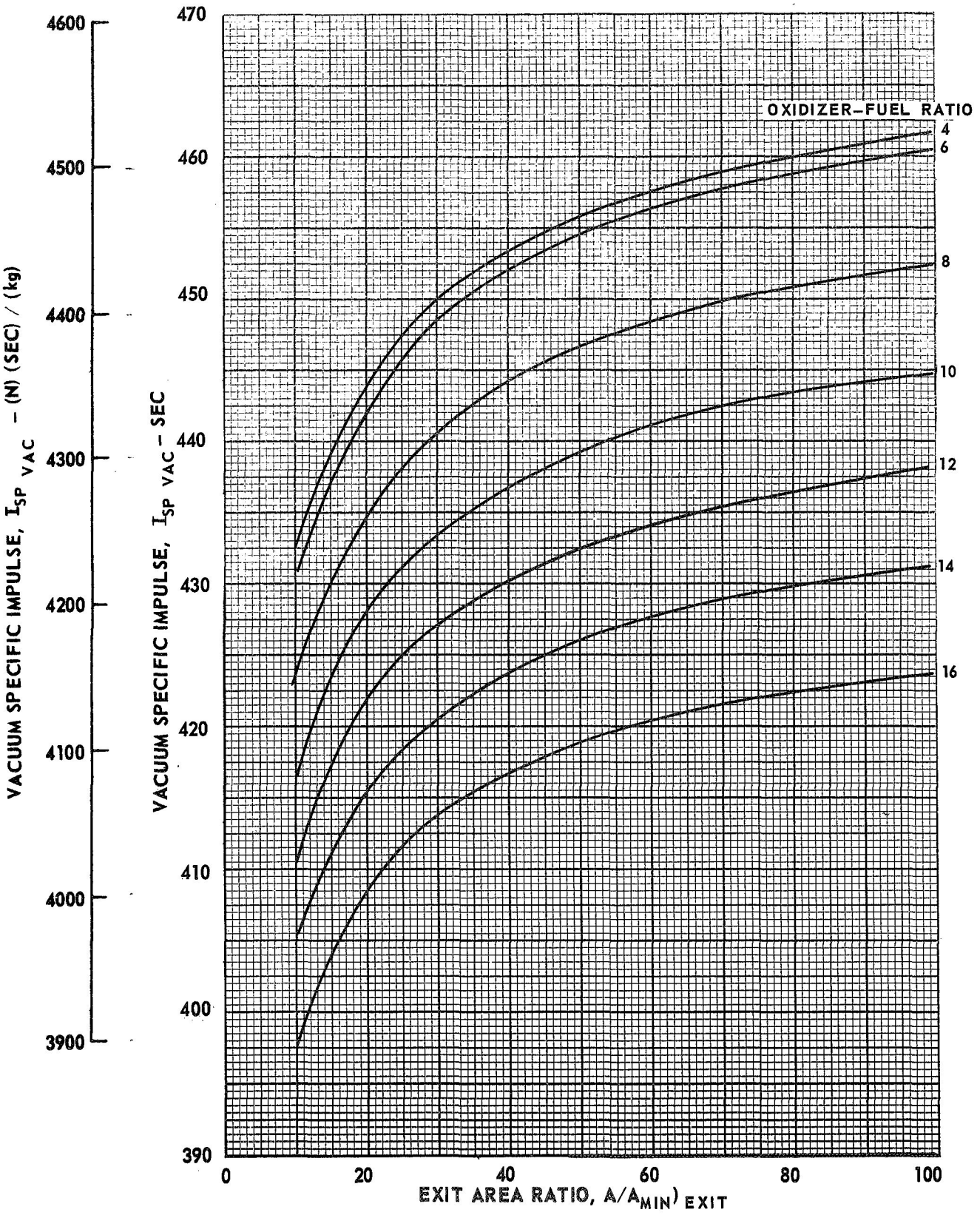

FIG. I-13

NORMALIZED GRAPHICAL SOLUTION FOR FREEZING AREA RATIO USING MODIFIED BRAY ANALYSIS

$H_2(\ell) - F_2(\ell)$

$P_C = 100$ PSIA ($6.895 \times 10^5 N/m^2$)

O/F = 8.0

NOTE: REACTION RATE CONSTANTS LISTED IN TABLE I-1

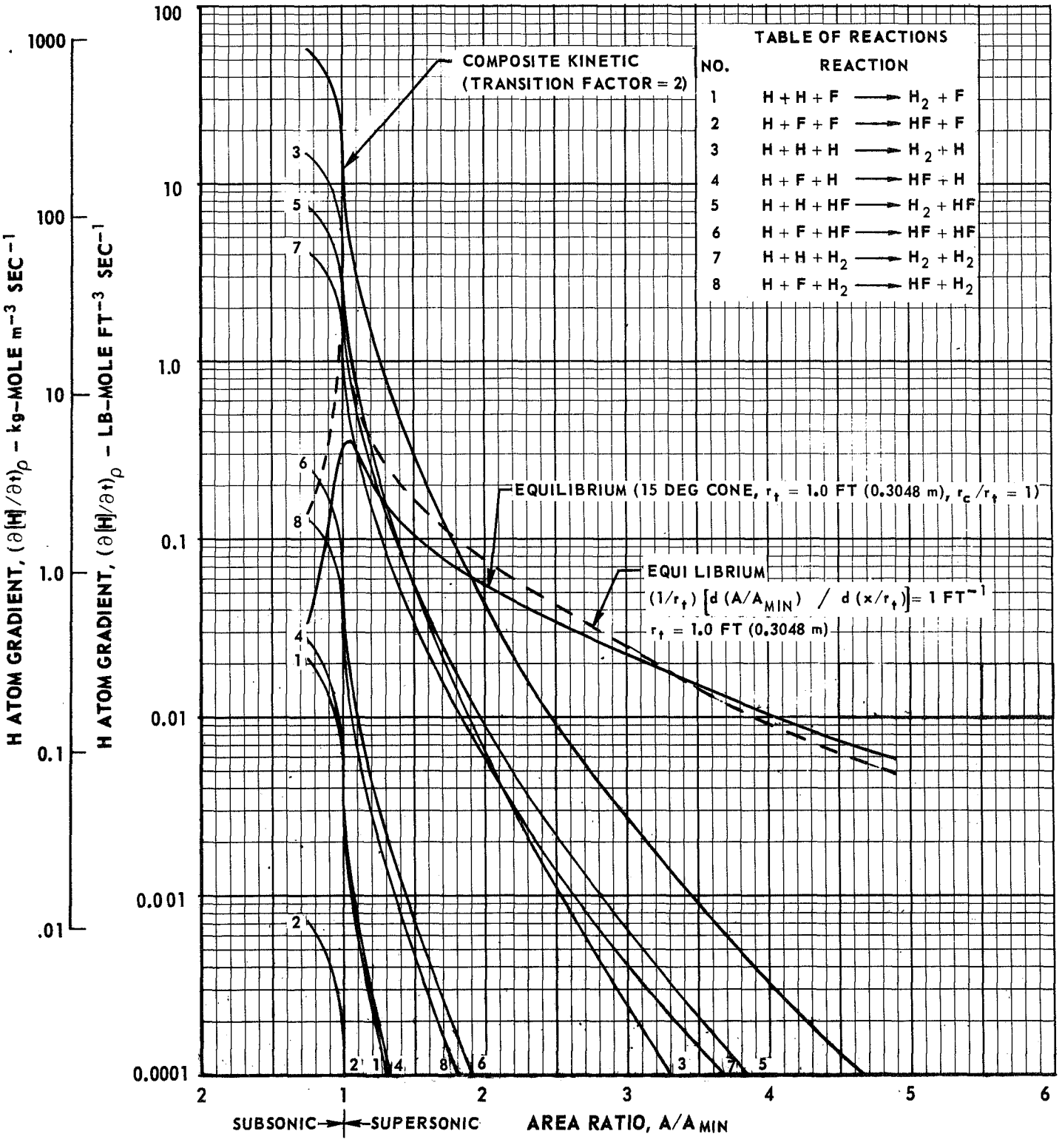

FIG. I-14

NORMALIZED GRAPHICAL SOLUTION FOR FREEZING AREA RATIO USING MODIFIED BRAY ANALYSIS

H_2 (ℓ) – F_2 (ℓ)

P_C = 100 PSIA (6.895×10^5 N/m^2)

O/F = 12.0

NOTE: REACTION RATE CONSTANTS LISTED IN TABLE I-1

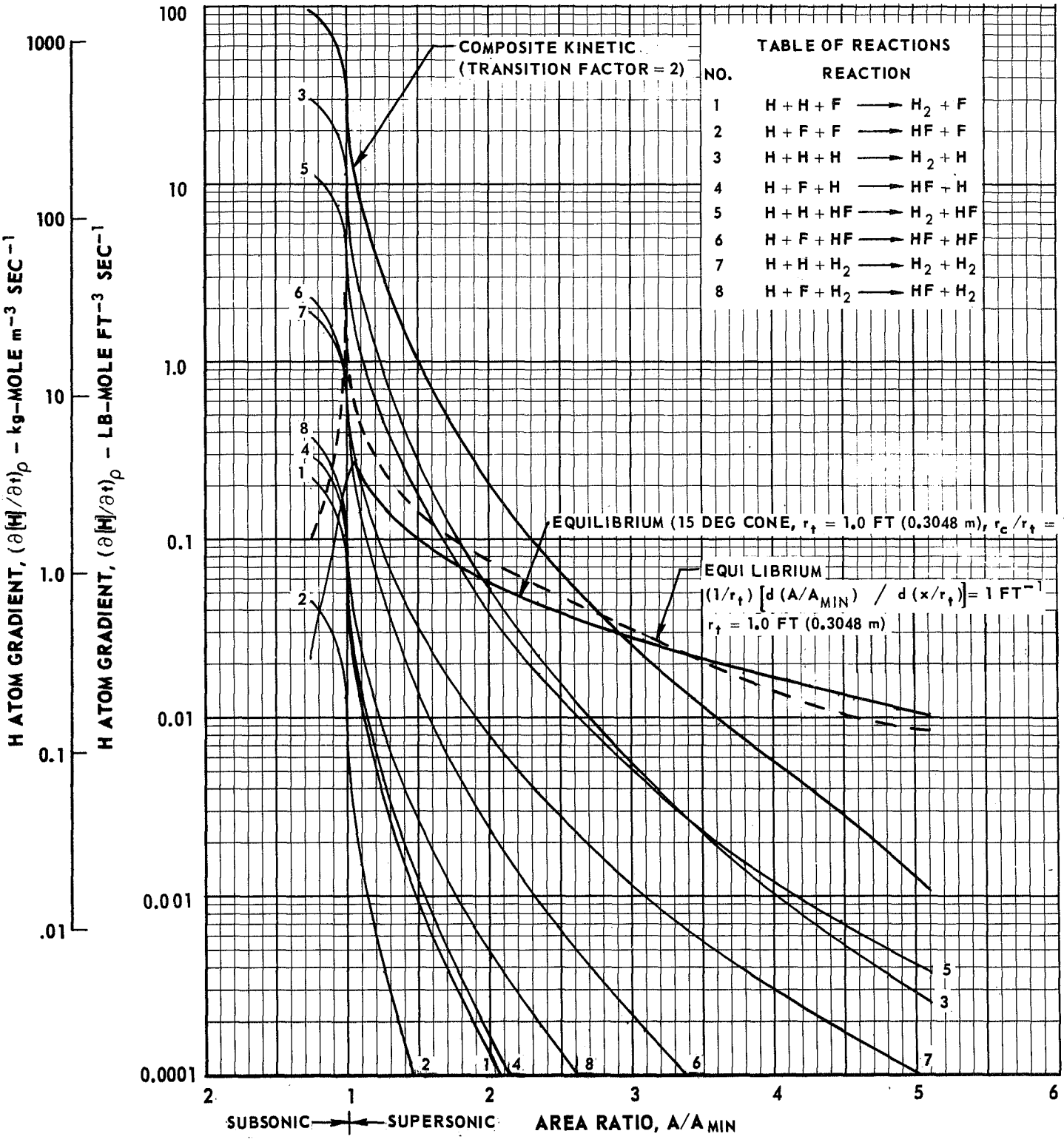

NORMALIZED GRAPHICAL SOLUTION FOR FREEZING AREA RATIO USING MODIFIED BRAY ANALYSIS

$H_2(\ell) - F_2(\ell)$

$P_C = 100$ PSIA (6.895×10^5 N/m^2)

O/F = 16.0

NOTE: REACTION RATE CONSTANTS LISTED IN TABLE I-1

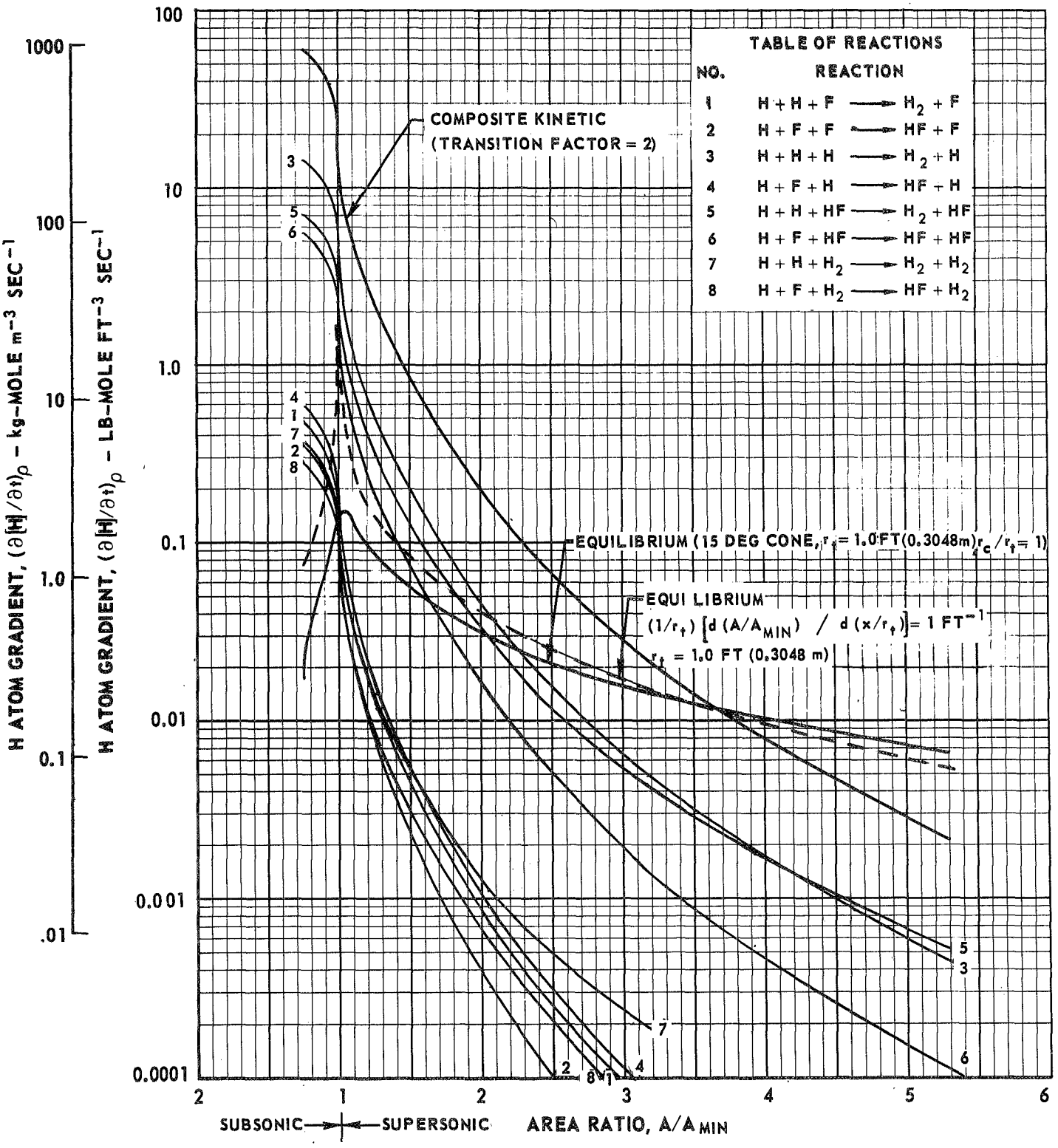

NORMALIZED GRAPHICAL SOLUTION FOR FREEZING AREA RATIO USING MODIFIED BRAY ANALYSIS

$H_2(\ell) - F_2(\ell)$

$P_C = 200$ PSIA (1.379×10^6 N/m^2).

O/F = 8.0

NOTE: REACTION RATE CONSTANTS LISTED IN TABLE I-1

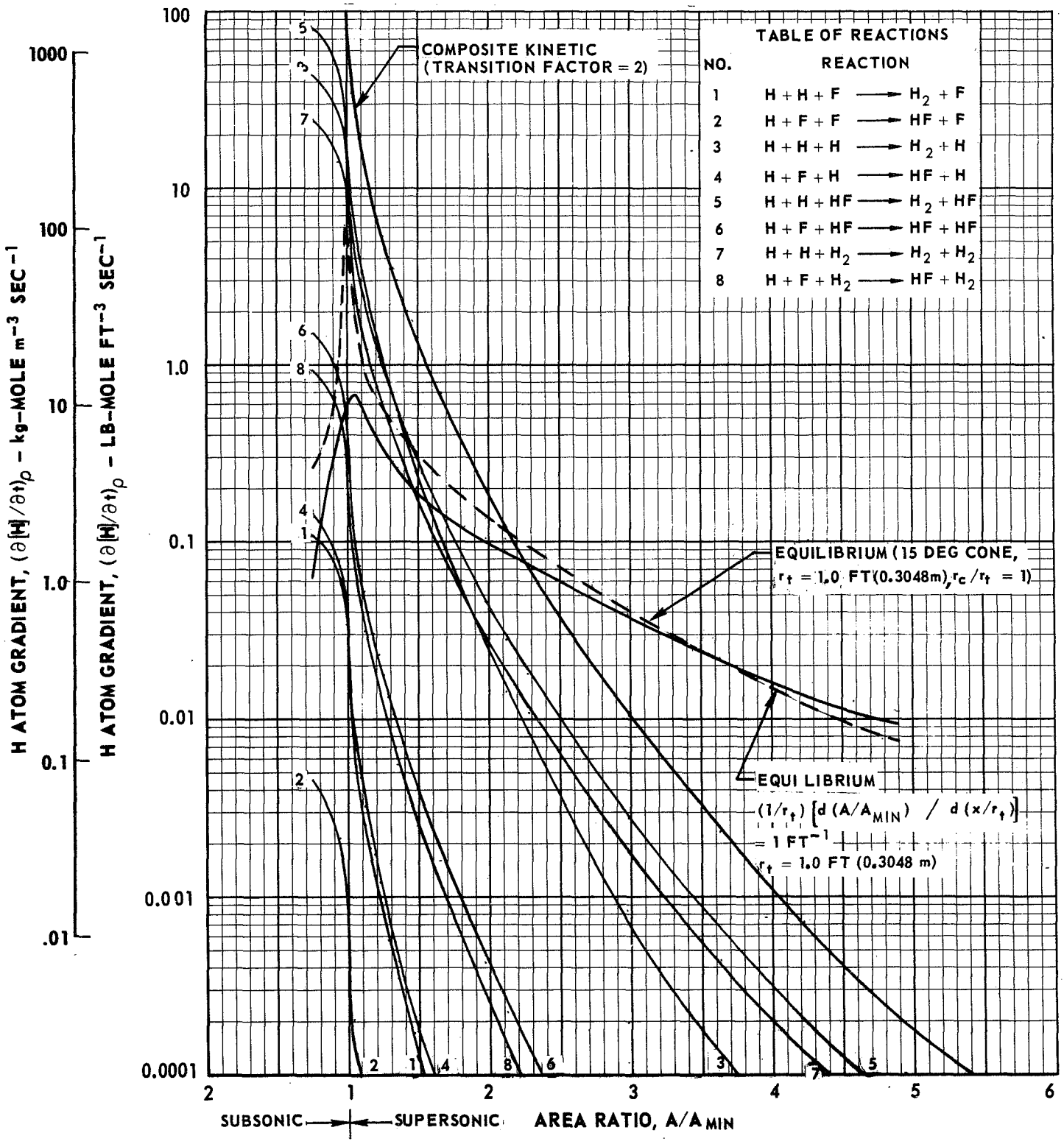

FIG. I-17

NORMALIZED GRAPHICAL SOLUTION FOR FREEZING AREA RATIO USING MODIFIED BRAY ANALYSIS

H_2 (ℓ) - F_2 (ℓ)

P_C = 200 PSIA (1.379X10^6 N/m^2)

O/F = 12.0

NOTE: REACTION RATE CONSTANTS LISTED IN TABLE I-1

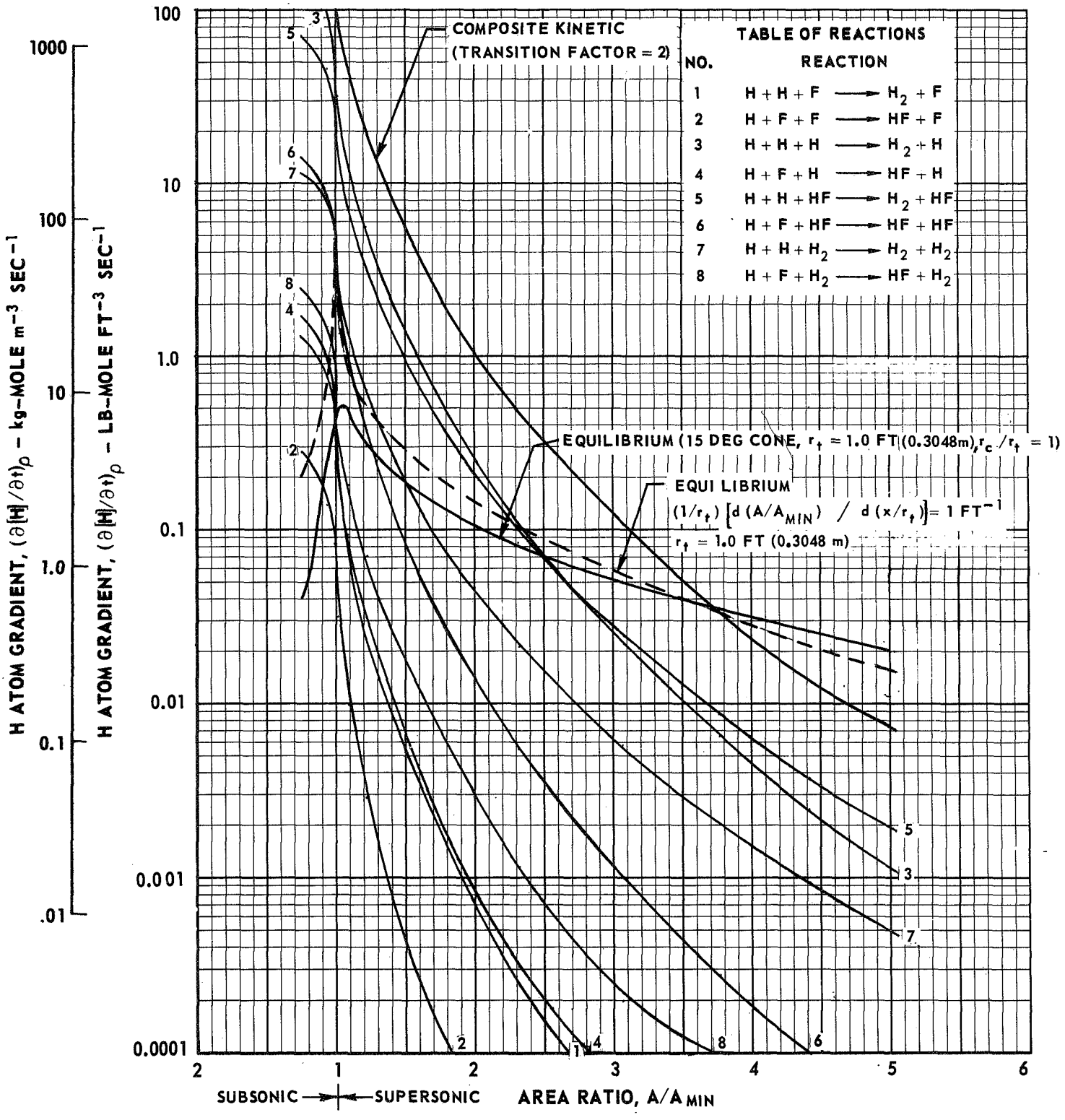

FIG. I-18

NORMALIZED GRAPHICAL SOLUTION FOR FREEZING AREA RATIO USING MODIFIED BRAY ANALYSIS

$H_2(\ell) - F_2(\ell)$

$P_C = 200$ PSIA (1.379×10^6 N/m^2)

O/F = 16.0

NOTE: REACTION RATE CONSTANTS LISTED IN TABLE I-1

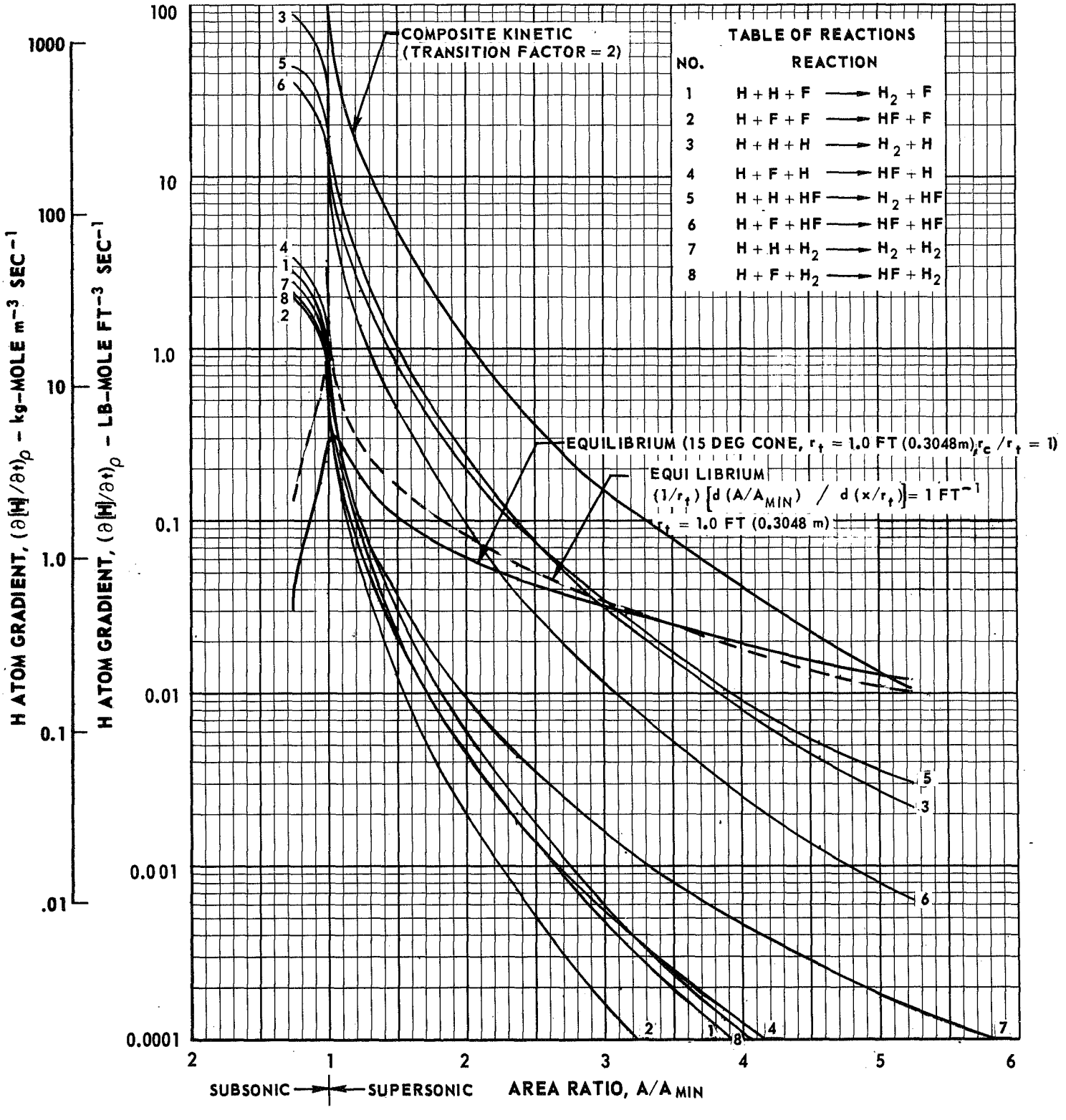

FIG. I-19

NORMALIZED GRAPHICAL SOLUTION FOR FREEZING AREA RATIO USING MODIFIED BRAY ANALYSIS

H_2 (ℓ) - F_2 (ℓ)

P_C = 300 PSIA (2.069×10^6 N/m^2)

O/F = 8.0

NOTE: REACTION RATE CONSTANTS LISTED IN TABLE I-1

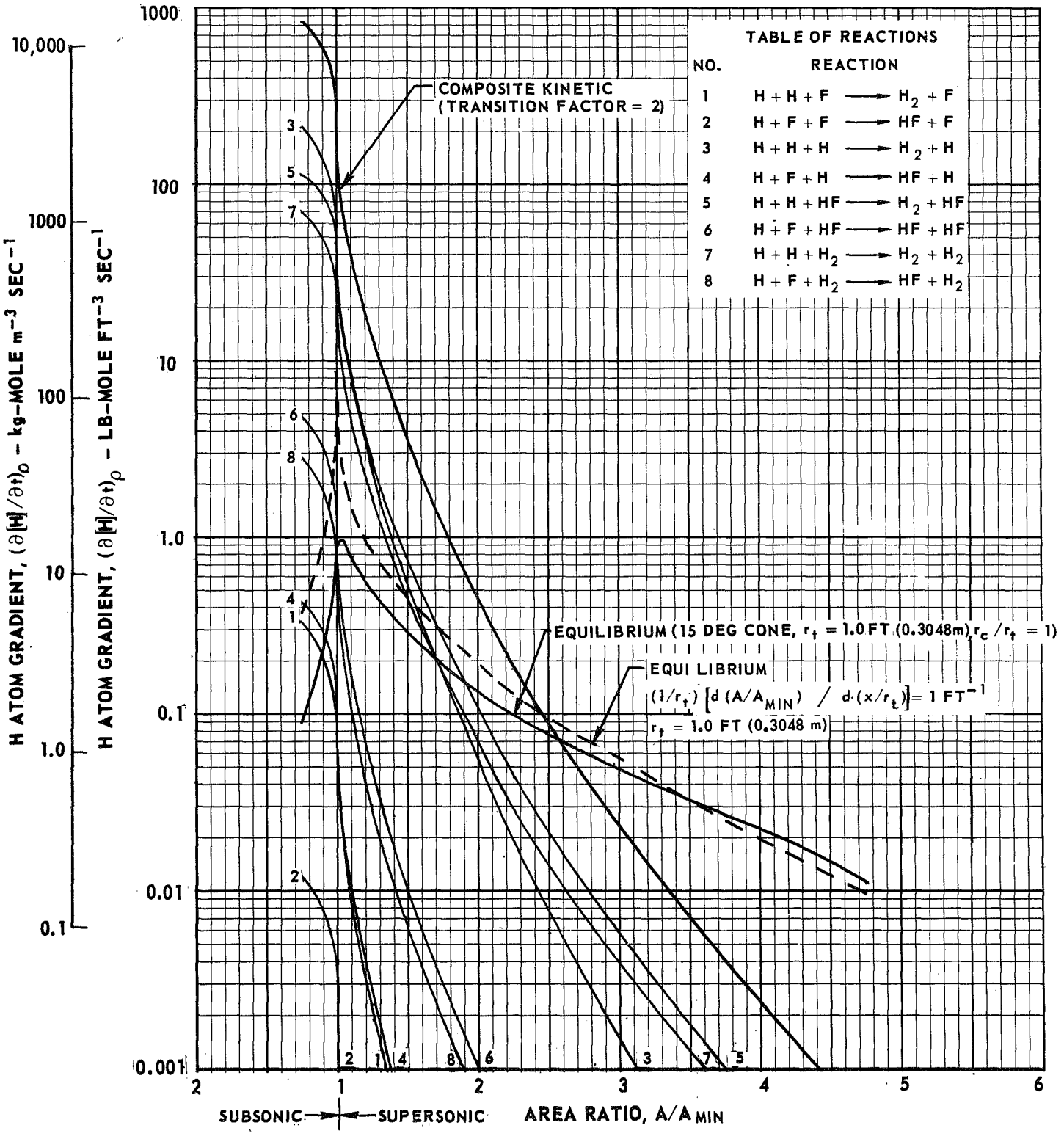

NORMALIZED GRAPHICAL SOLUTION FOR FREEZING AREA RATIO USING MODIFIED BRAY ANALYSIS

$H_2(\ell) - F_2(\ell)$

$P_C = 300$ PSIA (2.069×10^6 N/m^2)

O/F = 12.0

NOTE: REACTION RATE CONSTANTS LISTED IN TABLE I-1

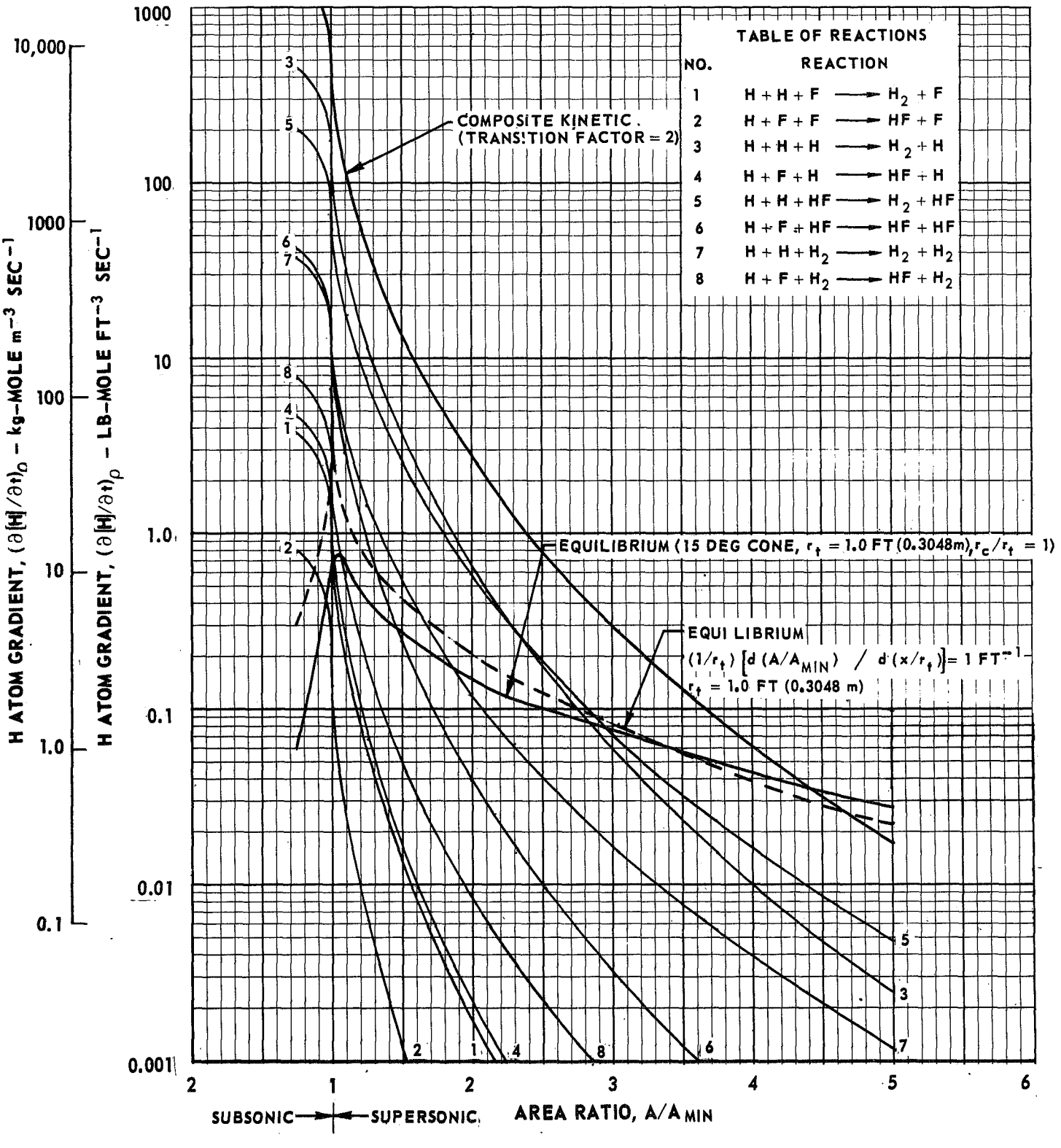

FIG. I-21

NORMALIZED GRAPHICAL SOLUTION FOR FREEZING AREA RATIO USING MODIFIED BRAY ANALYSIS

H_2 (ℓ) - F_2 (ℓ)

P_C = 300 PSIA (2.069×10^6 N/m^2)

O/F = 16.0

NOTE: REACTION RATE CONSTANTS LISTED IN TABLE I-1

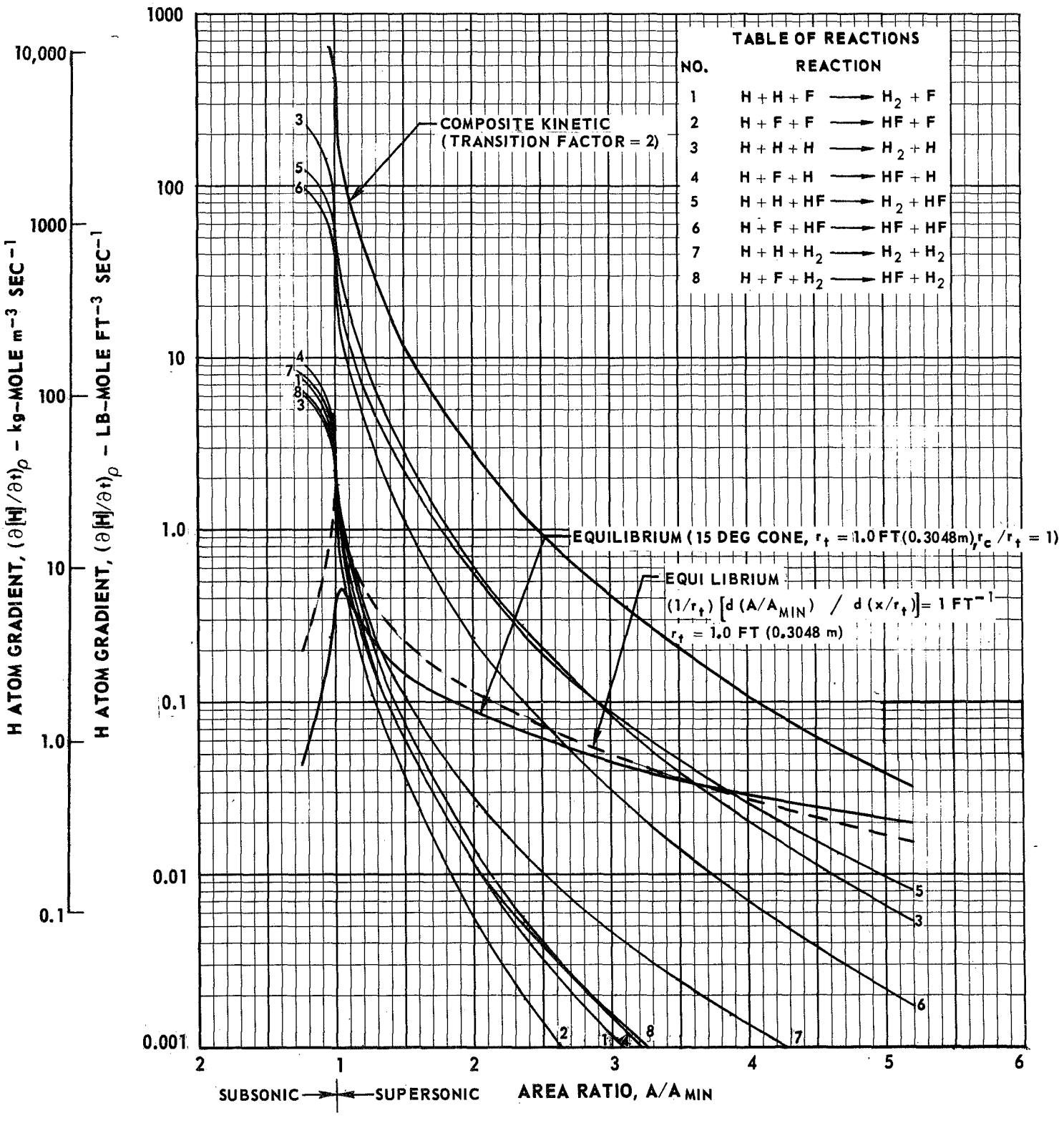

FIG. I-22

NORMALIZED GRAPHICAL SOLUTION FOR FREEZING AREA RATIO USING MODIFIED BRAY ANALYSIS

H_2 (ℓ) - F_2 (ℓ)

P_C = 500 PSIA ($3.448 \times 10^6 N/m^2$)

O/F = 8.0

NOTE: REACTION RATE CONSTANTS LISTED IN TABLE I-1

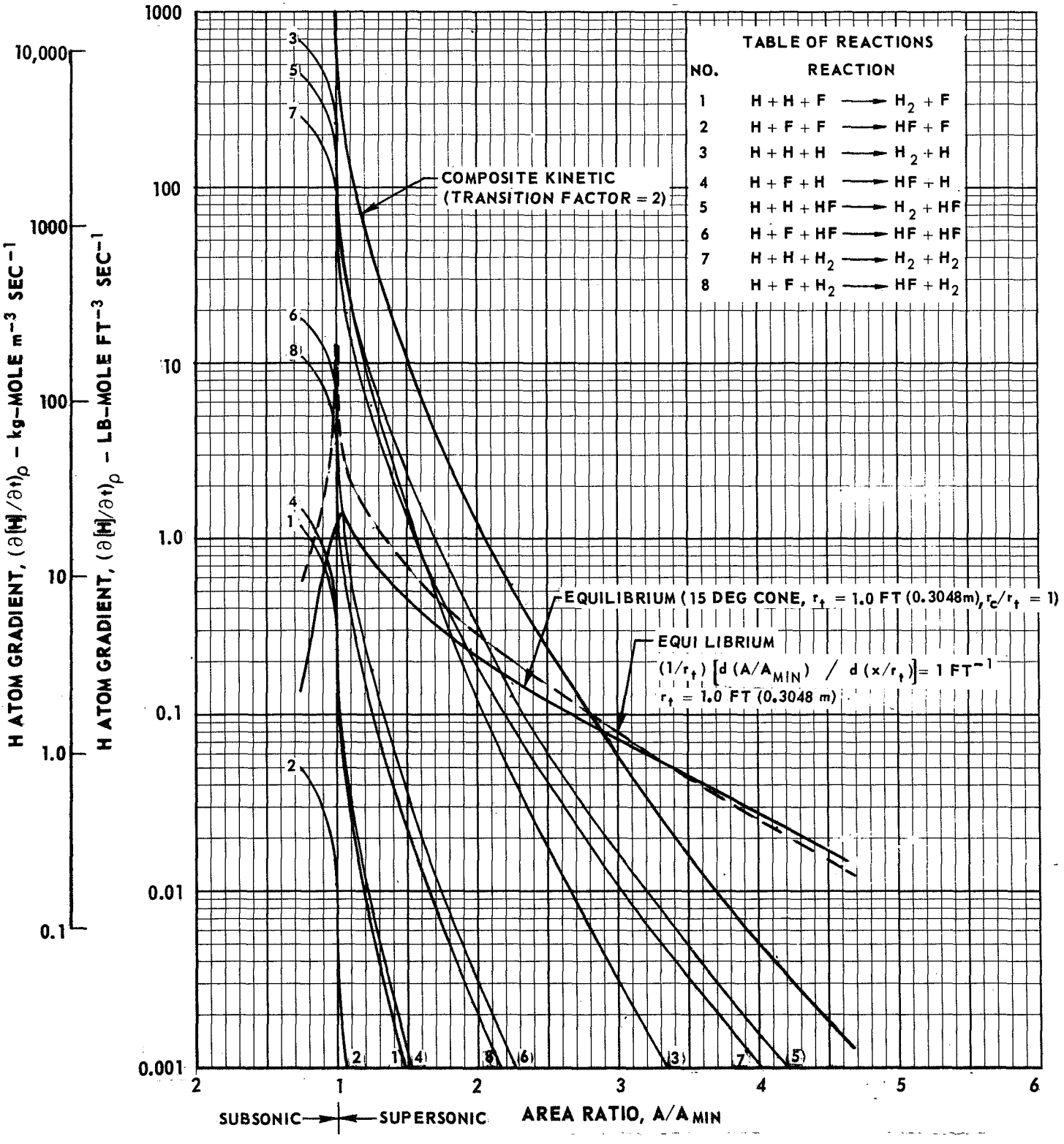

NORMALIZED GRAPHICAL SOLUTION FOR FREEZING AREA RATIO USING MODIFIED BRAY ANALYSIS

$H_2(\ell) - F_2(\ell)$

$P_C = 500$ PSIA ($3.448 \times 10^6 N/m^2$)

O/F = 12.0

NOTE: REACTION RATE CONSTANTS LISTED IN TABLE I-1

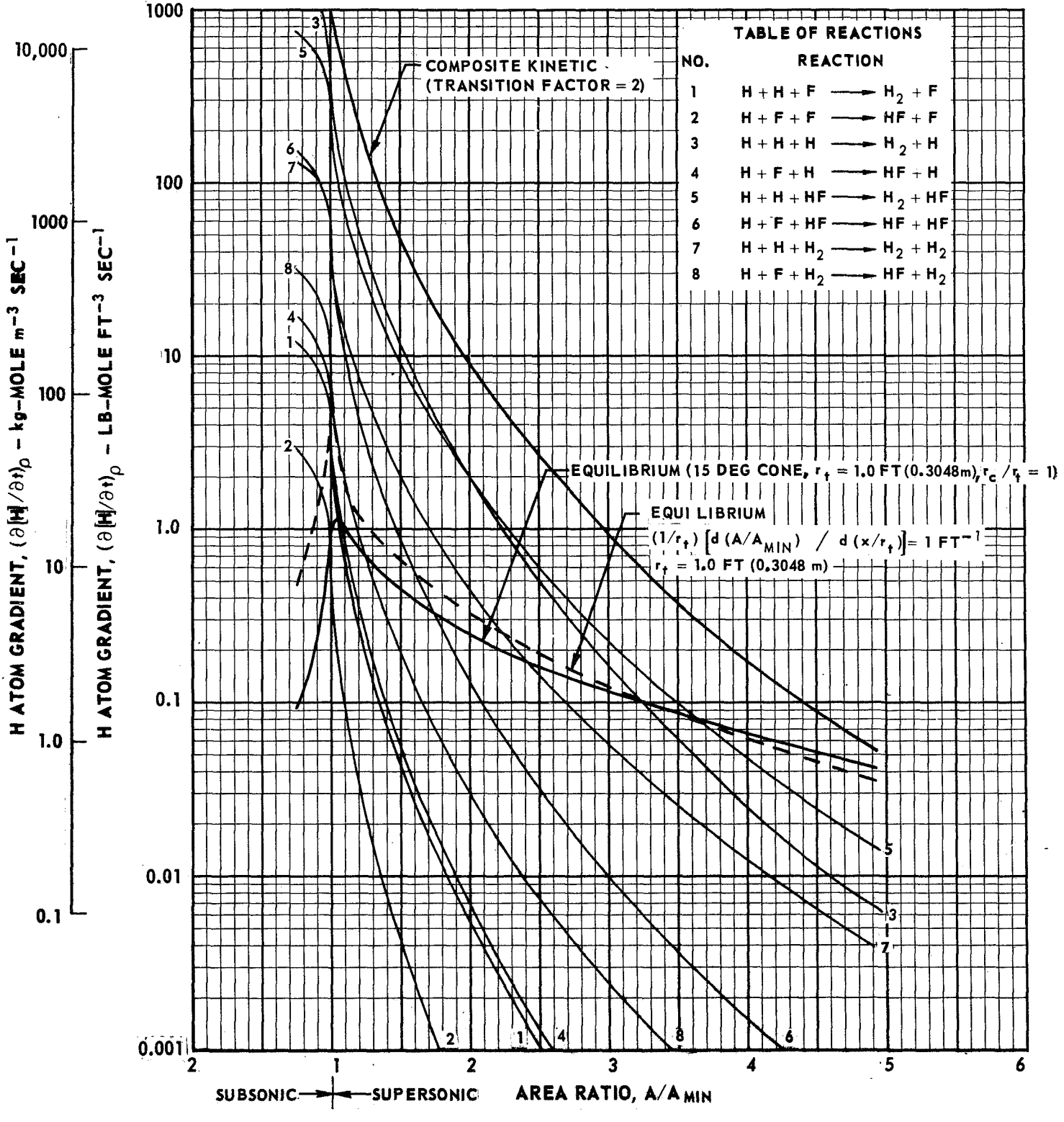

NORMALIZED GRAPHICAL SOLUTION FOR FREEZING AREA RATIO USING MODIFIED BRAY ANALYSIS

H_2 (ℓ) - F_2 (ℓ)

P_C = 500 PSIA (3.448×10^6 N/m^2)

O/F = 16.0

NOTE: REACTION RATE CONSTANTS LISTED IN TABLE I-1

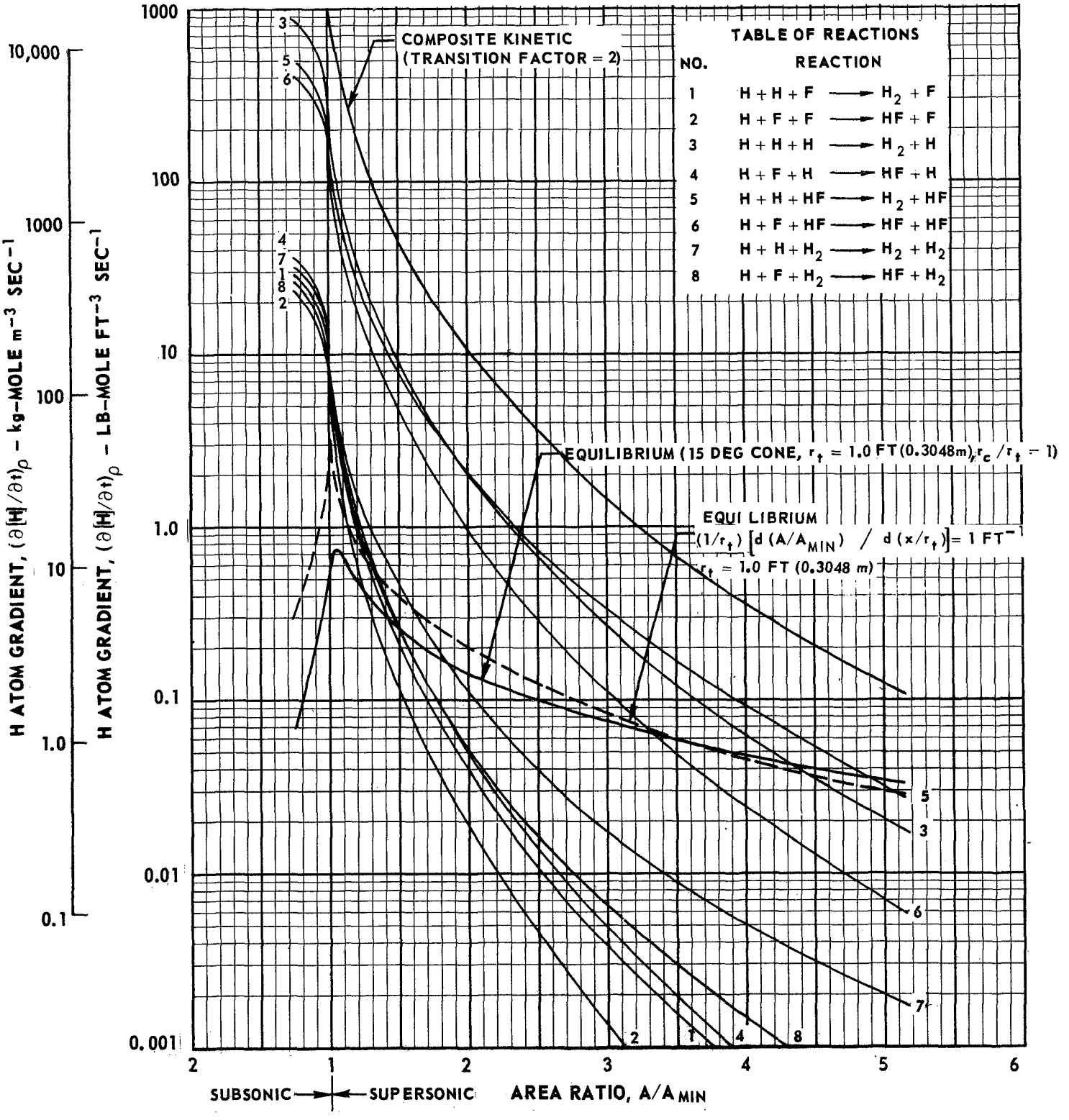

FIG. I-25

NORMALIZED GRAPHICAL SOLUTION FOR FREEZING AREA RATIO USING MODIFIED BRAY ANALYSIS

H_2 (ℓ) - F_2 (ℓ)

P_C = 750 PSIA (5.171X10^{6}N/m^2)

O/F = 8.0

NOTE: REACTION RATE CONSTANTS LISTED IN TABLE I-1

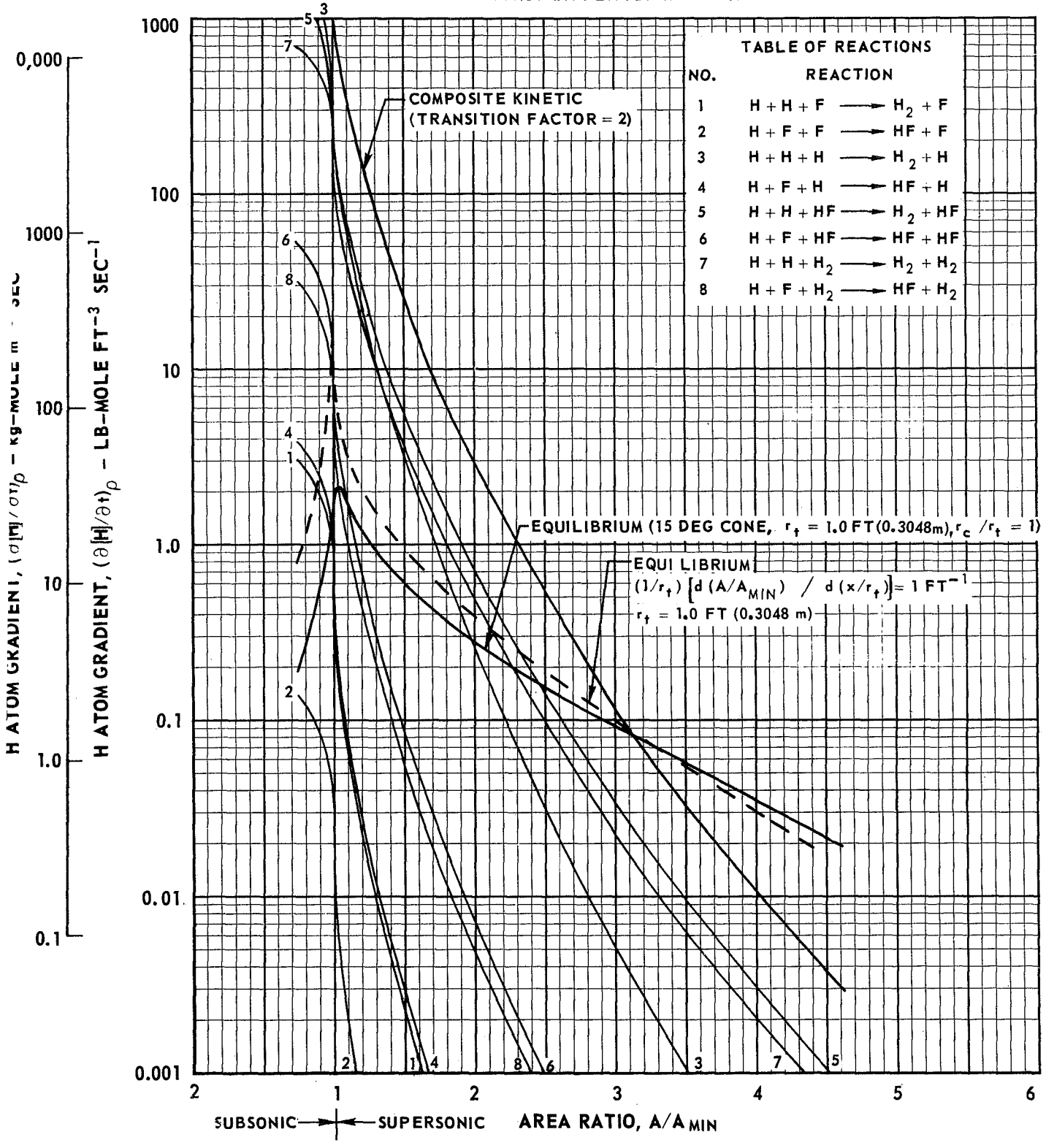

FIG. I-26

NORMALIZED GRAPHICAL SOLUTION FOR FREEZING AREA RATIO USING MODIFIED BRAY ANALYSIS

$H_2(\ell) - F_2(\ell)$

$P_C = 750$ PSIA (5.171×10^6 N/m^2)

O/F = 12.0

NOTE: REACTION RATE CONSTANTS LISTED IN TABLE I-1

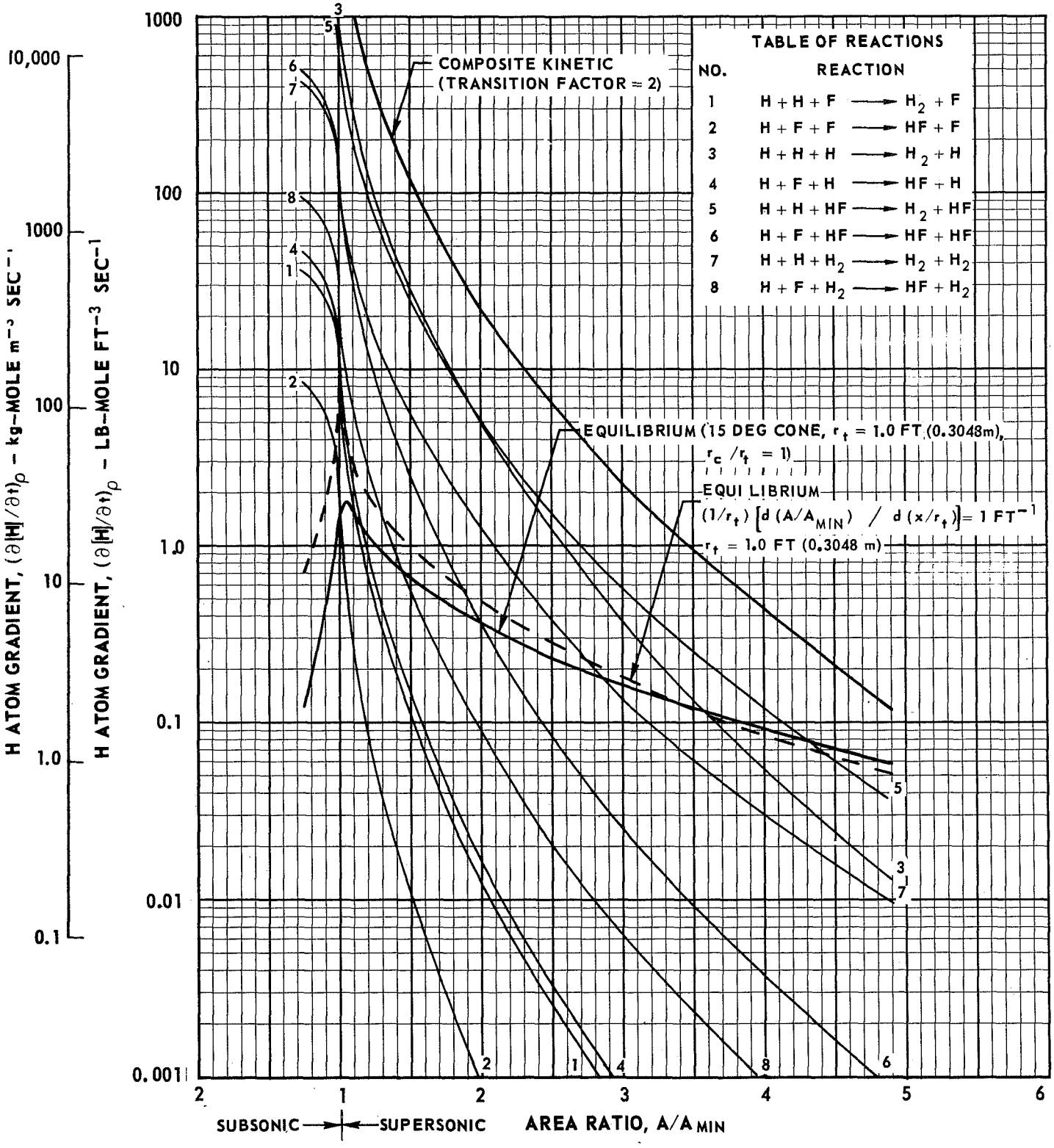

FIG. I-27

NORMALIZED GRAPHICAL SOLUTION FOR FREEZING AREA RATIO USING MODIFIED BRAY ANALYSIS

H_2 (ℓ) - F_2 (ℓ)

P_C = 750 PSIA (5.171X10^6 N/m^2)

O/F = 16.0

NOTE: REACTION RATE CONSTANTS LISTED IN TABLE I-1

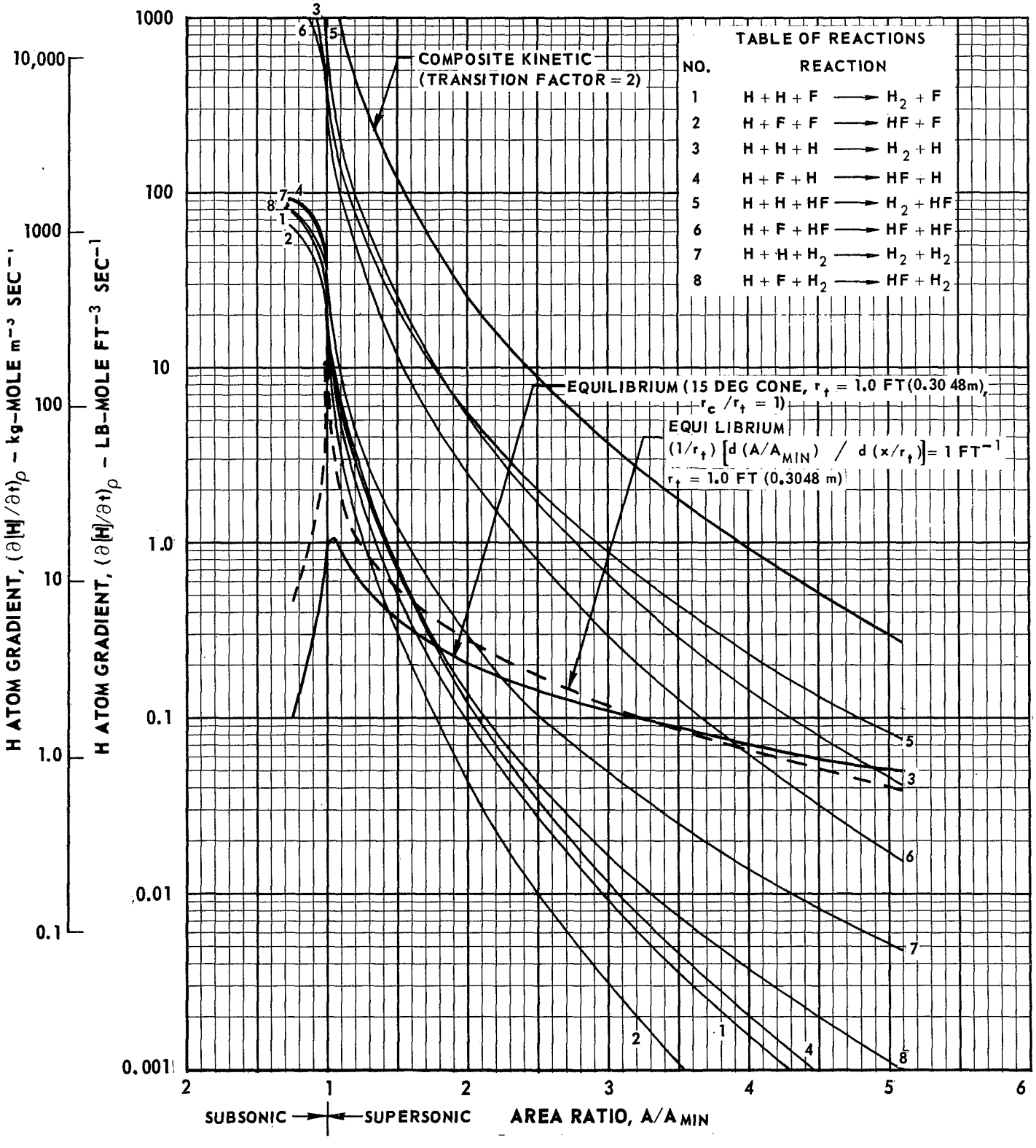

FIG. I–28

NORMALIZED GRAPHICAL SOLUTION FOR FREEZING AREA RATIO USING MODIFIED BRAY ANALYSIS

H_2 (ℓ) – F_2 (ℓ)

P_C =1000 PSIA (6.895×10^6 N/m^2)

O/F = 8.0

NOTE: REACTION RATE CONSTANTS LISTED IN TABLE I–1

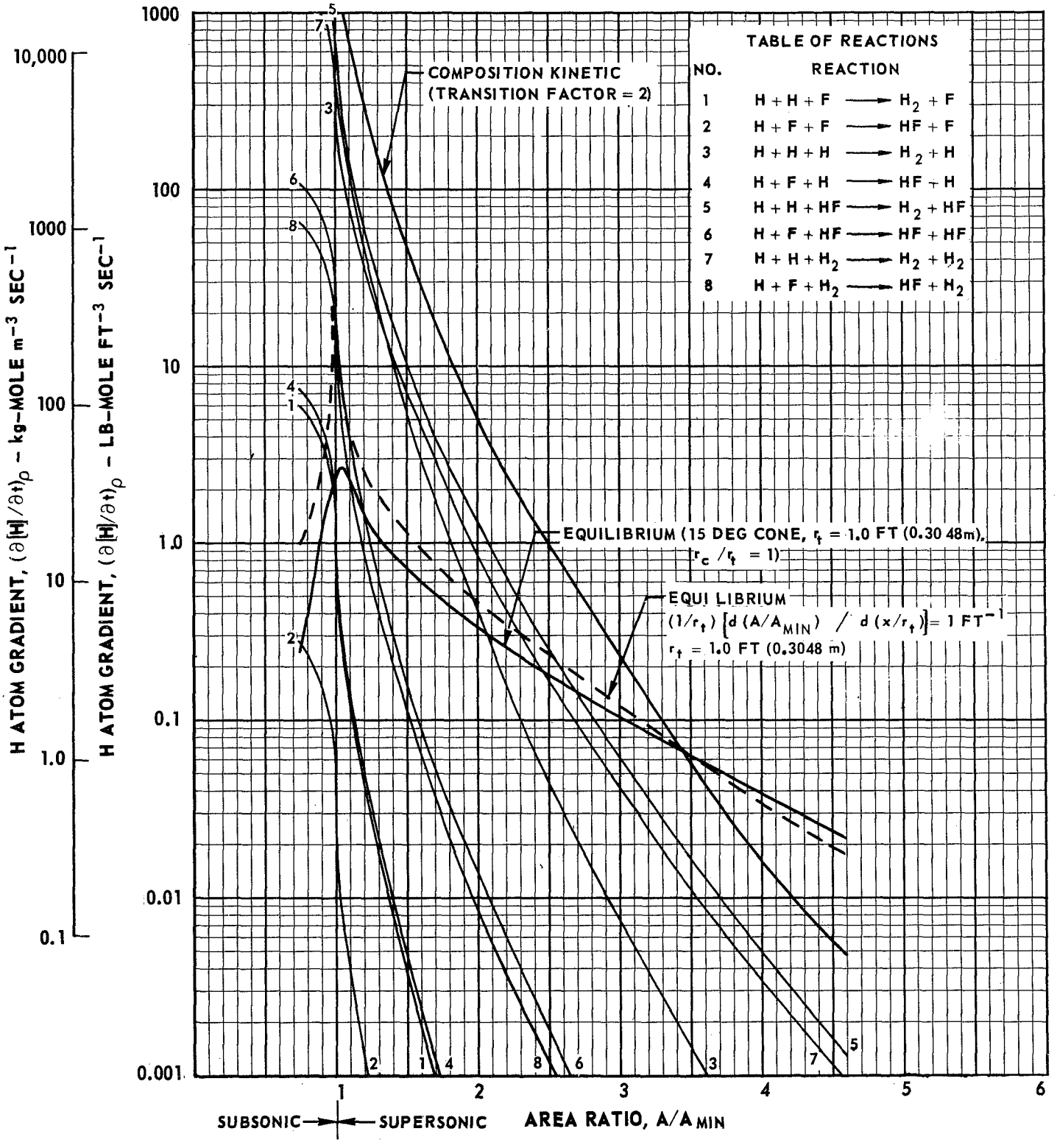

FIG. 1-29

NORMALIZED GRAPHICAL SOLUTION FOR FREEZING AREA RATIO USING MODIFIED BRAY ANALYSIS

$H_2(\ell) - F_2(\ell)$

P_C =1000 PSIA (6.895×10^6 N/m^2)

O/F = 12.0

NOTE: REACTION RATE CONSTANTS LISTED IN TABLE I-1

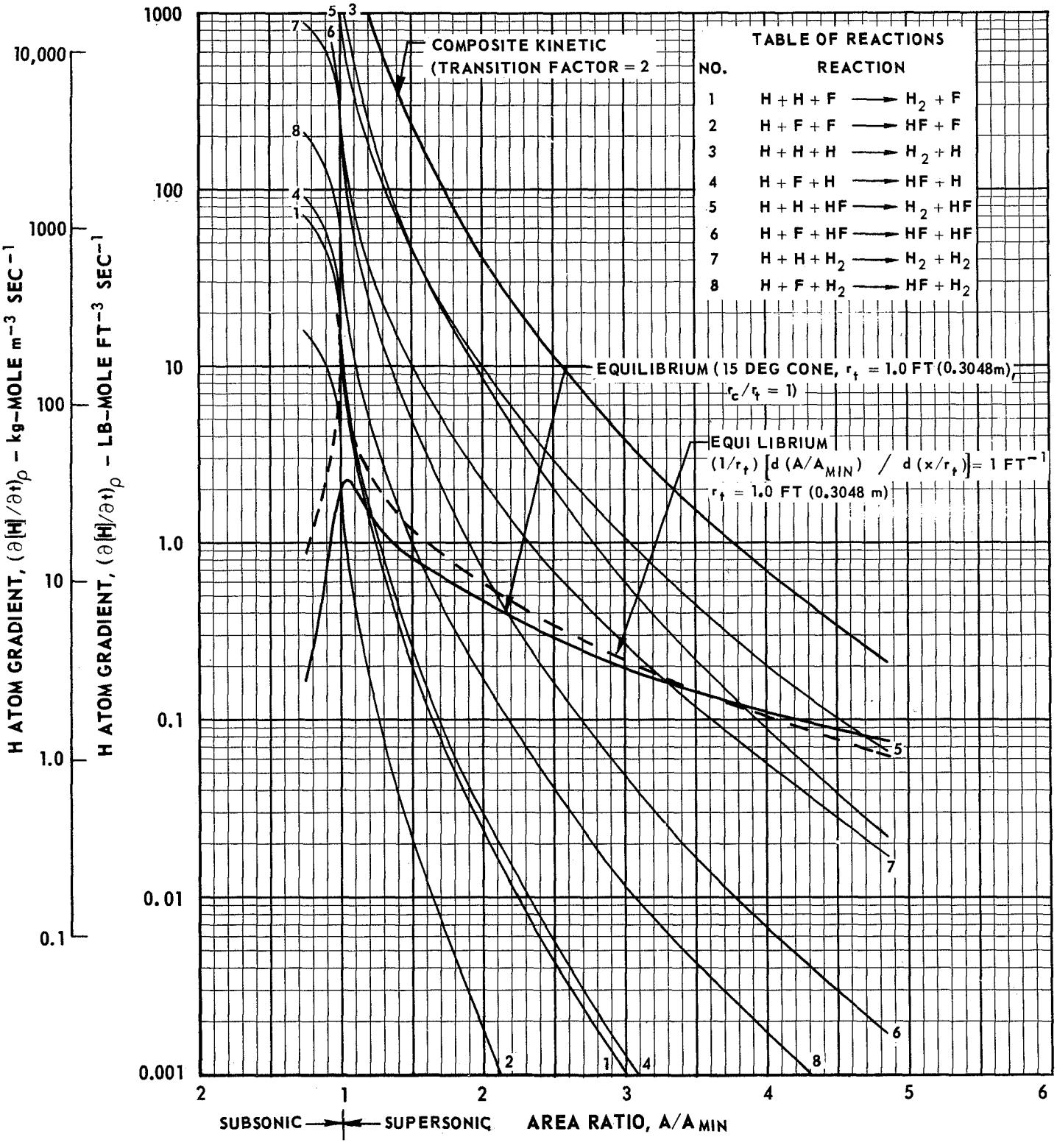

FIG. I–30

NORMALIZED GRAPHICAL SOLUTION FOR FREEZING AREA RATIO USING MODIFIED BRAY ANALYSIS

H_2 (ℓ) – F_2 (ℓ)

P_C =1000 PSIA (6.895X10 ^{6}N/m^2)

O/F = 16.0

NOTE: REACTION RATE CONSTANTS LISTED IN TABLE I–1

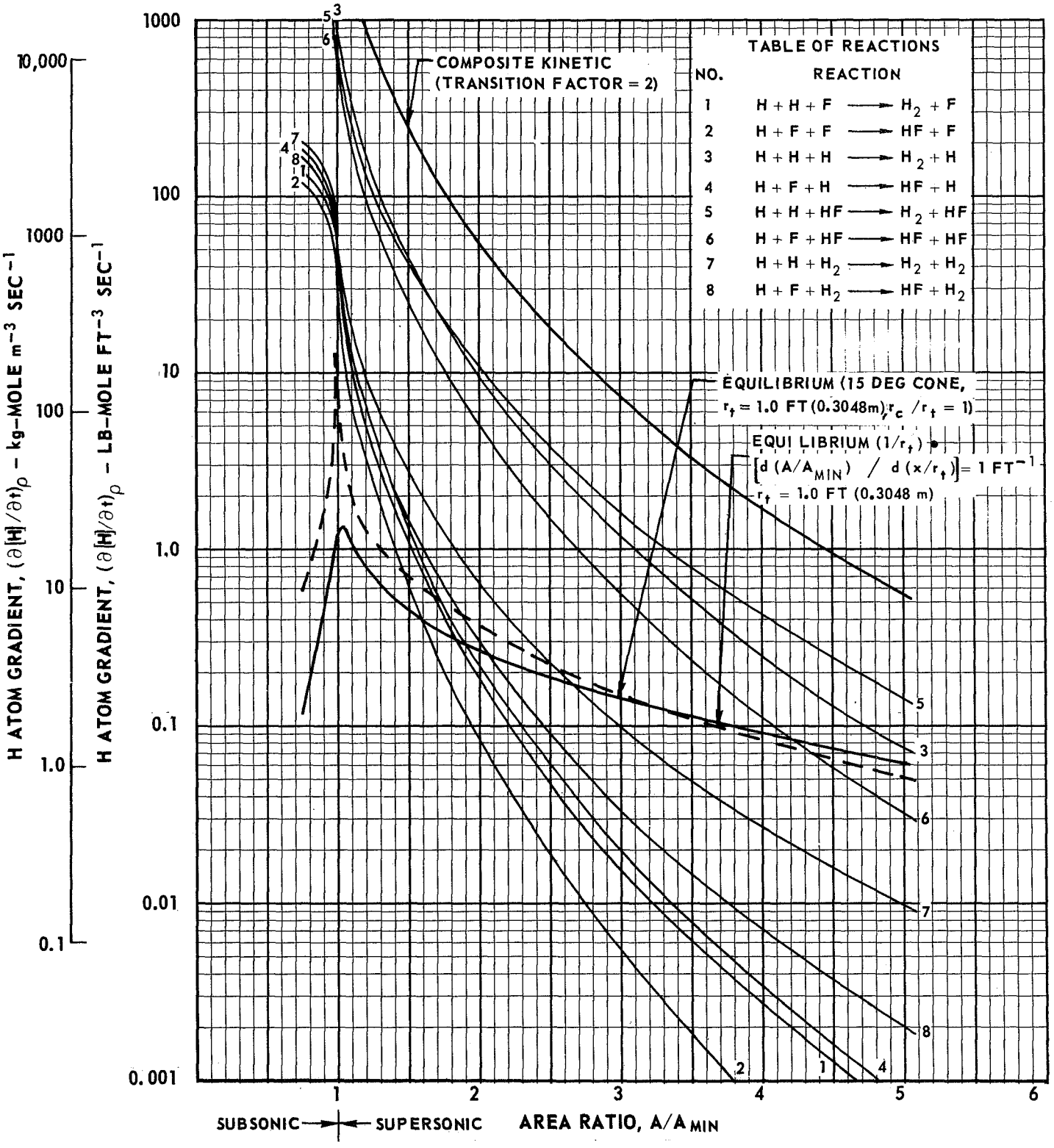

EFFECT OF FREEZING AREA RATIO ON NONEQUILIBRIUM PERFORMANCE FOR HYDROGEN-FLUORINE PROPELLANT SYSTEM

H_2 (ℓ) - F_2 (ℓ)

P_C = 100 PSIA ($6.895 \times 10^5 N/m^2$)

O/F = 8.0

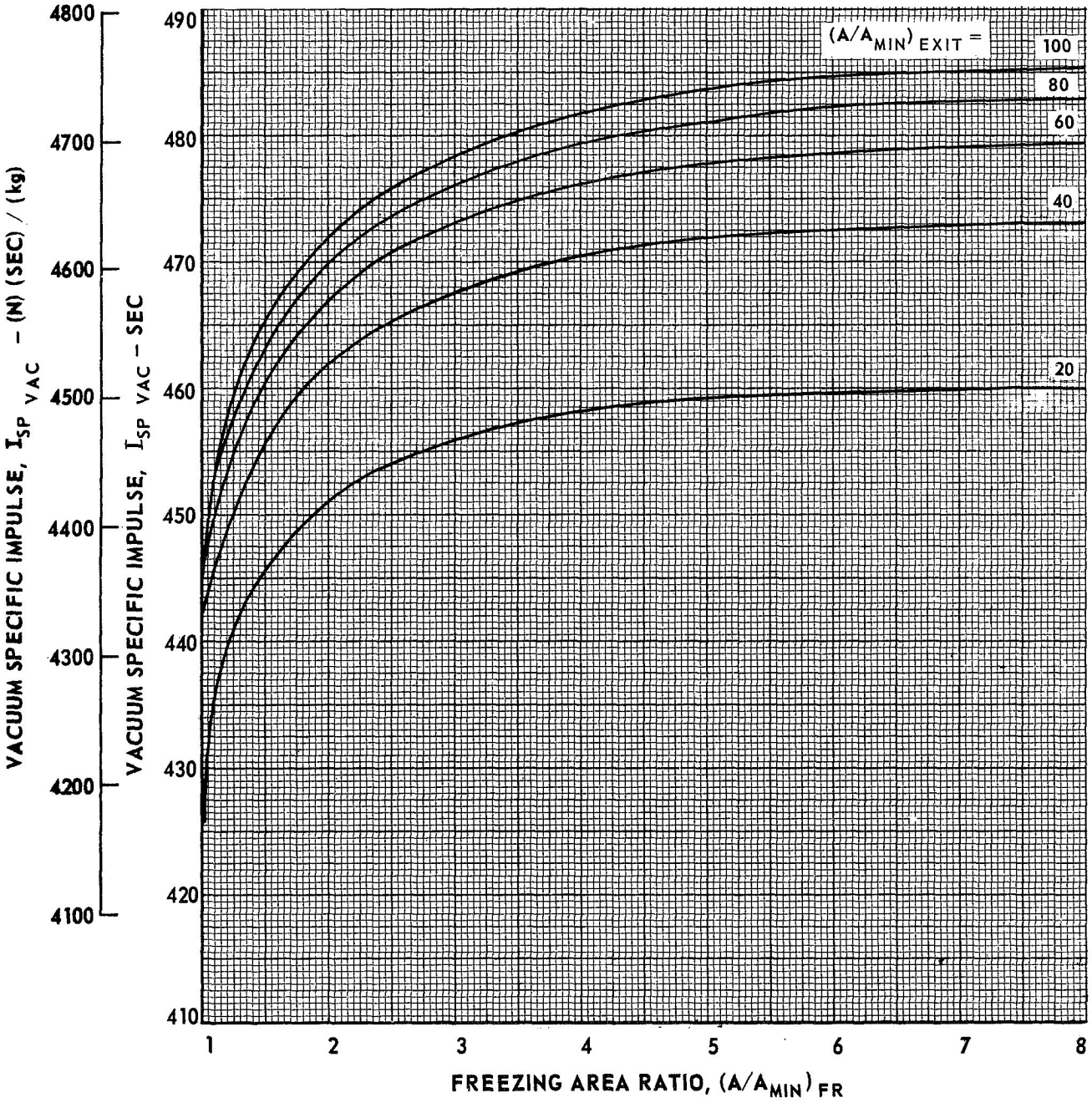

FIG. I-32

EFFECT OF FREEZING AREA RATIO ON NONEQUILIBRIUM PERFORMANCE FOR HYDROGEN PROPELLANT SYSTEM

H_2 (ℓ) – F_2 (ℓ)

P_C = 100 PSI ($6.895 \times 10^5 N/m^2$)

O/F = 12.0

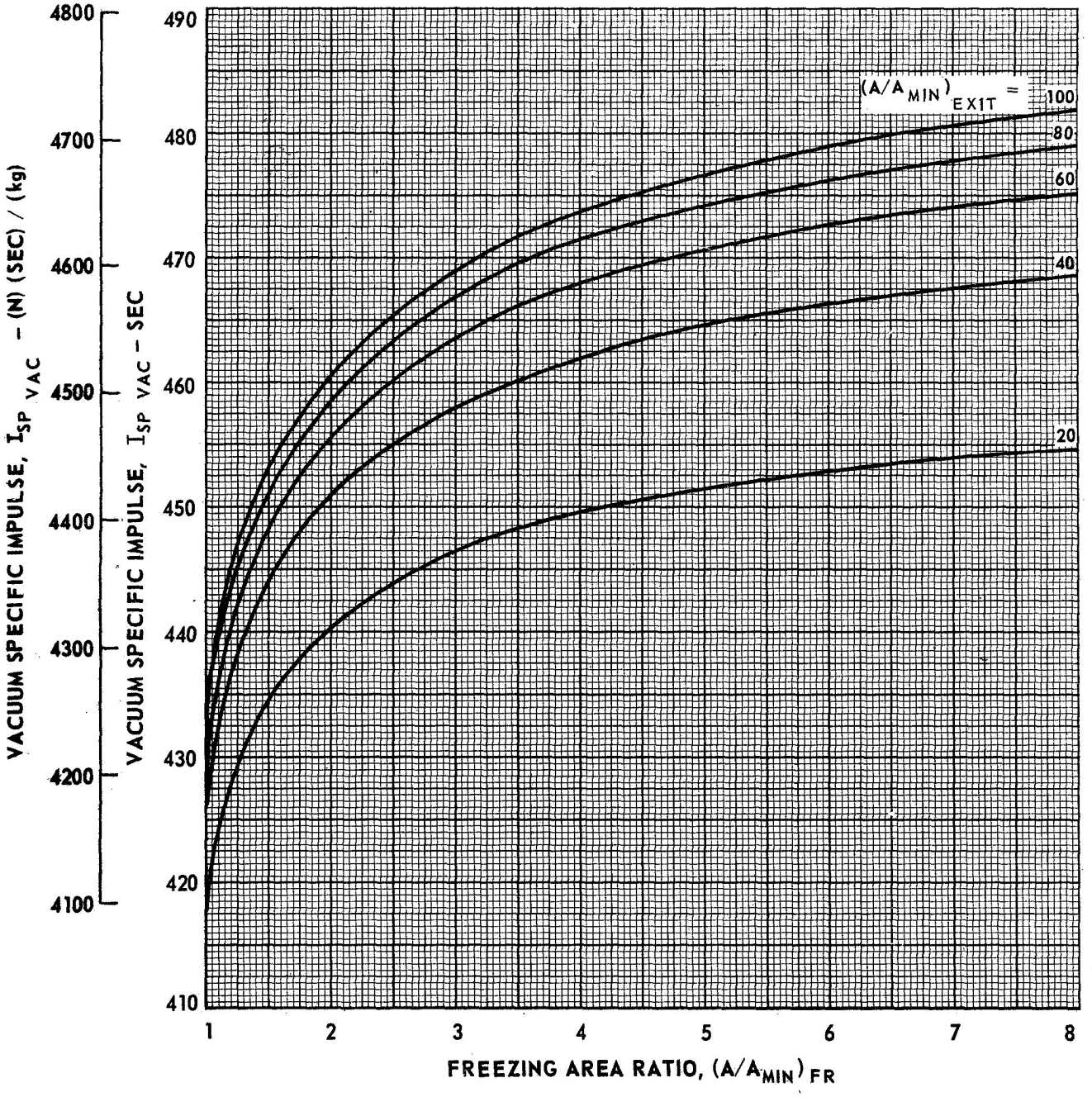

FIG. I-33

EFFECT OF FREEZING AREA RATIO ON NONEQUILIBRIUM PERFORMANCE FOR HYDROGEN-FLUORINE PROPELLANT SYSTEM

H_2 (ℓ) – F_2 (ℓ)

P_C = 100 PSIA (6.895X10^{5}N/m2)

O/F = 16.0

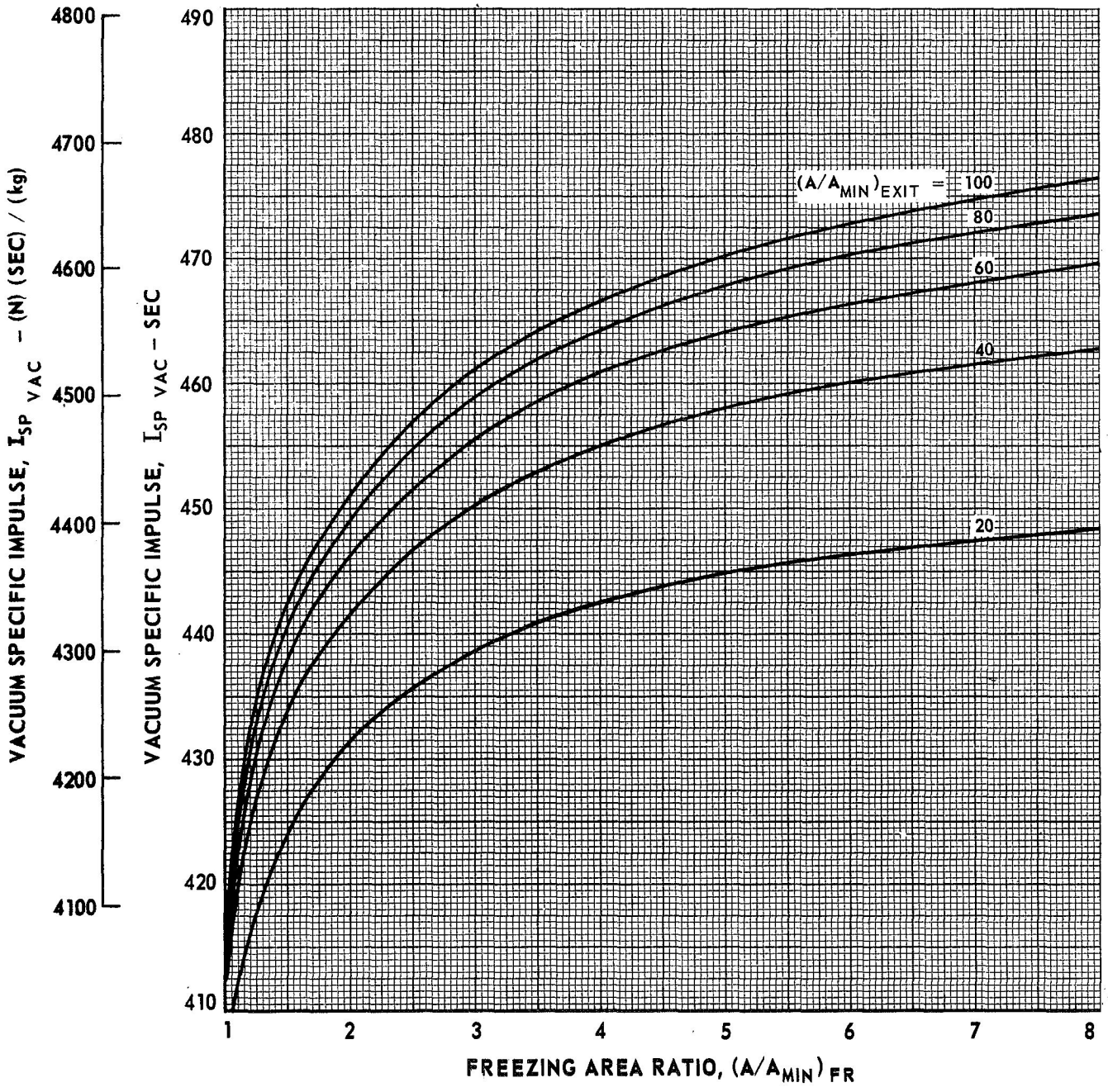

EFFECT OF FREEZING AREA RATIO ON NONEQUILIBRIUM PERFORMANCE FOR HYDROGEN-FLUORINE PROPELLANT SYSTEM

H_2 (ℓ) – F_2 (ℓ)

P_C = 200 PSIA (1.379 X 10^6 N/m^2)

O/F = 8.0

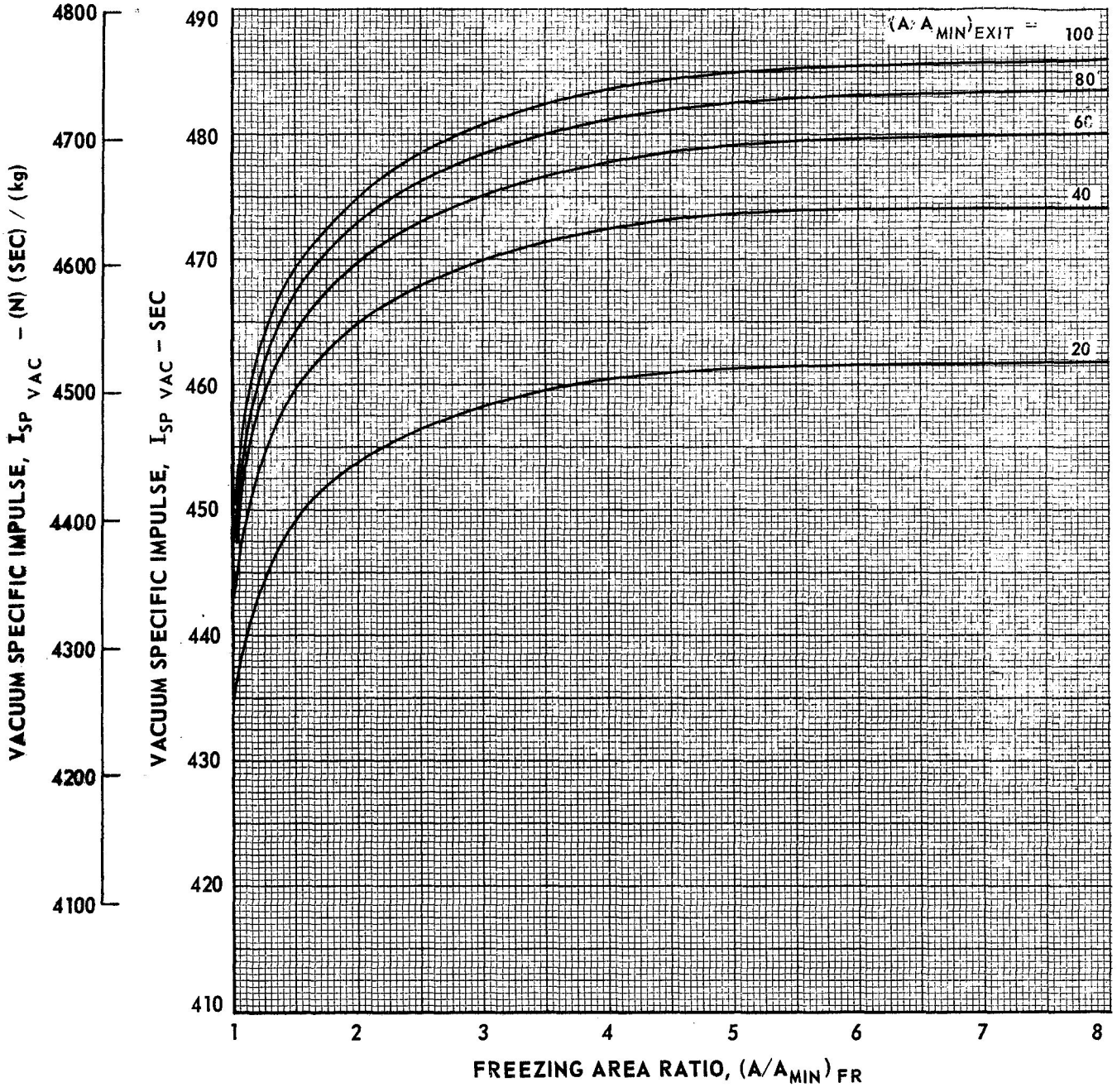

FIG. I-35

EFFECT OF FREEZING AREA RATIO ON NONEQUILIBRIUM PERFORMANCE FOR HYDROGEN-FLUORINE PROPELLANT SYSTEM

H_2 (ℓ) - F_2 (ℓ)

P_C = 200 PSIA (1.379X10^{6}N/m^2)

O/F = 12.0

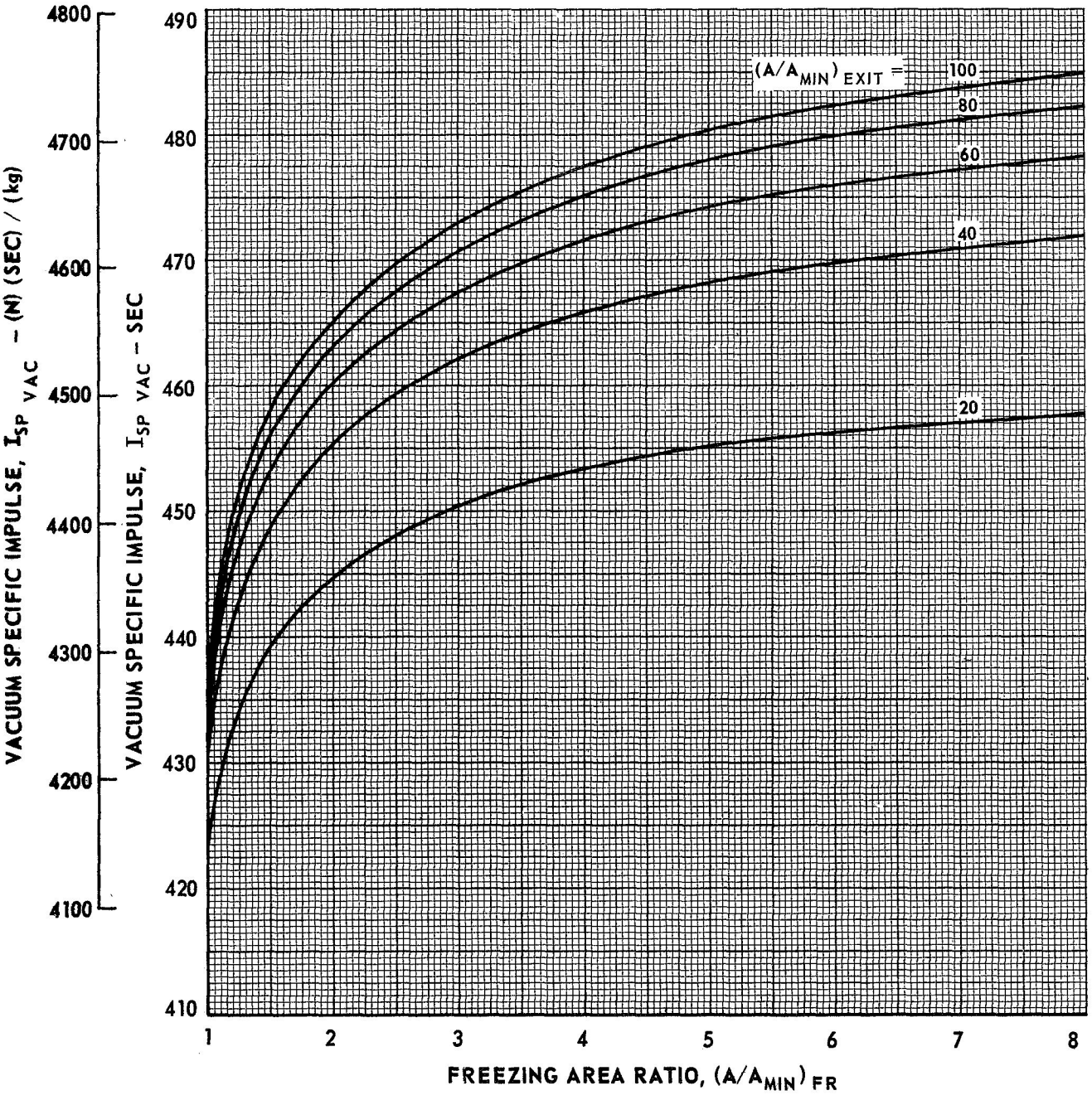

EFFECT OF FREEZING AREA RATIO ON NONEQUILIBRIUM PERFORMANCE FOR HYDROGEN-FLUORINE PROPELLANT SYSTEM

H_2 (ℓ) – F_2 (ℓ)

P_C = 200 PSIA (1.379 X 10^6 N/m^2)

O/F = 16.0

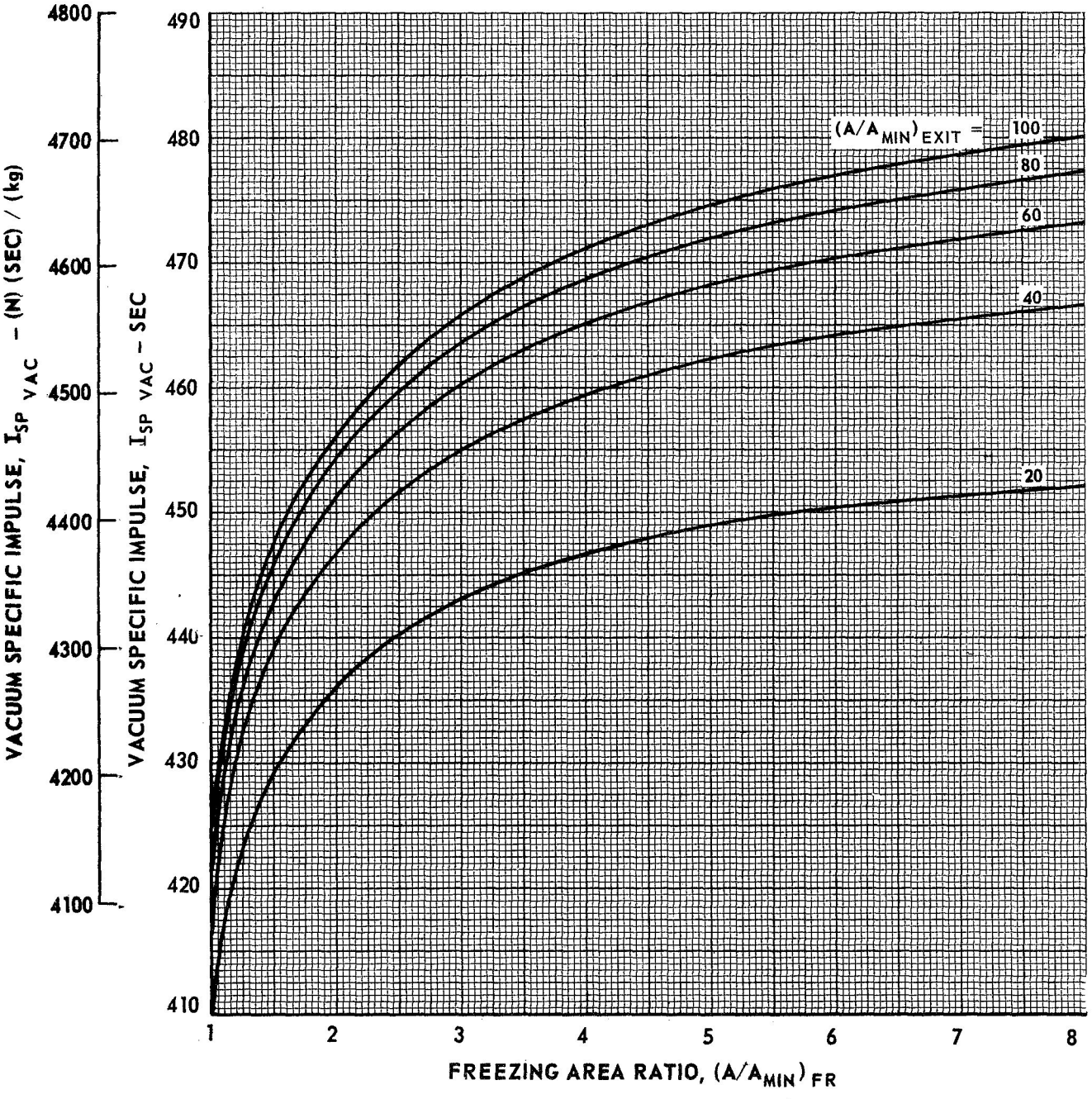

EFFECT OF FREEZING AREA RATIO ON NONEQUILIBRIUM PERFORMANCE FOR HYDROGEN-FLUORINE PROPELLANT SYSTEM

H_2 (ℓ) - F_2 (ℓ)

P_C = 300 PSIA (2.069 X 10^6 N/m^2)

O/F = 8.0

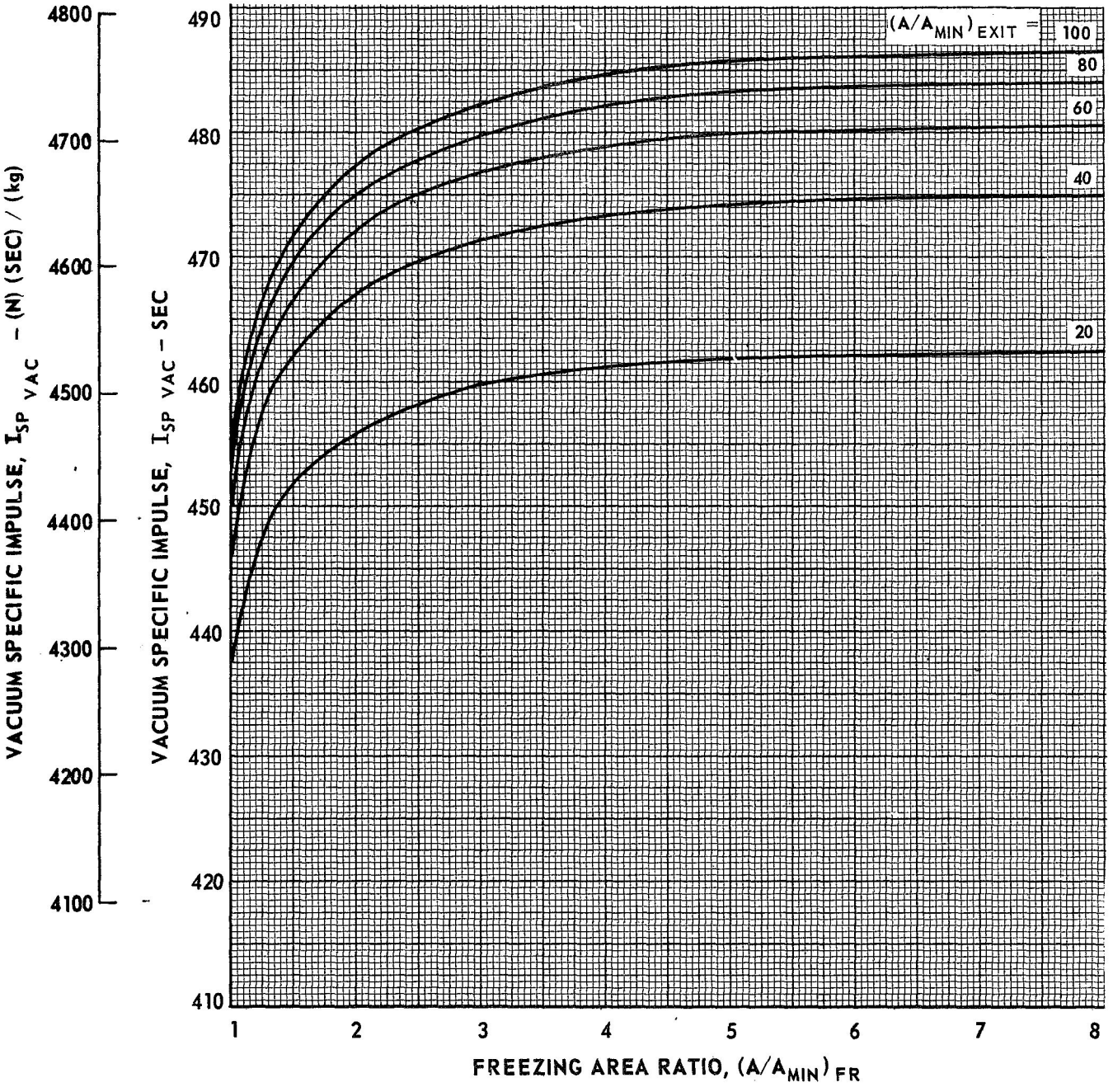

FIG. I-38

EFFECT OF FREEZING AREA RATIO ON NONEQUILIBRIUM PERFORMANCE FOR HYDROGEN-FLUORINE PROPELLANT SYSTEM

H_2 (ℓ) – F_2 (ℓ)

P_C = 300 PSIA (2.069 X 10^6 N/m^2)

O/F = 12.0

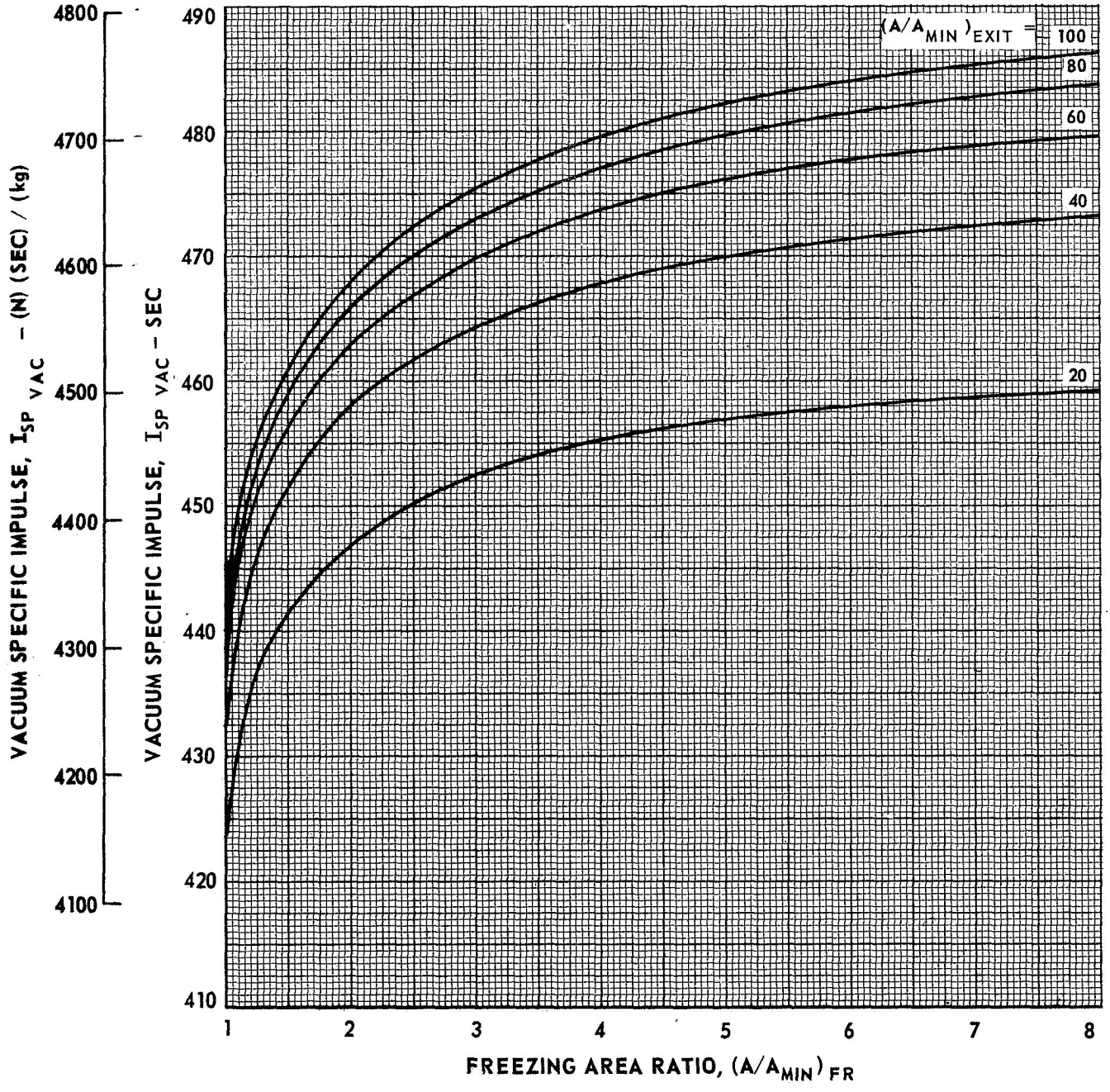

FIG. I-39

EFFECT OF FREEZING AREA RATIO ON NONEQUILIBRIUM PERFORMANCE FOR HYDROGEN-FLUORINE PROPELLANT SYSTEM

H_2 (ℓ) – F_2 (ℓ)

P_C = 300 PSIA (2.069 X 10^6 N/m^2)

O/F = 16.0

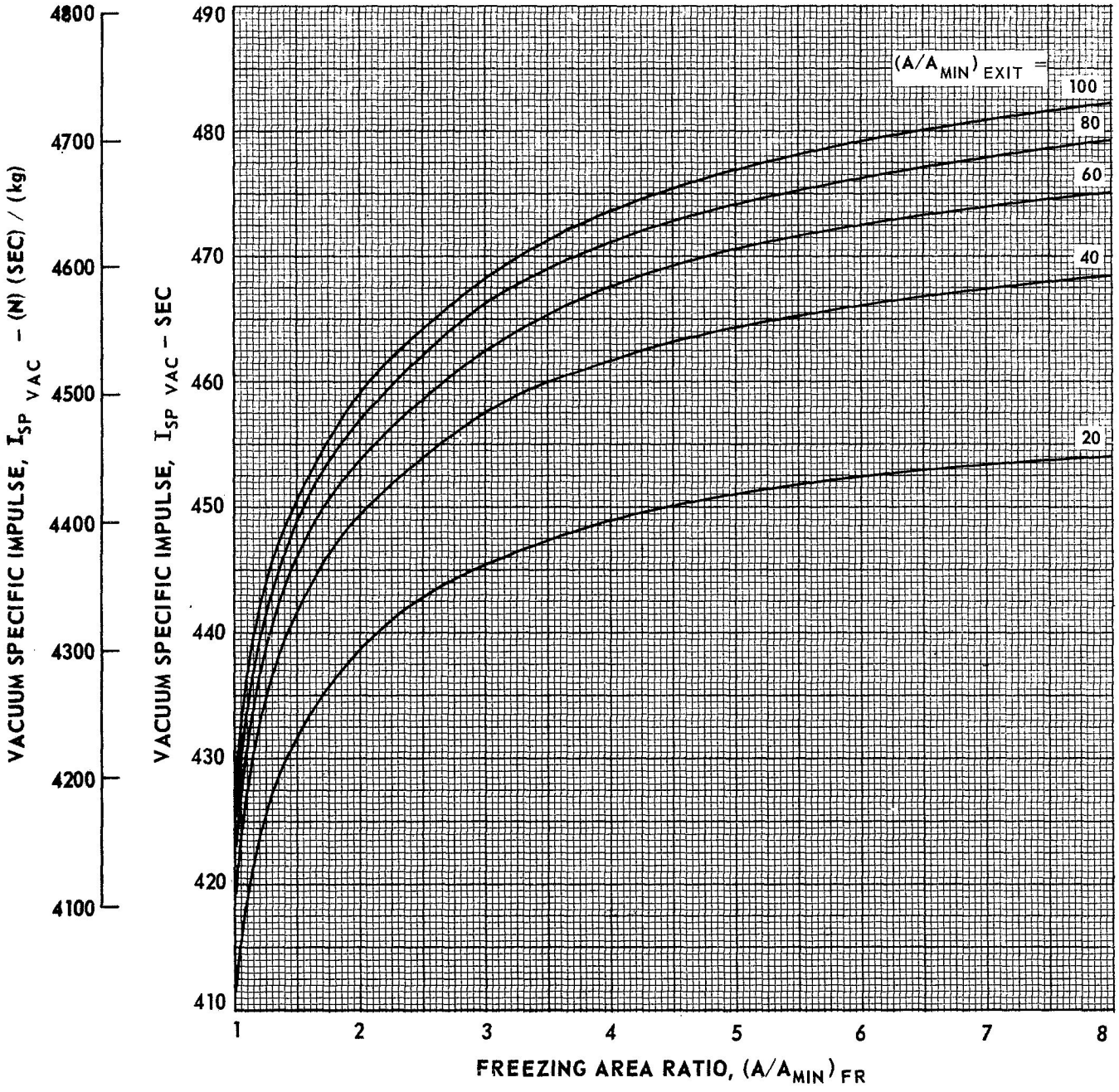

FIG. I-40

EFFECT OF FREEZING AREA RATIO ON NONEQUILIBRIUM PERFORMANCE FOR HYDROGEN-FLUORINE PROPELLANT SYSTEM

H_2 (ℓ) – F_2 (ℓ)

P_C = 500 PSIA (3.448 X 10^6 N/m^2)

O/F = 8.0

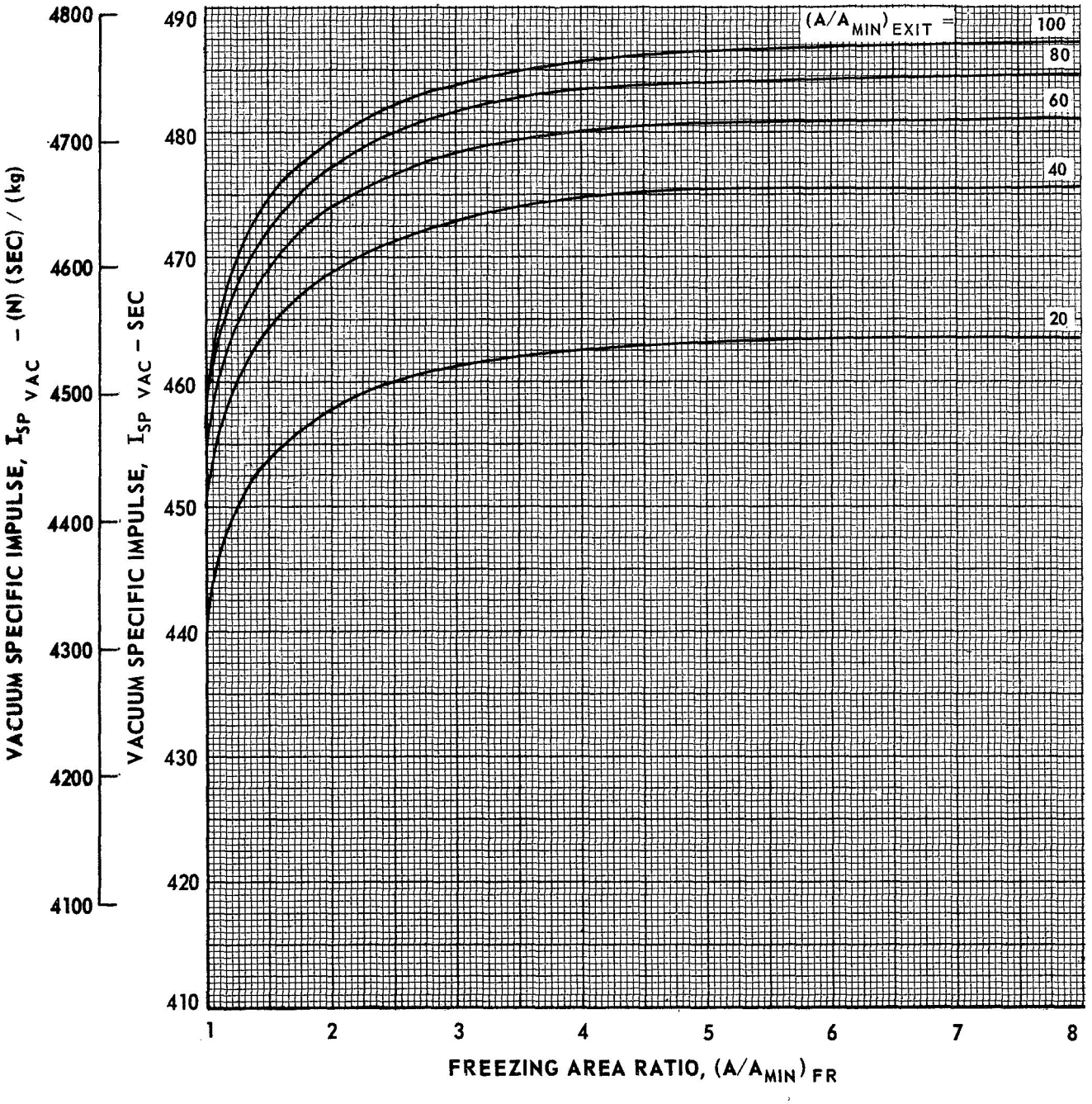

EFFECT OF FREEZING AREA RATIO ON NONEQUILIBRIUM PERFORMANCE FOR HYDROGEN-FLUORINE PROPELLANT SYSTEM

H_2 (ℓ) – F_2 (ℓ)

P_C = 500 PSIA (3.448 X 10^6 N/m^2)

O/F = 12.0

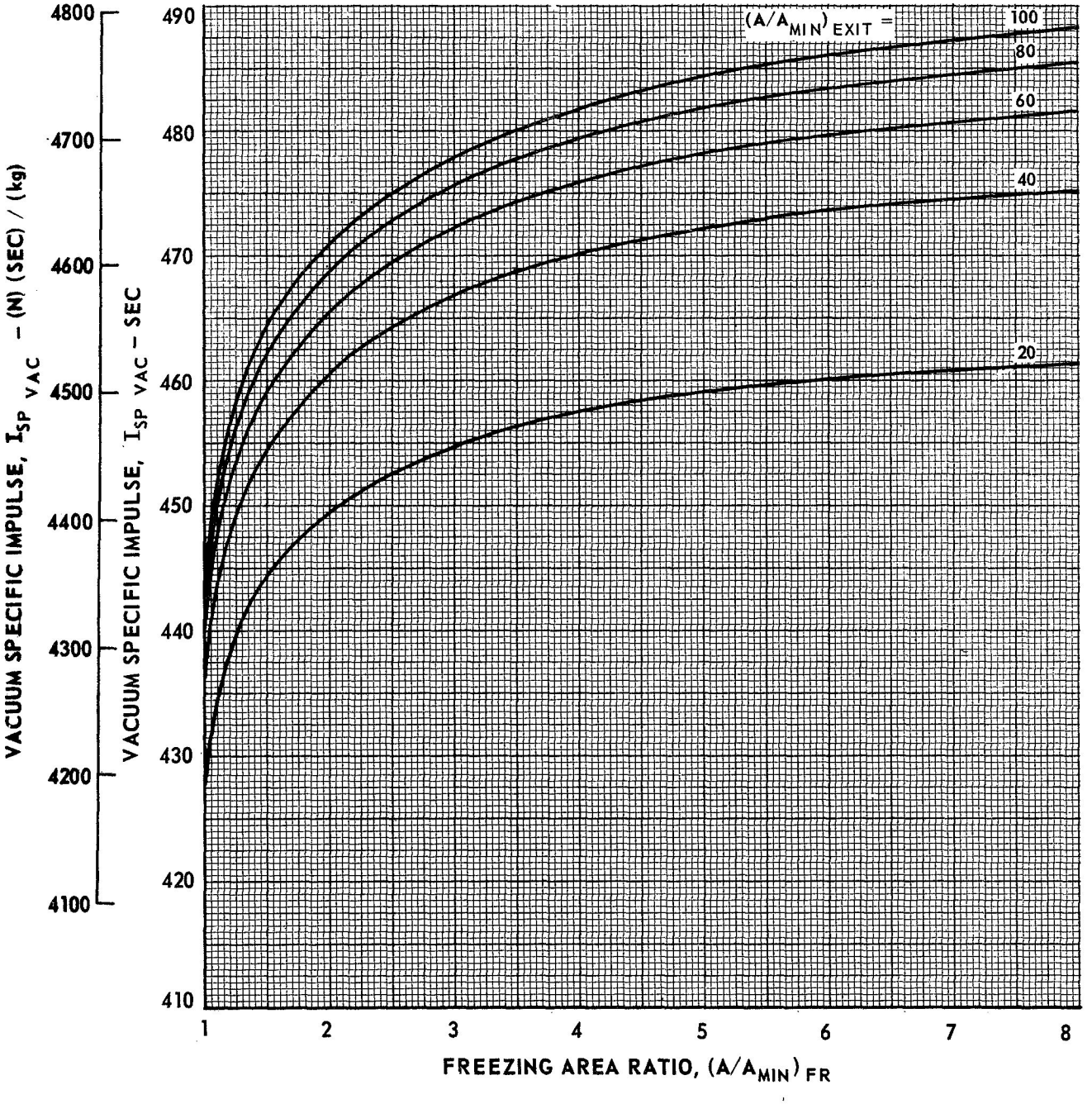

EFFECT OF FREEZING AREA RATIO ON NONEQUILIBRIUM PERFORMANCE FOR HYDROGEN-FLUORINE PROPELLANT SYSTEM

H_2 (ℓ) – F_2 (ℓ)

P_C = 500 PSIA (3.448 X 10^6 N/m^2)

O/F = 16.0

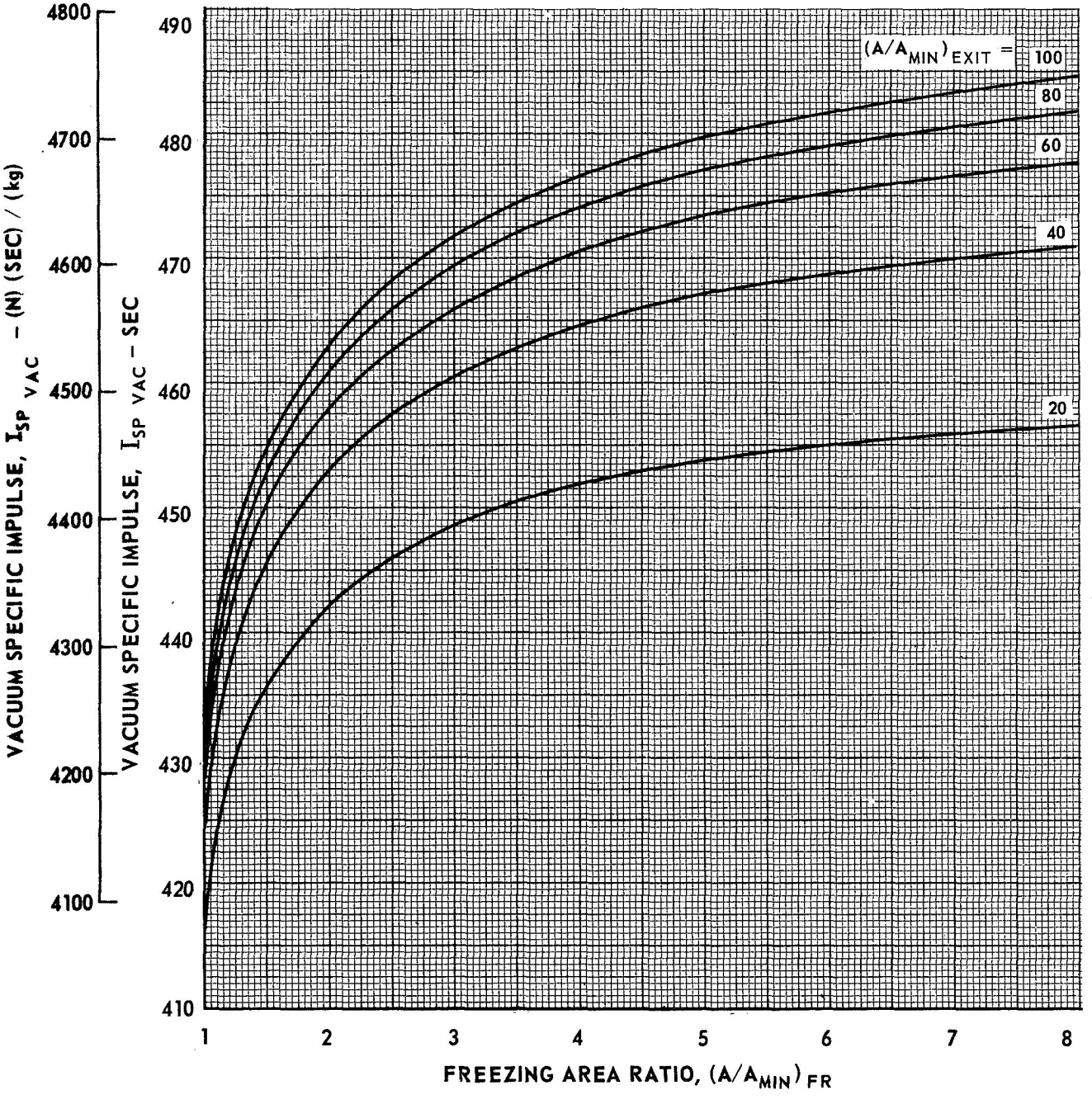

EFFECT OF FREEZING AREA RATIO ON NONEQUILIBRIUM PERFORMANCE FOR HYDROGEN-FLUORINE PROPELLANT SYSTEM

H_2 (ℓ) - F_2 (ℓ)

P_C = 750 PSIA (5.171 X 10^6 N/m^2)

O/F = 8.0

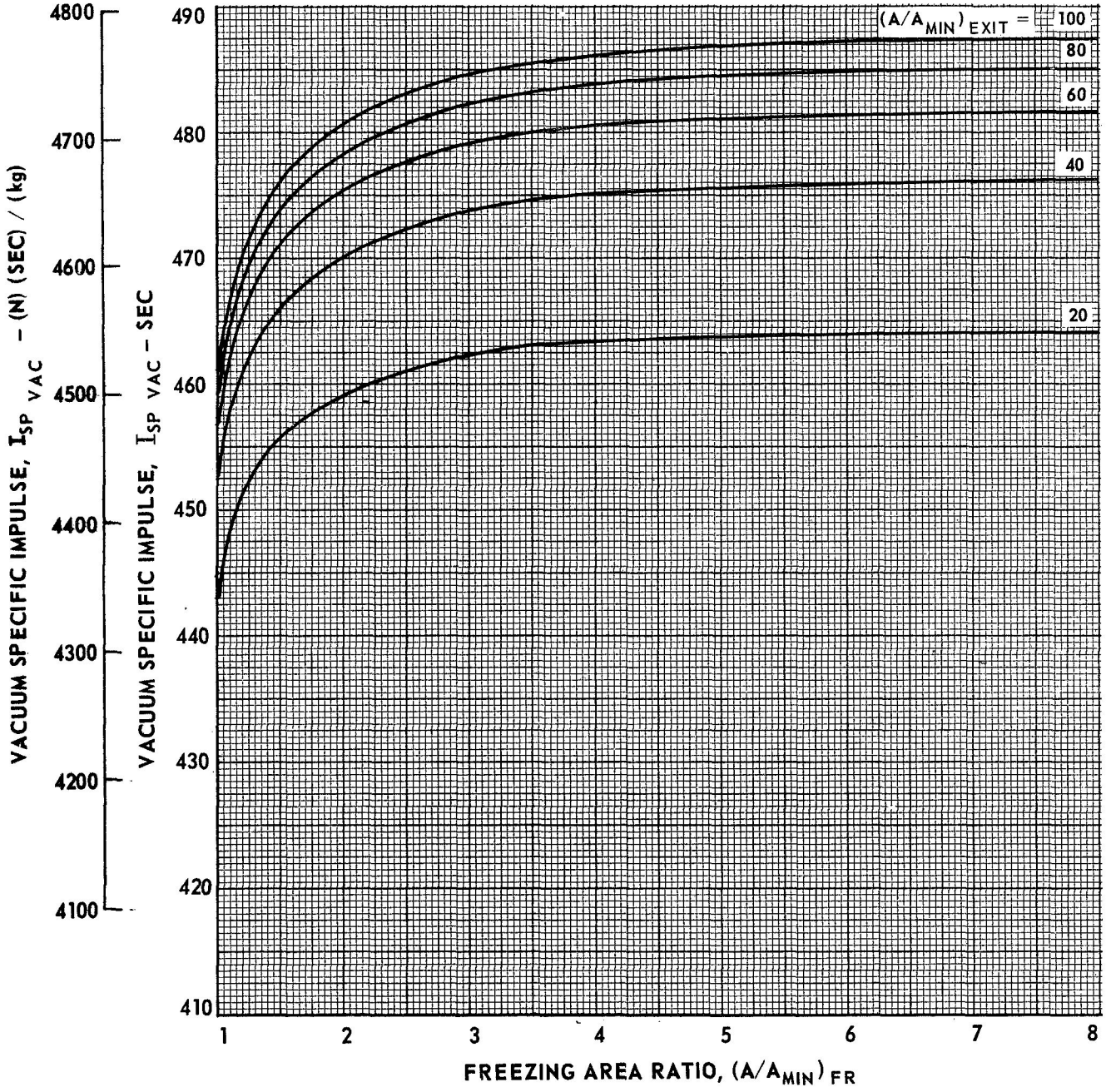

EFFECT OF FREEZING AREA RATIO ON NONEQUILIBRIUM PERFORMANCE FOR HYDROGEN-FLUORINE PROPELLANT SYSTEM

H_2 (ℓ) – F_2 (ℓ)

P_C = 750 PSIA (5.171 X 10^6 N/m^2)

O/F = 12.0

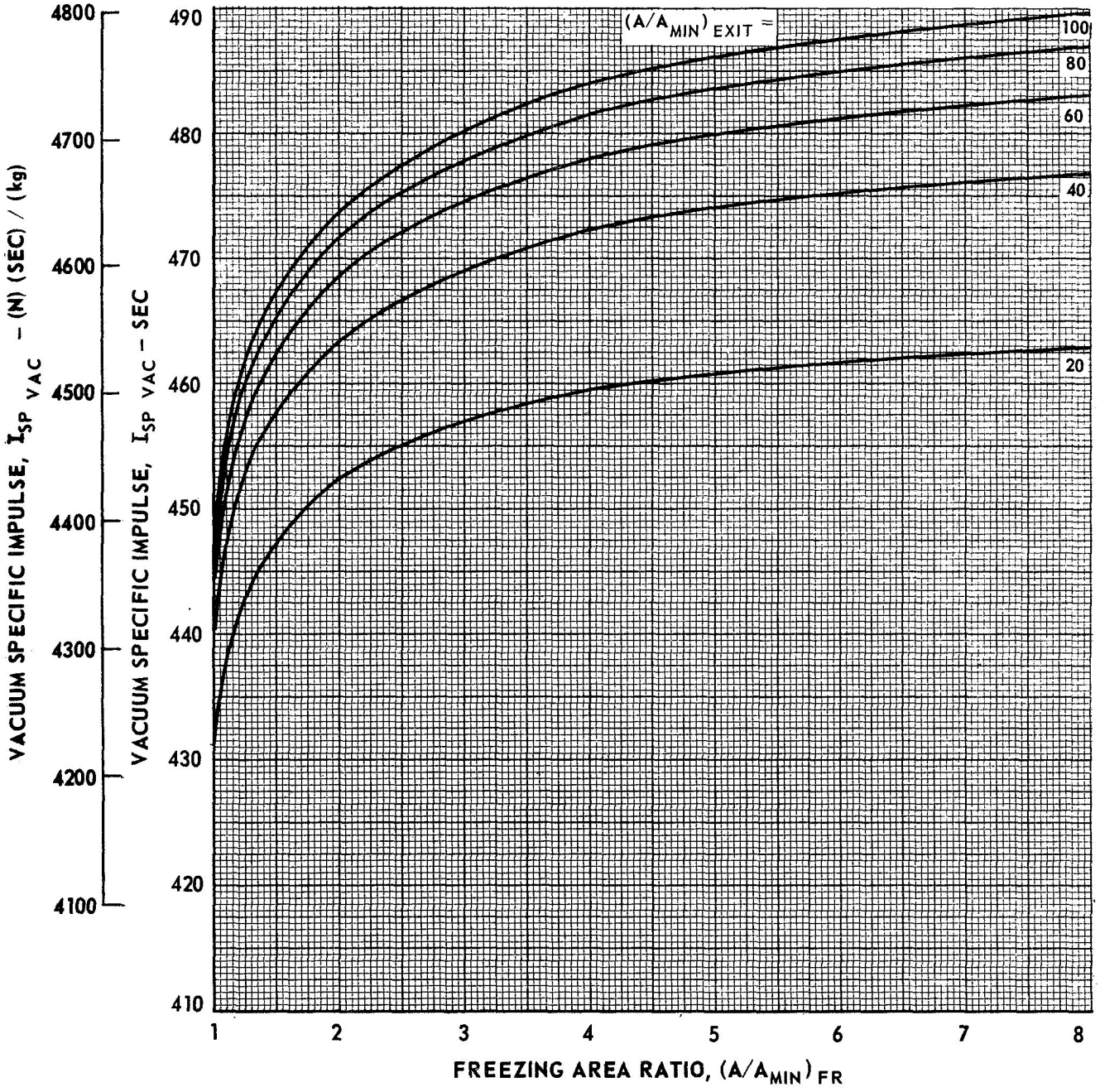

FIG. I-45

EFFECT OF FREEZING AREA RATIO ON NONEQUILIBRIUM PERFORMANCE FOR HYDROGEN-FLUORINE PROPELLANT SYSTEM

H_2 (ℓ) - F_2 (ℓ)

P_C = 750 PSIA (5.171 X 10^6 N/m^2)

O/F = 16.0

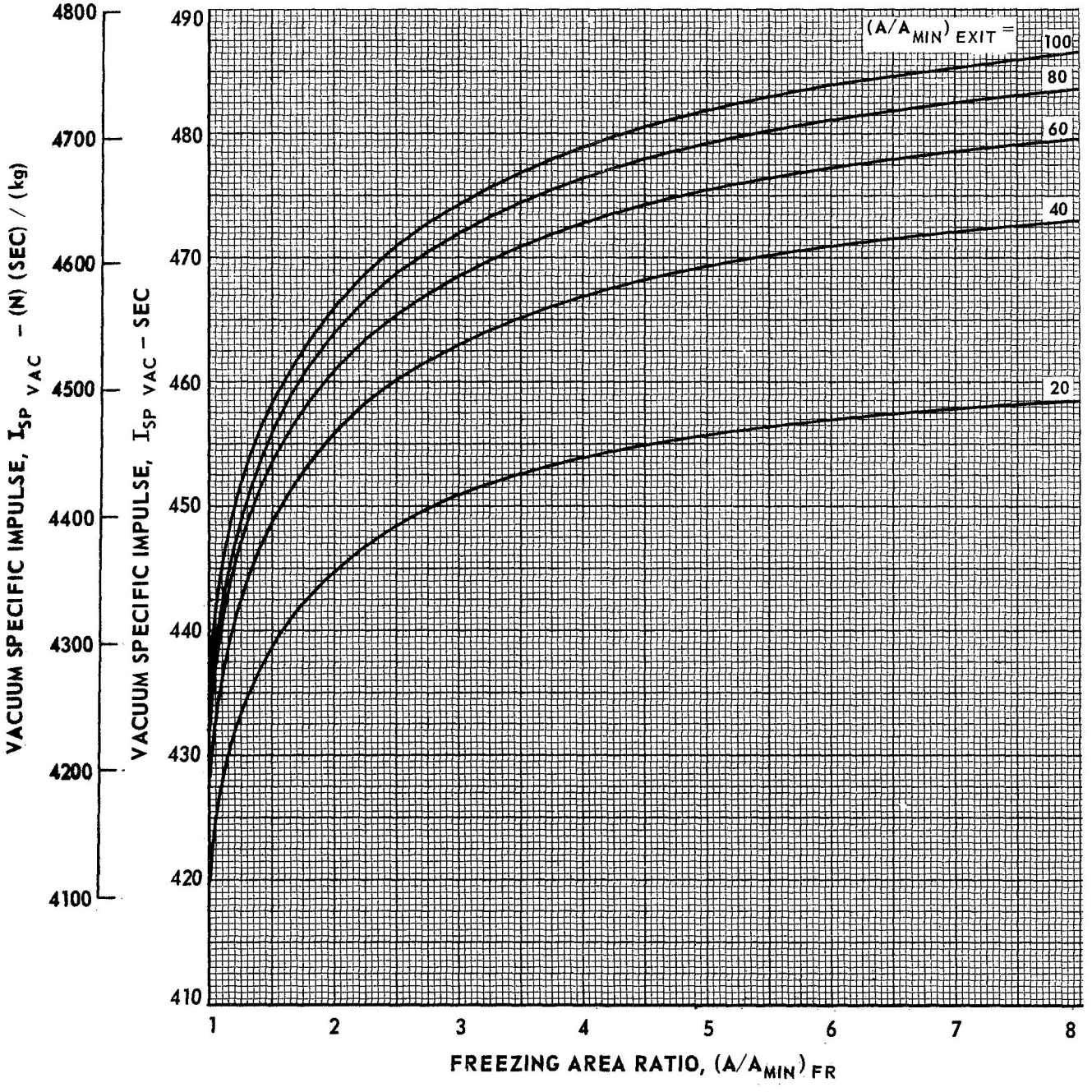

EFFECT OF FREEZING AREA RATIO ON NONEQUILIBRIUM PERFORMANCE FOR HYDROGEN-FLUORINE PROPELLANT SYSTEM

H_2 (ℓ) – F_2 (ℓ)

P_C = 1000 PSIA (6.895X10^{6}N/m^2)

O/F = 8.0

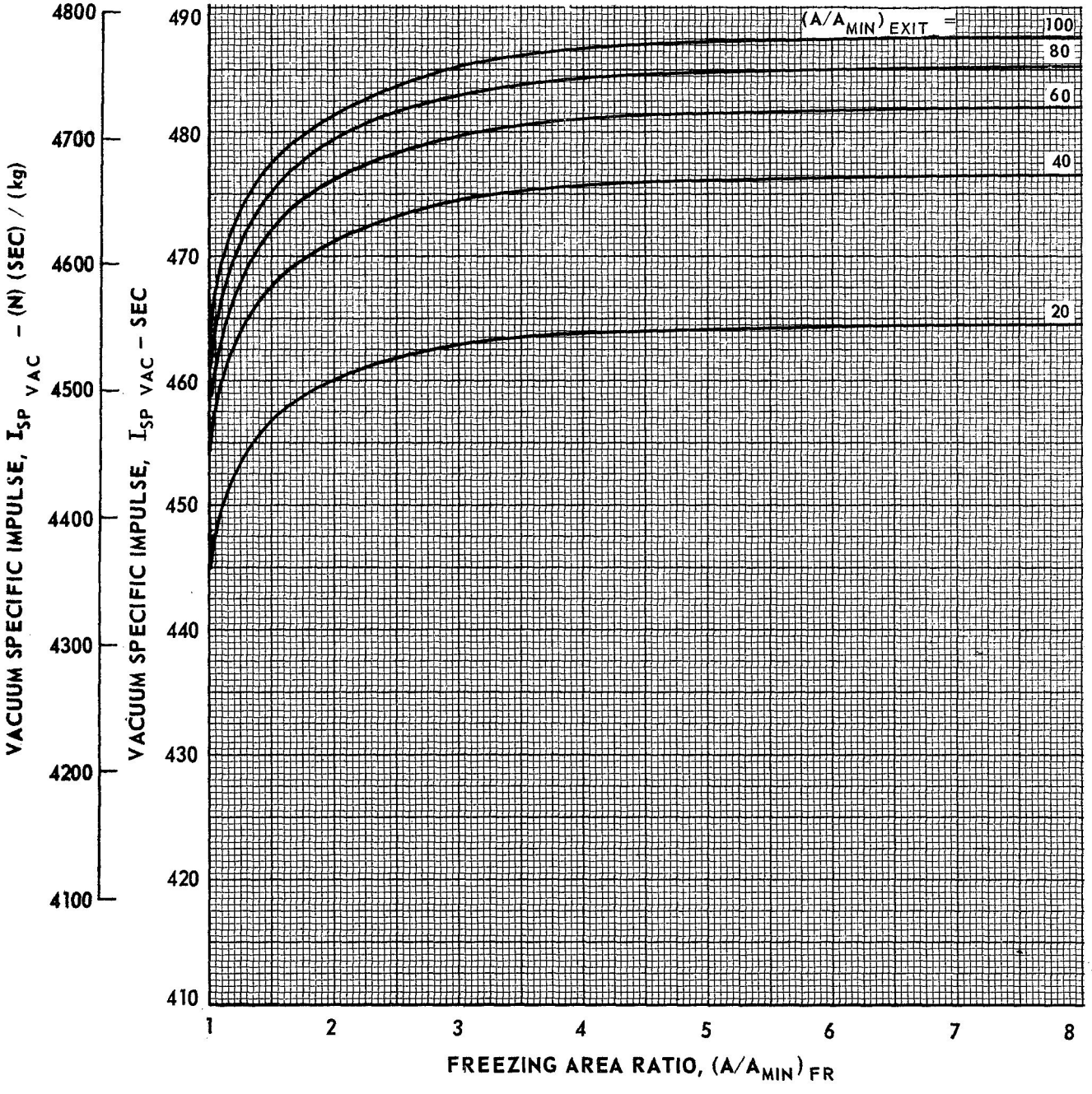

EFFECT OF FREEZING AREA RATIO ON NONEQUILIBRIUM PERFORMANCE FOR HYDROGEN-FLUORINE PROPELLANT SYSTEM

H_2 (ℓ) – F_2 (ℓ)

P_C = 1000 PSIA (6.895X10^{6}N/m^2)

O/F = 12.0

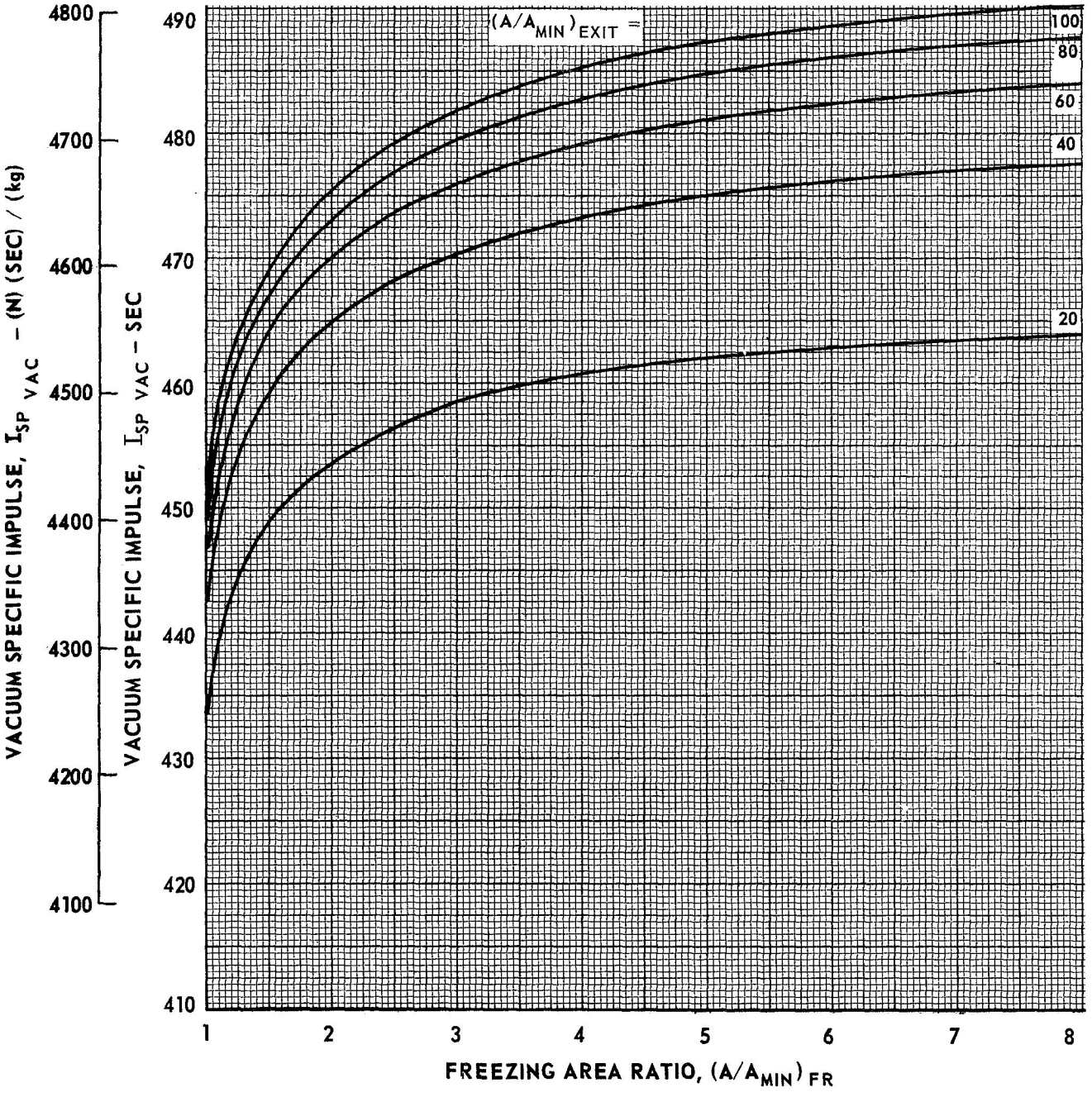

EFFECT OF FREEZING AREA RATIO ON NONEQUILIBRIUM PERFORMANCE FOR HYDROGEN-FLUORINE PROPELLANT SYSTEM

H_2 (ℓ) – F_2 (ℓ)

P_C = 1000 PSIA (6.895X10^6 N/m^2)

O/F = 16.0

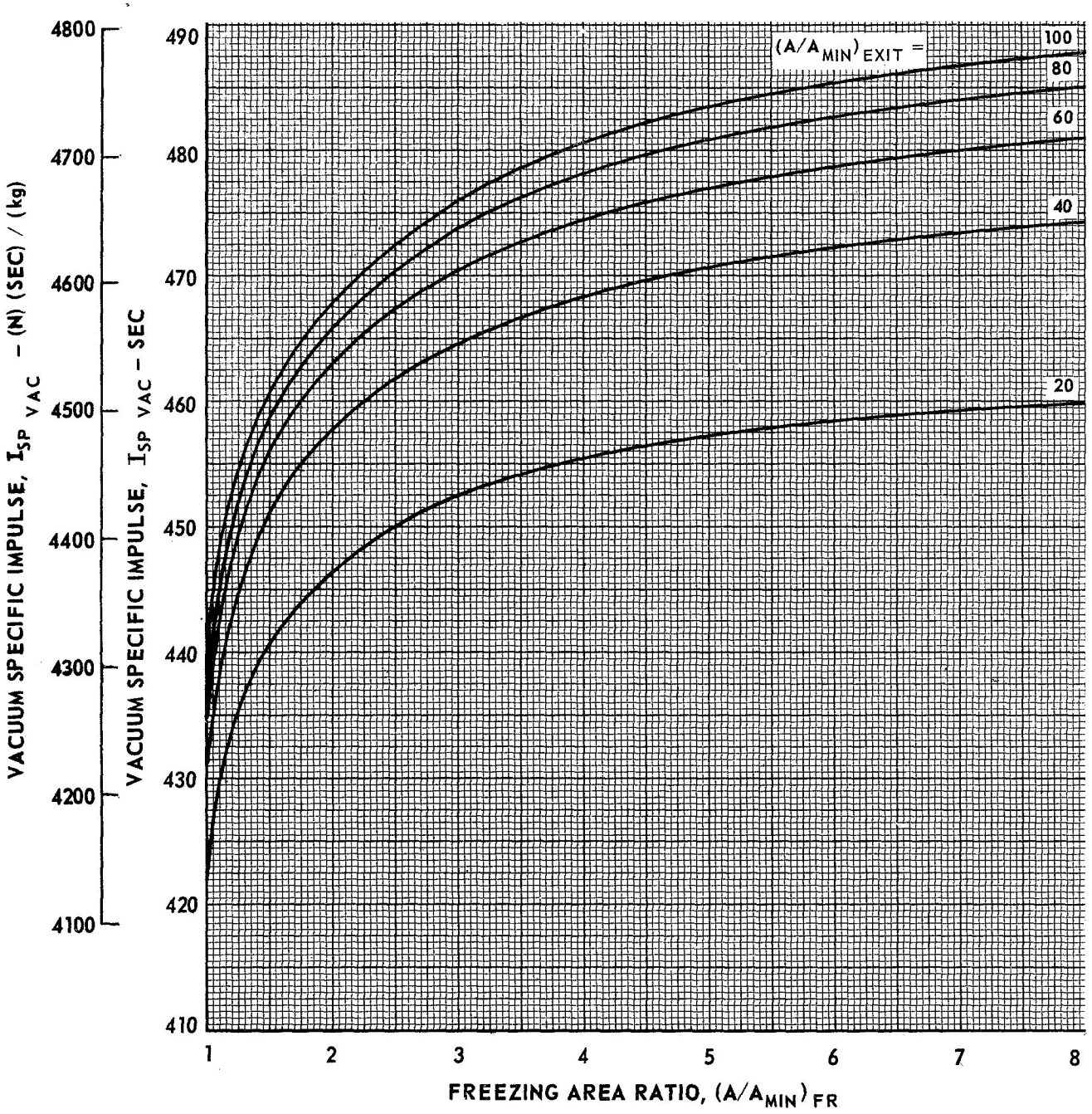

TABLE II-1

SUMMARY OF ELEMENTARY REACTIONS AND REACTION RATE CONSTANTS EMPLOYED IN $H_2 - O_2$ RECOMBINATION MECHANSIM

	REACTIONS	FORWARD RATE
	$H + H + A \rightleftharpoons H_2 + A$	$k_f = 4.62 \times 10^{14} T^{-1}$
	$H + OH + A \rightleftharpoons H_2O + A$	$k_f = 7.85 \times 10^{15} T^{-1}$
1	$H + H + H \rightleftharpoons H_2 + H$	$k_f = 20\ (4.62 \times 10^{14} T^{-1})$
2	$H + H + H_2 \rightleftharpoons H_2 + H_2$	$k_f = 2.5\ (4.62 \times 10^{15} T^{-1})$
3	$H + H + H_2O \rightleftharpoons H_2 + H_2O$	$K_f = 2.5\ (4.62 \times 10^{15} T^{-1})$
4	$H + OH + H_2O \rightleftharpoons H_2O + H_2O$	$k_f = 20\ (7.85 \times 10^{15} T^{-1})$
5	$H + OH + H_2 \rightleftharpoons H_2O + H_2$	$k_f = 3\ (7.85 \times 10^{15} T^{-1})$
6	$H + OH + H \rightleftharpoons H_2O + H$	$k_f = 3\ (7.85 \times 10^{15} T^{-1})$

NOTE: ALL RATES ARE EXPRESSED IN TERMS OF LB-MOLES, FT^3, SEC; AND T IS IN °R

TO CONVERT TO kg-MOLES, m^3, SEC, AND T IN °K; MULTIPLY ABOVE RATE BY 2.165×10^{-3}

TABLE II-2

EQUILIBRIUM AND FROZEN FLOW PROPERTIES AT

NOZZLE THROAT

$H_2(\ell) - O_2(\ell)$

	P_c-psia	OXIDIZER - FUEL WEIGHT RATIO					
		3.0	4.0	5.0	6.0	7.0	8.0
Equilibrium Mass Flow - W/A $\frac{\text{Lbm}}{\text{Ft}^2.\text{Sec}}$	100	58.2	58.7	60.4	62.6	65.0	67.5
	200	116.5	117.1	120.1	124.2	129.0	133.9
	300	174.7	175.5	179.6	185.6	192.6	199.9
	500	291.1	292.2	298.4	307.8	319.2	331.2
	750	436.7	437.9	446.6	460.1	476.6	494.6
	1000	582.2	583.7	594.6	611.9	633.6	657.4
Frozen Mass Flow - W/A $\frac{\text{Lbm}}{\text{Ft}^2.\text{Sec}}$	100	58.6	59.7	61.8	64.3	66.9	69.4
	200	117.0	118.8	122.6	127.3	132.4	137.4
	300	175.3	177.7	183.1	190.0	197.4	204.9
	500	292.0	295.2	303.6	314.4	326.5	339.0
	750	437.7	441.9	453.6	469.3	487.0	505.5
	1000	583.4	588.5	603.3	623.5	646.8	671.3
Frozen Specific Heat Ratio γ_{FR}	100	1.25	1.23	1.22	1.21	1.21	1.21
	200	1.25	1.23	1.22	1.21	1.21	1.21
	300	1.25	1.23	1.22	1.21	1.20	1.20
	500	1.25	1.23	1.21	1.21	1.20	1.20
	750	1.25	1.23	1.21	1.20	1.20	1.20
	1000	1.25	1.23	1.21	1.20	1.20	1.20

NOTE: P_c (psia) x $6.895 \times 10^3 = P_c$ (N/m^2)

Mass Flow ($\frac{\text{Lbm}}{\text{Ft}^2.\text{sec}}$) x 4.883 = Mass Flow ($\frac{\text{kg}}{\text{m}^2\ \text{sec}}$)

H910666-16

FIG. II-1

VARIATION OF EQUILIBRIUM VACUUM SPECIFIC IMPULSE WITH AREA RATIO

H_2 (ℓ) - O_2 (ℓ)

P_C = 100 PSIA ($6.895 \times 10^5 N/m^2$)

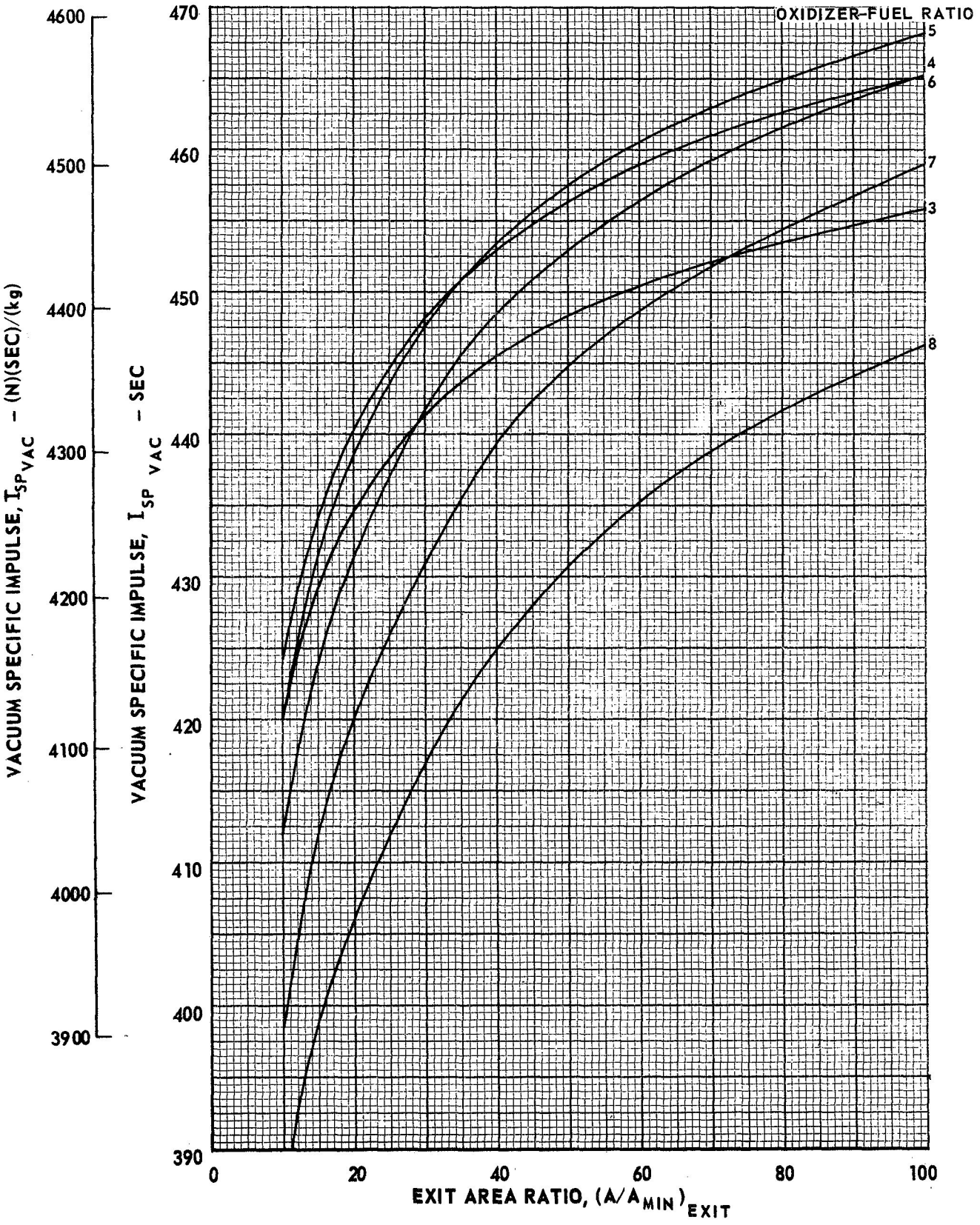

FIG. II-2

VARIATION OF FROZEN VACUUM SPECIFIC IMPULSE WITH AREA RATIO

H_2 (ℓ) - O_2 (ℓ)

P_C = 100 PSIA (6.895X10^{5}N/m^2)

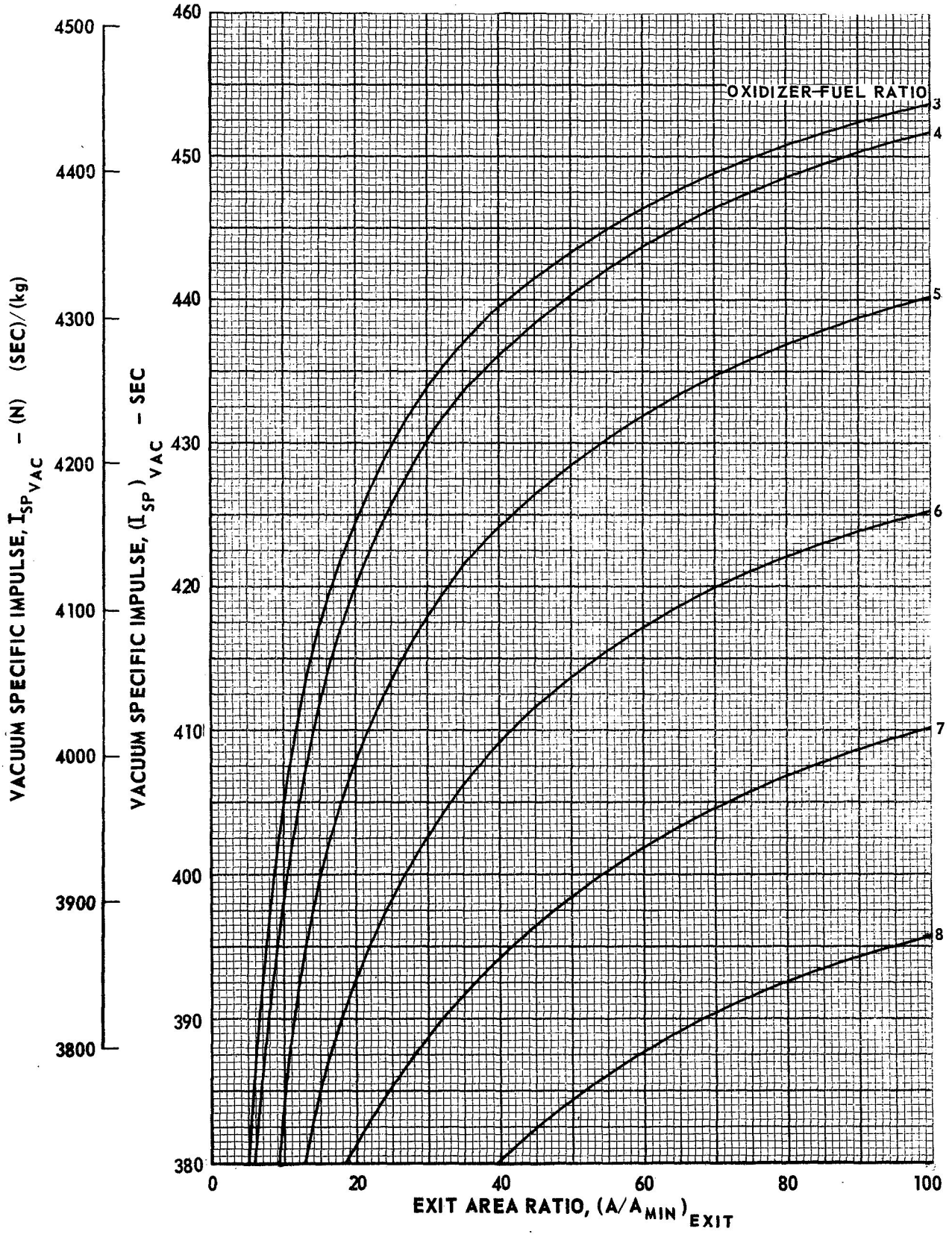

H910666-16

FIG. II-3

VARIATION OF EQUILIBRIUM VACUUM SPECIFIC IMPULSE WITH AREA RATIO

H_2 (ℓ) – O_2 (ℓ)

P_C = 200 PSIA (1.379×10^6 N/m^2)

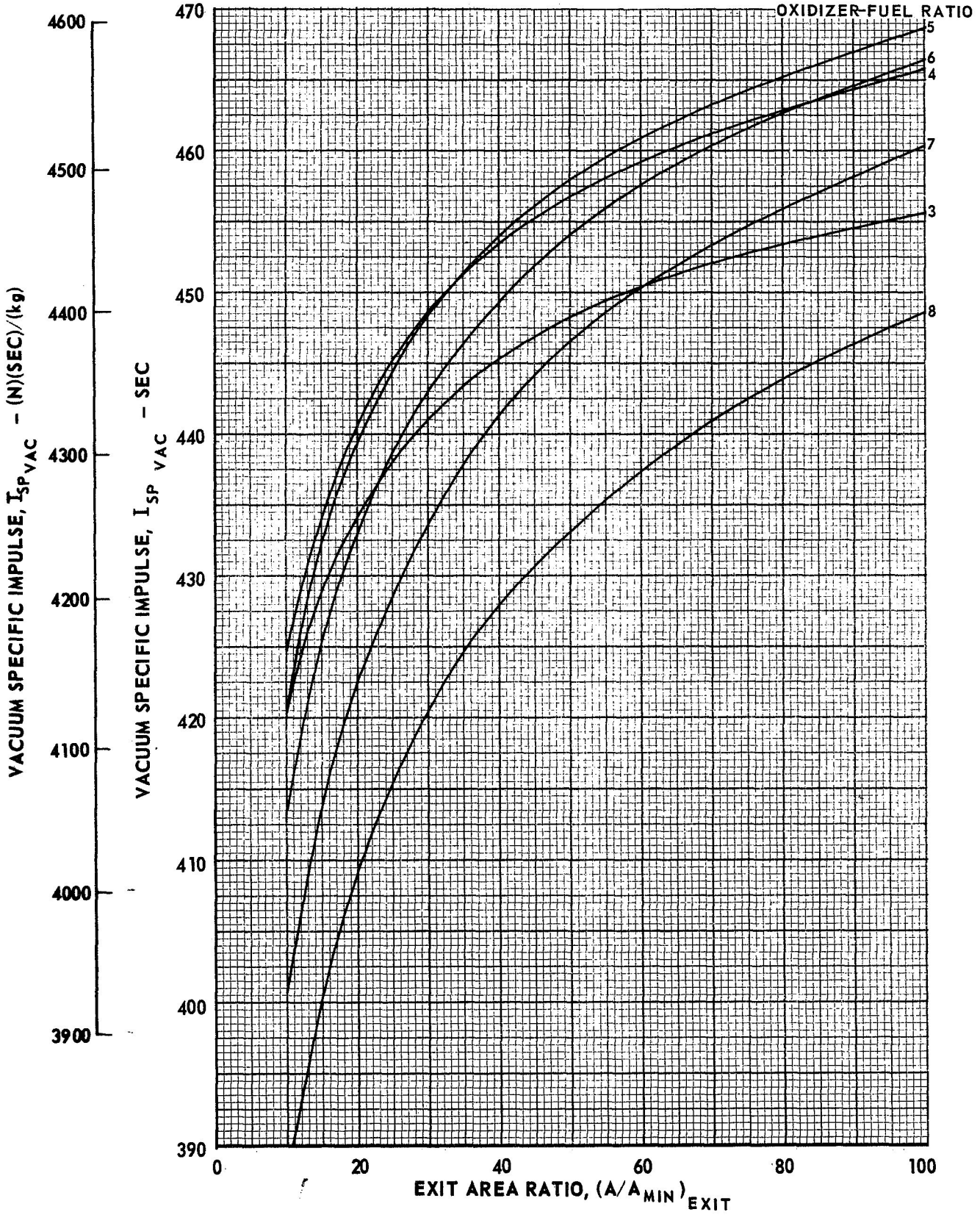

FIG. II-4

VARIATION OF FROZEN VACUUM SPECIFIC IMPULSE WITH AREA RATIO

H_2 (ℓ) - O_2 (ℓ)

P_C = 200 PSIA (1.379 X 10^6 N/m^2)

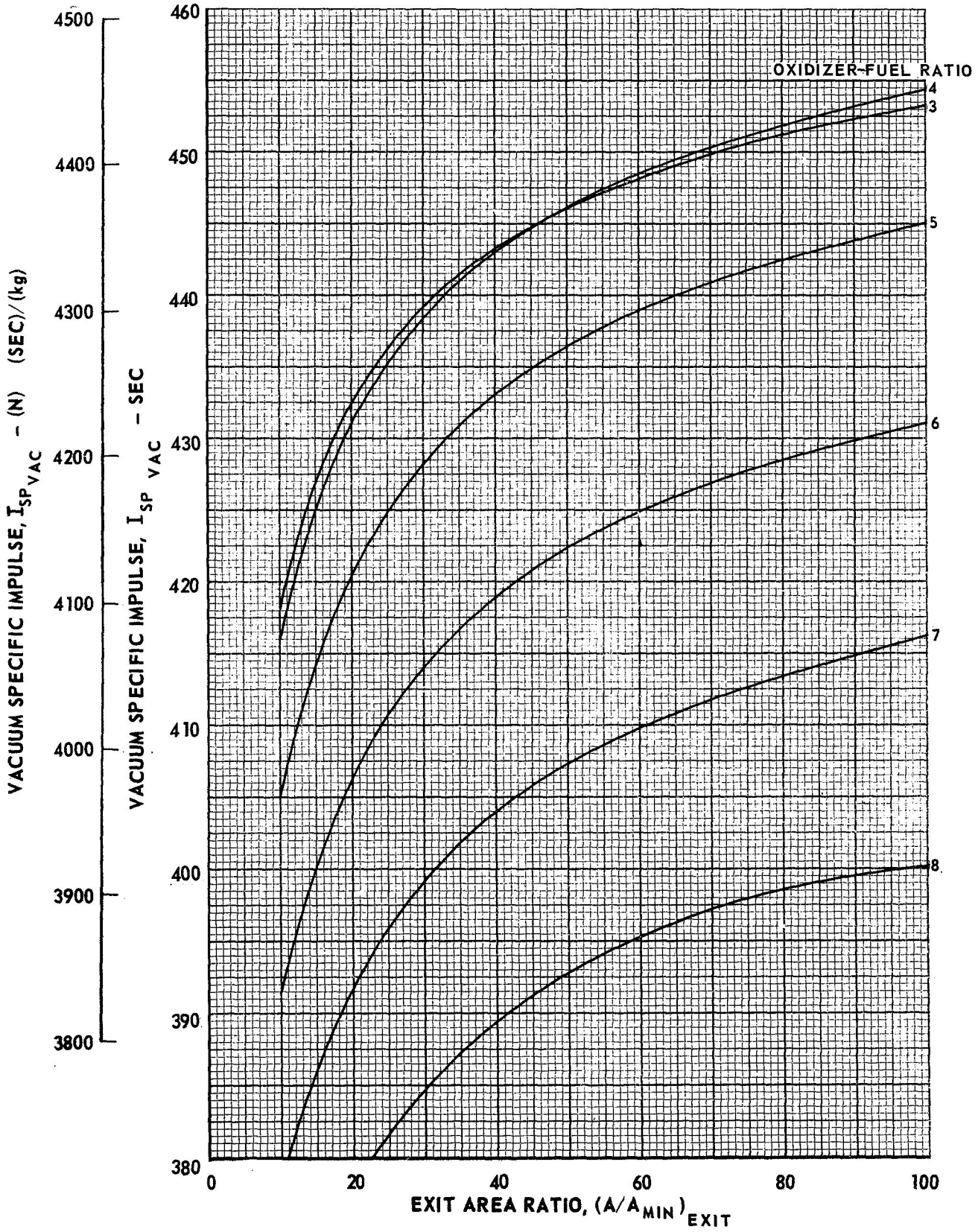

FIG. II-5

VARIATION OF EQUILIBRIUM VACUUM SPECIFIC IMPULSE WITH AREA RATIO

H_2 (ℓ) - O_2 (ℓ)

P_C = 300 PSIA (2.069×10^6 N/m^2)

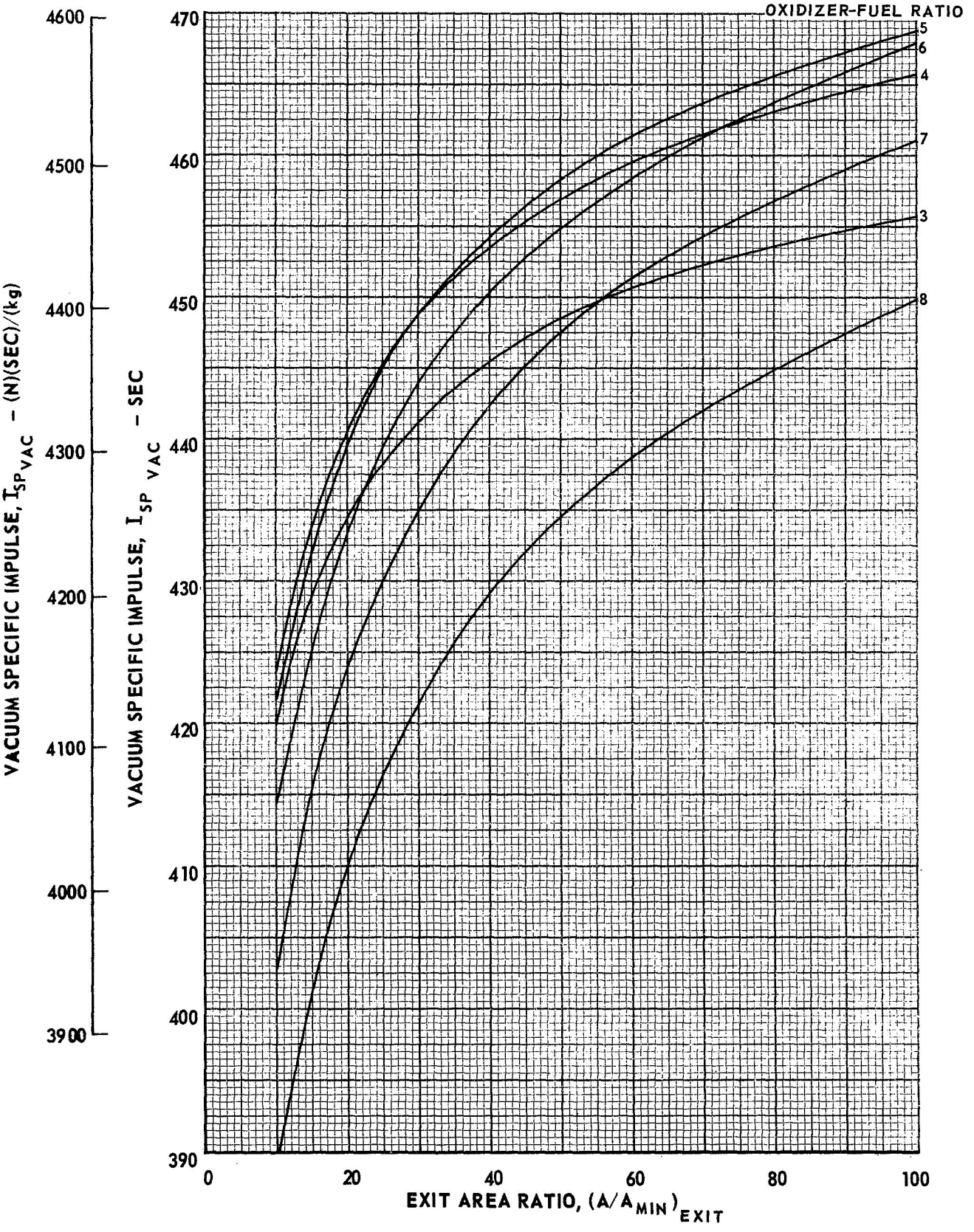

FIG. II-6

VARIATION OF FROZEN VACUUM SPECIFIC IMPULSE WITH AREA RATIO

H_2 (ℓ) - O_2 (ℓ)

P_C = 300 PSIA (2.069X10^6 N/m^2)

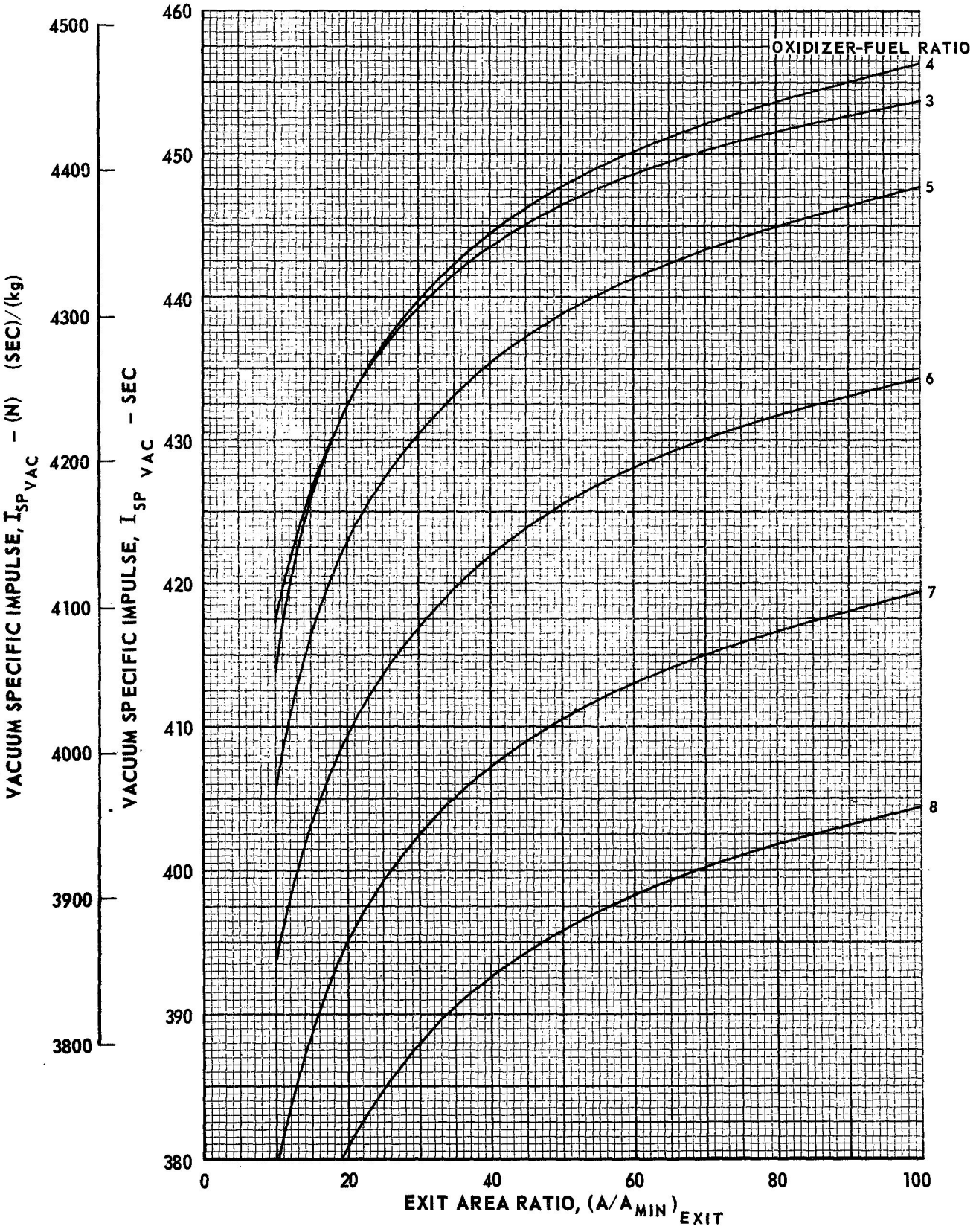

H910666-16

FIG. II-7

VARIATION OF EQUILIBRIUM VACUUM SPECIFIC IMPULSE WITH AREA RATIO

H_2 (ℓ) – O_2 (ℓ)

P_C = 500 PSIA (3.448X10^{6}N/m^2)

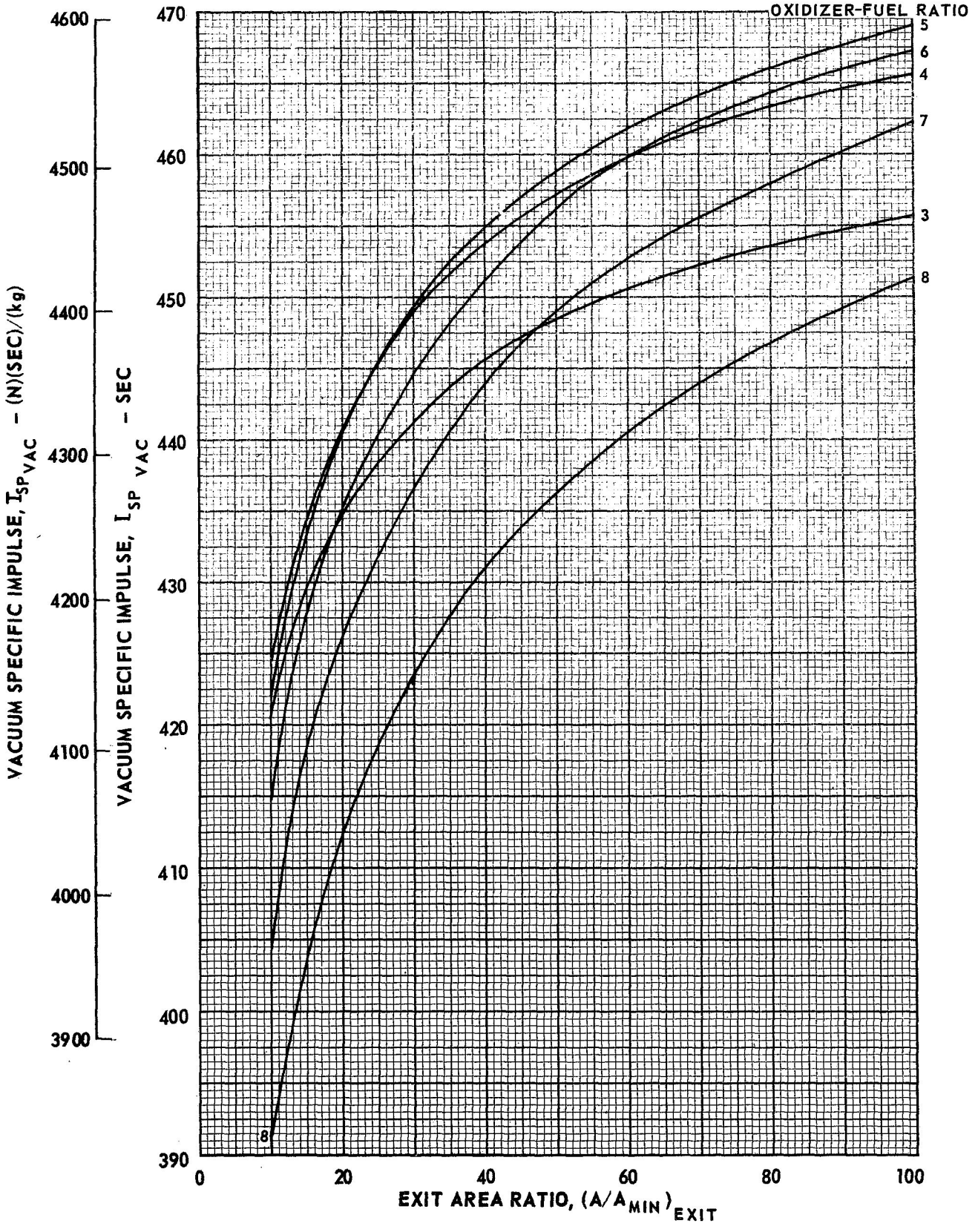

FIG. II-8

VARIATION OF FROZEN VACUUM SPECIFIC IMPULSE WITH AREA RATIO

H_2 (ℓ) - O_2 (ℓ)

P_C = 500 PSIA (3.448X10^{6}N/m^2)

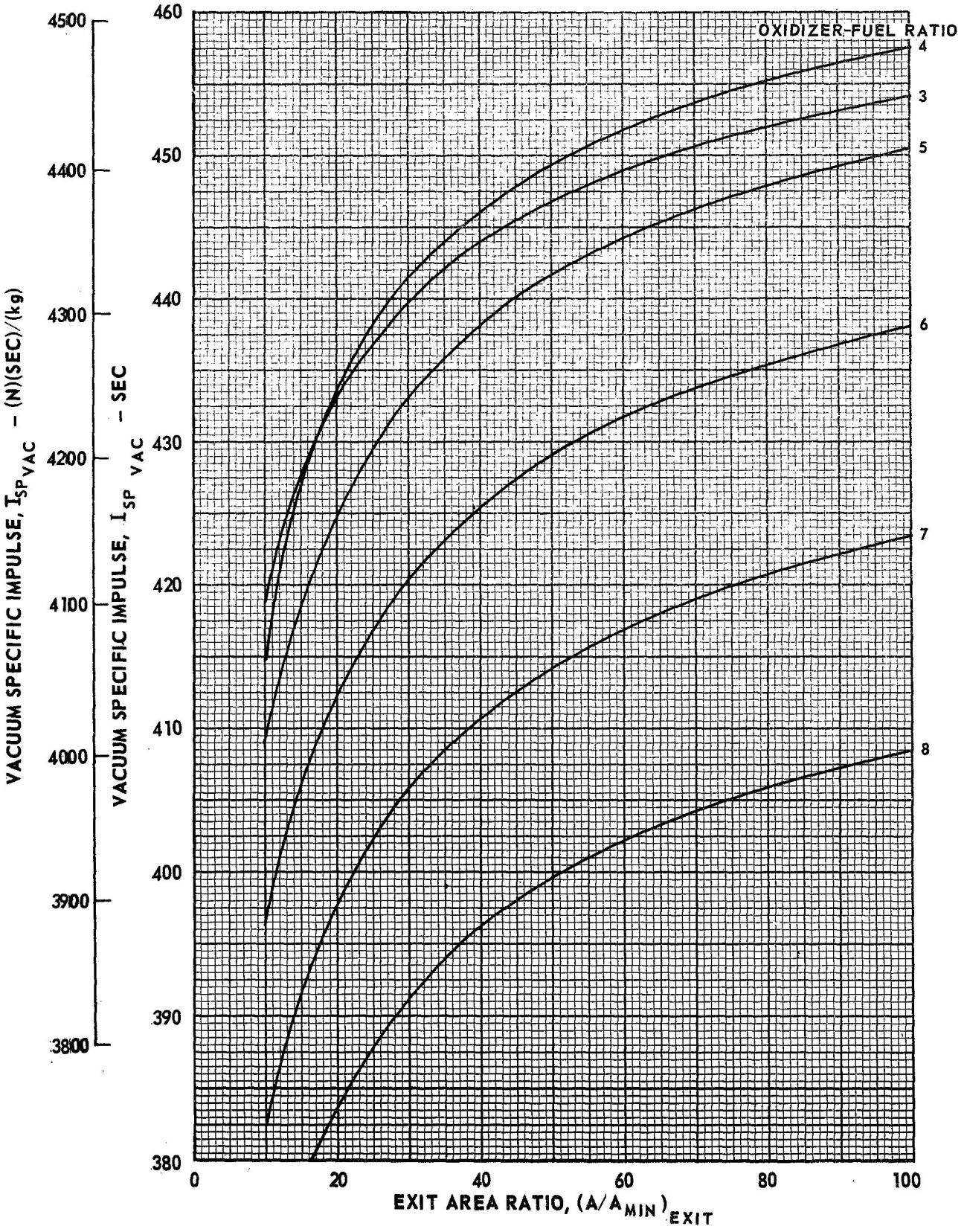

H910666-16

FIG. II-9

VARIATION OF EQUILIBRIUM VACUUM SPECIFIC IMPULSE WITH AREA RATIO

H_2 (ℓ) - O_2 (ℓ)

P_C = 750 PSIA (5.171X10^{6}N/m^2)

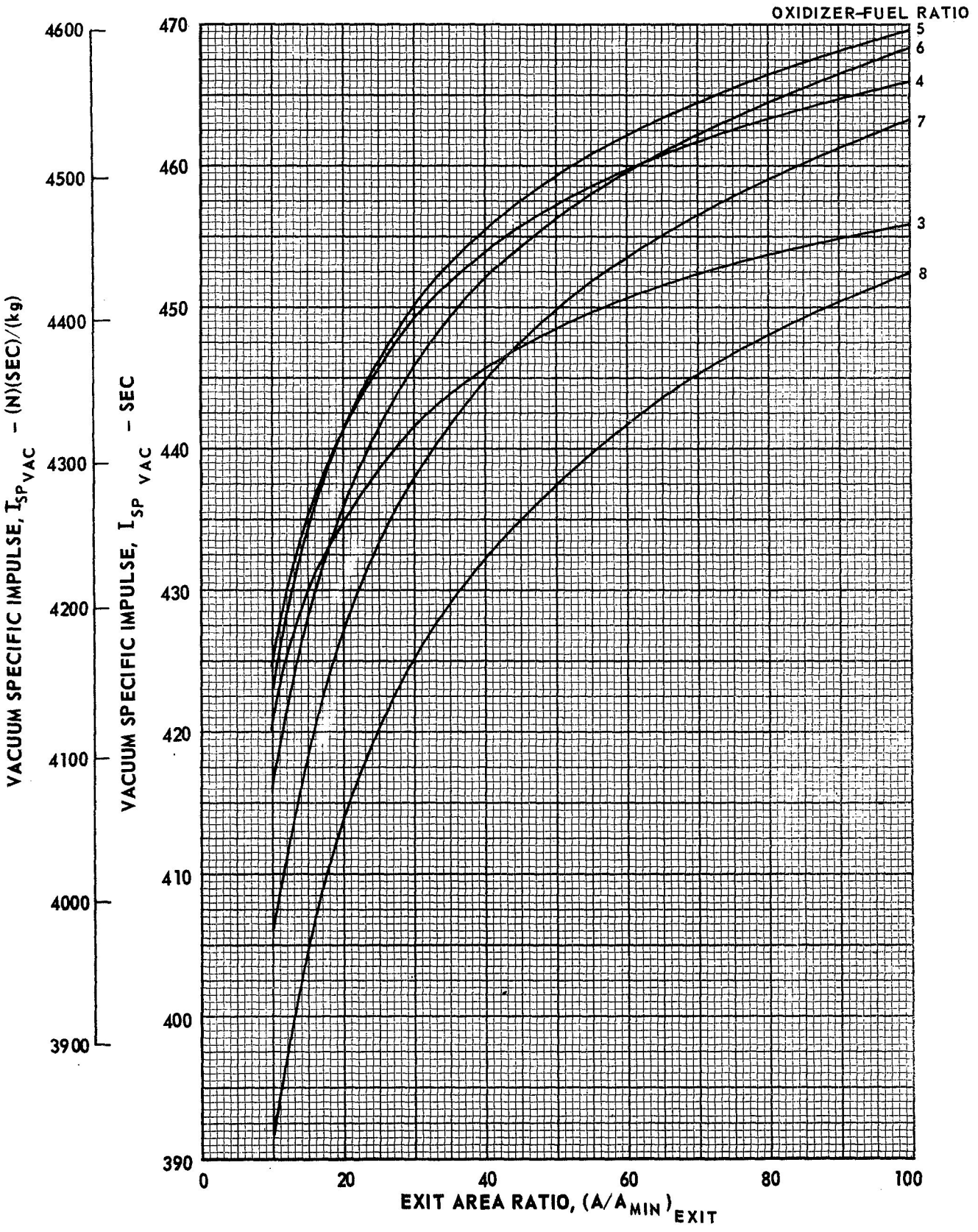

FIG. II-10

VARIATION OF FROZEN VACUUM SPECIFIC IMPULSE WITH AREA RATIO

H_2 (ℓ) - O_2 (ℓ)

P_C = 750 PSIA (5.171X10^{6}N/m^2)

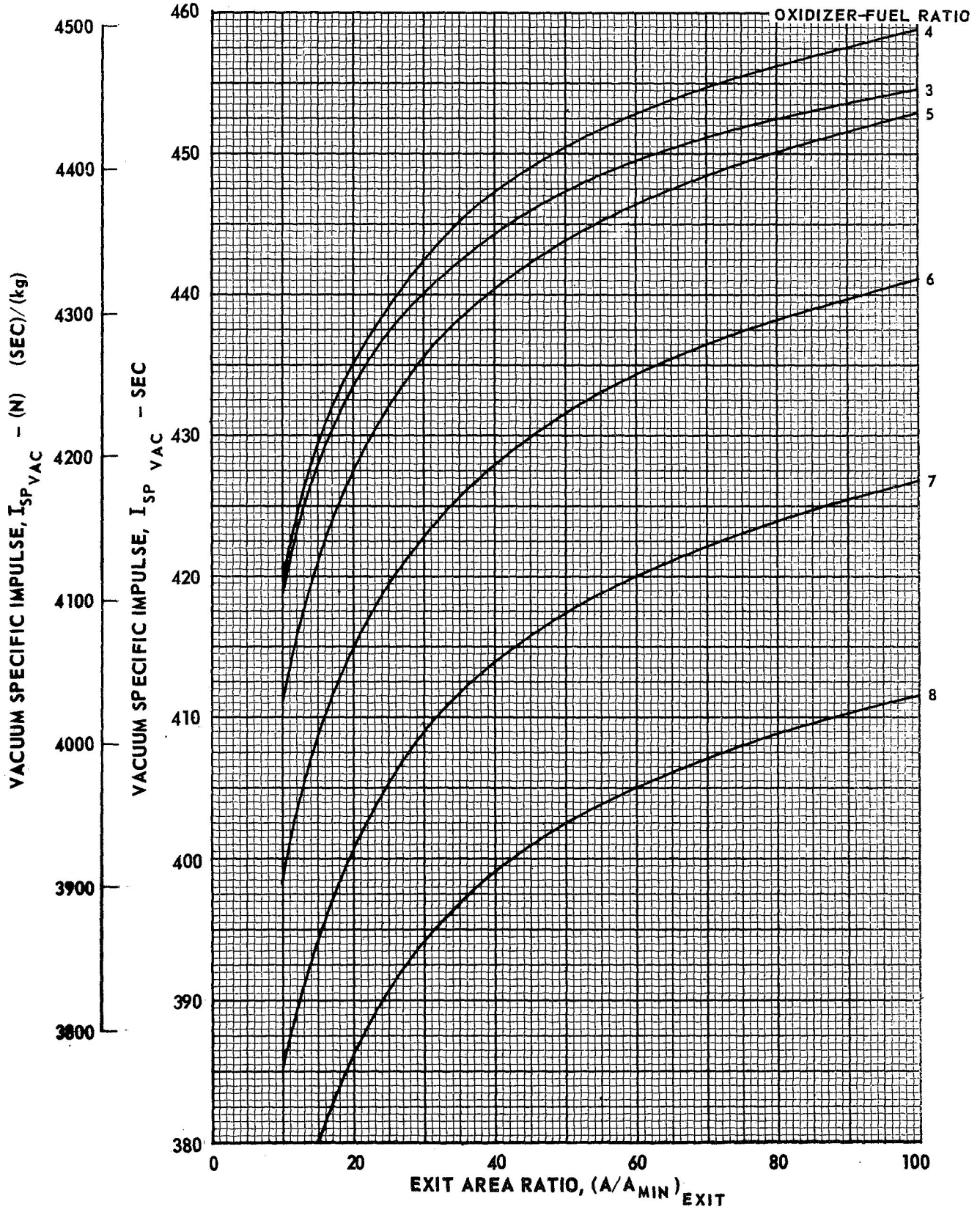

FIG. II-11

VARIATION OF EQUILIBRIUM VACUUM SPECIFIC IMPULSE WITH AREA RATIO

H_2 (ℓ) - O_2 (ℓ)

P_C = 1000 PSIA (6.895X10^{6}N/m^2)

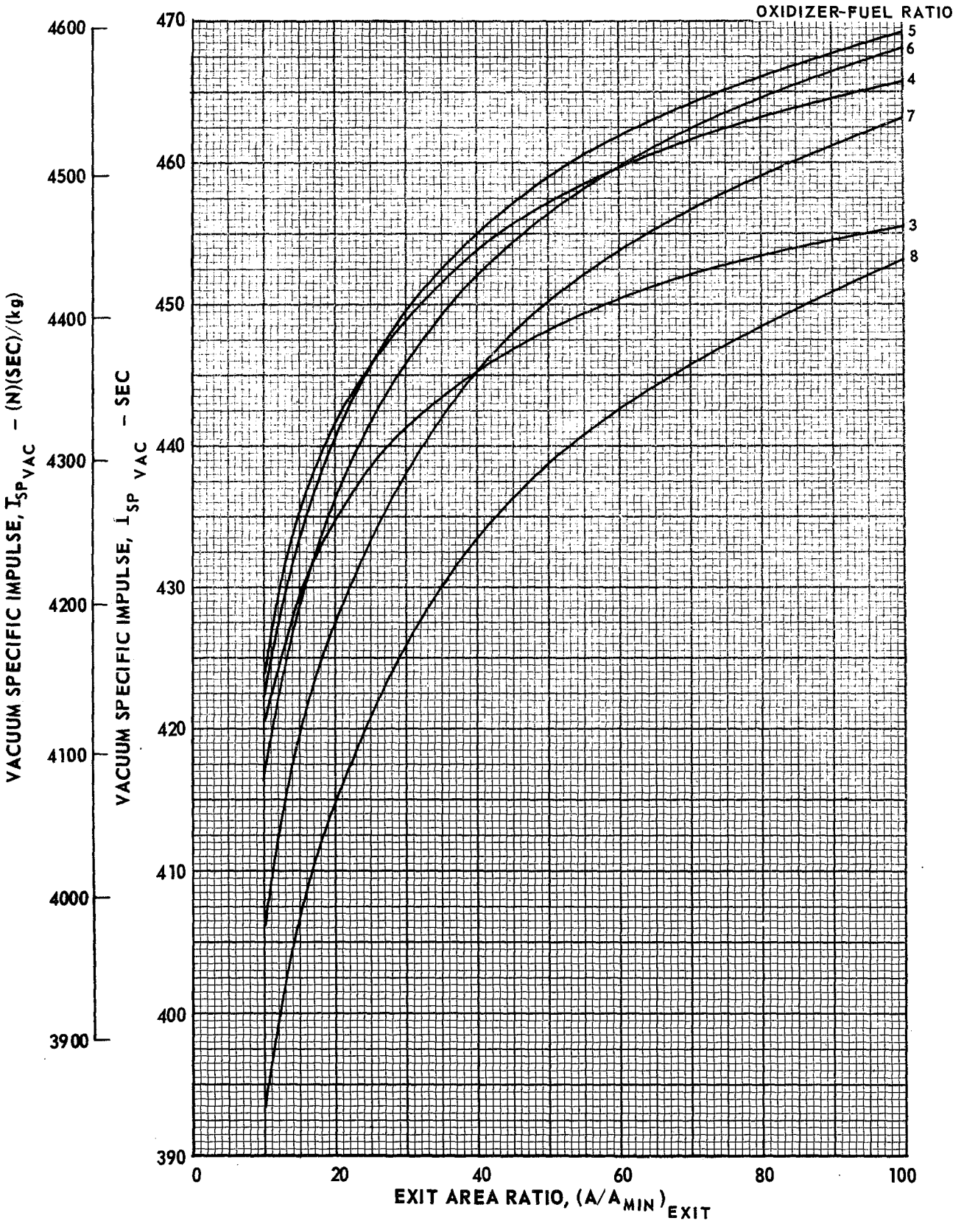

FIG. II-12

VARIATION OF FROZEN VACUUM SPECIFIC IMPULSE WITH AREA RATIO

H_2 (ℓ) – O_2 (ℓ)

P_C = 1000 PSIA (6.895X10^{6}N/m^2)

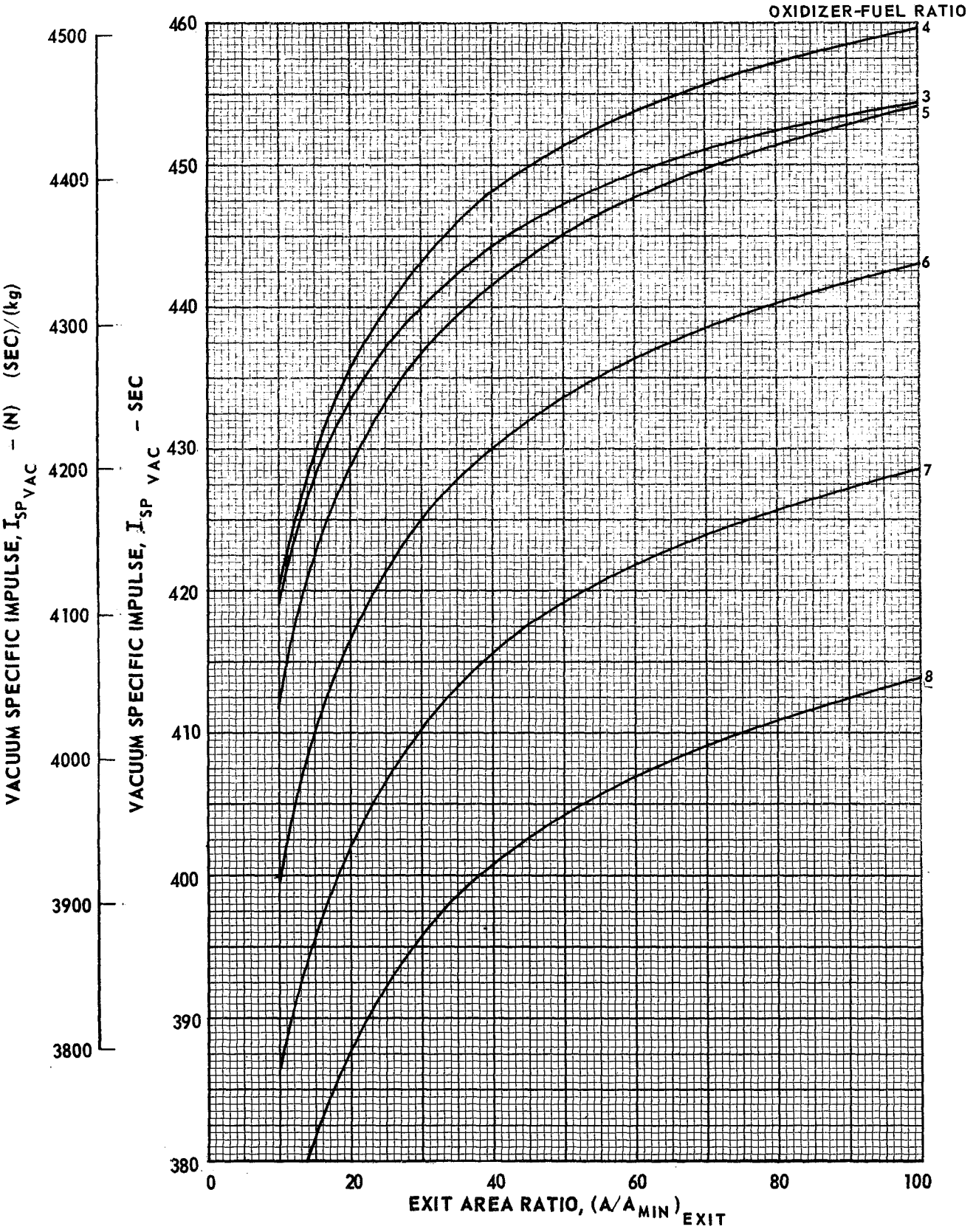

FIG. II-13

NORMALIZED GRAPHICAL SOLUTION FOR FREEZING AREA RATIO USING MODIFIED BRAY ANALYSIS

$H_2(\ell) - O_2(\ell)$

$P_C = 100$ PSIA ($6.895 \times 10^5 N/m^2$)

O/F = 4.00

NOTE: REACTION RATE CONSTANTS LISTED IN TABLE II-1

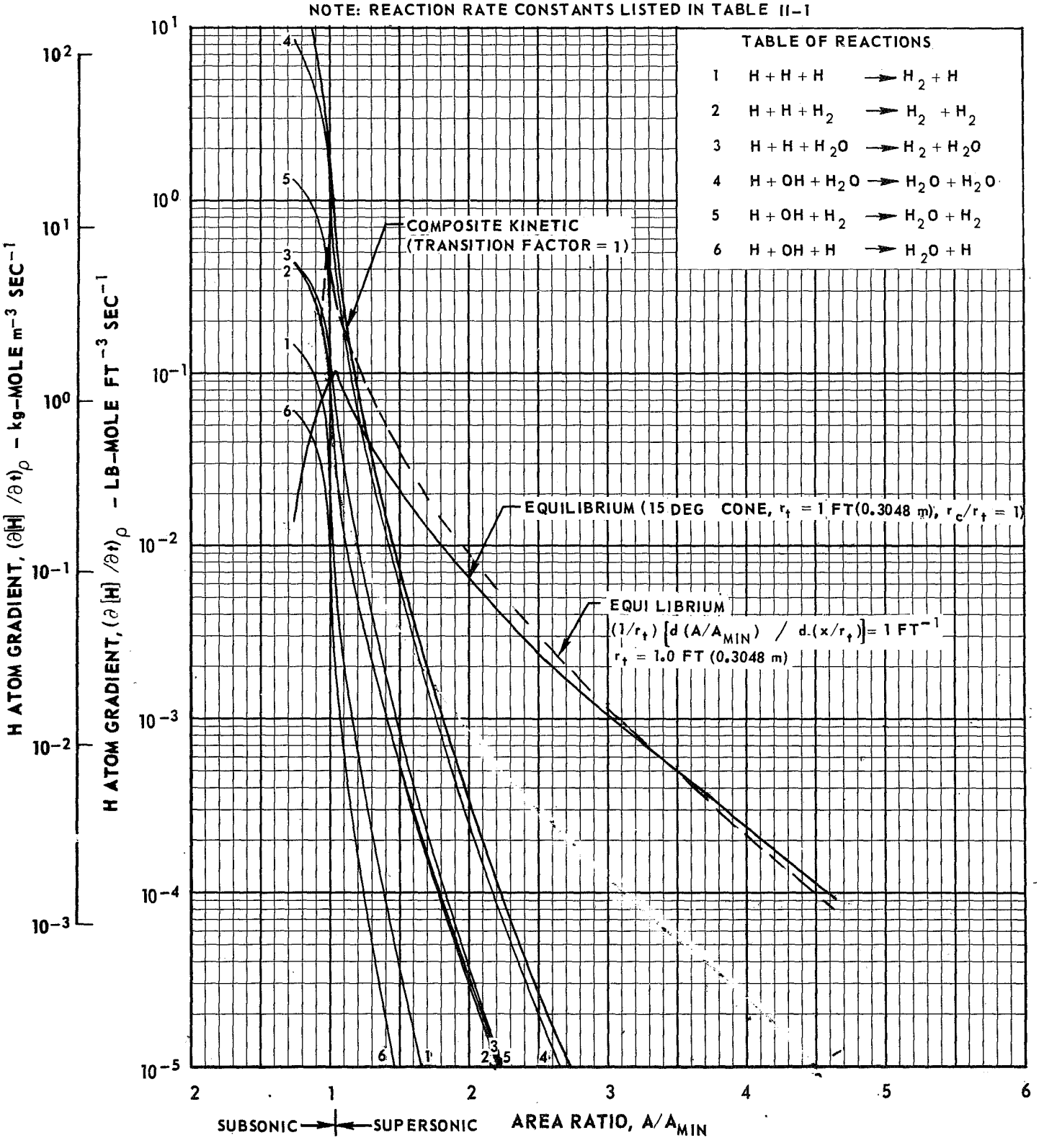

FIG. II-14

NORMALIZED GRAPHICAL SOLUTION FOR FREEZING AREA RATIO USING MODIFIED BRAY ANALYSIS

$H_2(\ell) - O_2(\ell)$

$P_C = 100$ PSIA ($6.895 \times 10^5 N/m^2$)

O/F = 6.00

NOTE: REACTION RATE CONSTANTS LISTED IN TABLE II-1

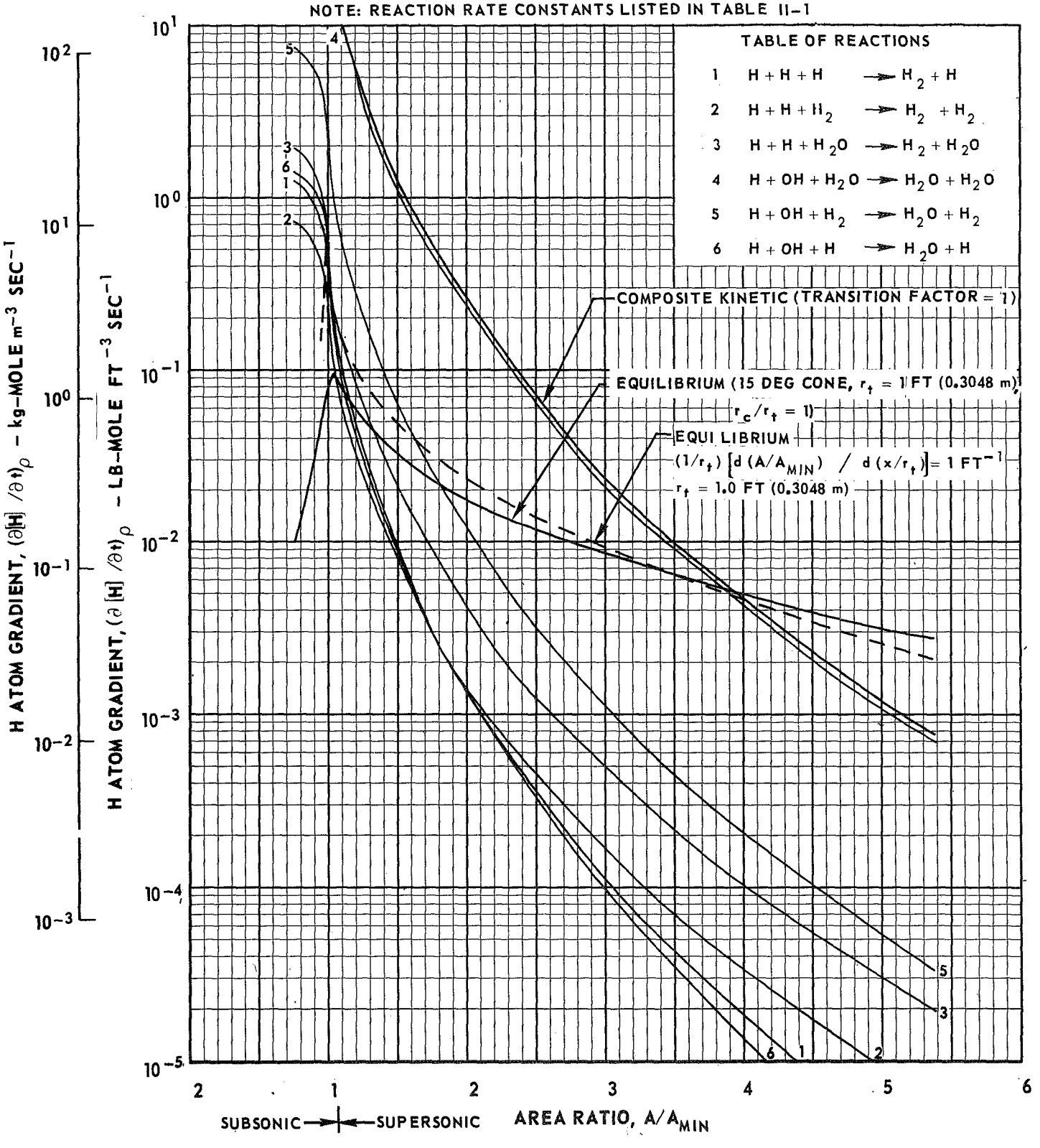

FIG. II-15

NORMALIZED GRAPHICAL SOLUTION FOR FREEZING AREA RATIO USING MODIFIED BRAY ANALYSIS

$H_2(\ell) - O_2(\ell)$

$P_C = 100$ PSIA (6.895×10^5 N/m^2)

O/F = 8.00

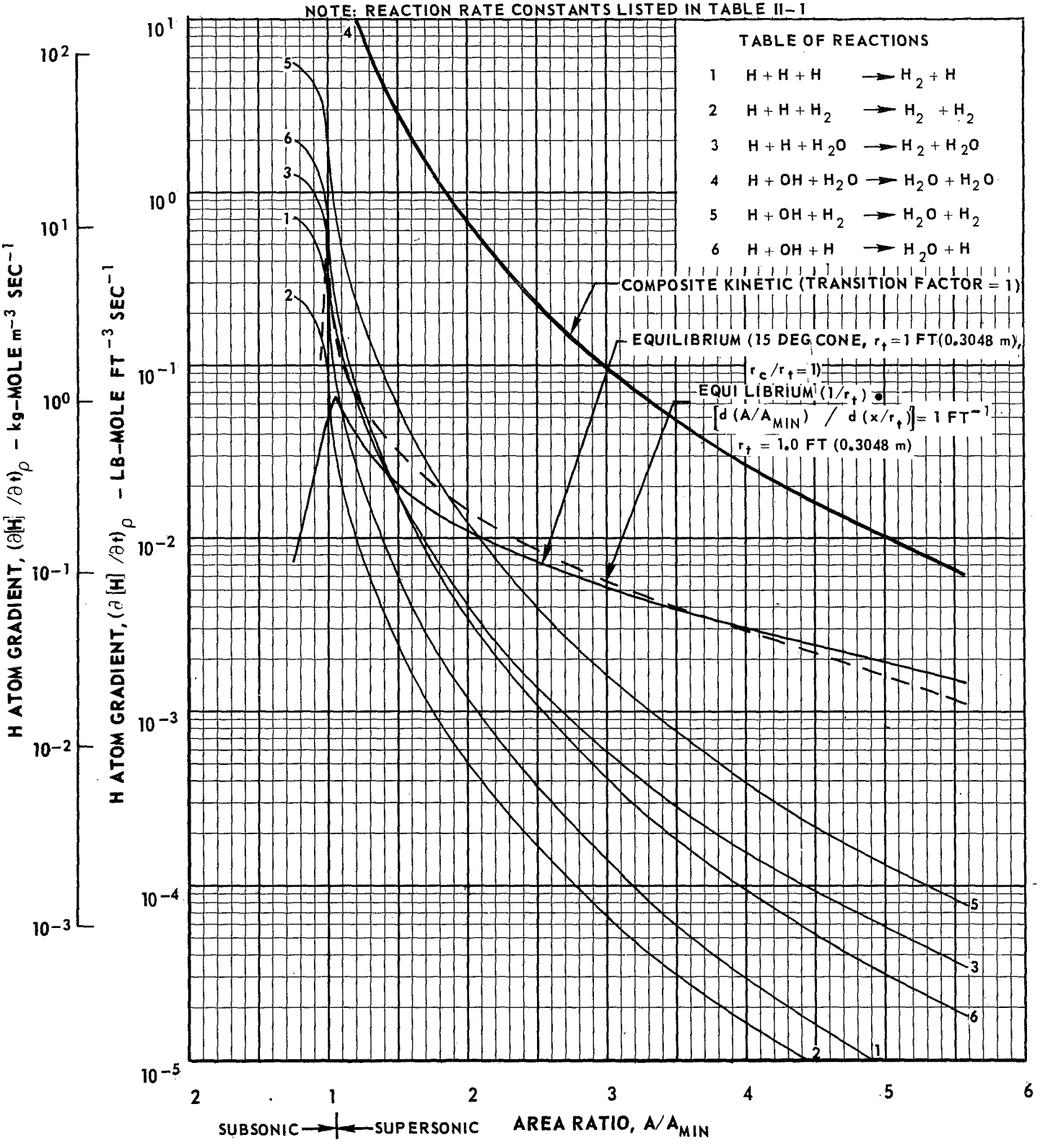

FIG. II-16

NORMALIZED GRAPHICAL SOLUTION FOR FREEZING AREA RATIO USING MODIFIED BRAY ANALYSIS

$H_2(\ell) - O_2(\ell)$

$P_C = 200$ PSIA $(1.379 \times 10^6 N/m^2)$

O/F = 4.00

NOTE: REACTION RATE CONSTANTS LISTED IN TABLE III-1

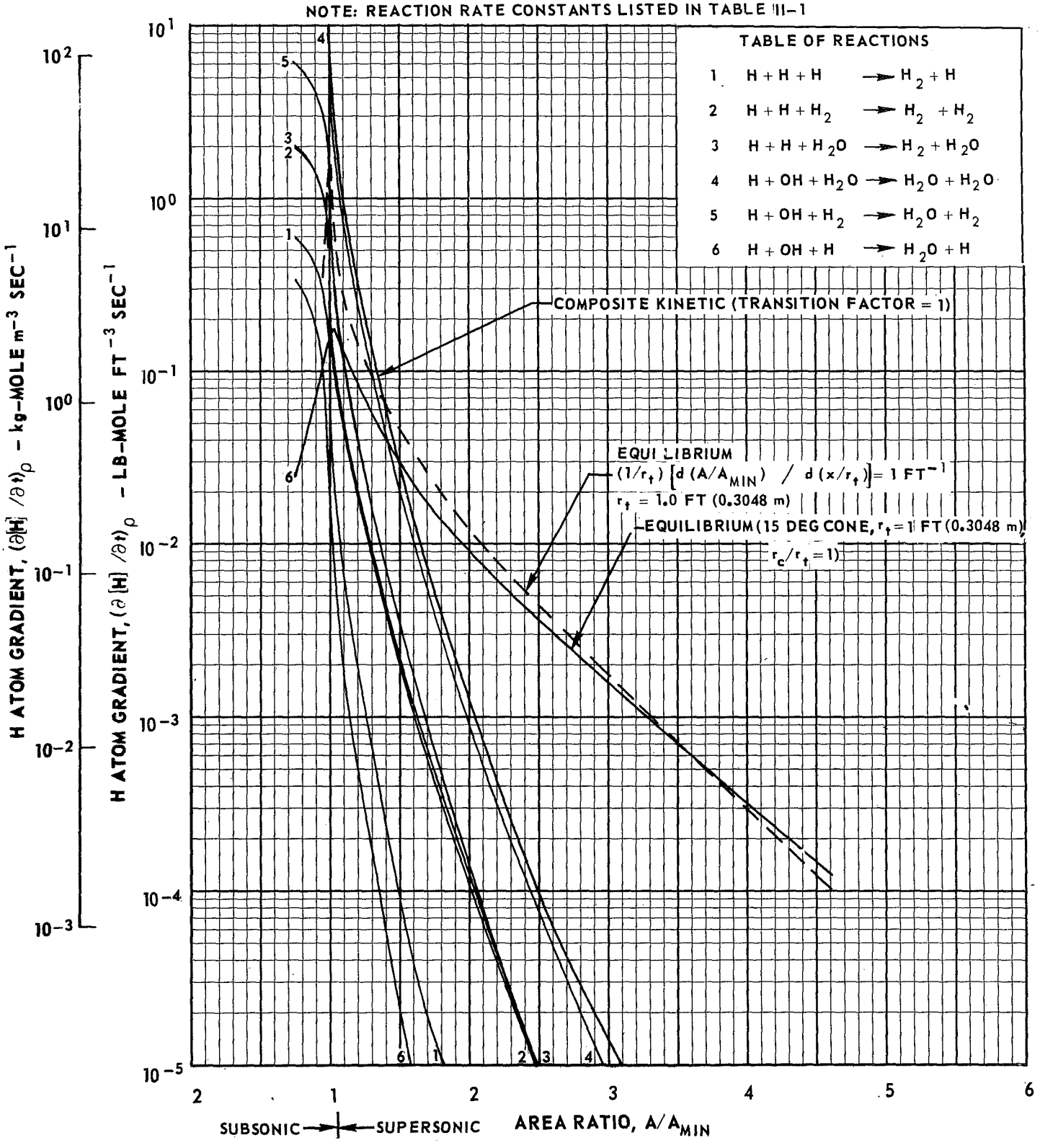

FIG. II-17

NORMALIZED GRAPHICAL SOLUTION FOR FREEZING AREA RATIO USING MODIFIED BRAY ANALYSIS

$H_2(\ell) - O_2(\ell)$

$P_C = 200$ PSIA (1.379×10^6 N/m^2)

O/F = 6.00

NOTE: REACTION RATE CONSTANTS LISTED IN TABLE II-1

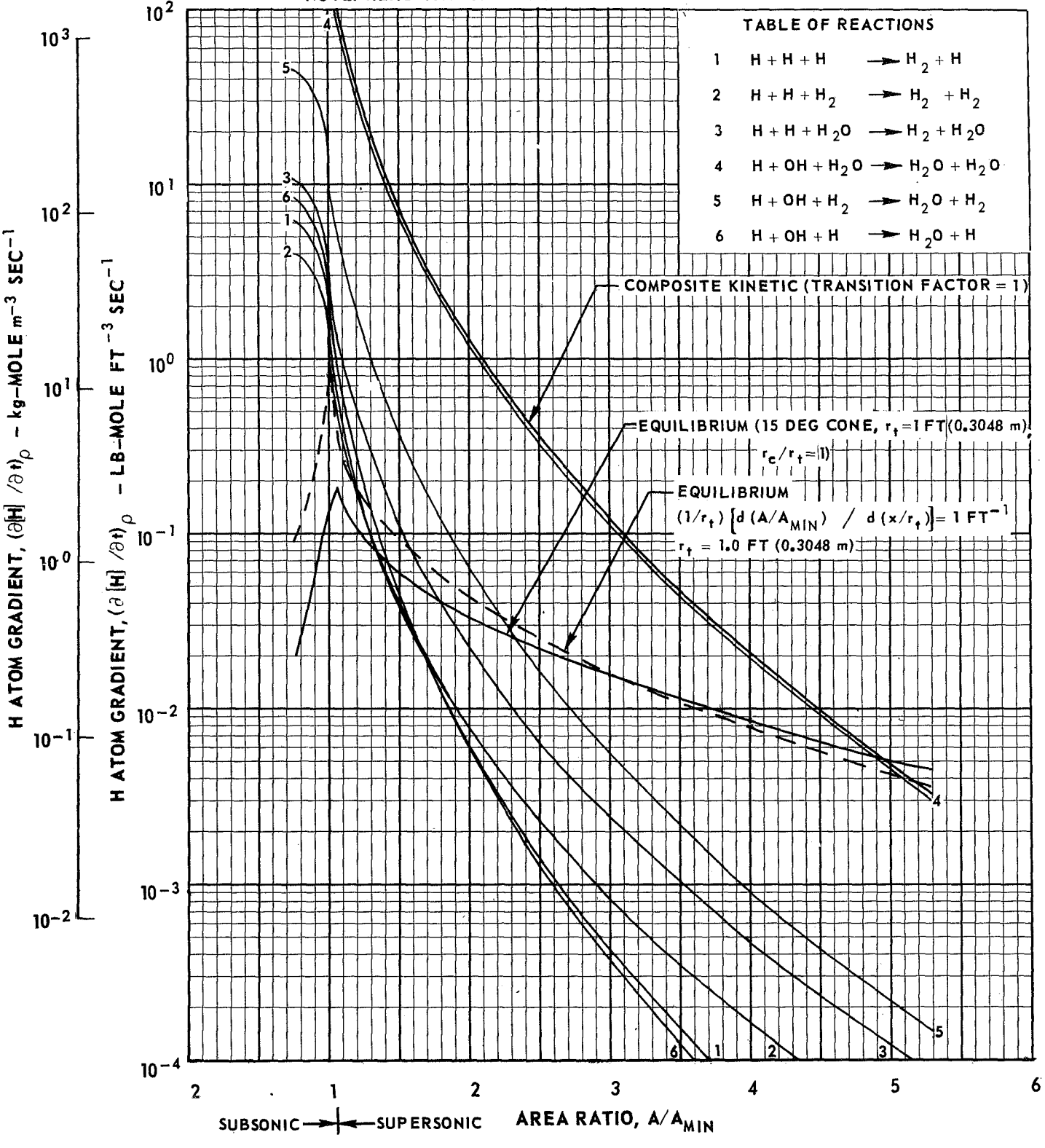

FIG. II-18

NORMALIZED GRAPHICAL SOLUTION FOR FREEZING AREA RATIO USING MODIFIED BRAY ANALYSIS

$H_2(\ell) - O_2(\ell)$

$P_C = 200$ PSIA ($1.379 \times 10^6 N/m^2$)

O/F = 8.00

NOTE: REACTION RATE CONSTANTS LISTED IN TABLE II-1

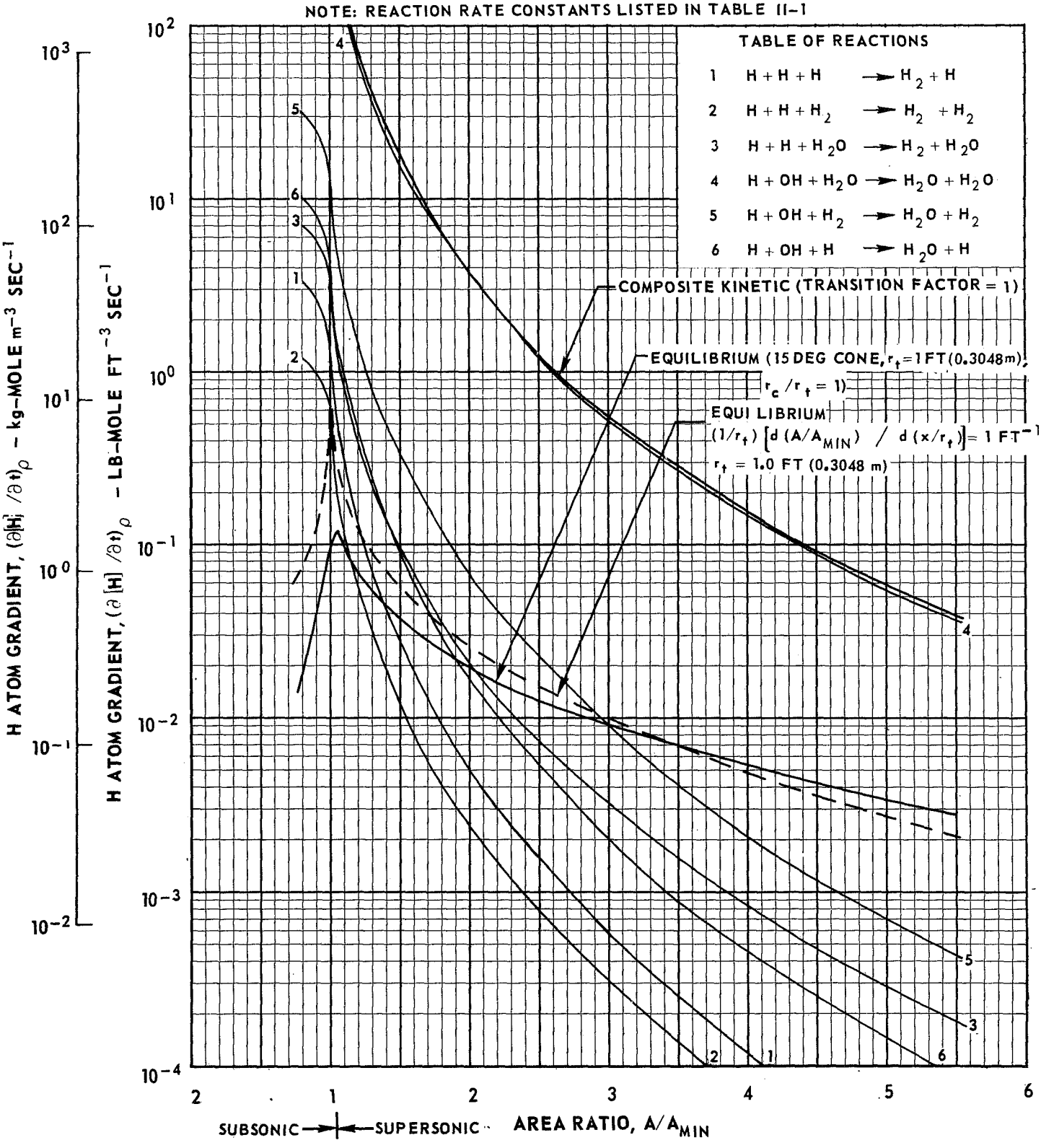

FIG. II-19

NORMALIZED GRAPHICAL SOLUTION FOR FREEZING AREA RATIO USING MODIFIED BRAY ANALYSIS

$H_2(\ell) - O_2(\ell)$

$P_C = 300$ PSIA (2.069×10^6 N/m^2)

O/F = 4.00

NOTE: REACTION RATE CONSTANTS LISTED IN TABLE II-1

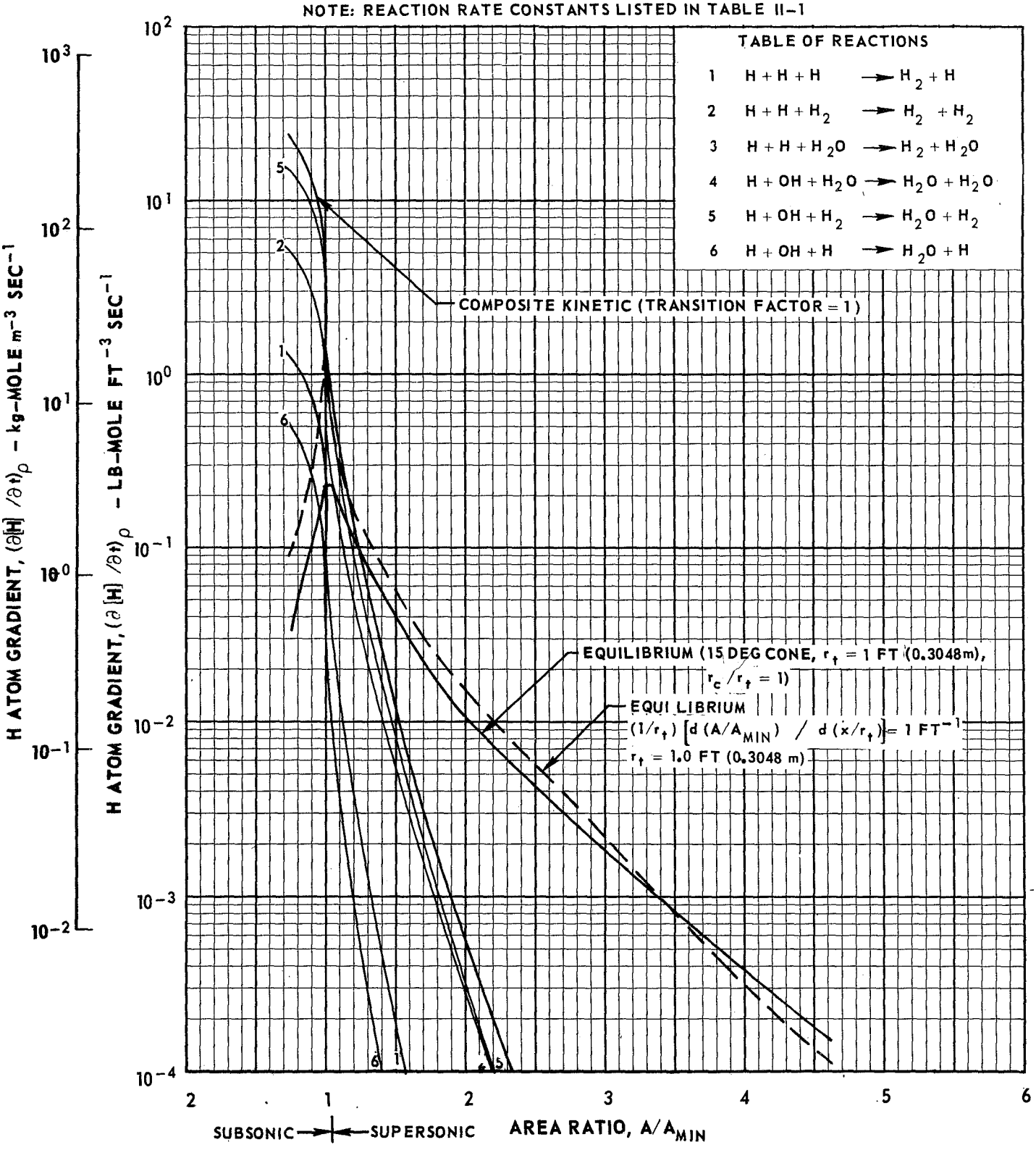

FIG. II-20

NORMALIZED GRAPHICAL SOLUTION FOR FREEZING AREA RATIO USING MODIFIED BRAY ANALYSIS

$H_2(\ell) - O_2(\ell)$

$P_C = 300$ PSIA (2.069×10^6 N/m^2)

O/F = 6.00

NOTE: REACTION RATE CONSTANTS LISTED IN TABLE II-1

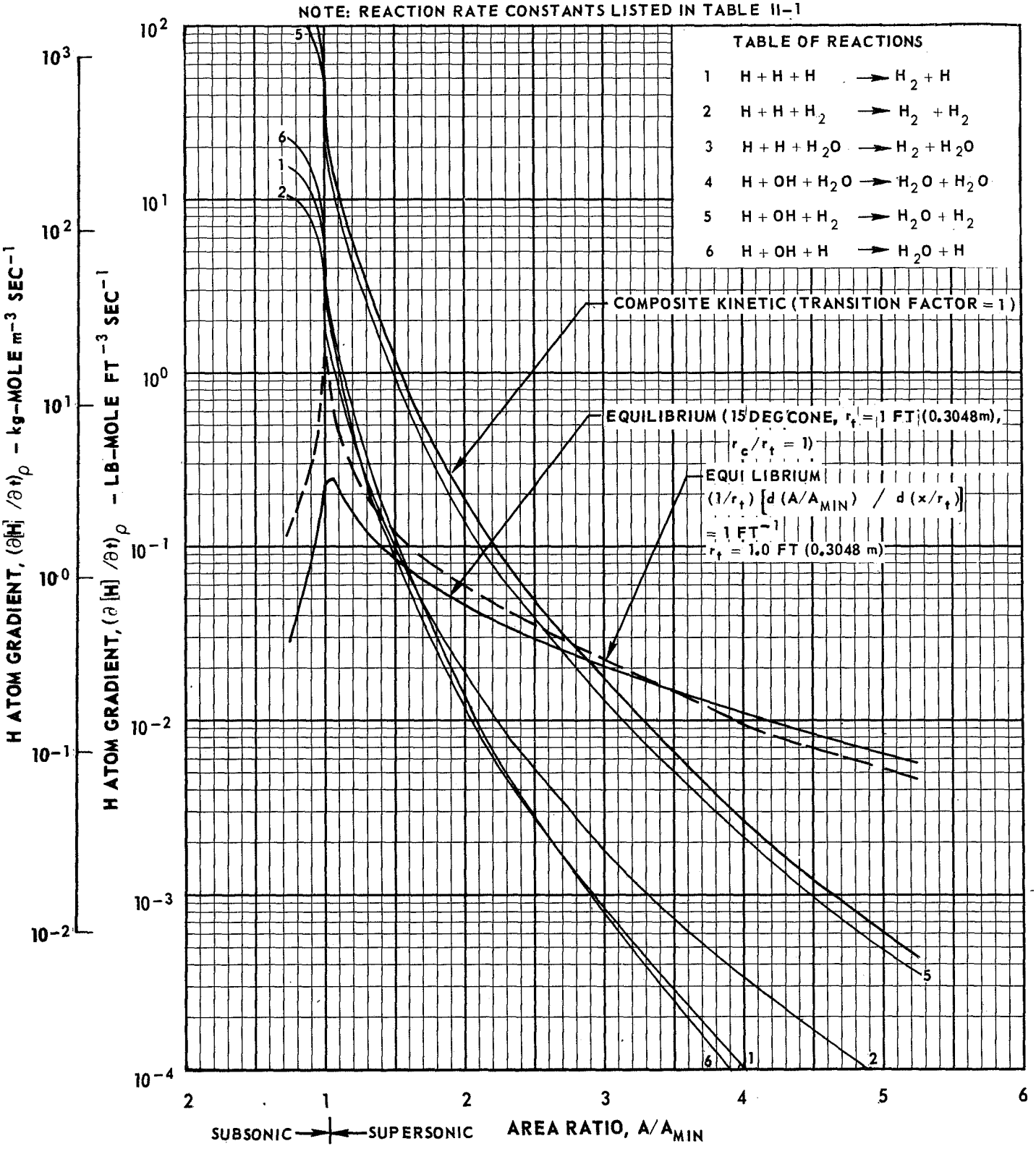

FIG. II-21

NORMALIZED GRAPHICAL SOLUTION FOR FREEZING AREA RATIO USING MODIFIED BRAY ANALYSIS

$H_2(\ell) - O_2(\ell)$

$P_C = 300$ PSIA ($2.069 \times 10^6 N/m^2$)

O/F = 8.00

NOTE: REACTION RATE CONSTANTS LISTED IN TABLE II-1

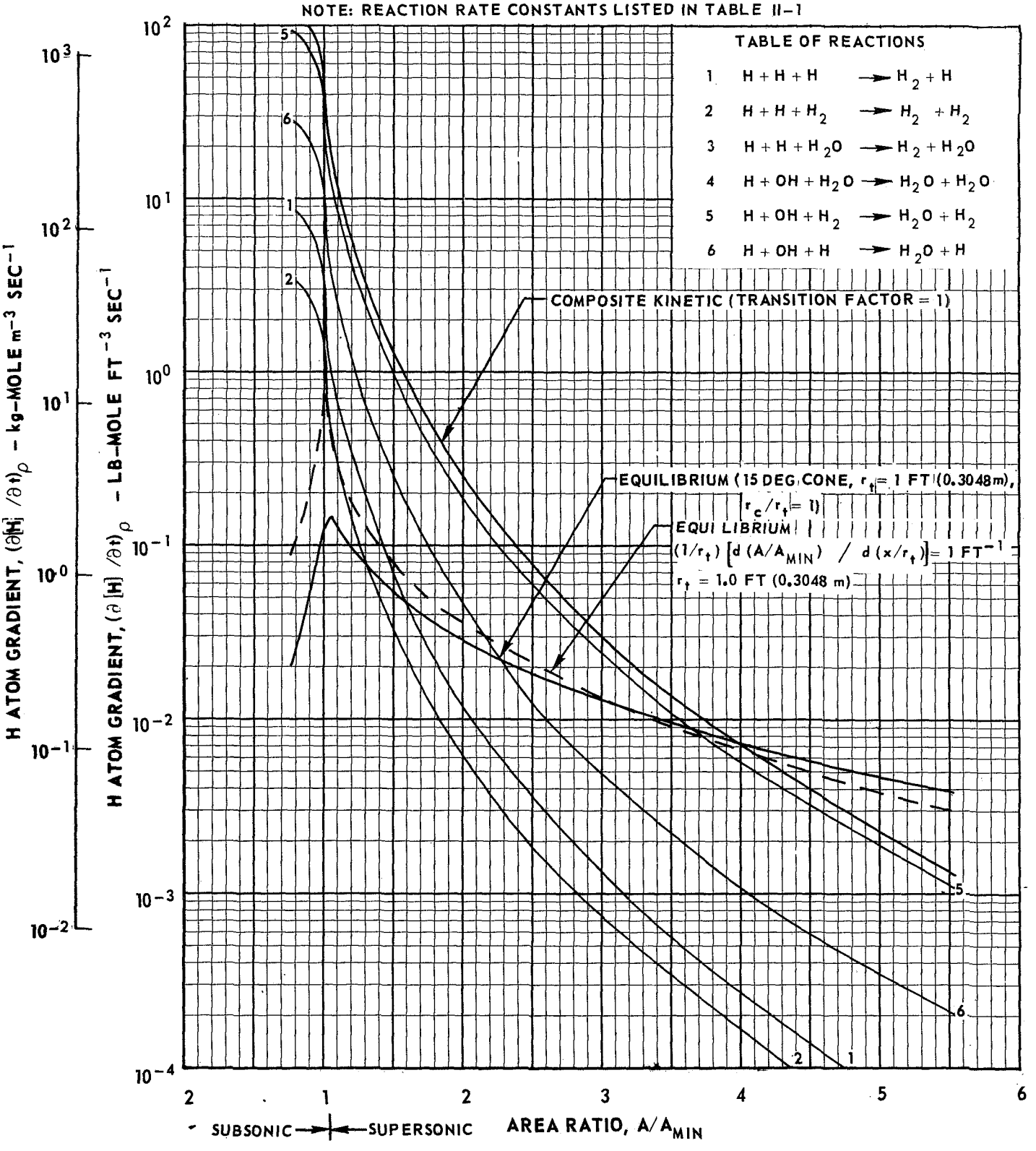

FIG. II-22

NORMALIZED GRAPHICAL SOLUTION FOR FREEZING AREA RATIO USING MODIFIED BRAY ANALYSIS

$H_2(\ell) - O_2(\ell)$

$P_C = 500$ PSIA (3.448×10^6 N/m^2)

O/F = 4.00

NOTE: REACTION RATE CONSTANTS LISTED IN TABLE II-1

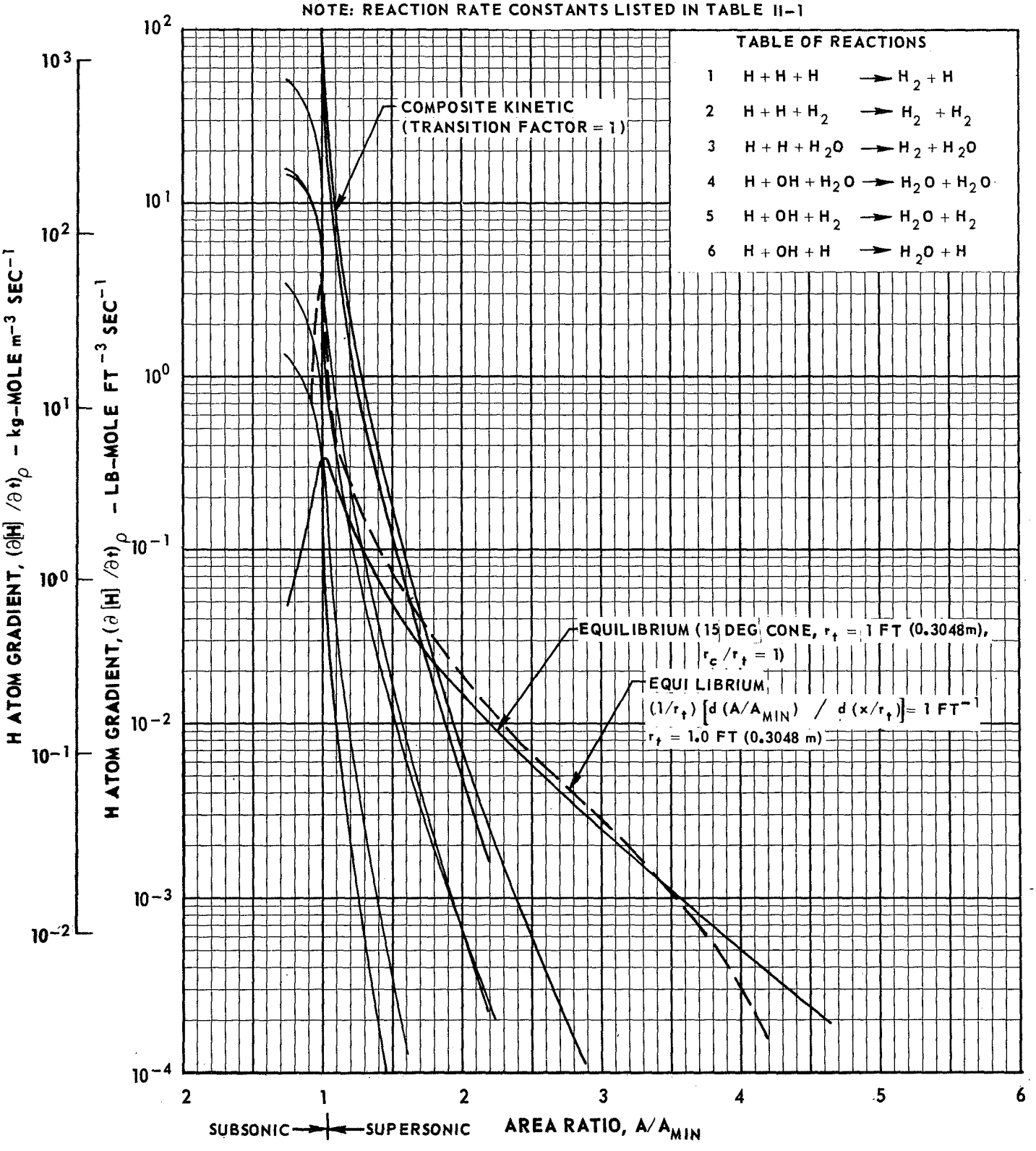

FIG. II-23

NORMALIZED GRAPHICAL SOLUTION FOR FREEZING AREA RATIO USING MODIFIED BRAY ANALYSIS

$H_2(\ell) - O_2(\ell)$

$P_C = 500$ PSIA (3.448×10^6 N/m^2)

O/F = 6.00

NOTE: REACTION RATE CONSTANTS LISTED IN TABLE II-1

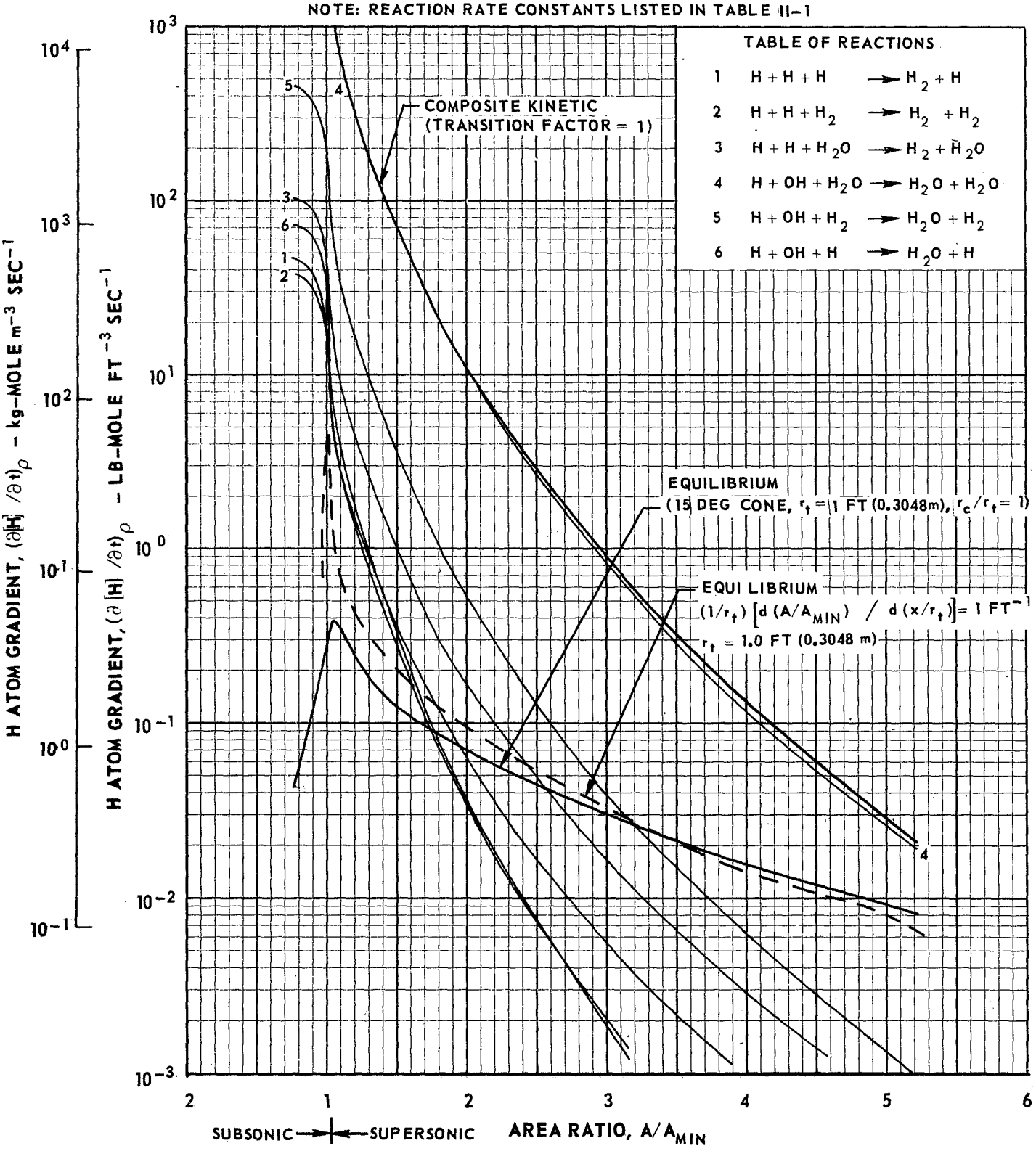

FIG. II-24

NORMALIZED GRAPHICAL SOLUTION FOR FREEZING AREA RATIO USING MODIFIED BRAY ANALYSIS

$H_2(\ell) - O_2(\ell)$

$P_C = 500$ PSIA $(3.448 \times 10^6 N/m^2)$

O/F = 8.00

NOTE: REACTION RATE CONSTANTS LISTED IN TABLE II-1

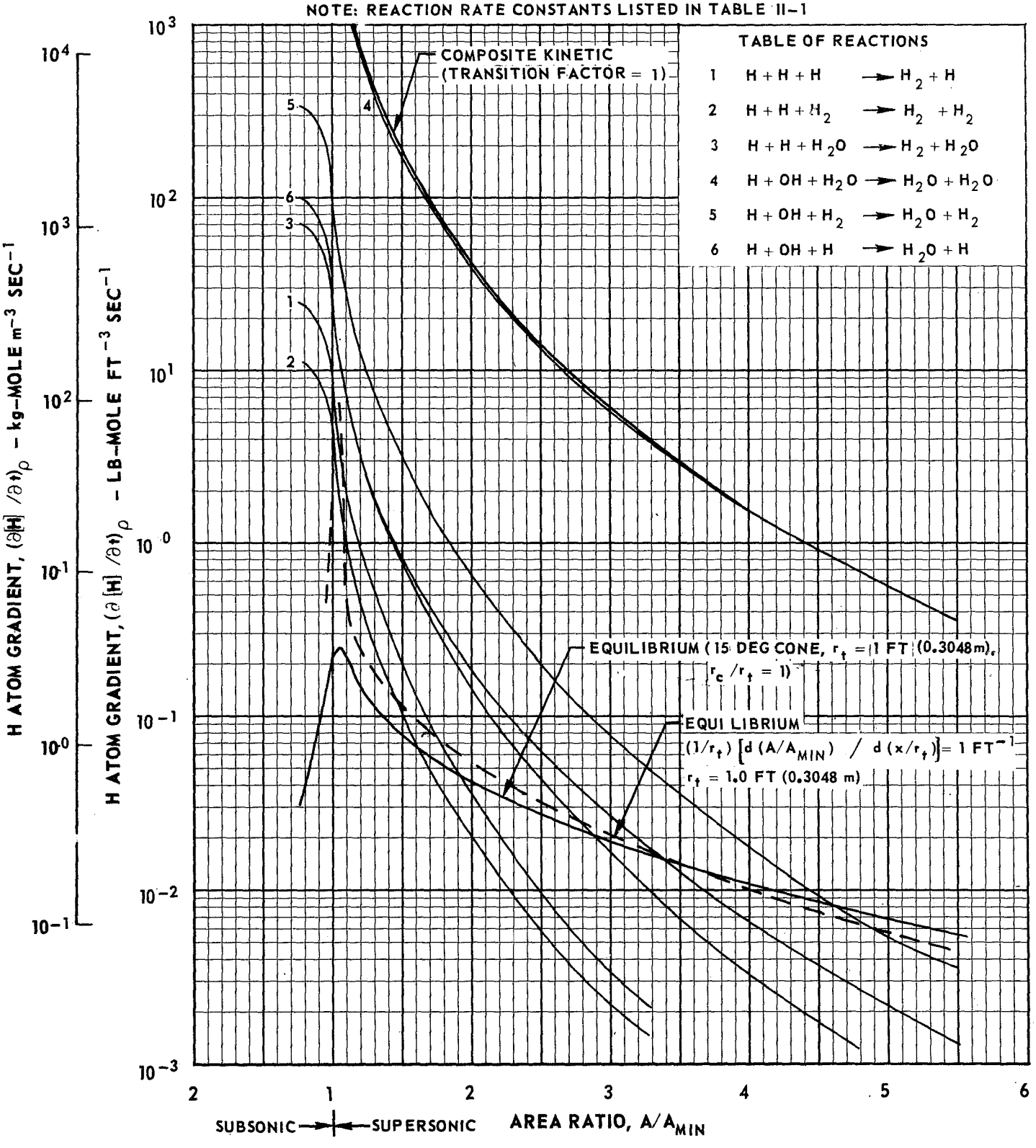

FIG. II-25

NORMALIZED GRAPHICAL SOLUTION FOR FREEZING AREA RATIO USING MODIFIED BRAY ANALYSIS

$H_2(\ell) - O_2(\ell)$

$P_C = 750$ PSIA (5.171×10^6 N/m^2)

O/F = 4.00

NOTE: REACTION RATE CONSTANTS LISTED IN TABLE II-1

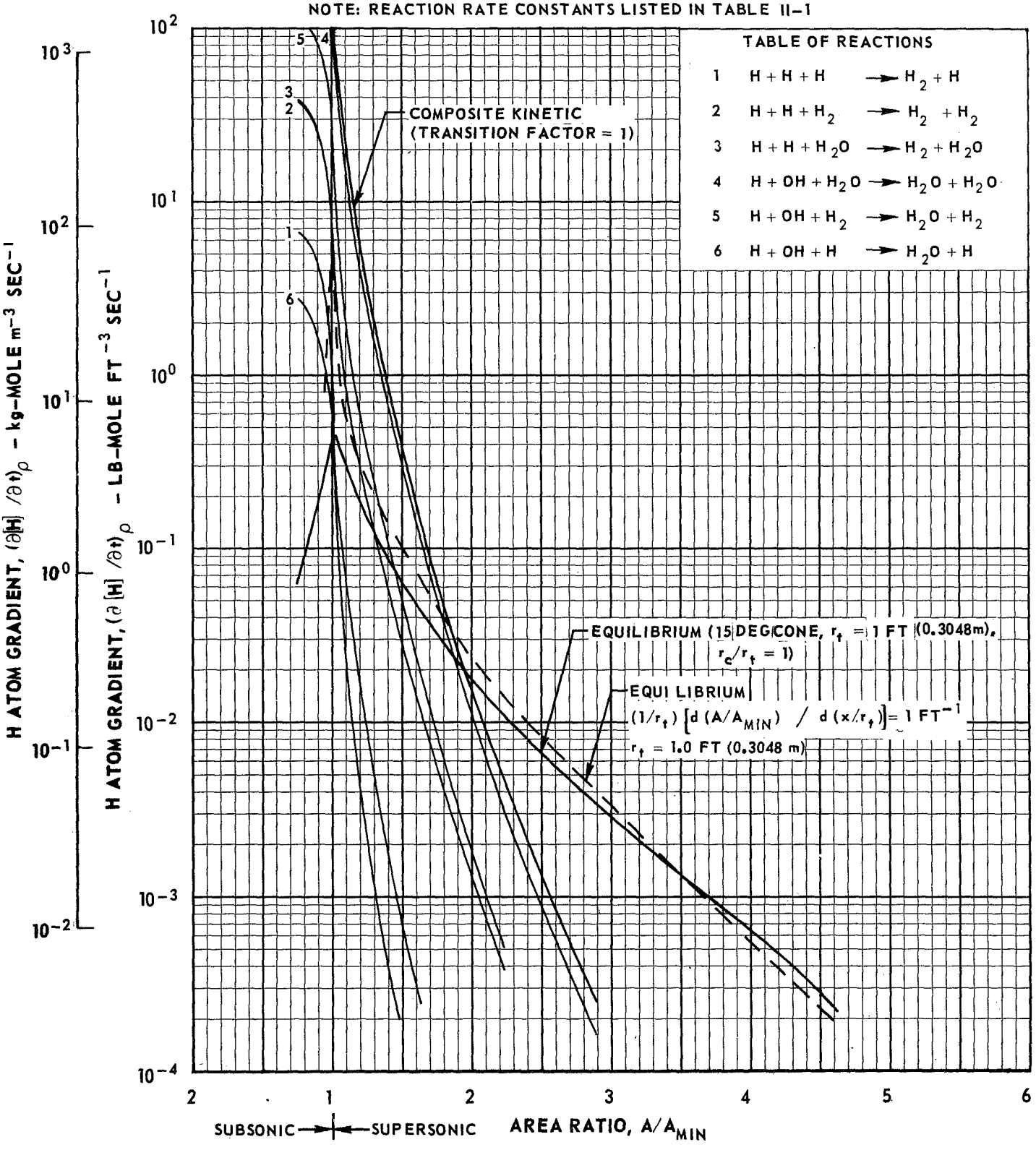

FIG. II-26

NORMALIZED GRAPHICAL SOLUTION FOR FREEZING AREA RATIO USING MODIFIED BRAY ANALYSIS

$H_2(\ell) - O_2(\ell)$

$P_C = 750$ PSIA (5.171×10^6 N/m2)

O/F = 6.00

NOTE: REACTION RATE CONSTANTS LISTED IN TABLE II-1

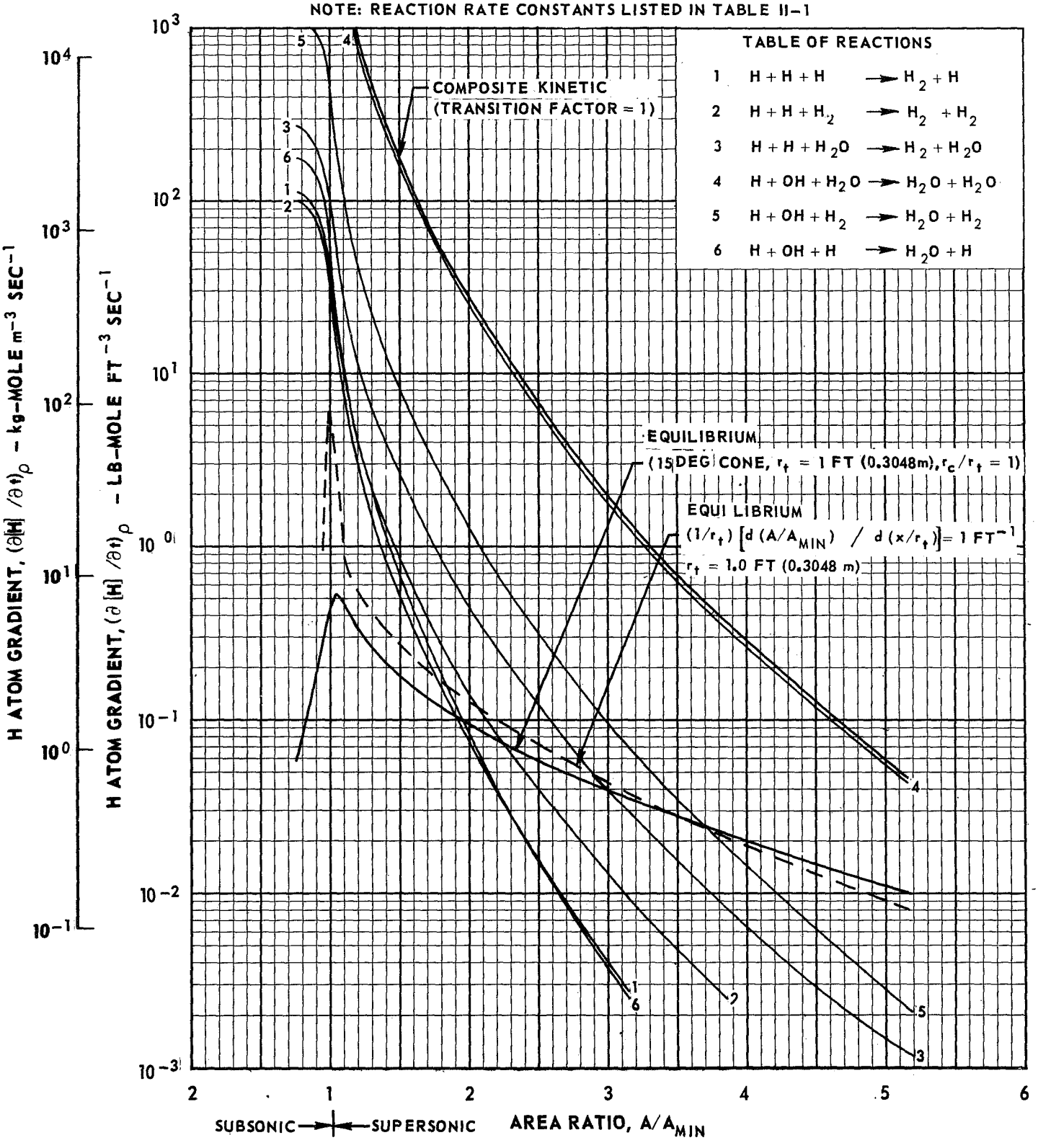

FIG. II-27

NORMALIZED GRAPHICAL SOLUTION FOR FREEZING AREA RATIO USING MODIFIED BRAY ANALYSIS

$H_2(\ell) - O_2(\ell)$

$P_C = 750$ PSIA ($5.171 \times 10^6 N/m^2$)

O/F = 8.00

NOTE: REACTION RATE CONSTANTS LISTED IN TABLE II-1

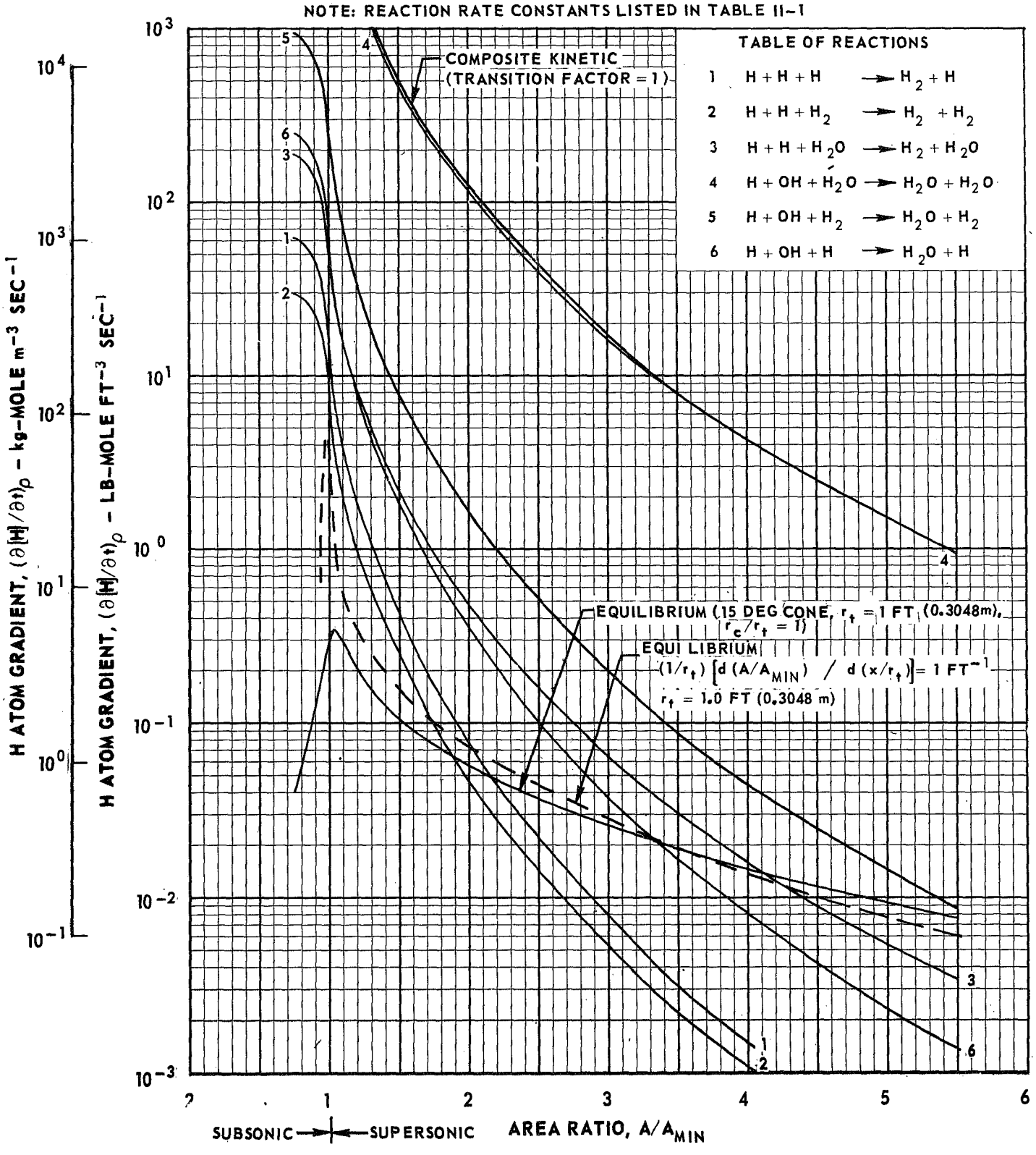

FIG. II-28

NORMALIZED GRAPHICAL SOLUTION FOR FREEZING AREA RATIO USING MODIFIED BRAY ANALYSIS

$H_2(\ell) - O_2(\ell)$

$P_C = 1000$ PSIA (6.895×10^6 N/m^2)

O/F = 4.00

NOTE: REACTION RATE CONSTANTS LISTED IN TABLE II-1

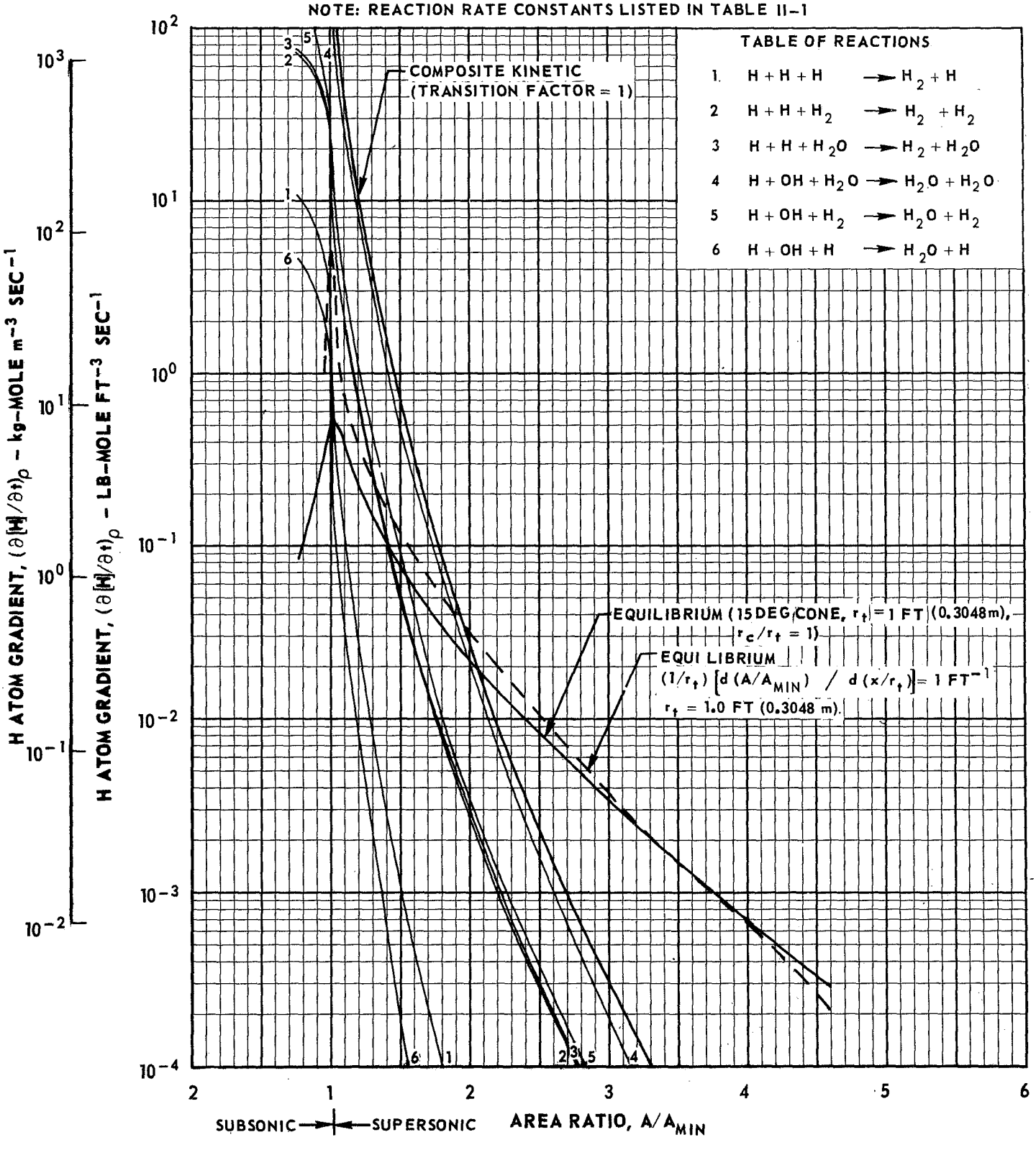

FIG. II-29

NORMALIZED GRAPHICAL SOLUTION FOR FREEZING AREA RATIO USING MODIFIED BRAY ANALYSIS

$H_2(\ell) - O_2(\ell)$

$P_C = 1000$ PSIA $(6.895 \times 10^6 N/m^2)$

O/F = 6.00

NOTE: REACTION RATE CONSTANTS LISTED IN TABLE II-1

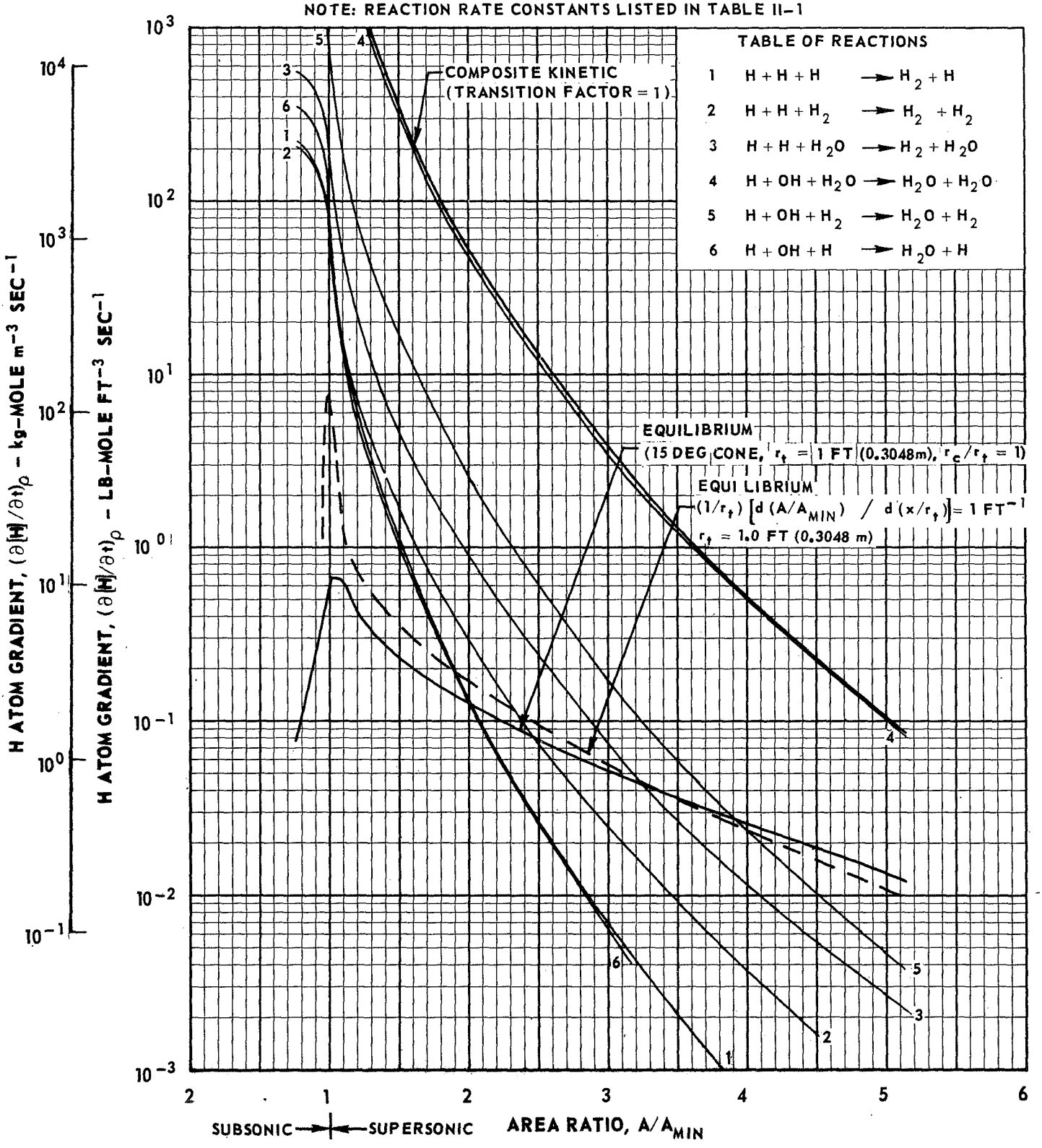

FIG. II-30

NORMALIZED GRAPHICAL SOLUTION FOR FREEZING AREA RATIO USING MODIFIED BRAY ANALYSIS

$H_2(\ell) - O_2(\ell)$

$P_C = 1000$ PSIA $(6.895 \times 10^6 N/m^2)$

O/F = 8.00

NOTE: REACTION RATE CONSTANTS LISTED IN TABLE II-1

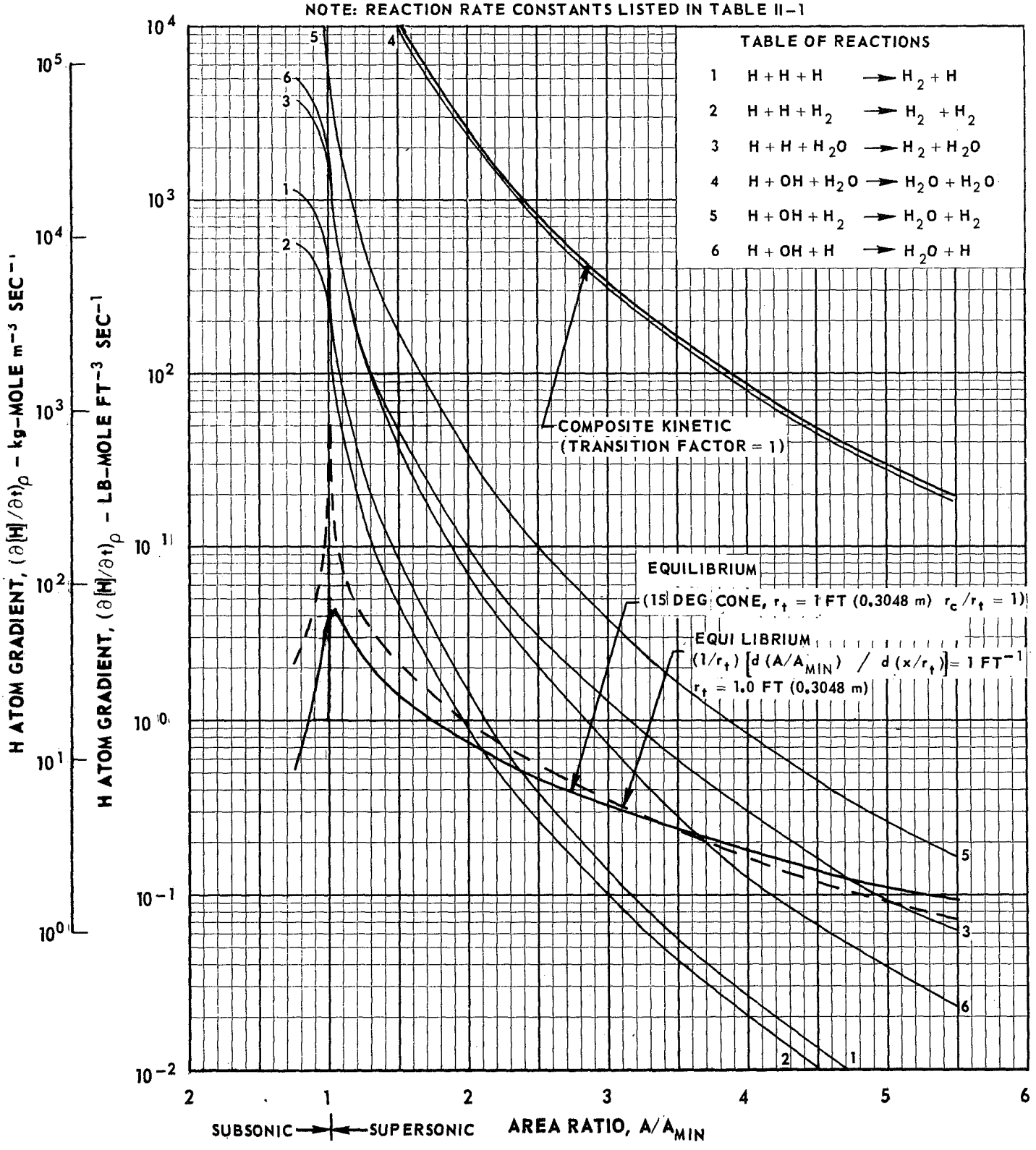

EFFECT OF FREEZING AREA RATIO ON NONEQUILIBRIUM PERFORMANCE FOR HYDROGEN-OXYGEN PROPELLANT SYSTEM

$H_2(\ell) - O_2(\ell)$

P_C = 100 PSIA ($6.895 \times 10^5 N/m^2$)

O/F = 4.00

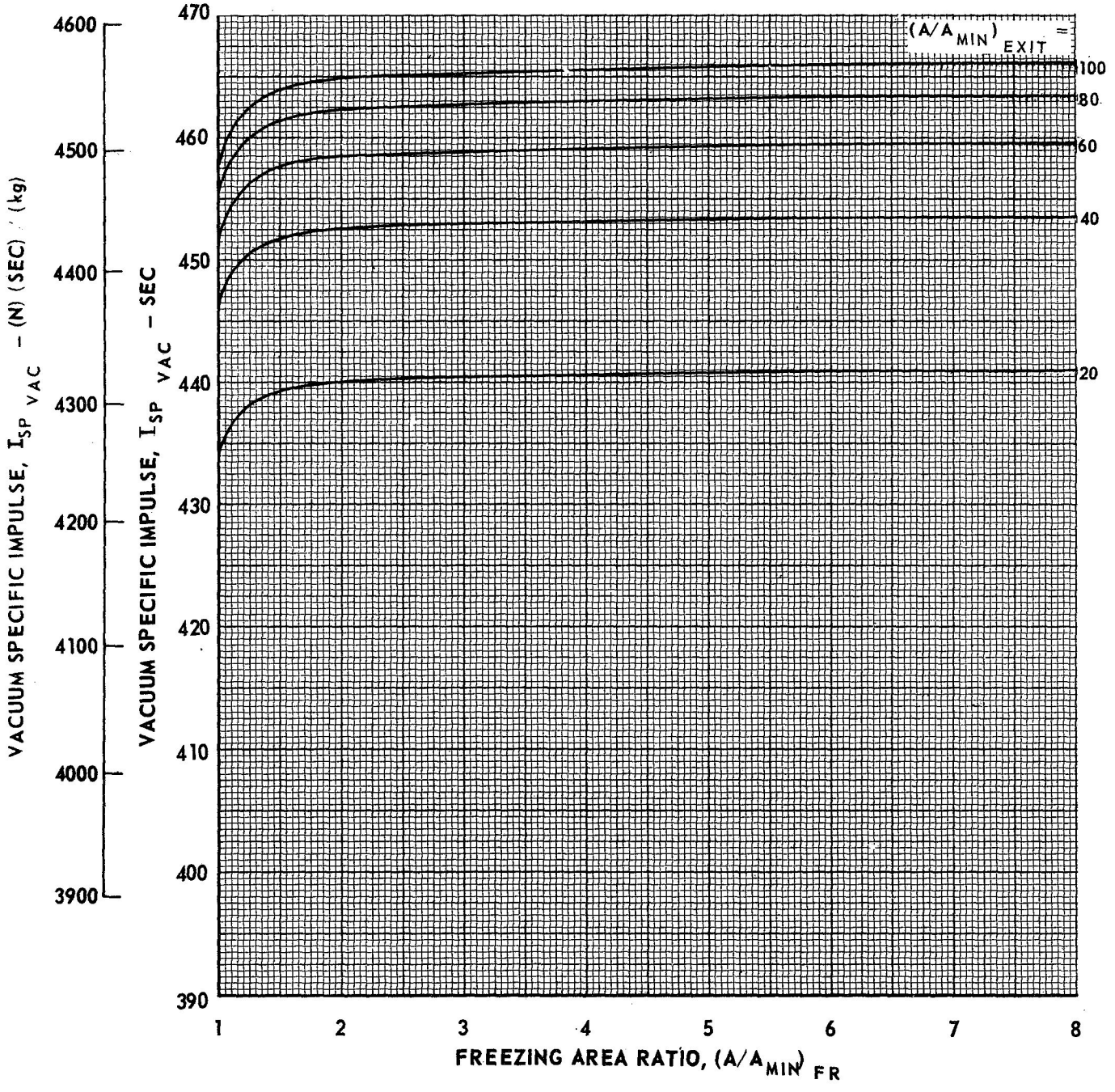

EFFECT OF FREEZING AREA RATIO ON NONEQUILIBRIUM PERFORMANCE FOR HYDROGEN-OXYGEN PROPELLANT SYSTEM

$H_2(\ell) - O_2(\ell)$

P_C = 100 PSIA (6.895X10^{5}N/m^2)

O/F = 6.00

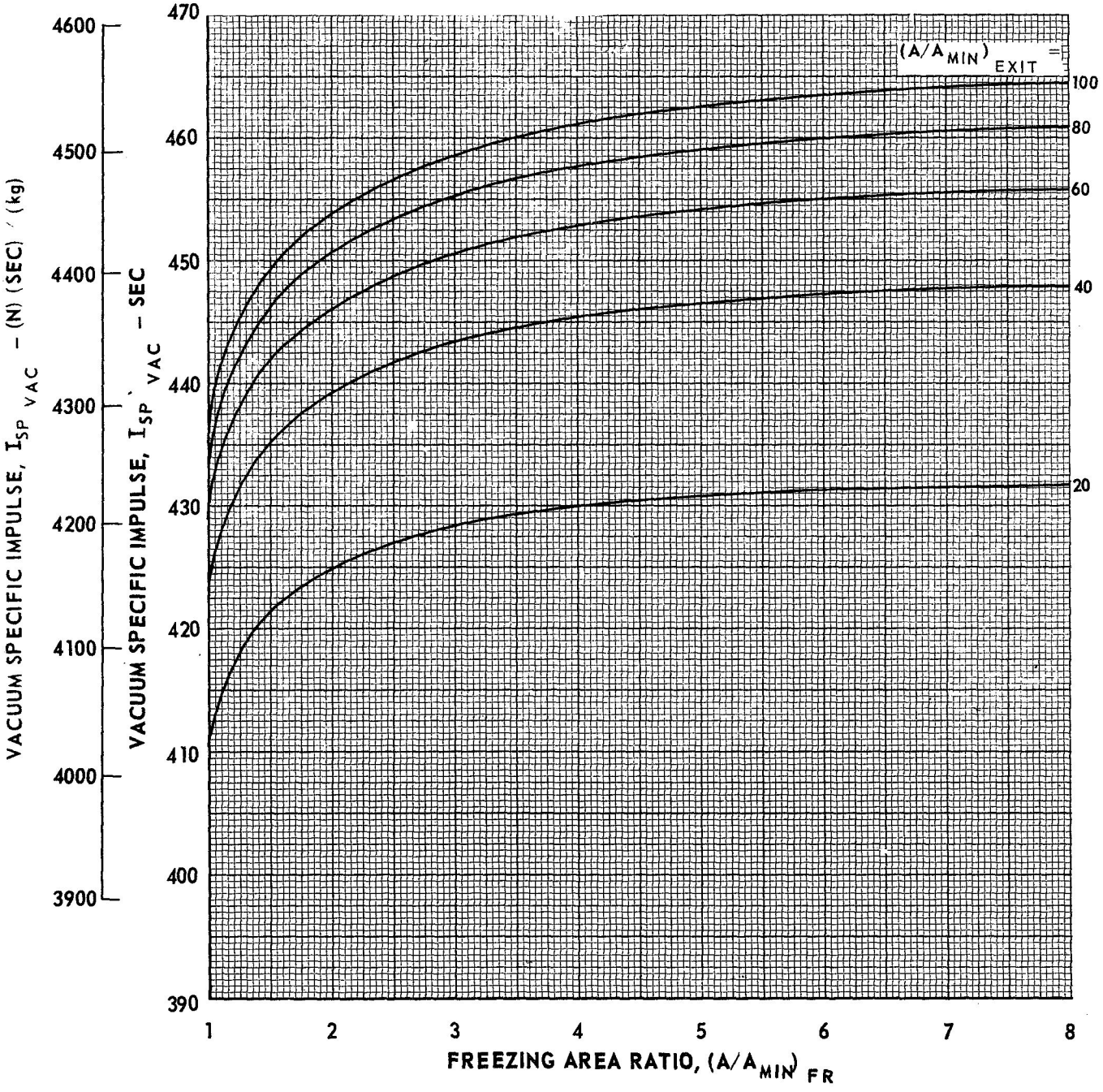

FIG. II-33

EFFECT OF FREEZING AREA RATIO ON NONEQUILIBRIUM PERFORMANCE FOR HYDROGEN-OXYGEN PROPELLANT SYSTEM

$H_2(\ell) - O_2(\ell)$

$P_C = 100$ PSIA ($6.895 \times 10^5 N/m^2$)

O/F = 8.00

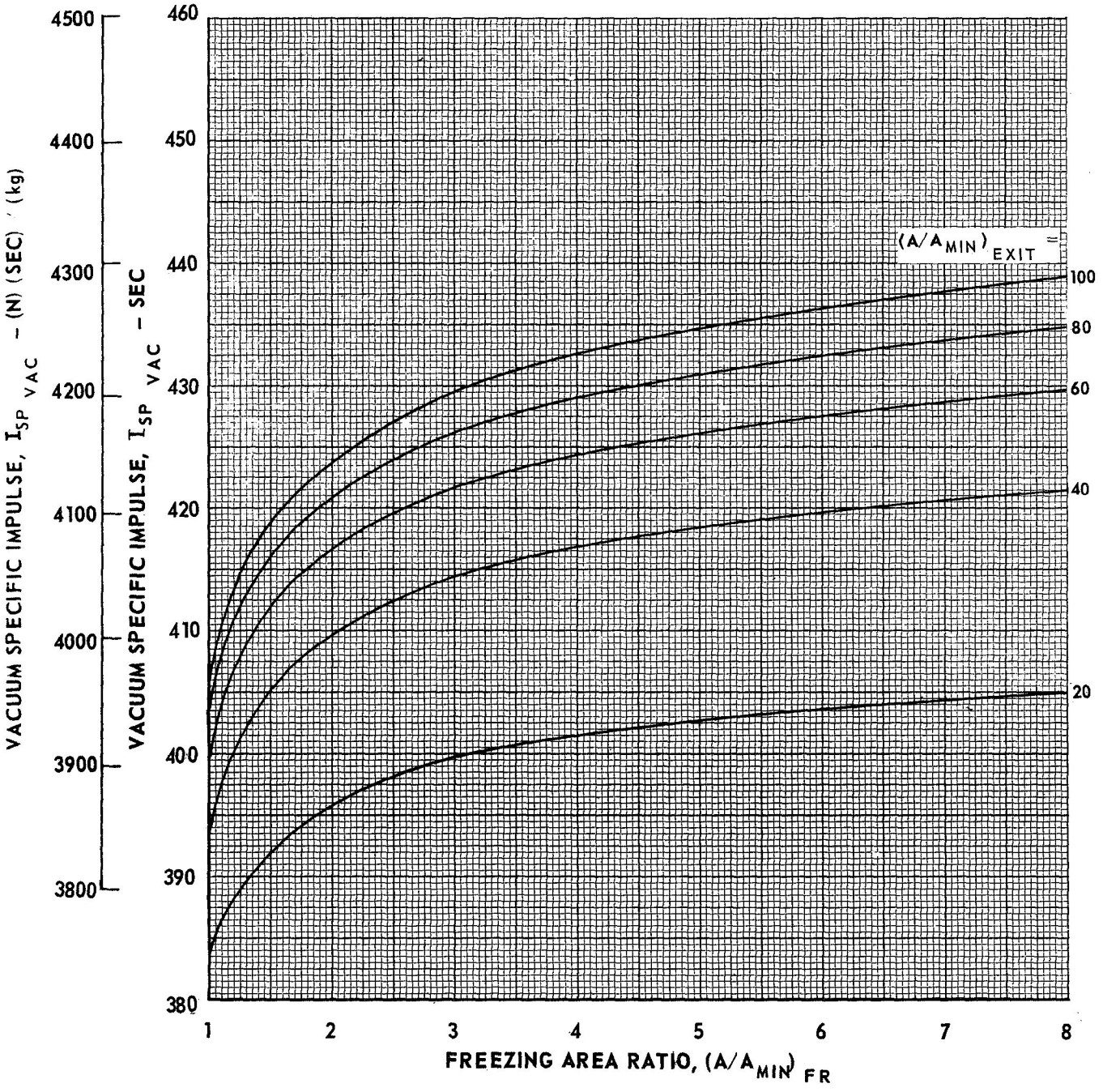

EFFECT OF FREEZING AREA RATIO ON NONEQUILIBRIUM PERFORMANCE FOR HYDROGEN-OXYGEN PROPELLANT SYSTEM

$H_2(\ell) - O_2(\ell)$

P_C = 200 PSIA (1.379X10^{6}N/m^2)

O/F = 4.00

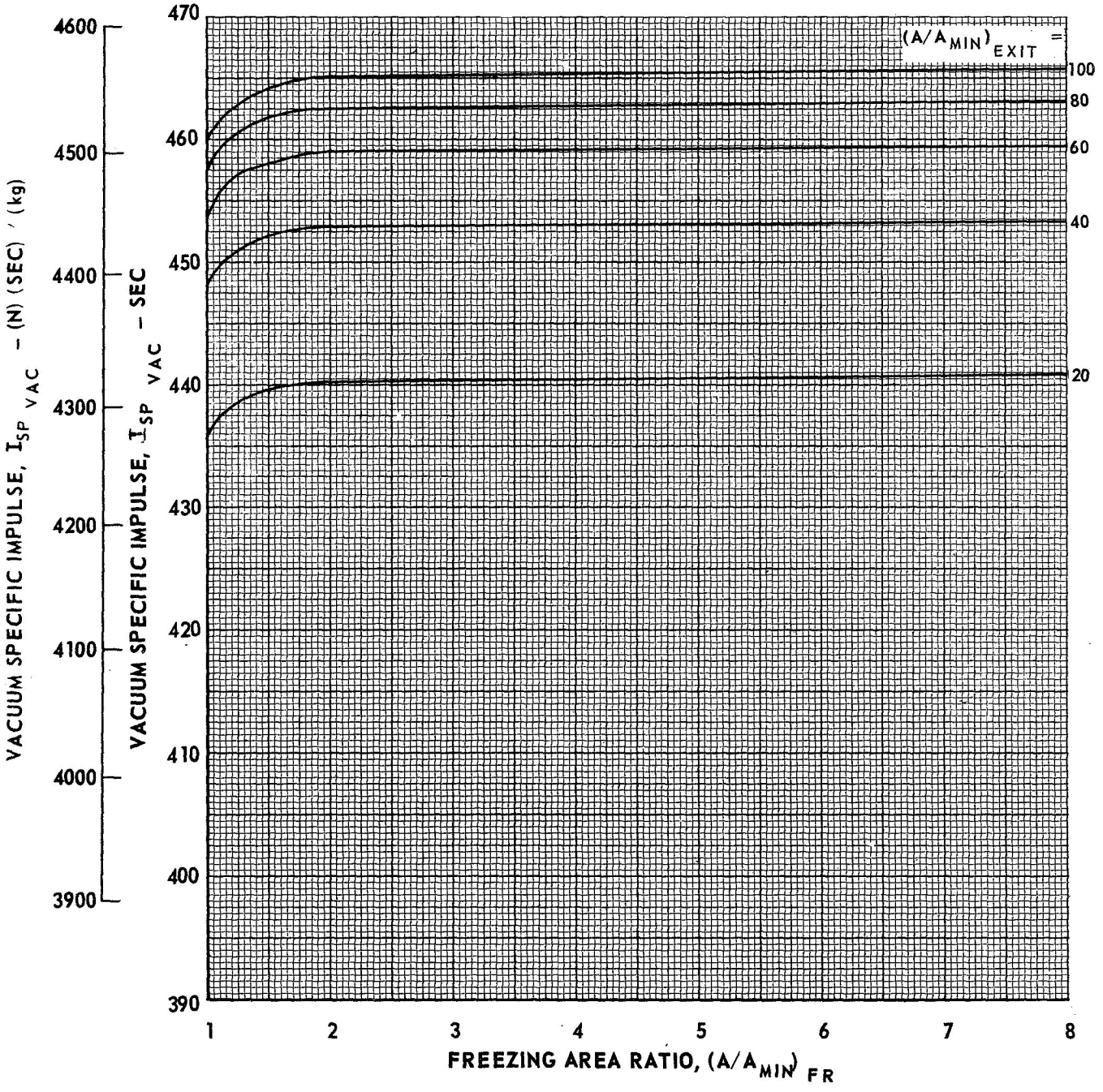

EFFECT OF FREEZING AREA RATIO ON NONEQUILIBRIUM PERFORMANCE FOR HYDROGEN-OXYGEN PROPELLANT SYSTEM

$H_2(\ell) - O_2(\ell)$

P_C = 200 PSIA ($1.379 \times 10^6 N/m^2$)

O/F = 6.00

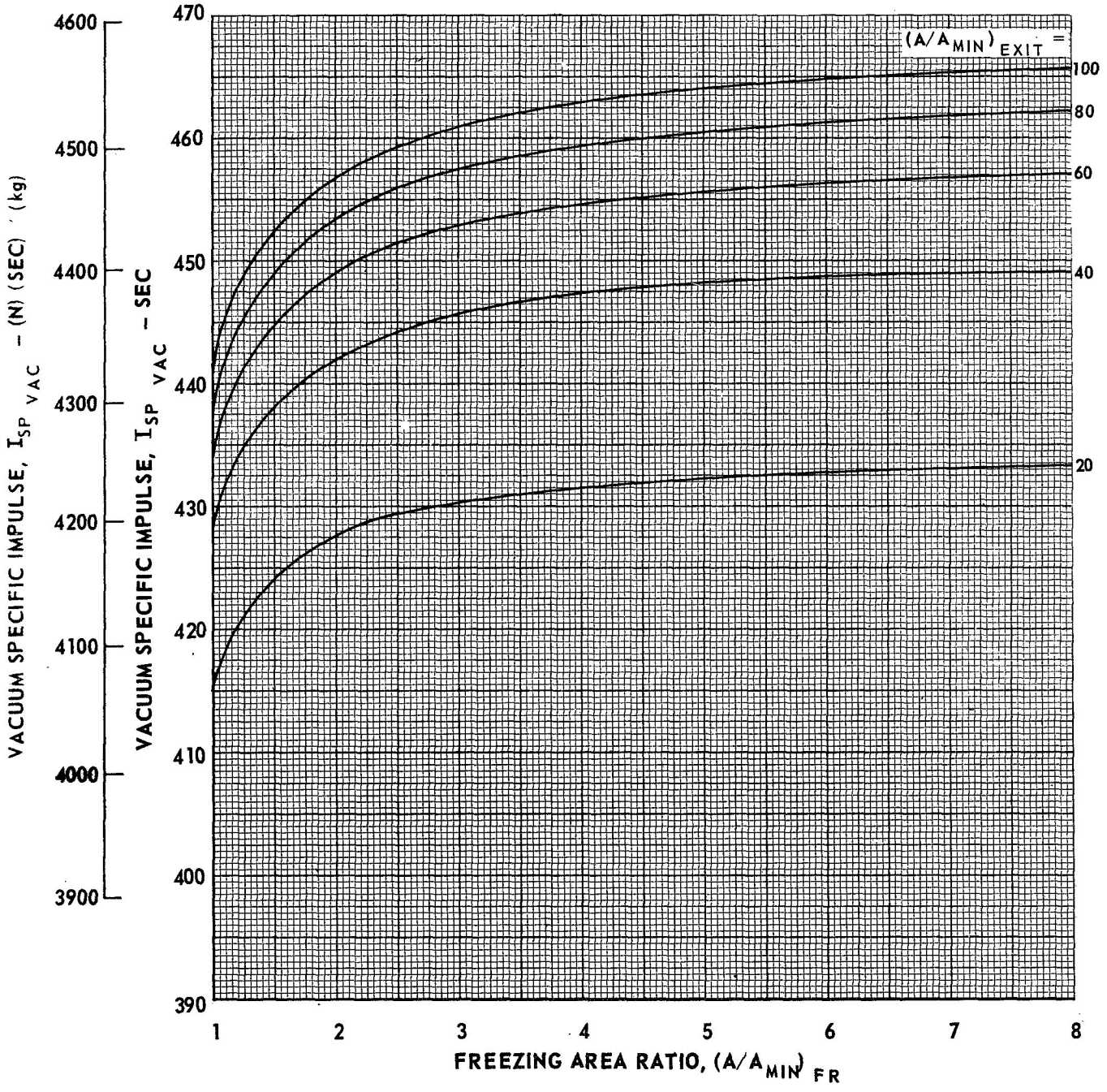

EFFECT OF FREEZING AREA RATIO ON NONEQUILIBRIUM PERFORMANCE FOR HYDROGEN-OXYGEN PROPELLANT SYSTEM

$H_2(\ell) - O_2(\ell)$

P_C = 200 PSIA, (1.379X10^{6}N/m^2)

O/F = 8.00

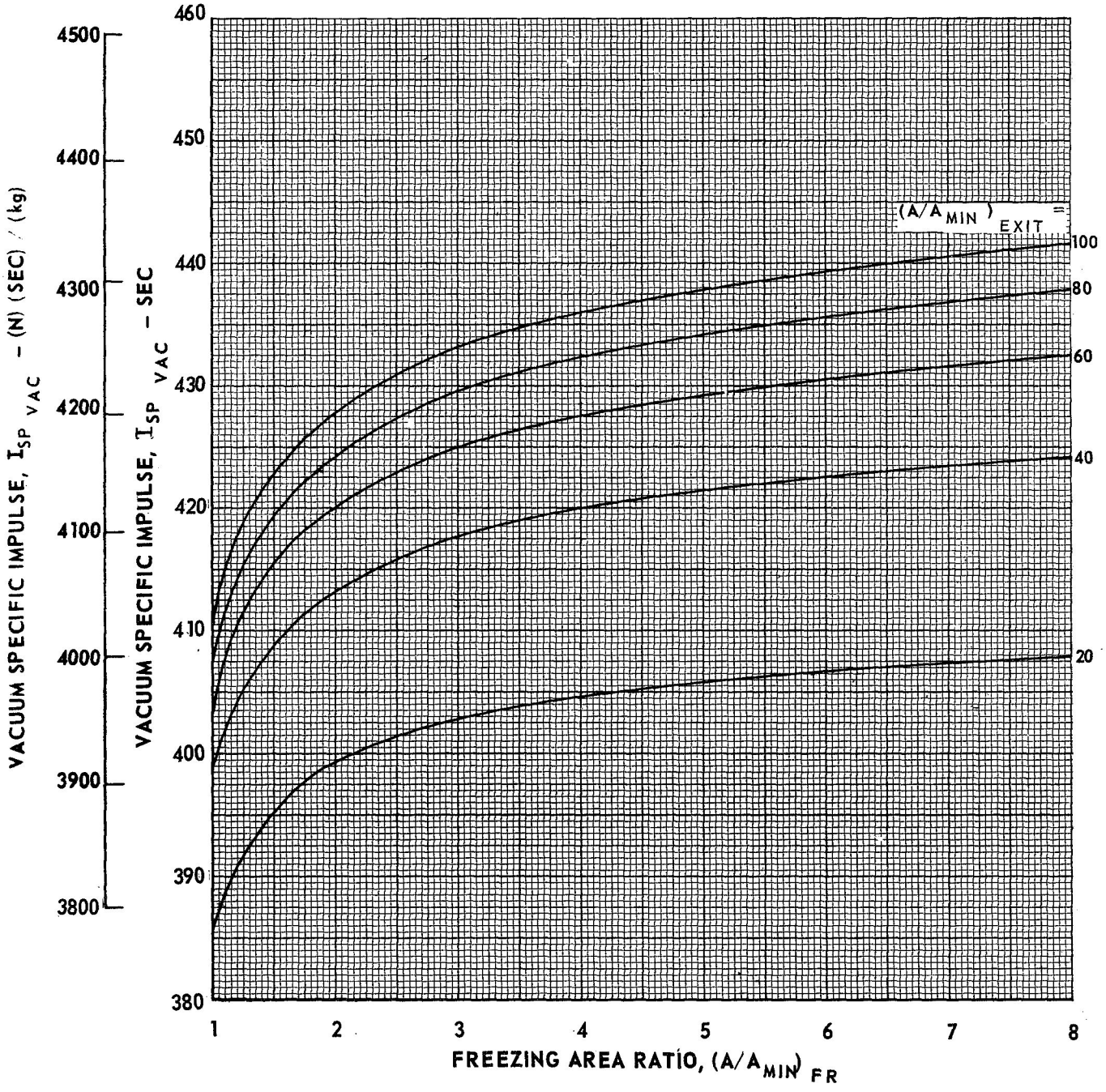

EFFECT OF FREEZING AREA RATIO ON NONEQUILIBRIUM PERFORMANCE FOR HYDROGEN-OXYGEN PROPELLANT SYSTEM

$H_2(\ell) - O_2(\ell)$

P_C = 300 PSIA (2.069X10^6 N/m^2)

O/F = 4.00

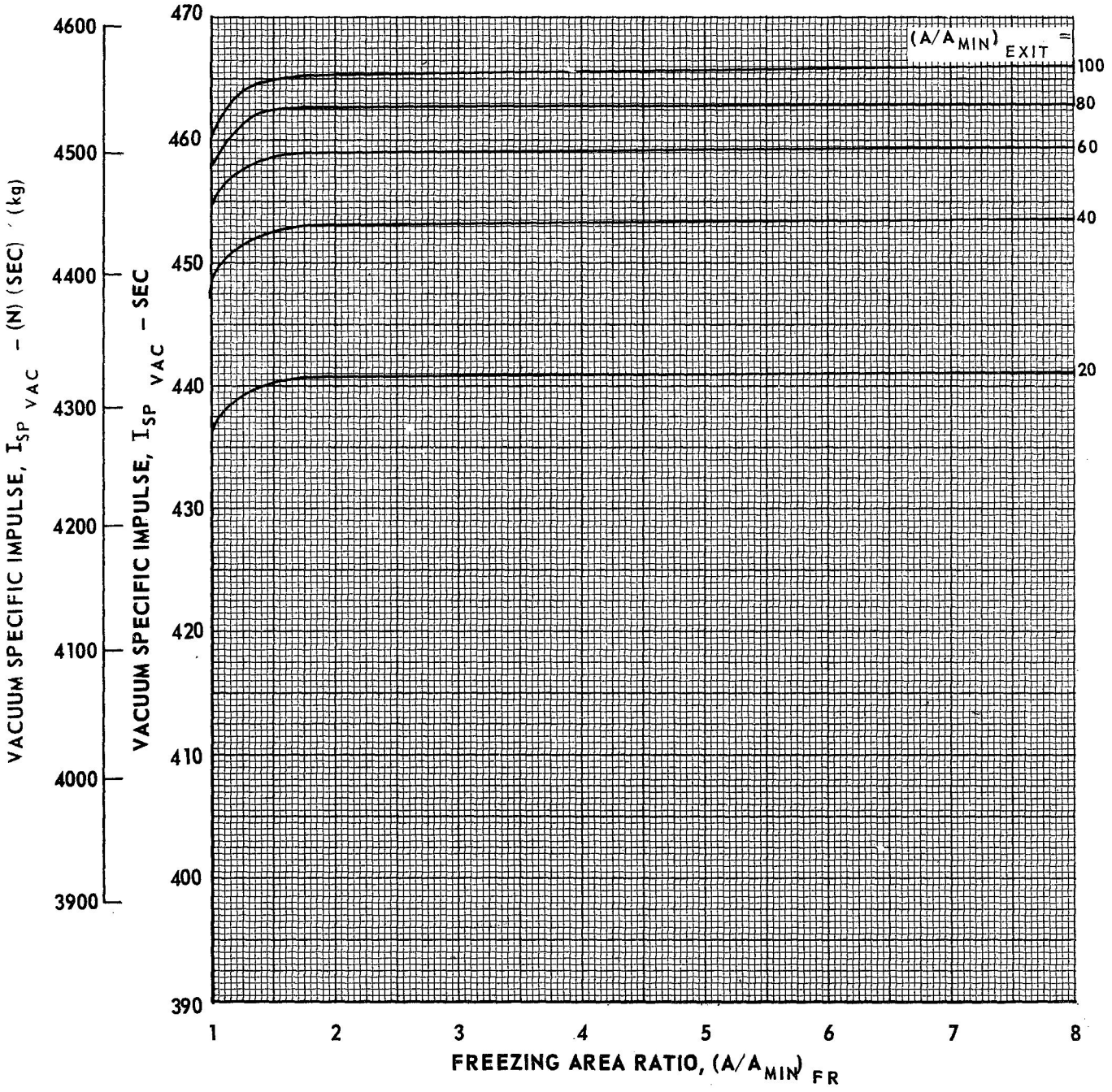

EFFECT OF FREEZING AREA RATIO ON NONEQUILIBRIUM PERFORMANCE FOR HYDROGEN-OXYGEN PROPELLANT SYSTEM

$H_2(\ell) - O_2(\ell)$

$P_C = 300$ PSIA $(2.069 \times 10^6 N/m^2)$

O/F = 6.00

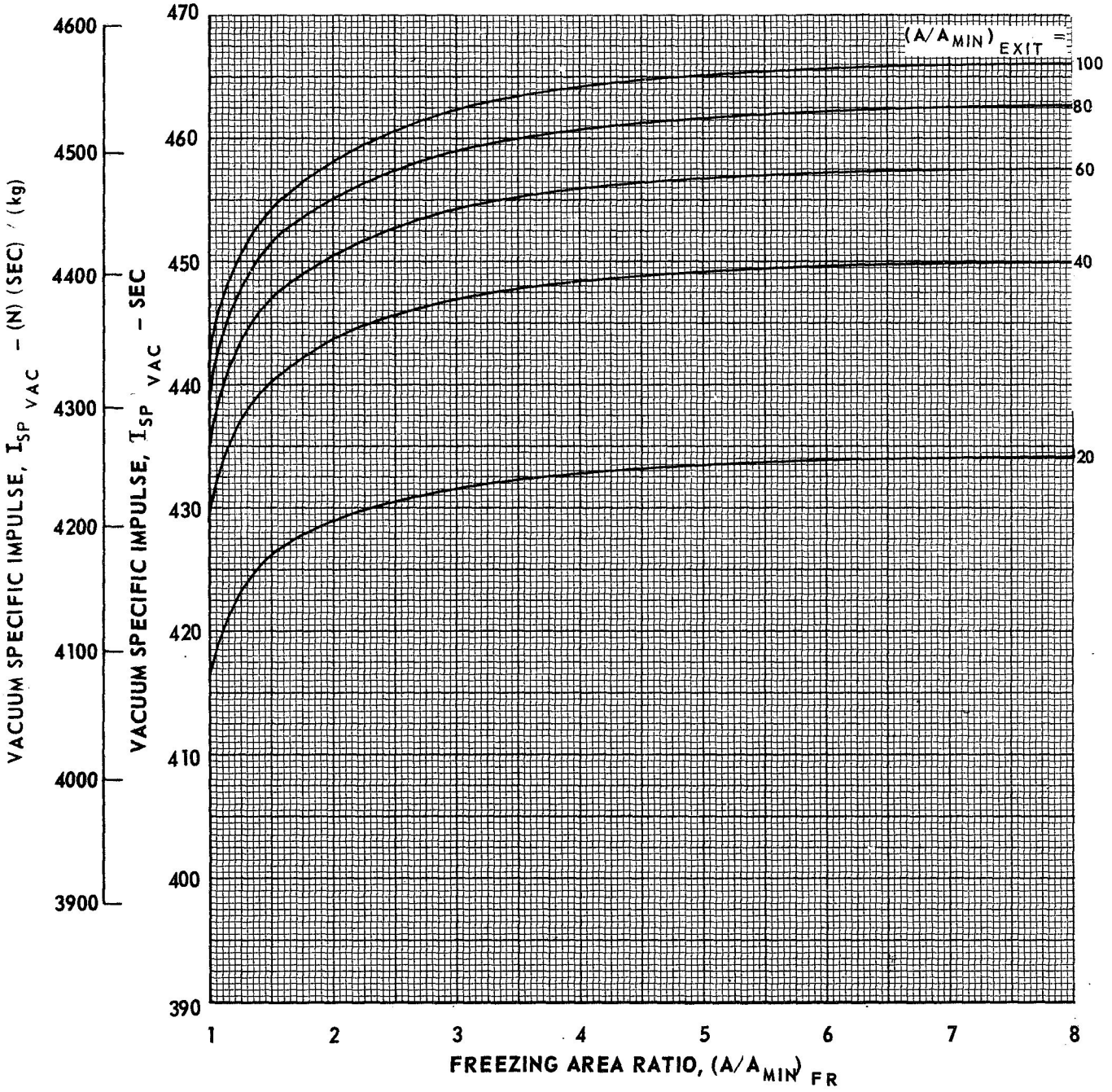

EFFECT OF FREEZING AREA RATIO ON NONEQUILIBRIUM PERFORMANCE FOR HYDROGEN-OXYGEN PROPELLANT SYSTEM

$H_2(\ell) - O_2(\ell)$

P_C = 300 PSIA (2.069X10^6 N/m^2)

O/F = 8.00

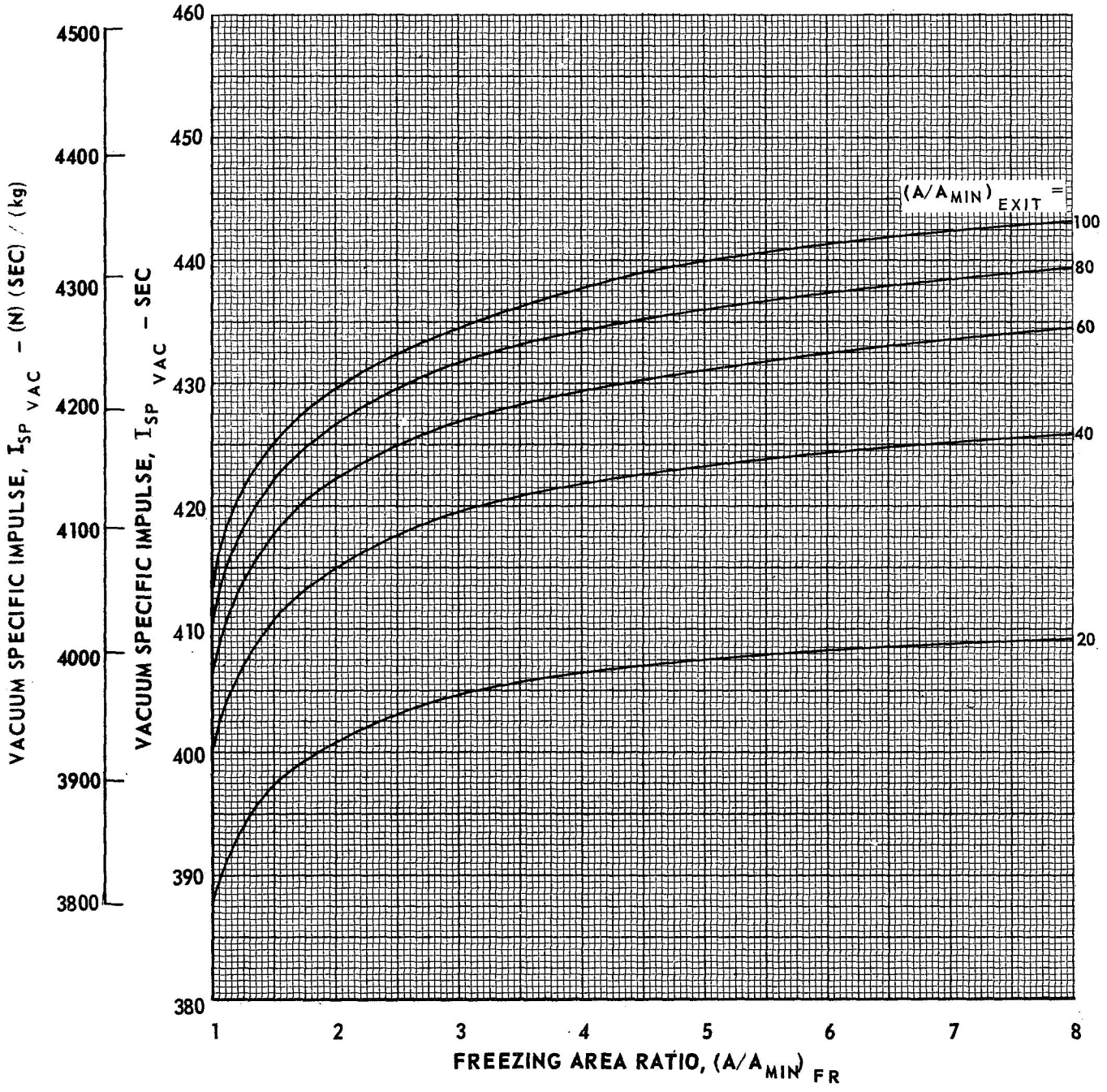

EFFECT OF FREEZING AREA RATIO ON NONEQUILIBRIUM PERFORMANCE FOR HYDROGEN-OXYGEN PROPELLANT SYSTEM

$H_2(\ell) - O_2(\ell)$

P_C = 500 PSIA (3.448X10^{6}N/m^2)

O/F = 4.00

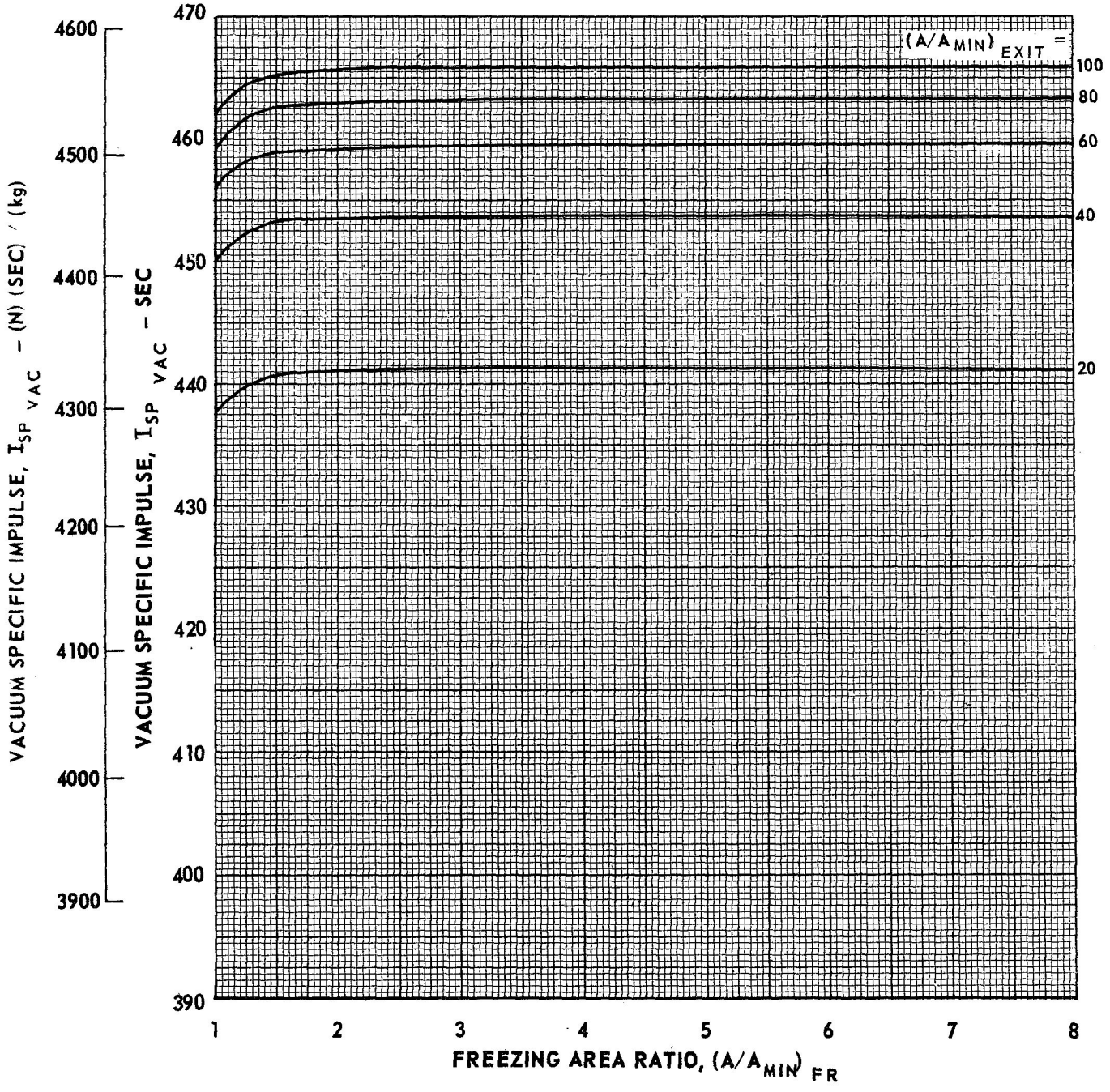

FIG. II-41

EFFECT OF FREEZING AREA RATIO ON NONEQUILIBRIUM PERFORMANCE FOR HYDROGEN-OXYGEN PROPELLANT SYSTEM

$H_2(\ell) - O_2(\ell)$

P_C = 500 PSIA (3.448X10^{6}N/m^2)

O/F = 6.00

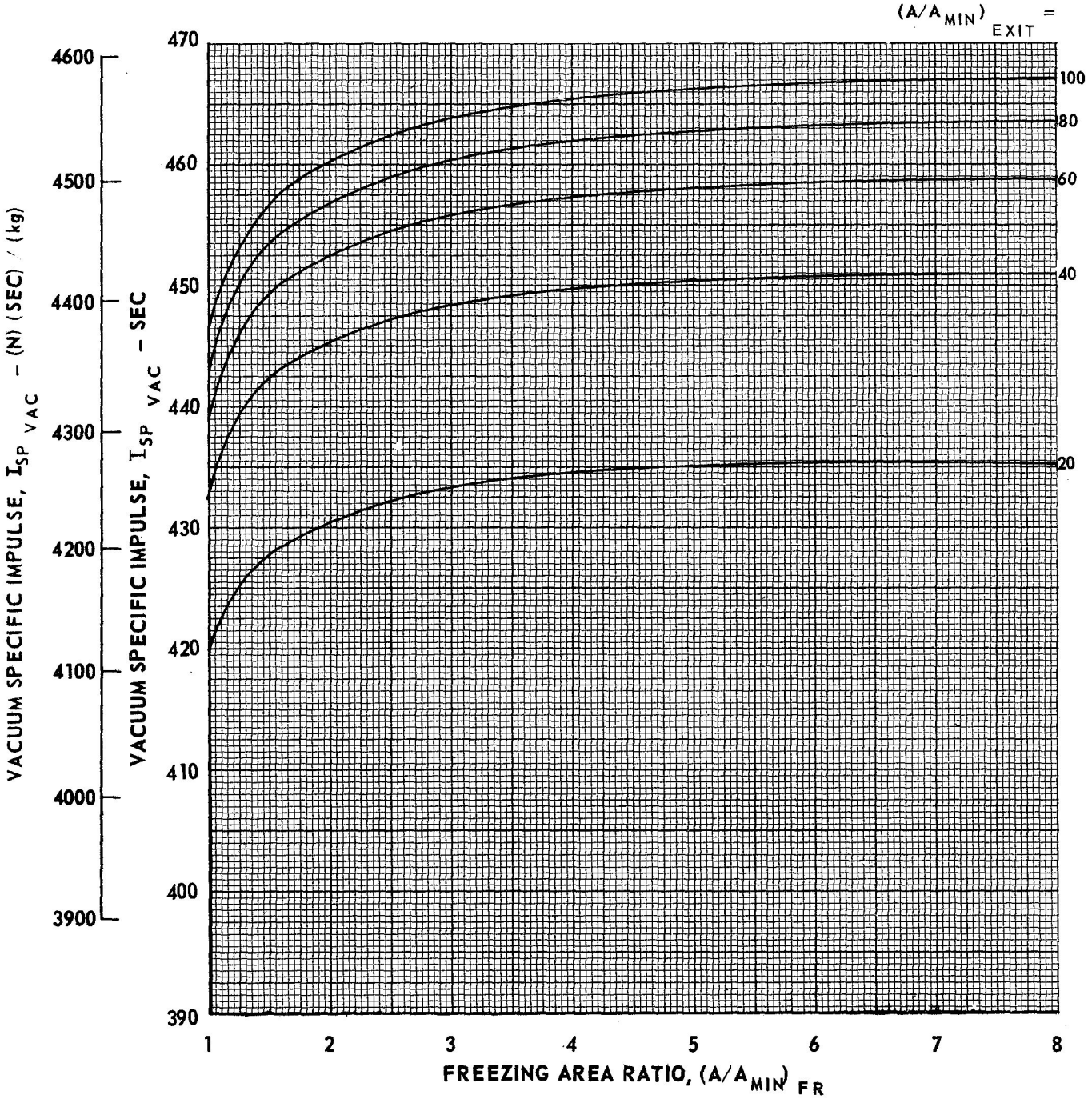

EFFECT OF FREEZING AREA RATIO ON NONEQUILIBRIUM PERFORMANCE FOR HYDROGEN-OXYGEN PROPELLANT SYSTEM

$H_2(\ell) - O_2(\ell)$

P_C = 500 PSIA ($3.448 \times 10^6 N/m^2$)

O/F = 8.00

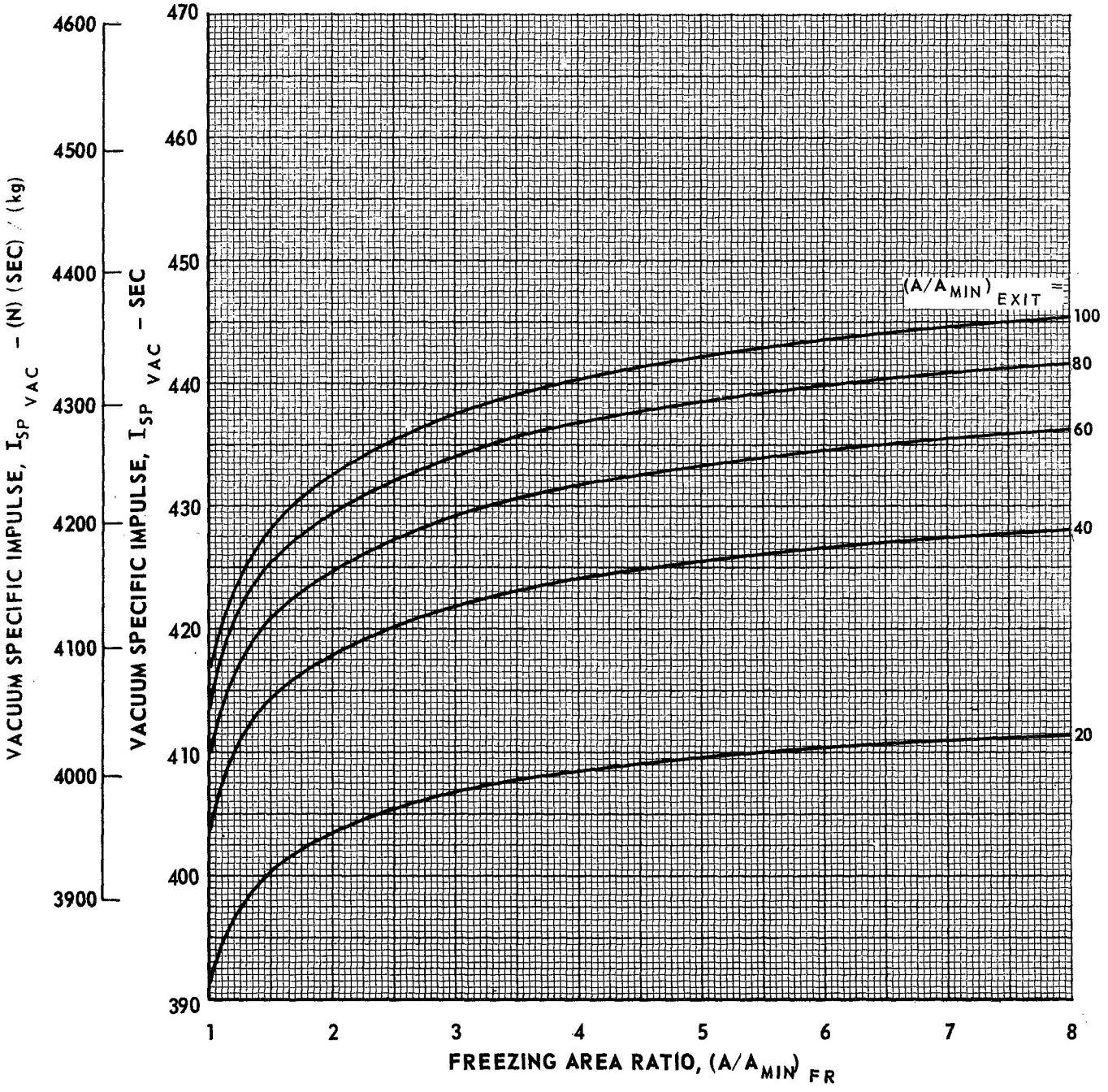

EFFECT OF FREEZING AREA RATIO ON NONEQUILIBRIUM PERFORMANCE FOR HYDROGEN-OXYGEN PROPELLANT SYSTEM

$H_2(\ell) - O_2(\ell)$

P_C = 750 PSIA (5.171X10^{6}N/m^2)

O/F = 4.00

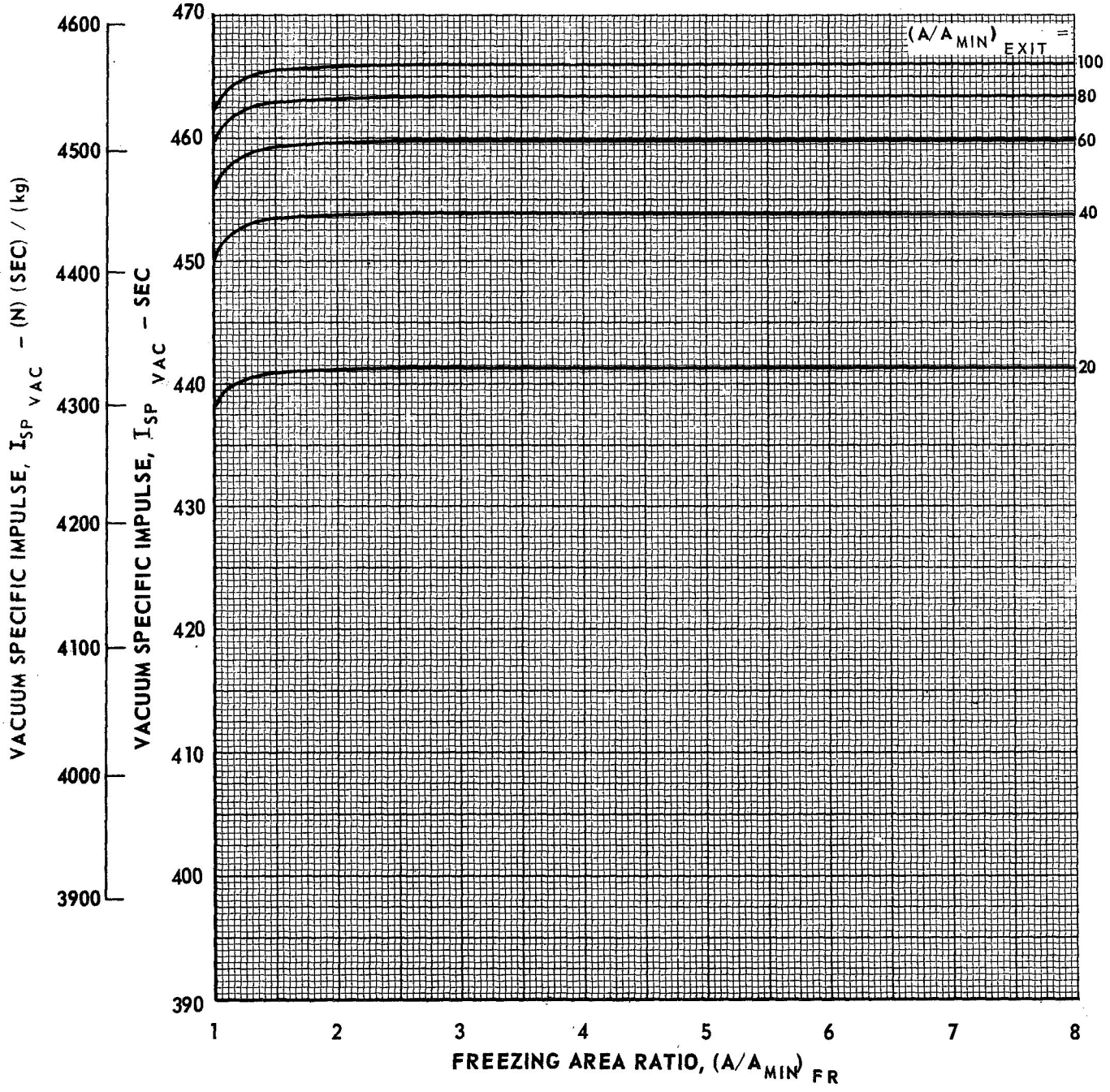

EFFECT OF FREEZING AREA RATIO ON NONEQUILIBRIUM PERFORMANCE FOR HYDROGEN-OXYGEN PROPELLANT SYSTEM

$H_2(\ell) - O_2(\ell)$

$P_C = 750$ PSIA $(5.171 \times 10^6 N/m^2)$

O/F = 6.00

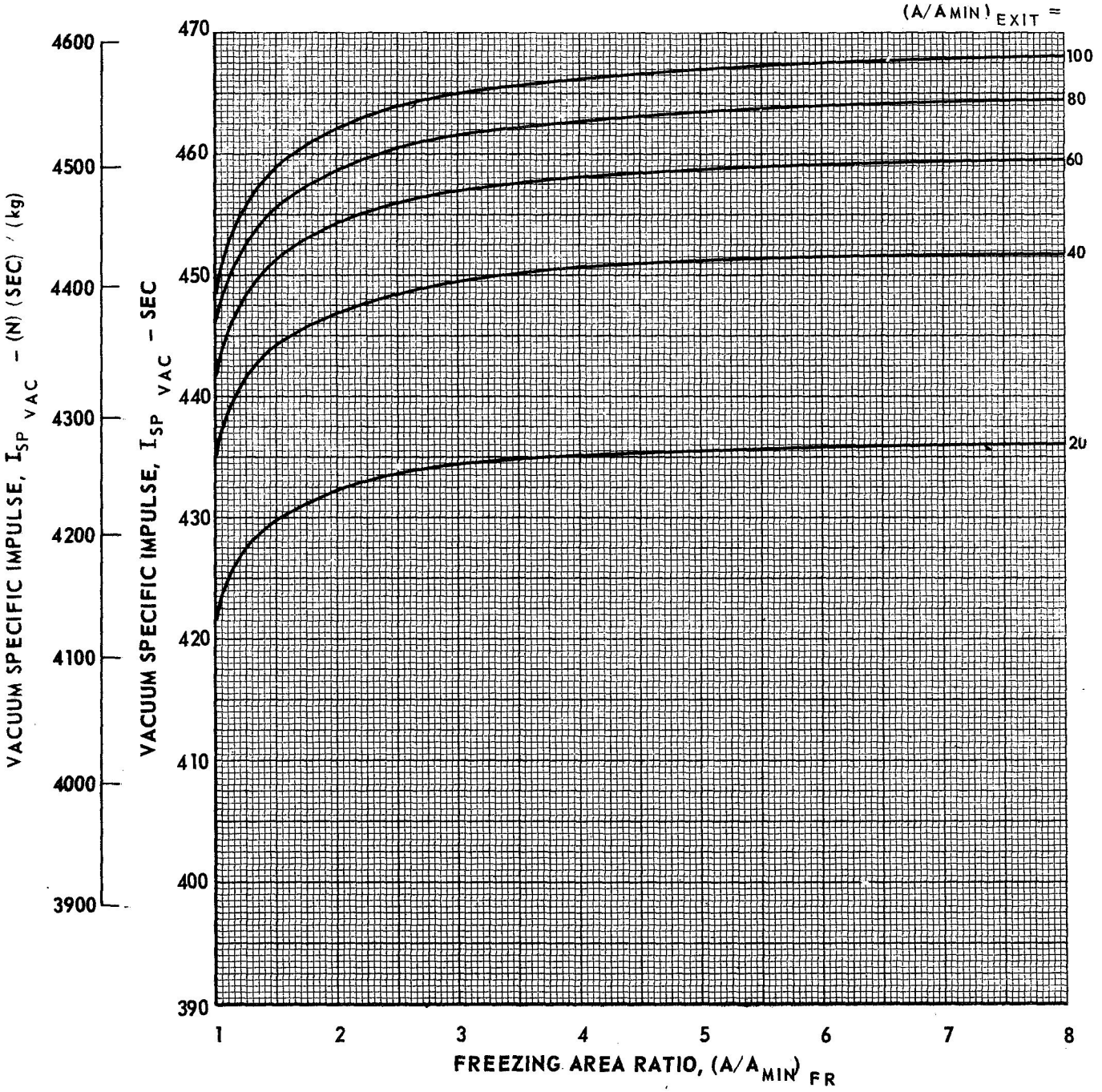

EFFECT OF FREEZING AREA RATIO ON NONEQUILIBRIUM PERFORMANCE FOR HYDROGEN-OXYGEN PROPELLANT SYSTEM

$H_2(\ell) - O_2(\ell)$

$P_C = 750$ PSIA $(5.171 \times 10^6 N/m^2)$

O/F = 8.00

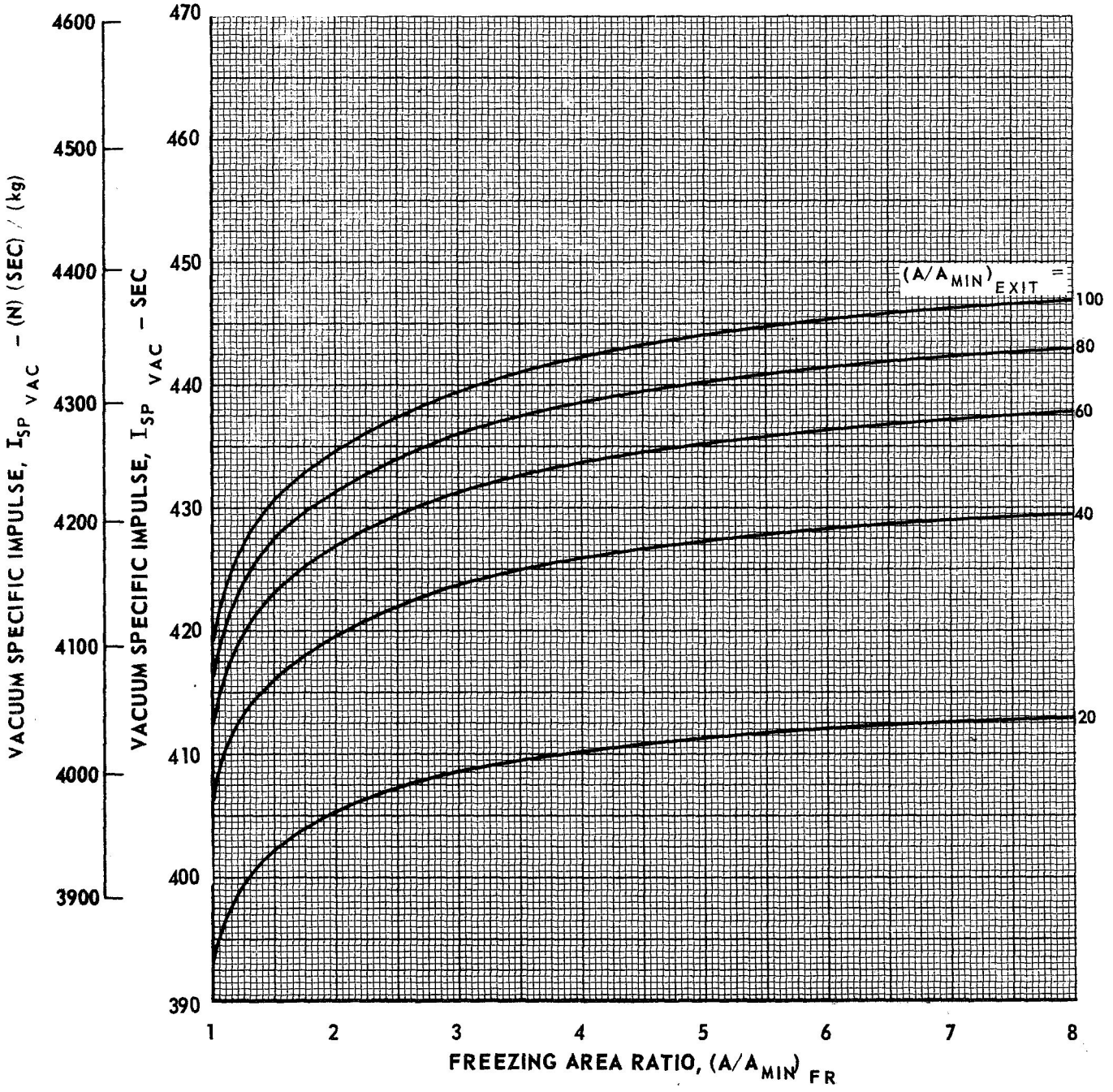

EFFECT OF FREEZING AREA RATIO ON NONEQUILIBRIUM PERFORMANCE FOR HYDROGEN-OXYGEN PROPELLANT SYSTEM

$H_2(\ell) - O_2(\ell)$

P_C = 1000 PSIA (6.895X10^{6}N/m^2)

O/F = 4.00

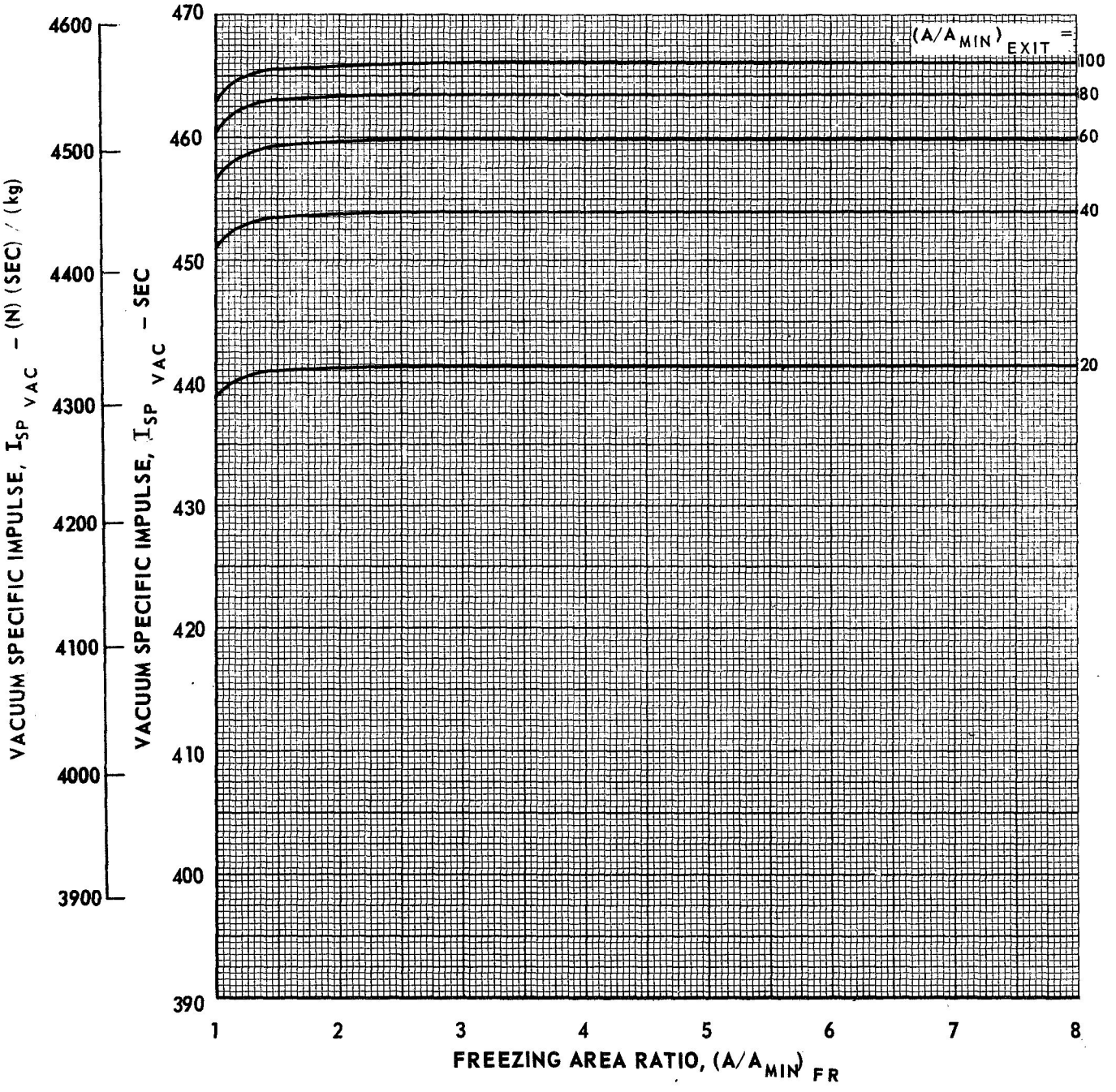

FIG. II-47

EFFECT OF FREEZING AREA RATIO ON NONEQUILIBRIUM PERFORMANCE FOR HYDROGEN-OXYGEN PROPELLANT SYSTEM

$H_2(\ell) - O_2(\ell)$

$P_C = 1000$ PSIA (6.895×10^6 N/m^2)

O/F = 6.00

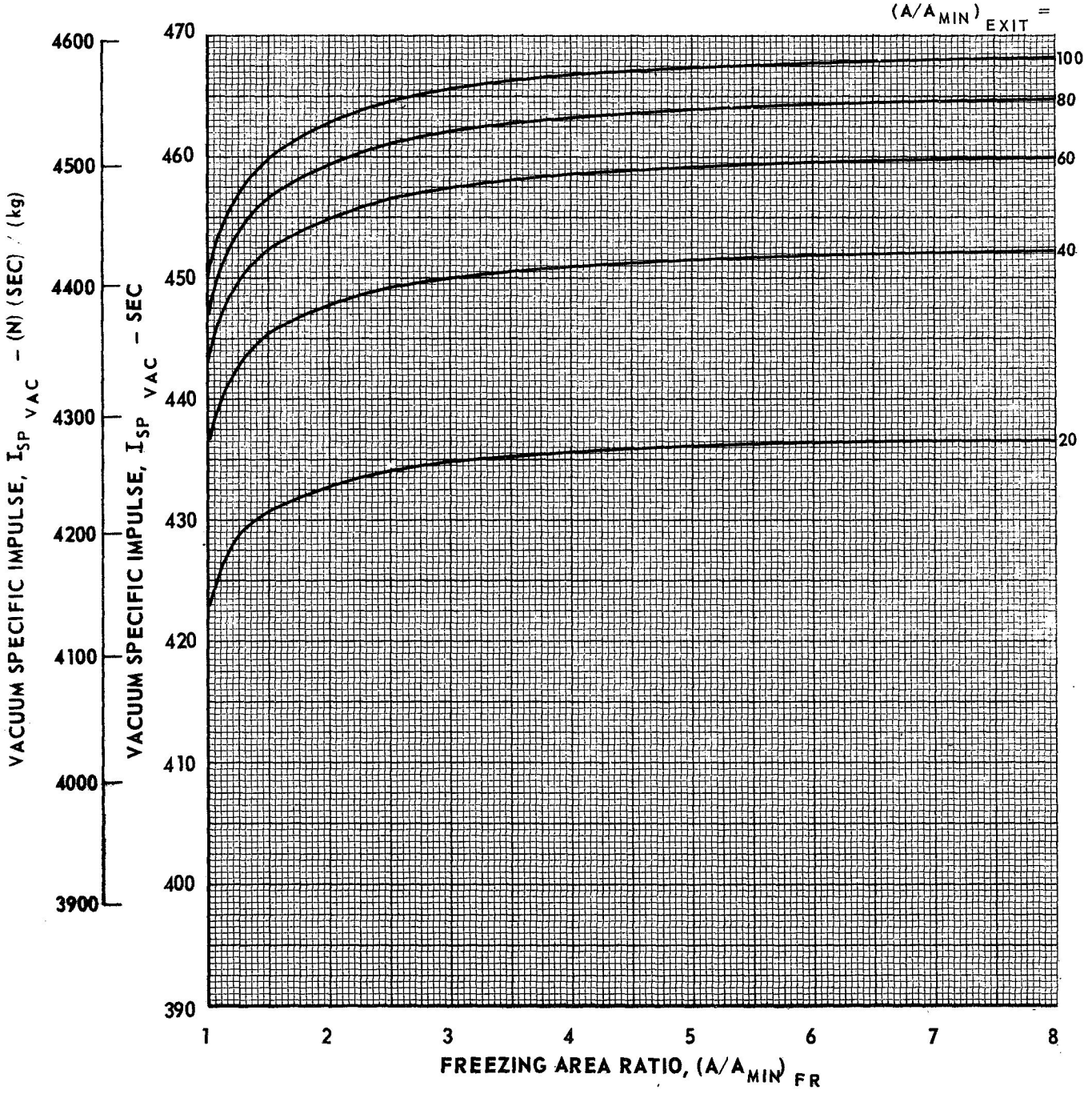

FIG. II-48

EFFECT OF FREEZING AREA RATIO ON NONEQUILIBRIUM PERFORMANCE FOR HYDROGEN-OXYGEN PROPELLANT SYSTEM

$H_2(\ell) - O_2(\ell)$

$P_C = 1000$ PSIA $(6.895 \times 10^6 N/m^2)$

O/F = 8.00

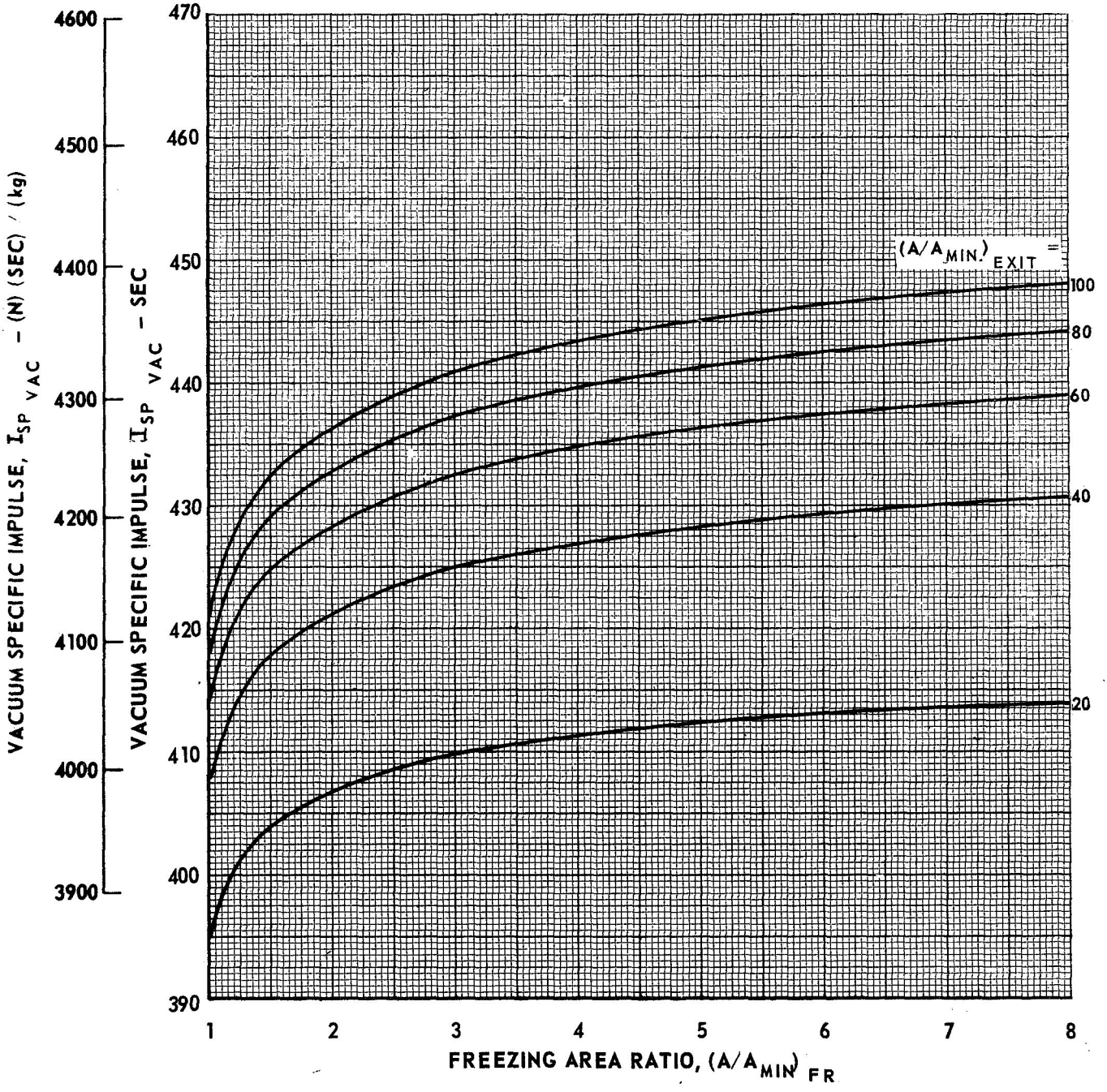

TABLE III-1
SUMMARY OF ELEMENTARY REACTIONS AND REACTION RATE CONSTANTS EMPLOYED IN CH_4 - FLOX RECOMBINATION MECHANISM

	REACTION			FORWARD RATE
	$H + H + H$	$\rightleftharpoons$	$H_2 + H$	$k_f = 4.62 \times 10^{-14} T^{-1}$
1	$H + H + H$	$\rightleftharpoons$	$H_2 + H$	$k_f = 20\,(4.62 \times 10^{-14} T^{-1})$
2	$H + H + H_2$	$\rightleftharpoons$	$H_2 + H_2$	$k_f = 2.5\,(4.62 \times 10^{-14} T^{-1})$
3	$H + H + HF$	$\rightleftharpoons$	$H_2 + HF$	$k_f = 2.5\,(4.62 \times 10^{-14} T^{-1})$
4	$H + H + CO_2$	$\rightleftharpoons$	$H_2 + CO_2$	$k_f = 2.0\,(4.62 \times 10^{-14} T^{-1})$
5	$H + H + CO$	$\rightleftharpoons$	$H_2 + CO$	$k_f = 2.0\,(4.62 \times 10^{-14} T^{-1})$
6	$H + H + H_2O$	$\rightleftharpoons$	$H_2 + H_2O$	$k_f = 2.5\,(4.62 \times 10^{-14} T^{-1})$
	$H + F + M$	$\rightleftharpoons$	$HF + M$	$k_f = 1.155 \times 10^{15} T^{-1}$
7	$H + F + H$	$\rightleftharpoons$	$HF + H$	$k_f = 1\,(1.155 \times 10^{15} T^{-1})$
8	$H + F + H_2$	$\rightleftharpoons$	$HF + H_2$	$k_f = 2.5\,(1.155 \times 10^{15} T^{-1})$
9	$H + F + HF$	$\rightleftharpoons$	$HF + HF$	$k_f = 2.5\,(1.155 \times 10^{15} T^{-1})$
10	$H + F + CO_2$	$\rightleftharpoons$	$HF + CO_2$	$k_f = 2.0\,(1.155 \times 10^{15} T^{-1})$
11	$H + F + CO$	$\rightleftharpoons$	$HF + CO$	$k_f = 2.0\,(1.155 \times 10^{15} T^{-1})$
12	$H + F + H_2O$	$\rightleftharpoons$	$HF + H_2O$	$k_f = 2.5\,(1.155 \times 10^{15} T^{-1})$
	$H + OH + M$	$\rightleftharpoons$	$H_2O + M$	$k_f = 7.85 \times 10^{15} T^{-1}$
13	$H + OH + H$	$\rightleftharpoons$	$H_2O + H$	$k_f = 3\,(7.85 \times 10^{15} T^{-1})$
14	$H + OH + H_2$	$\rightleftharpoons$	$H_2O + H_2$	$k_f = 3\,(7.85 \times 10^{15} T^{-1})$
15	$H + OH + HF$	$\rightleftharpoons$	$H_2O + HF$	$k_f = 3\,(7.85 \times 10^{15} T^{-1})$
16	$H + OH + CO_2$	$\rightleftharpoons$	$H_2O + CO_2$	$k_f = 10\,(7.85 \times 10^{15} T^{-1})$
17	$H + OH + CO$	$\rightleftharpoons$	$H_2O + CO$	$k_f = 3\,(7.85 \times 10^{15} T^{-1})$
18	$H + OH + H_2O$	$\rightleftharpoons$	$H_2O + H_2O$	$k_f = 20\,(7.85 \times 10^{15} T^{-1})$

NOTE: ALL RATES ARE EXPRESSED IN TERMS OF LB-MOLES, FT^3, SEC; AND T IS IN $^\circ R$

TO CONVERT TO kg-MOLES, m^3, SEC, AND T IN $^\circ K$; MULTIPLY ABOVE RATE BY 2.165×10^{-3}

TABLE III-2

EQUILIBRIUM AND FROZEN FLOW PROPERTIES AT NOZZLE THROAT

CH_4 - FLOX (82.6% F_2)

	P_c - psia	OXIDIZER - FUEL WEIGHT RATIO						
		3.5	4.0	4.5	5.0	5.5	6.0	6.5
Equilibrium Mass Flow - W/A $\frac{Lbm}{Ft^2.Sec}$	100	68.9	70.0	70.5	67.0	66.7	67.1	68.0
	200	137.2	138.9	139.8	132.7	132.0	---	134.6
	300	205.5	207.4	---	197.9	196.9	198.0	200.8
	500	342.0	343.9	345.8	327.7	325.9	327.7	332.4
	750	512.9	513.9	516.5	489.1	486.2	488.8	496.0
	1000	682.5	667.7	---	649.9	645.8	649.2	659.0
Frozen Mass Flow - W/A $\frac{Lbm}{Ft^2.Sec}$	100	72.1	71.2	70.6	70.3	70.2	70.7	71.6
	200	142.8	140.9	139.6	138.9	138.6	---	141.4
	300	213.0	210.0	208.0	206.8	206.4	207.8	210.6
	500	352.6	347.3	343.8	341.6	340.8	343.0	347.8
	750	526.3	517.9	512.4	508.9	507.5	510.7	517.9
	1000	699.3	687.8	680.2	675.3	673.2	677.4	687.1
Frozen Specific Heat Ratio γ_{FR}	100	1.29	1.30	1.31	1.32	1.33	1.33	1.34
	200	1.28	1.30	1.31	1.32	1.32	---	1.33
	300	1.28	1.29	1.30	1.31	1.32	1.33	1.33
	500	1.28	1.29	1.30	1.31	1.32	1.32	1.33
	750	1.28	1.29	1.30	1.31	1.32	1.32	1.32
	1000	1.28	1.29	1.30	1.30	1.31	1.32	1.32

NOTE: P_c (psia) x $6.895 \times 10^3 = P_c$ (N/m^2)

Mass Flow $\left(\frac{Lbm}{Ft^2.sec} \right) \times 4.883 =$ Mass Flow $\left(\frac{kg}{m^2\ sec} \right)$

FIG. III-1

VARIATION OF EQUILIBRIUM VACUUM SPECIFIC IMPULSE WITH AREA RATIO

CH_4 - FLOX (82.6% F_2)

P_C = 100 PSIA (6.895 X 10^5 N/m^2)

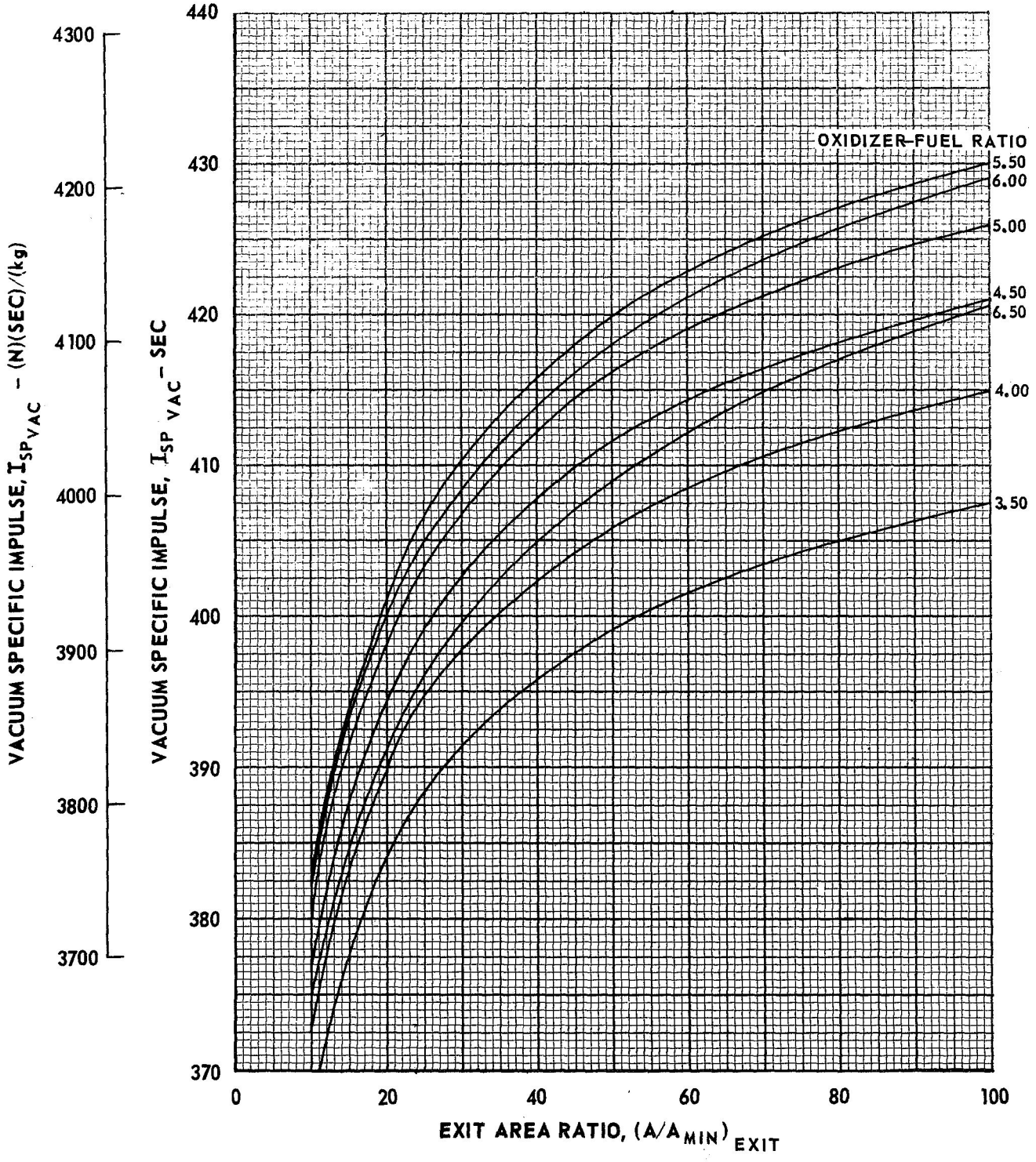

FIG. III-2

VARIATION OF FROZEN VACUUM SPECIFIC IMPULSE WITH AREA RATIO

CH_4 - FLOX (82.6% F_2)

P_C = 100 PSIA (6.895 X 10^5 N/m^2)

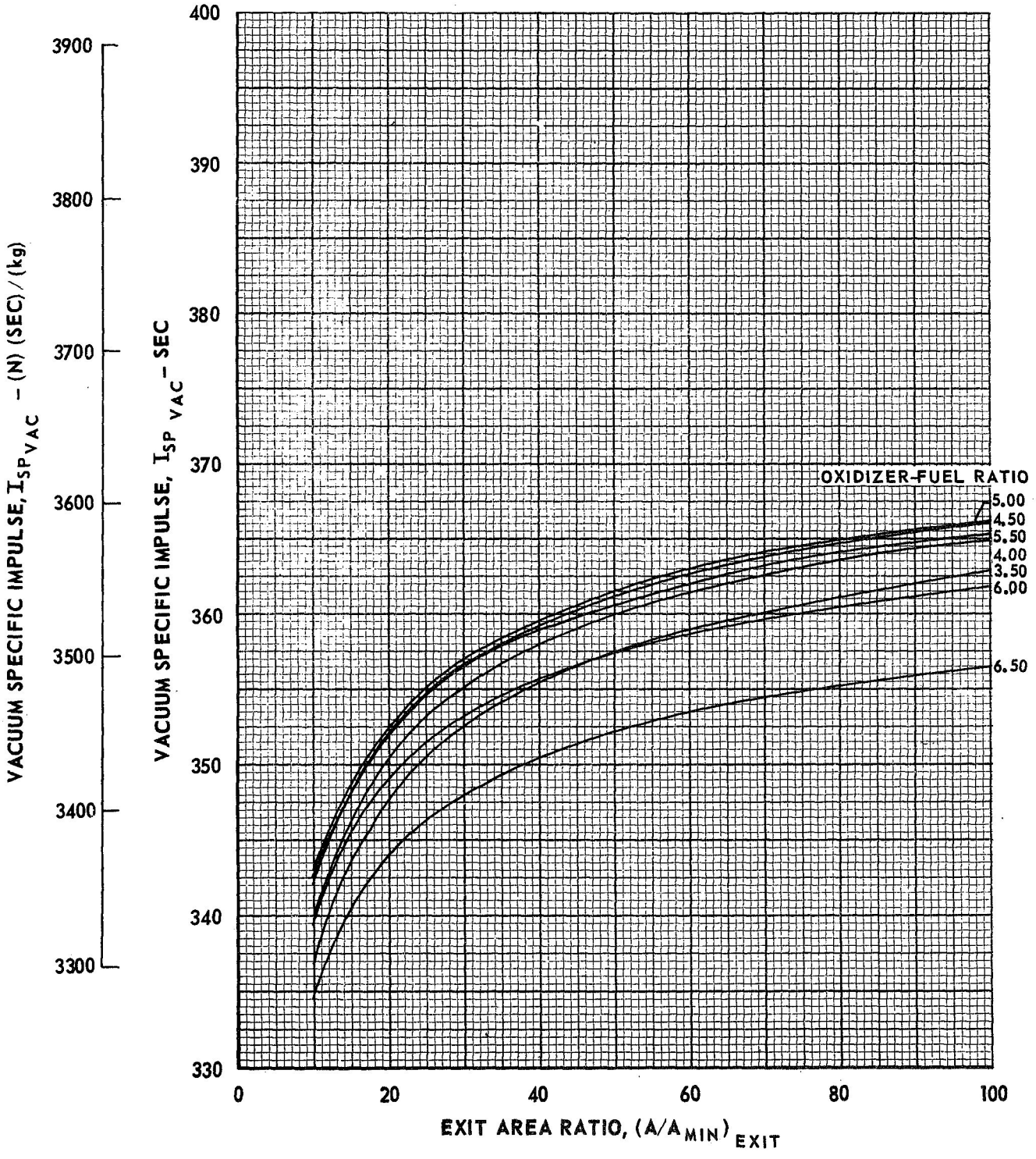

FIG. III-3

VARIATION OF EQUILIBRIUM VACUUM SPECIFIC IMPULSE WITH AREA RATIO

CH_4 - FLOX (82.6% F_2)

P_C = 200 PSIA (1.379 X 10^6 N/m^2)

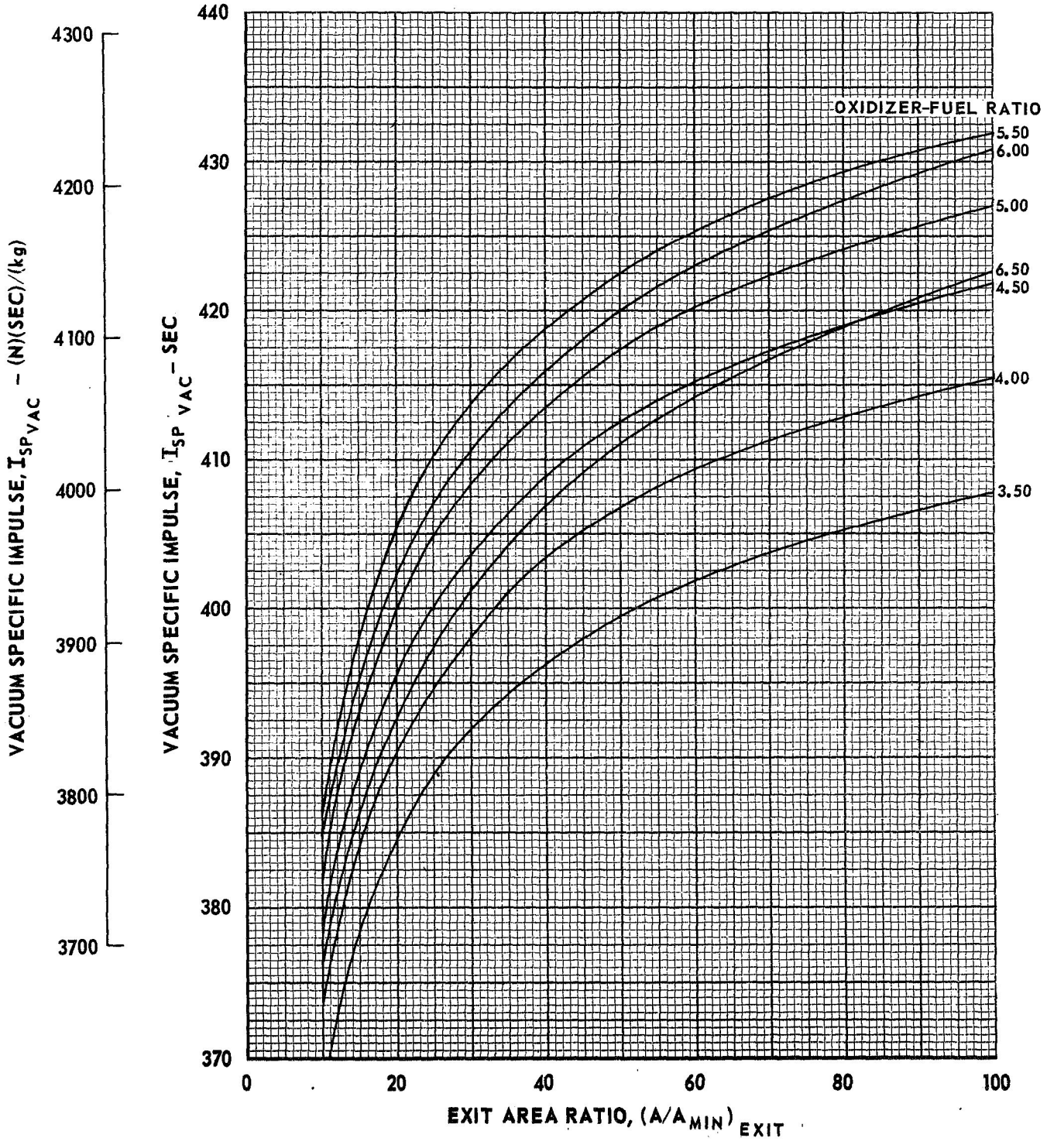

FIG. III-4

VARIATION OF FROZEN VACUUM SPECIFIC IMPULSE WITH AREA RATIO

CH_4 - FLOX (82.6% F_2)

P_C = 200 PSIA (1.379 X 10^6 N/m^2)

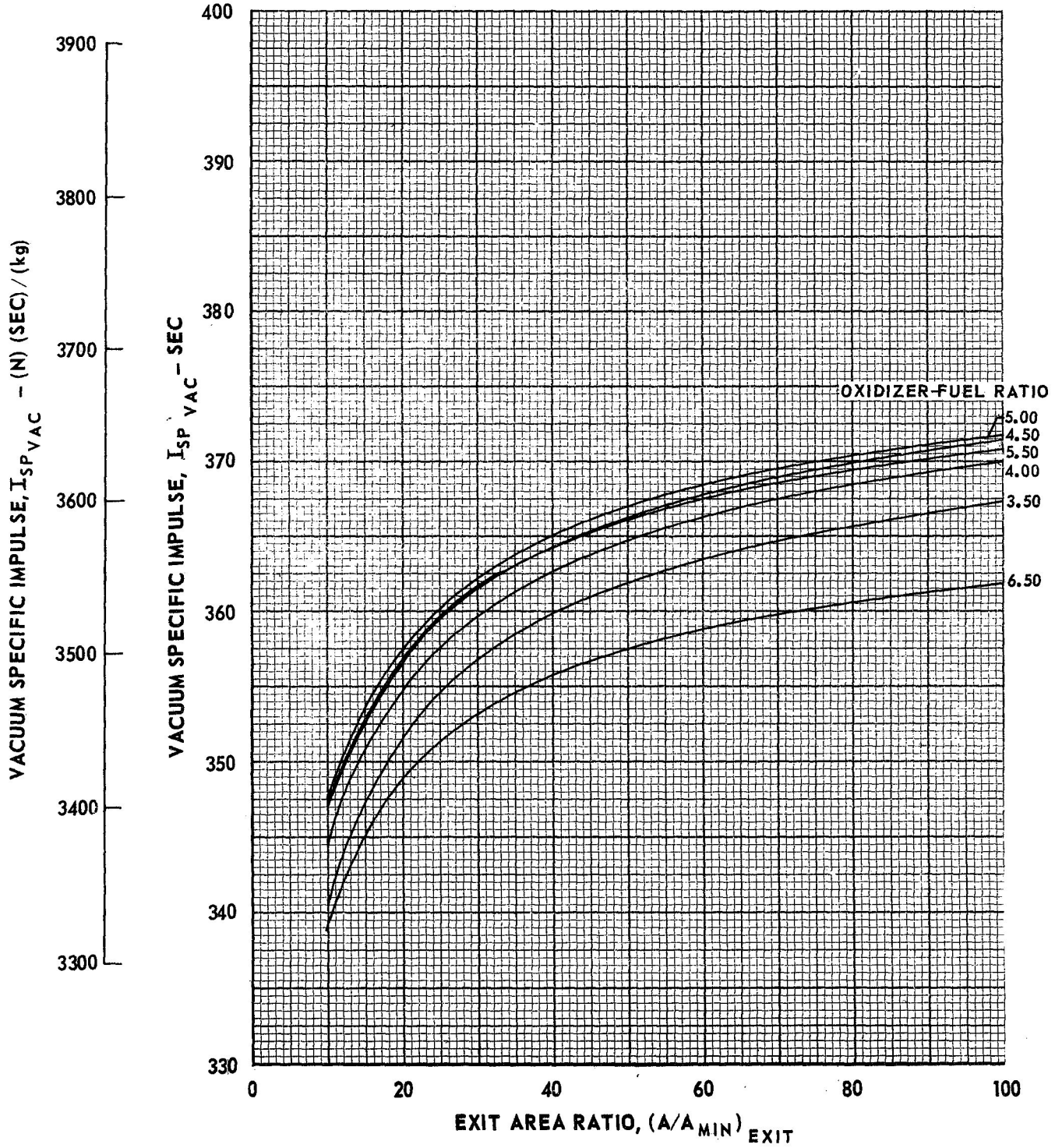

FIG. III–5

VARIATION OF EQUILIBRIUM VACUUM SPECIFIC IMPULSE WITH AREA RATIO

CH_4 – FLOX (82.6% F_2)

P_C = 300 PSIA (2.069 X 10^6 N/m^2)

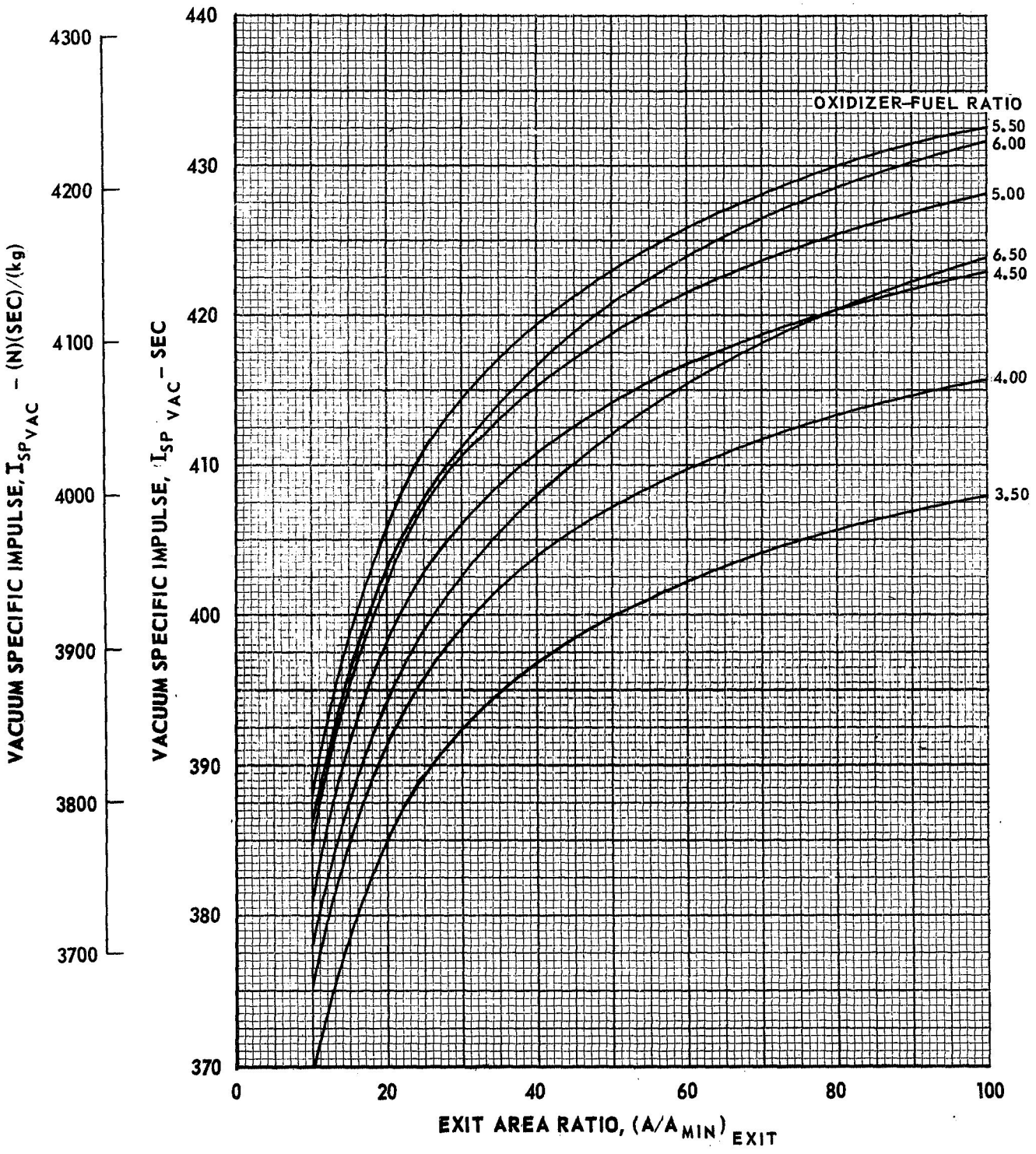

FIG. III-6

VARIATION OF FROZEN VACUUM SPECIFIC IMPULSE WITH AREA RATIO

CH_4 - FLOX (82.6% F_2)

P_C = 300 PSIA (2.069 X 10^6 N/m^2)

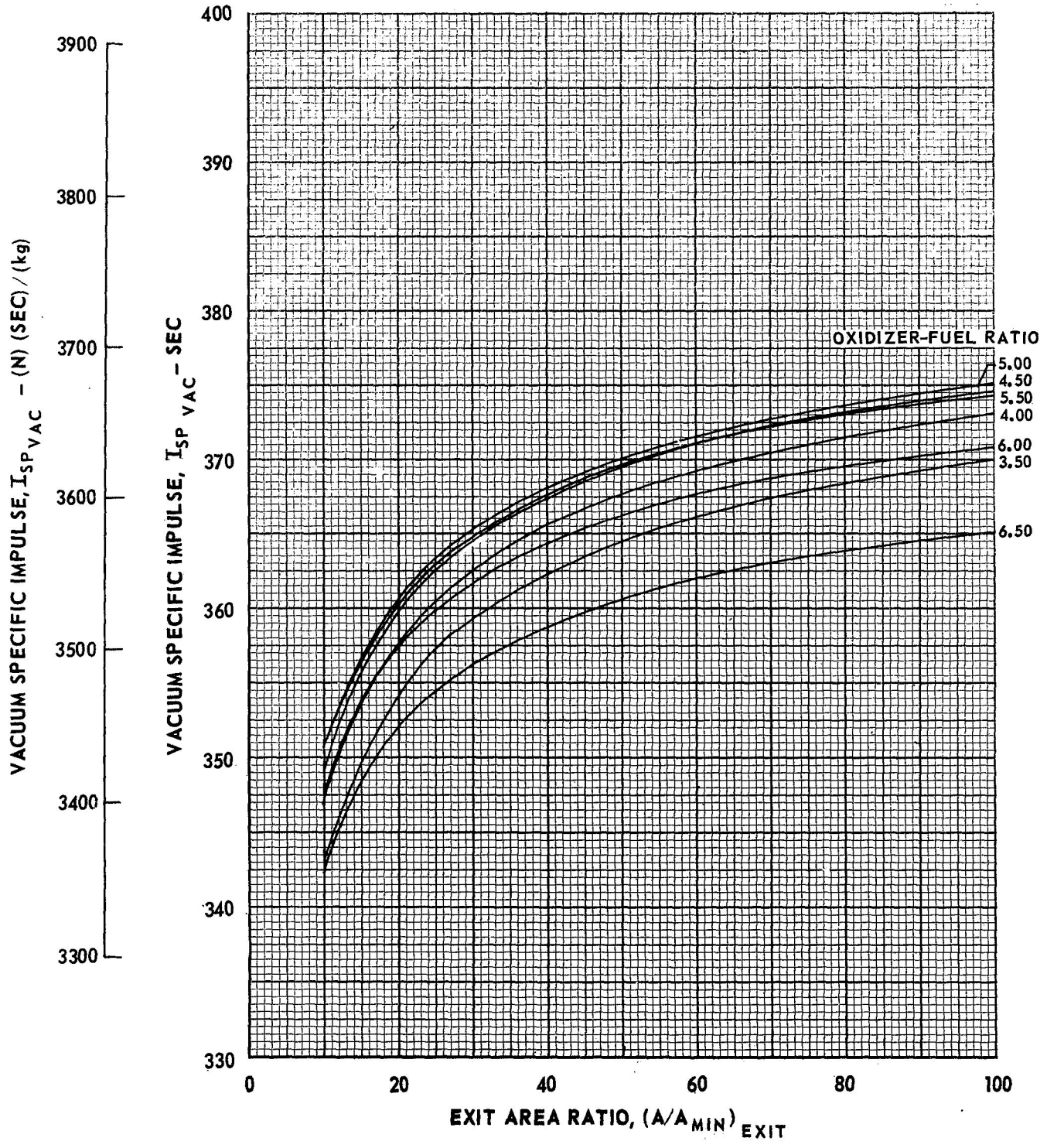

FIG. III-7

VARIATION OF EQUILIBRIUM VACUUM SPECIFIC IMPULSE WITH AREA RATIO

CH_4 - FLOX (82.6% F_2)

P_C = 500 PSIA (3.448 X 10^6 N/m^2)

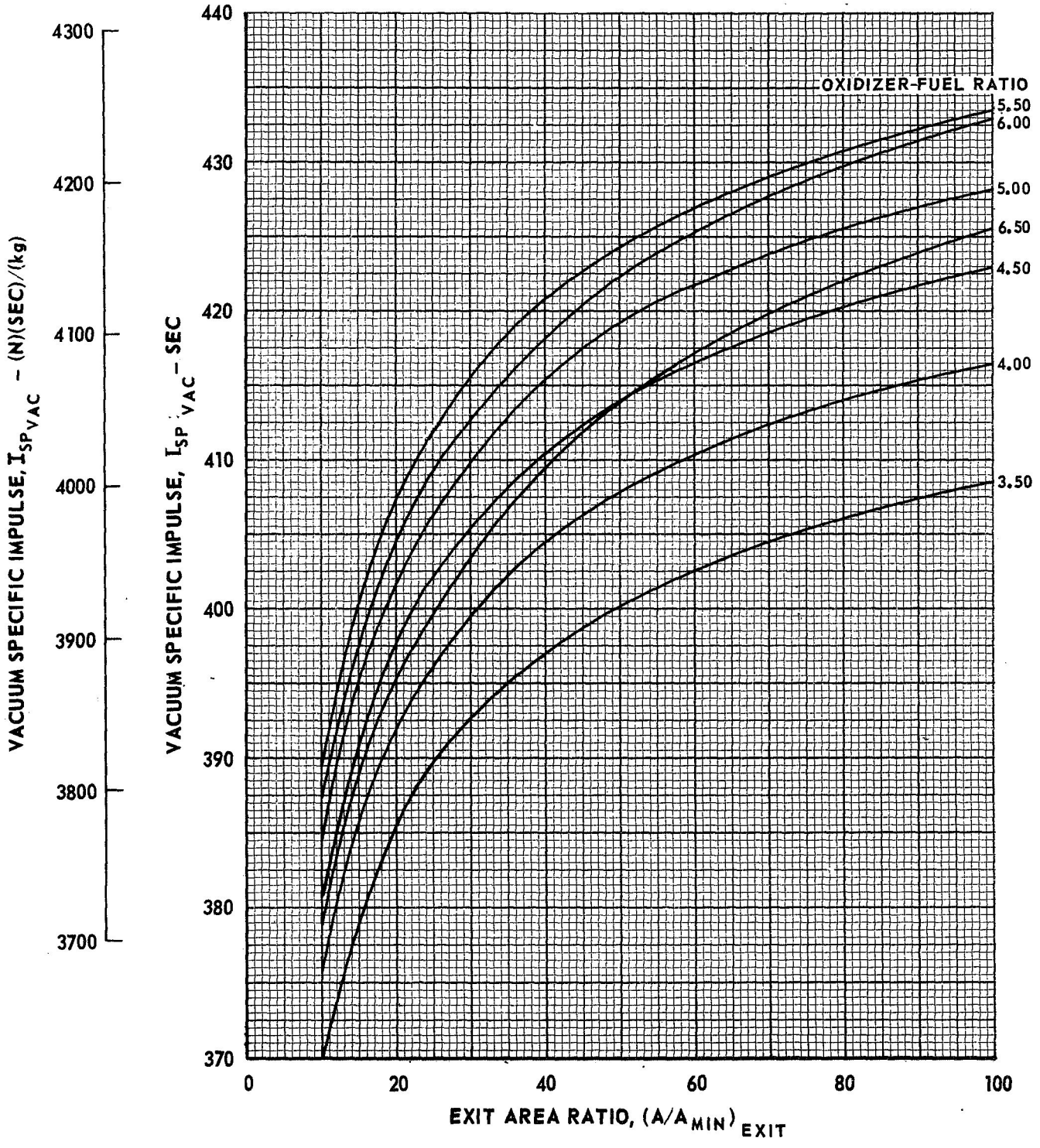

FIG. III-8

VARIATION OF FROZEN VACUUM SPECIFIC IMPULSE WITH AREA RATIO

CH_4 - FLOX (82.6% F_2)

P_C = 500 PSIA (3.448 X 10^6 N/m^2)

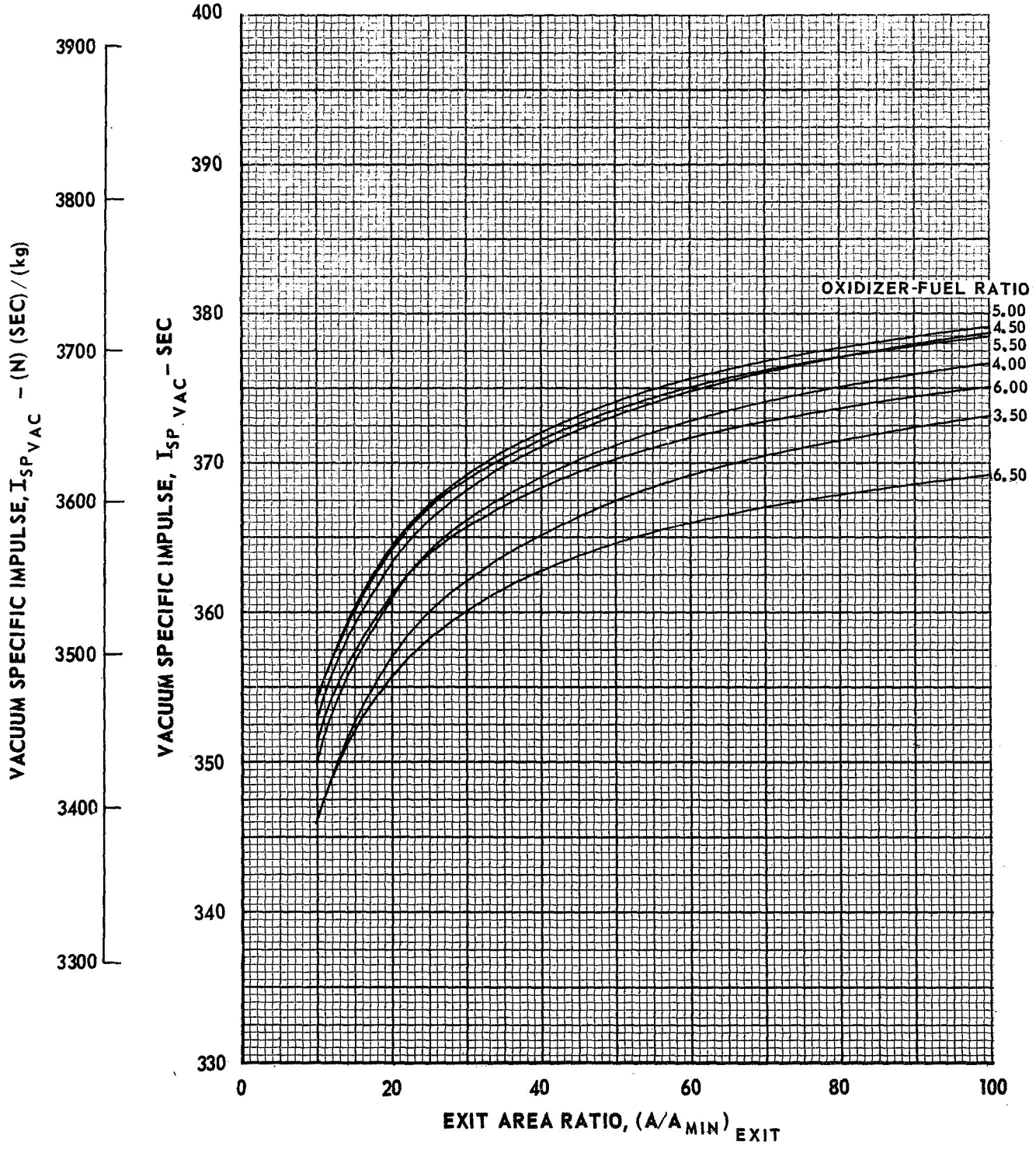

FIG. III-9

VARIATION OF EQUILIBRIUM VACUUM SPECIFIC IMPULSE WITH AREA RATIO

CH_4 – FLOX (82.6% F_2)

P_C = 750 PSIA (5.171 X 10^6 N/m^2)

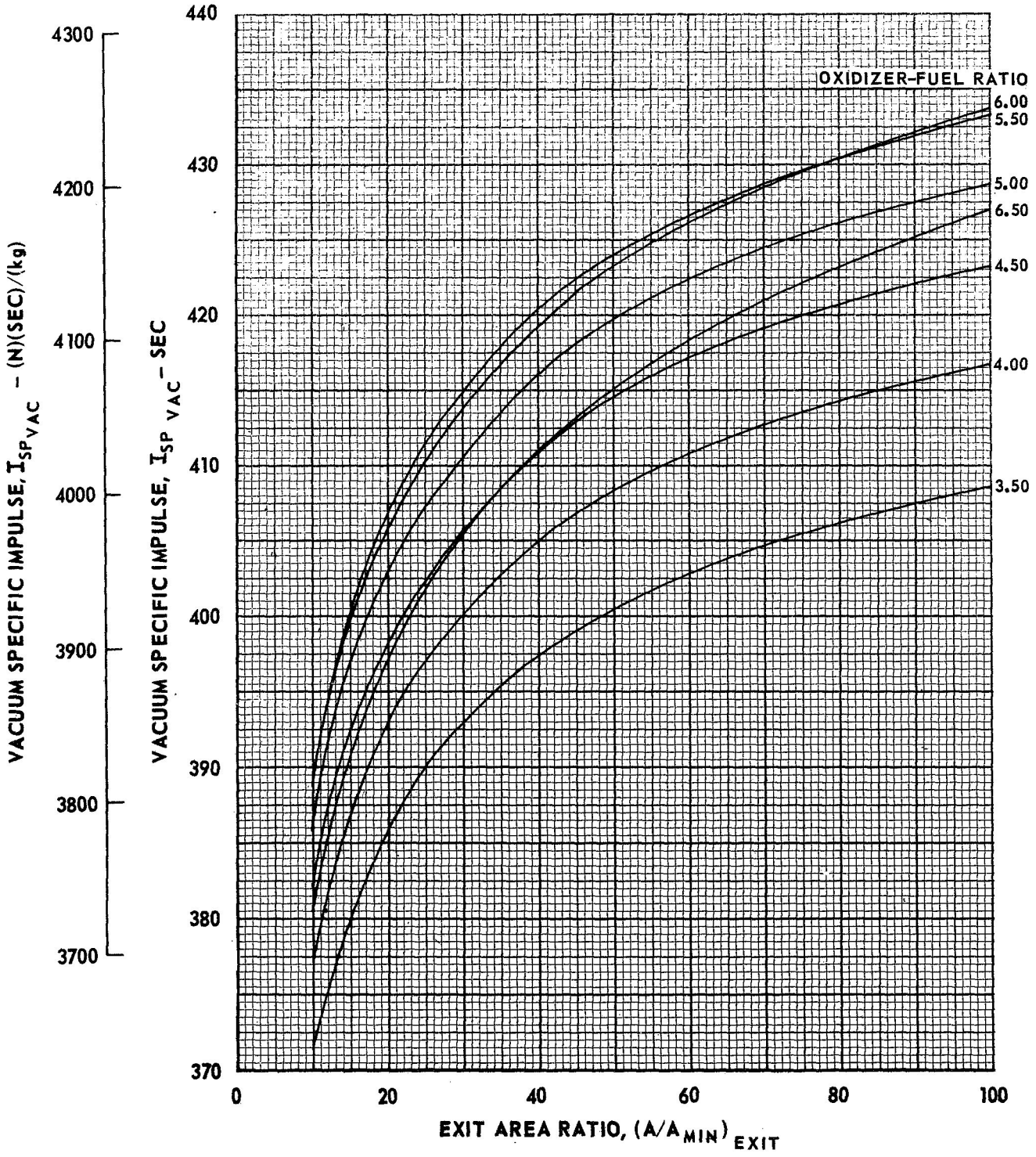

FIG. III-10

VARIATION OF FROZEN VACUUM SPECIFIC IMPULSE WITH AREA RATIO

CH_4 - FLOX (82.6% F_2)

P_C = 750 PSIA (5.171 X 10^6 N/m^2)

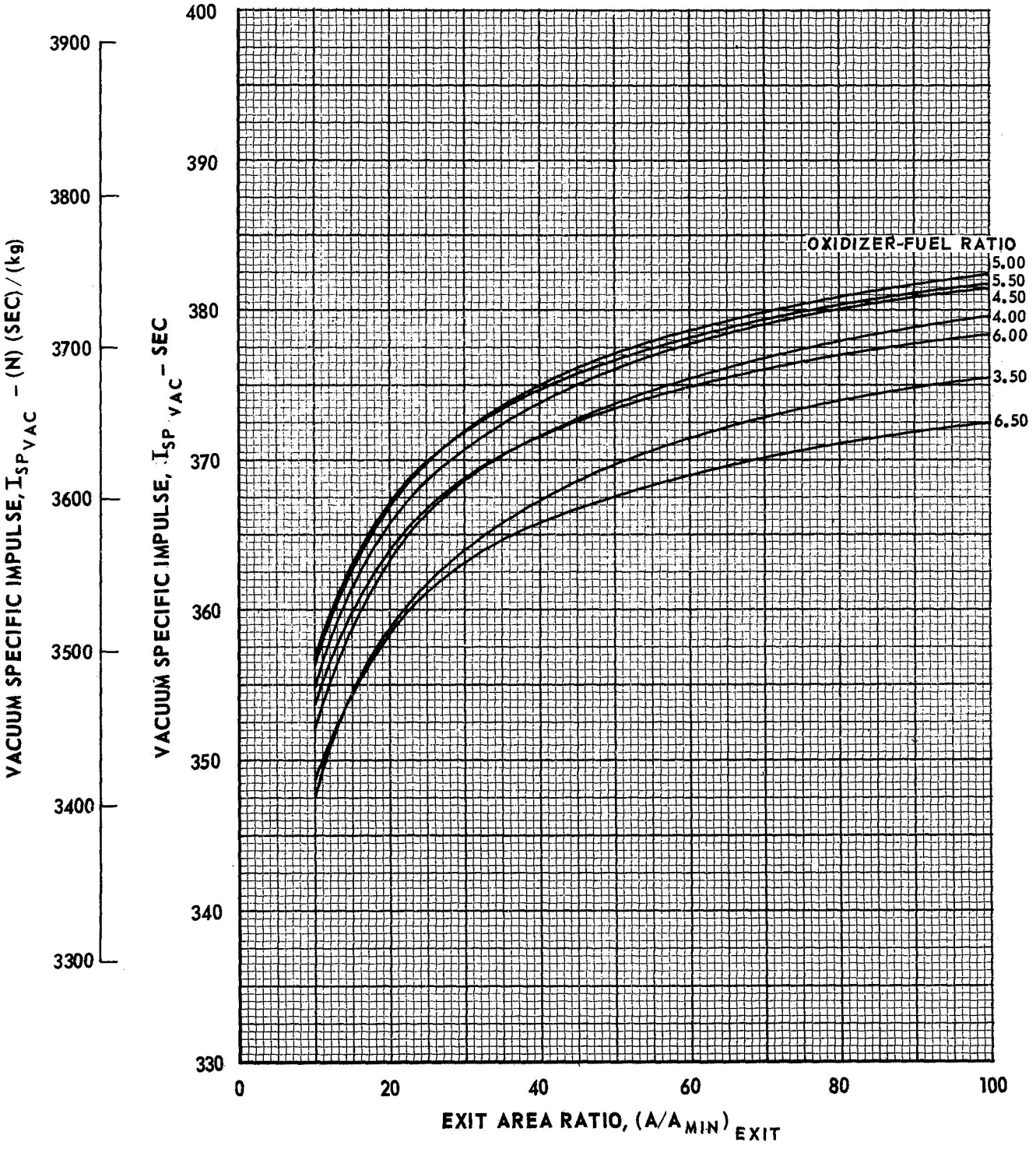

FIG. III-11

VARIATION OF EQUILIBRIUM VACUUM SPECIFIC IMPULSE WITH AREA RATIO

CH_4 - FLOX (82.6% F_2)

P_C = 1000 PSIA (6.895 X 10^6 N/m^2)

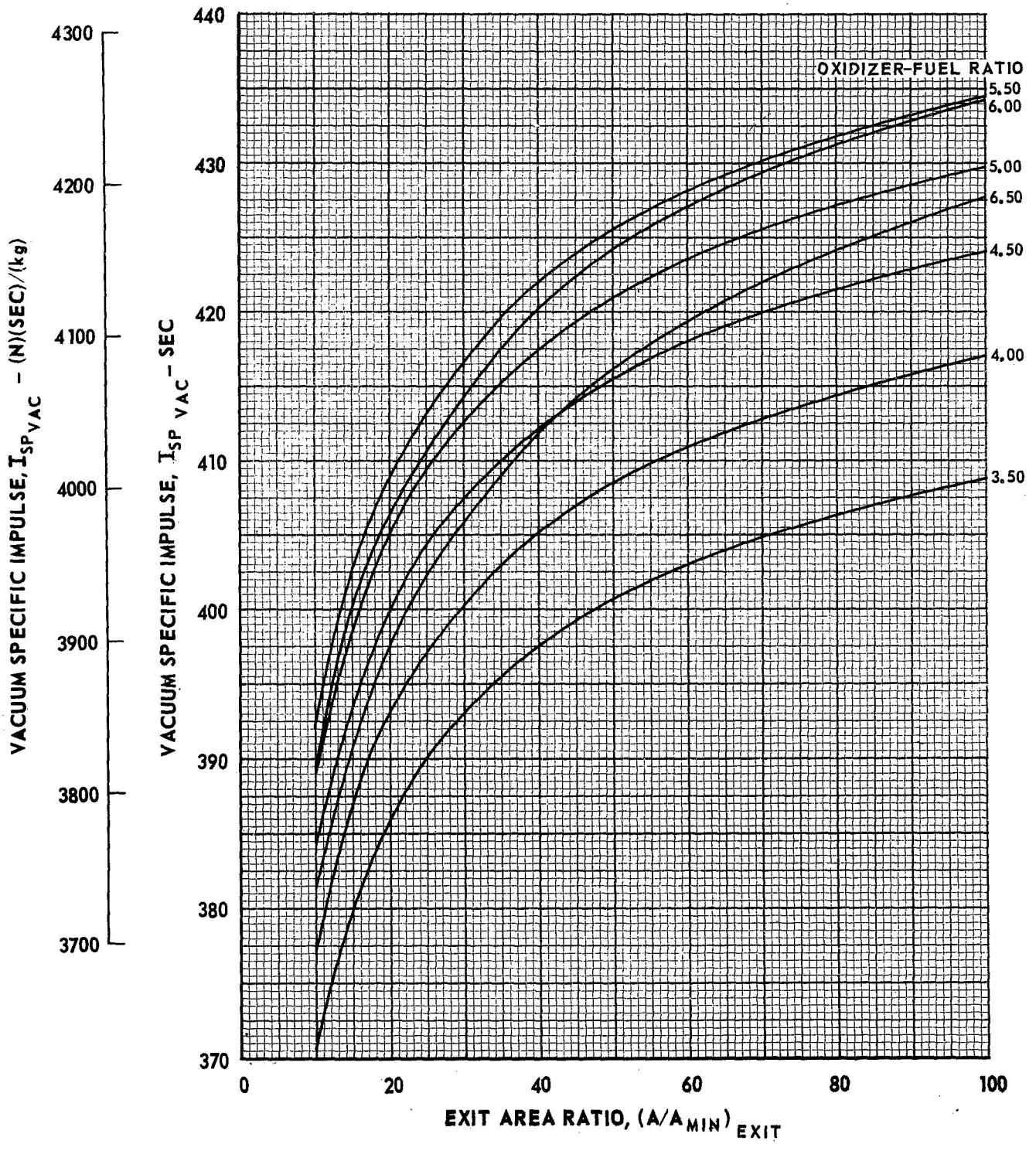

FIG. III-12

VARIATION OF FROZEN VACUUM SPECIFIC IMPULSE WITH AREA RATIO

CH_4 - FLOX (82.6% F_2)

P_C =1000 PSIA (6.895 X 10^6 N/m^2)

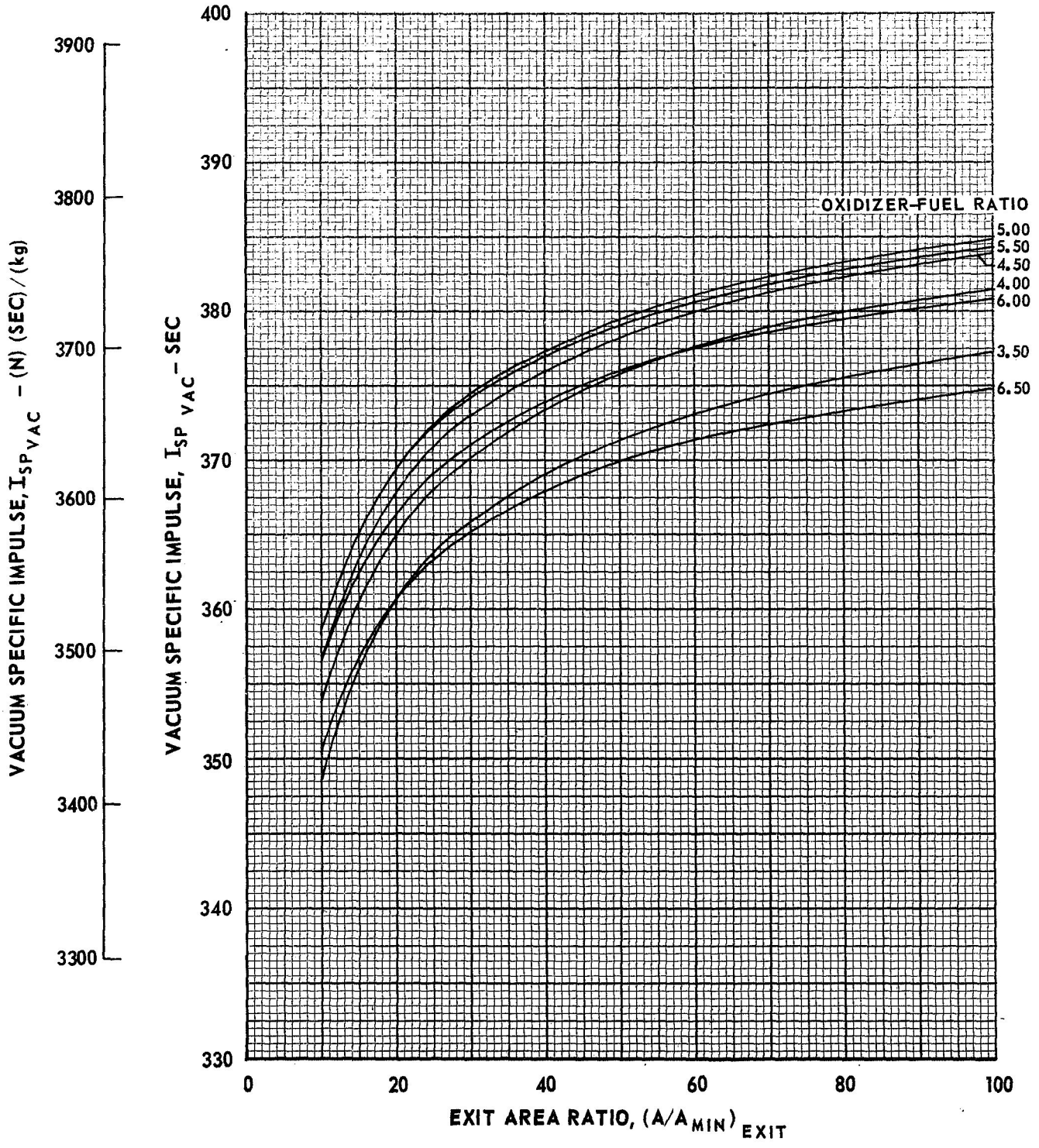

FIG. III-13

NORMALIZED GRAPHICAL SOLUTION FOR FREEZING AREA RATIO USING MODIFIED BRAY ANALYSIS

CH_4 - FLOX (82.6% F_2)

P_C = 100 PSIA ($6.895 \times 10^5 N/m^2$)

O/F = 3.50

NOTE: REACTION RATE CONSTANTS LISTED IN TABLE III-1

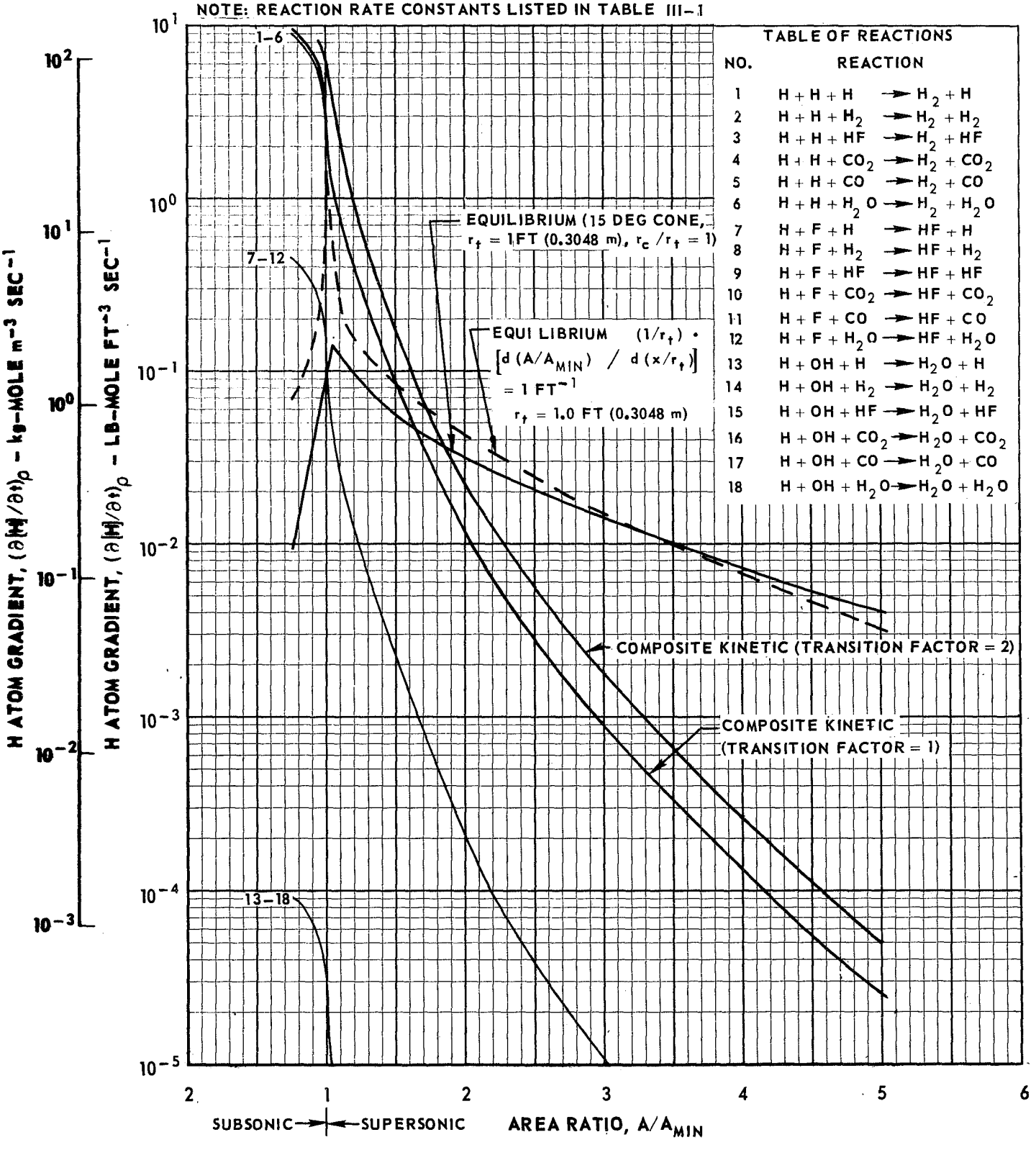

TABLE OF REACTIONS

NO.	REACTION
1	$H + H + H \rightarrow H_2 + H$
2	$H + H + H_2 \rightarrow H_2 + H_2$
3	$H + H + HF \rightarrow H_2 + HF$
4	$H + H + CO_2 \rightarrow H_2 + CO_2$
5	$H + H + CO \rightarrow H_2 + CO$
6	$H + H + H_2O \rightarrow H_2 + H_2O$
7	$H + F + H \rightarrow HF + H$
8	$H + F + H_2 \rightarrow HF + H_2$
9	$H + F + HF \rightarrow HF + HF$
10	$H + F + CO_2 \rightarrow HF + CO_2$
11	$H + F + CO \rightarrow HF + CO$
12	$H + F + H_2O \rightarrow HF + H_2O$
13	$H + OH + H \rightarrow H_2O + H$
14	$H + OH + H_2 \rightarrow H_2O + H_2$
15	$H + OH + HF \rightarrow H_2O + HF$
16	$H + OH + CO_2 \rightarrow H_2O + CO_2$
17	$H + OH + CO \rightarrow H_2O + CO$
18	$H + OH + H_2O \rightarrow H_2O + H_2O$

FIG. III-14

NORMALIZED GRAPHICAL SOLUTION FOR FREEZING AREA RATIO USING MODIFIED BRAY ANALYSIS

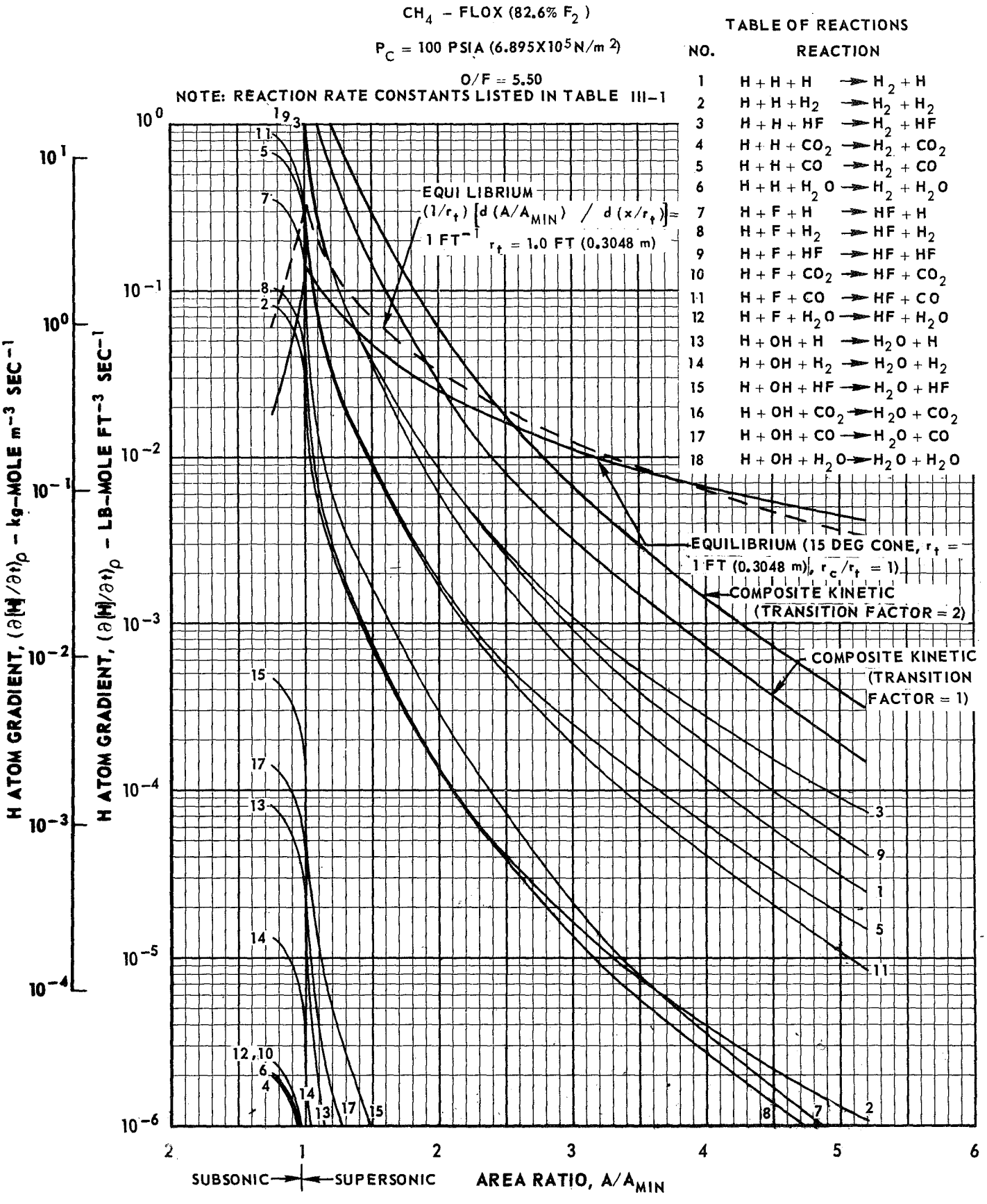

FIG. III-15

NORMALIZED GRAPHICAL SOLUTION FOR FREEZING AREA RATIO USING MODIFIED BRAY ANALYSIS

CH_4 - FLOX (82.6% F_2)

P_C = 100 PSIA (6.895×10^5 N/m^2)

O/F = 6.50

NOTE: REACTION RATE CONSTANTS LISTED IN TABLE III-1

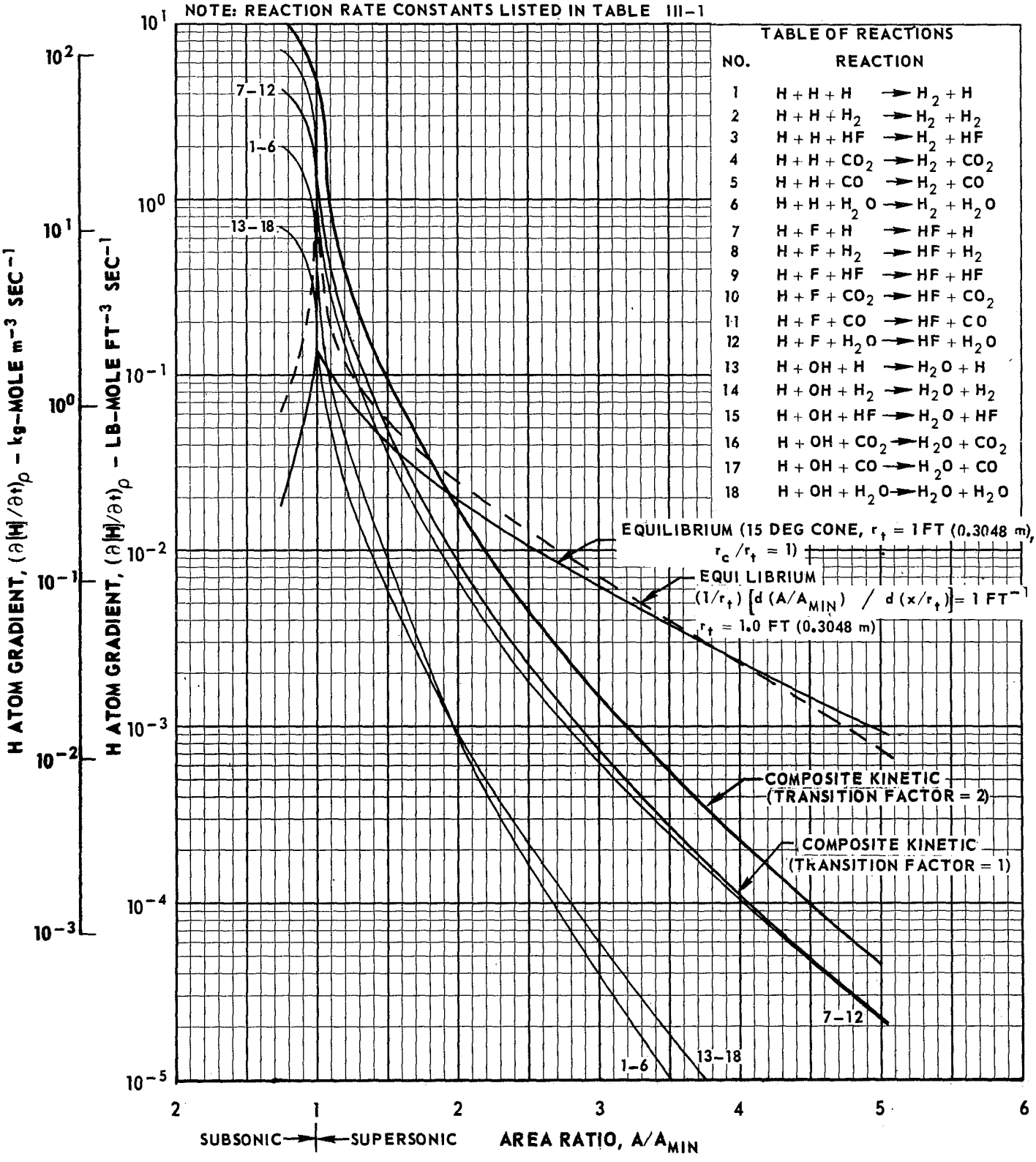

TABLE OF REACTIONS

NO.	REACTION
1	$H + H + H \rightarrow H_2 + H$
2	$H + H + H_2 \rightarrow H_2 + H_2$
3	$H + H + HF \rightarrow H_2 + HF$
4	$H + H + CO_2 \rightarrow H_2 + CO_2$
5	$H + H + CO \rightarrow H_2 + CO$
6	$H + H + H_2O \rightarrow H_2 + H_2O$
7	$H + F + H \rightarrow HF + H$
8	$H + F + H_2 \rightarrow HF + H_2$
9	$H + F + HF \rightarrow HF + HF$
10	$H + F + CO_2 \rightarrow HF + CO_2$
11	$H + F + CO \rightarrow HF + CO$
12	$H + F + H_2O \rightarrow HF + H_2O$
13	$H + OH + H \rightarrow H_2O + H$
14	$H + OH + H_2 \rightarrow H_2O + H_2$
15	$H + OH + HF \rightarrow H_2O + HF$
16	$H + OH + CO_2 \rightarrow H_2O + CO_2$
17	$H + OH + CO \rightarrow H_2O + CO$
18	$H + OH + H_2O \rightarrow H_2O + H_2O$

FIG. III-16

NORMALIZED GRAPHICAL SOLUTION FOR FREEZING AREA RATIO USING MODIFIED BRAY ANALYSIS

CH_4 - FLOX (82.6% F_2)

P_C = 200 PSIA ($1.379 \times 10^6 N/m^2$)

O/F = 3.50

NOTE: REACTION RATE CONSTANTS LISTED IN TABLE III-1

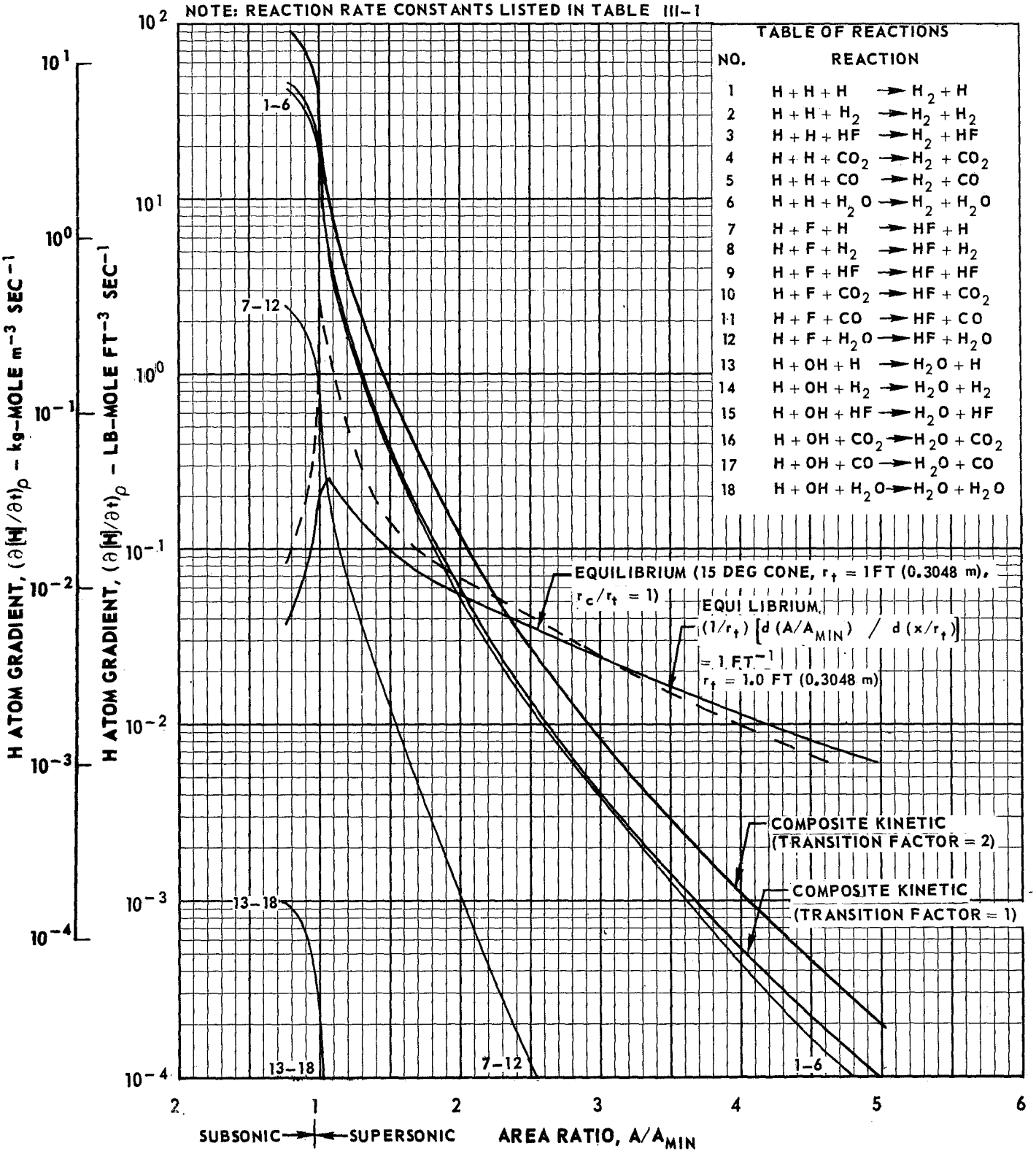

FIG. III-17

NORMALIZED GRAPHICAL SOLUTION FOR FREEZING AREA RATIO USING MODIFIED BRAY ANALYSIS

CH_4 - FLOX (82.6% F_2)

P_C = 200 PSIA (1.379×10^6 N/m^2)

O/F = 5.50

NOTE: REACTION RATE CONSTANTS LISTED IN TABLE III-1

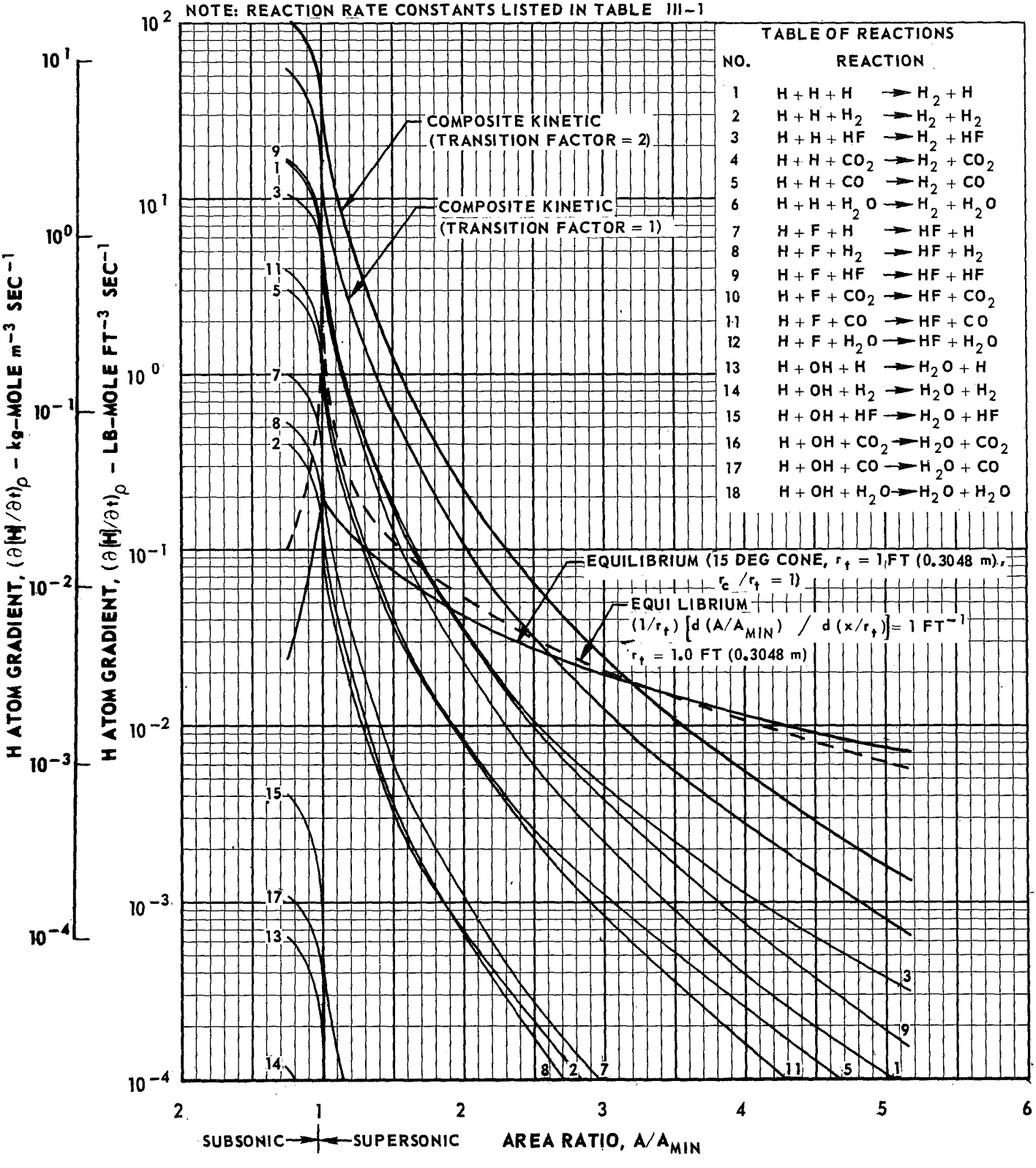

TABLE OF REACTIONS

NO.	REACTION
1	$H + H + H \rightarrow H_2 + H$
2	$H + H + H_2 \rightarrow H_2 + H_2$
3	$H + H + HF \rightarrow H_2 + HF$
4	$H + H + CO_2 \rightarrow H_2 + CO_2$
5	$H + H + CO \rightarrow H_2 + CO$
6	$H + H + H_2O \rightarrow H_2 + H_2O$
7	$H + F + H \rightarrow HF + H$
8	$H + F + H_2 \rightarrow HF + H_2$
9	$H + F + HF \rightarrow HF + HF$
10	$H + F + CO_2 \rightarrow HF + CO_2$
11	$H + F + CO \rightarrow HF + CO$
12	$H + F + H_2O \rightarrow HF + H_2O$
13	$H + OH + H \rightarrow H_2O + H$
14	$H + OH + H_2 \rightarrow H_2O + H_2$
15	$H + OH + HF \rightarrow H_2O + HF$
16	$H + OH + CO_2 \rightarrow H_2O + CO_2$
17	$H + OH + CO \rightarrow H_2O + CO$
18	$H + OH + H_2O \rightarrow H_2O + H_2O$

FIG. III-18

NORMALIZED GRAPHICAL SOLUTION FOR FREEZING AREA RATIO USING MODIFIED BRAY ANALYSIS

CH_4 - FLOX (82.6% F_2)

P_C = 200 PSIA (1.379X10^6 N/m^2)

O/F = 6.50

NOTE: REACTION RATE CONSTANTS LISTED IN TABLE III-1

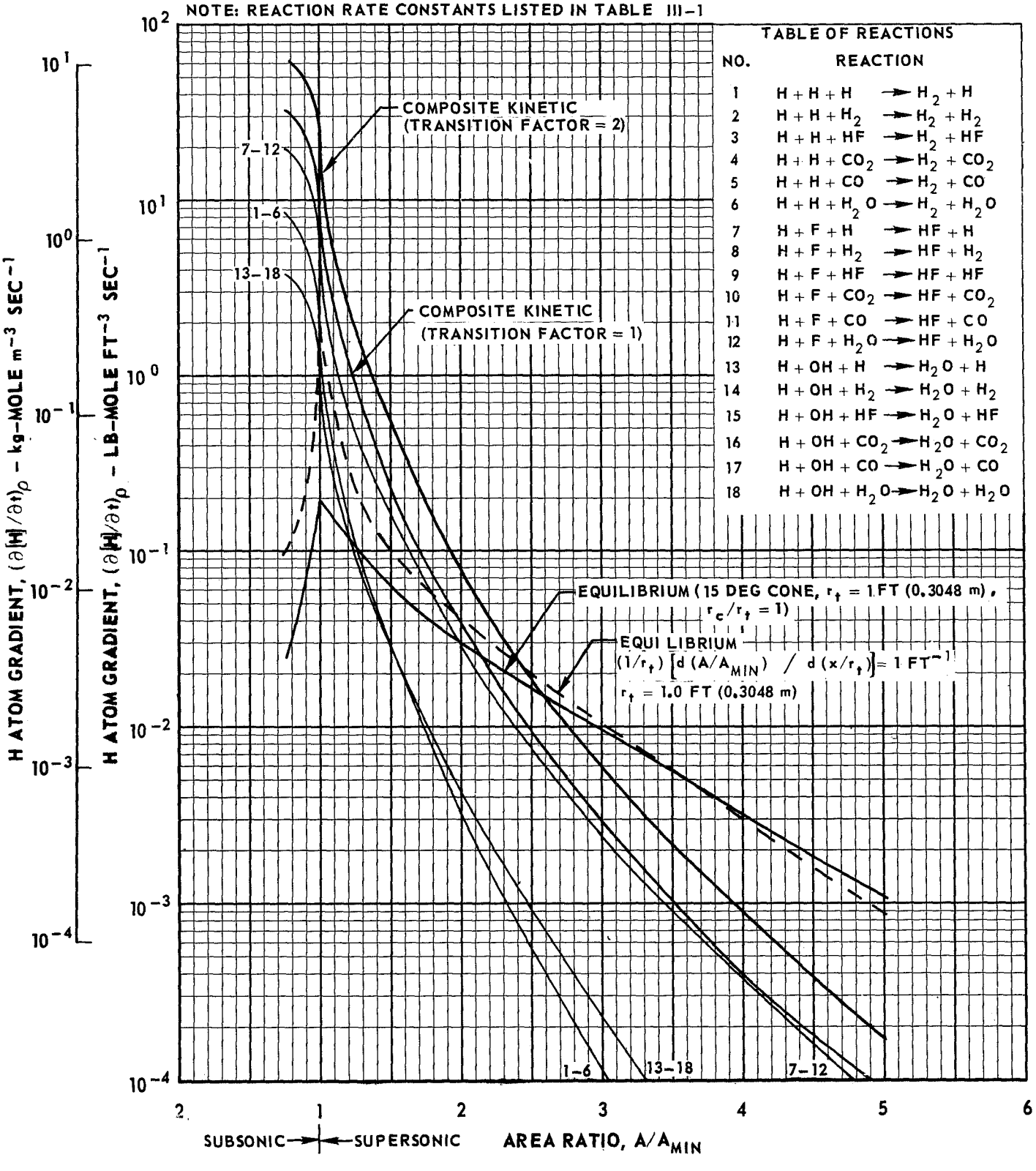

FIG. III-19

NORMALIZED GRAPHICAL SOLUTION FOR FREEZING AREA RATIO USING MODIFIED BRAY ANALYSIS

CH_4 - FLOX (82.6% F_2)

P_C = 300 PSIA (2.069X10 ^{6}N/m ^{2})

O/F = 3.50

NOTE: REACTION RATE CONSTANTS LISTED IN TABLE III-1

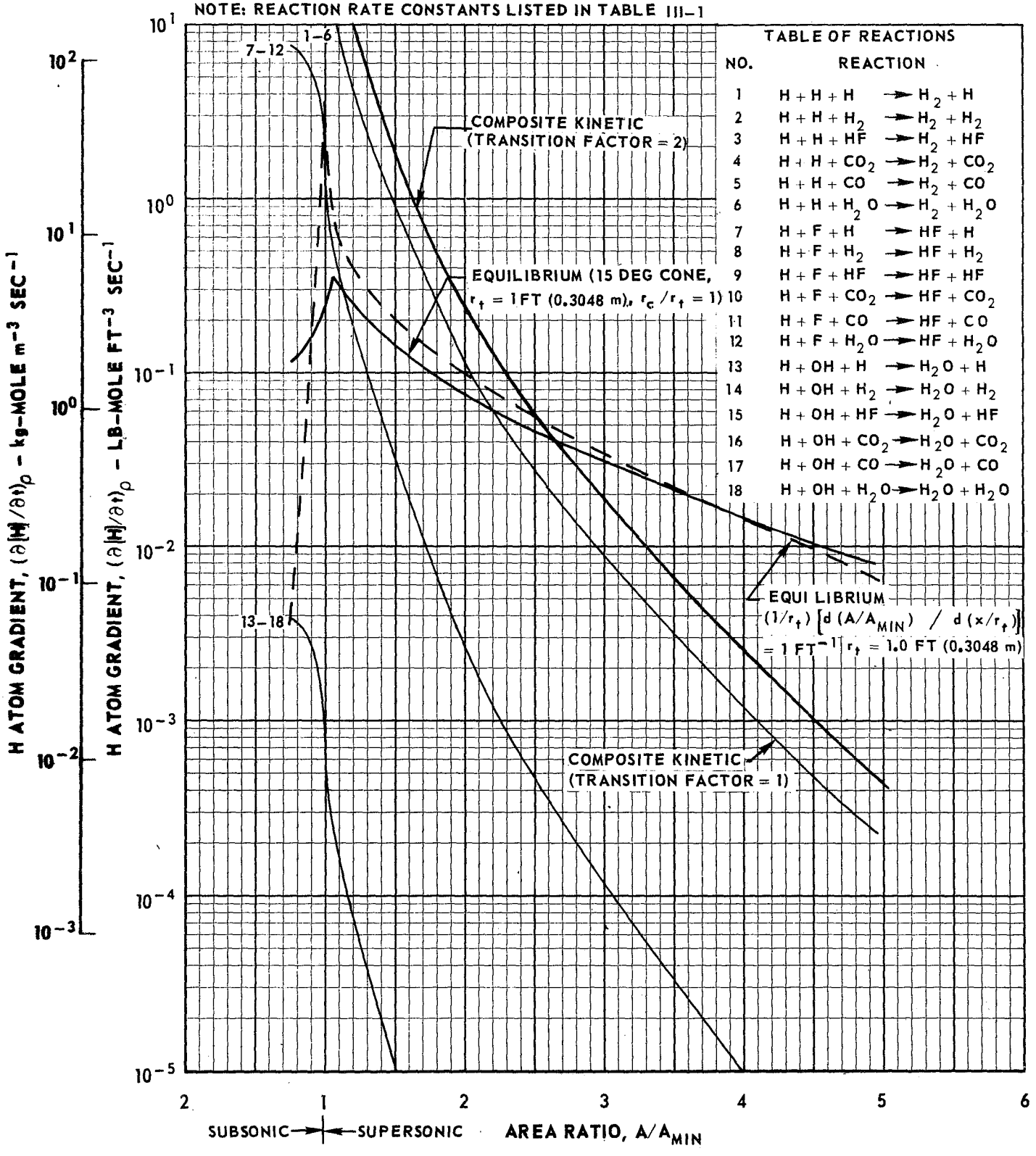

TABLE OF REACTIONS

NO.	REACTION
1	$H + H + H \rightarrow H_2 + H$
2	$H + H + H_2 \rightarrow H_2 + H_2$
3	$H + H + HF \rightarrow H_2 + HF$
4	$H + H + CO_2 \rightarrow H_2 + CO_2$
5	$H + H + CO \rightarrow H_2 + CO$
6	$H + H + H_2O \rightarrow H_2 + H_2O$
7	$H + F + H \rightarrow HF + H$
8	$H + F + H_2 \rightarrow HF + H_2$
9	$H + F + HF \rightarrow HF + HF$
10	$H + F + CO_2 \rightarrow HF + CO_2$
11	$H + F + CO \rightarrow HF + CO$
12	$H + F + H_2O \rightarrow HF + H_2O$
13	$H + OH + H \rightarrow H_2O + H$
14	$H + OH + H_2 \rightarrow H_2O + H_2$
15	$H + OH + HF \rightarrow H_2O + HF$
16	$H + OH + CO_2 \rightarrow H_2O + CO_2$
17	$H + OH + CO \rightarrow H_2O + CO$
18	$H + OH + H_2O \rightarrow H_2O + H_2O$

FIG. III-20

NORMALIZED GRAPHICAL SOLUTION FOR FREEZING AREA RATIO USING MODIFIED BRAY ANALYSIS

CH_4 - FLOX (82.6% F_2)

P_C = 300 PSIA (2.069X10^{6}N/m^2)

O/F = 5.50

NOTE: REACTION RATE CONSTANTS LISTED IN TABLE III-1

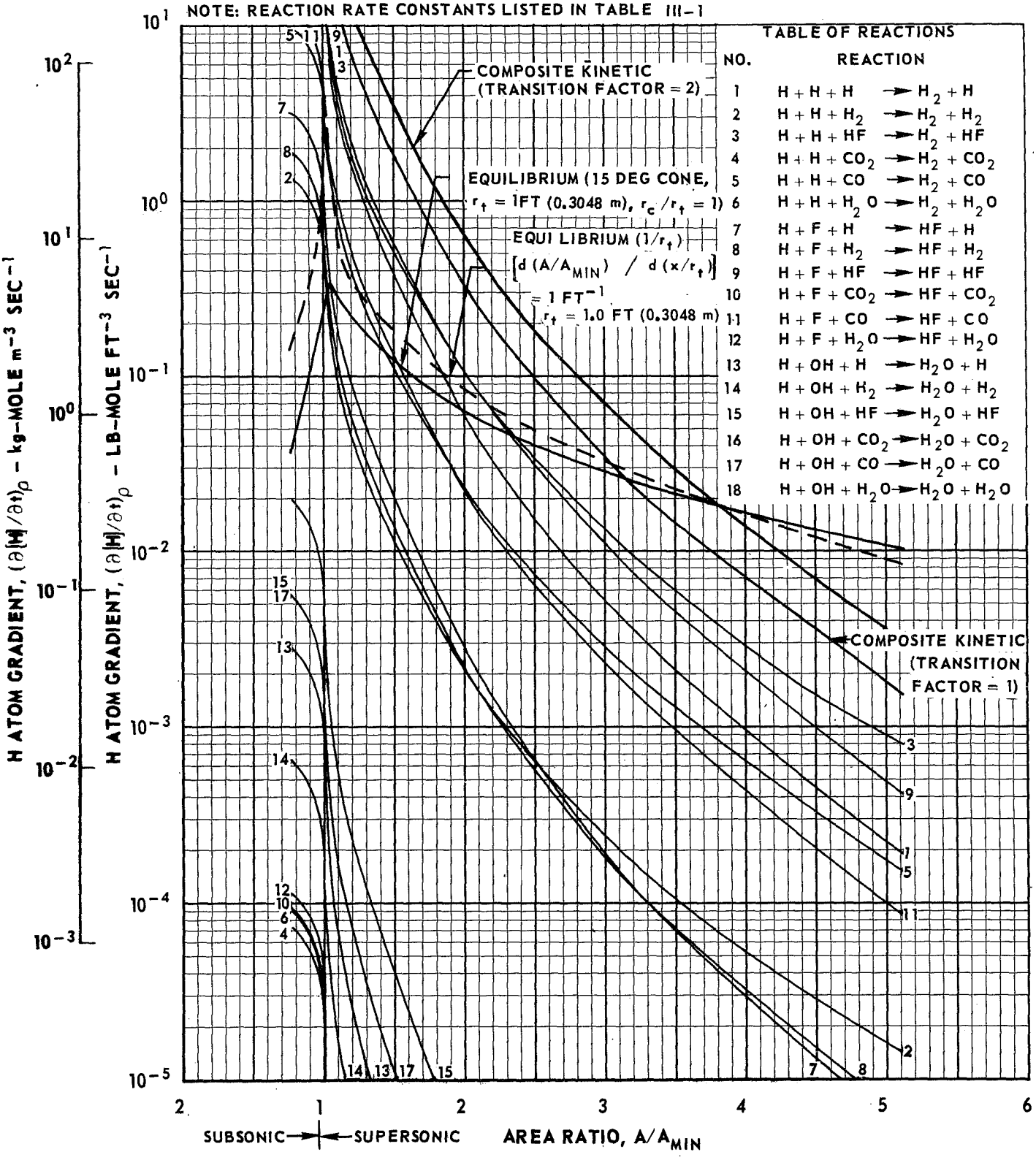

TABLE OF REACTIONS

NO.	REACTION
1	H + H + H → H_2 + H
2	H + H + H_2 → H_2 + H_2
3	H + H + HF → H_2 + HF
4	H + H + CO_2 → H_2 + CO_2
5	H + H + CO → H_2 + CO
6	H + H + H_2O → H_2 + H_2O
7	H + F + H → HF + H
8	H + F + H_2 → HF + H_2
9	H + F + HF → HF + HF
10	H + F + CO_2 → HF + CO_2
11	H + F + CO → HF + CO
12	H + F + H_2O → HF + H_2O
13	H + OH + H → H_2O + H
14	H + OH + H_2 → H_2O + H_2
15	H + OH + HF → H_2O + HF
16	H + OH + CO_2 → H_2O + CO_2
17	H + OH + CO → H_2O + CO
18	H + OH + H_2O → H_2O + H_2O

FIG. III-21

NORMALIZED GRAPHICAL SOLUTION FOR FREEZING AREA RATIO USING MODIFIED BRAY ANALYSIS

CH_4 - FLOX (82.6% F_2)

P_C = 300 PSIA (2.069X10 ^{6}N/m^2)

O/F = 6.50

NOTE: REACTION RATE CONSTANTS LISTED IN TABLE III-1

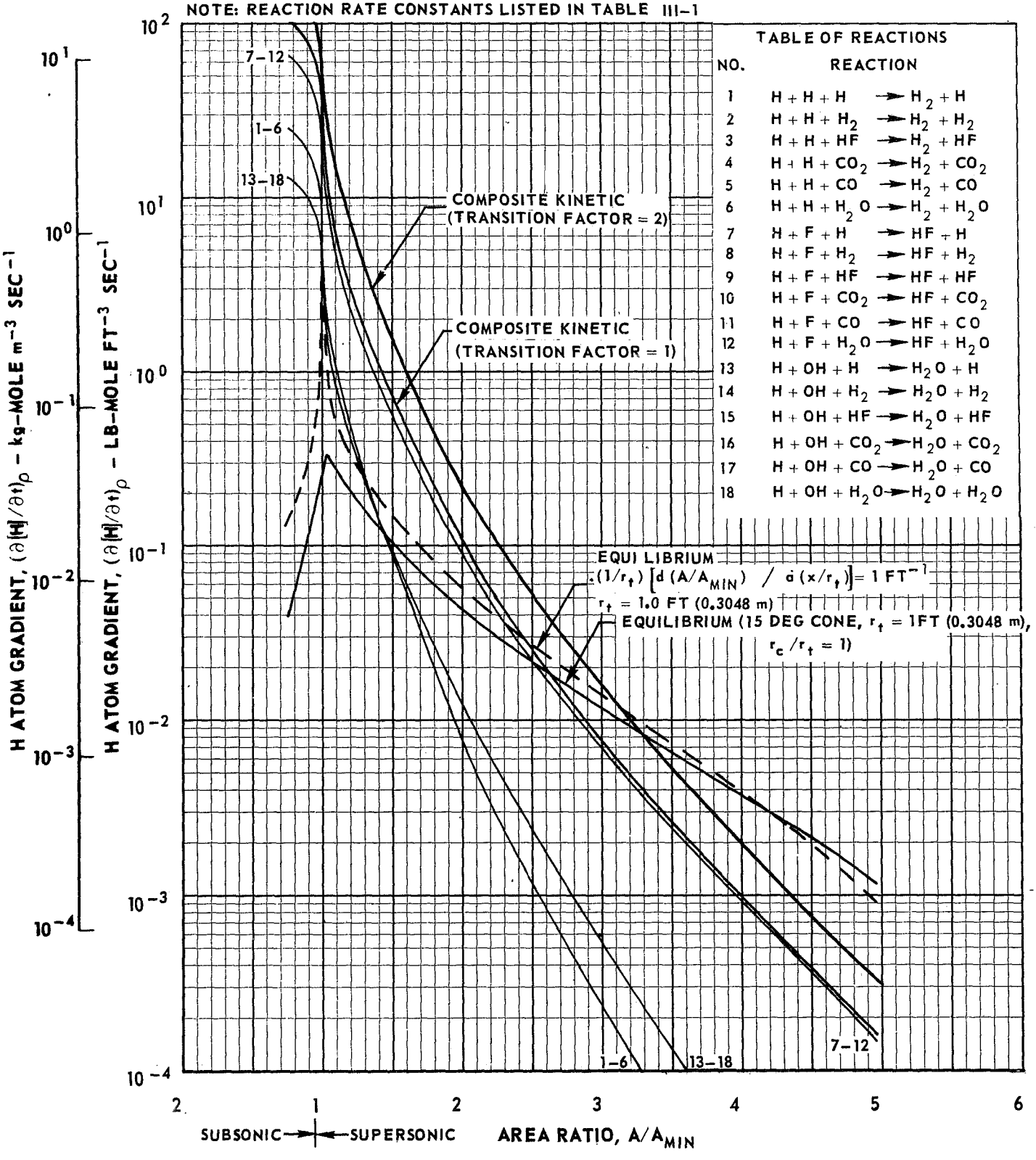

FIG. III-22

NORMALIZED GRAPHICAL SOLUTION FOR FREEZING AREA RATIO USING MODIFIED BRAY ANALYSIS

CH_4 - FLOX (82.6% F_2)

P_C = 500 PSIA (3.448×10^6 N/m^2)

O/F = 3.50

NOTE: REACTION RATE CONSTANTS LISTED IN TABLE III-1

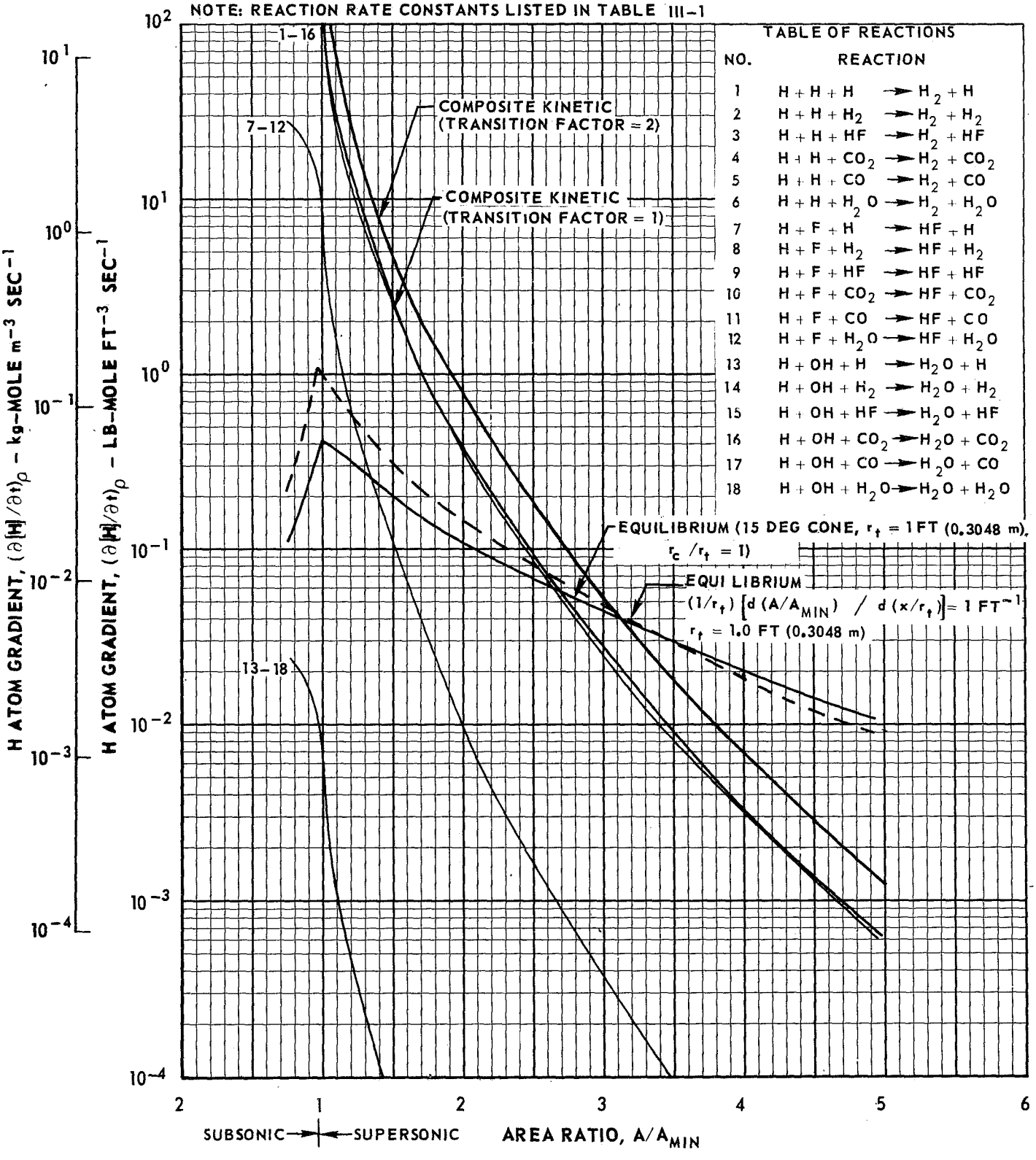

TABLE OF REACTIONS

NO.	REACTION
1	$H + H + H \rightarrow H_2 + H$
2	$H + H + H_2 \rightarrow H_2 + H_2$
3	$H + H + HF \rightarrow H_2 + HF$
4	$H + H + CO_2 \rightarrow H_2 + CO_2$
5	$H + H + CO \rightarrow H_2 + CO$
6	$H + H + H_2O \rightarrow H_2 + H_2O$
7	$H + F + H \rightarrow HF + H$
8	$H + F + H_2 \rightarrow HF + H_2$
9	$H + F + HF \rightarrow HF + HF$
10	$H + F + CO_2 \rightarrow HF + CO_2$
11	$H + F + CO \rightarrow HF + CO$
12	$H + F + H_2O \rightarrow HF + H_2O$
13	$H + OH + H \rightarrow H_2O + H$
14	$H + OH + H_2 \rightarrow H_2O + H_2$
15	$H + OH + HF \rightarrow H_2O + HF$
16	$H + OH + CO_2 \rightarrow H_2O + CO_2$
17	$H + OH + CO \rightarrow H_2O + CO$
18	$H + OH + H_2O \rightarrow H_2O + H_2O$

FIG. III-23

NORMALIZED GRAPHICAL SOLUTION FOR FREEZING AREA RATIO USING MODIFIED BRAY ANALYSIS

CH_4 - FLOX (82.6% F_2)

P_C = 500 PSIA (3.448×10^6 N/m^2)

O/F = 5.50

NOTE: REACTION RATE CONSTANTS LISTED IN TABLE III-1

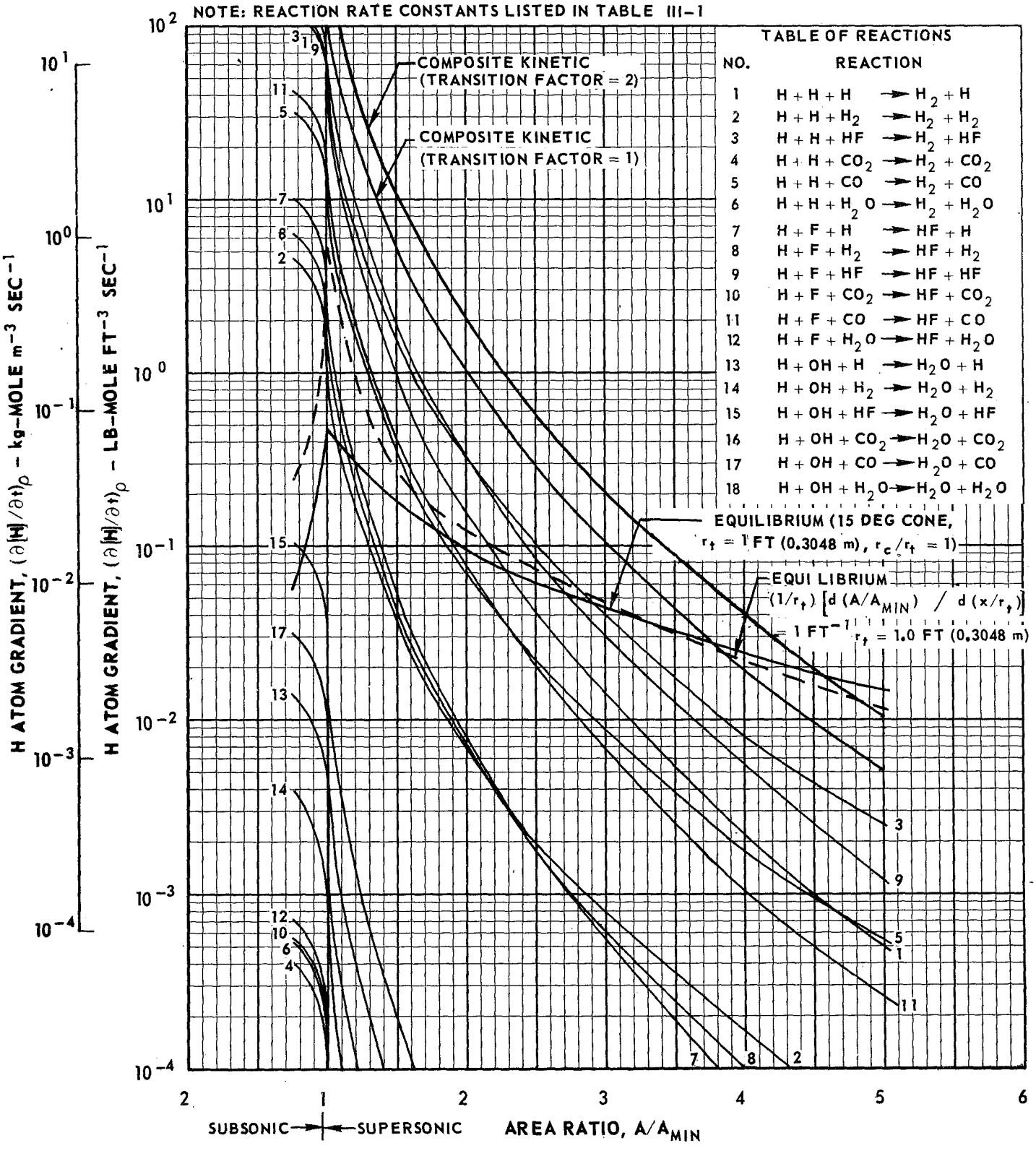

TABLE OF REACTIONS

NO.	REACTION
1	$H + H + H \rightarrow H_2 + H$
2	$H + H + H_2 \rightarrow H_2 + H_2$
3	$H + H + HF \rightarrow H_2 + HF$
4	$H + H + CO_2 \rightarrow H_2 + CO_2$
5	$H + H + CO \rightarrow H_2 + CO$
6	$H + H + H_2O \rightarrow H_2 + H_2O$
7	$H + F + H \rightarrow HF + H$
8	$H + F + H_2 \rightarrow HF + H_2$
9	$H + F + HF \rightarrow HF + HF$
10	$H + F + CO_2 \rightarrow HF + CO_2$
11	$H + F + CO \rightarrow HF + CO$
12	$H + F + H_2O \rightarrow HF + H_2O$
13	$H + OH + H \rightarrow H_2O + H$
14	$H + OH + H_2 \rightarrow H_2O + H_2$
15	$H + OH + HF \rightarrow H_2O + HF$
16	$H + OH + CO_2 \rightarrow H_2O + CO_2$
17	$H + OH + CO \rightarrow H_2O + CO$
18	$H + OH + H_2O \rightarrow H_2O + H_2O$

FIG. III-24

NORMALIZED GRAPHICAL SOLUTION FOR FREEZING AREA RATIO USING MODIFIED BRAY ANALYSIS

CH_4 – FLOX (82.6% F_2)

P_C = 500 PSIA (3.448X10^{6}N/m^2)

O/F = 6.50

NOTE: REACTION RATE CONSTANTS LISTED IN TABLE III-1

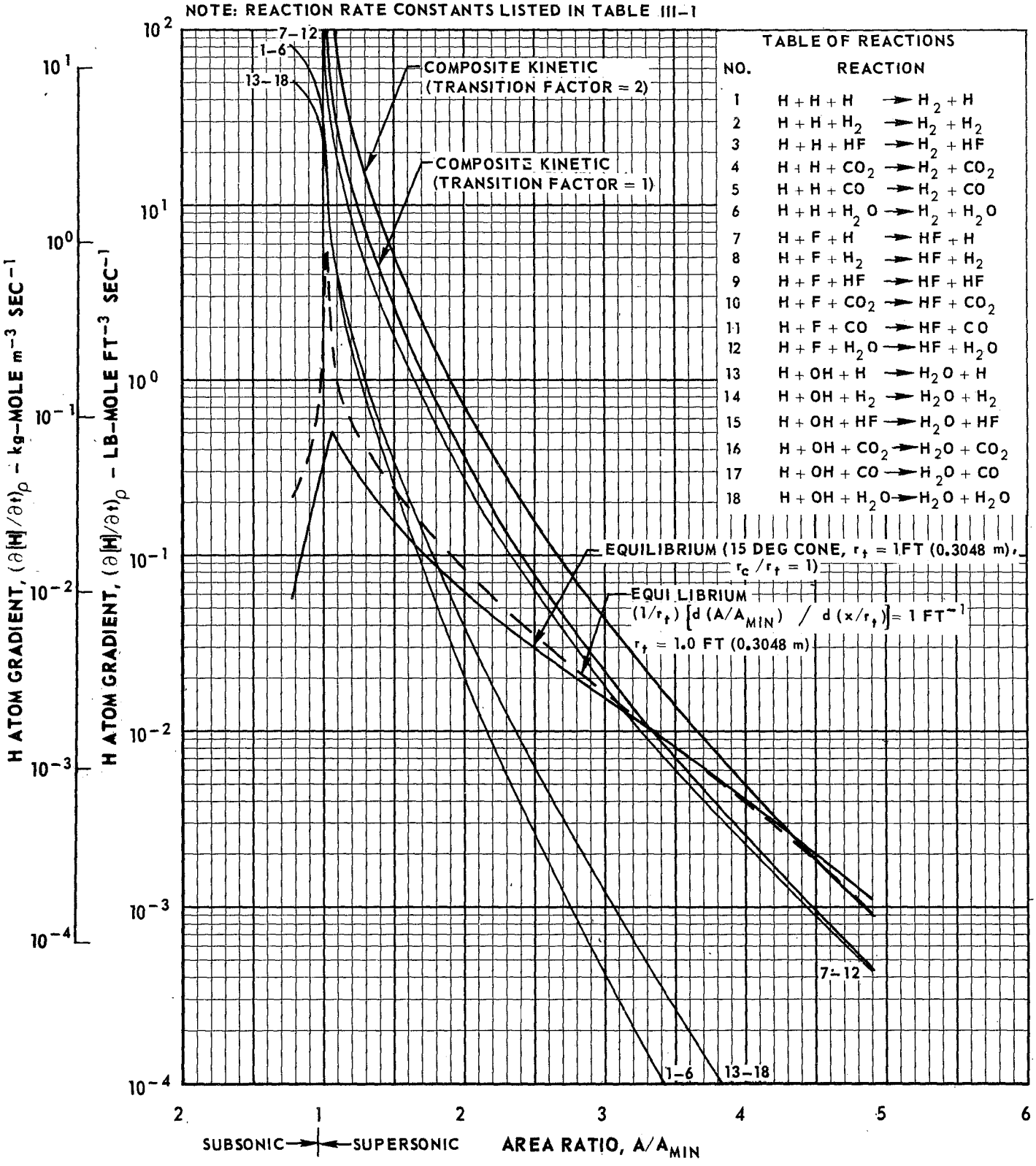

TABLE OF REACTIONS

NO.	REACTION
1	$H + H + H \rightarrow H_2 + H$
2	$H + H + H_2 \rightarrow H_2 + H_2$
3	$H + H + HF \rightarrow H_2 + HF$
4	$H + H + CO_2 \rightarrow H_2 + CO_2$
5	$H + H + CO \rightarrow H_2 + CO$
6	$H + H + H_2O \rightarrow H_2 + H_2O$
7	$H + F + H \rightarrow HF + H$
8	$H + F + H_2 \rightarrow HF + H_2$
9	$H + F + HF \rightarrow HF + HF$
10	$H + F + CO_2 \rightarrow HF + CO_2$
11	$H + F + CO \rightarrow HF + CO$
12	$H + F + H_2O \rightarrow HF + H_2O$
13	$H + OH + H \rightarrow H_2O + H$
14	$H + OH + H_2 \rightarrow H_2O + H_2$
15	$H + OH + HF \rightarrow H_2O + HF$
16	$H + OH + CO_2 \rightarrow H_2O + CO_2$
17	$H + OH + CO \rightarrow H_2O + CO$
18	$H + OH + H_2O \rightarrow H_2O + H_2O$

FIG. III-25

NORMALIZED GRAPHICAL SOLUTION FOR FREEZING AREA RATIO USING MODIFIED BRAY ANALYSIS

CH_4 - FLOX (82.6% F_2)

$P_C = 750$ PSIA ($5.171 \times 10^6 N/m^2$)

O/F = 3.50

NOTE: REACTION RATE CONSTANTS LISTED IN TABLE III-1

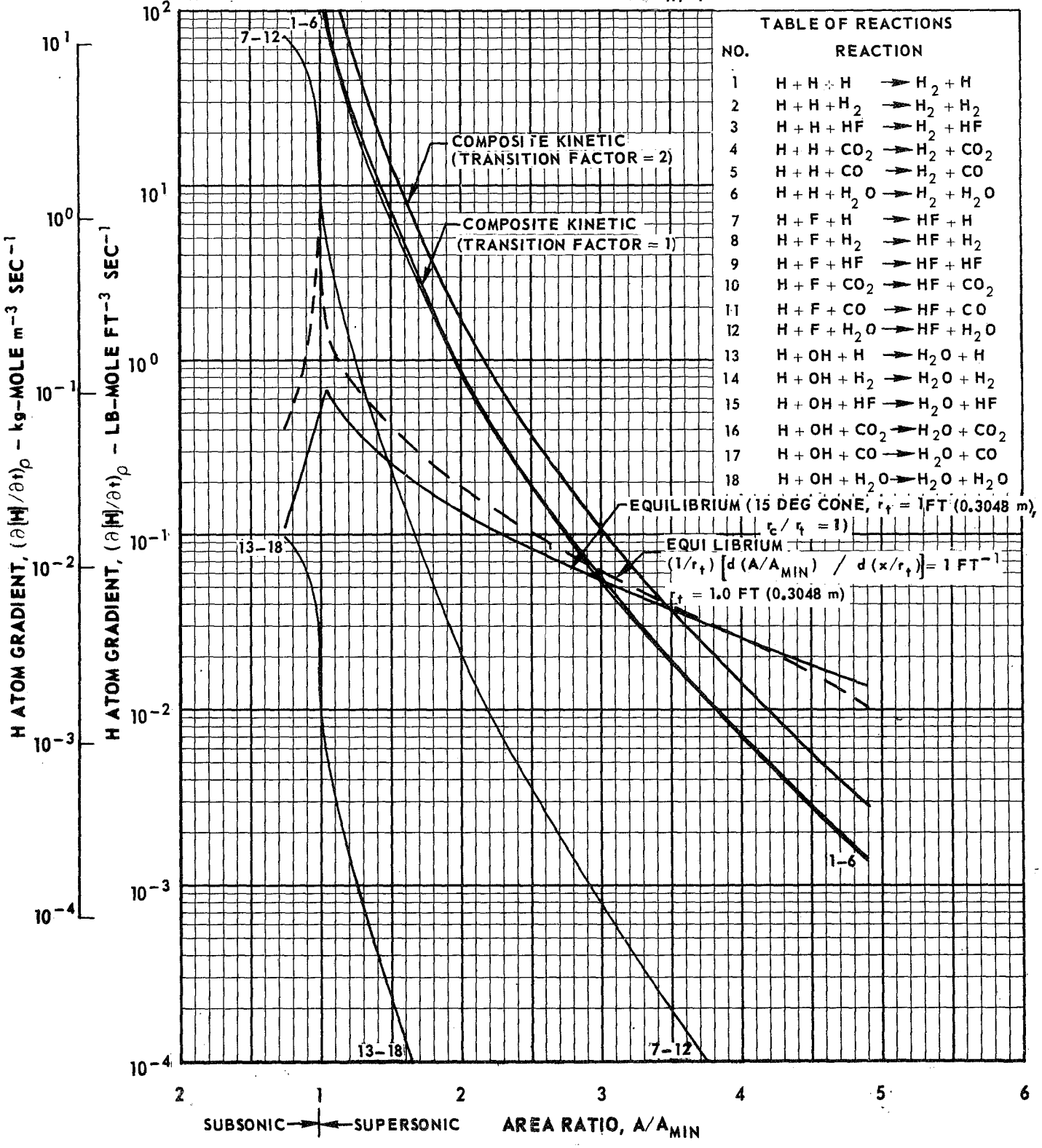

FIG. III-26

NORMALIZED GRAPHICAL SOLUTION FOR FREEZING AREA RATIO USING MODIFIED BRAY ANALYSIS

CH_4 - FLOX (82.6% F_2)

P_C = 750 PSIA (5.171X10^6 N/m^2)

O/F = 5.50

NOTE: REACTION RATE CONSTANTS LISTED IN TABLE III-1

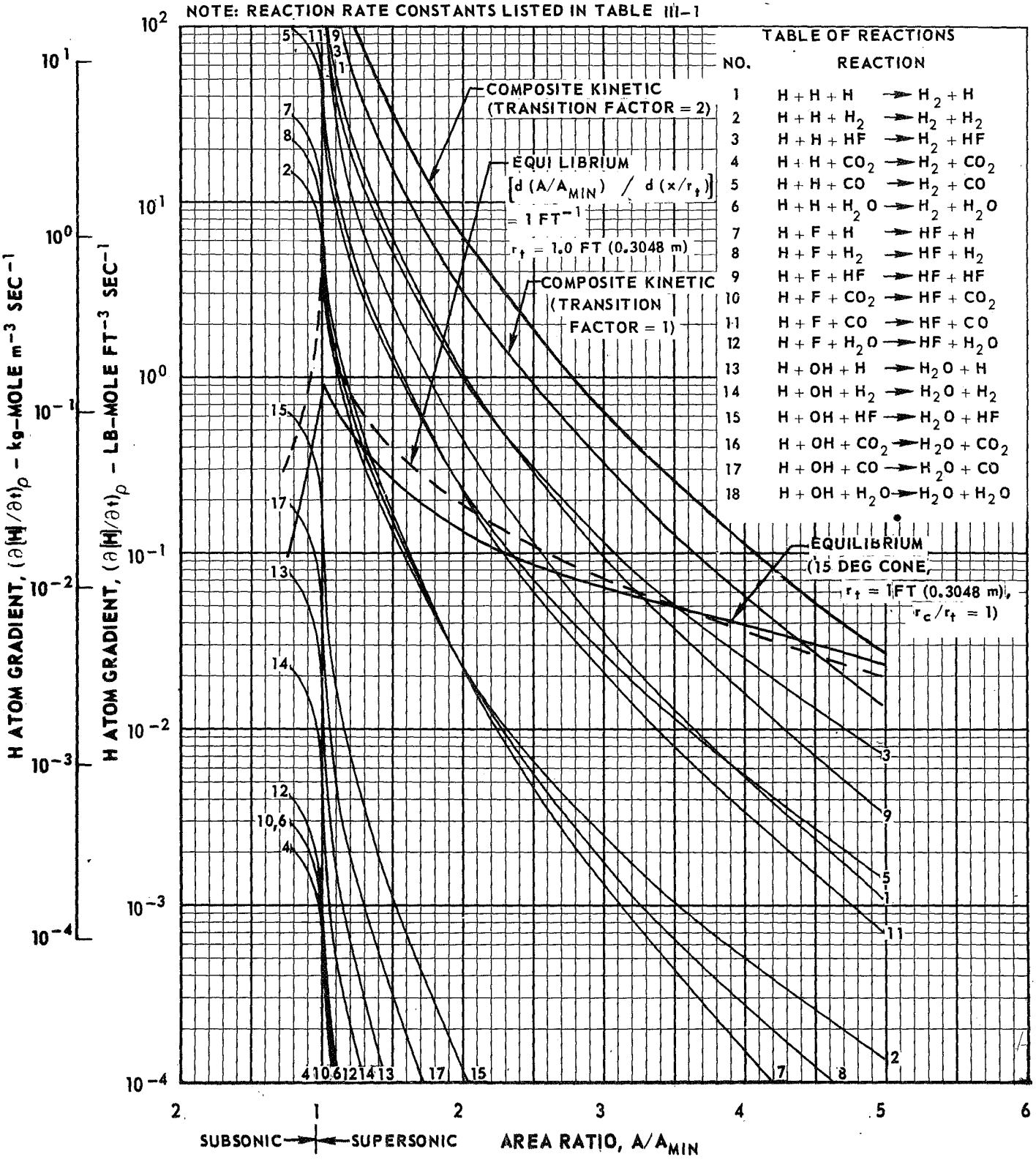

FIG. III-27

NORMALIZED GRAPHICAL SOLUTION FOR FREEZING AREA RATIO USING MODIFIED BRAY ANALYSIS

CH_4 - FLOX (82.6% F_2)

P_C = 750 PSIA (5.171X10 ^{6}N/m^2)

O/F = 6.50

NOTE: REACTION RATE CONSTANTS LISTED IN TABLE III-1

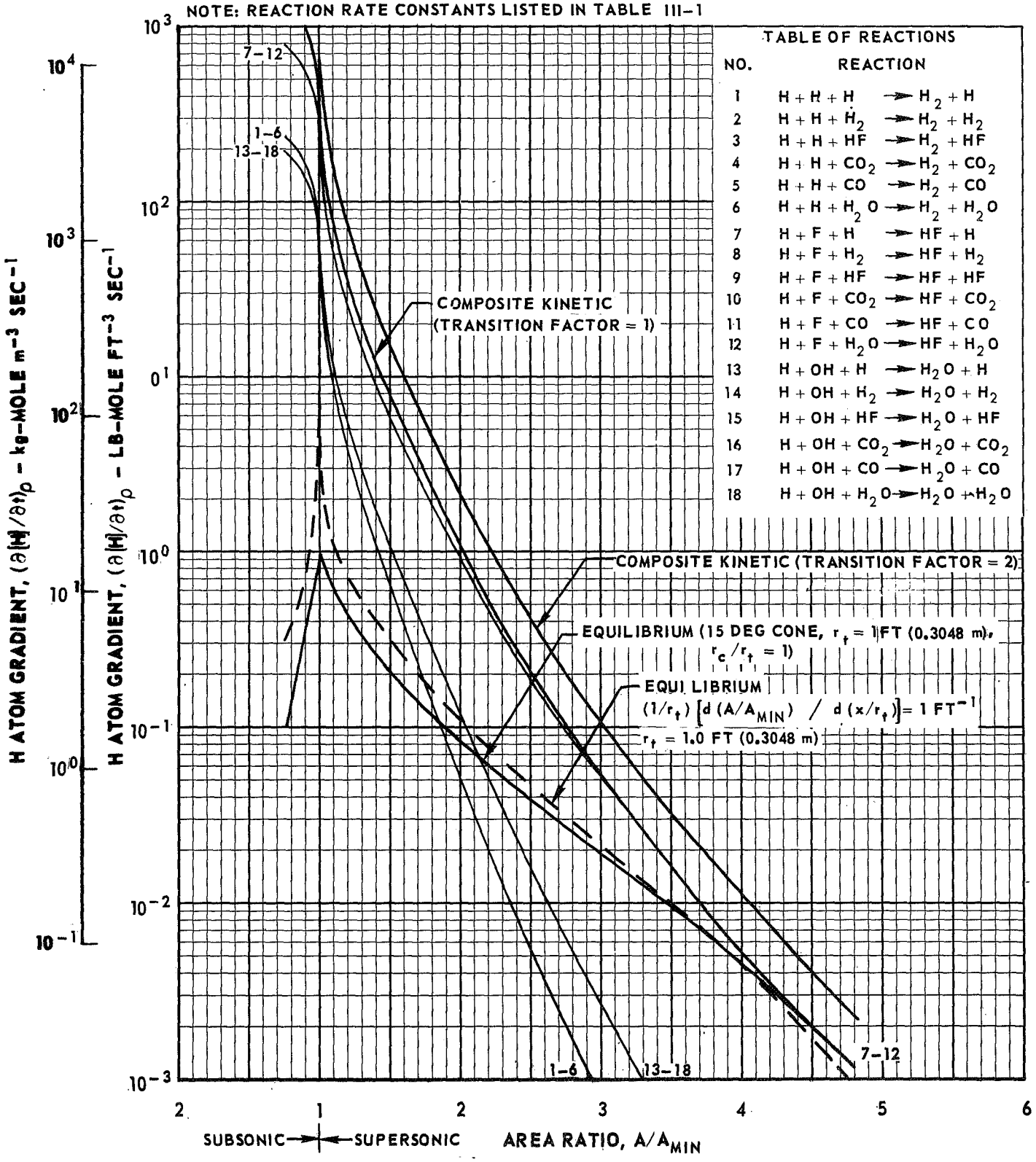

NORMALIZED GRAPHICAL SOLUTION FOR FREEZING AREA RATIO USING MODIFIED BRAY ANALYSIS

CH_4 – FLOX (82.6% F_2)

P_C = 1000 PSIA ($6.895 \times 10^6 N/m^2$)

O/F = 4.00

NOTE: REACTION RATE CONSTANTS LISTED IN TABLE III-1

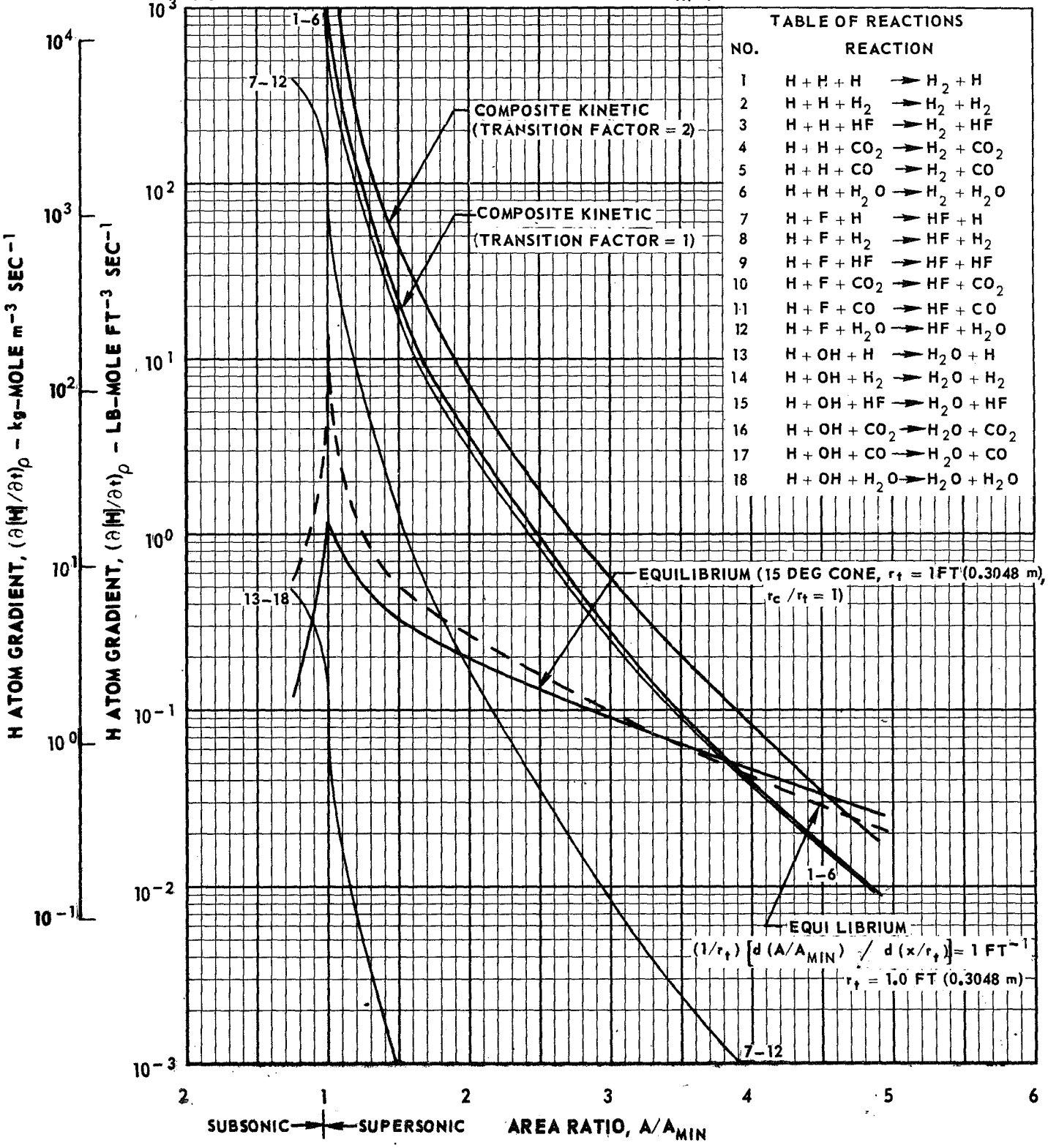

TABLE OF REACTIONS

NO.	REACTION
1	$H + H + H \rightarrow H_2 + H$
2	$H + H + H_2 \rightarrow H_2 + H_2$
3	$H + H + HF \rightarrow H_2 + HF$
4	$H + H + CO_2 \rightarrow H_2 + CO_2$
5	$H + H + CO \rightarrow H_2 + CO$
6	$H + H + H_2O \rightarrow H_2 + H_2O$
7	$H + F + H \rightarrow HF + H$
8	$H + F + H_2 \rightarrow HF + H_2$
9	$H + F + HF \rightarrow HF + HF$
10	$H + F + CO_2 \rightarrow HF + CO_2$
11	$H + F + CO \rightarrow HF + CO$
12	$H + F + H_2O \rightarrow HF + H_2O$
13	$H + OH + H \rightarrow H_2O + H$
14	$H + OH + H_2 \rightarrow H_2O + H_2$
15	$H + OH + HF \rightarrow H_2O + HF$
16	$H + OH + CO_2 \rightarrow H_2O + CO_2$
17	$H + OH + CO \rightarrow H_2O + CO$
18	$H + OH + H_2O \rightarrow H_2O + H_2O$

FIG. III-29

NORMALIZED GRAPHICAL SOLUTION FOR FREEZING AREA RATIO USING MODIFIED BRAY ANALYSIS

CH_4 - FLOX (82.6% F_2)

P_C = 1000 PSIA (6.895×10^6 N/m2)

O/F = 6.00

NOTE: REACTION RATE CONSTANTS LISTED IN TABLE III-1

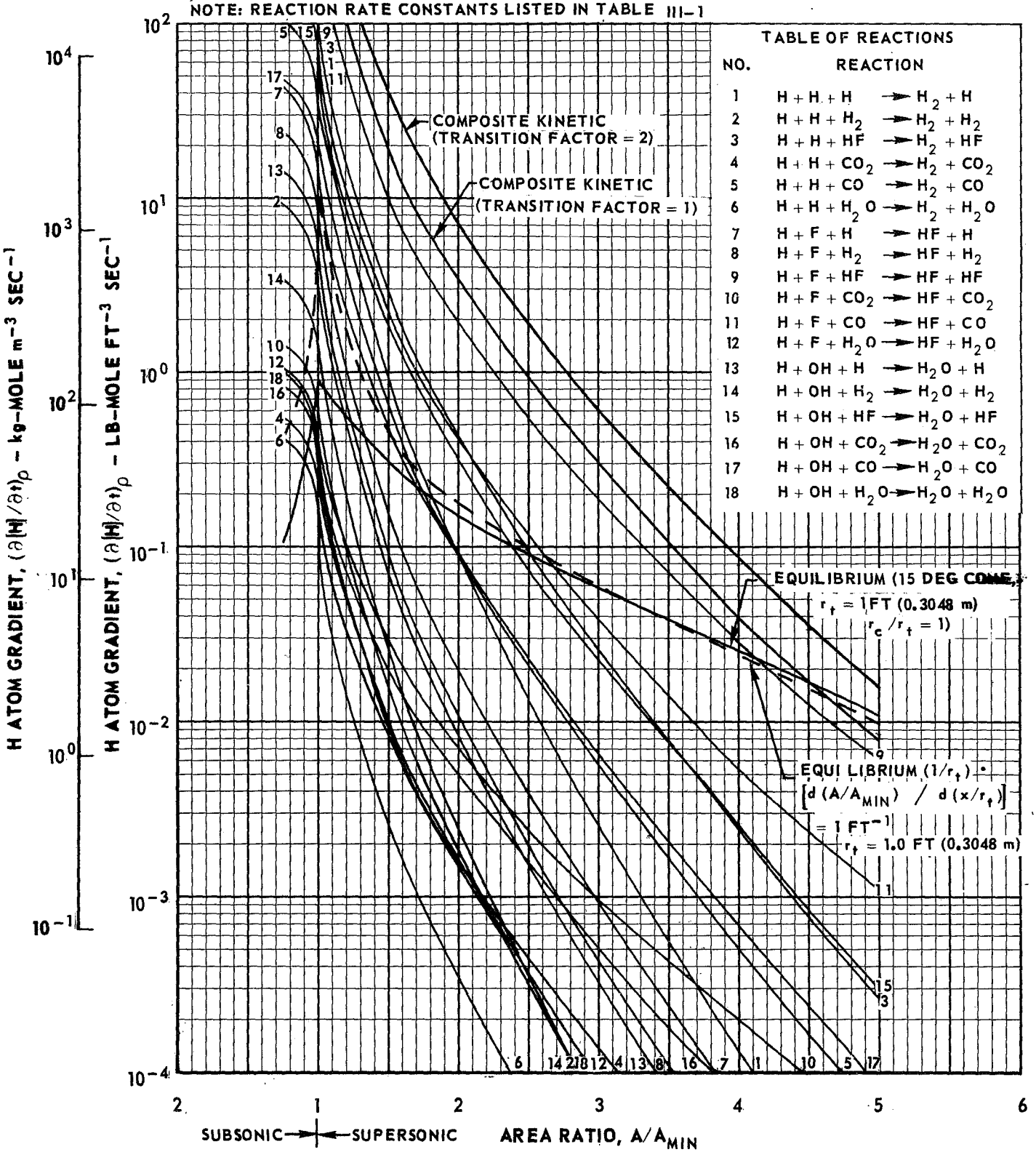

TABLE OF REACTIONS

NO.	REACTION
1	$H + H + H \rightarrow H_2 + H$
2	$H + H + H_2 \rightarrow H_2 + H_2$
3	$H + H + HF \rightarrow H_2 + HF$
4	$H + H + CO_2 \rightarrow H_2 + CO_2$
5	$H + H + CO \rightarrow H_2 + CO$
6	$H + H + H_2O \rightarrow H_2 + H_2O$
7	$H + F + H \rightarrow HF + H$
8	$H + F + H_2 \rightarrow HF + H_2$
9	$H + F + HF \rightarrow HF + HF$
10	$H + F + CO_2 \rightarrow HF + CO_2$
11	$H + F + CO \rightarrow HF + CO$
12	$H + F + H_2O \rightarrow HF + H_2O$
13	$H + OH + H \rightarrow H_2O + H$
14	$H + OH + H_2 \rightarrow H_2O + H_2$
15	$H + OH + HF \rightarrow H_2O + HF$
16	$H + OH + CO_2 \rightarrow H_2O + CO_2$
17	$H + OH + CO \rightarrow H_2O + CO$
18	$H + OH + H_2O \rightarrow H_2O + H_2O$

FIG. III-30

NORMALIZED GRAPHICAL SOLUTION FOR FREEZING AREA RATIO USING MODIFIED BRAY ANALYSIS

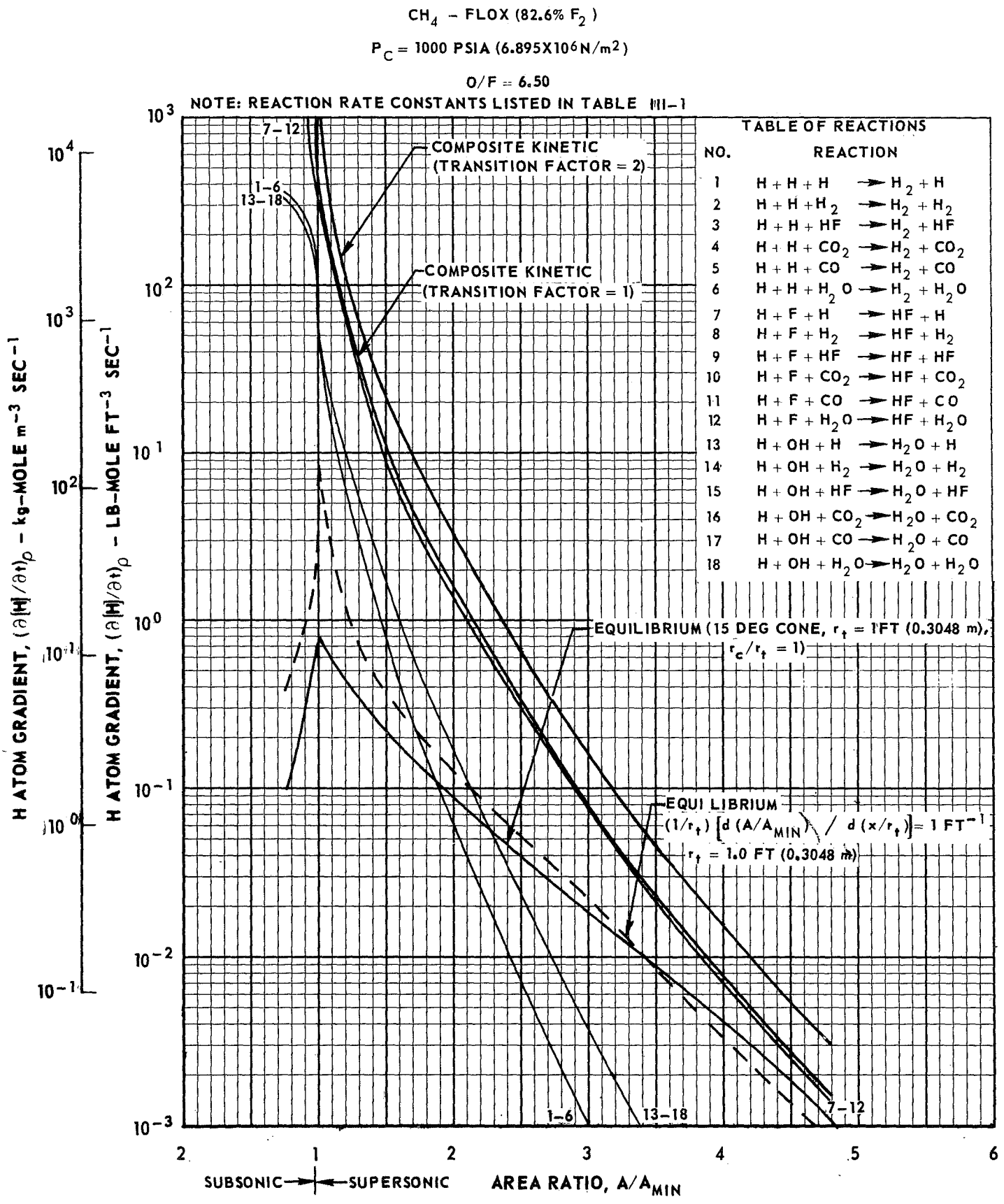

FIG. III-31

EFFECT OF FREEZING AREA RATIO ON NONEQUILIBRIUM PERFORMANCE FOR METHANE - FLOX PROPELLANT SYSTEM

CH_4 - FLOX (82.6% F_2)

P_C = 100 PSIA (6.895 X 10^5 N/m^2)

O/F = 3.50

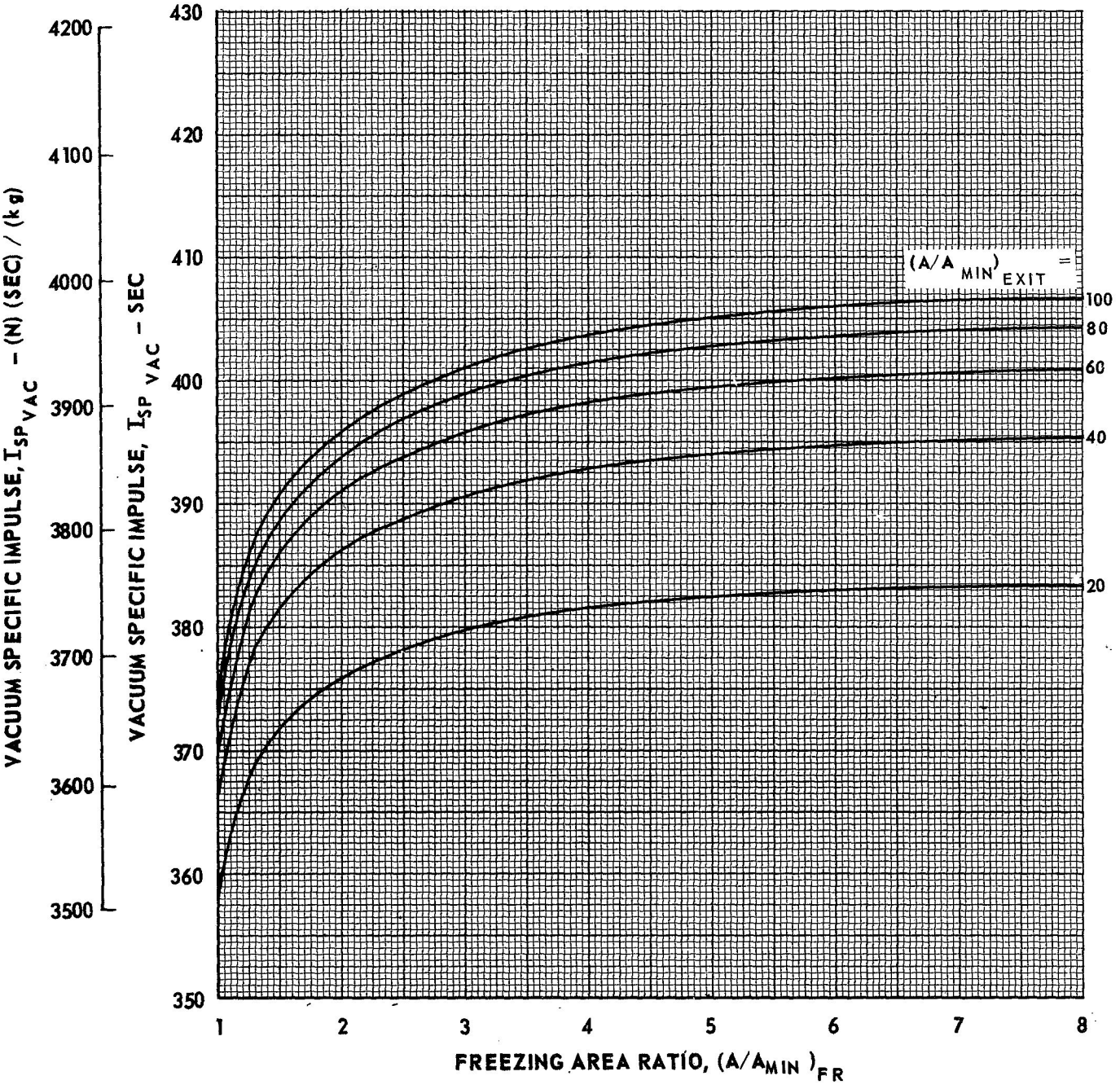

FIG. III-32

EFFECT OF FREEZING AREA RATIO ON NONEQUILIBRIUM PERFORMANCE FOR METHANE - FLOX PROPELLANT SYSTEM

CH_4 - FLOX (82.6% F_2)

P_C = 100 PSIA (6.895 X 10^5 N/m^2)

O/F = 5.5

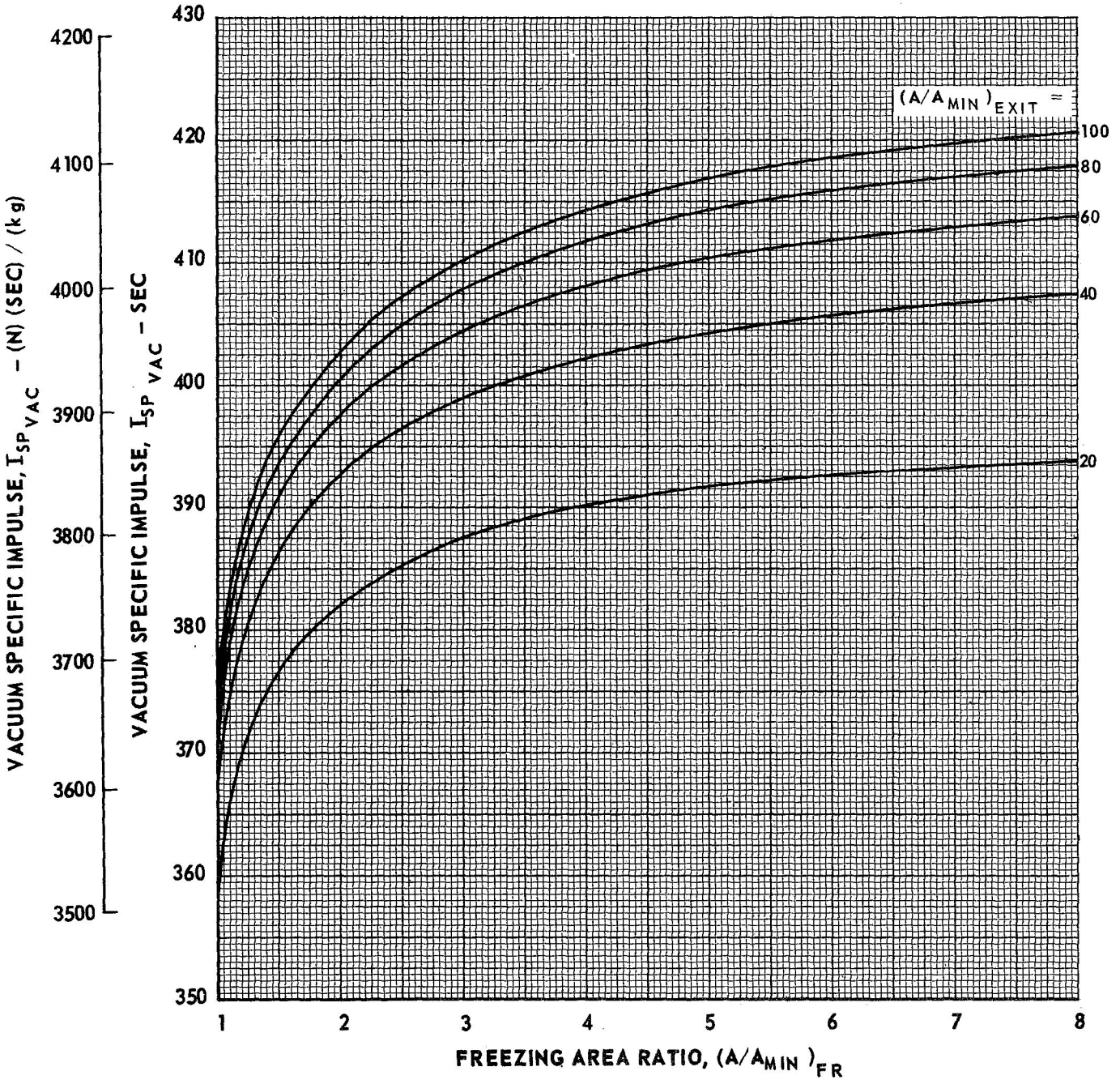

FIG. III-33

EFFECT OF FREEZING AREA RATIO ON NONEQUILIBRIUM PERFORMANCE FOR METHANE - FLOX PROPELLANT SYSTEM

CH_4 - FLOX (82.6% F_2)

P_C = 100 PSIA (6.895X10^5 N/m2)

O/F = 6.50

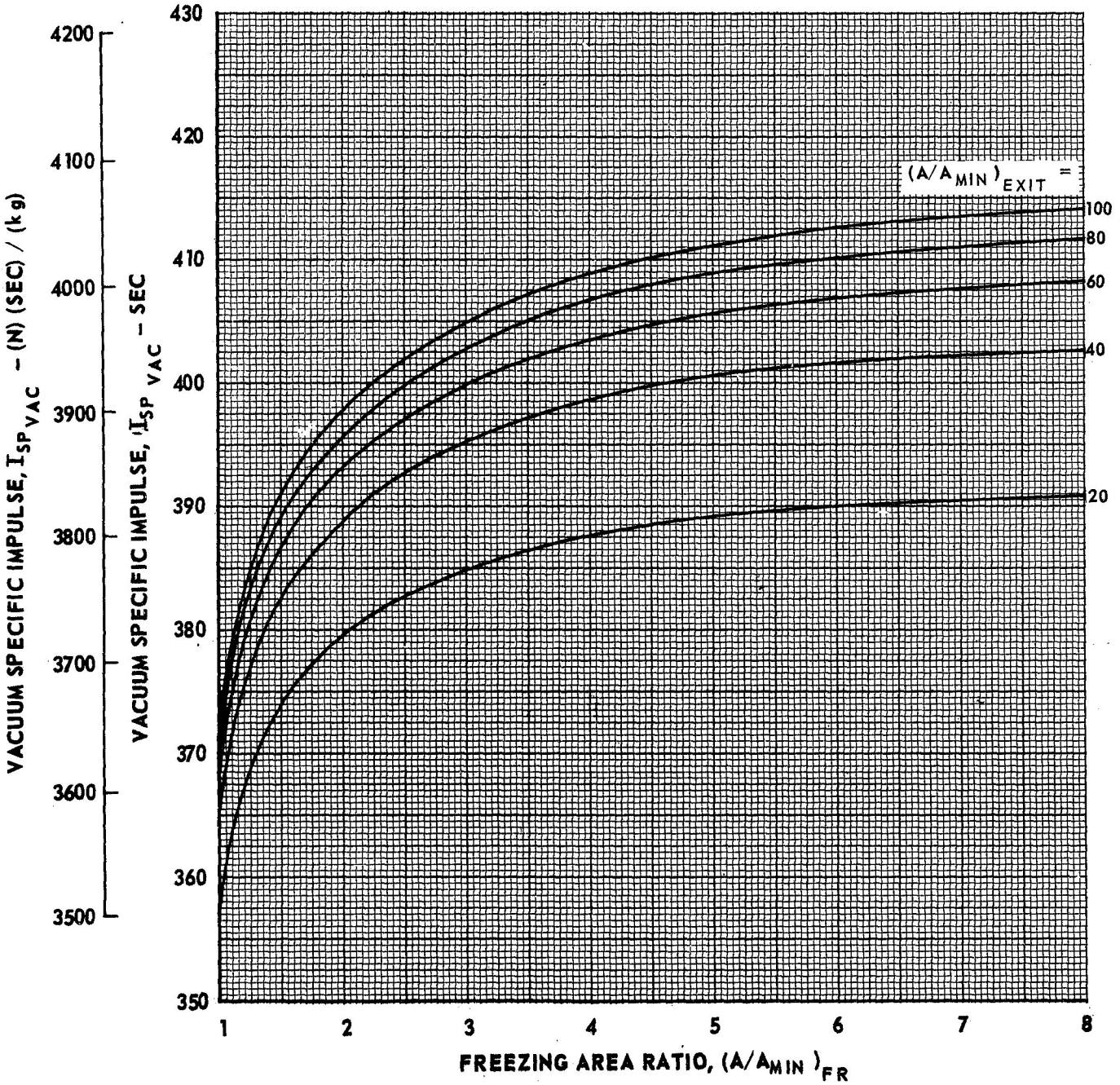

FIG. III-34

EFFECT OF FREEZING AREA RATIO ON NONEQUILIBRIUM PERFORMANCE FOR METHANE - FLOX PROPELLANT SYSTEM

CH_4 - FLOX (82.6% F_2)

P_C = 200 PSIA (1.379 X 10^6 N/m^2)

O/F = 3.50

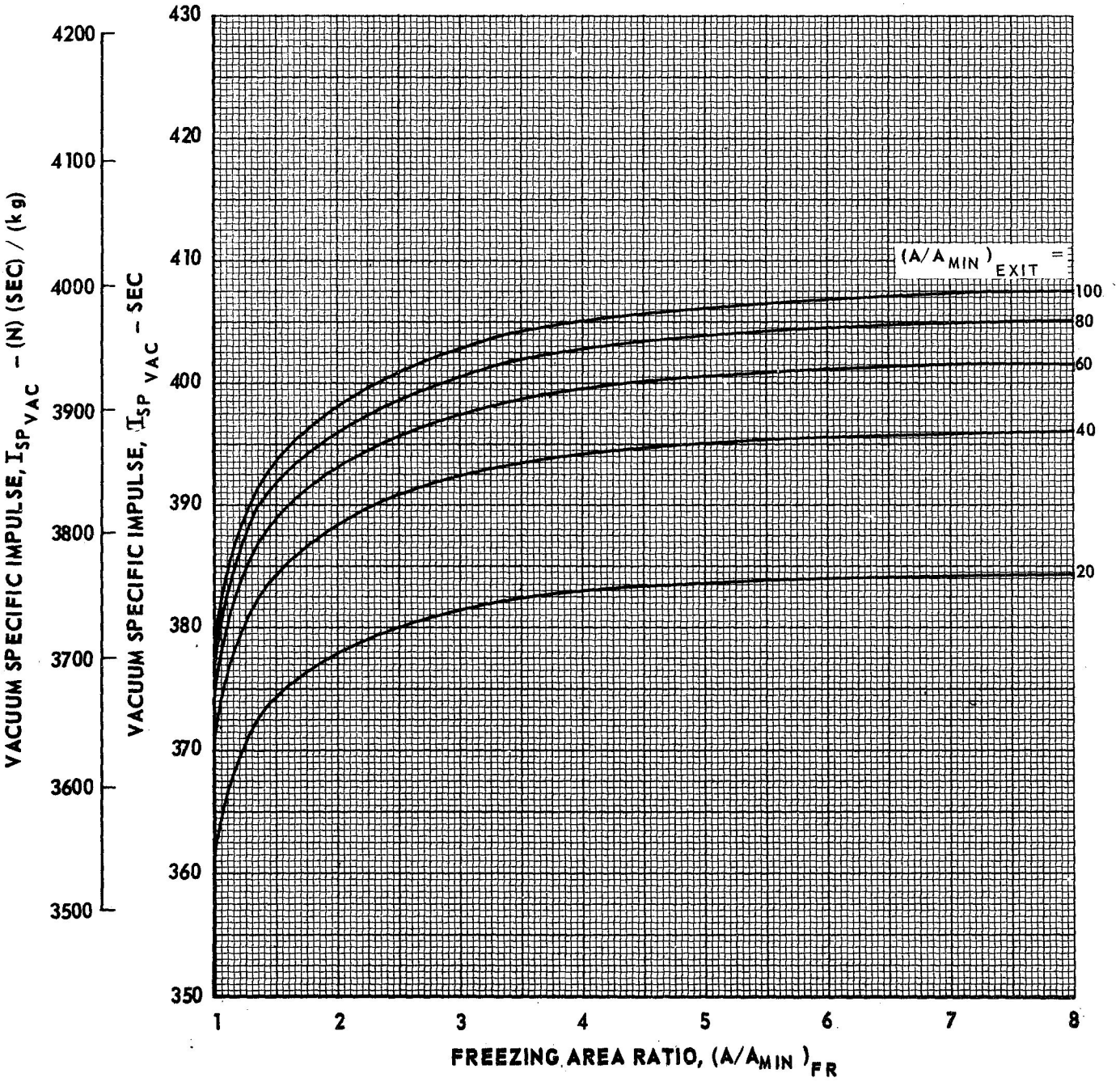

FIG. III–35

EFFECT OF FREEZING AREA RATIO ON NONEQUILIBRIUM PERFORMANCE FOR METHANE – FLOX PROPELLANT SYSTEM

CH_4 – FLOX (82.6% F_2)

P_C = 200 PSIA (1.379 X 10^6 N/m^2)

O/F = 5.50

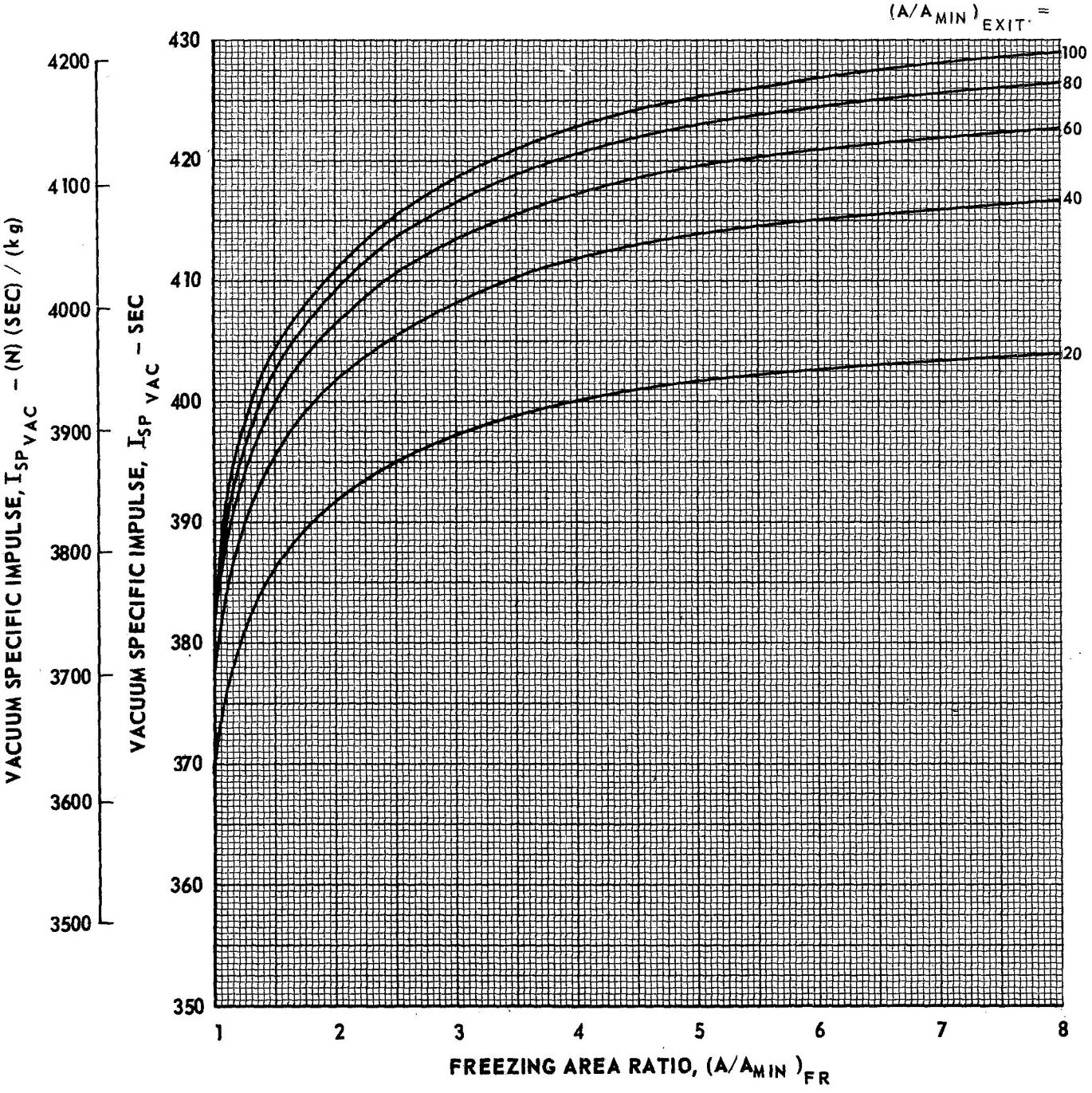

FIG. III-36

EFFECT OF FREEZING AREA RATIO ON NONEQUILIBRIUM PERFORMANCE FOR METHANE - FLOX PROPELLANT SYSTEM

CH_4 - FLOX (82.6% F_2)

P_C = 200 PSIA ($1.379 \times 10^6 N/m^2$)

O/F = 6.50

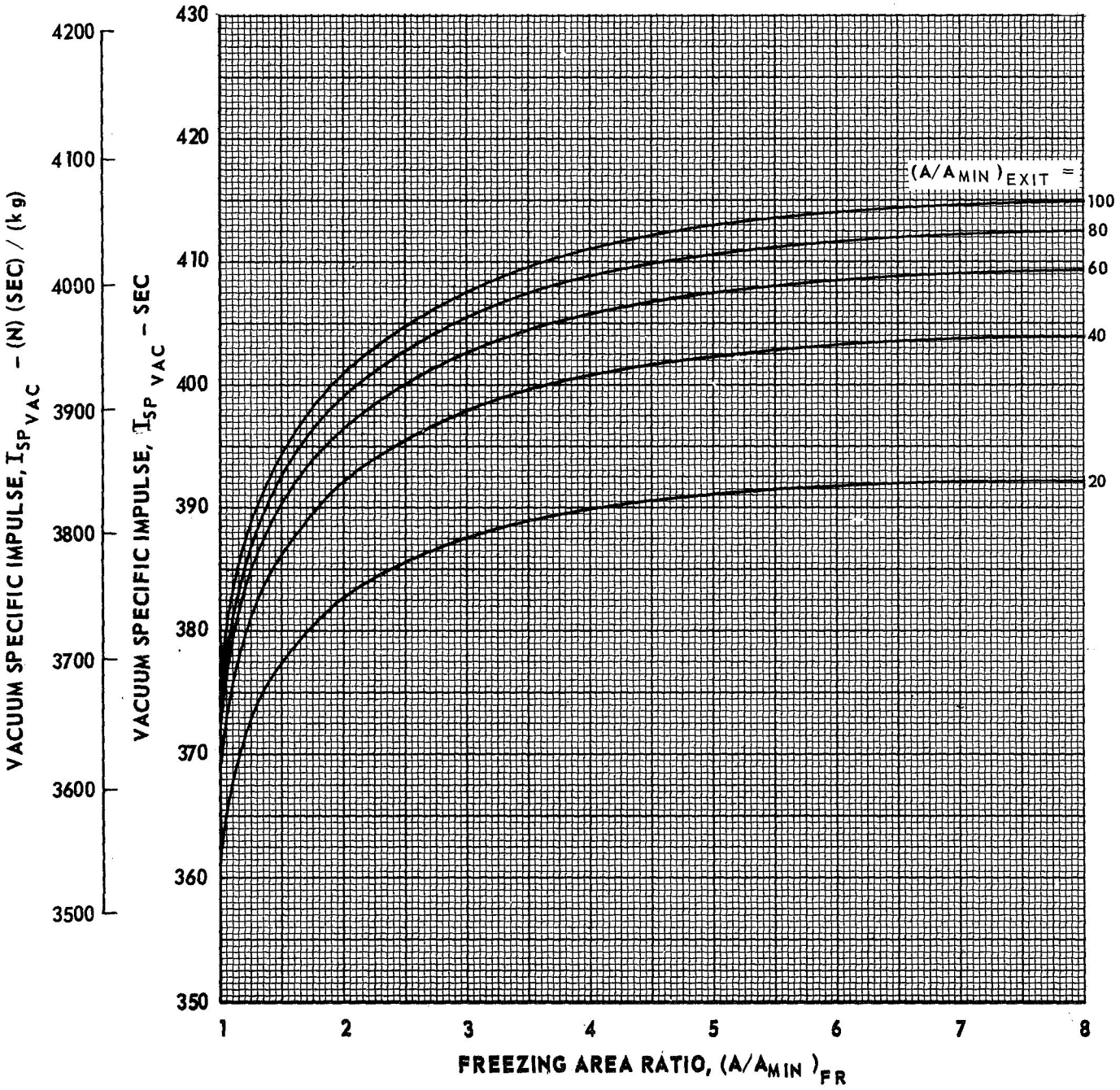

FIG. III-37

EFFECT OF FREEZING AREA RATIO ON NONEQUILIBRIUM PERFORMANCE FOR METHANE - FLOX PROPELLANT SYSTEM

CH_4 - FLOX (82.6% F_2)

P_C = 300 PSIA (2.069 X 10^6 N/m^2)

O/F = 3.50

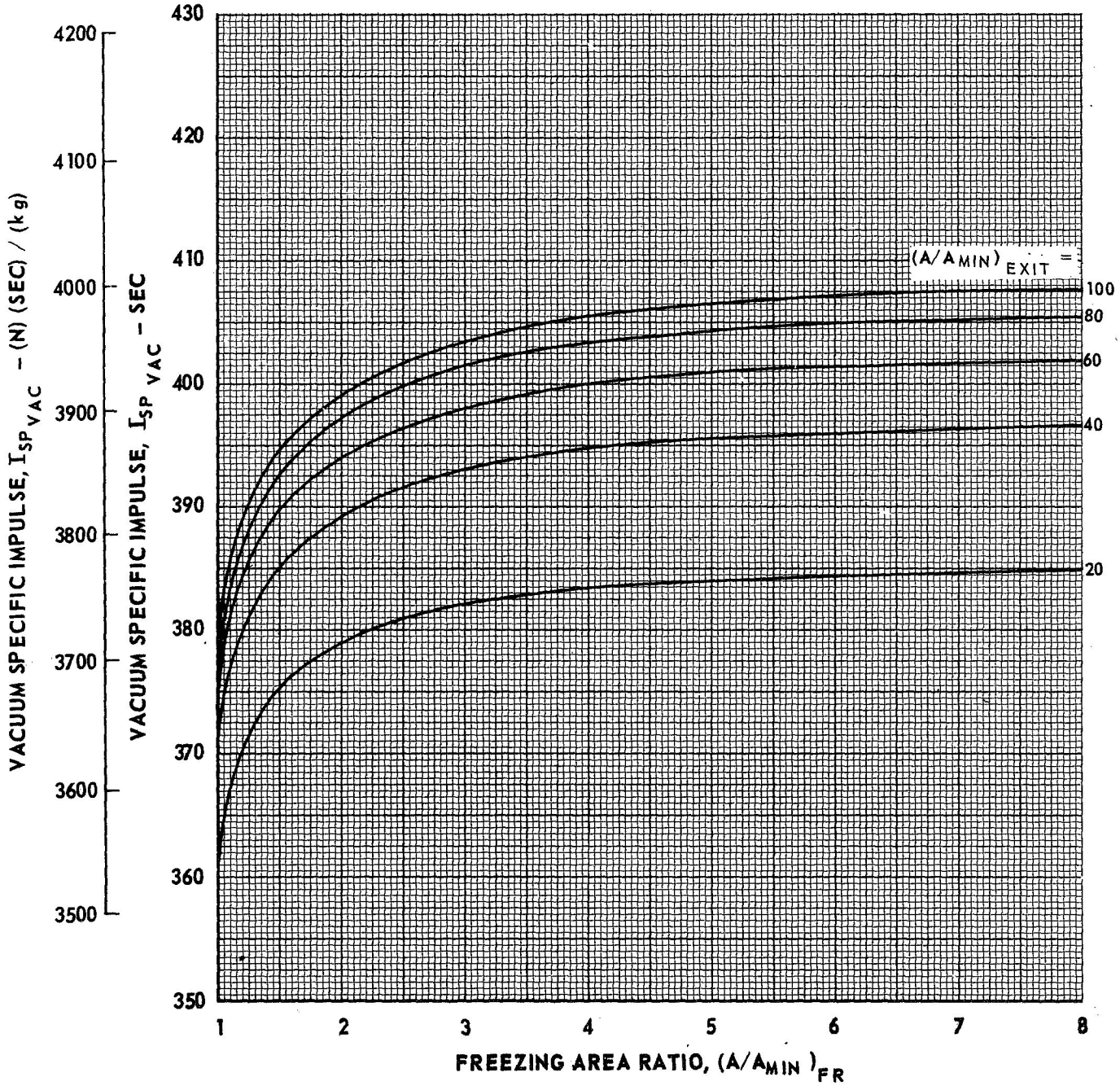

FIG. III-38

EFFECT OF FREEZING AREA RATIO ON NONEQUILIBRIUM PERFORMANCE FOR METHANE - FLOX PROPELLANT SYSTEM

CH_4 - FLOX (82.6% F_2)

P_C = 300 PSIA (2.069 X 10^6 N/m^2)

O/F = 5.50

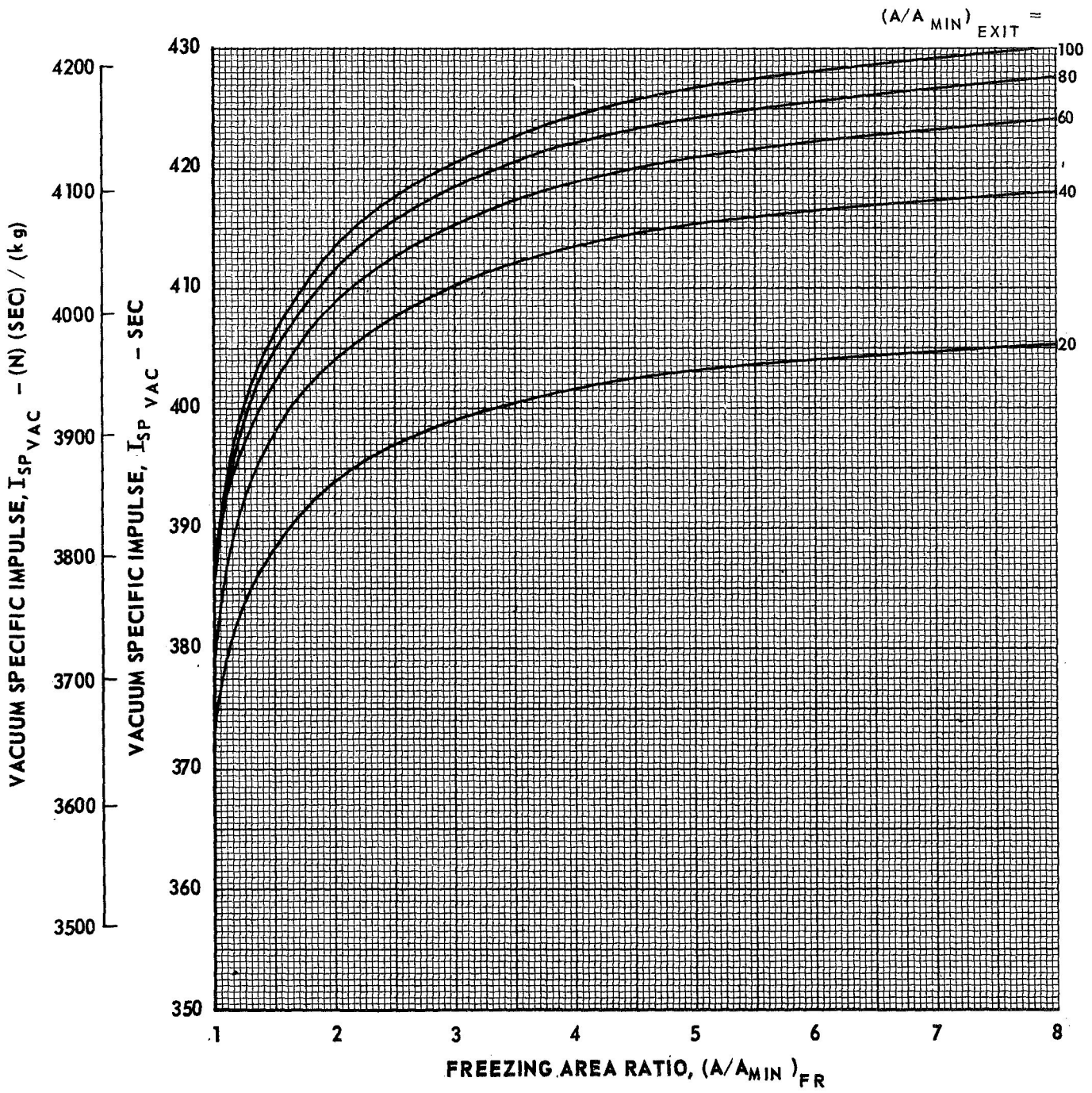

FIG. III-39

EFFECT OF FREEZING AREA RATIO ON NONEQUILIBRIUM PERFORMANCE FOR METHANE - FLOX PROPELLANT SYSTEM

CH_4 - FLOX (82.6% F_2)

P_C = 300 PSIA (2.069 X 10^6 N/m^2)

O/F = 6.50

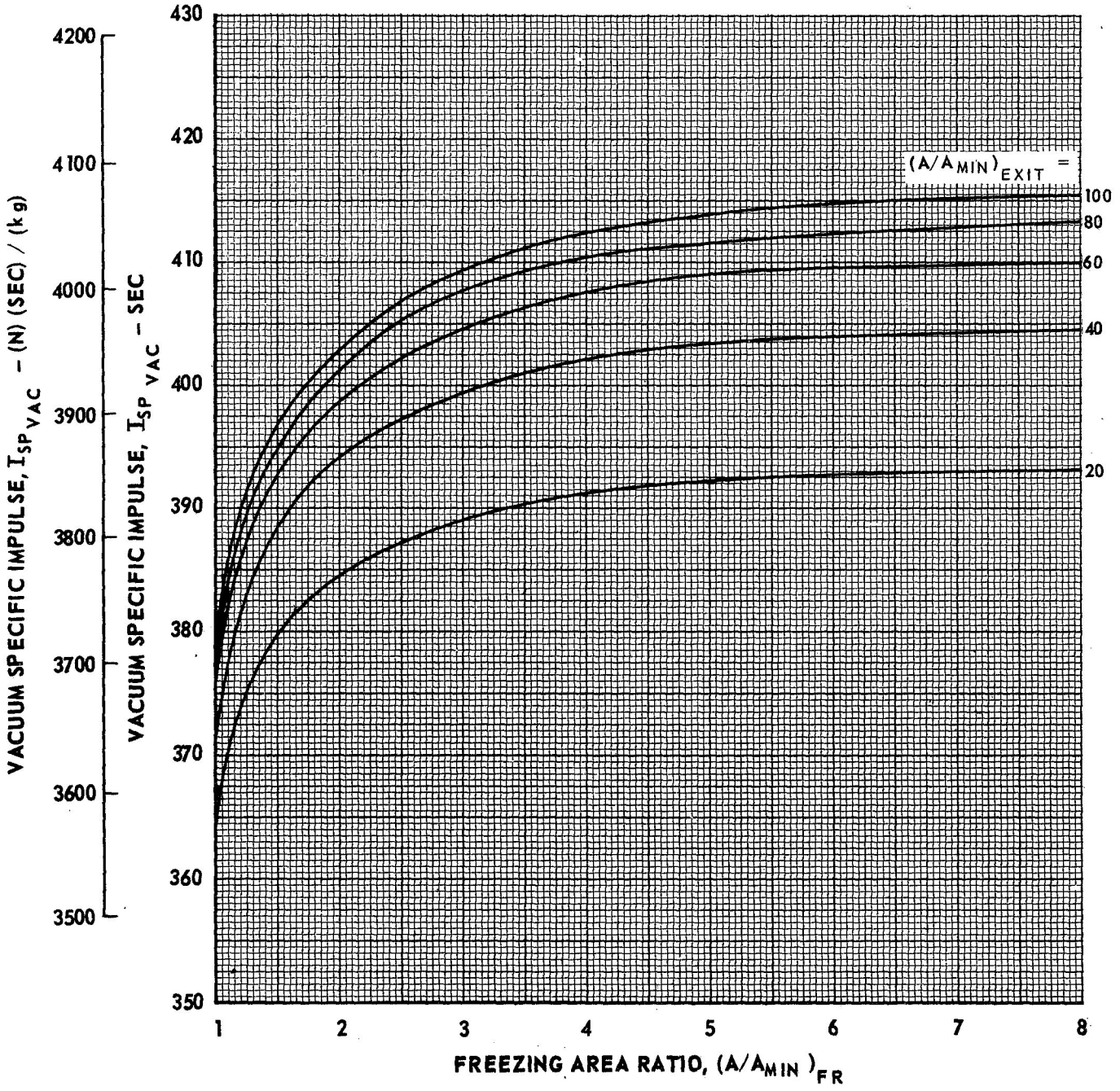

FIG. III-40

EFFECT OF FREEZING AREA RATIO ON NONEQUILIBRIUM PERFORMANCE FOR METHANE - FLOX PROPELLANT SYSTEM

CH_4 - FLOX (82.6% F_2)

P_C = 500 PSIA (3.448 X 10^6 N/m^2)

O/F = 3.50

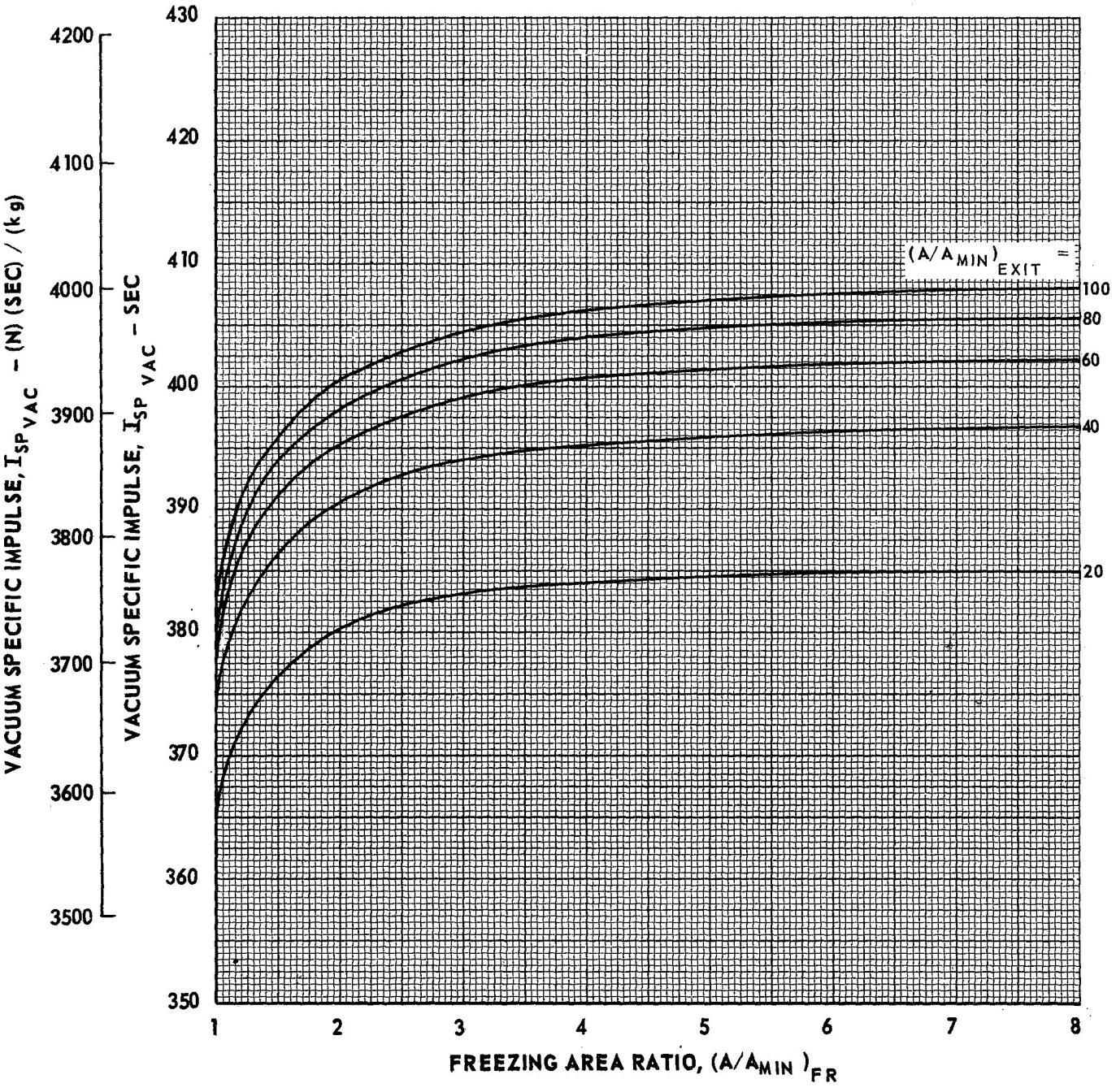

FIG. III-41

EFFECT OF FREEZING AREA RATIO ON NONEQUILIBRIUM PERFORMANCE FOR METHANE - FLOX PROPELLANT SYSTEM

CH_4 - FLOX (82.6% F_2)

P_C = 500 PSIA (3.448 X 10^6 N/m^2)

O/F = 5.50

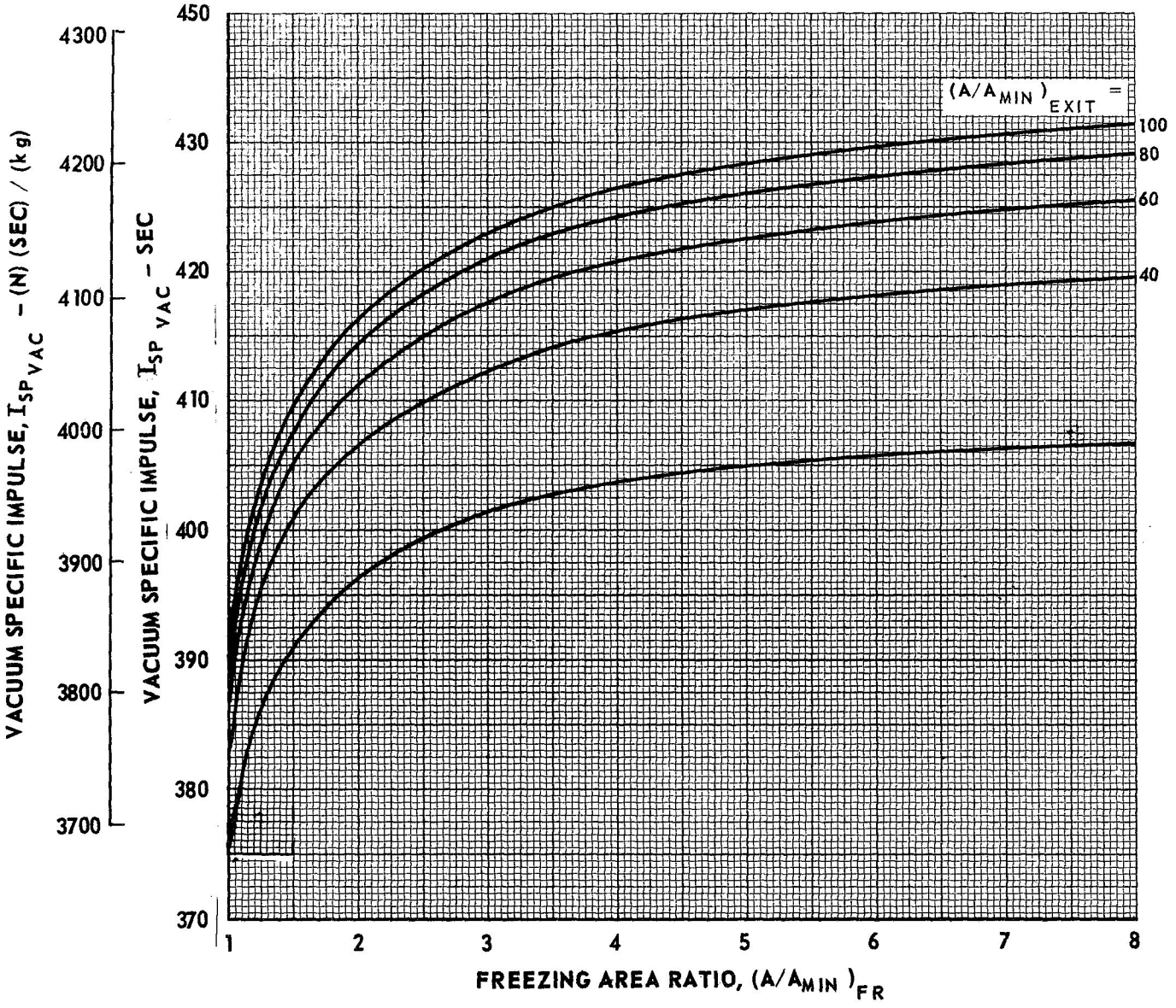

FIG. III-42

EFFECT OF FREEZING AREA RATIO ON NONEQUILIBRIUM PERFORMANCE FOR METHANE - FLOX PROPELLANT SYSTEM

CH_4 - FLOX (82.6% F_2)

P_C = 500 PSIA (3.448 X 10^6 N/m^2)

O/F = 6.50

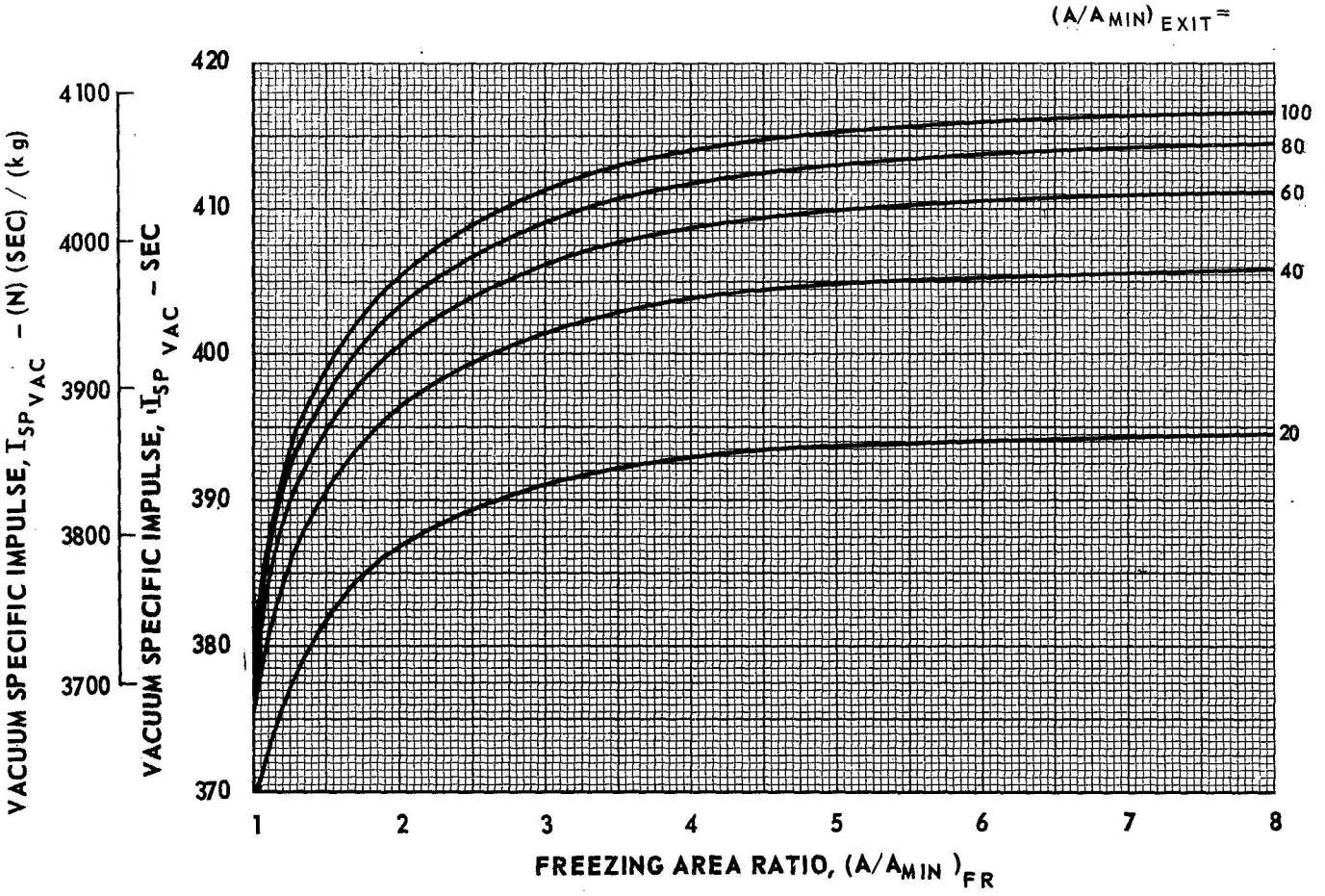

FIG. III-43

EFFECT OF FREEZING AREA RATIO ON NONEQUILIBRIUM PERFORMANCE FOR METHANE - FLOX PROPELLANT SYSTEM

CH_4 - FLOX (82.6% F_2)

P_C = 750 PSIA (5.171 X 10^6 N/m^2)

O/F = 3.50

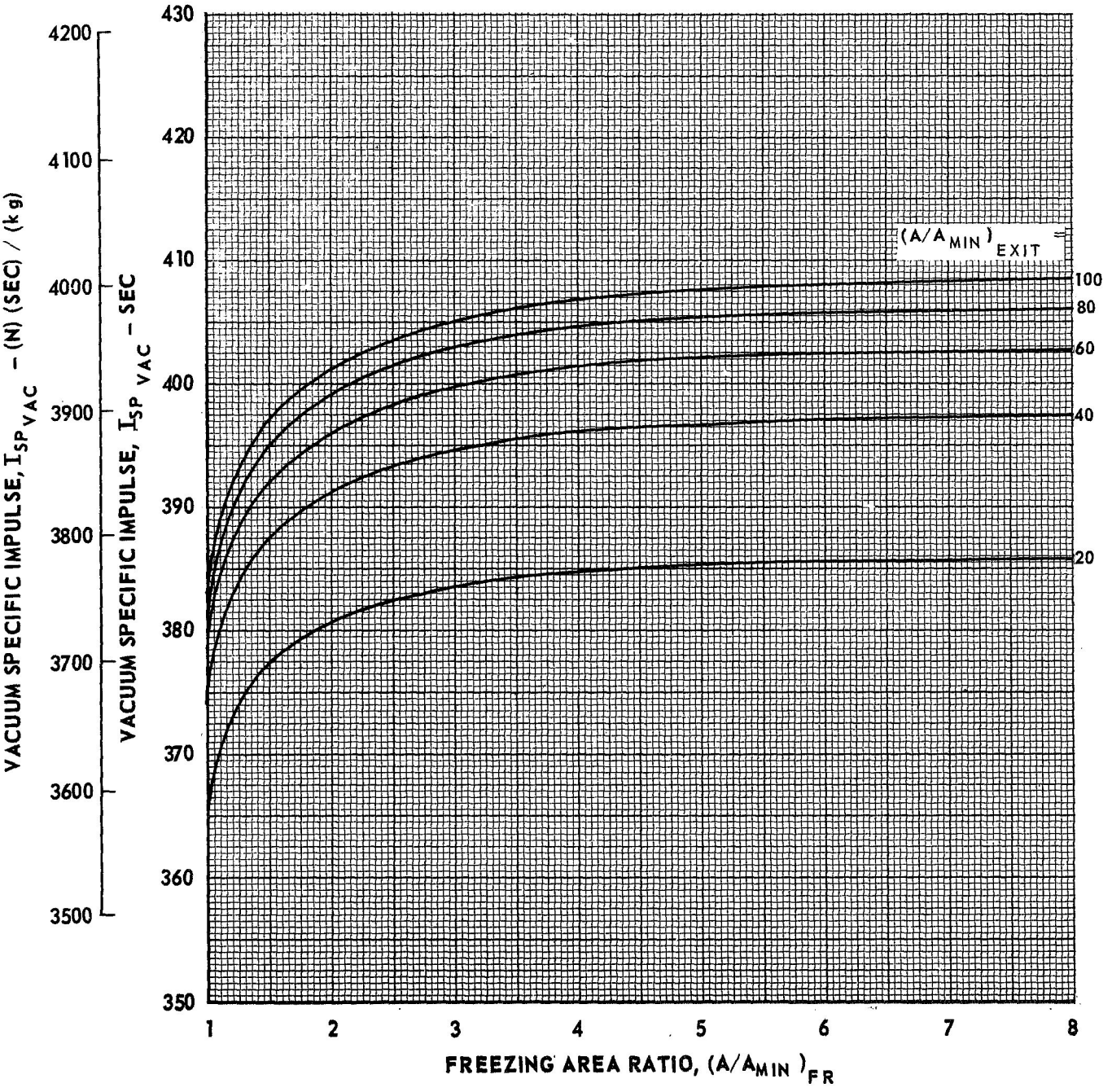

FIG. III-44

EFFECT OF FREEZING AREA RATIO ON NONEQUILIBRIUM PERFORMANCE FOR METHANE - FLOX PROPELLANT SYSTEM

CH_4 - FLOX (82.6% F_2)

P_C = 750 PSIA (5.171 X 10^6 N/m^2)

O/F = 5.50

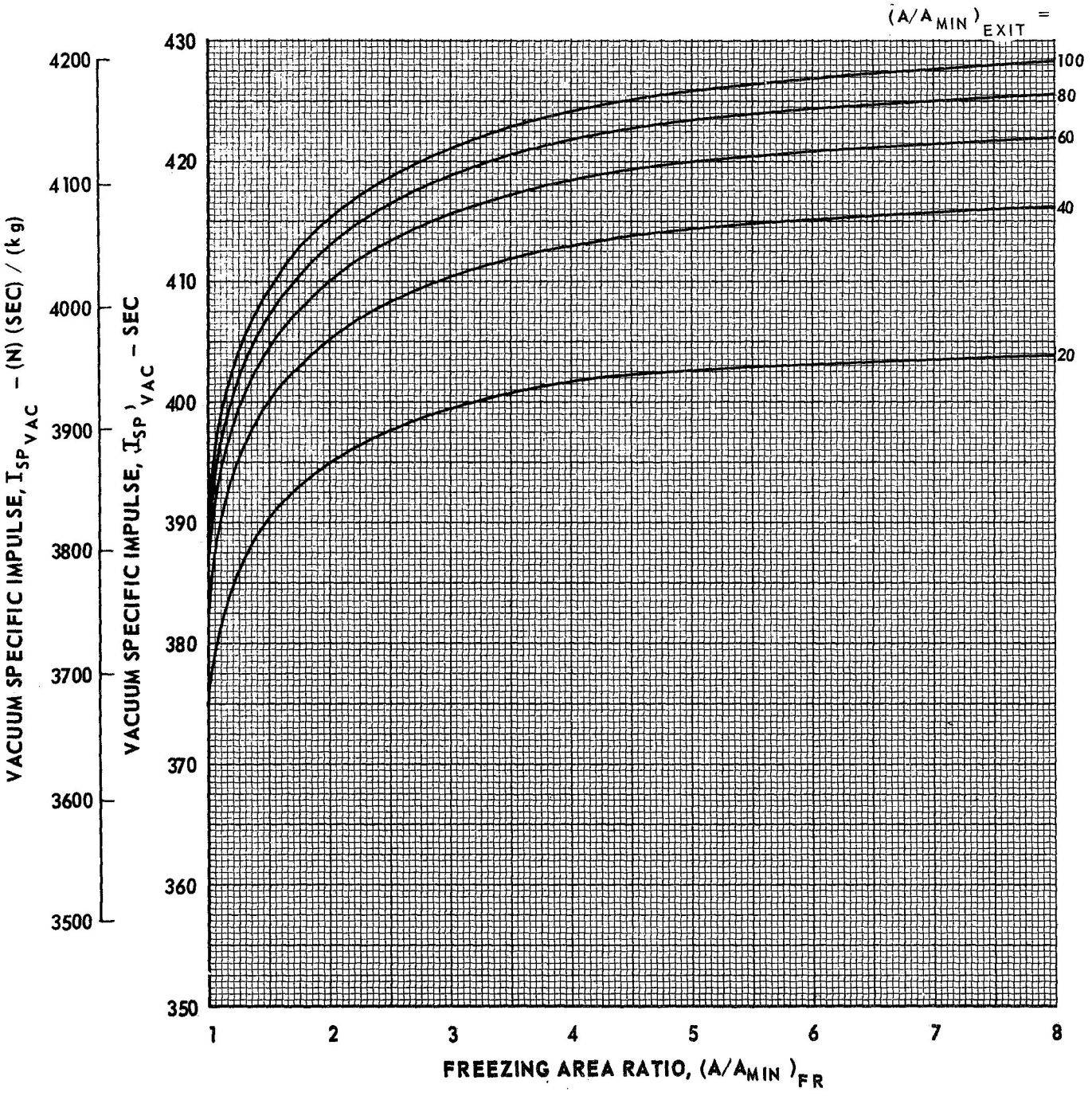

FIG. III-45

EFFECT OF FREEZING AREA RATIO ON NONEQUILIBRIUM PERFORMANCE FOR METHANE - FLOX PROPELLANT SYSTEM

CH_4 - FLOX (82.6% F_2)

P_C = 750 PSIA (5.171 X 10^6 N/m^2)

O/F = 6.50

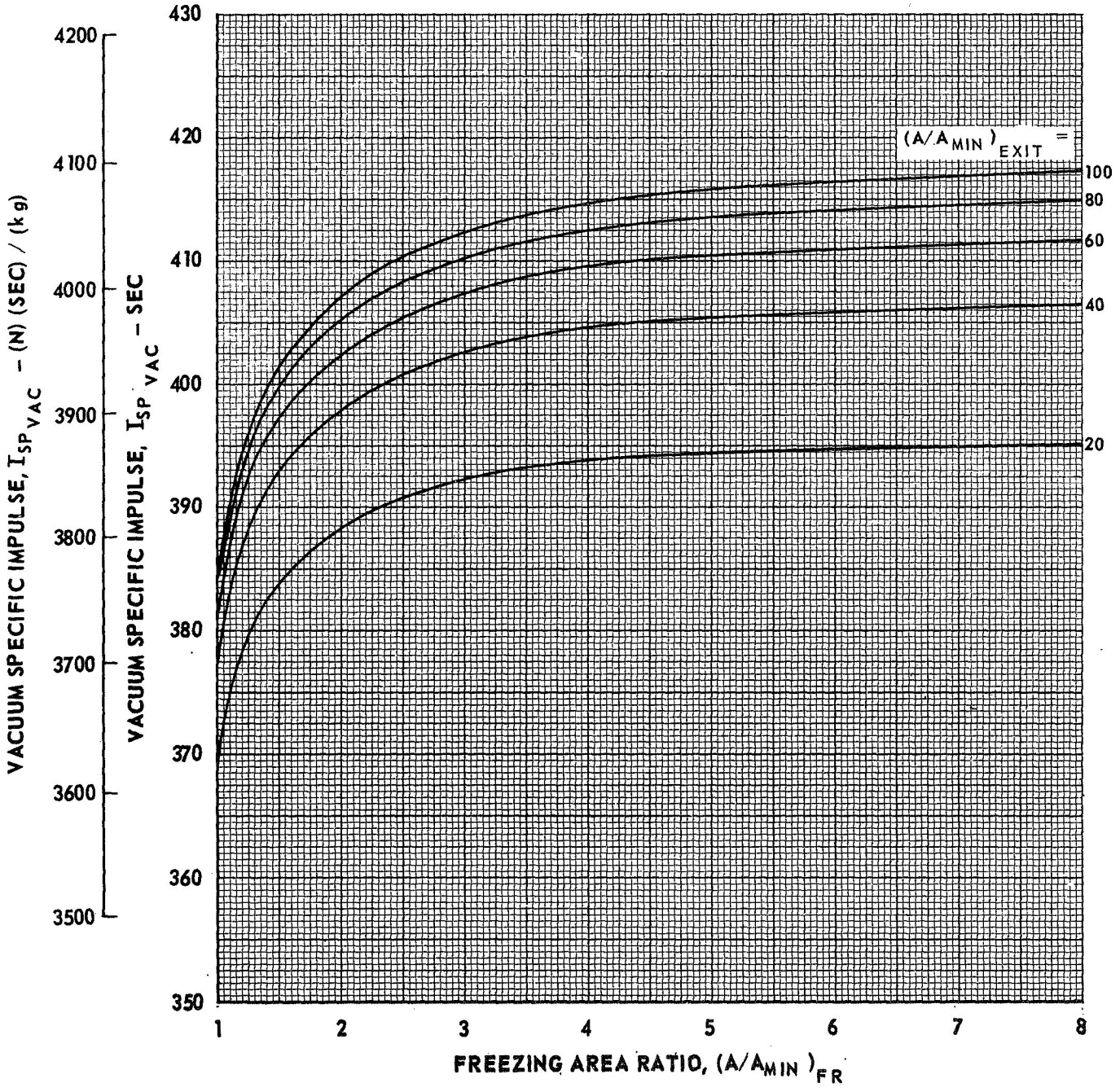

FIG. III-46

EFFECT OF FREEZING AREA RATIO ON NONEQUILIBRIUM PERFORMANCE FOR METHANE - FLOX PROPELLANT SYSTEM

CH_4 - FLOX (82.6% F_2)

P_C = 1000 PSIA (6.895 X 10^6 N/m^2)

O/F = 4.00

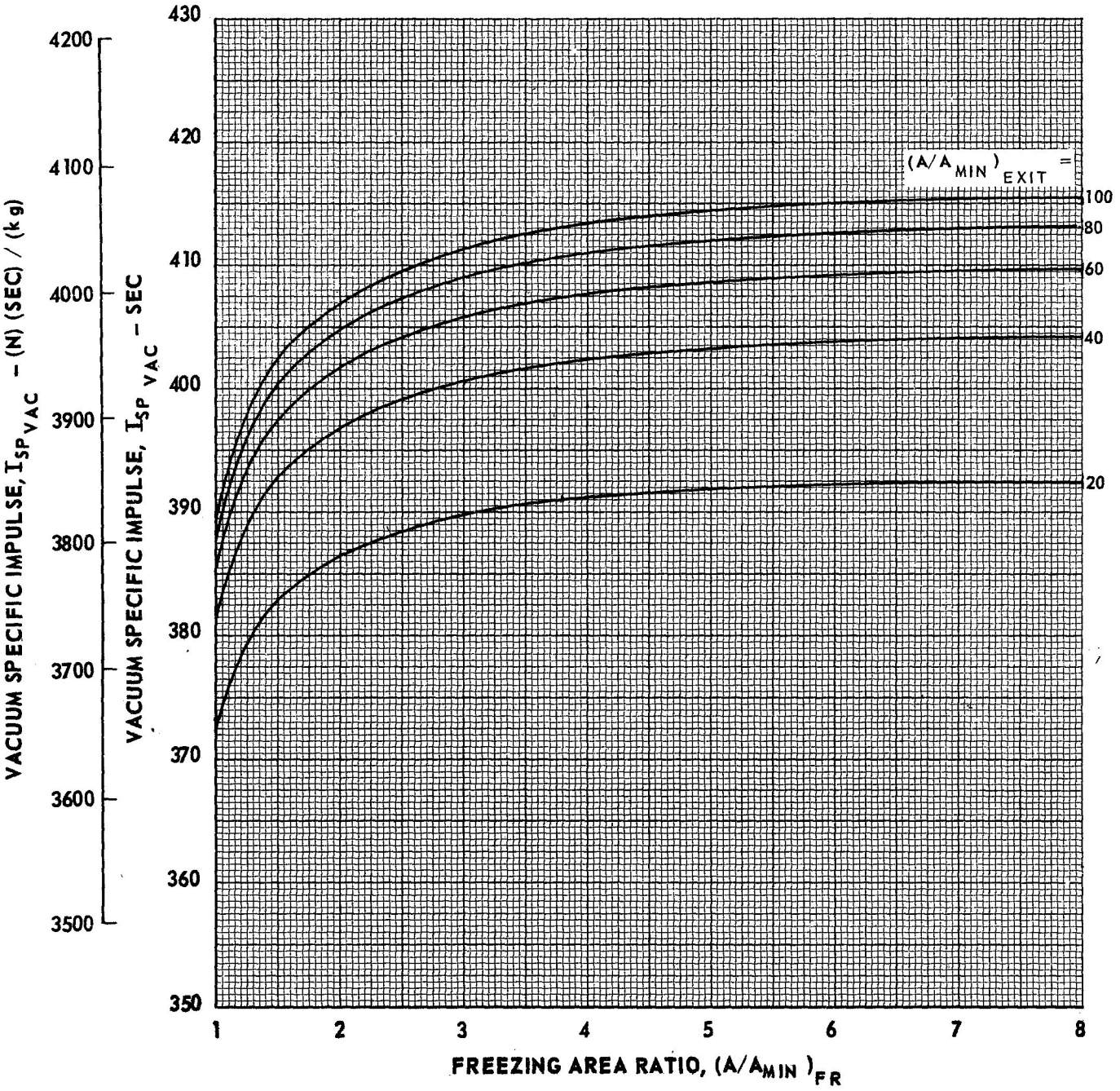

FIG. III-47

EFFECT OF FREEZING AREA RATIO ON NONEQUILIBRIUM PERFORMANCE FOR METHANE - FLOX PROPELLANT SYSTEM

CH_4 - FLOX (82.6% F_2)

P_C = 1000 PSIA (6.895 X 10^6 N/m^2)

O/F = 6.00

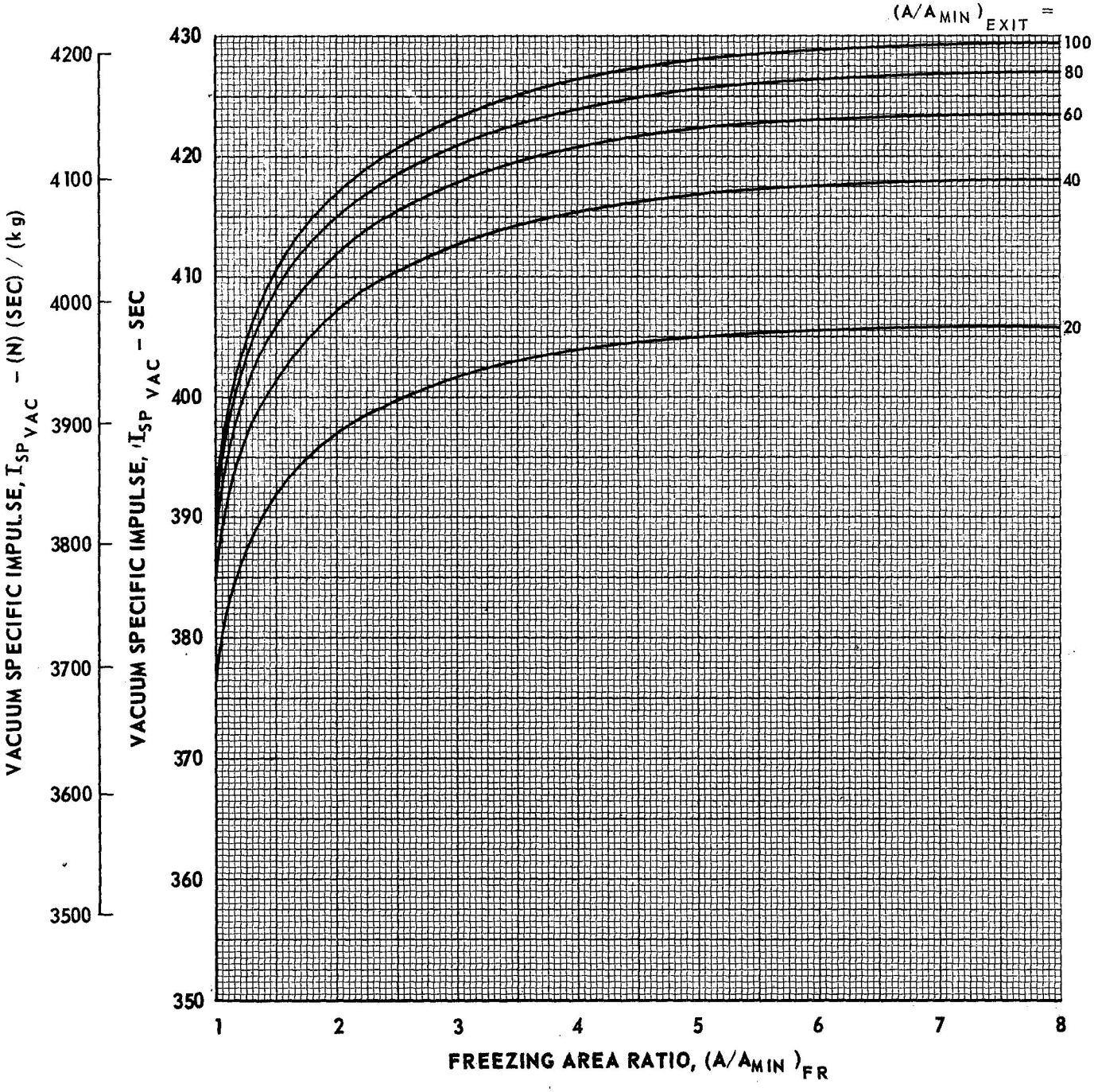

FIG. III-48

EFFECT OF FREEZING AREA RATIO ON NONEQUILIBRIUM PERFORMANCE FOR METHANE - FLOX PROPELLANT SYSTEM

CH_4 - FLOX (82.6% F_2)

P_C = 1000 PSIA (6.895 X 10^6 N/m^2)

O/F = 6.50

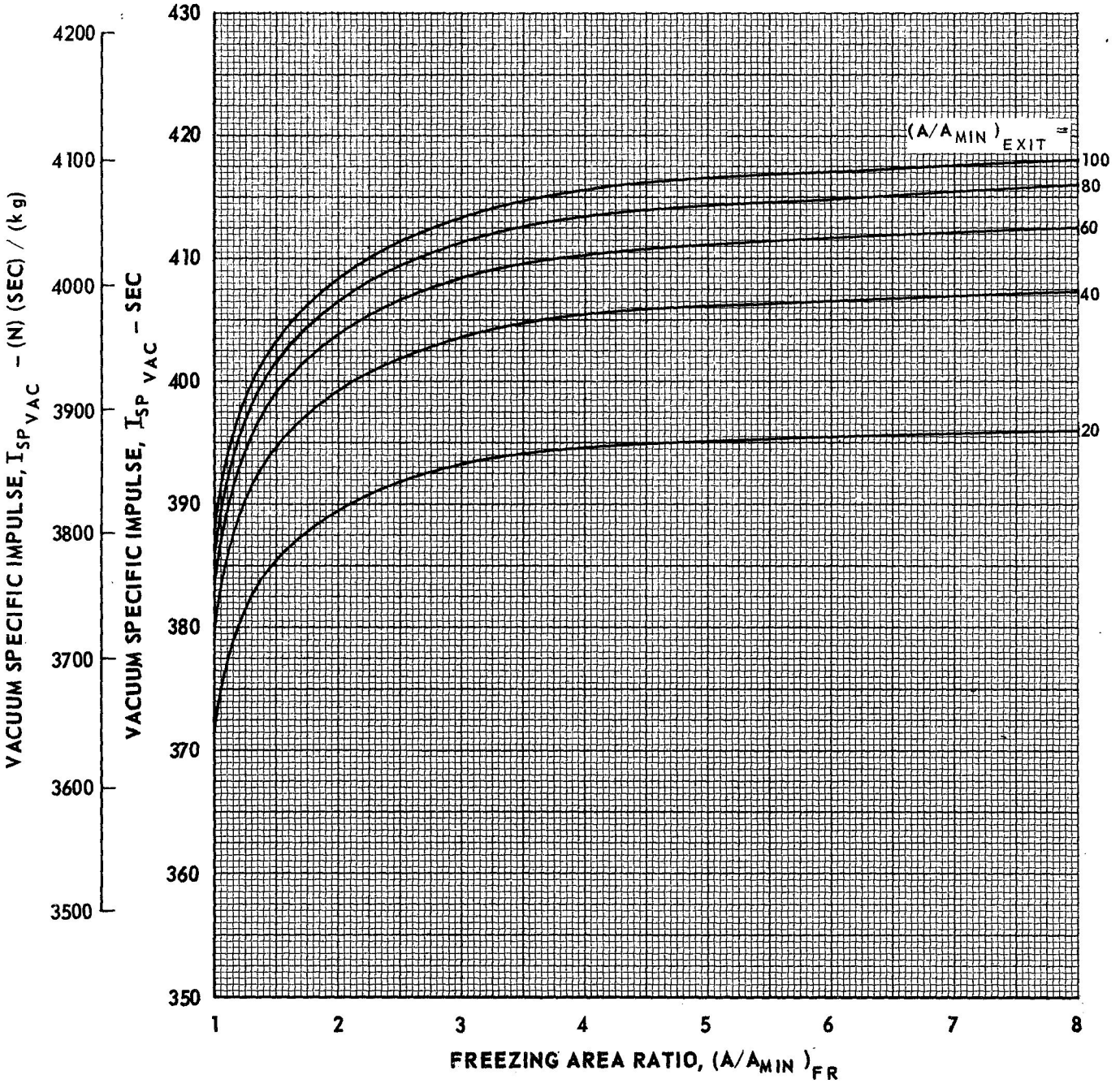

TABLE IV - 1

SUMMARY OF ELEMENTARY REACTIONS AND REACTION RATE CONSTANTS EMPLOYED IN AEROZINE 50-N_2O_4 RECOMBINATION MECHANISM

	REACTION	FORWARD RATE
	$H + H + M \rightleftharpoons H_2 + M$	$K_f = 4.62 \times 10^{14} T^{-1}$
1	$H + H + H \rightleftharpoons H_2 + H$	$K_f = 2 (4.62 \times 10^{14} T^{-1})$
2	$H + H + H_2 \rightleftharpoons H_2 + H_2$	$K_f = 2.5 (4.62 \times 10^{14} T^{-1})$
3	$H + H + H_2O \rightleftharpoons H_2 + H_2O$	$K_f = 2.5 (4.62 \times 10^{14} T^{-1})$
4	$H + H + CO_2 \rightleftharpoons H_2 + CO_2$	$K_f = 2 (4.62 \times 10^{14} T^{-1})$
5	$H + H + CO \rightleftharpoons H_2 + CO$	$K_f = 2 (4.62 \times 10^{14} T^{-1})$
6	$H + H + N_2 \rightleftharpoons H_2 + N_2$	$K_f = 2 (4.62 \times 10^{14} T^{-1})$
	$H + OH + M \rightleftharpoons H_2O + M$	$K_f = 7.85 \times 10^{15} T^{-1}$
7	$H + OH + H \rightleftharpoons H_2O + H$	$K_f = 3 (7.85 \times 10^{15} T^{-1})$
8	$H + OH + H_2 \rightleftharpoons H_2O + H_2O$	$K_f = 3 (7.85 \times 10^{15} T^{-1})$
9	$H + OH + H_2O \rightleftharpoons H_2O + H_2O$	$K_f = 20 (7.85 \times 10^{15} T^{-1})$
10	$H + OH + CO_2 \rightleftharpoons H_2O + CO$	$K_f = 10 (7.85 \times 10^{15} T^{-1})$
11	$H + OH + CO \rightleftharpoons H_2O + CO$	$K_f = 3 (7.85 \times 10^{15} T^{-1})$
12	$H + OH + N_2 \rightleftharpoons H_2O + N_2$	$K_f = 3 (7.85 \times 10^{15} T^{-1})$

NOTE: ALL RATES ARE EXPRESSED IN TERMS OF LB-MOLES, FT^3, SEC; AND T IS IN $^\circ R$

TO CONVERT TO kg-MOLES, m^3, SEC, AND T IN $^\circ K$; MULTIPLY ABOVE RATE BY 2.165×10^{-3}

TABLE IV-2

EQUILIBRIUM AND FROZEN FLOW PROPERTIES AT NOZZLE THROAT

AEROZINE 50 (ℓ) - N_2O_4(ℓ)

	P_c-psia	OXIDIZER - FUEL WEIGHT RATIO					
		1.25	1.50	1.75	2.00	2.25	2.50
Equilibrium Mass Flow - $\frac{W/A\ Lbm}{Ft^2.Sec}$	100	81.8	81.0	81.5	82.6	84.1	85.7
	200	163.4	161.5	161.9	164.1	167.0	170.2
	300	245.0	241.8	242.1	245.2	249.5	254.3
	500	408.1	402.2	402.1	406.6	413.8	421.8
	750	612.0	602.6	601.5	607.8	618.4	630.5
	1000	8.15.8	802.8	800.6	808.4	822.3	828.6
Frozen Mass Flow - $\frac{W/A\ Lbm}{Ft^2.Sec}$	100	83.1	83.0	83.9	85.2	86.8	88.4
	200	165.5	164.9	166.3	168.9	172.0	175.2
	300	247.7	246.4	248.3	252.0	256.7	261.5
	500	411.9	409.0	411.5	417.4	425.0	433.1
	750	616.8	611.6	614.6	623.1	634.4	646.7
	1000	821.6	813.8	817.1	828.1	843.0	859.5
Frozen Specific Heat Ratio γ_{FR}	100	1.25	1.24	1.23	1.23	1.23	1.23
	200	1.25	1.24	1.23	1.23	1.23	1.23
	300	1.25	1.24	1.23	1.23	1.23	1.23
	500	1.25	1.24	1.23	1.23	1.22	1.22
	750	1.25	1.23	1.23	1.22	1.22	1.22
	1000	1.25	1.23	1.23	1.22	1.22	1.22

NOTE: P_c (psia) x $6.895 \times 10^3 = P_c$ (N/m^2)

Mass Flow ($\frac{Lbm}{Ft^2.sec}$) x 4.883 = Mass Flow ($\frac{kg}{m^2\ sec}$)

FIG. IV-1

VARIATION OF EQUILIBRIUM VACUUM SPECIFIC IMPULSE WITH AREA RATIO

AEROZINE 50 (ℓ) – N_2O_4 (ℓ)

P_C = 100 PSIA (6.895X10^{5}N/m^2)

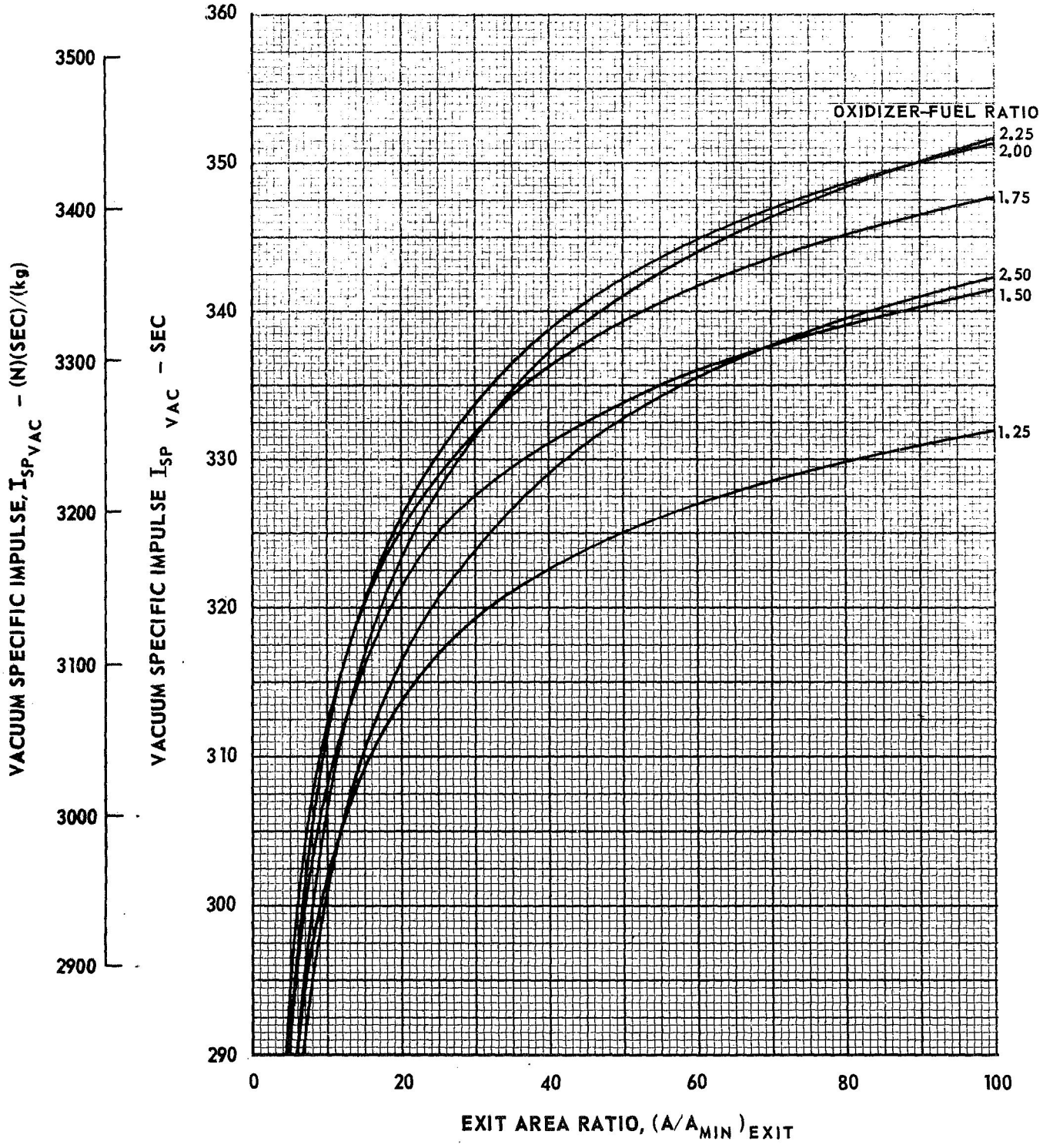

FIG. IV-2

VARIATION OF FROZEN VACUUM SPECIFIC IMPULSE WITH AREA RATIO

AEROZINE 50 (ℓ) - N_2O_4 (ℓ)

P_C = 100 PSIA (6.895×10^5 N/m^2)

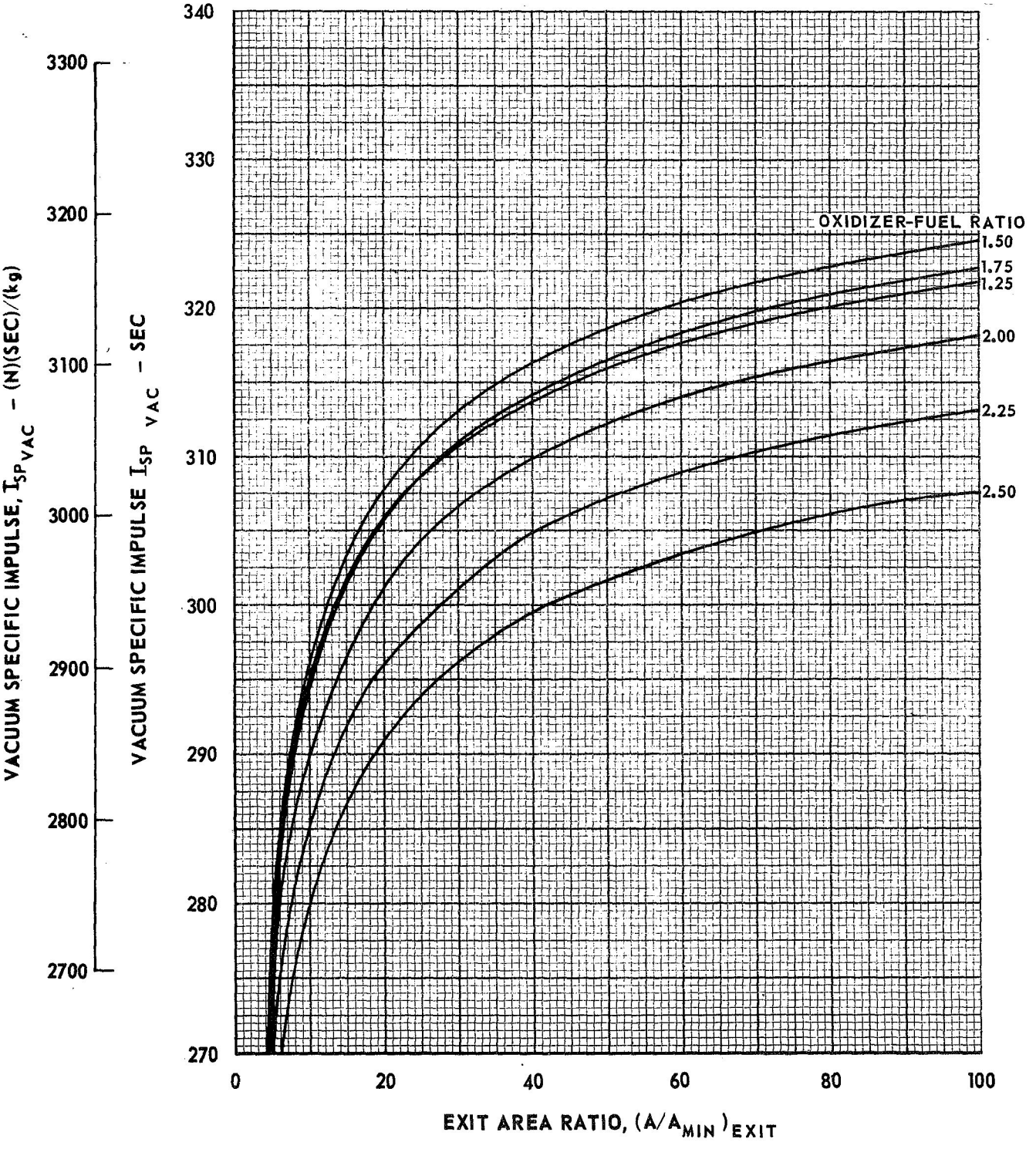

FIG. IV–3

VARIATION OF EQUILIBRIUM VACUUM SPECIFIC IMPULSE WITH AREA RATIO

AEROZINE 50 (ℓ) – N_2O_4 (ℓ)

P_C = 200 PSIA (1.379X10^{6}N/m^2)

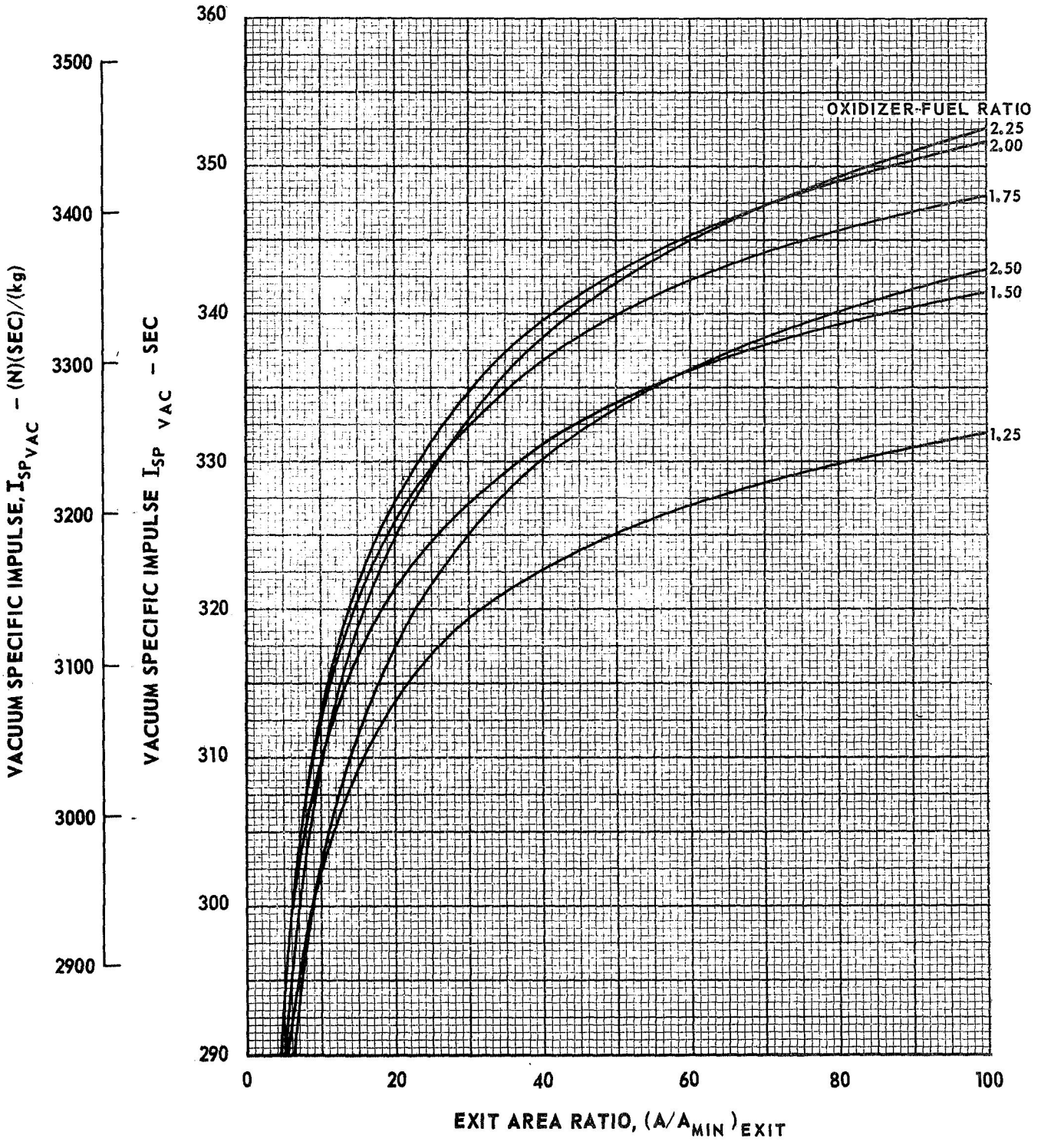

FIG. IV-4

VARIATION OF FROZEN VACUUM SPECIFIC IMPULSE WITH AREA RATIO

AEROZINE 50 (ℓ) - N_2O_4 (ℓ)

P_C = 200 PSIA (1.379X10^6 N/m^2)

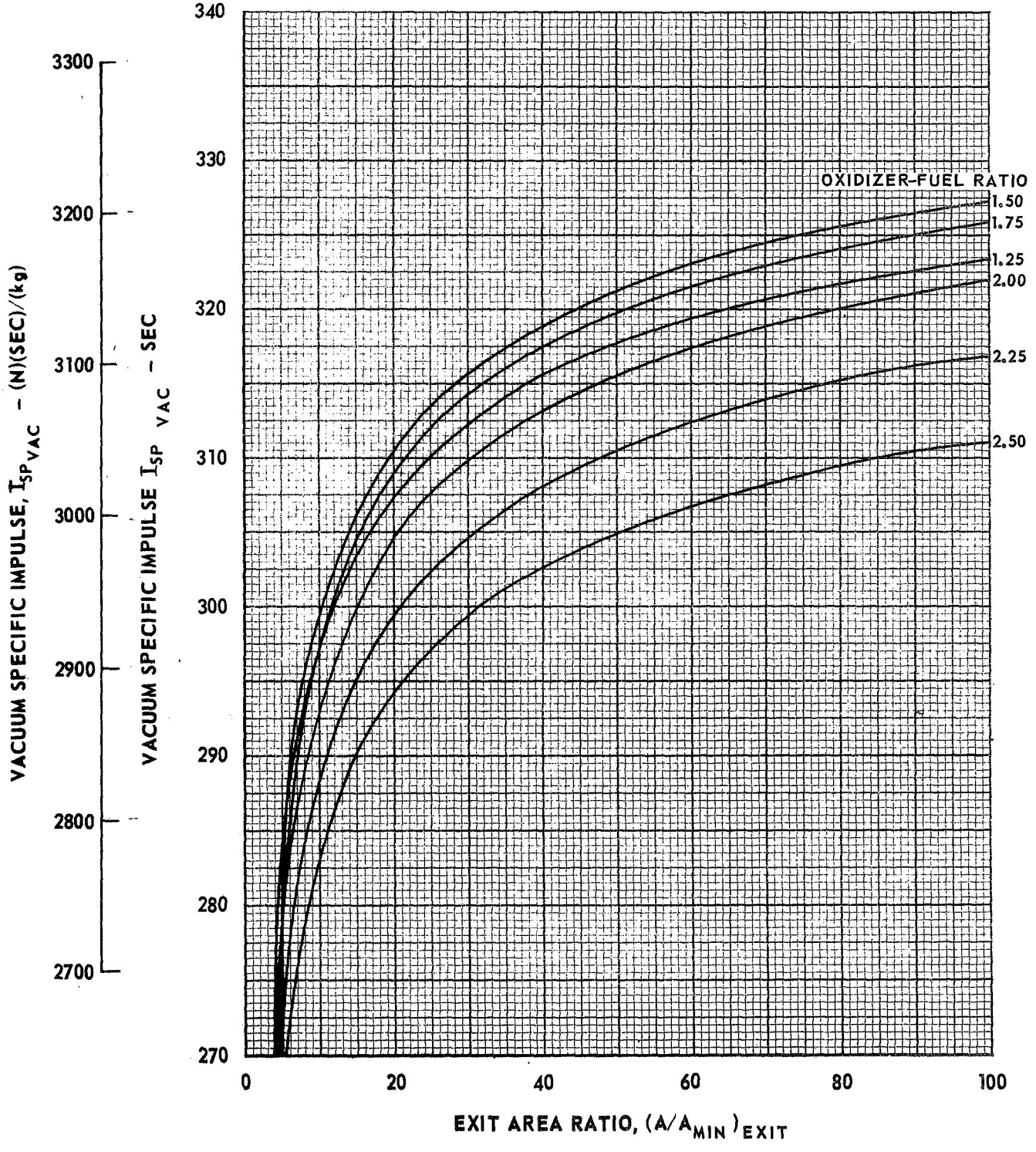

FIG. IV–5

VARIATION OF EQUILIBRIUM VACUUM SPECIFIC IMPULSE WITH AREA RATIO

AEROZINE 50 (ℓ) – N_2O_4 (ℓ)

P_C = 300 PSIA (2.069X10^{6}N/m^2)

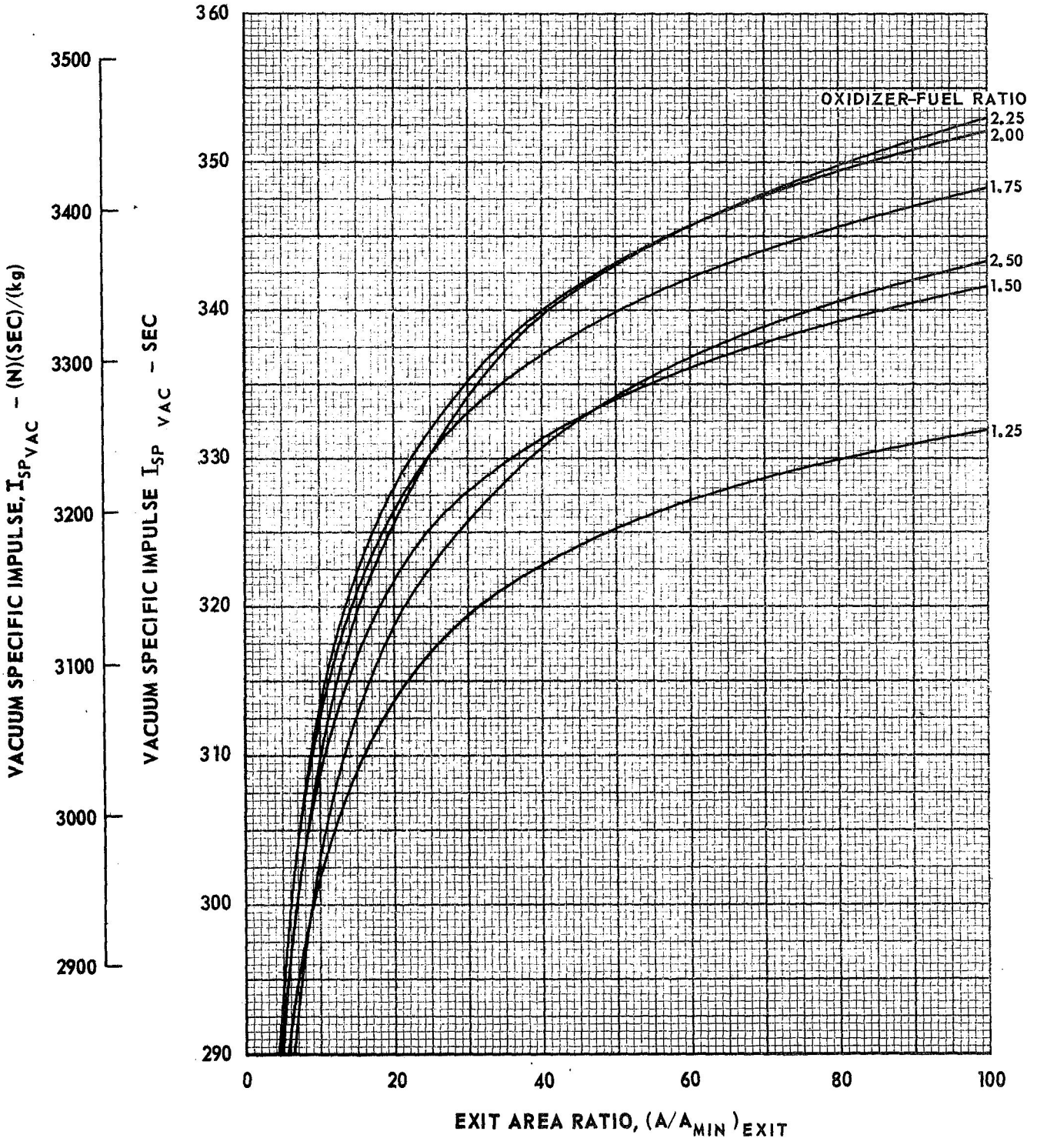

FIG. IV-6

VARIATION OF FROZEN VACUUM SPECIFIC IMPULSE WITH AREA RATIO

AEROZINE 50 (ℓ) – N_2O_4 (ℓ)

P_C = 300 PSIA (2.069X10^{6}N/m^2)

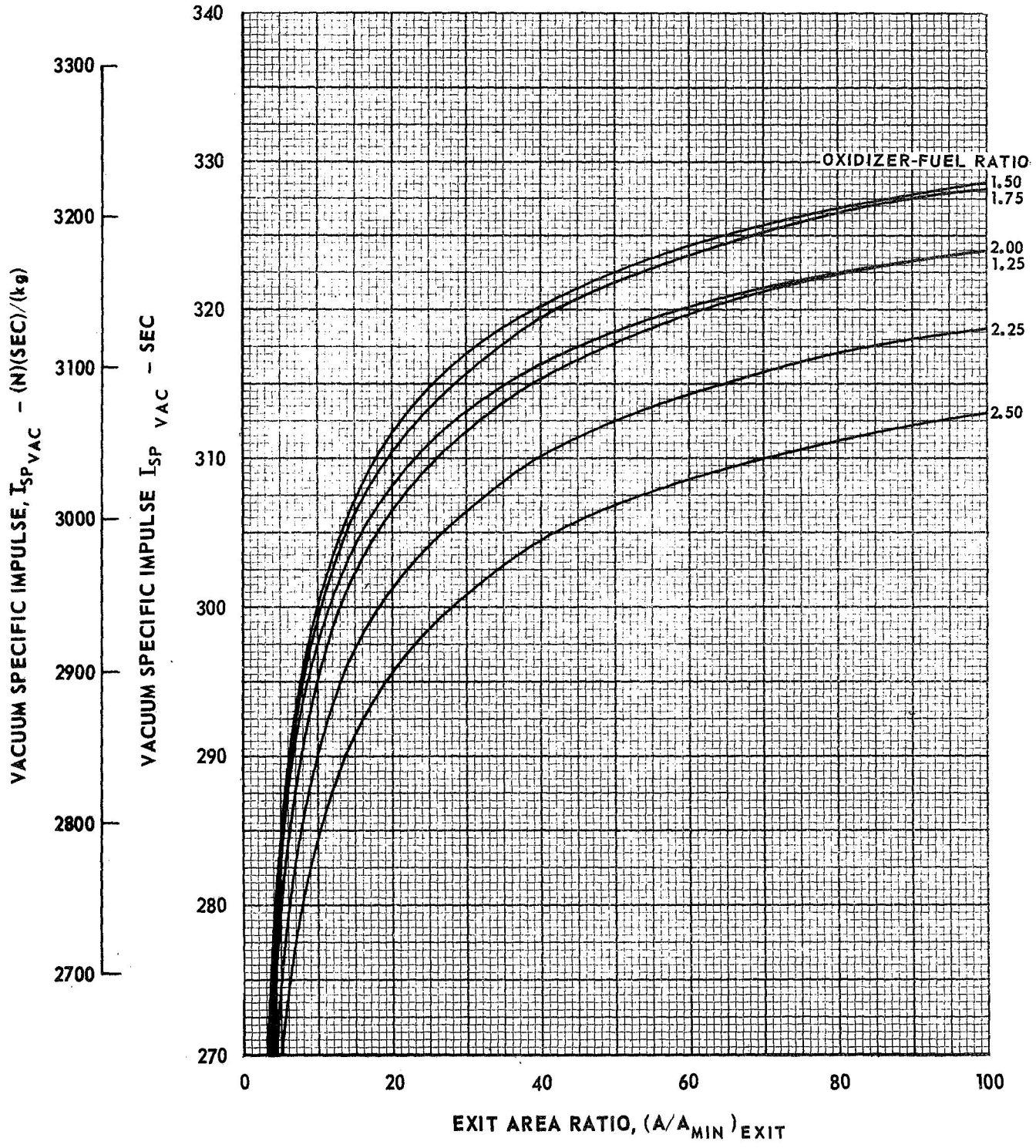

FIG. IV–7

VARIATION OF EQUILIBRIUM VACUUM SPECIFIC IMPULSE WITH AREA RATIO

AEROZINE 50 (ℓ) – N_2O_4 (ℓ)

P_C = 500 PSIA (3.448X10^{6}N/m^2)

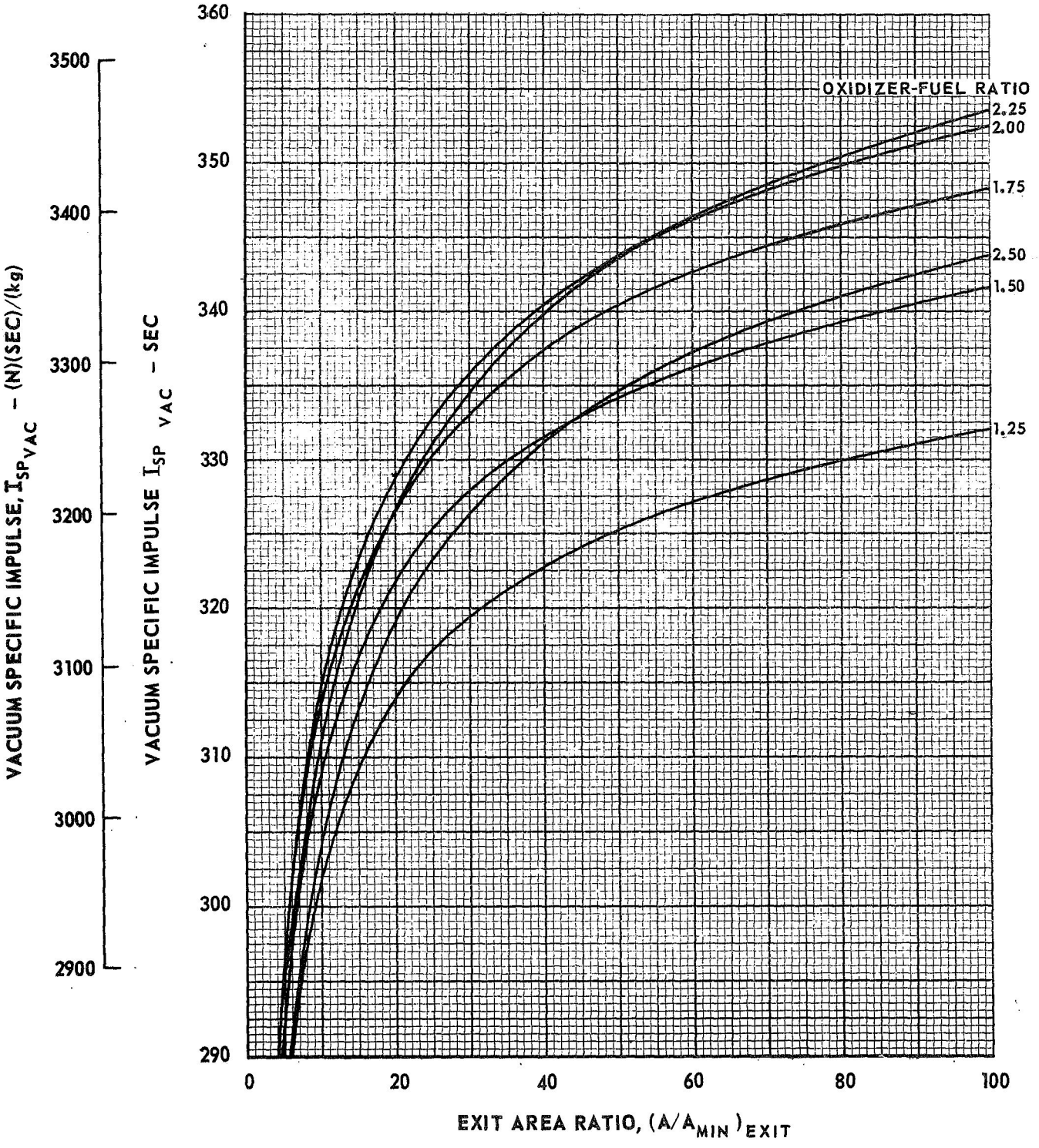

FIG. IV-8

VARIATION OF FROZEN VACUUM SPECIFIC IMPULSE WITH AREA RATIO

AEROZINE 50 (ℓ) - N_2O_4 (ℓ)

P_C = 500 PSIA (3.448X10^6 N/m^2)

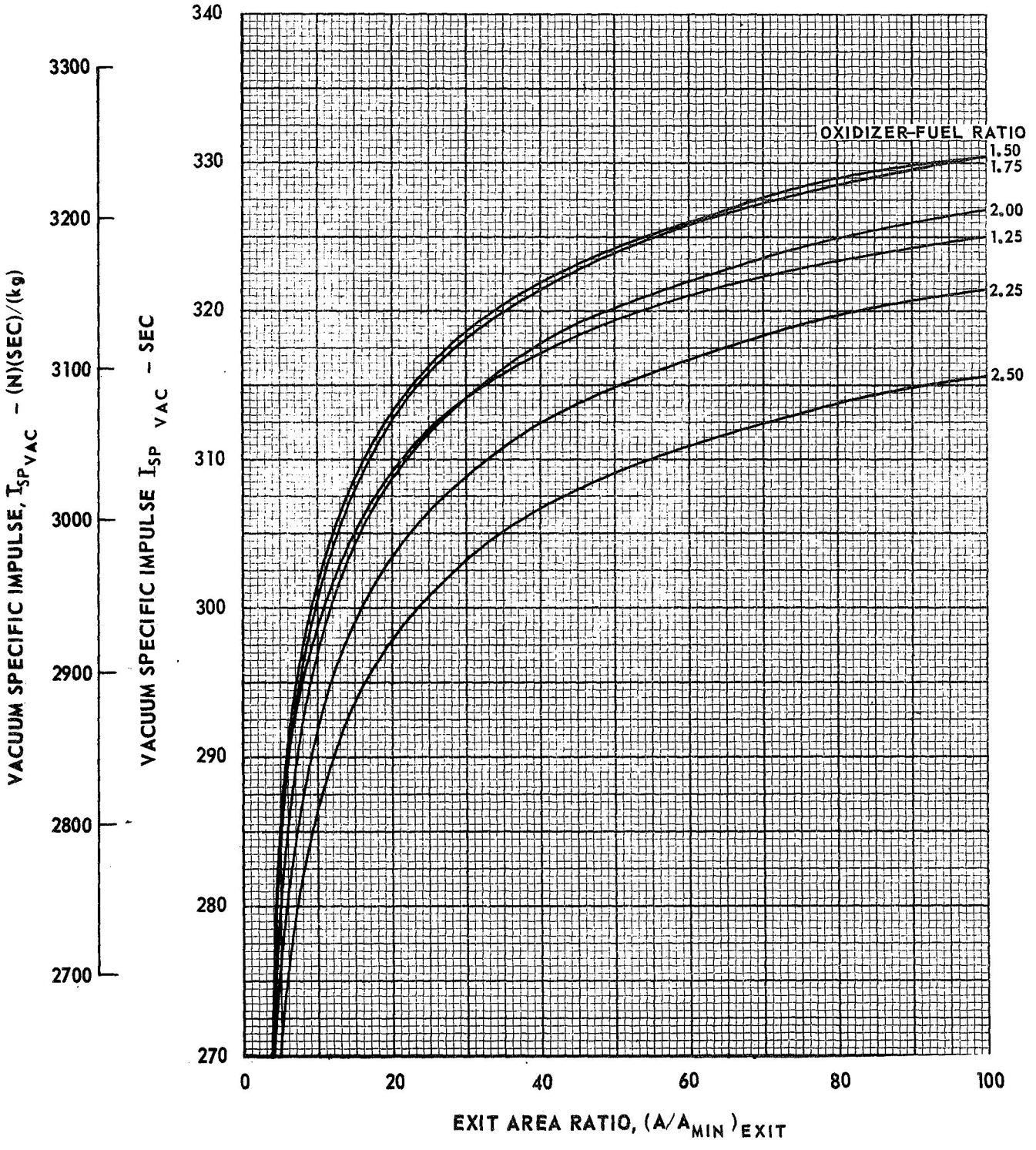

FIG. IV-9

VARIATION OF EQUILIBRIUM VACUUM SPECIFIC IMPULSE WITH AREA RATIO

AEROZINE 50 (ℓ) – N_2O_4 (ℓ)

P_C = 750 PSIA (5.171X10^{6}N/m^2)

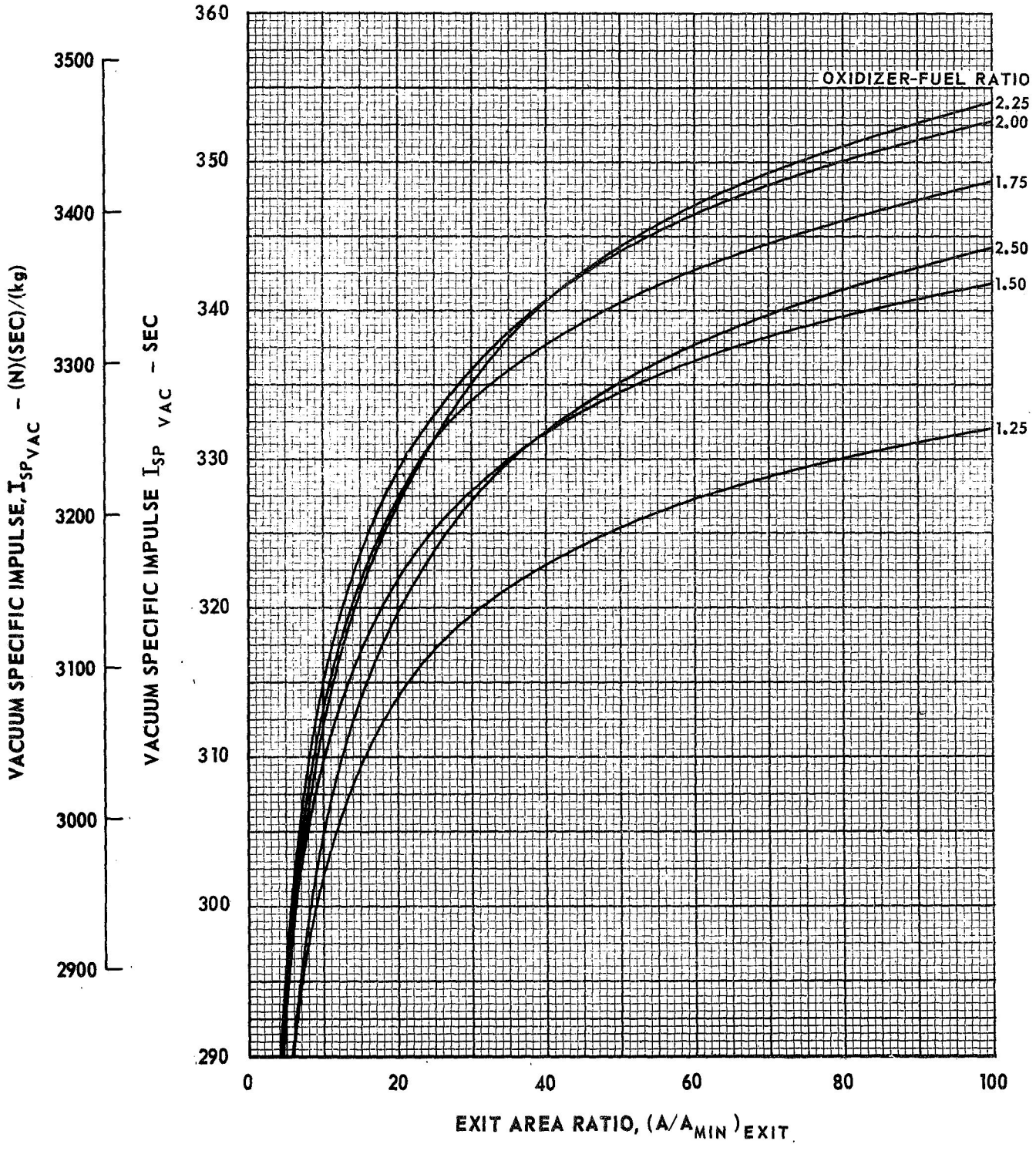

FIG. IV-10

VARIATION OF FROZEN VACUUM SPECIFIC IMPULSE WITH AREA RATIO

AEROZINE 50 (ℓ) – N_2O_4 (ℓ)

P_C = 750 PSIA (5.171X10^{6}N/m^2)

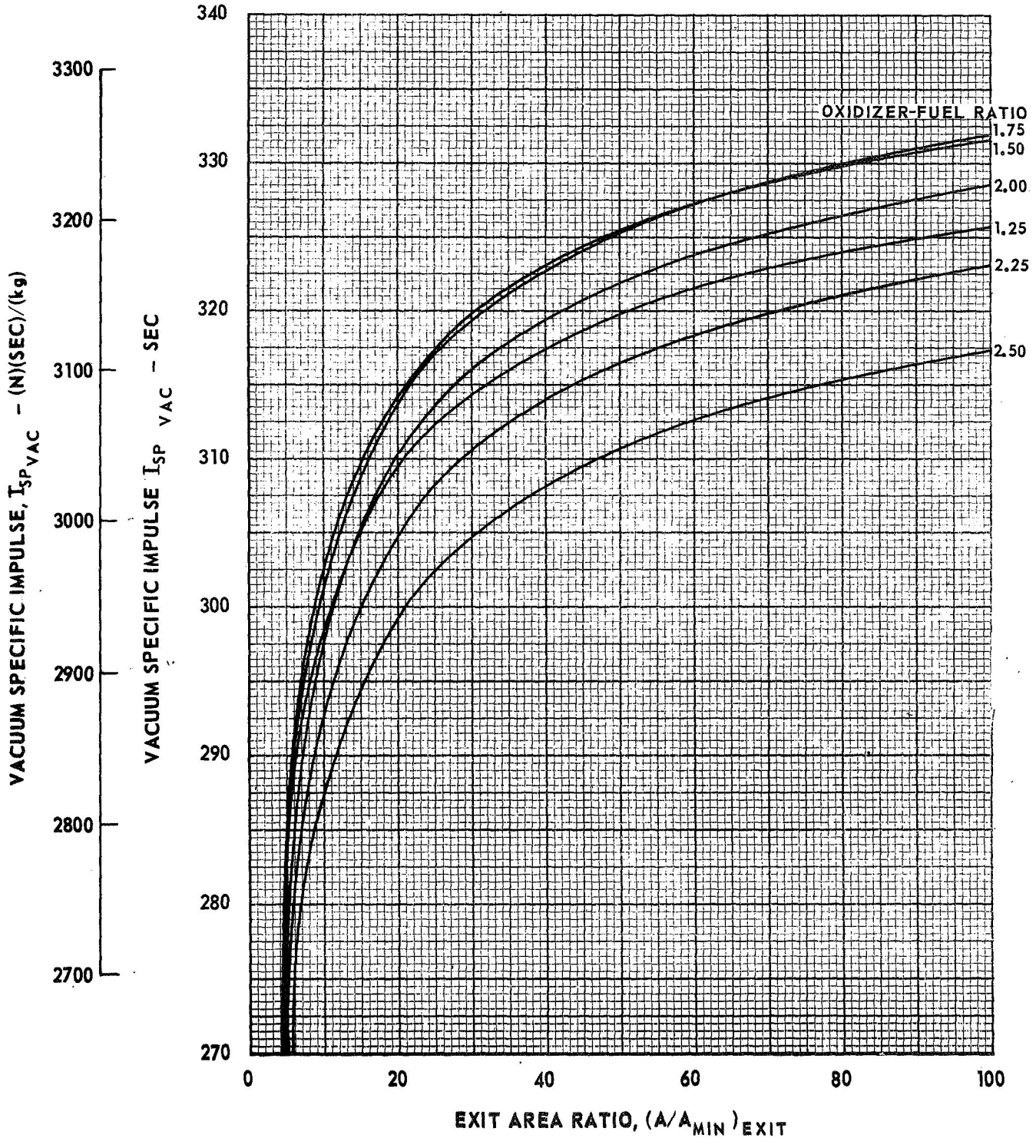

FIG. IV–11

VARIATION OF EQUILIBRIUM VACUUM SPECIFIC IMPULSE WITH AREA RATIO

AEROZINE 50 (ℓ) – N_2O_4 (ℓ)

P_C =1000 PSIA (6.895X10^6 N/m^2)

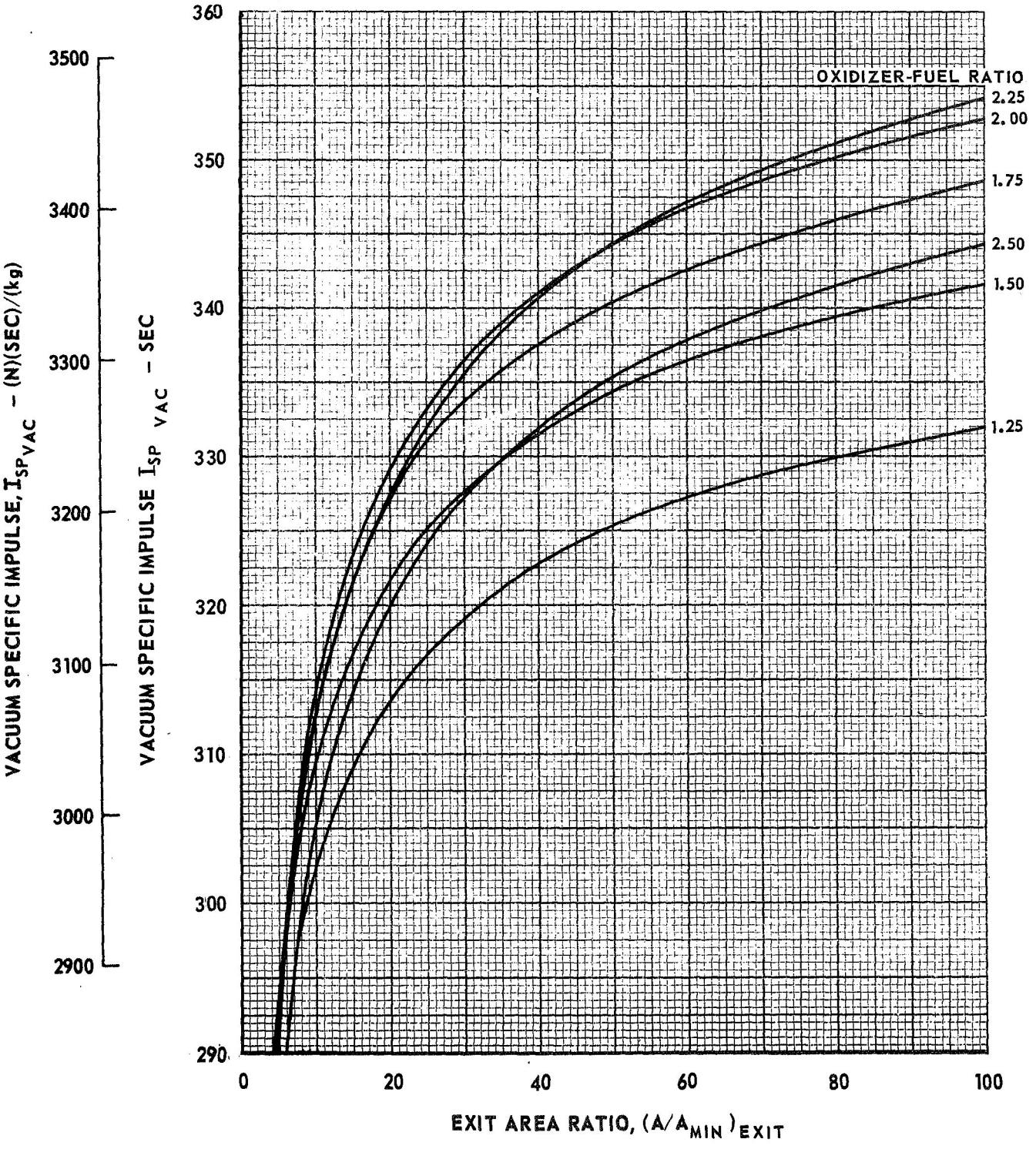

FIG. IV–12

VARIATION OF FROZEN VACUUM SPECIFIC IMPULSE WITH AREA RATIO

AEROZINE 50 (ℓ) – N_2O_4 (ℓ)

P_C = 1000 PSIA (6.895X10^6 N/m^2)

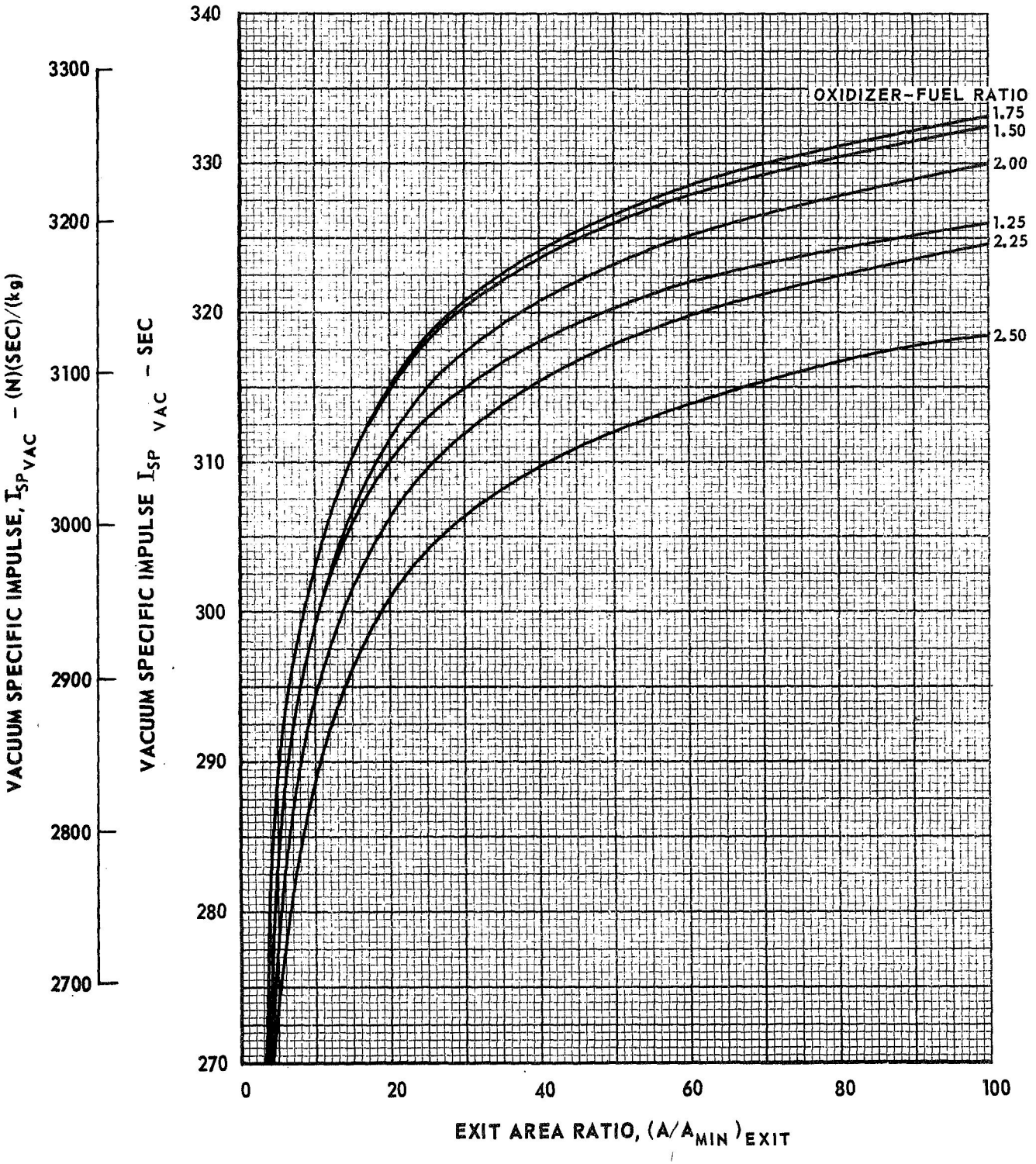

FIG. IV-13

NORMALIZED GRAPHICAL SOLUTION FOR FREEZING AREA RATIO USING MODIFIED BRAY ANALYSIS

AEROZINE 50 (ℓ) - N_2O_4 (ℓ)

P_C = 100 PSIA (6.895 X 10^5 N/m^2)

O/F = 1.50

NOTE: REACTION RATE CONSTANTS LISTED IN TABLE IV-1

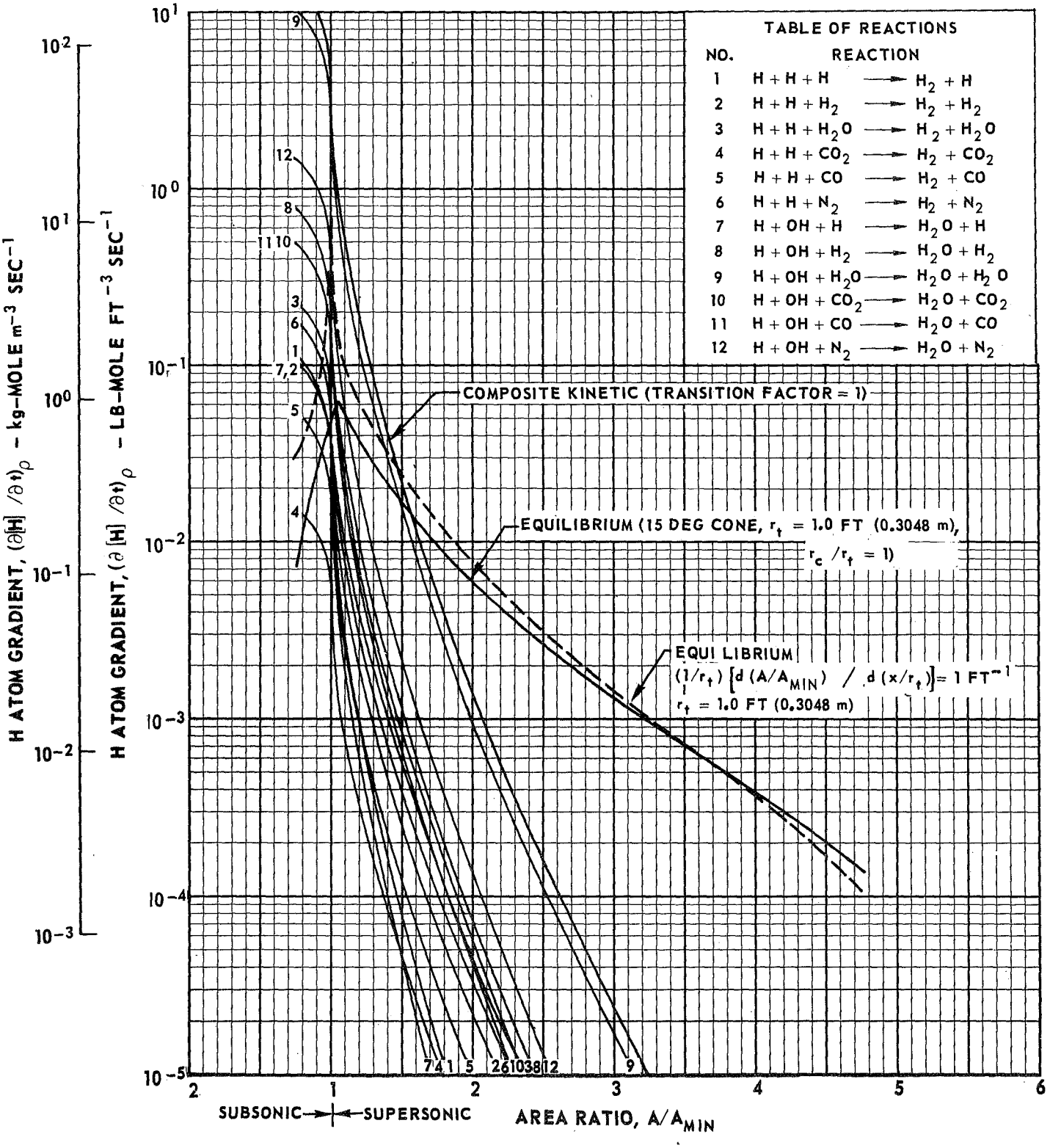

FIG. IV-14

NORMALIZED GRAPHICAL SOLUTION FOR FREEZING AREA RATIO USING MODIFIED BRAY ANALYSIS

AEROZINE 50 (ℓ) - N_2O_4 (ℓ)

P_C = 100 PSIA (6.895 X 10^5 N/m^2)

O/F = 2.00

NOTE: REACTION RATE CONSTANTS LISTED IN TABLE IV-1

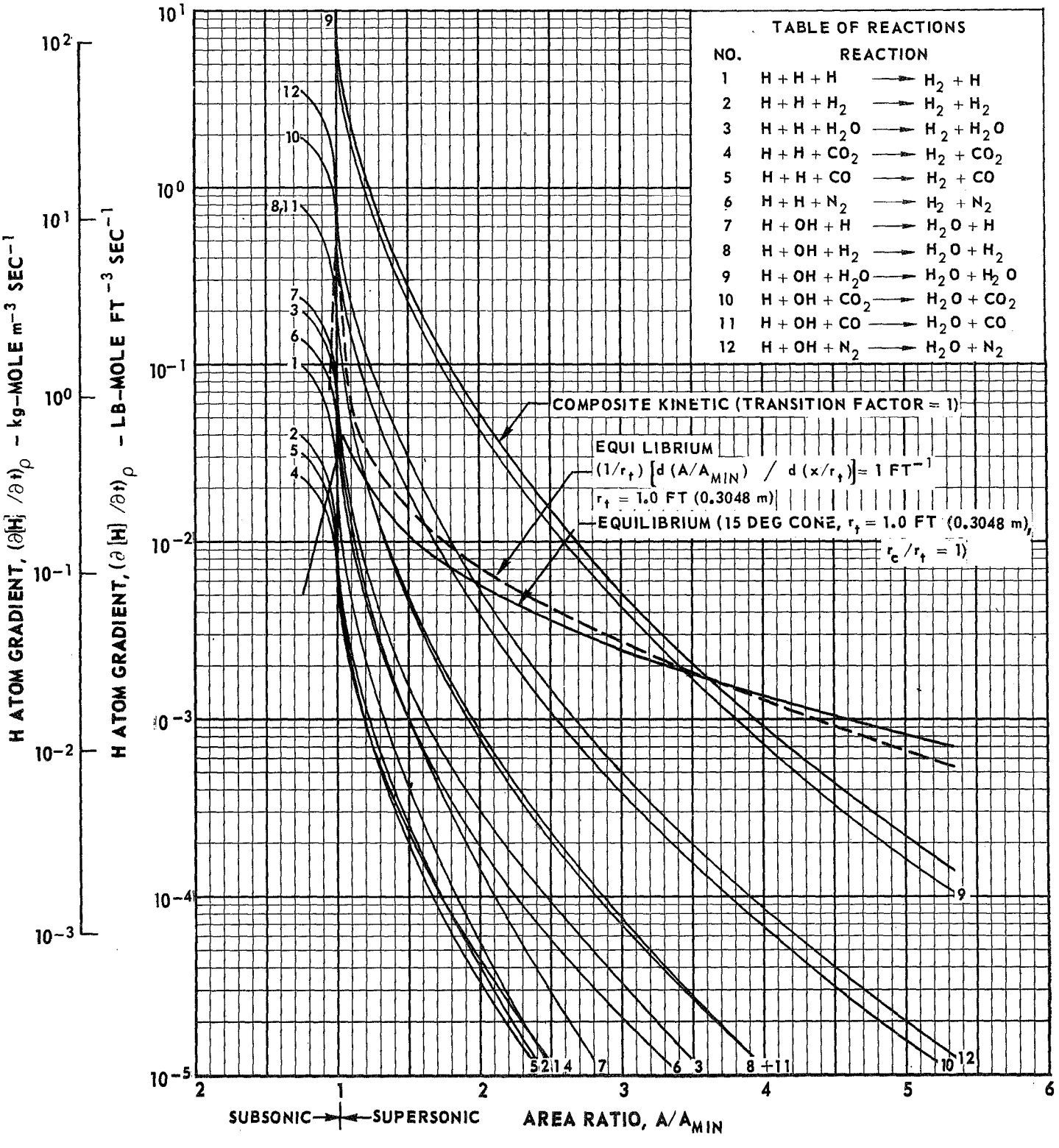

FIG. IV-15

NORMALIZED GRAPHICAL SOLUTION FOR FREEZING AREA RATIO USING MODIFIED BRAY ANALYSIS

AEROZINE 50 (ℓ) - N_2O_4 (ℓ)

P_C = 100 PSIA (6.895×10^5 N/m^2)

O/F = 2.50

NOTE: REACTION RATE CONSTANTS LISTED IN TABLE IV-1

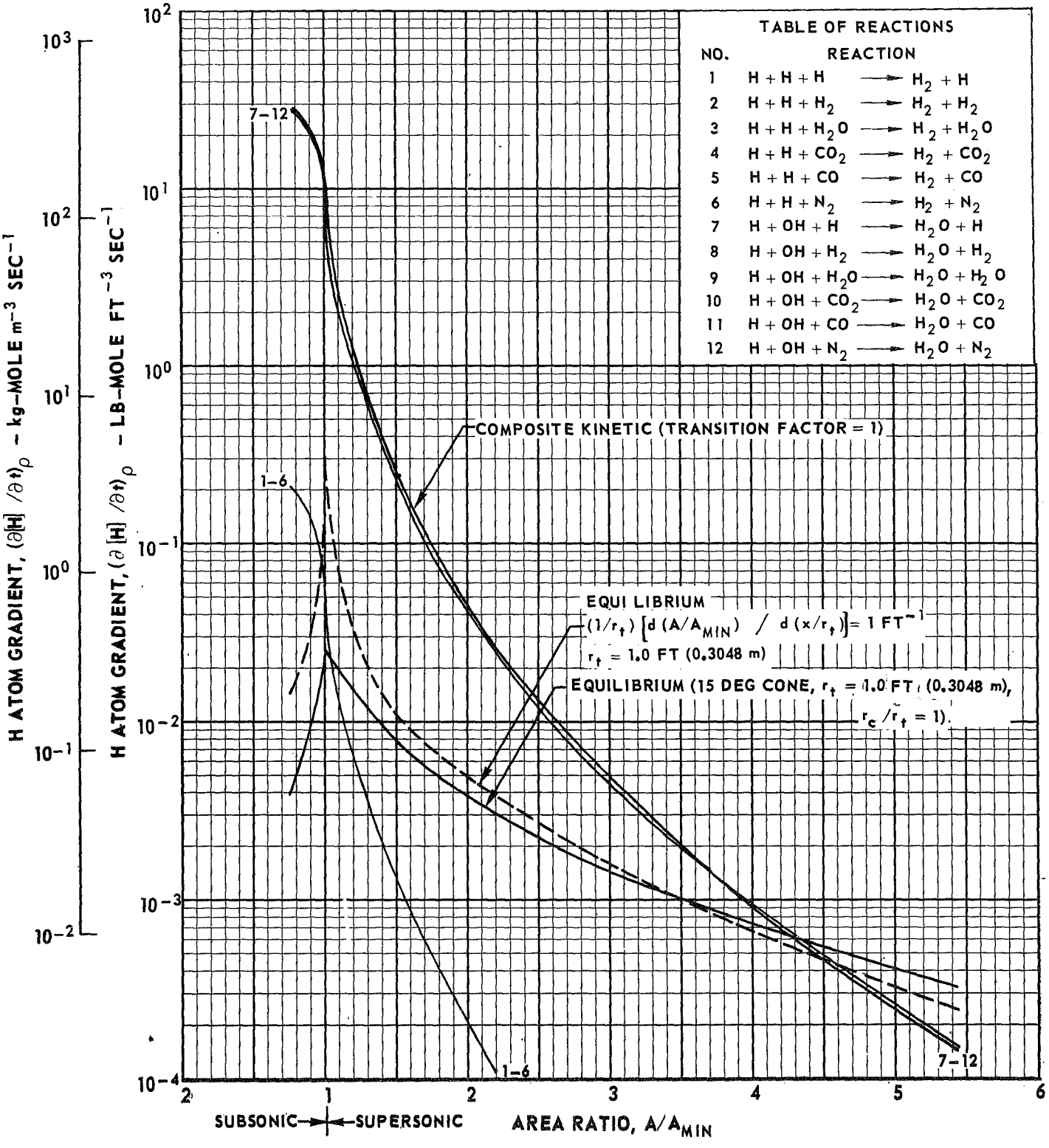

FIG. IV-16

NORMALIZED GRAPHICAL SOLUTION FOR FREEZING AREA RATIO USING MODIFIED BRAY ANALYSIS

AEROZINE 50 (ℓ) - N_2O_4 (ℓ)

P_C = 200 PSIA (1.379 X 10^6 N/m^2)

O/F = 1.50

NOTE: REACTION RATE CONSTANTS LISTED IN TABLE IV-1

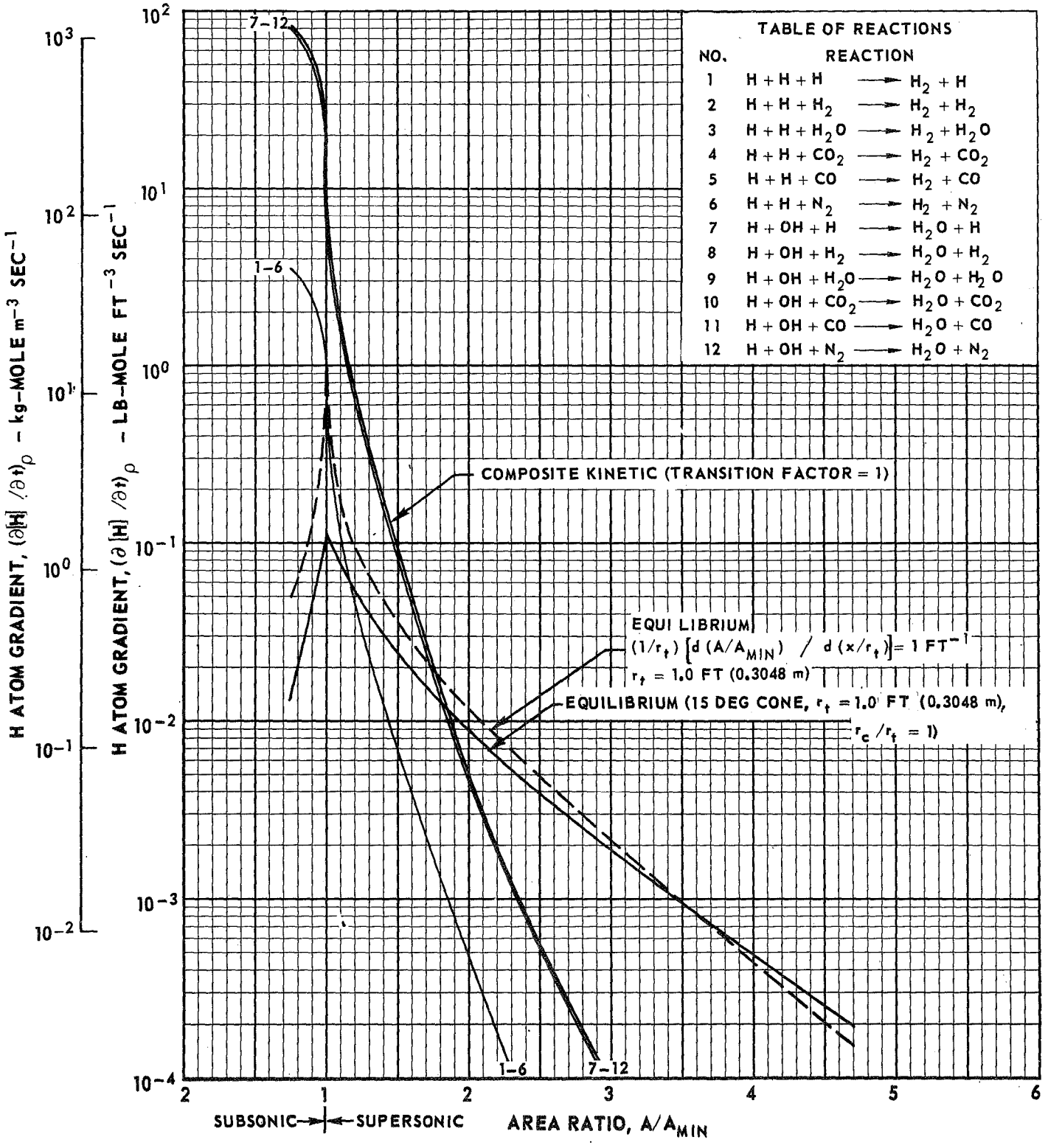

FIG. IV-17

NORMALIZED GRAPHICAL SOLUTION FOR FREEZING AREA RATIO USING MODIFIED BRAY ANALYSIS

AEROZINE 50 (ℓ) - N_2O_4 (ℓ)

P_C = 200 PSIA (1.379 X 10^6 N/m^2)

O/F = 2.00

NOTE: REACTION RATE CONSTANTS LISTED IN TABLE IV-1

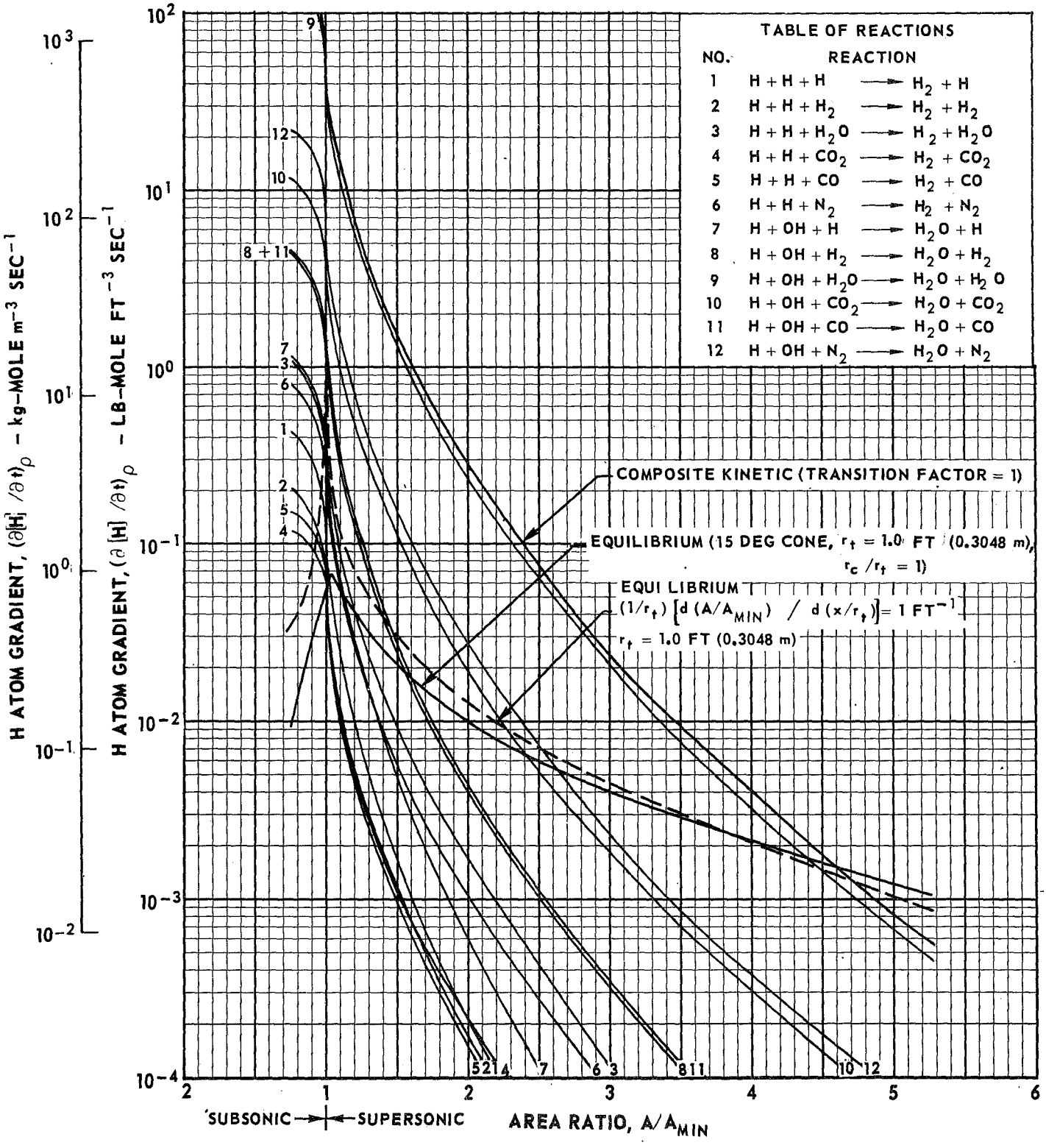

FIG. IV-18

NORMALIZED GRAPHICAL SOLUTION FOR FREEZING AREA RATIO USING MODIFIED BRAY ANALYSIS

AEROZINE 50 (ℓ) - N_2O_4 (ℓ)

P_C = 200 PSIA (1.379 X 10^6 N/m^2)

O/F = 2.50

NOTE: REACTION RATE CONSTANTS LISTED IN TABLE IV-1

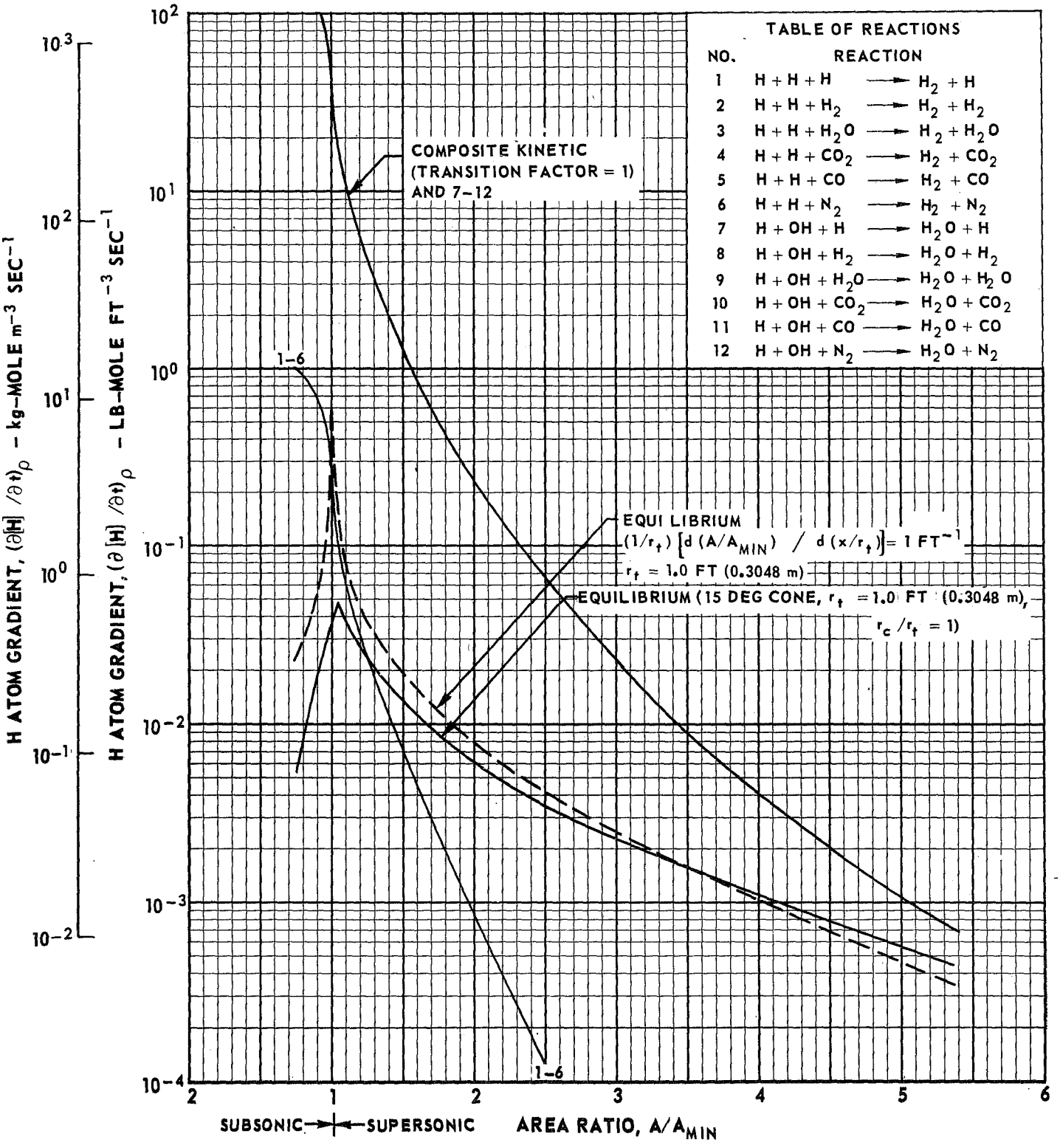

NORMALIZED GRAPHICAL SOLUTION FOR FREEZING AREA RATIO USING MODIFIED BRAY ANALYSIS

AEROZINE 50 (ℓ) - N_2O_4 (ℓ)

P_C = 300 PSIA (2.069 X 10^6 N/m^2)

O/F = 1.50

NOTE: REACTION RATE CONSTANTS LISTED IN TABLE IV-1

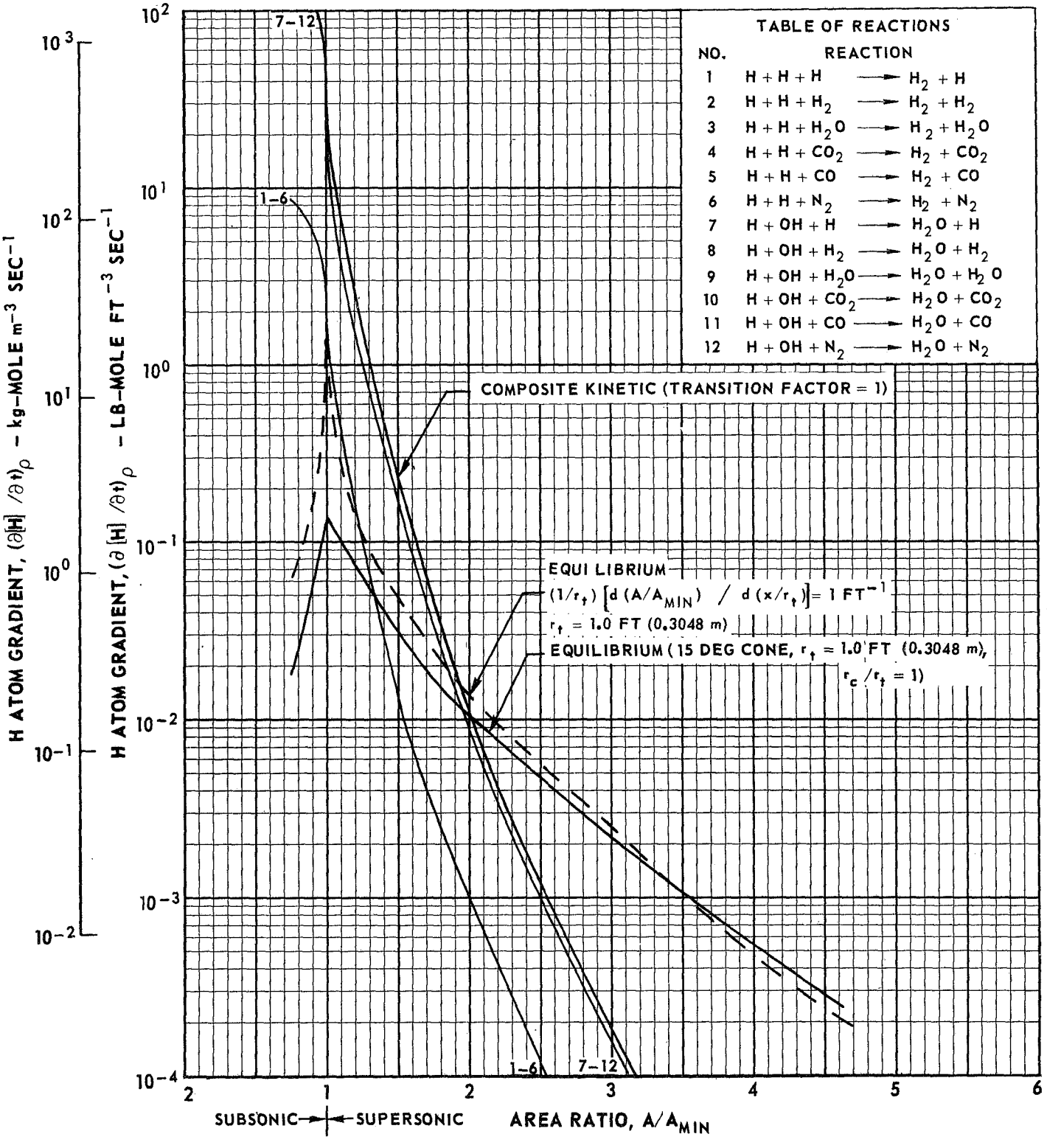

FIG. IV-20

NORMALIZED GRAPHICAL SOLUTION FOR FREEZING AREA RATIO USING MODIFIED BRAY ANALYSIS

AEROZINE 50 (ℓ) - N_2O_4 (ℓ)

P_C = 300 PSIA (2.069 X 10^6 N/m^2)

O/F = 2.00

NOTE: REACTION RATE CONSTANTS LISTED IN TABLE IV-1

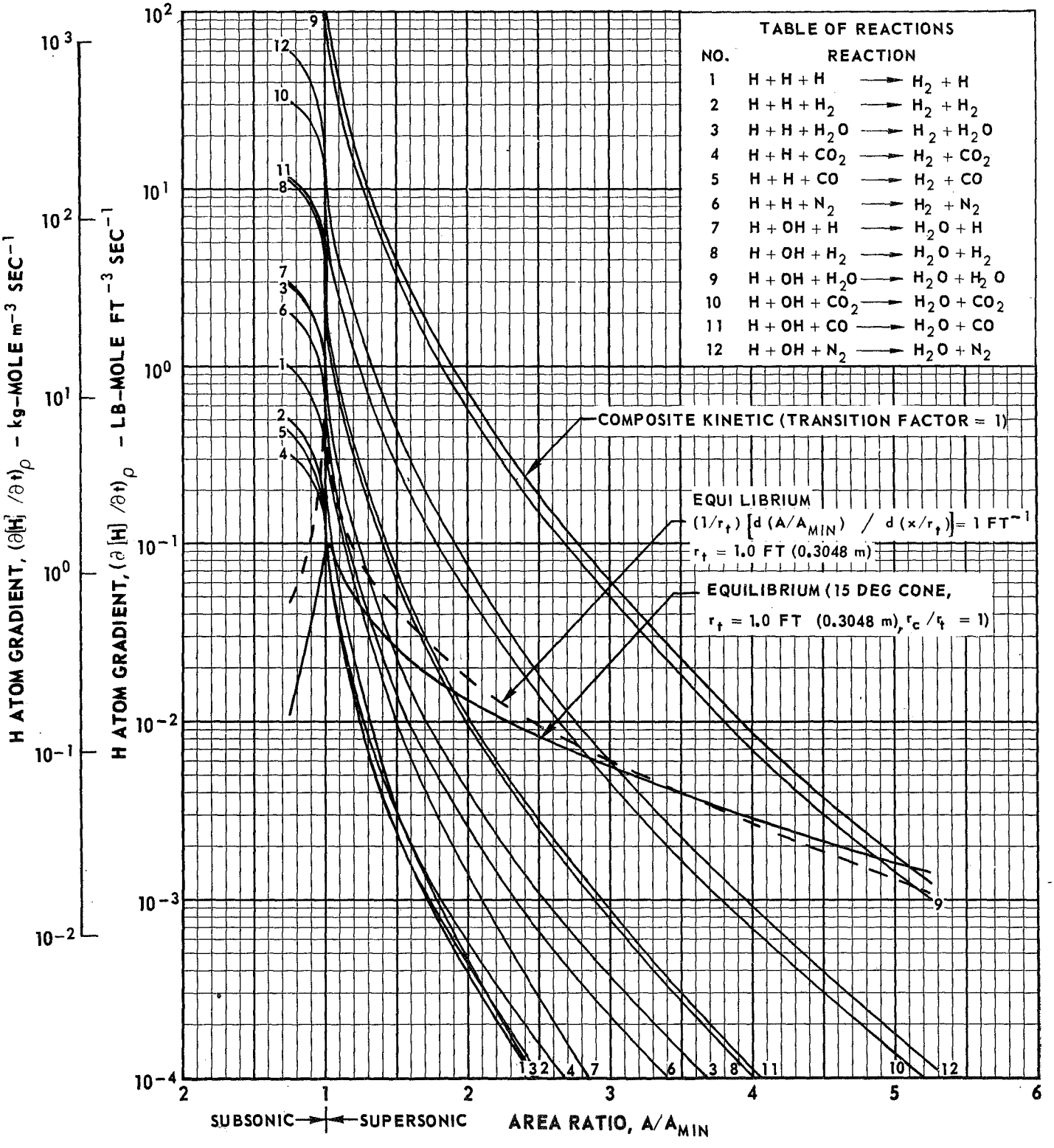

FIG. IV-21

NORMALIZED GRAPHICAL SOLUTION FOR FREEZING AREA RATIO USING MODIFIED BRAY ANALYSIS

AEROZINE 50 (ℓ) - N_2O_4 (ℓ)

P_C = 300 PSIA (2.069 X 10^6 N/m^2)

O/F = 2.50

NOTE: REACTION RATE CONSTANTS LISTED IN TABLE IV-1

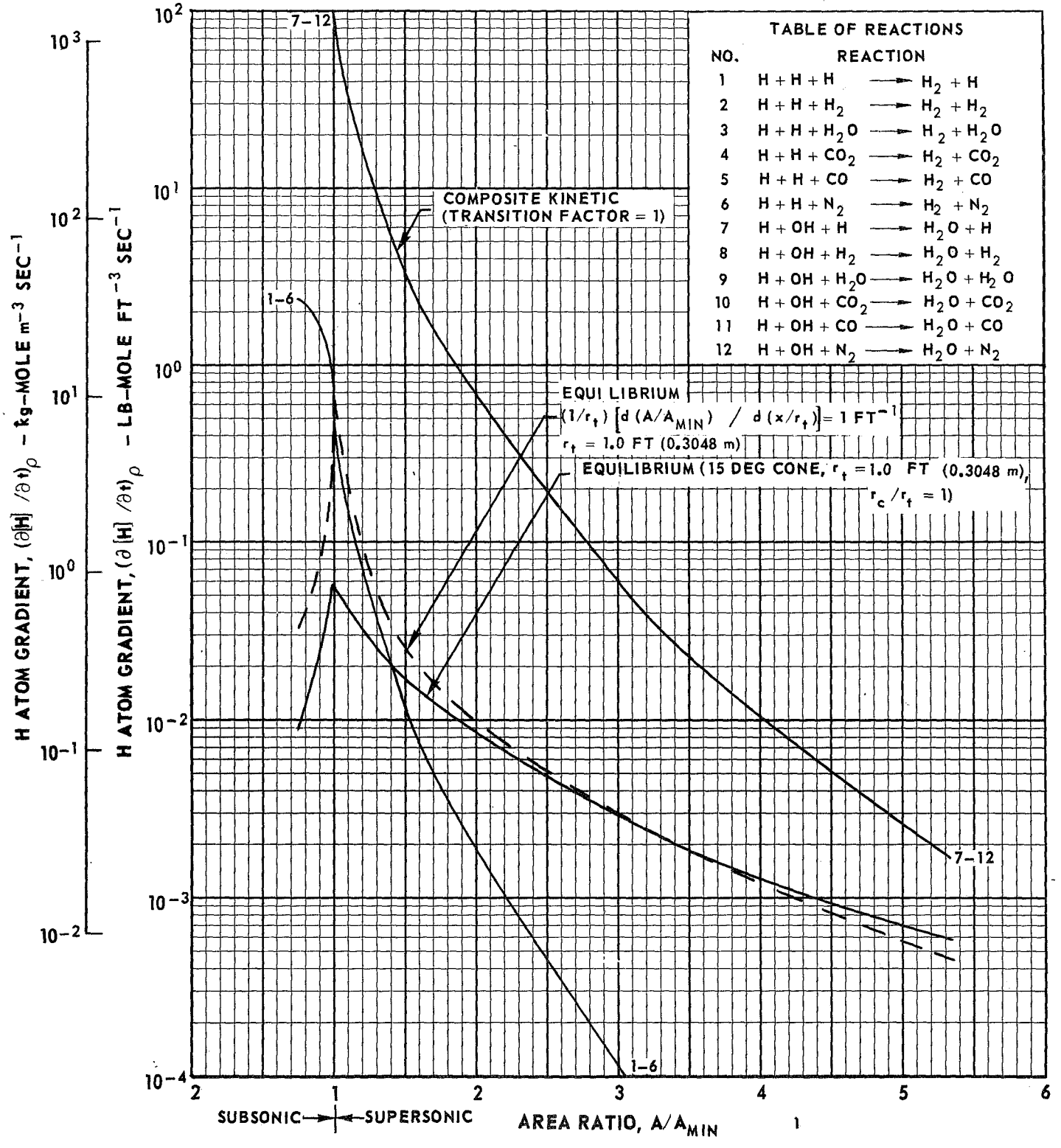

FIG. IV-22

NORMALIZED GRAPHICAL SOLUTION FOR FREEZING AREA RATIO USING MODIFIED BRAY ANALYSIS

AEROZINE 50 (ℓ) – N_2O_4 (ℓ)

P_C = 500 PSIA (3.448×10^6 N/m^2)

O/F = 1.50

NOTE: REACTION RATE CONSTANTS LISTED IN TABLE IV-1

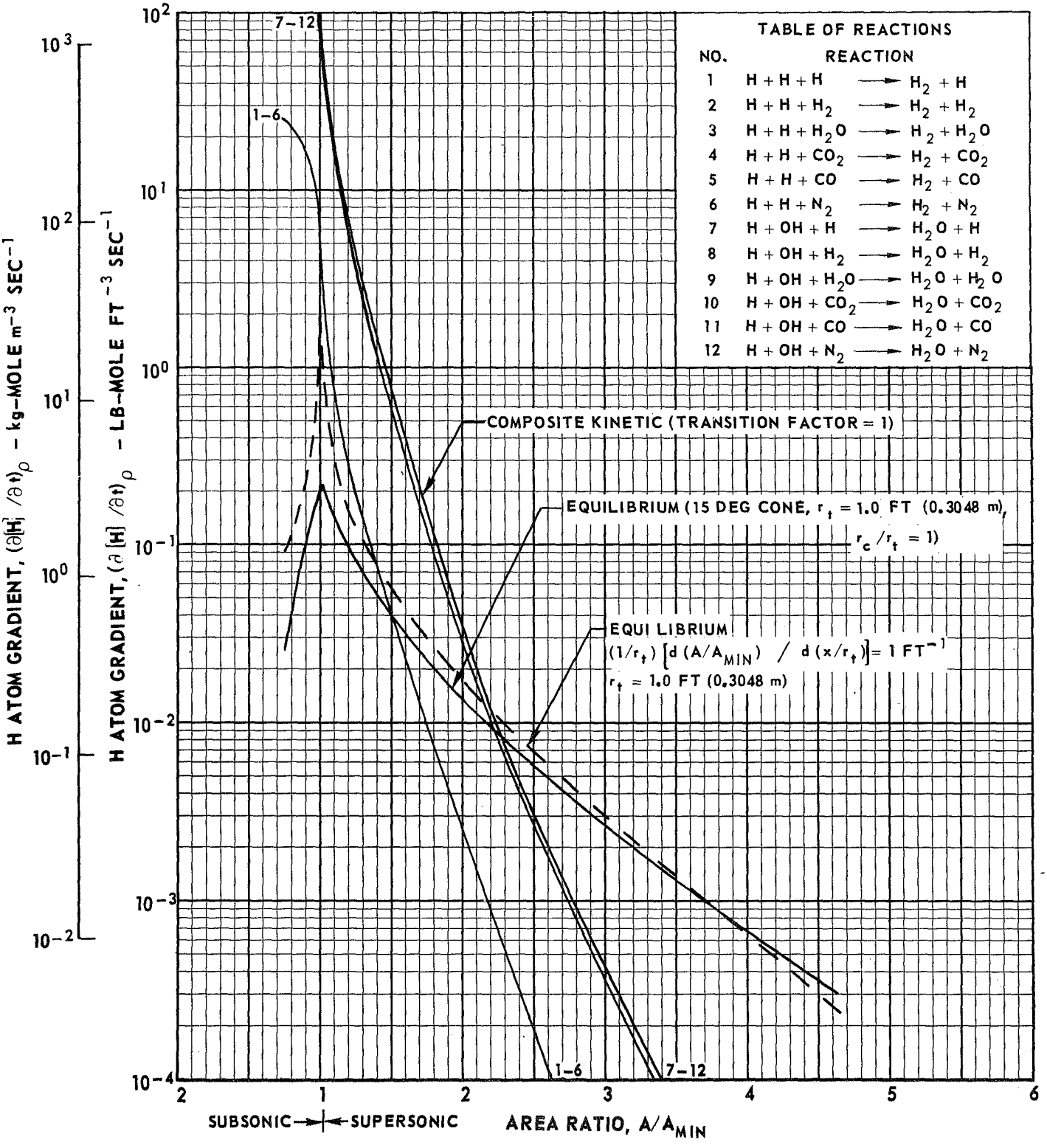

FIG. IV-23

NORMALIZED GRAPHICAL SOLUTION FOR FREEZING AREA RATIO USING MODIFIED BRAY ANALYSIS

AEROZINE 50 (ℓ) - N_2O_4 (ℓ)

P_C = 500 PSIA (3.448 X 10^6 N/m^2)

O/F = 2.00

NOTE: REACTION RATE CONSTANTS LISTED IN TABLE IV-1

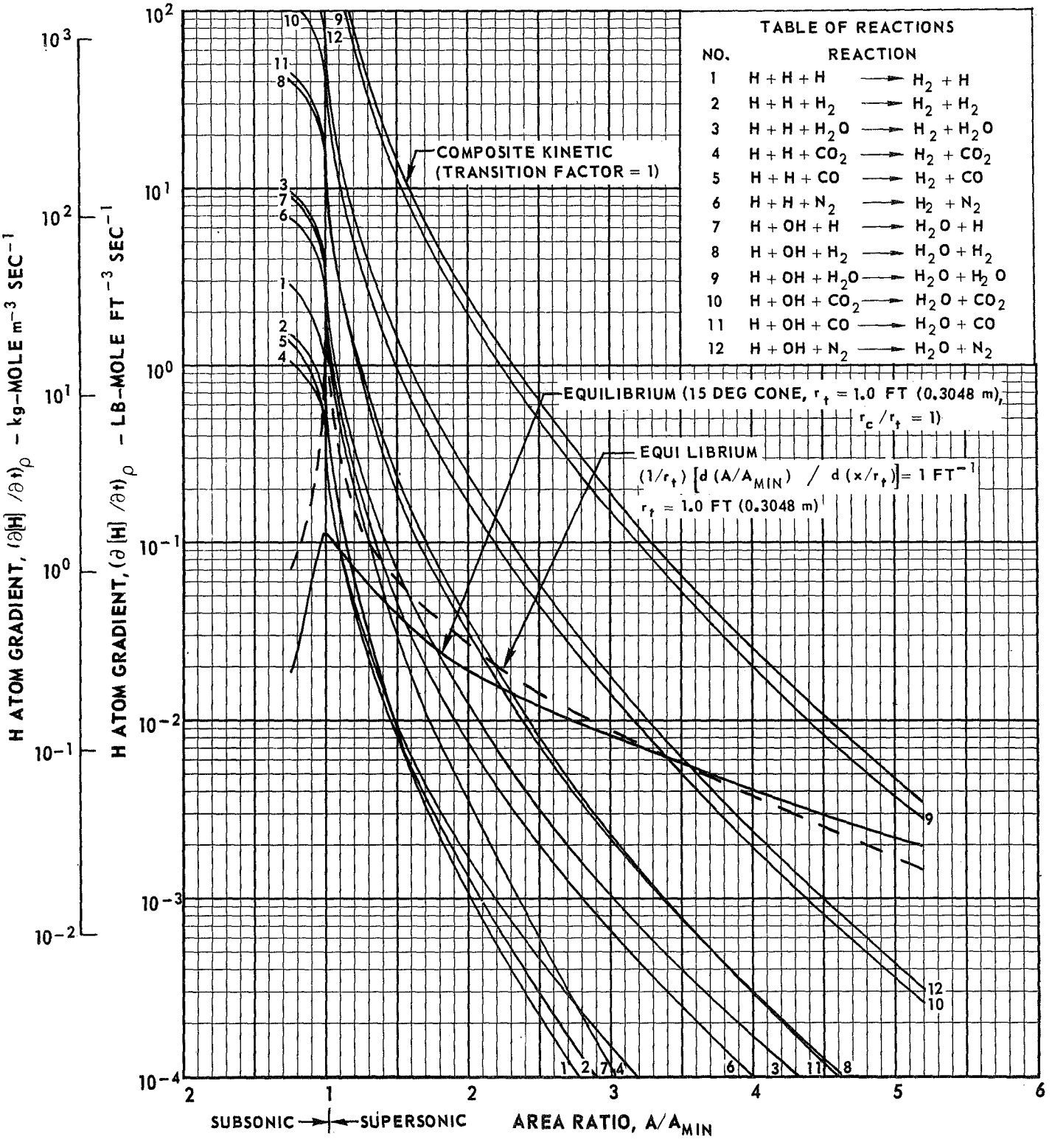

FIG. IV-24

NORMALIZED GRAPHICAL SOLUTION FOR FREEZING AREA RATIO USING MODIFIED BRAY ANALYSIS

AEROZINE 50 (ℓ) - N_2O_4 (ℓ)

P_C = 500 PSIA (3.448 X 10^6 N/m^2)

O/F = 2.50

NOTE: REACTION RATE CONSTANTS LISTED IN TABLE IV-1

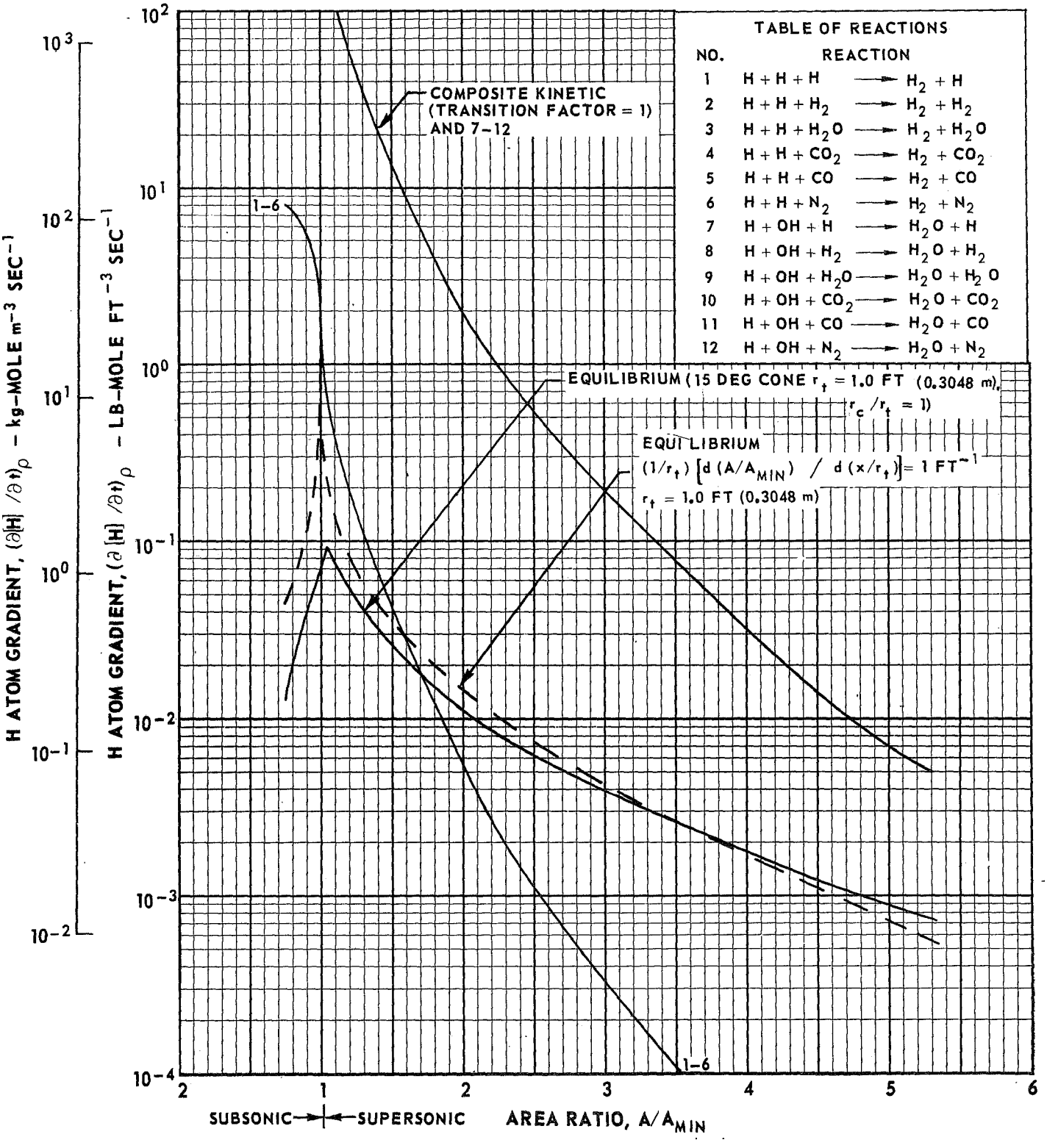

FIG. IV-25

NORMALIZED GRAPHICAL SOLUTION FOR FREEZING AREA RATIO USING MODIFIED BRAY ANALYSIS

AEROZINE 50 (ℓ) - N_2O_4 (ℓ)

P_C = 750 PSIA (5.171 X 10^6 N/m^2)

O/F = 1.50

NOTE: REACTION RATE CONSTANTS LISTED IN TABLE IV-1

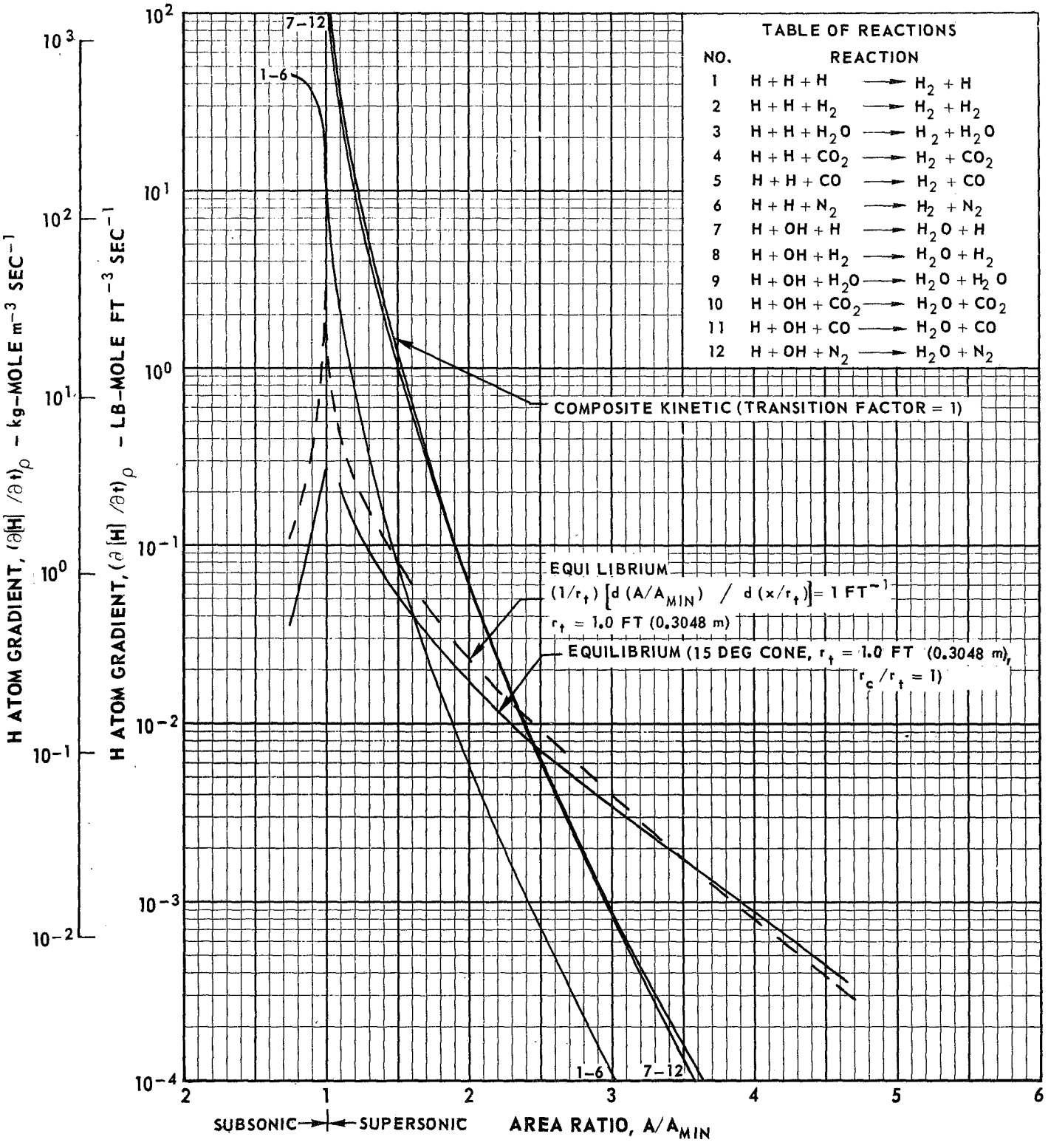

FIG. IV-26

NORMALIZED GRAPHICAL SOLUTION FOR FREEZING AREA RATIO USING MODIFIED BRAY ANALYSIS

AEROZINE 50 (ℓ) - N_2O_4 (ℓ)

P_C = 750 PSIA (5.171 X 10^6 N/m^2)

O/F = 2.00

NOTE: REACTION RATE CONSTANTS LISTED IN TABLE IV-1

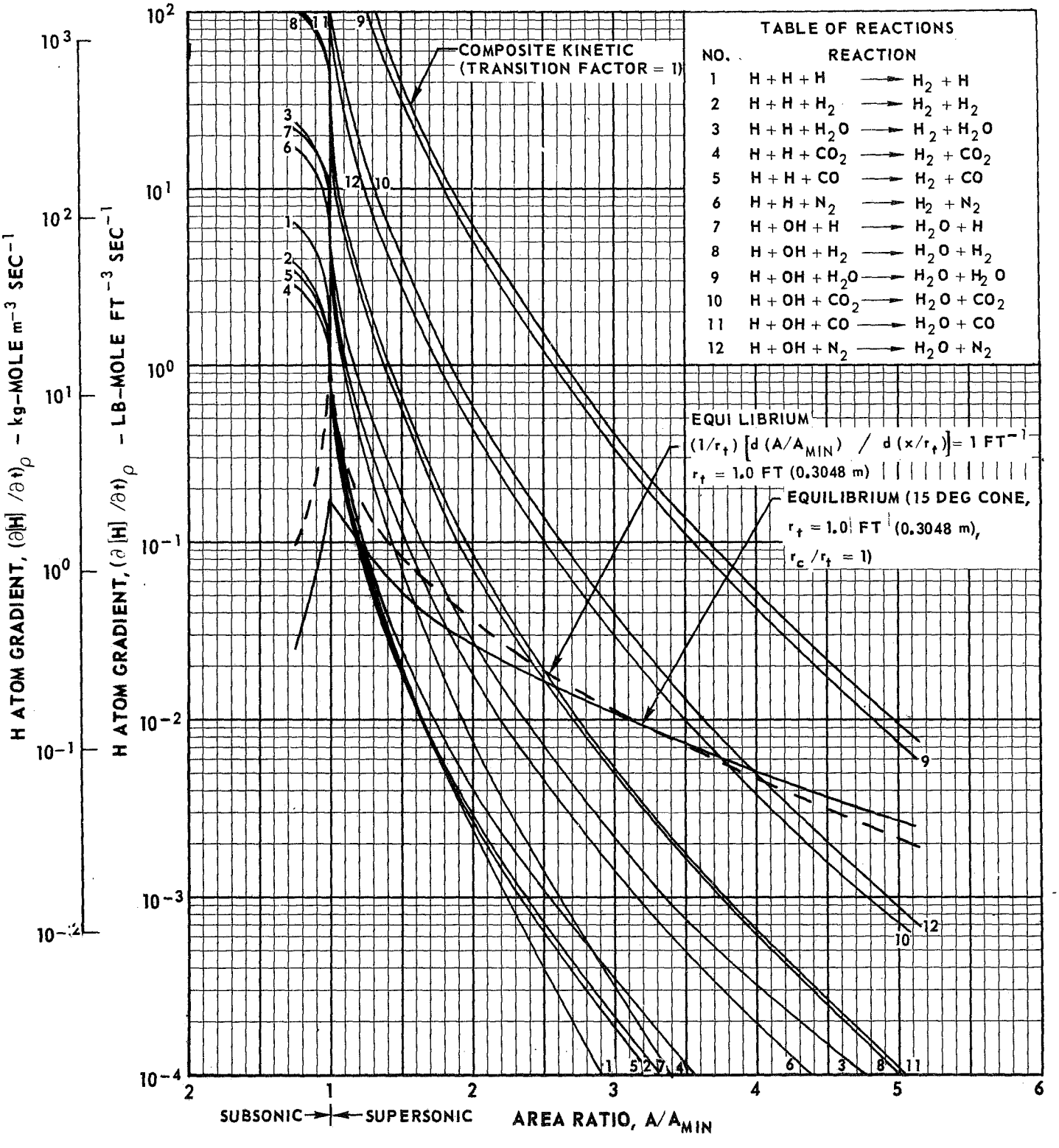

FIG. IV-27

NORMALIZED GRAPHICAL SOLUTION FOR FREEZING AREA RATIO USING MODIFIED BRAY ANALYSIS

AEROZINE 50 (ℓ) – N_2O_4 (ℓ)

P_C = 750 PSIA (5.171 X 10^6 N/m^2)

O/F = 2.50

NOTE: REACTION RATE CONSTANTS LISTED IN TABLE IV-1

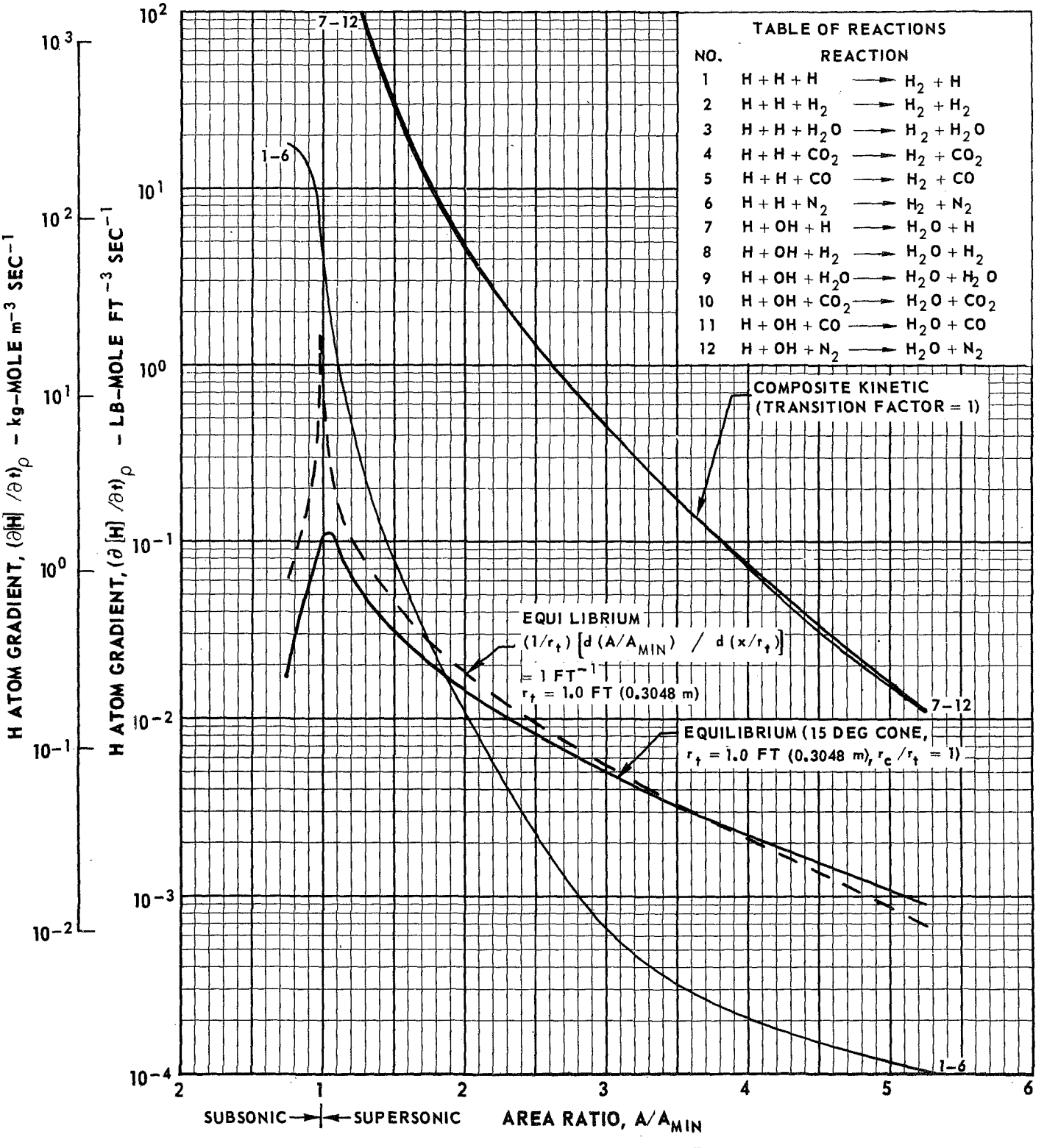

FIG. IV-28

NORMALIZED GRAPHICAL SOLUTION FOR FREEZING AREA RATIO USING MODIFIED BRAY ANALYSIS

AEROZINE 50 (ℓ) - N_2O_4 (ℓ)

P_C = 1000 PSIA (6.895×10^6 N/m^2)

O/F = 1.50

NOTE: REACTION RATE CONSTANTS LISTED IN TABLE IV-1

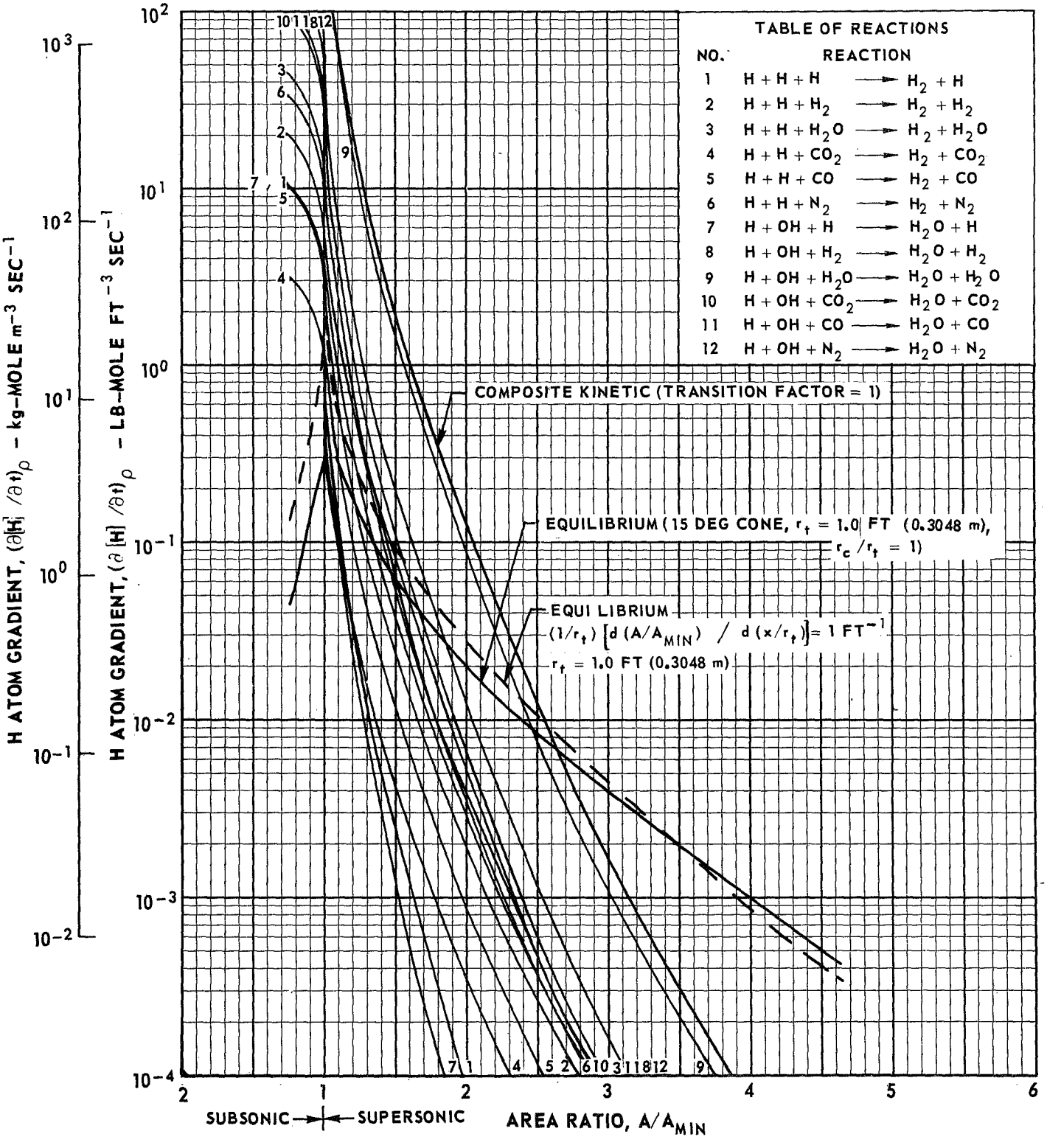

FIG. IV-29

NORMALIZED GRAPHICAL SOLUTION FOR FREEZING AREA RATIO USING MODIFIED BRAY ANALYSIS

AEROZINE 50 (ℓ) - N_2O_4 (ℓ)

P_C = 1000 PSIA (6.895 X 10^6 N/m^2)

O/F = 2.00

NOTE: REACTION RATE CONSTANTS LISTED IN TABLE IV-1

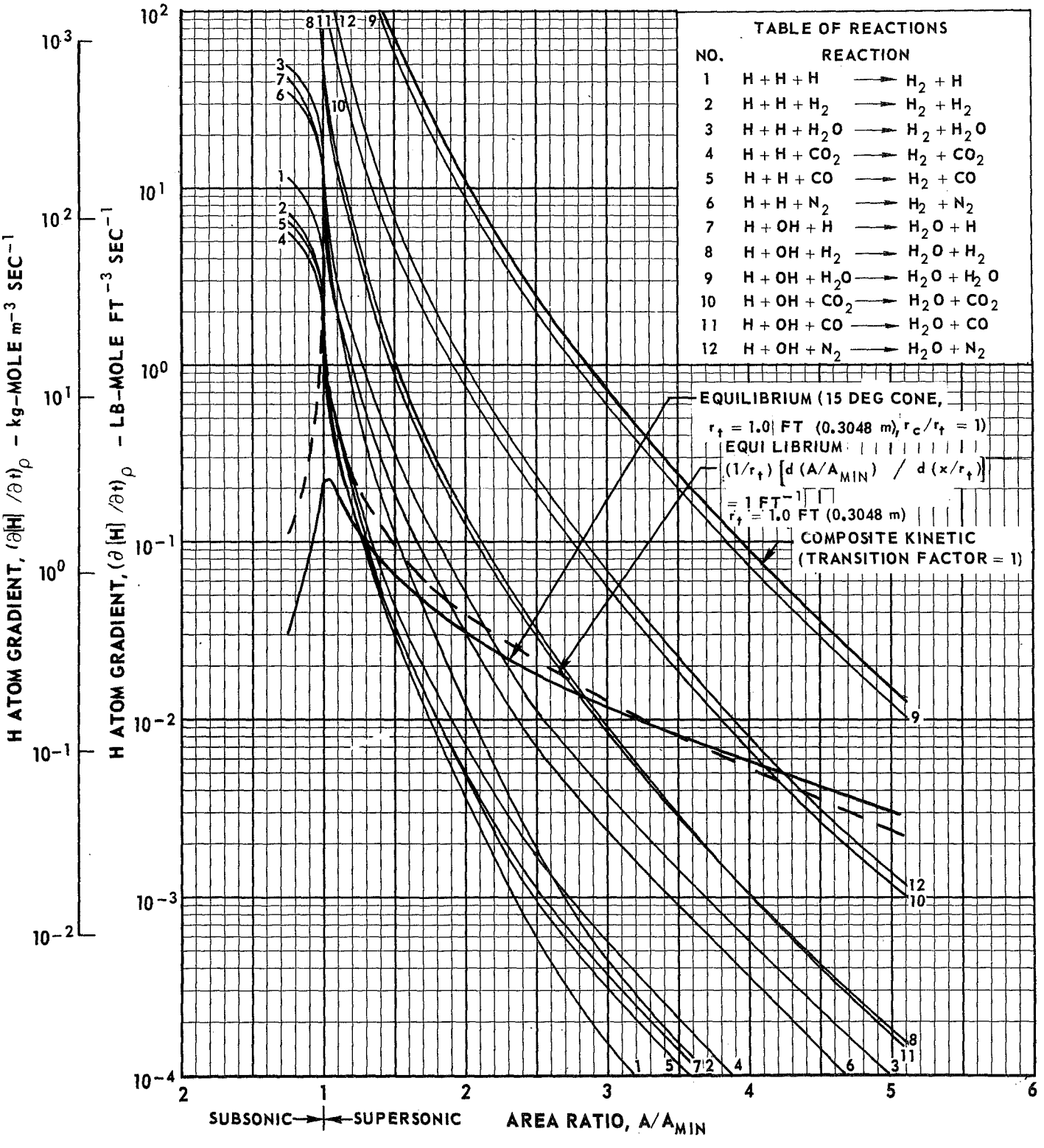

FIG. IV-30

NORMALIZED GRAPHICAL SOLUTION FOR FREEZING AREA RATIO USING MODIFIED BRAY ANALYSIS

AEROZINE 50 (ℓ) - N_2O_4 (ℓ)

P_C = 1000 PSIA (6.895 X 10^6 N/m^2)

O/F = 2.50

NOTE: REACTION RATE CONSTANTS LISTED IN TABLE IV-1

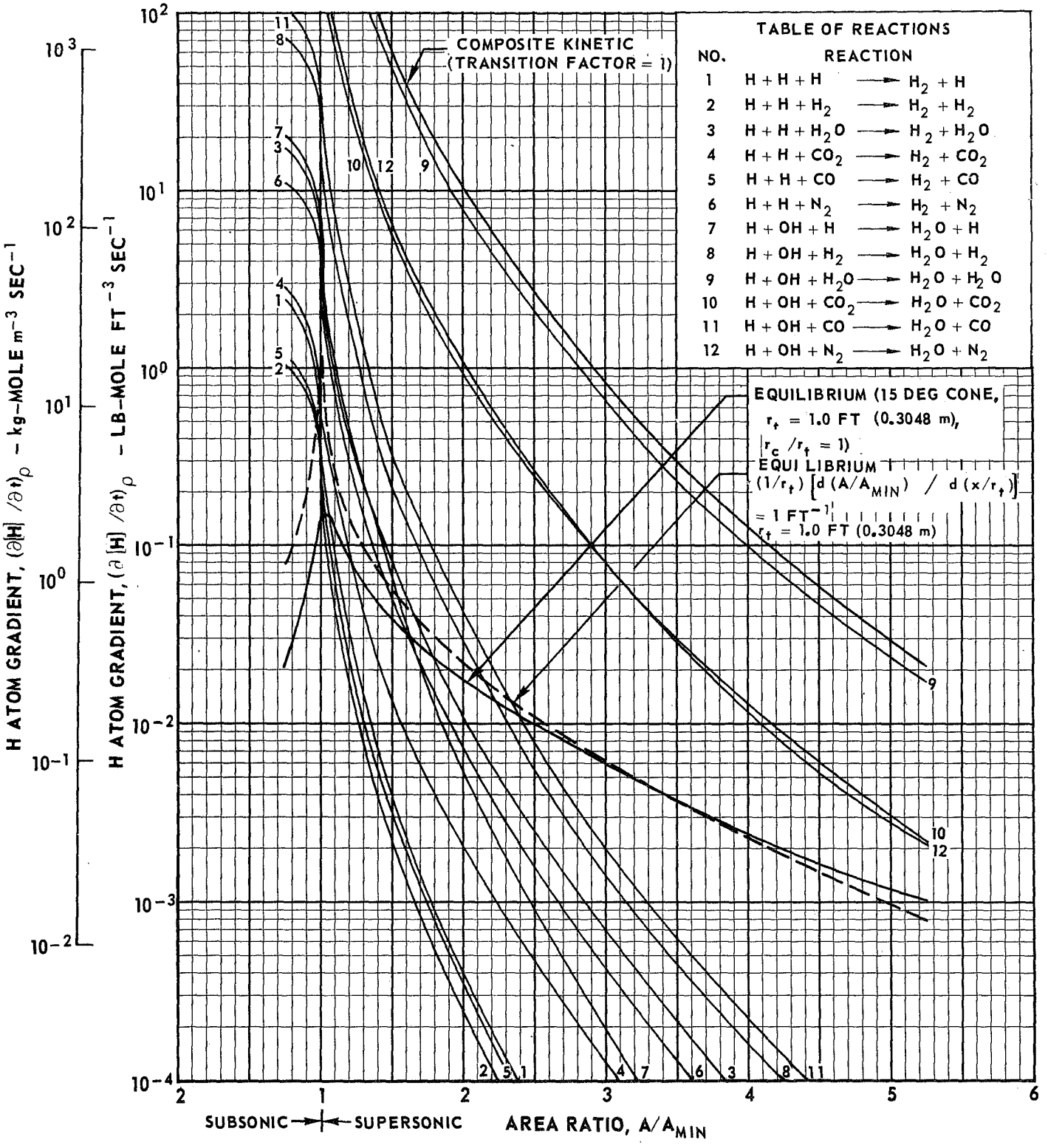

TABLE OF REACTIONS

NO.	REACTION
1	$H + H + H \longrightarrow H_2 + H$
2	$H + H + H_2 \longrightarrow H_2 + H_2$
3	$H + H + H_2O \longrightarrow H_2 + H_2O$
4	$H + H + CO_2 \longrightarrow H_2 + CO_2$
5	$H + H + CO \longrightarrow H_2 + CO$
6	$H + H + N_2 \longrightarrow H_2 + N_2$
7	$H + OH + H \longrightarrow H_2O + H$
8	$H + OH + H_2 \longrightarrow H_2O + H_2$
9	$H + OH + H_2O \longrightarrow H_2O + H_2O$
10	$H + OH + CO_2 \longrightarrow H_2O + CO_2$
11	$H + OH + CO \longrightarrow H_2O + CO$
12	$H + OH + N_2 \longrightarrow H_2O + N_2$

FIG. IV-31

EFFECT OF FREEZING AREA RATIO ON NONEQUILIBRIUM PERFORMANCE FOR AEROZINE – N_2O_4 PROPELLANT SYSTEM

AEROZINE 50 (ℓ) – N_2 O_4 (ℓ)

P_C = 100 PSIA (6.895×10^5 N/m^2)

O/F = 1.50

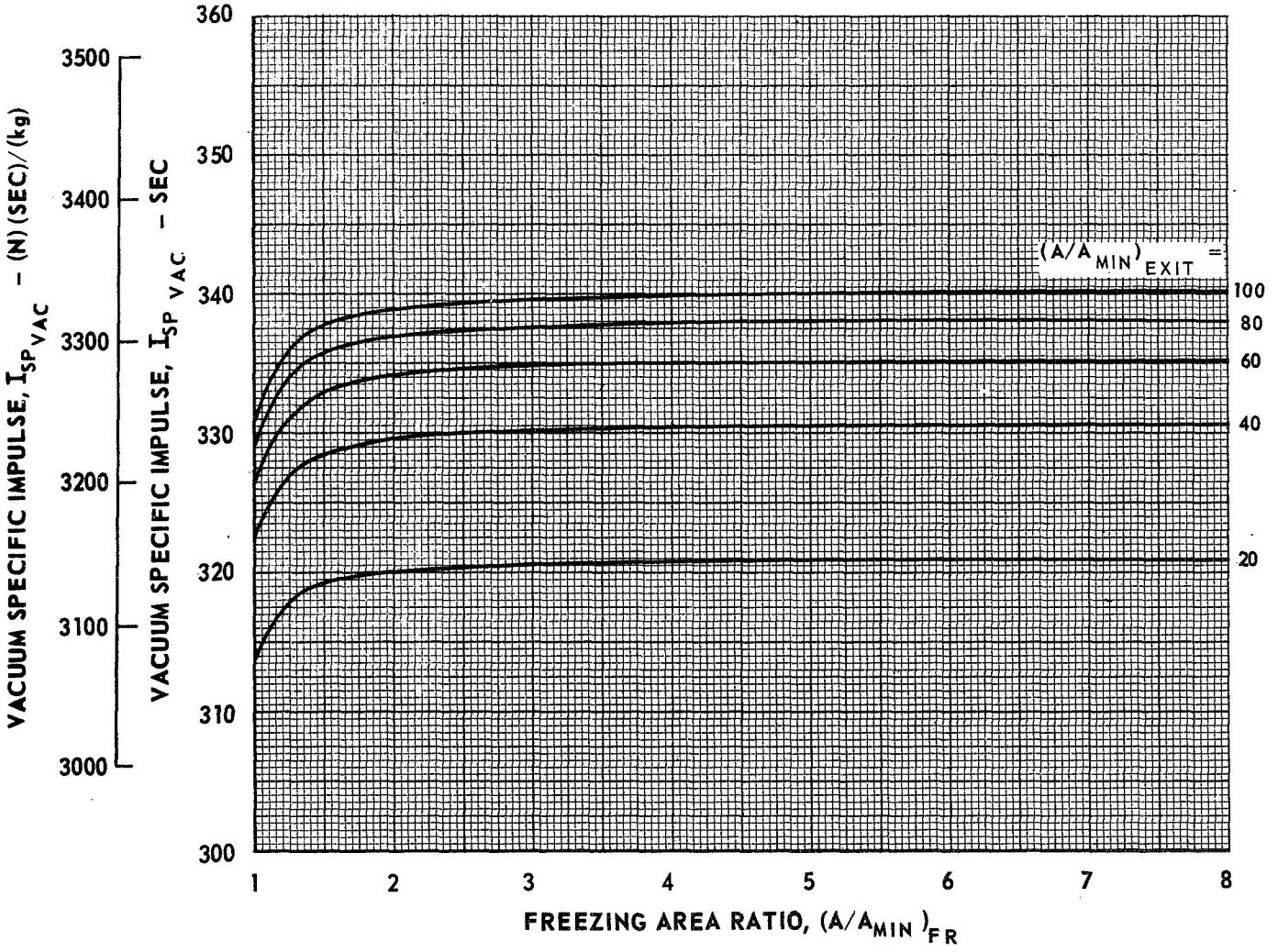

FIG. IV-32

EFFECT OF FREEZING AREA RATIO ON NONEQUILIBRIUM PERFORMANCE FOR AEROZINE - N_2O_4 PROPELLANT SYSTEM

AEROZINE 50 (ℓ) - N_2O_4 (ℓ)

P_C = 100 PSIA (6.895×10^5 N/m^2)

O/F = 2.00

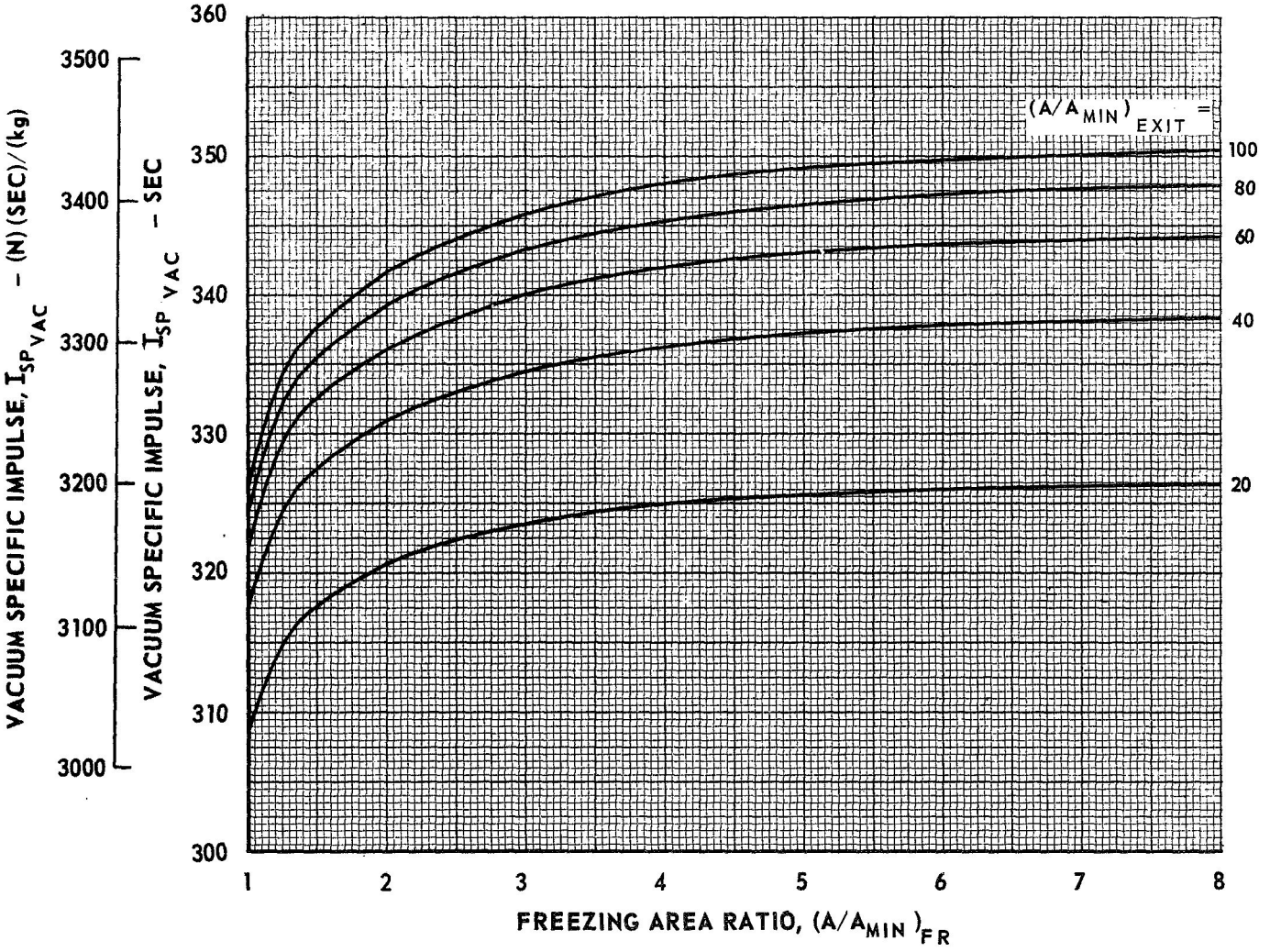

FIG. IV-33

EFFECT OF FREEZING AREA RATIO ON NONEQUILIBRIUM PERFORMANCE FOR AEROZINE $-N_2O_4$ PROPELLANT SYSTEM

AEROZINE 50 (ℓ) - N_2 O_4 (ℓ)

P_C = 100 PSIA (6.895×10^5 N/m^2)

O/F = 2.50

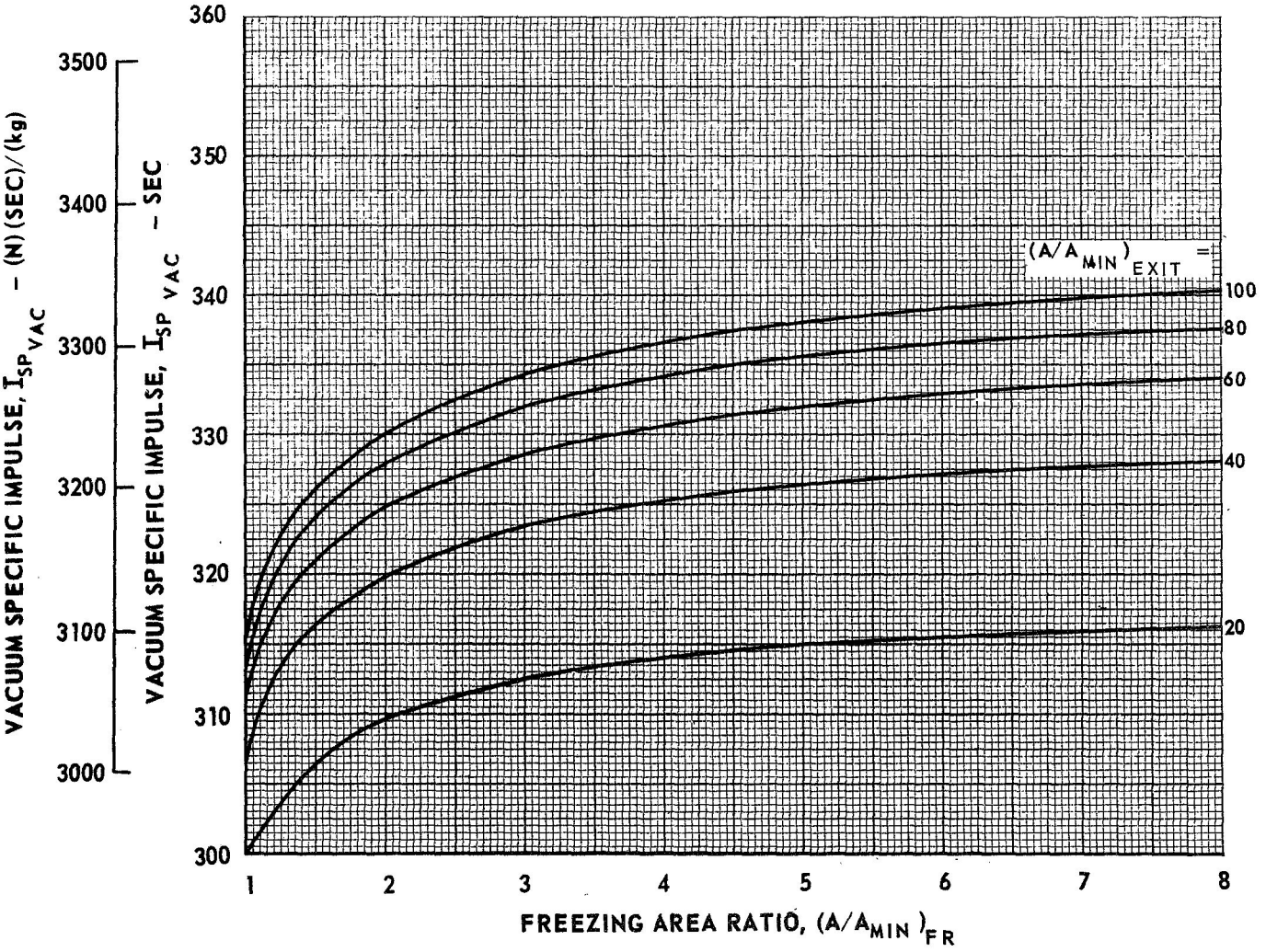

FIG. IV–34

EFFECT OF FREEZING AREA RATIO ON NONEQUILIBRIUM PERFORMANCE FOR AEROZINE – N_2O_4 PROPELLANT SYSTEM

AEROZINE 50 (ℓ) – N_2O_4 (ℓ)

P_C = 200 PSIA (1.379×10^6 N/m^2)

O/F = 1.50

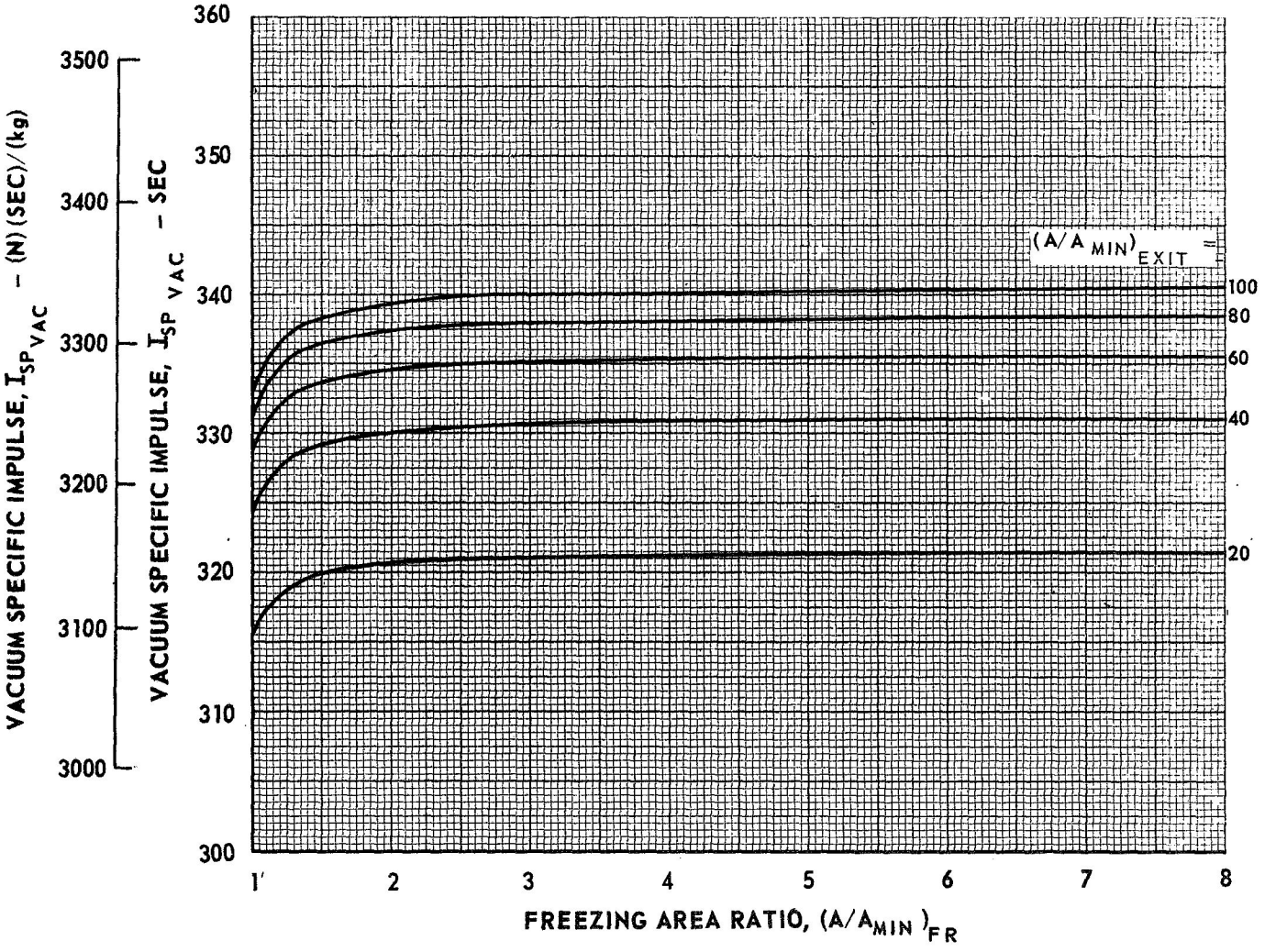

FIG. IV-35

EFFECT OF FREEZING AREA RATIO ON NONEQUILIBRIUM PERFORMANCE FOR AEROZINE - N_2O_4 PROPELLANT SYSTEM

AEROZINE 50 (ℓ) - N_2O_4 (ℓ)

P_C = 200 PSIA (1.379X10^6 N/m^2)

O/F = 2.00

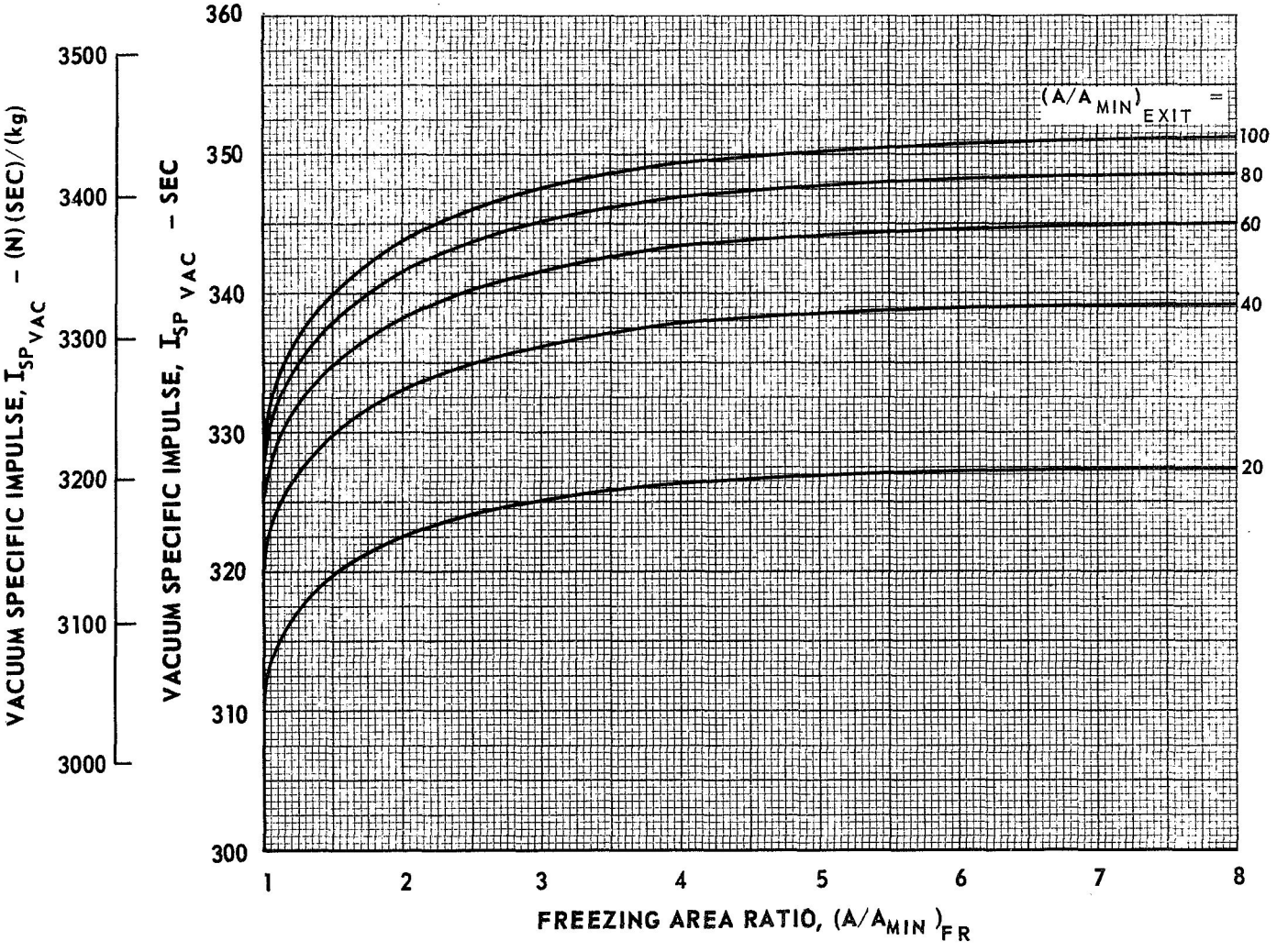

FIG. IV-36

EFFECT OF FREEZING AREA RATIO ON NONEQUILIBRIUM PERFORMANCE FOR AEROZINE - N_2O_4 PROPELLANT SYSTEM

AEROZINE 50 (ℓ) - N_2O_4 (ℓ)

P_C = 200 PSIA ($1.379 \times 10^6 N/m^2$)

O/F = 2.50

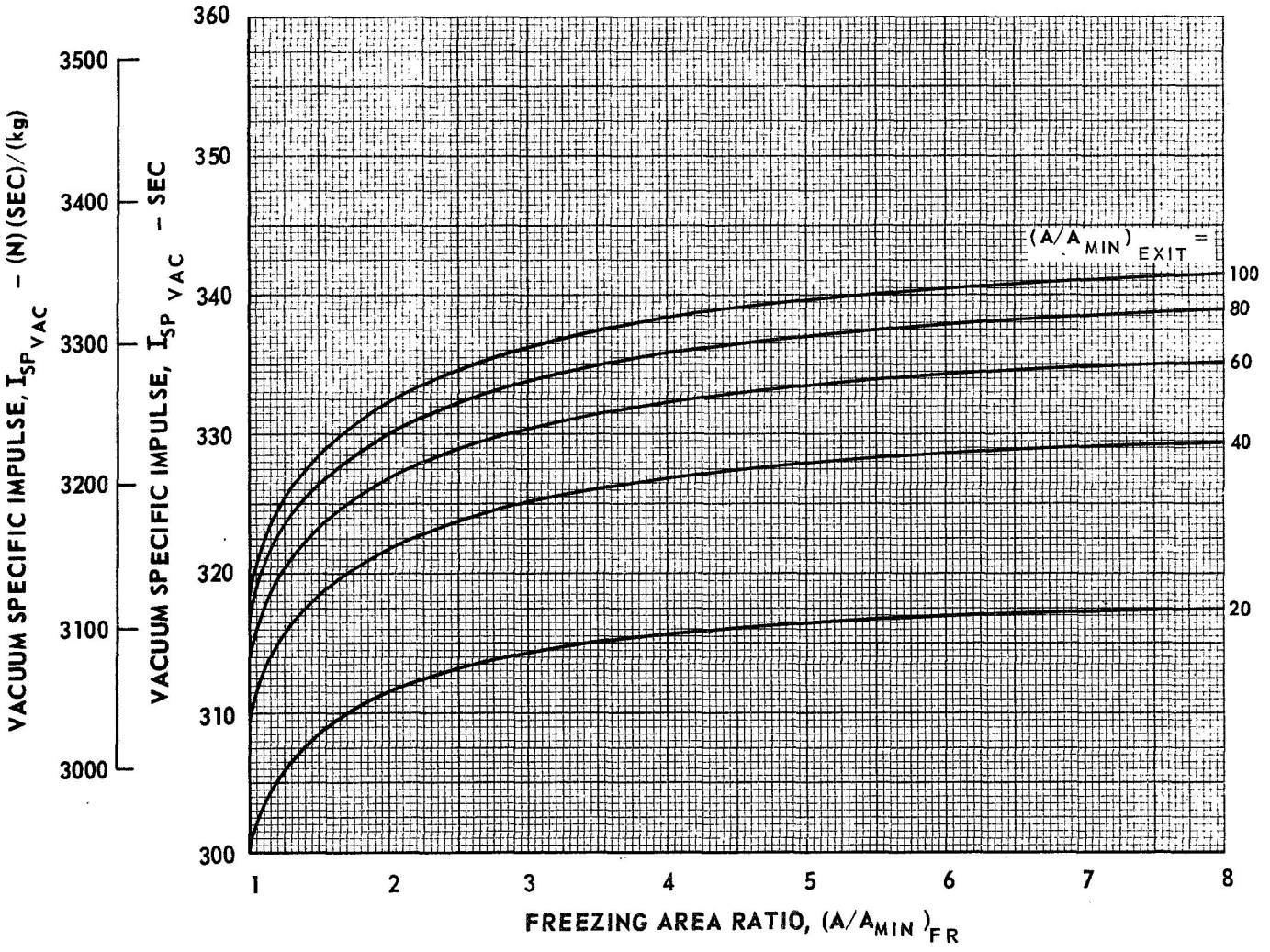

EFFECT OF FREEZING AREA RATIO ON NONEQUILIBRIUM PERFORMANCE FOR AEROZINE - N_2O_4 PROPELLANT SYSTEM

AEROZINE 50 (ℓ) - N_2O_4 (ℓ)

P_C = 300 PSIA ($2.069 \times 10^6 N/m^2$)

O/F = 1.50

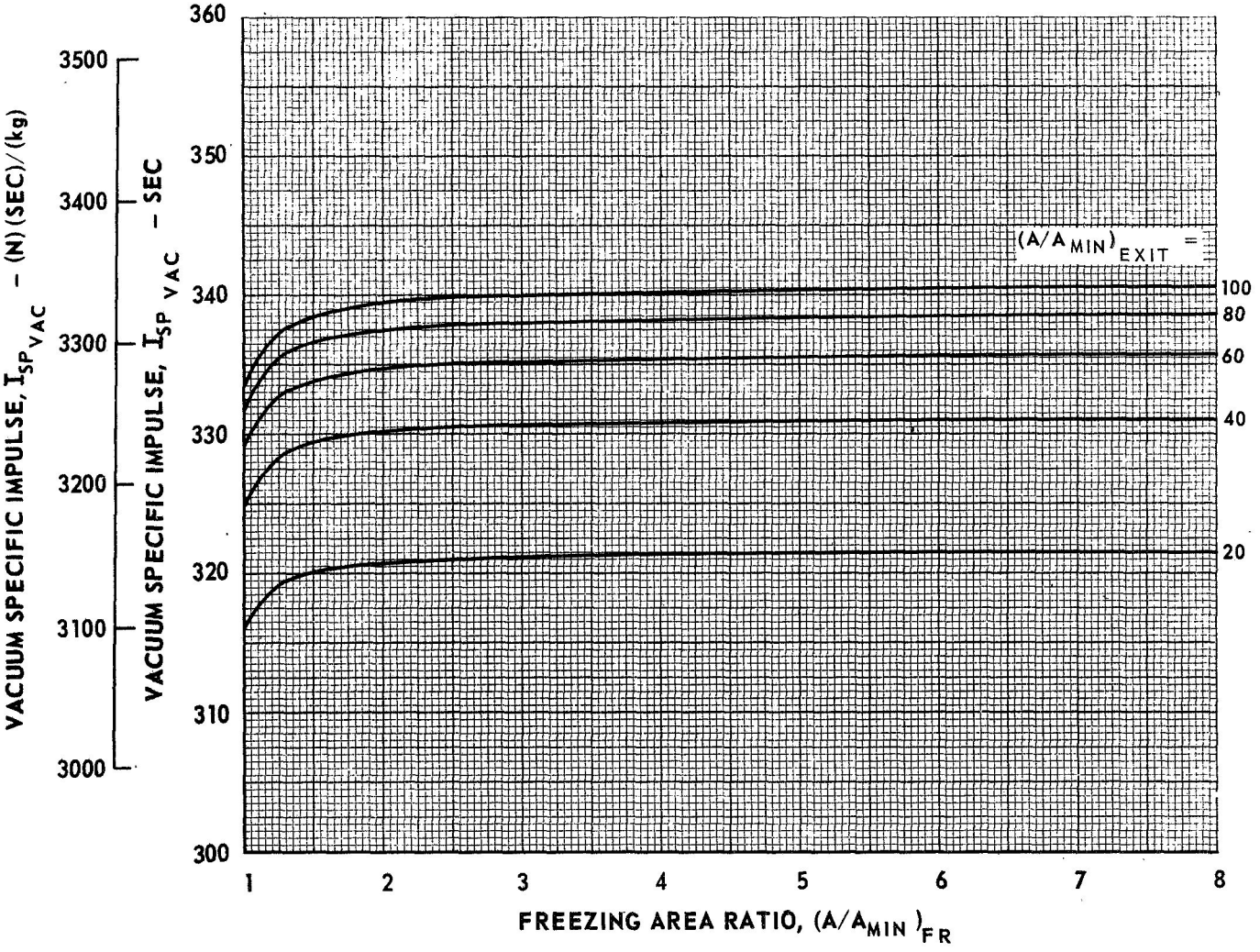

FIG. IV-38

EFFECT OF FREEZING AREA RATIO ON NONEQUILIBRIUM PERFORMANCE FOR AEROZINE - N_2O_4 PROPELLANT SYSTEM

AEROZINE 50 (ℓ) - N_2O_4 (ℓ)

P_C = 300 PSIA ($2.069 \times 10^6 N/m^2$)

O/F = 2.00

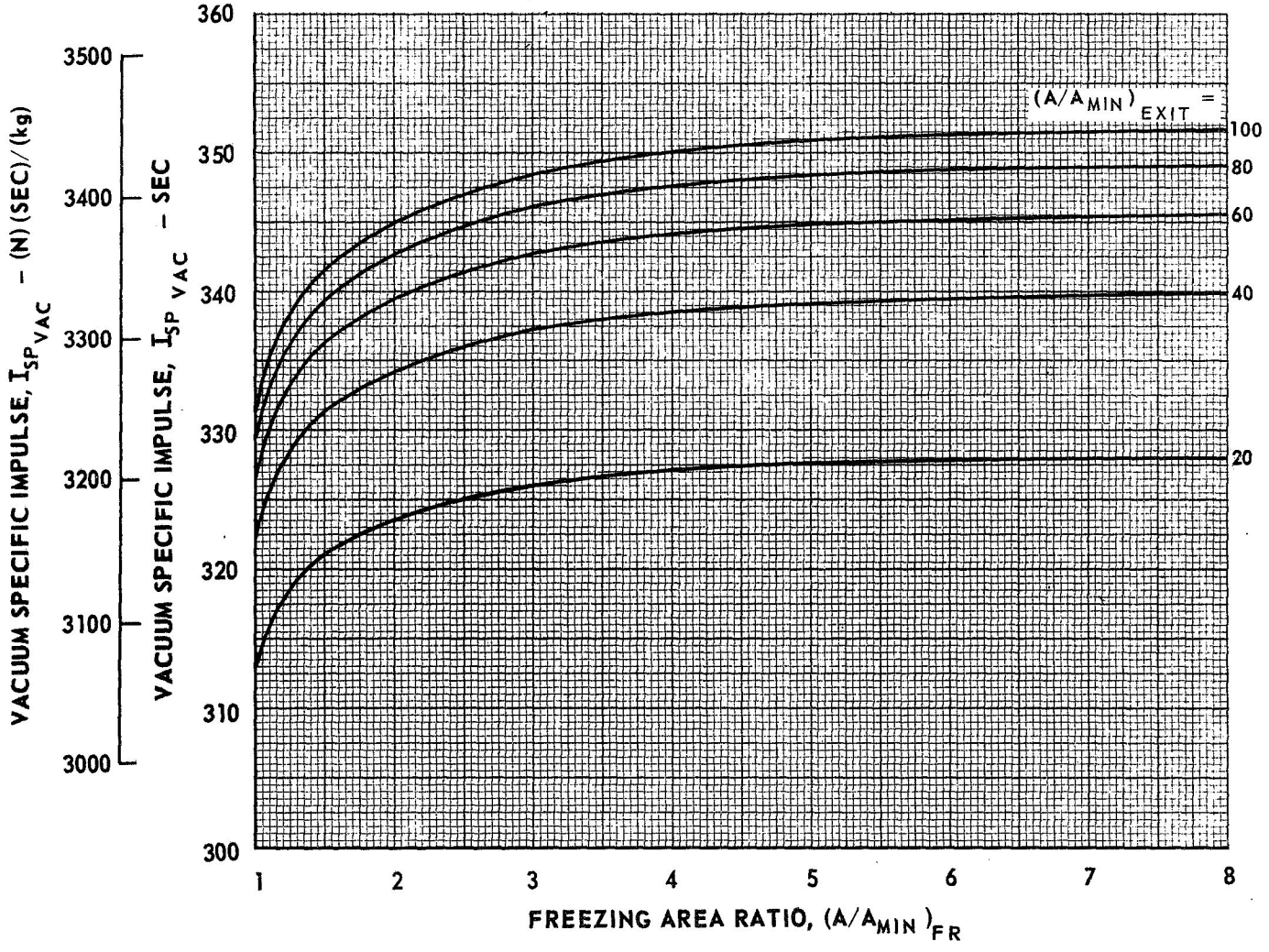

FIG. IV-39

EFFECT OF FREEZING AREA RATIO ON NONEQUILIBRIUM PERFORMANCE FOR AEROZINE $-N_2O_4$ PROPELLANT SYSTEM

AEROZINE 50 (ℓ) - N_2 O_4 (ℓ)

P_C = 300 PSIA (2.069 X 10^6 N/m^2)

O/F = 2.50

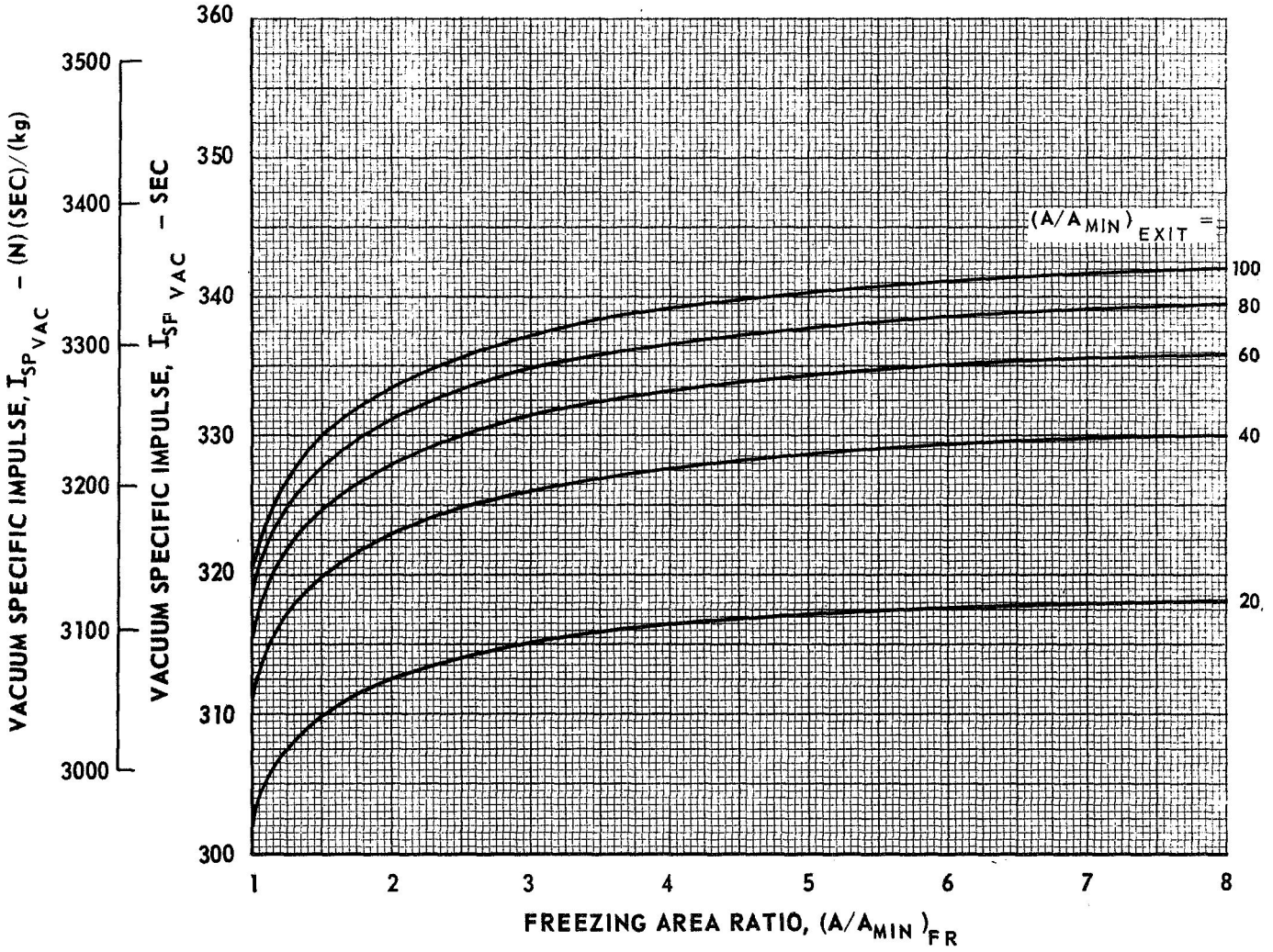

FIG. IV-40

EFFECT OF FREEZING AREA RATIO ON NONEQUILIBRIUM PERFORMANCE FOR AEROZINE - N_2O_4 PROPELLANT SYSTEM

AEROZINE 50 (ℓ) - N_2O_4 (ℓ)

P_C = 500 PSIA (3.448X10^{6}N/m^2)

O/F = 1.50

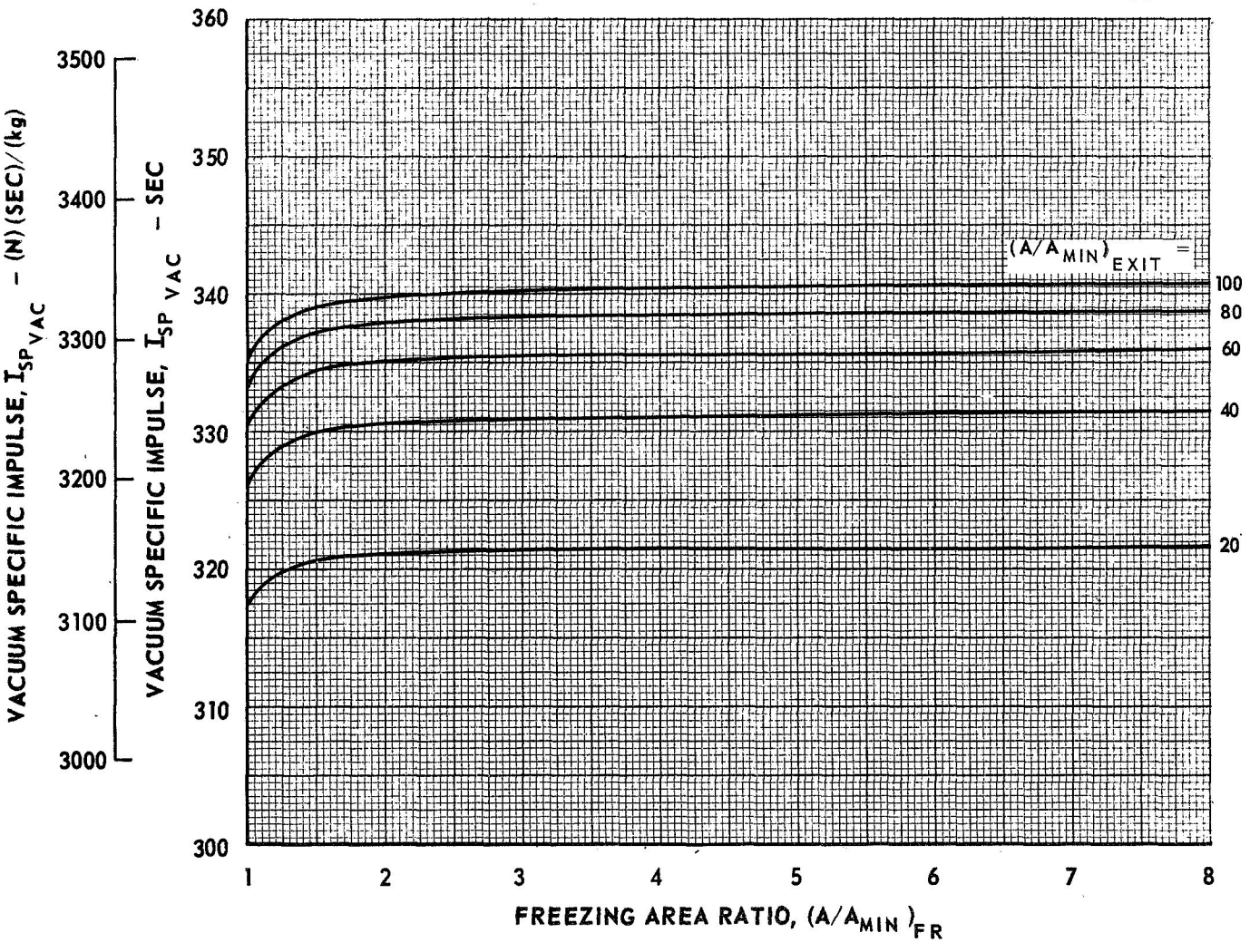

FIG. IV-41

EFFECT OF FREEZING AREA RATIO ON NONEQUILIBRIUM PERFORMANCE FOR AEROZINE $-N_2O_4$ PROPELLANT SYSTEM

AEROZINE 50 (ℓ) - N_2O_4 (ℓ)

P_C = 500 PSIA (3.448×10^6 N/m^2)

O/F = 2.00

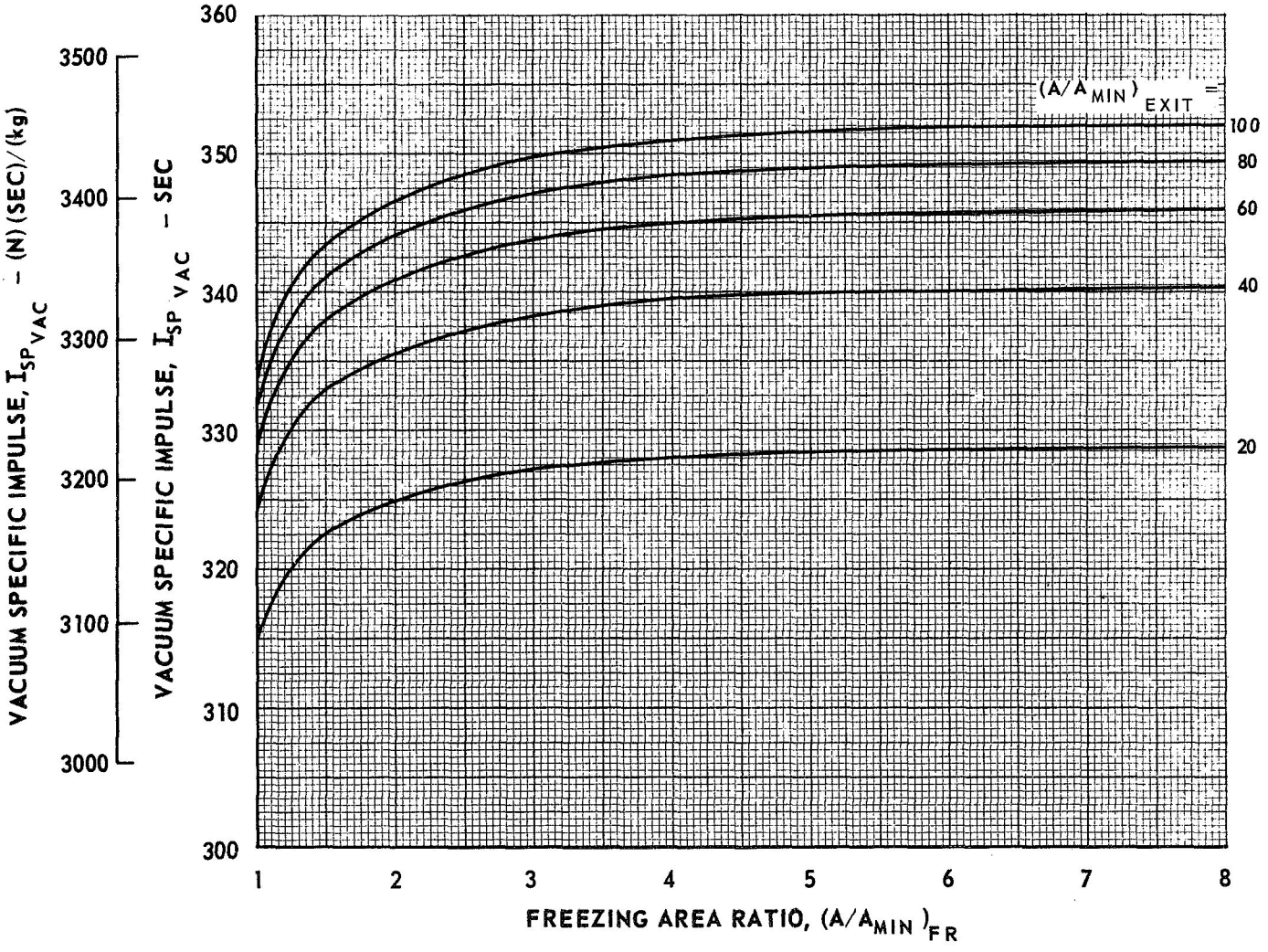

FIG. IV-42

EFFECT OF FREEZING AREA RATIO ON NONEQUILIBRIUM PERFORMANCE FOR AEROZINE - N_2O_4 PROPELLANT SYSTEM

AEROZINE 50 (ℓ) - N_2 O_4 (ℓ)

P_C = 500 PSIA (3.448X10 ^{6}N/m ^{2})

O/F = 2.50

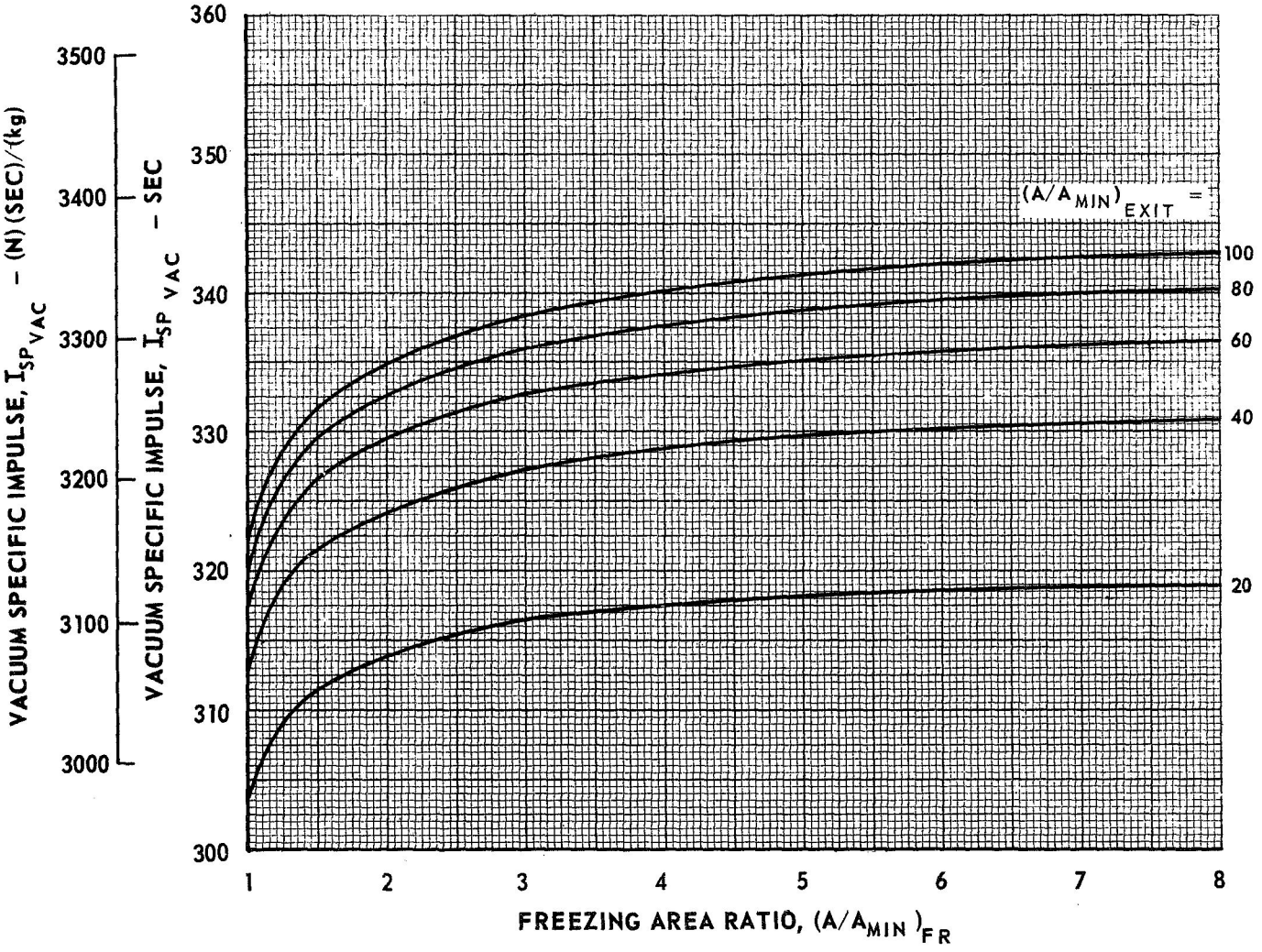

FIG. IV-43

EFFECT OF FREEZING AREA RATIO ON NONEQUILIBRIUM PERFORMANCE FOR AEROZINE - N_2O_4 PROPELLANT SYSTEM

AEROZINE 50 (ℓ) - N_2O_4 (ℓ)

P_C = 750 PSIA ($5.171 \times 10^6 N/m^2$)

O/F = 1.50

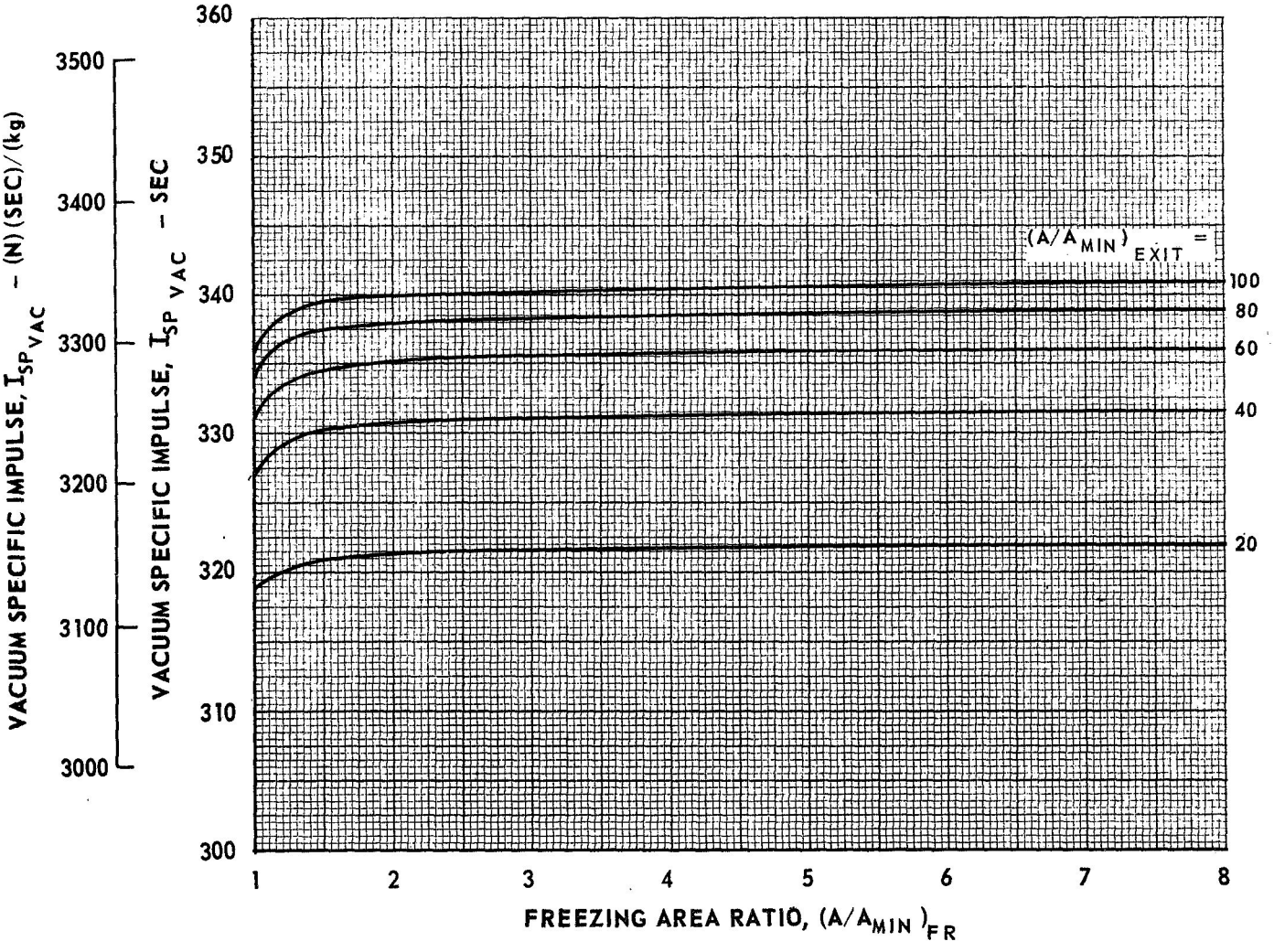

EFFECT OF FREEZING AREA RATIO ON NONEQUILIBRIUM PERFORMANCE FOR AEROZINE $-N_2O_4$ PROPELLANT SYSTEM

AEROZINE 50 (ℓ) – N_2O_4 (ℓ)

P_C = 750 PSIA (5.171×10^6 N/m^2)

O/F = 2.00

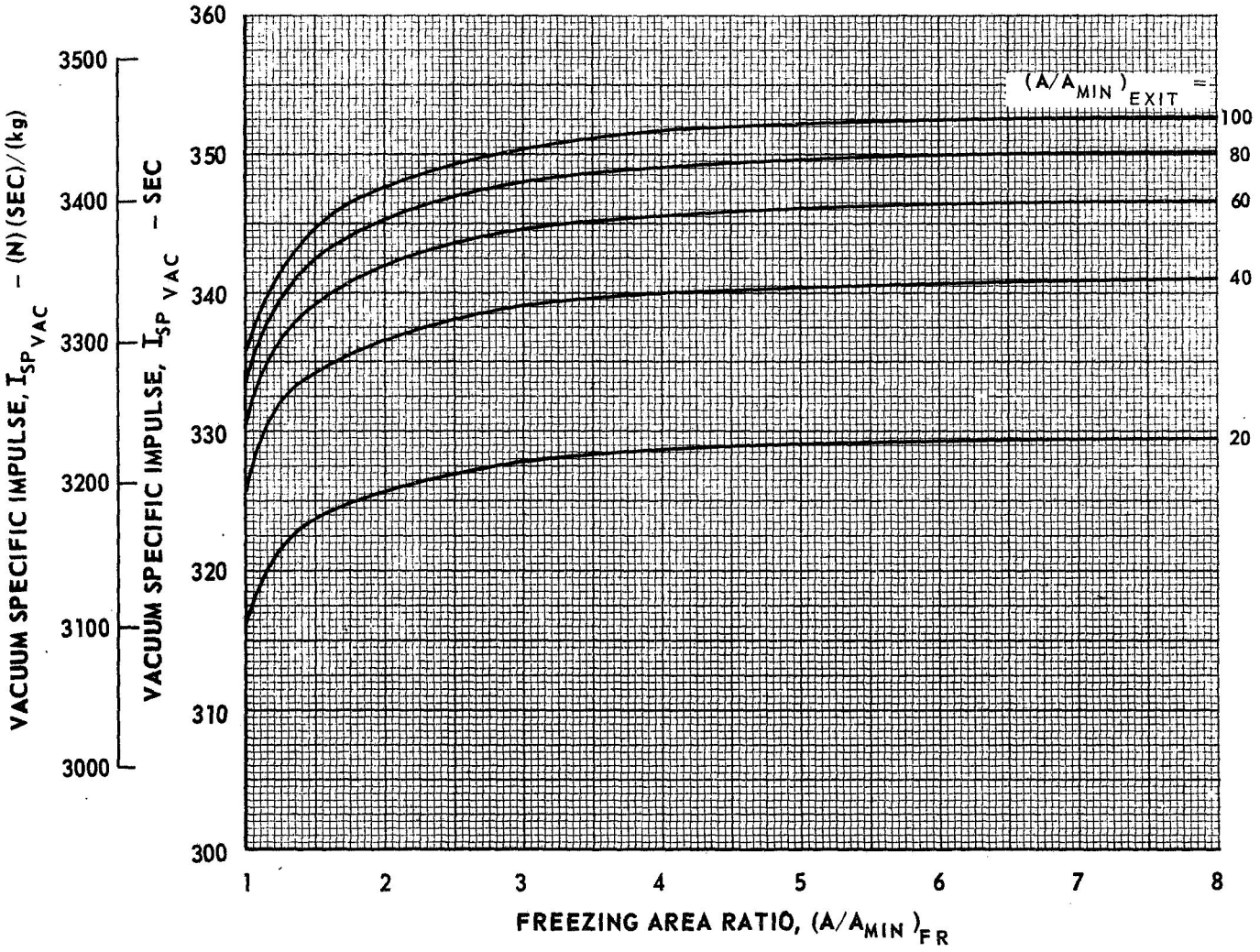

FIG. IV-45

EFFECT OF FREEZING AREA RATIO ON NONEQUILIBRIUM PERFORMANCE FOR AEROZINE - N_2O_4 PROPELLANT SYSTEM

AEROZINE 50 (ℓ) - N_2O_4 (ℓ)

P_C = 750 PSIA (5.171X10^6 N/m^2)

O/F = 2.50

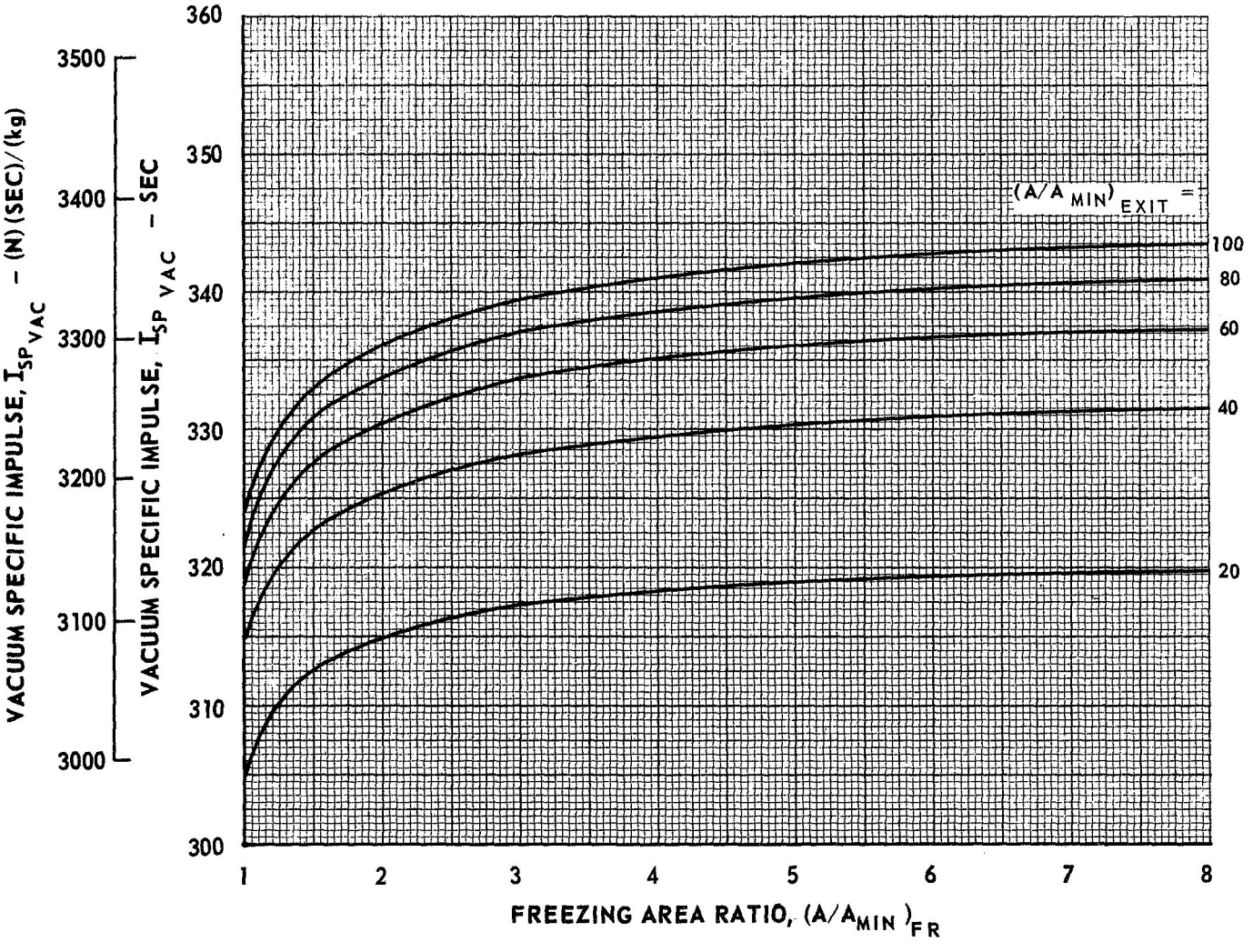

FIG. IV-46

EFFECT OF FREEZING AREA RATIO ON NONEQUILIBRIUM PERFORMANCE FOR AEROZINE - N_2O_4 PROPELLANT SYSTEM

AEROZINE 50 (ℓ) - N_2O_4 (ℓ)

P_C=1000 PSIA ($6.895 \times 10^6 N/m^2$)

O/F = 1.50

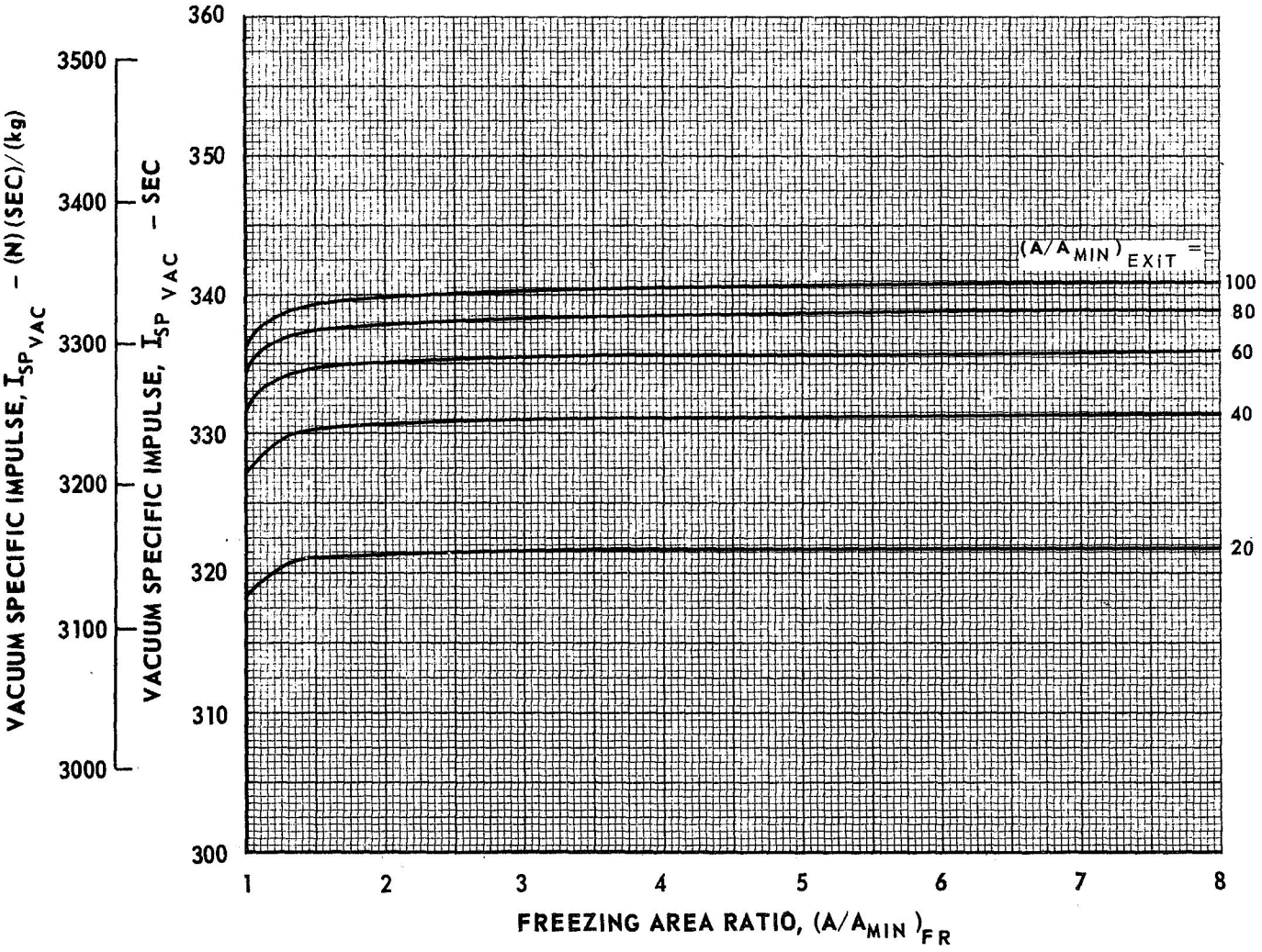

FIG. IV-47

EFFECT OF FREEZING AREA RATIO ON NONEQUILIBRIUM PERFORMANCE FOR AEROZINE - N_2O_4 PROPELLANT SYSTEM

AEROZINE 50 (ℓ) - N_2O_4 (ℓ)

P_C=1000 PSIA (6.895×10^6 N/m^2)

O/F = 2.00

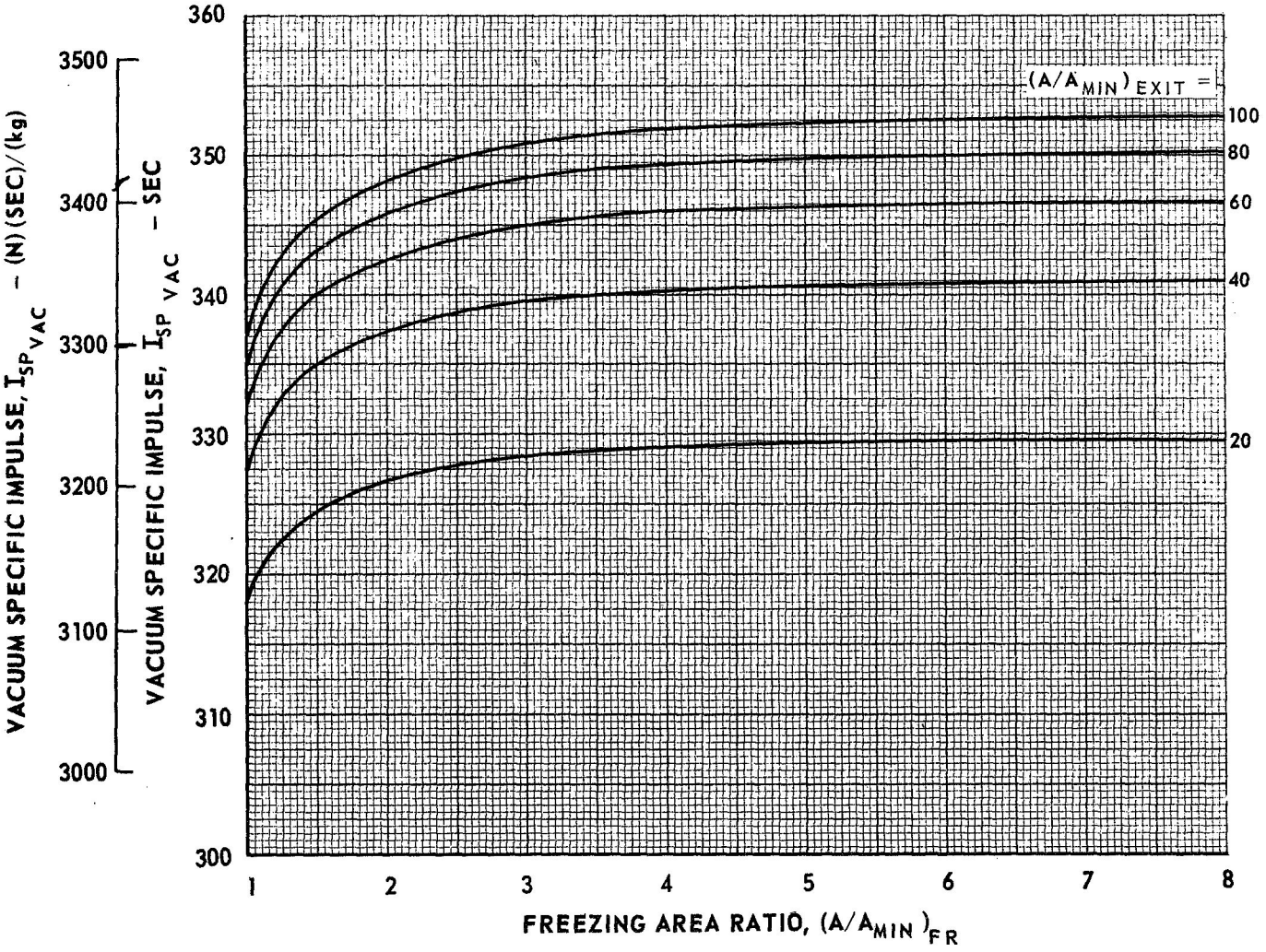

FIG. IV-48

EFFECT OF FREEZING AREA RATIO ON NONEQUILIBRIUM PERFORMANCE FOR AEROZINE - N_2O_4 PROPELLANT SYSTEM

AEROZINE 50 (ℓ) - N_2O_4 (ℓ)

P_C = 1000 PSIA (6.895×10^6 N/m^2)

O/F = 2.50

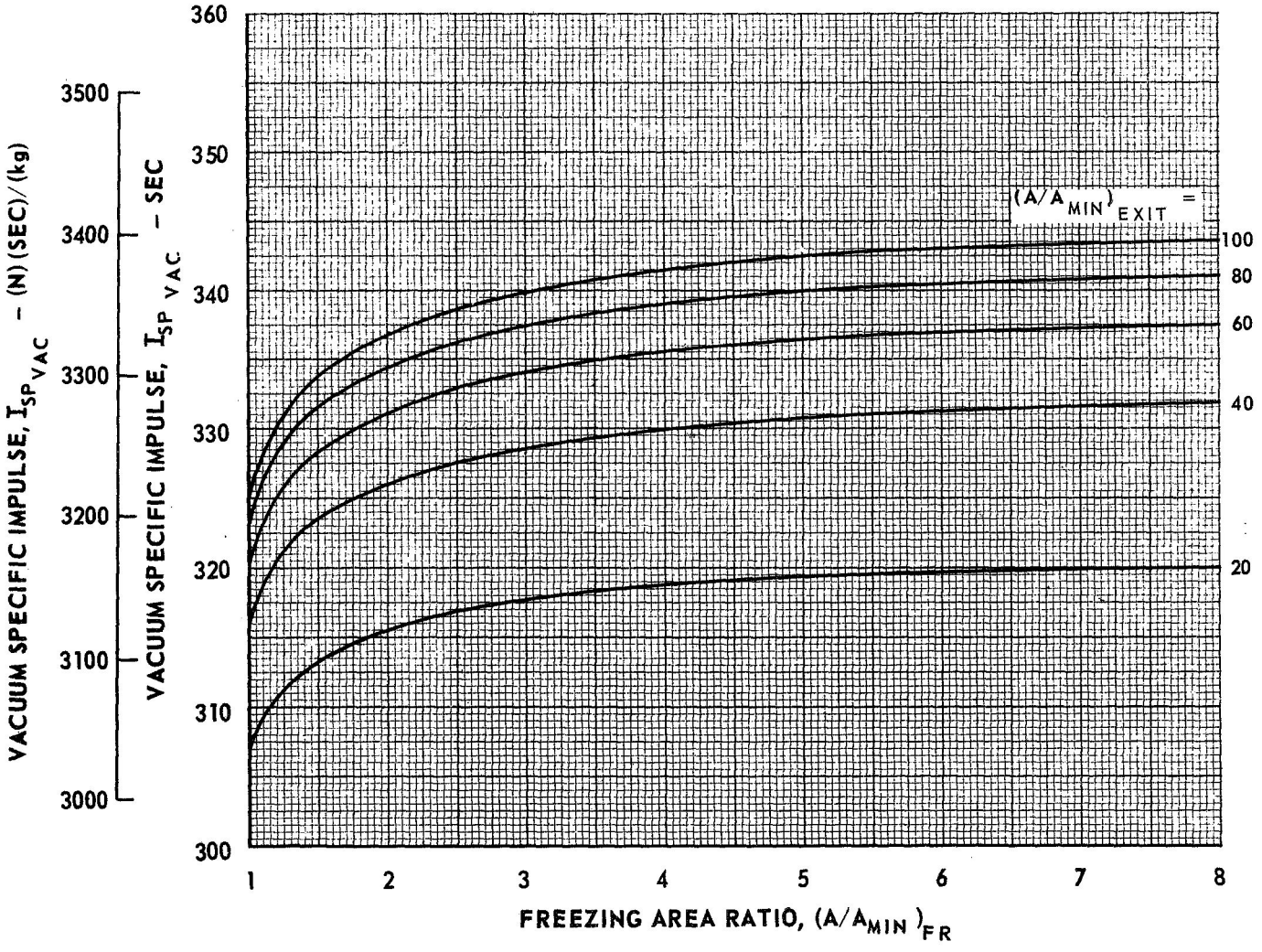

TABLE V-1
SUMMARY OF ELEMENTARY REACTIONS AND REACTION RATE CONSTANTS EMPLOYED IN B_2H_6-OF_2 RECOMBINATION MECHANISM

	REACTION		FORWARD RATE
	$H + H + A \rightarrow$	$H_2 + A$	$k_f = 4.62 \times 10^{14} T^{-1}$
1	$H + H + H \rightarrow$	$H_2 + H$	$k_f = 2.0\ (4.62 \times 10^{14} T^{-1})$
2	$H + H + H_2 \rightarrow$	$H_2 + H_2$	$k_f = 2.5\ (4.62 \times 10^{14} T^{-1})$
3	$H + H + HF \rightarrow$	$H_2 + HF$	$k_f = 2.5\ (4.62 \times 10^{14} T^{-1})$
4	$H + H + BOF \rightarrow$	$H_2 + BOF$	$k_f = 2.0 (4.62 \times 10^{14} T^{-1})$
5	$H + H + BF \rightarrow$	$H_2 + BF$	$k_f = 2.0\ (4.62 \times 10^{14} T^{-1})$
6	$H + H + H_2O \rightarrow$	$H_2 + H_2O$	$k_f = 2.5\ (4.62 \times 10^{14} T^{-1})$
	$H + F + A \rightarrow$	$HF + A$	$k_f = 1.155 \times 10^{15} T^{-1}$
7	$H + F + H \rightarrow$	$HF + H$	$k_f = 1\ (1.155 \times 10^{15} T^{-1})$
8	$H + F + H_2 \rightarrow$	$HF + H_2$	$k_f = 2.5\ (1.155 \times 10^{15} T^{-1})$
9	$H + F + HF \rightarrow$	$HF + HF$	$k_f = 2.5\ (1.155 \times 10^{15} T^{-1})$
10	$H + F + BOF \rightarrow$	$HF + BOF$	$k_f = 2.0\ (1.155 \times 10^{15} T^{-1})$
11	$H + F + BF \rightarrow$	$HF + BF$	$k_f = 2.0\ (1.155 \times 10^{15} T^{-1})$
12	$H + F + H_2O \rightarrow$	$HF + H_2O$	$k_f = 2.5\ (1.155 \times 10^{15} T^{-1})$
	$H + OH + A \rightarrow$	$H_2O + A$	$k_f = 7.85 \times 10^{15} T^{-1}$
13	$H + OH + H \rightarrow$	$H_2O + H$	$k_f = 3\ (7.85 \times 10^{15} T^{-1})$
14	$H + OH + H_2 \rightarrow$	$H_2O + H_2$	$k_f = 3\ (7.85 \times 10^{15} T^{-1})$
15	$H + OH + HF \rightarrow$	$H_2O + HF$	$k_f = 3\ (7.85 \times 10^{15} T^{-1})$
16	$H + OH + BOF \rightarrow$	$H_2O + BOF$	$k_f = 10\ (7.85 \times 10^{15} T^{-1})$
17	$H + OH + BF \rightarrow$	$H_2O + BF$	$k_f = 3\ (7.85 \times 10^{15} T^{-1})$
18	$H + OH + H_2O \rightarrow$	$H_2O + H_2O$	$k_f = 20\ (7.85 \times 10^{15} T^{-1})$

NOTE: ALL RATES EXPRESSED IN TERMS OF LB-MOLES, FT^3, SEC; AND T IS IN °R

TO CONVERT TO Kg-MOLES, M^3, SEC, AND T IN °K, MULTIPLY ABOVE RATE BY 2.165×10^{-3}

TABLE V-2

EQUILIBRIUM AND FROZEN PROPERTIES AT

NOZZLE THROAT

$B_2H_6(\ell)$ - $OF_2(\ell)$

	P_c-psia	OXIDIZER - FUEL WEIGHT RATIO						
		2.5	3.0	3.5	4.0	4.5	5.0	5.5
Equilibrium Mass Flow = $\frac{Lbm}{Ft^2.Sec}$	50	33.54	33.16	32.92	32.90	33.07	33.33	33.61
	100	66.46	65.68	65.20	65.16	65.49	65.98	--
	250	164.2	162.2	161.0	160.9	161.6	162.7	164.1
	500	325.7	321.4	319.1	318.7	320.1	322.3	324.8
Frozen Mass Flow - $\frac{Lbm}{Ft^2.Sec}$	50	34.90	34.56	34.40	34.47	34.72	35.03	35.36
	100	68.98	68.27	67.96	68.11	68.57	69.17	--
	250	169.9	168.0	167.2	167.5	168.6	170.0	171.6
	500	336.1	332.2	330.6	331.1	333.1	335.7	338.7
Frozen Specific Heat Ratio	50	1.278	1.286	1.292	1.293	1.300	1.303	1.303
	100	1.274	1.281	1.287	1.291	1.294	1.298	--
	250	1.264	1.271	1.276	1.281	1.284	1.288	1.291
	500	1.263	1.269	1.274	1.278	1.282	1.282	1.288

NOTE: P_c (psia) x 6.895 x 10^3 = P_c (N/m^2)

Mass Flow ($\frac{Lbm}{Ft^2.sec}$) x 4.883 = Mass Flow ($\frac{kg}{m^2\ sec}$)

FIG. V-1

VARIATION OF EQUILIBRIUM VACUUM SPECIFIC IMPULSE WITH AREA RATIO

B_2H_6 (ℓ) – OF_2 (ℓ)

P_C = 50 PSIA (3.448 X 10^5 N/m^2)

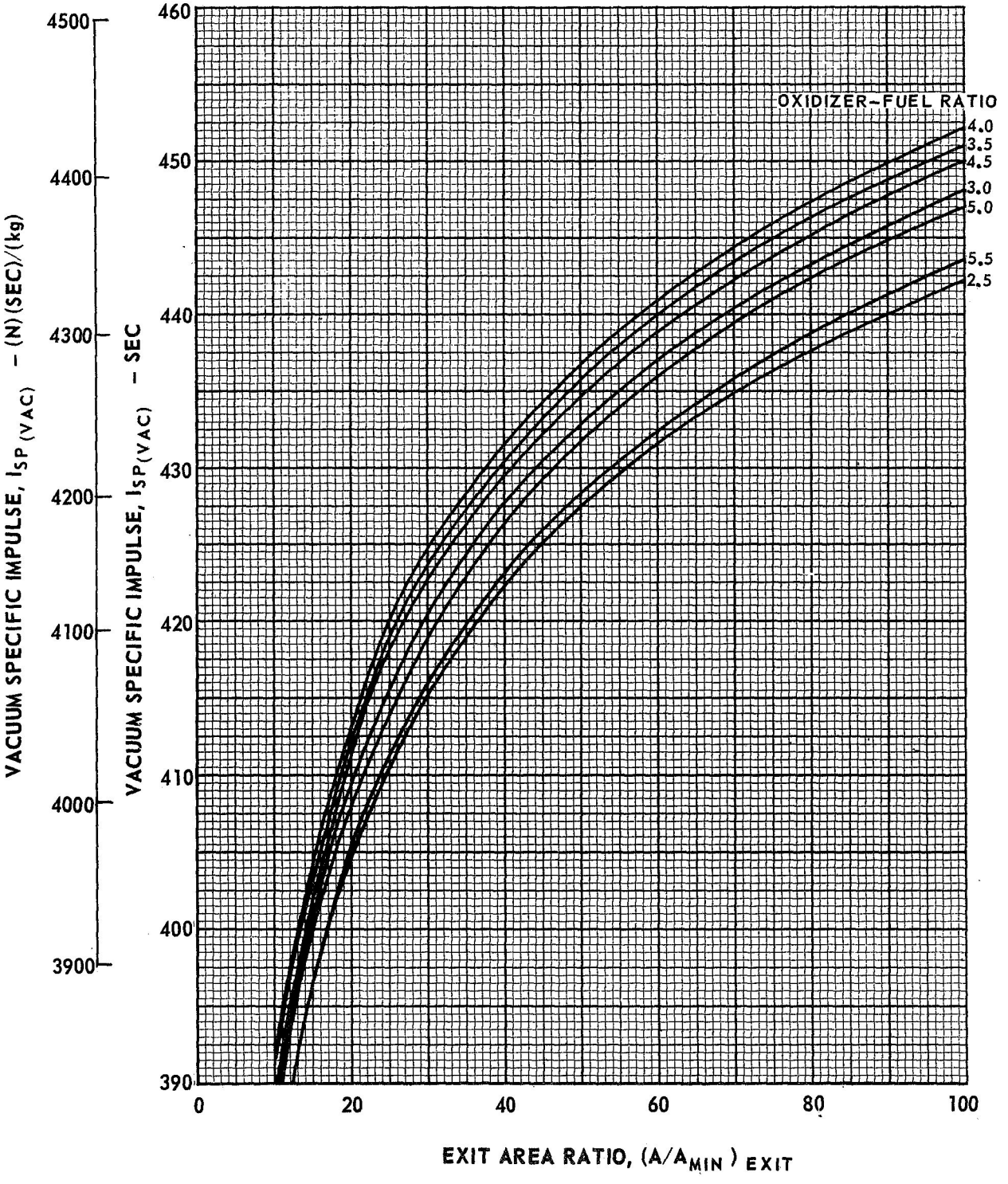

FIG. V-2

VARIATION OF FROZEN VACUUM SPECIFIC IMPULSE WITH AREA RATIO

B_2H_6 (ℓ) – OF_2 (ℓ)

P_C = 50 PSIA (3.448 X 10^5 N/m^2)

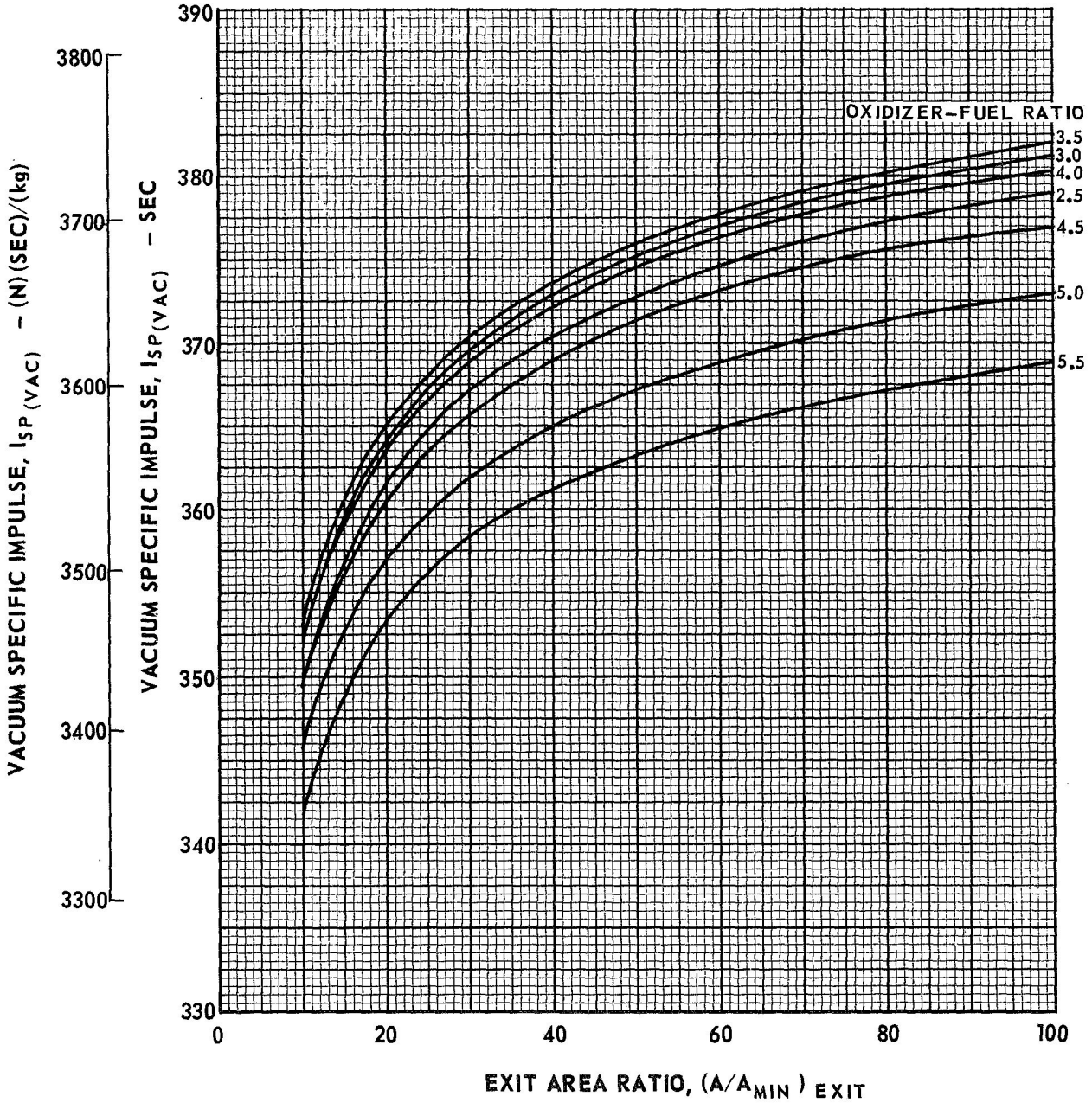

VARIATION OF EQUILIBRIUM VACUUM SPECIFIC IMPULSE WITH AREA RATIO

B_2H_6 (ℓ) – OF_2 (ℓ)

P_C =100 PSIA (6.895 X 10^5 N/m^2)

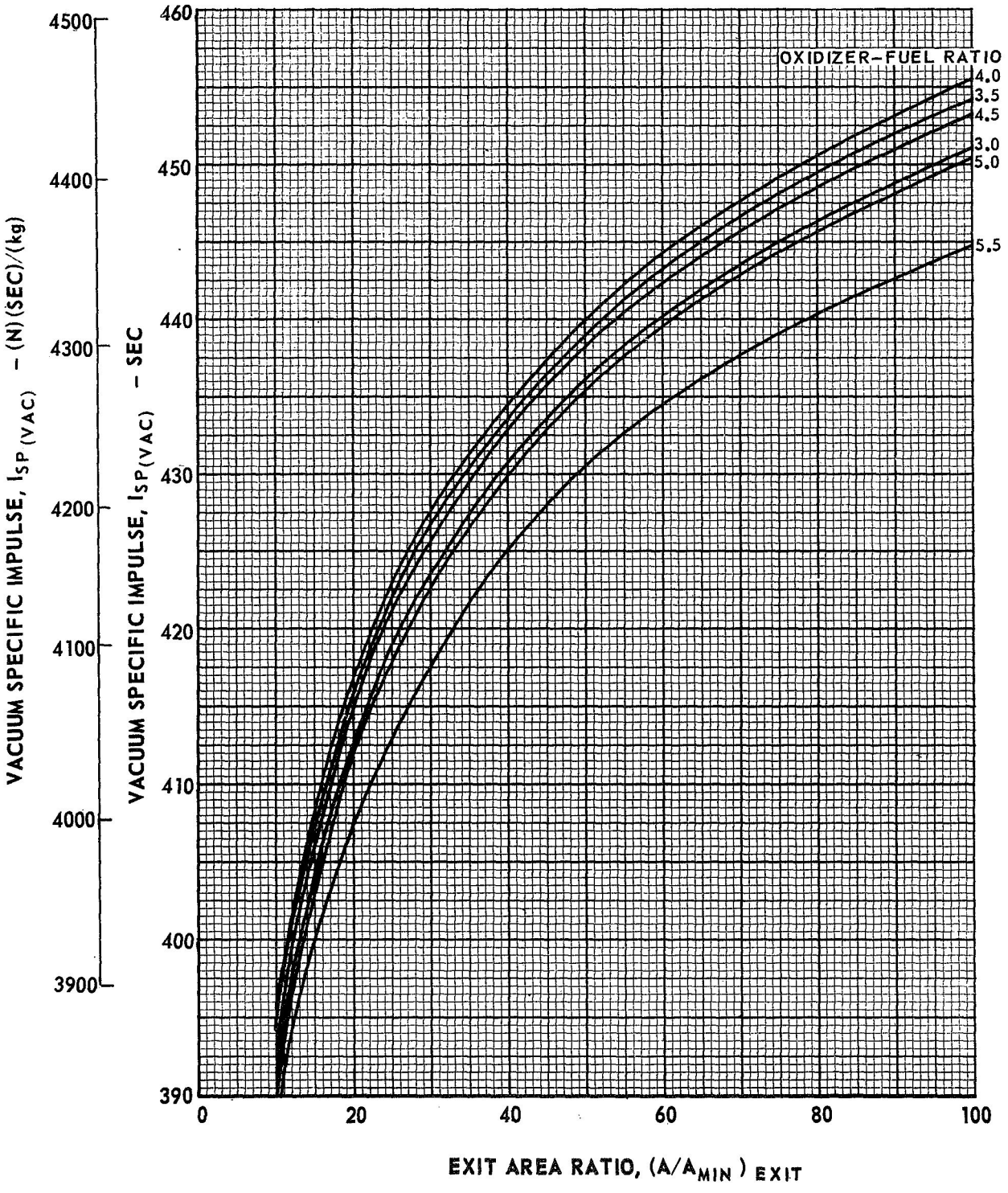

VARIATION OF FROZEN VACUUM SPECIFIC IMPULSE WITH AREA RATIO

B_2H_6 (ℓ) – OF_2 (ℓ)

P_C = 100 PSIA (6.895 X 10^5 N/m^2)

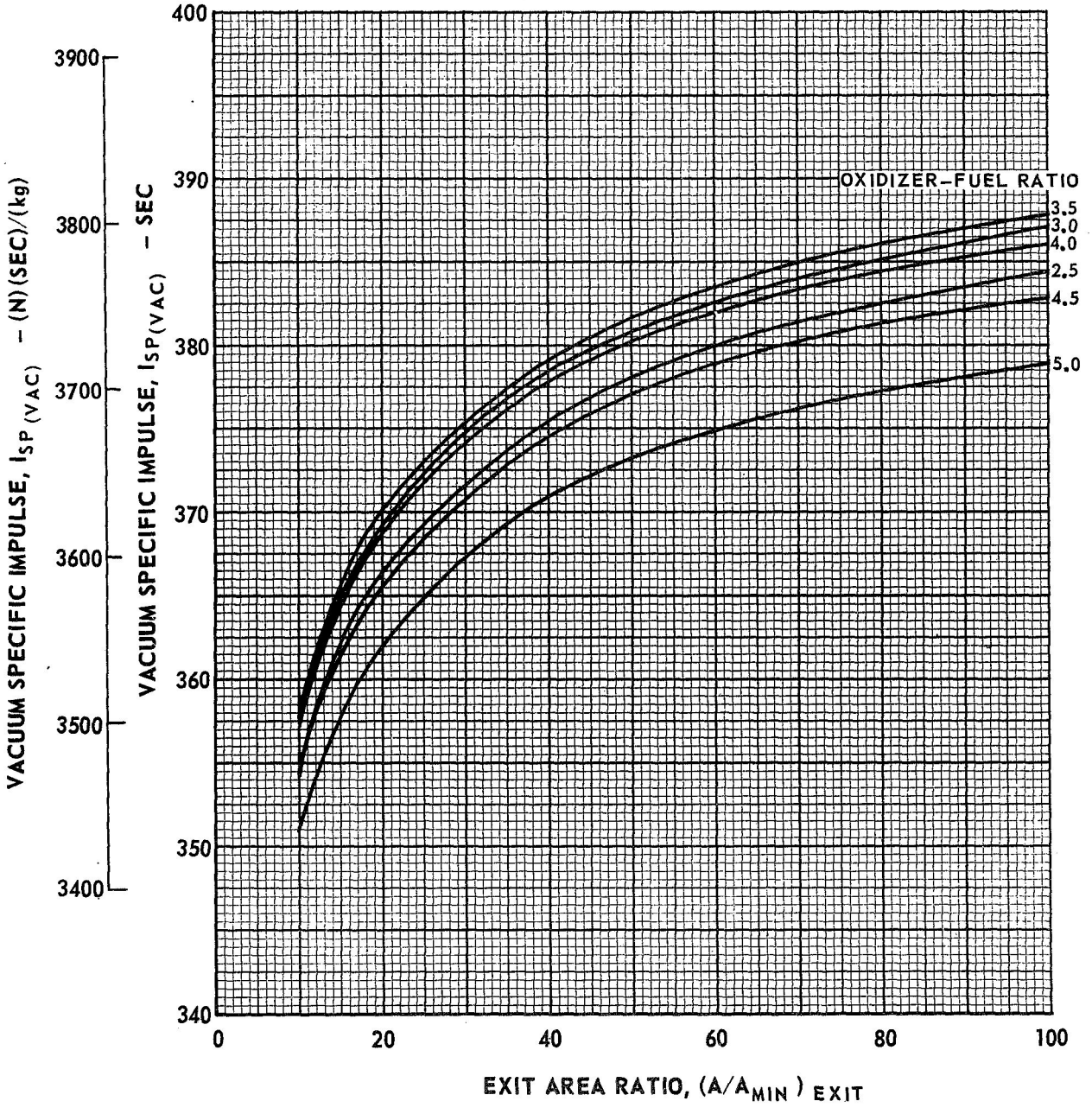

FIG. V-5

VARIATION OF EQUILIBRIUM VACUUM SPECIFIC IMPULSE WITH AREA RATIO

B_2H_6 (ℓ) – OF_2 (ℓ)

P_C = 250 PSIA (1.724 X 10^6 N/m^2)

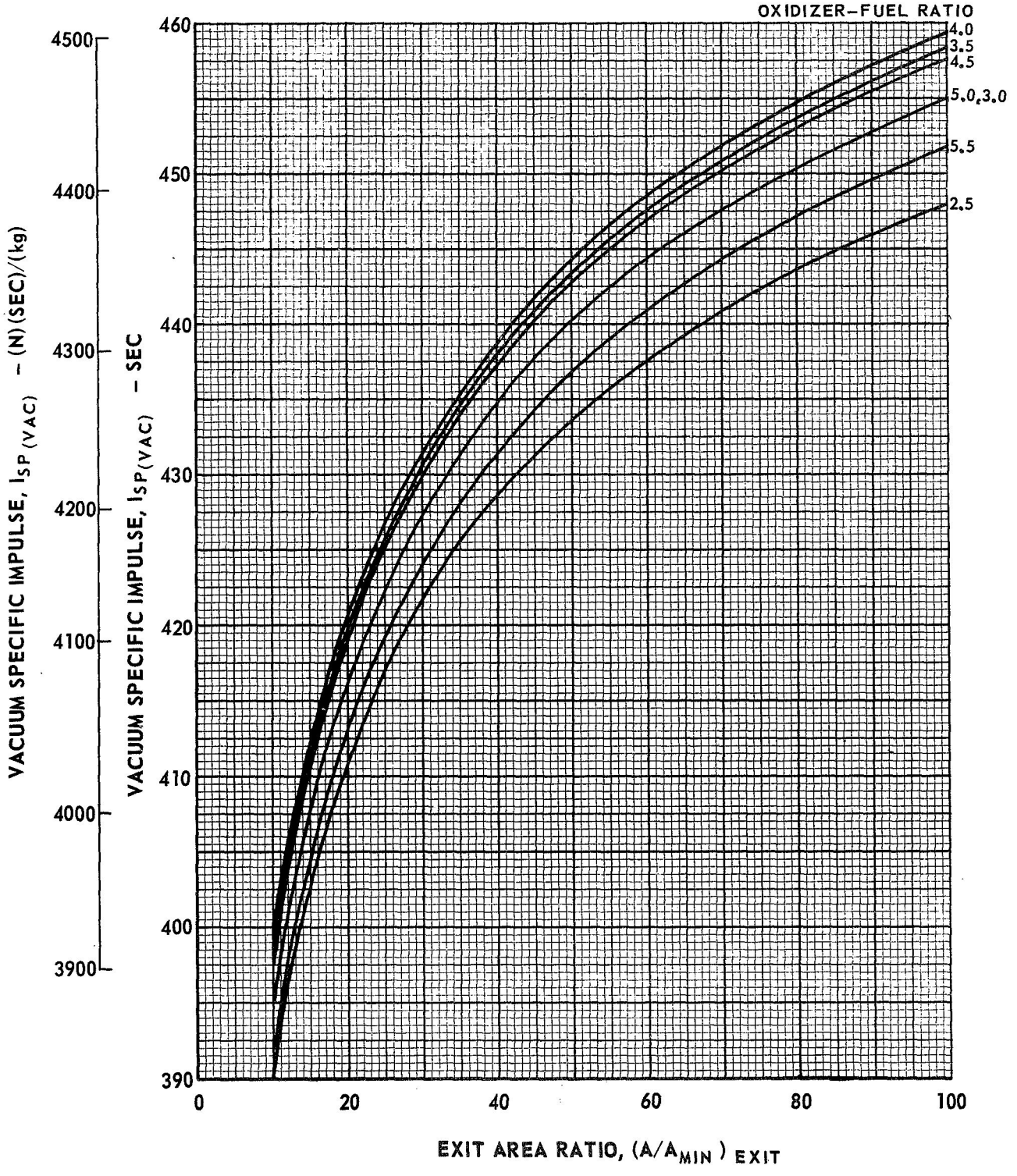

VARIATION OF FROZEN VACUUM SPECIFIC IMPULSE WITH AREA RATIO

B_2H_6 (ℓ) – OF_2 (ℓ)

P_C = 250 PSIA (1.724 X 10^6 N/m^2)

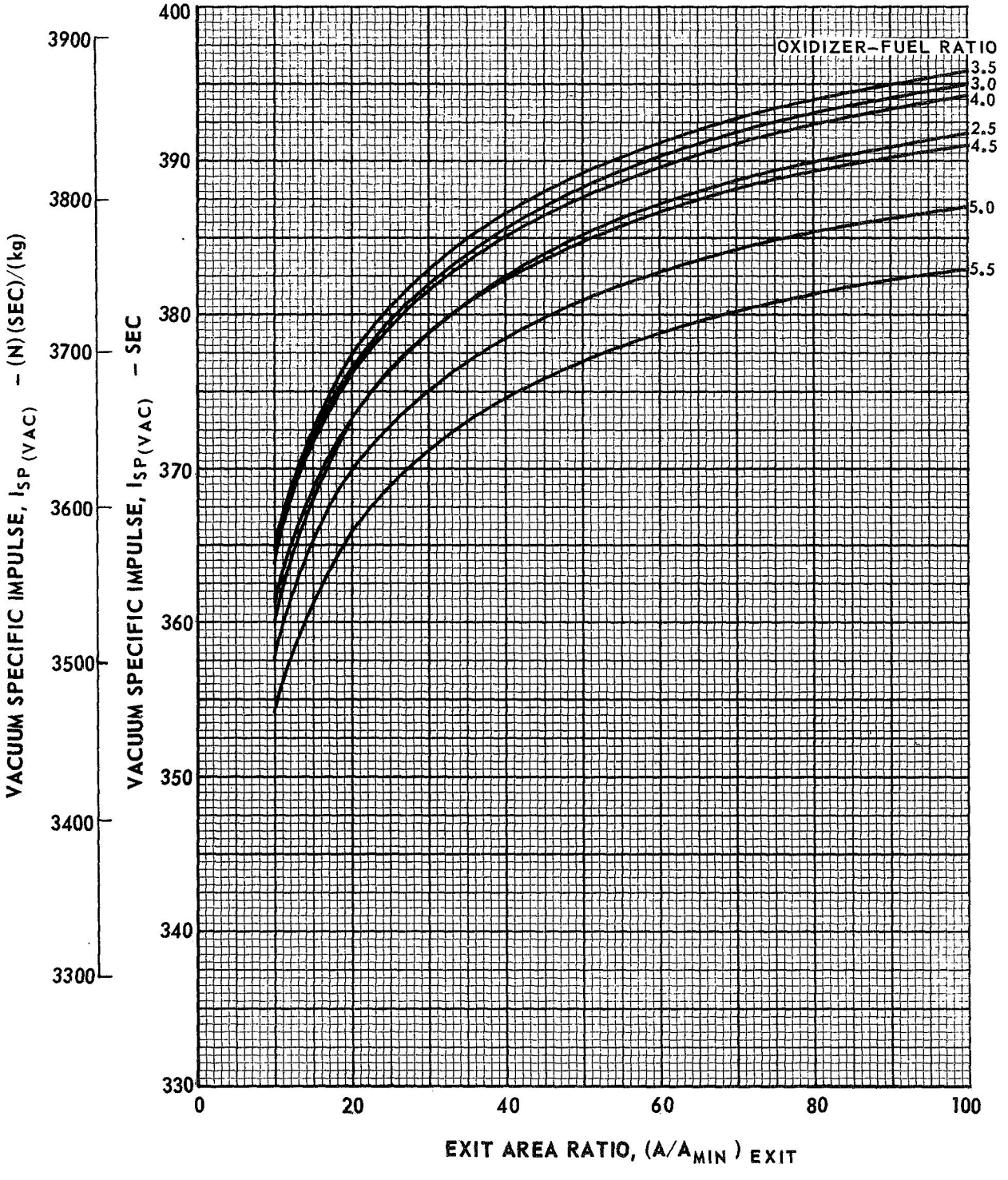

VARIATION OF EQUILIBRIUM VACUUM SPECIFIC IMPULSE WITH AREA RATIO

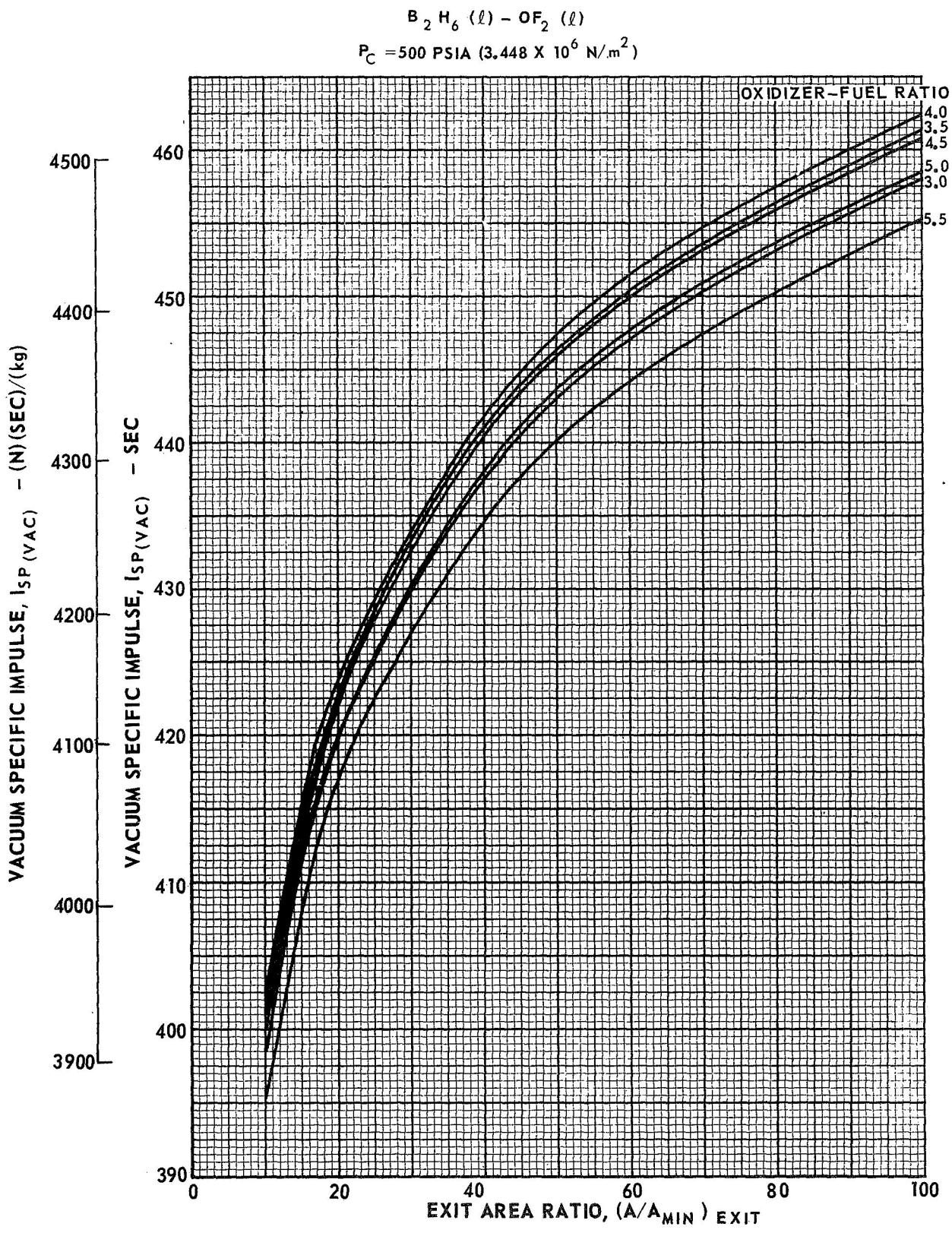

FIG. V-8

VARIATION OF FROZEN VACUUM SPECIFIC IMPULSE WITH AREA RATIO

B_2H_6 (ℓ) - OF_2 (ℓ)

P_C = 500 PSIA (3.488 X 10^6 N/m^2)

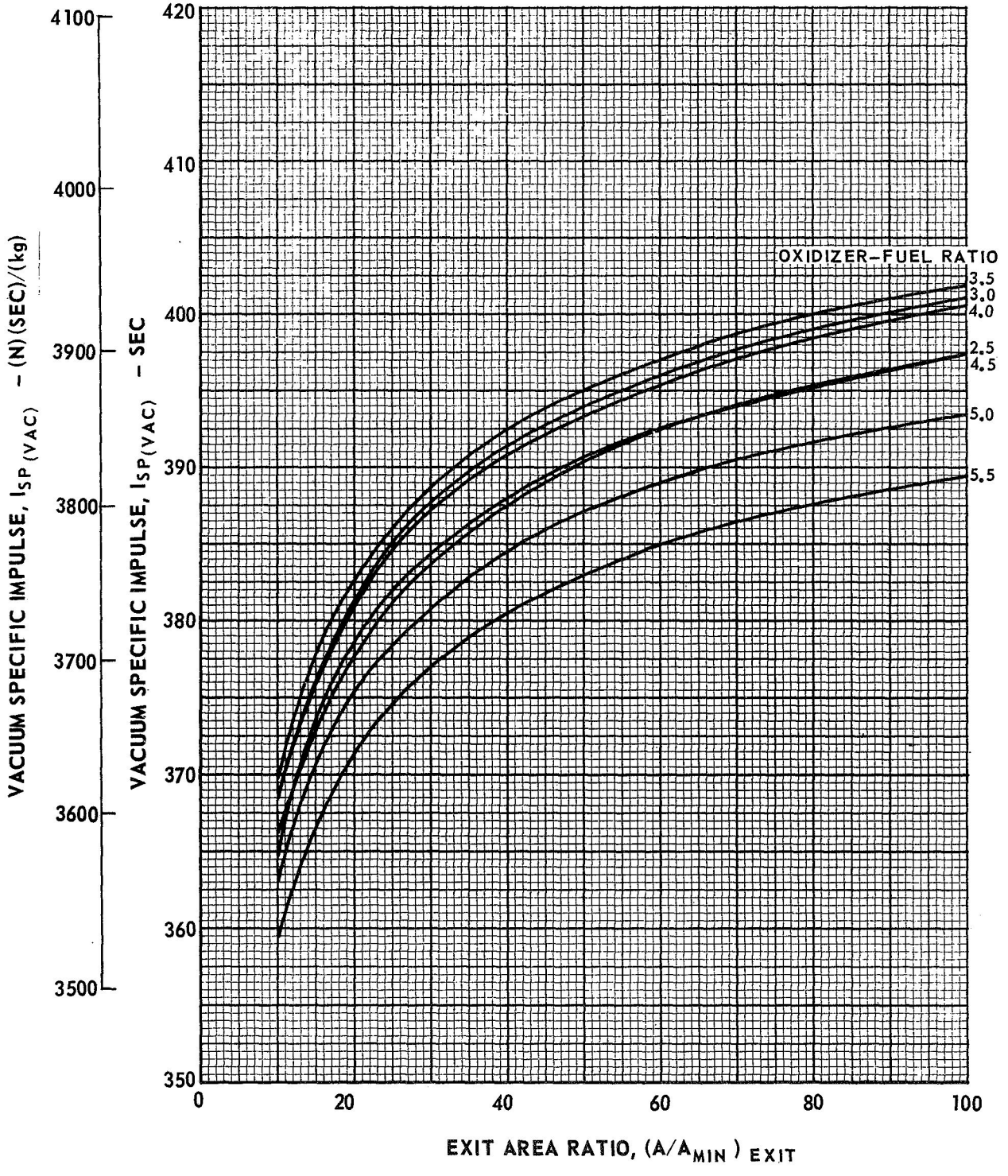

FIG. V-9

NORMALIZED GRAPHICAL SOLUTION FOR FREEZING AREA RATIO USING MODIFIED BRAY ANALYSIS

$B_2H_6(\ell) - OF_2(\ell)$

$P_C = 50$ PSIA (3.448×10^5 N/m^2)

O/F = 3.0

NOTE: REACTION RATE CONSTANTS LISTED IN TABLE V-1

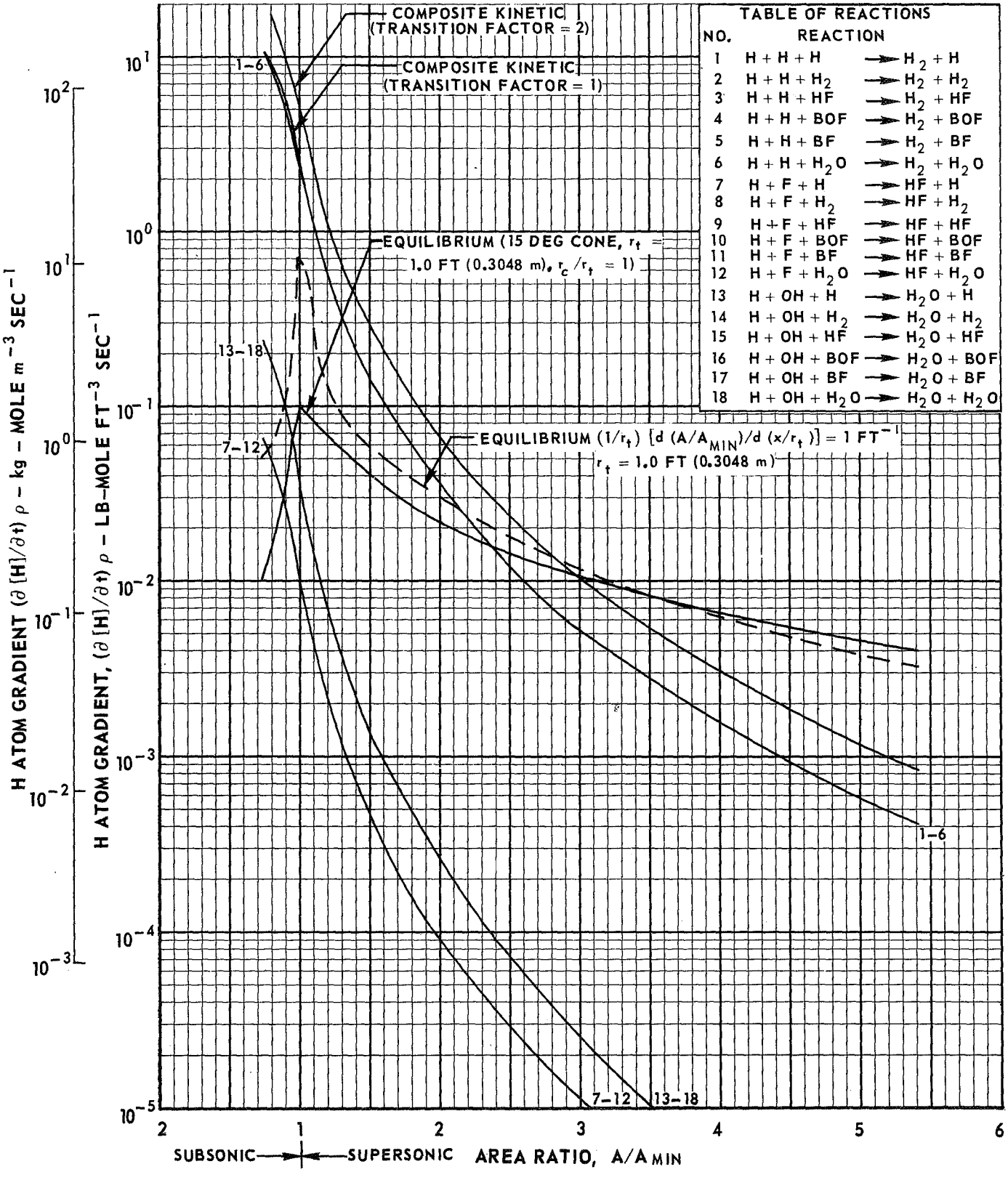

TABLE OF REACTIONS

NO.	REACTION
1	$H + H + H \rightarrow H_2 + H$
2	$H + H + H_2 \rightarrow H_2 + H_2$
3	$H + H + HF \rightarrow H_2 + HF$
4	$H + H + BOF \rightarrow H_2 + BOF$
5	$H + H + BF \rightarrow H_2 + BF$
6	$H + H + H_2O \rightarrow H_2 + H_2O$
7	$H + F + H \rightarrow HF + H$
8	$H + F + H_2 \rightarrow HF + H_2$
9	$H + F + HF \rightarrow HF + HF$
10	$H + F + BOF \rightarrow HF + BOF$
11	$H + F + BF \rightarrow HF + BF$
12	$H + F + H_2O \rightarrow HF + H_2O$
13	$H + OH + H \rightarrow H_2O + H$
14	$H + OH + H_2 \rightarrow H_2O + H_2$
15	$H + OH + HF \rightarrow H_2O + HF$
16	$H + OH + BOF \rightarrow H_2O + BOF$
17	$H + OH + BF \rightarrow H_2O + BF$
18	$H + OH + H_2O \rightarrow H_2O + H_2O$

FIG. V-10

NORMALIZED GRAPHICAL SOLUTION FOR FREEZING AREA RATIO USING MODIFIED BRAY ANALYSIS

$B_2H_6(\ell) - OF_2(\ell)$

$P_C = 50$ PSIA (3.448×10^5 N/m^2)

O/F = 3.5

NOTE: REACTION RATE CONSTANTS LISTED IN TABLE V-1

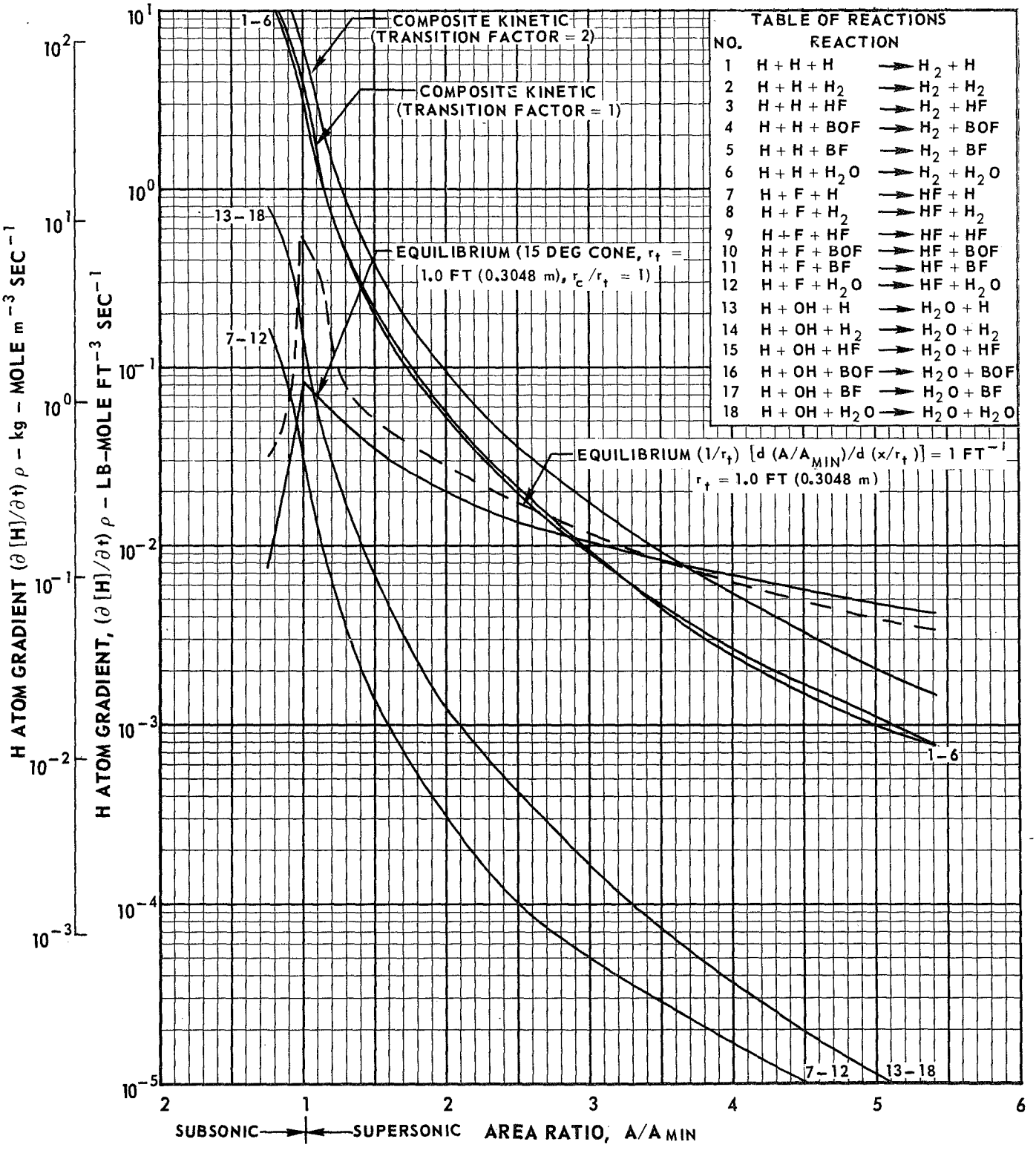

FIG. V-11

NORMALIZED GRAPHICAL SOLUTION FOR FREEZING AREA RATIO USING MODIFIED BRAY ANALYSIS

$B_2H_6(\ell) - OF_2(\ell)$

$P_C = 50$ PSIA (3.448×10^5 N/m^2)

O/F = 4.0

NOTE: REACTION RATE CONSTANTS LISTED IN TABLE V-1

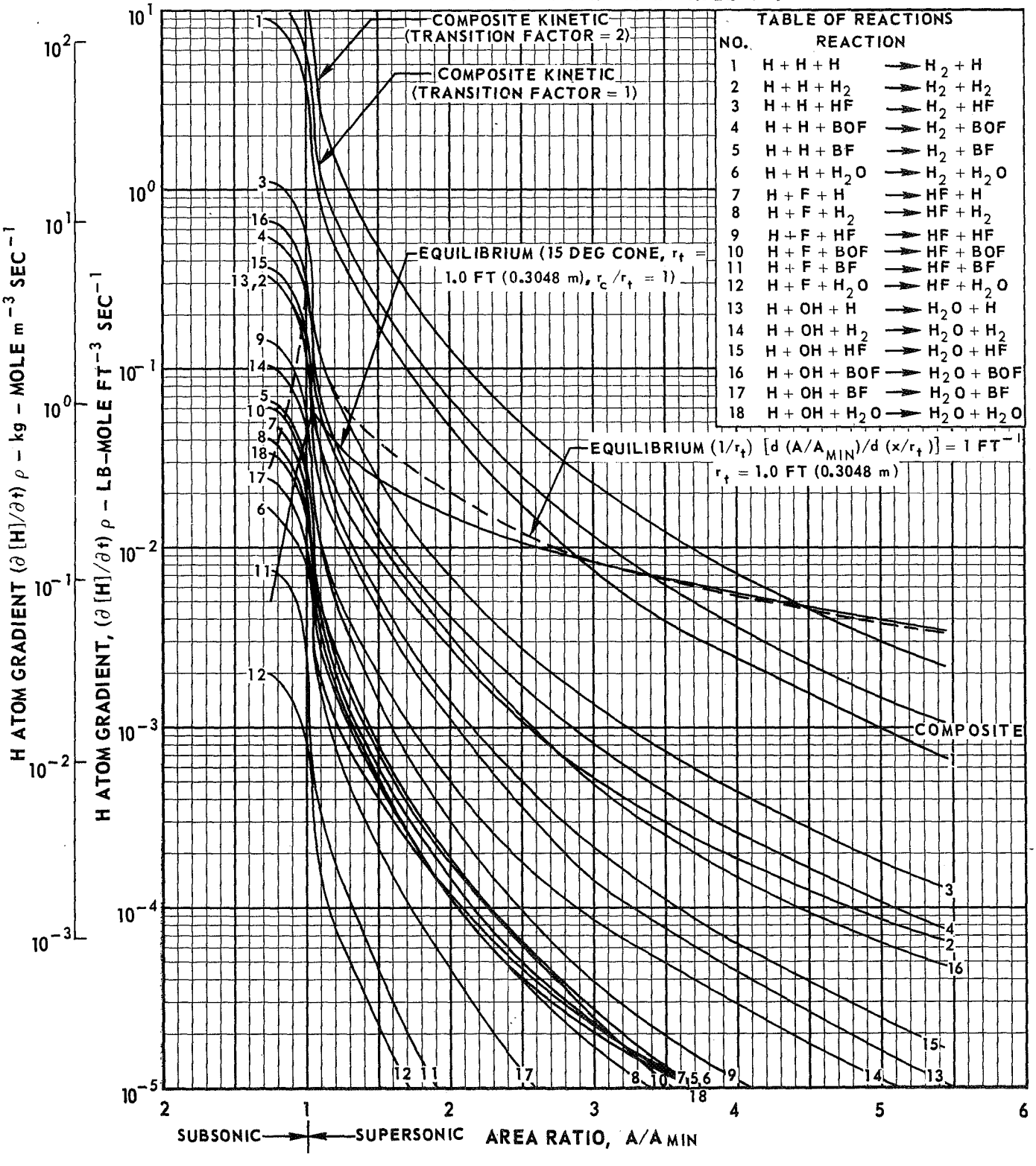

FIG. V-12

NORMALIZED GRAPHICAL SOLUTION FOR FREEZING AREA RATIO USING MODIFIED BRAY ANALYSIS

$B_2H_6(\ell) - OF_2(\ell)$

$P_C = 50$ PSIA (3.448×10^5 N/m^2)

O/F = 4.5

NOTE: REACTION RATE CONSTANTS LISTED IN TABLE V-1

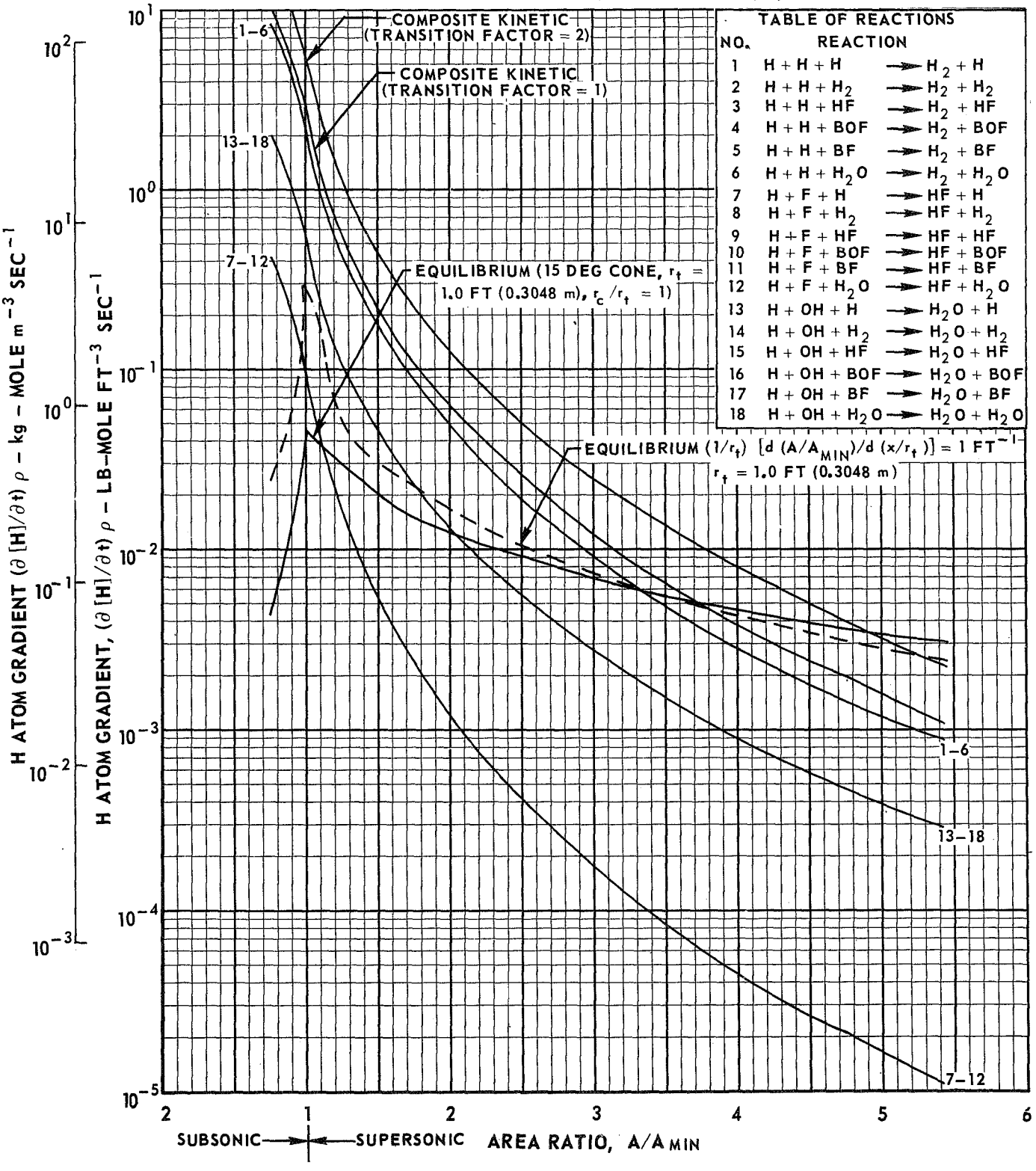

FIG. V-13

NORMALIZED GRAPHICAL SOLUTION FOR FREEZING AREA RATIO USING MODIFIED BRAY ANALYSIS

$B_2H_6(\ell) - OF_2(\ell)$

P_C = 100 PSIA (3.448 X 10^5 N/m^2)

O/F = 3.0

NOTE: REACTION RATE CONSTANTS LISTED IN TABLE V-1

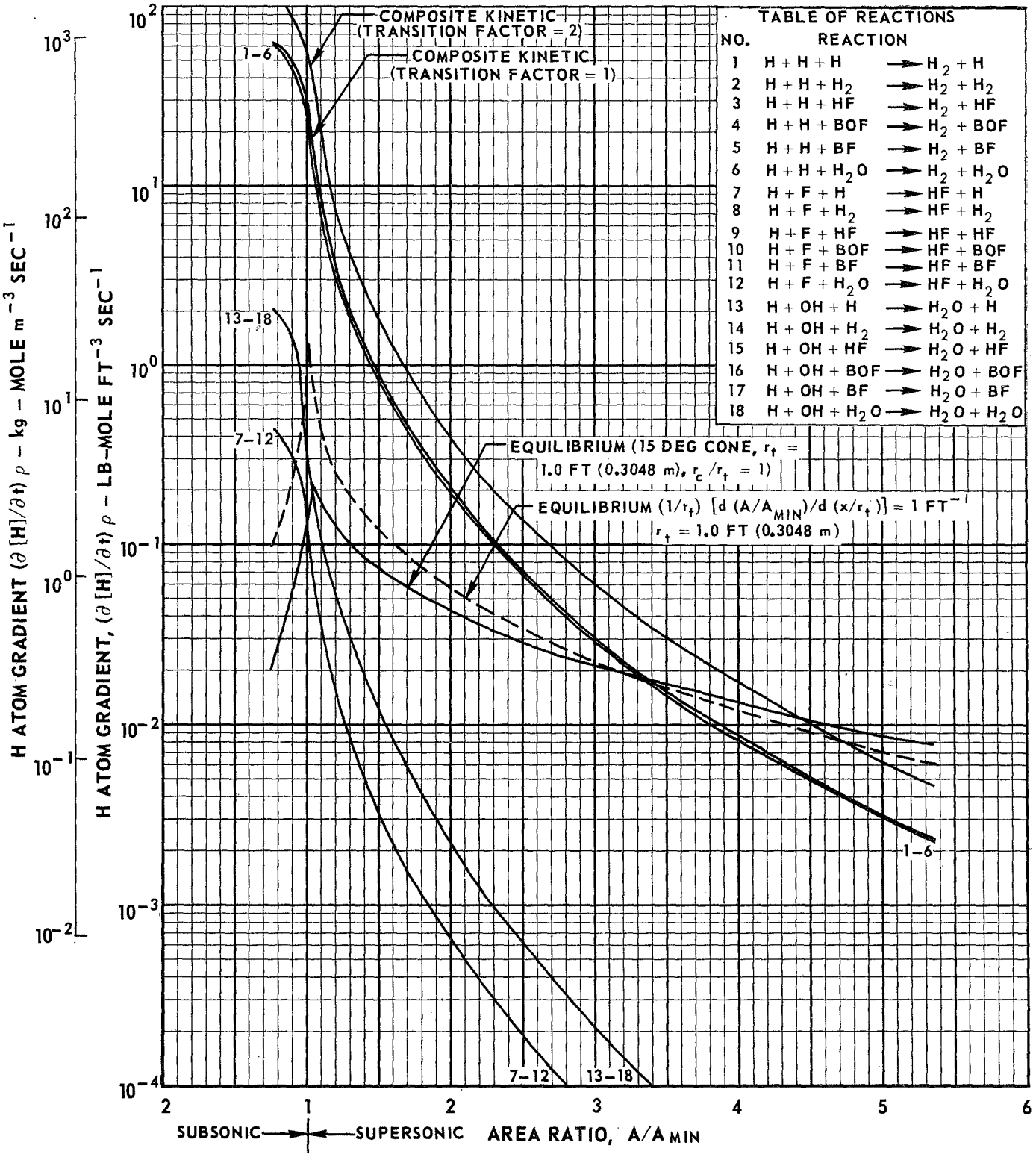

TABLE OF REACTIONS

NO.	REACTION
1	H + H + H → H_2 + H
2	H + H + H_2 → H_2 + H_2
3	H + H + HF → H_2 + HF
4	H + H + BOF → H_2 + BOF
5	H + H + BF → H_2 + BF
6	H + H + H_2O → H_2 + H_2O
7	H + F + H → HF + H
8	H + F + H_2 → HF + H_2
9	H + F + HF → HF + HF
10	H + F + BOF → HF + BOF
11	H + F + BF → HF + BF
12	H + F + H_2O → HF + H_2O
13	H + OH + H → H_2O + H
14	H + OH + H_2 → H_2O + H_2
15	H + OH + HF → H_2O + HF
16	H + OH + BOF → H_2O + BOF
17	H + OH + BF → H_2O + BF
18	H + OH + H_2O → H_2O + H_2O

FIG. V-14

NORMALIZED GRAPHICAL SOLUTION FOR FREEZING AREA RATIO USING MODIFIED BRAY ANALYSIS

B_2H_6 (ℓ) – OF_2 (ℓ)

P_C = 100 PSIA (3.448 X 10^5 N/m^2)

O/F = 3.5

NOTE: REACTION RATE CONSTANTS LISTED IN TABLE V-1

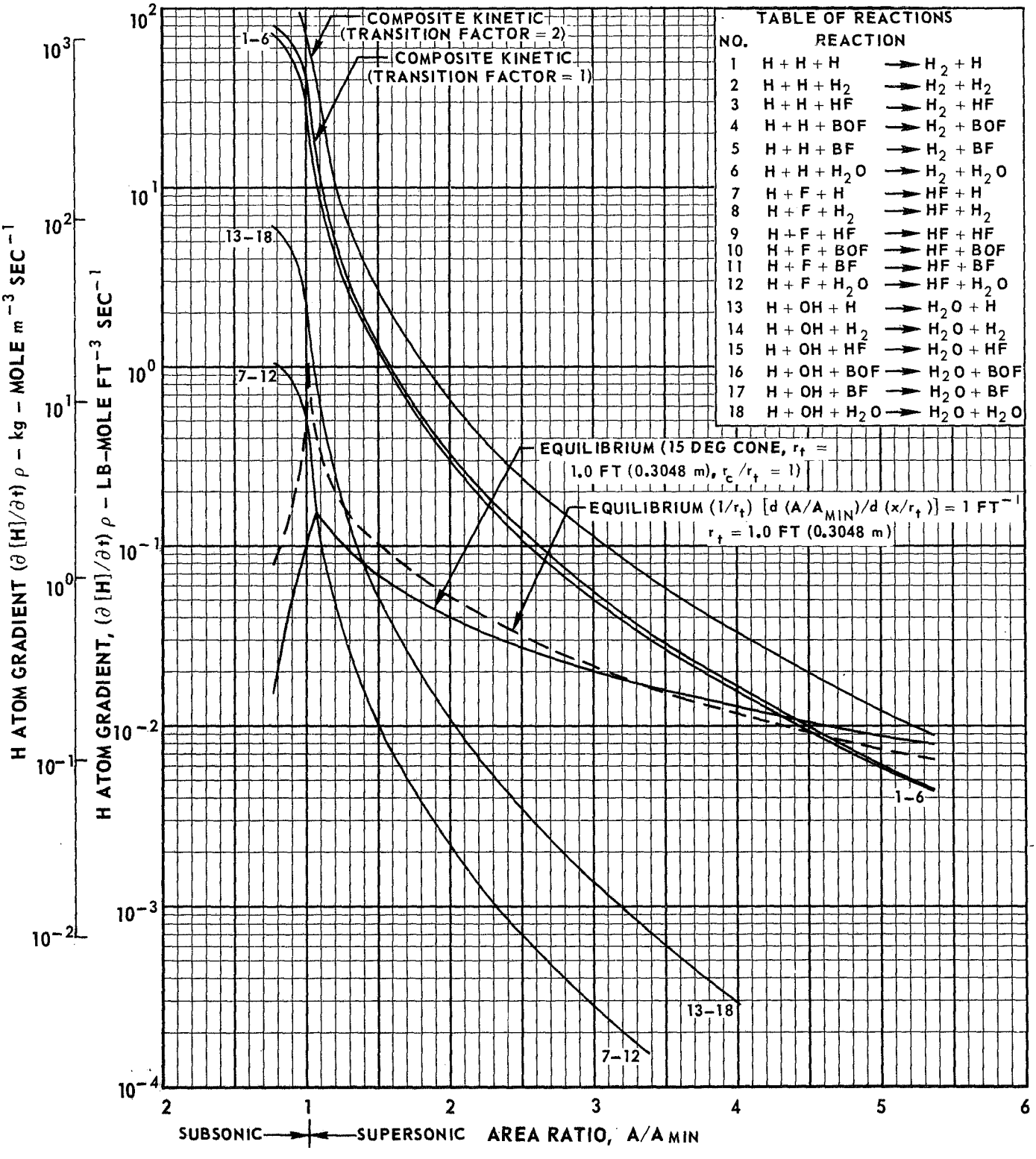

FIG. V-15

NORMALIZED GRAPHICAL SOLUTION FOR FREEZING AREA RATIO USING MODIFIED BRAY ANALYSIS

$B_2H_6(\ell) - OF_2(\ell)$

$P_C = 100$ PSIA (3.448×10^5 N/m^2)

O/F = 4.0

NOTE: REACTION RATE CONSTANTS LISTED IN TABLE V-1

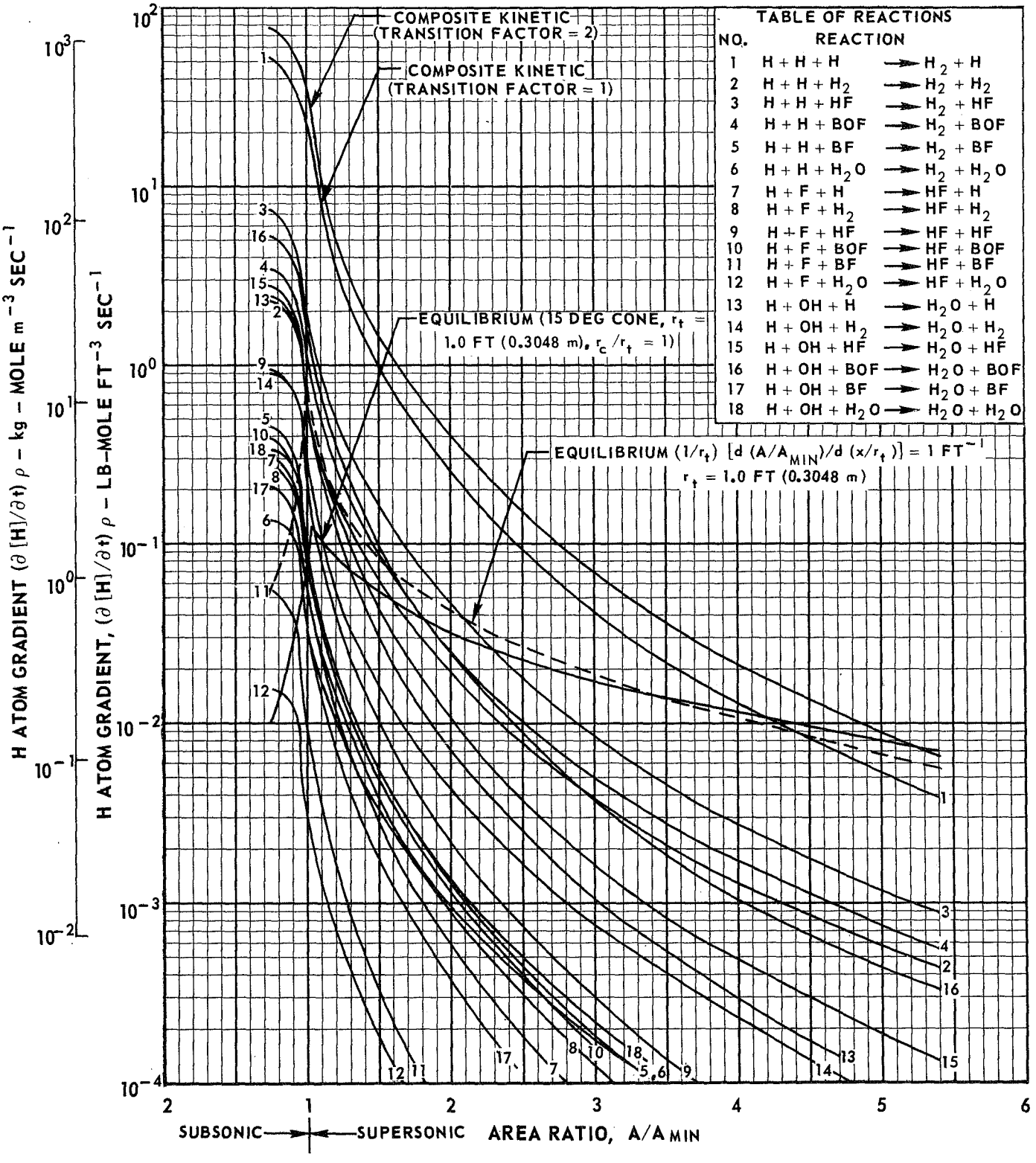

TABLE OF REACTIONS

NO.	REACTION
1	$H + H + H \rightarrow H_2 + H$
2	$H + H + H_2 \rightarrow H_2 + H_2$
3	$H + H + HF \rightarrow H_2 + HF$
4	$H + H + BOF \rightarrow H_2 + BOF$
5	$H + H + BF \rightarrow H_2 + BF$
6	$H + H + H_2O \rightarrow H_2 + H_2O$
7	$H + F + H \rightarrow HF + H$
8	$H + F + H_2 \rightarrow HF + H_2$
9	$H + F + HF \rightarrow HF + HF$
10	$H + F + BOF \rightarrow HF + BOF$
11	$H + F + BF \rightarrow HF + BF$
12	$H + F + H_2O \rightarrow HF + H_2O$
13	$H + OH + H \rightarrow H_2O + H$
14	$H + OH + H_2 \rightarrow H_2O + H_2$
15	$H + OH + HF \rightarrow H_2O + HF$
16	$H + OH + BOF \rightarrow H_2O + BOF$
17	$H + OH + BF \rightarrow H_2O + BF$
18	$H + OH + H_2O \rightarrow H_2O + H_2O$

FIG. V-16

NORMALIZED GRAPHICAL SOLUTION FOR FREEZING AREA RATIO USING MODIFIED BRAY ANALYSIS

B_2H_6 (ℓ) – OF_2 (ℓ)

P_C = 100 PSIA (3.448 X 10^5 N/m^2)

O/F = 4.5

NOTE: REACTION RATE CONSTANTS LISTED IN TABLE V-1

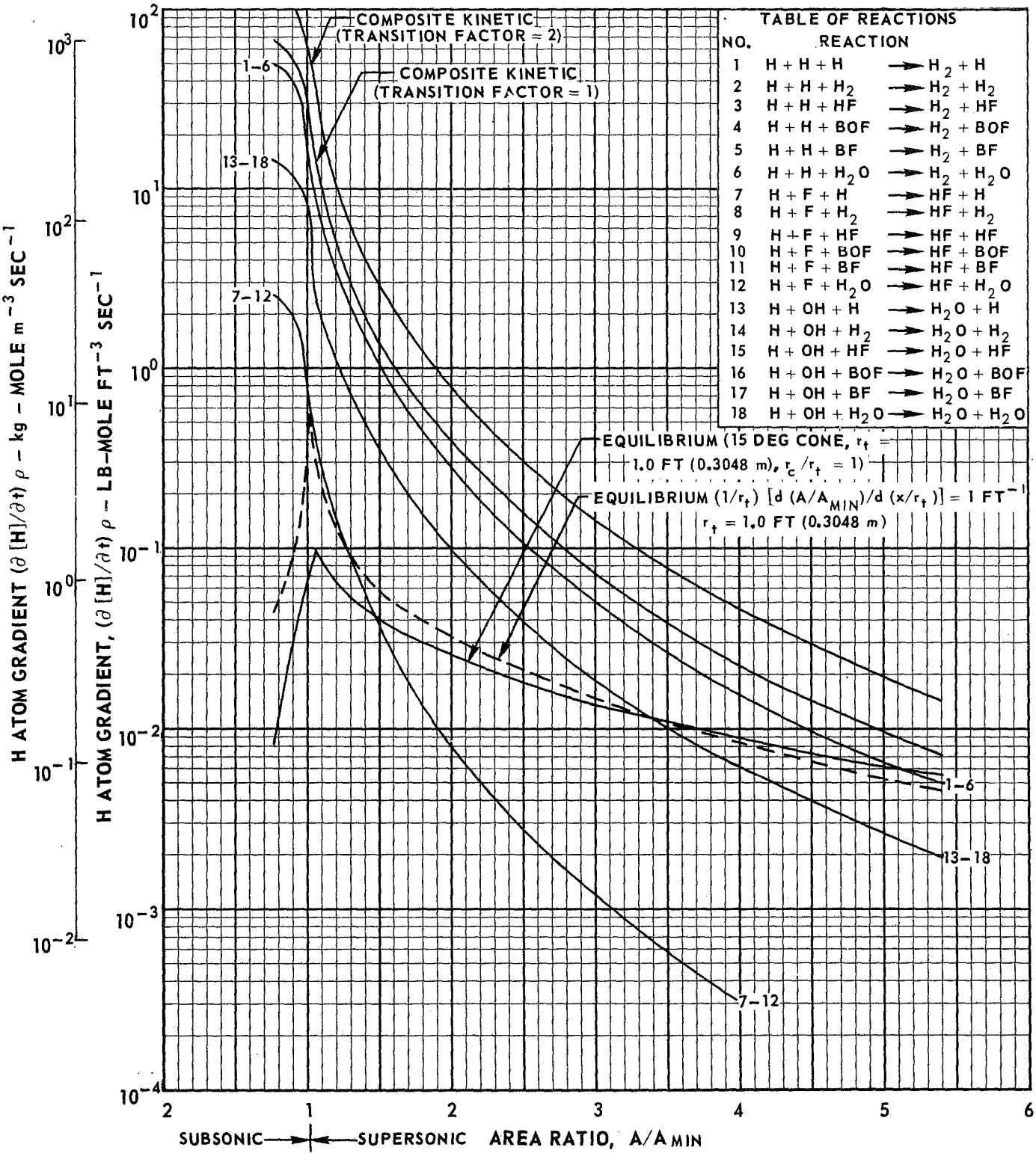

TABLE OF REACTIONS

NO.	REACTION
1	H + H + H → H_2 + H
2	H + H + H_2 → H_2 + H_2
3	H + H + HF → H_2 + HF
4	H + H + BOF → H_2 + BOF
5	H + H + BF → H_2 + BF
6	H + H + H_2O → H_2 + H_2O
7	H + F + H → HF + H
8	H + F + H_2 → HF + H_2
9	H + F + HF → HF + HF
10	H + F + BOF → HF + BOF
11	H + F + BF → HF + BF
12	H + F + H_2O → HF + H_2O
13	H + OH + H → H_2O + H
14	H + OH + H_2 → H_2O + H_2
15	H + OH + HF → H_2O + HF
16	H + OH + BOF → H_2O + BOF
17	H + OH + BF → H_2O + BF
18	H + OH + H_2O → H_2O + H_2O

FIG. V-17

NORMALIZED GRAPHICAL SOLUTION FOR FREEZING AREA RATIO USING MODIFIED BRAY ANALYSIS

$B_2H_6(\ell) - OF_2(\ell)$

P_C = 250 PSIA (3.448 X 10^5 N/m^2)

O/F = 3.0

NOTE: REACTION RATE CONSTANTS LISTED IN TABLE V-1

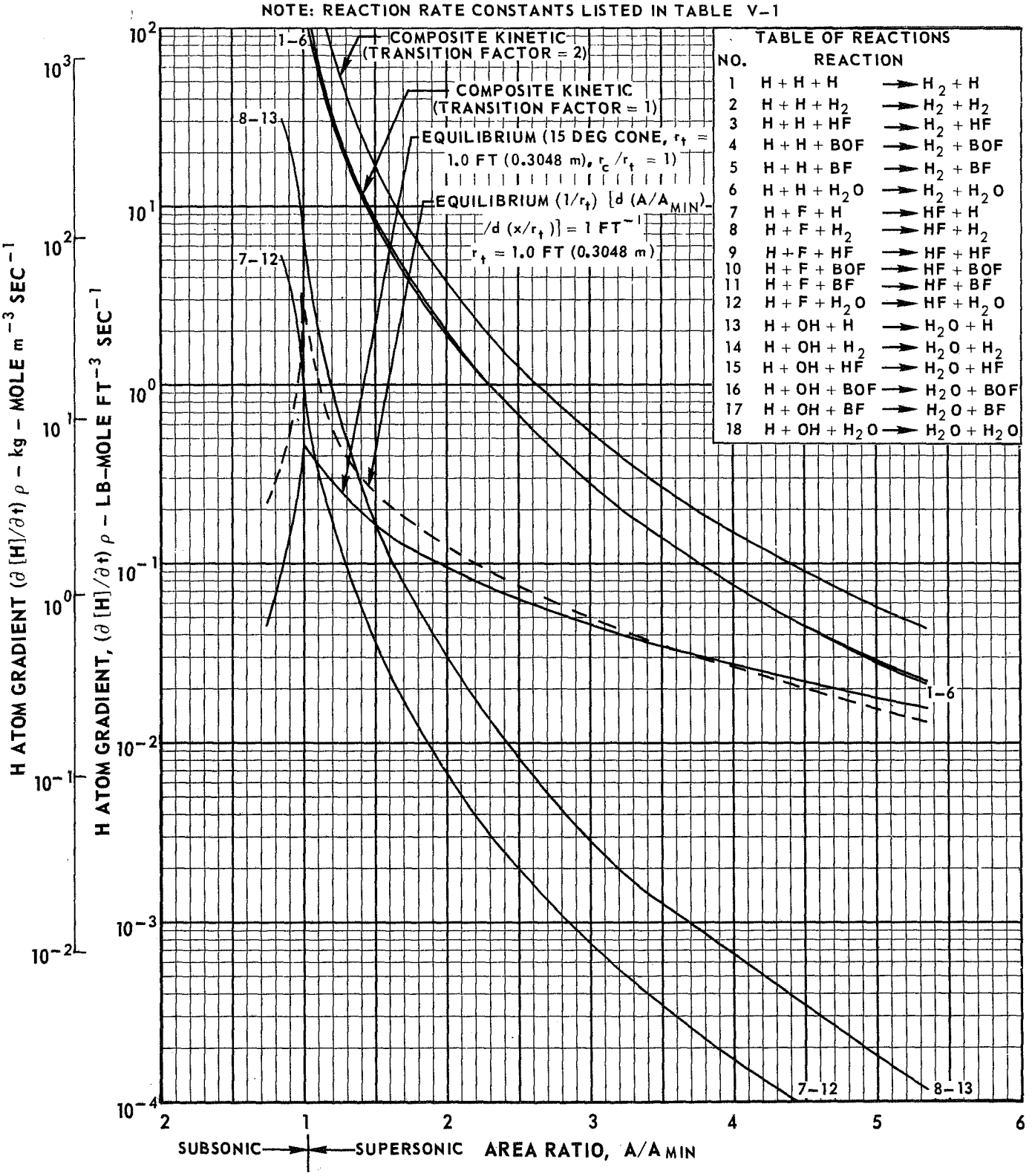

TABLE OF REACTIONS

NO.	REACTION
1	$H + H + H \rightarrow H_2 + H$
2	$H + H + H_2 \rightarrow H_2 + H_2$
3	$H + H + HF \rightarrow H_2 + HF$
4	$H + H + BOF \rightarrow H_2 + BOF$
5	$H + H + BF \rightarrow H_2 + BF$
6	$H + H + H_2O \rightarrow H_2 + H_2O$
7	$H + F + H \rightarrow HF + H$
8	$H + F + H_2 \rightarrow HF + H_2$
9	$H + F + HF \rightarrow HF + HF$
10	$H + F + BOF \rightarrow HF + BOF$
11	$H + F + BF \rightarrow HF + BF$
12	$H + F + H_2O \rightarrow HF + H_2O$
13	$H + OH + H \rightarrow H_2O + H$
14	$H + OH + H_2 \rightarrow H_2O + H_2$
15	$H + OH + HF \rightarrow H_2O + HF$
16	$H + OH + BOF \rightarrow H_2O + BOF$
17	$H + OH + BF \rightarrow H_2O + BF$
18	$H + OH + H_2O \rightarrow H_2O + H_2O$

FIG. V-18

NORMALIZED GRAPHICAL SOLUTION FOR FREEZING AREA RATIO USING MODIFIED BRAY ANALYSIS

B_2H_6 (ℓ) – OF_2 (ℓ)

P_C = 250 PSIA (3.448 X 10^5 N/m^2)

O/F = 3.5

NOTE: REACTION RATE CONSTANTS LISTED IN TABLE V-1

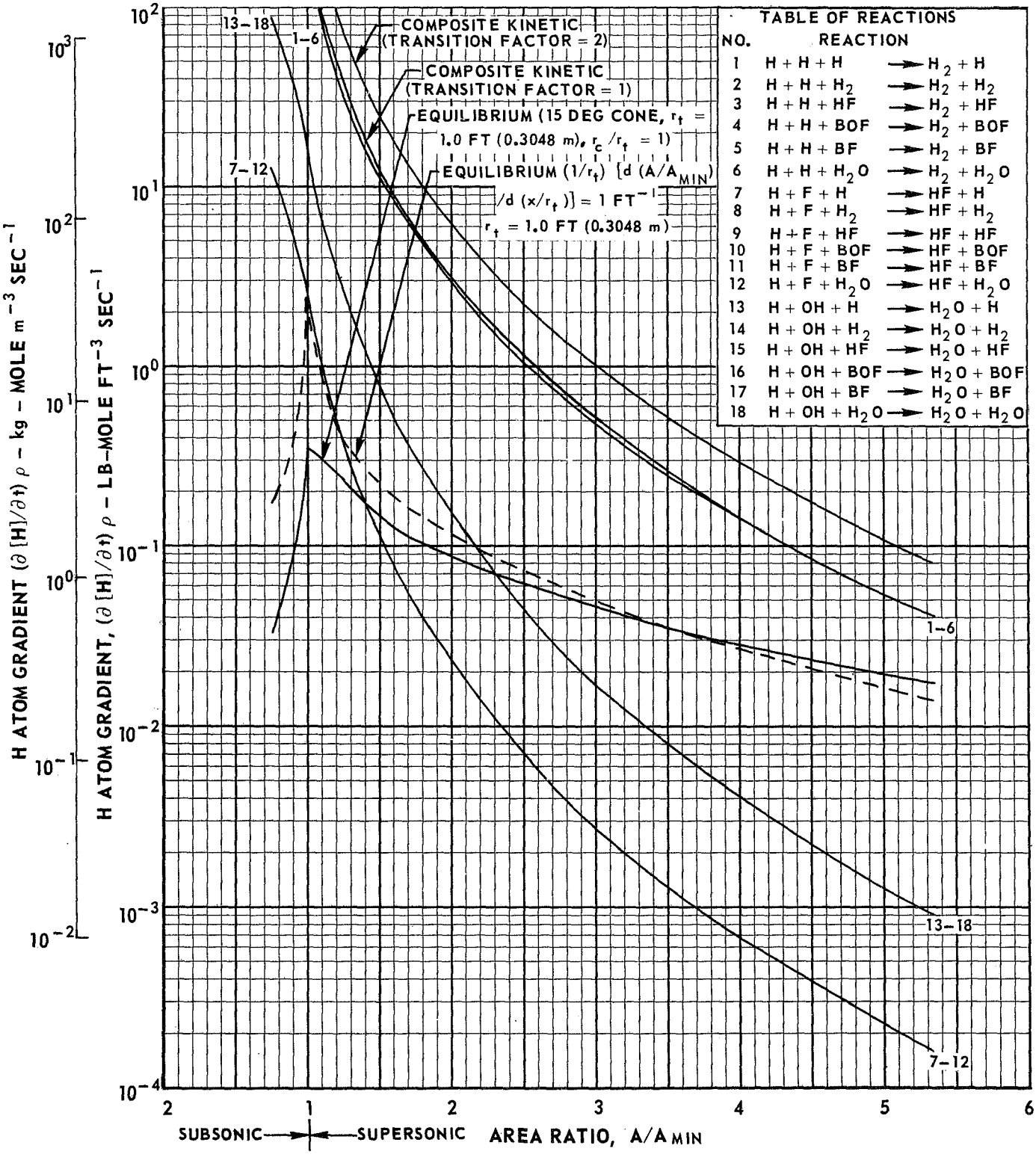

FIG. V-19

NORMALIZED GRAPHICAL SOLUTION FOR FREEZING AREA RATIO USING MODIFIED BRAY ANALYSIS

$B_2H_6(\ell) - OF_2(\ell)$

$P_C = 250$ PSIA (3.448×10^5 N/m^2)

O/F = 4.0

NOTE: REACTION RATE CONSTANTS LISTED IN TABLE V-1

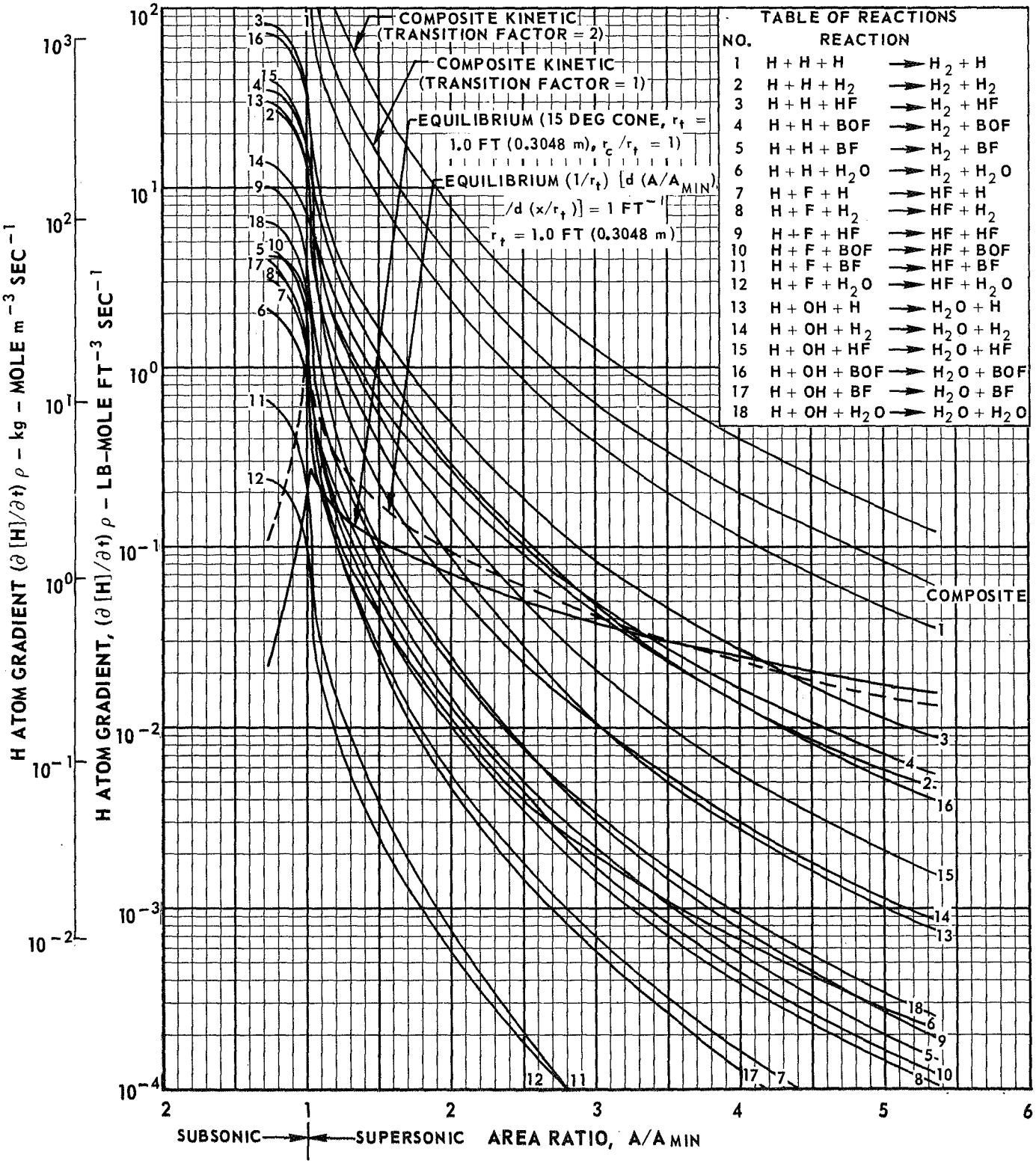

FIG. V-20

NORMALIZED GRAPHICAL SOLUTION FOR FREEZING AREA RATIO USING MODIFIED BRAY ANALYSIS

$B_2H_6(\ell) - OF_2(\ell)$

$P_C = 250$ PSIA (3.448×10^5 N/m^2)

O/F = 4.5

NOTE: REACTION RATE CONSTANTS LISTED IN TABLE V-1

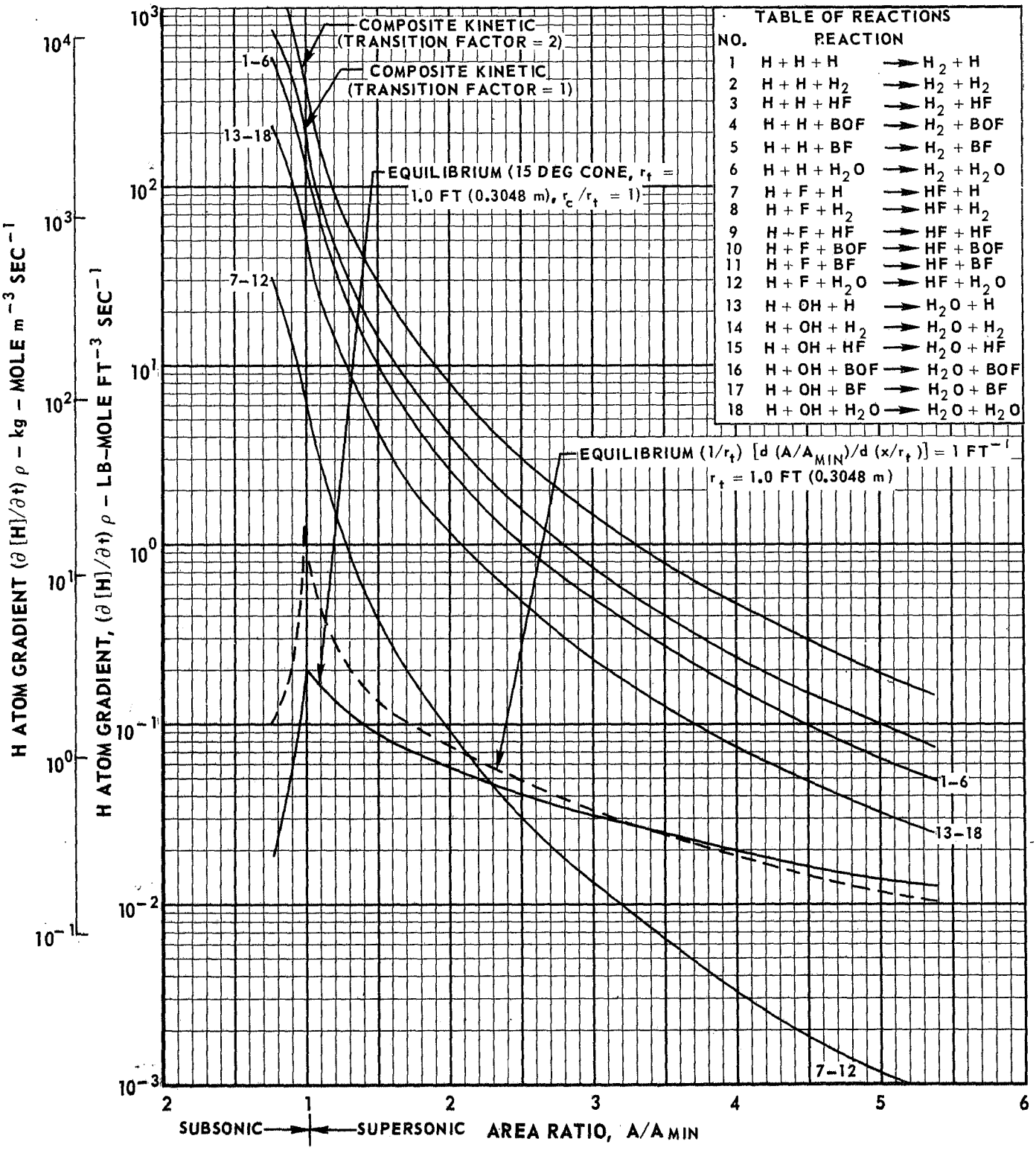

TABLE OF REACTIONS

NO.	REACTION
1	$H + H + H \rightarrow H_2 + H$
2	$H + H + H_2 \rightarrow H_2 + H_2$
3	$H + H + HF \rightarrow H_2 + HF$
4	$H + H + BOF \rightarrow H_2 + BOF$
5	$H + H + BF \rightarrow H_2 + BF$
6	$H + H + H_2O \rightarrow H_2 + H_2O$
7	$H + F + H \rightarrow HF + H$
8	$H + F + H_2 \rightarrow HF + H_2$
9	$H + F + HF \rightarrow HF + HF$
10	$H + F + BOF \rightarrow HF + BOF$
11	$H + F + BF \rightarrow HF + BF$
12	$H + F + H_2O \rightarrow HF + H_2O$
13	$H + OH + H \rightarrow H_2O + H$
14	$H + OH + H_2 \rightarrow H_2O + H_2$
15	$H + OH + HF \rightarrow H_2O + HF$
16	$H + OH + BOF \rightarrow H_2O + BOF$
17	$H + OH + BF \rightarrow H_2O + BF$
18	$H + OH + H_2O \rightarrow H_2O + H_2O$

FIG. V-21

NORMALIZED GRAPHICAL SOLUTION FOR FREEZING AREA RATIO USING MODIFIED BRAY ANALYSIS

$B_2H_6(\ell) - OF_2(\ell)$

$P_C = 500$ PSIA (3.448×10^5 N/m^2)

O/F = 3.0

NOTE: REACTION RATE CONSTANTS LISTED IN TABLE V-1

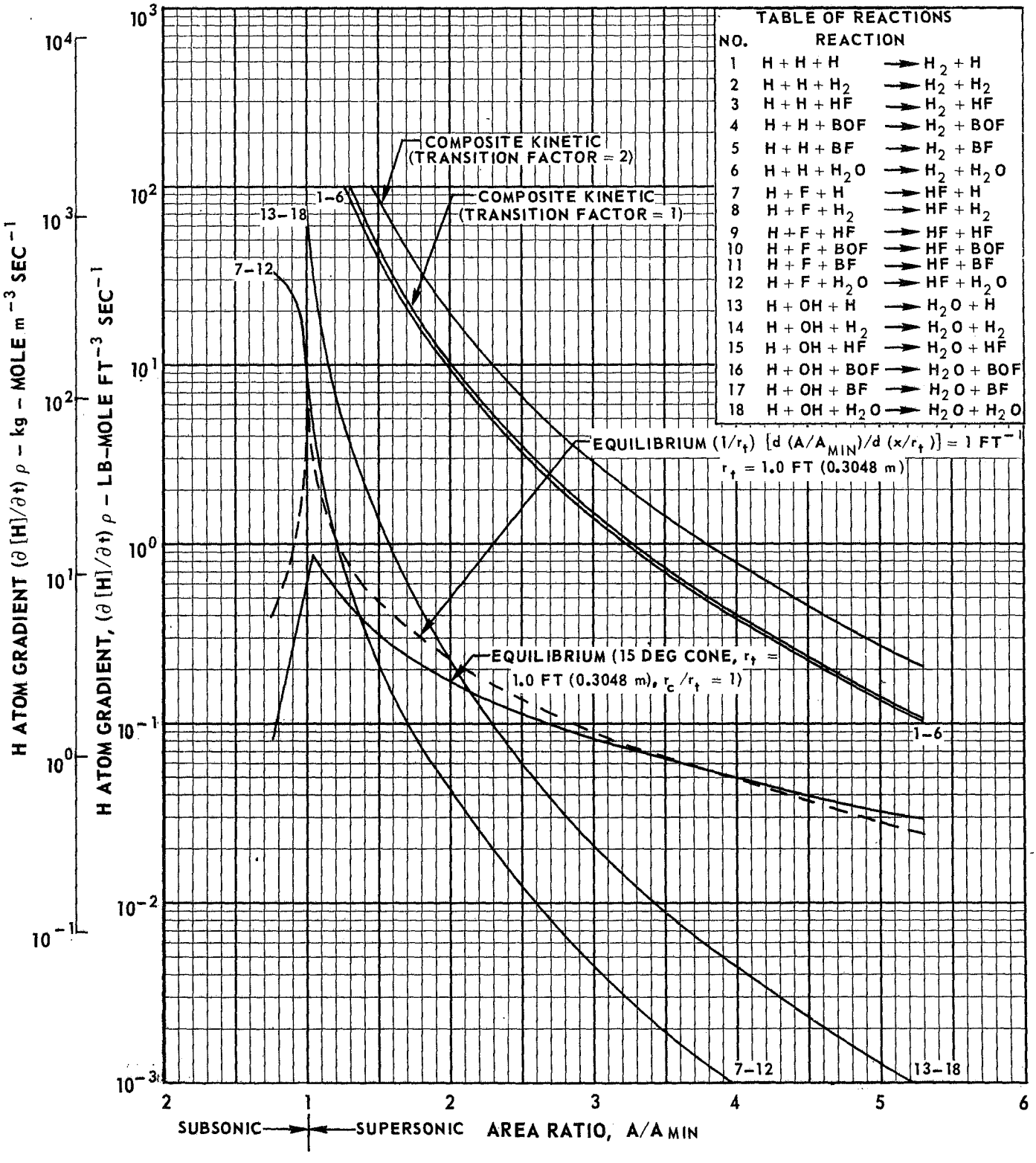

FIG. V-22

NORMALIZED GRAPHICAL SOLUTION FOR FREEZING AREA RATIO USING MODIFIED BRAY ANALYSIS

B_2H_6 (ℓ) – OF_2 (ℓ)

P_C = 500 PSIA (3.448 X 10^5 N/m^2)

O/F = 3.5

NOTE: REACTION RATE CONSTANTS LISTED IN TABLE V-1

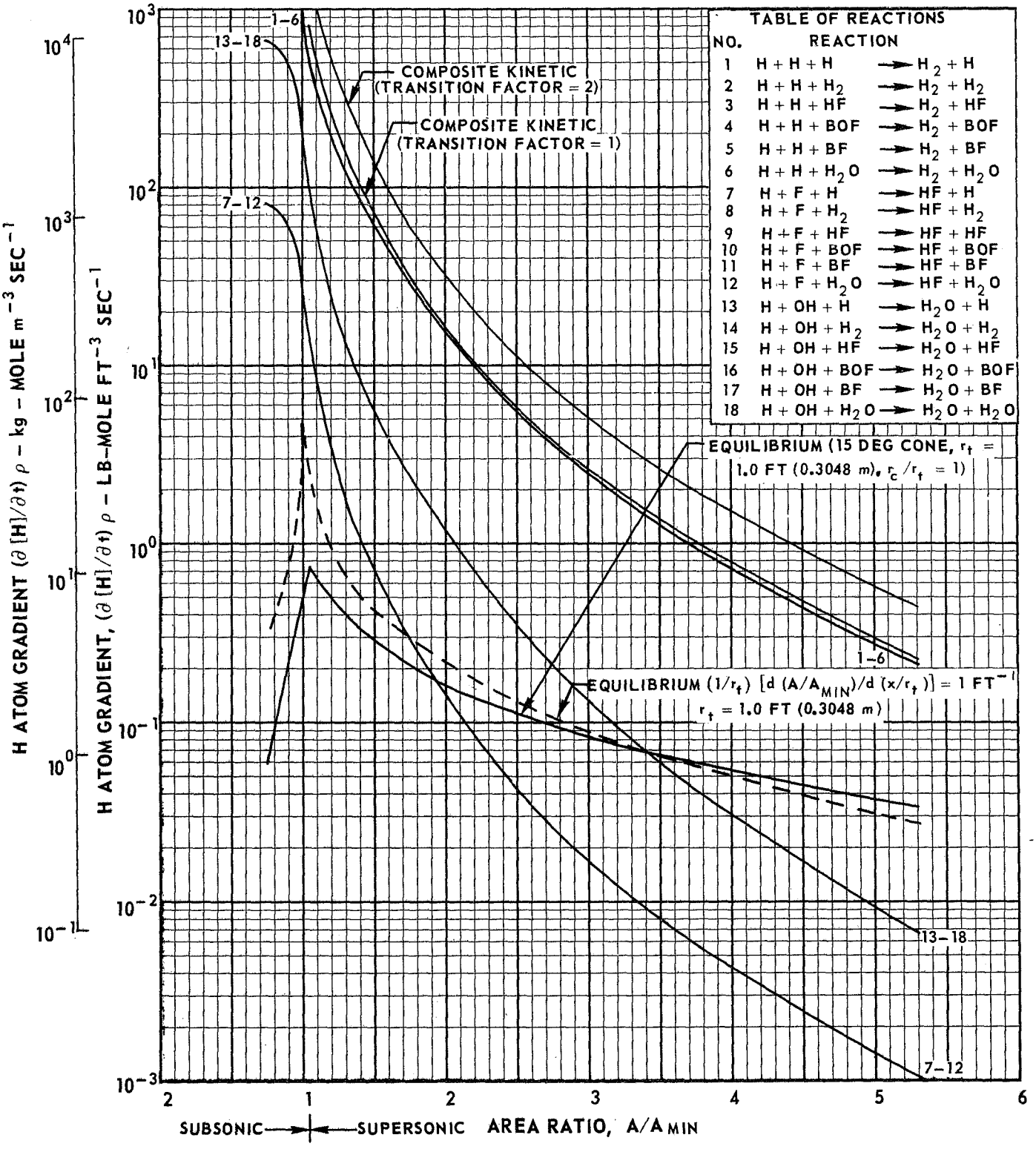

FIG. V-23

NORMALIZED GRAPHICAL SOLUTION FOR FREEZING AREA RATIO USING MODIFIED BRAY ANALYSIS

$B_2H_6(\ell) - OF_2(\ell)$

$P_C = 500$ PSIA (3.448×10^5 N/m^2)

O/F = 4.0

NOTE: REACTION RATE CONSTANTS LISTED IN TABLE V-1

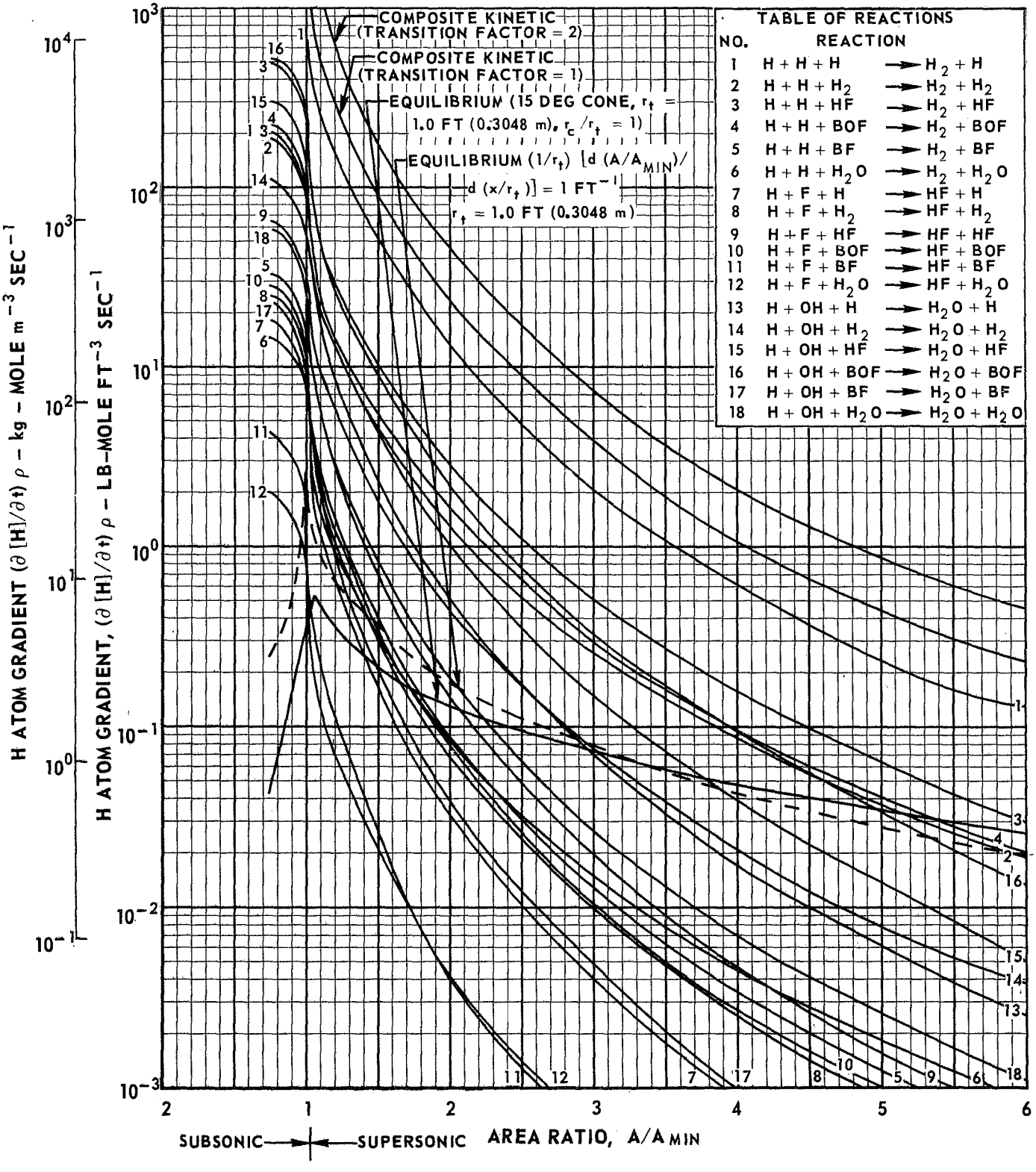

TABLE OF REACTIONS

NO.	REACTION
1	$H + H + H \rightarrow H_2 + H$
2	$H + H + H_2 \rightarrow H_2 + H_2$
3	$H + H + HF \rightarrow H_2 + HF$
4	$H + H + BOF \rightarrow H_2 + BOF$
5	$H + H + BF \rightarrow H_2 + BF$
6	$H + H + H_2O \rightarrow H_2 + H_2O$
7	$H + F + H \rightarrow HF + H$
8	$H + F + H_2 \rightarrow HF + H_2$
9	$H + F + HF \rightarrow HF + HF$
10	$H + F + BOF \rightarrow HF + BOF$
11	$H + F + BF \rightarrow HF + BF$
12	$H + F + H_2O \rightarrow HF + H_2O$
13	$H + OH + H \rightarrow H_2O + H$
14	$H + OH + H_2 \rightarrow H_2O + H_2$
15	$H + OH + HF \rightarrow H_2O + HF$
16	$H + OH + BOF \rightarrow H_2O + BOF$
17	$H + OH + BF \rightarrow H_2O + BF$
18	$H + OH + H_2O \rightarrow H_2O + H_2O$

FIG. V-24

NORMALIZED GRAPHICAL SOLUTION FOR FREEZING AREA RATIO USING MODIFIED BRAY ANALYSIS

B_2H_6 (ℓ) – OF_2 (ℓ)

P_C = 500 PSIA (3.448 X 10^5 N/m^2)

O/F = 4.5

NOTE: REACTION RATE CONSTANTS LISTED IN TABLE V-1

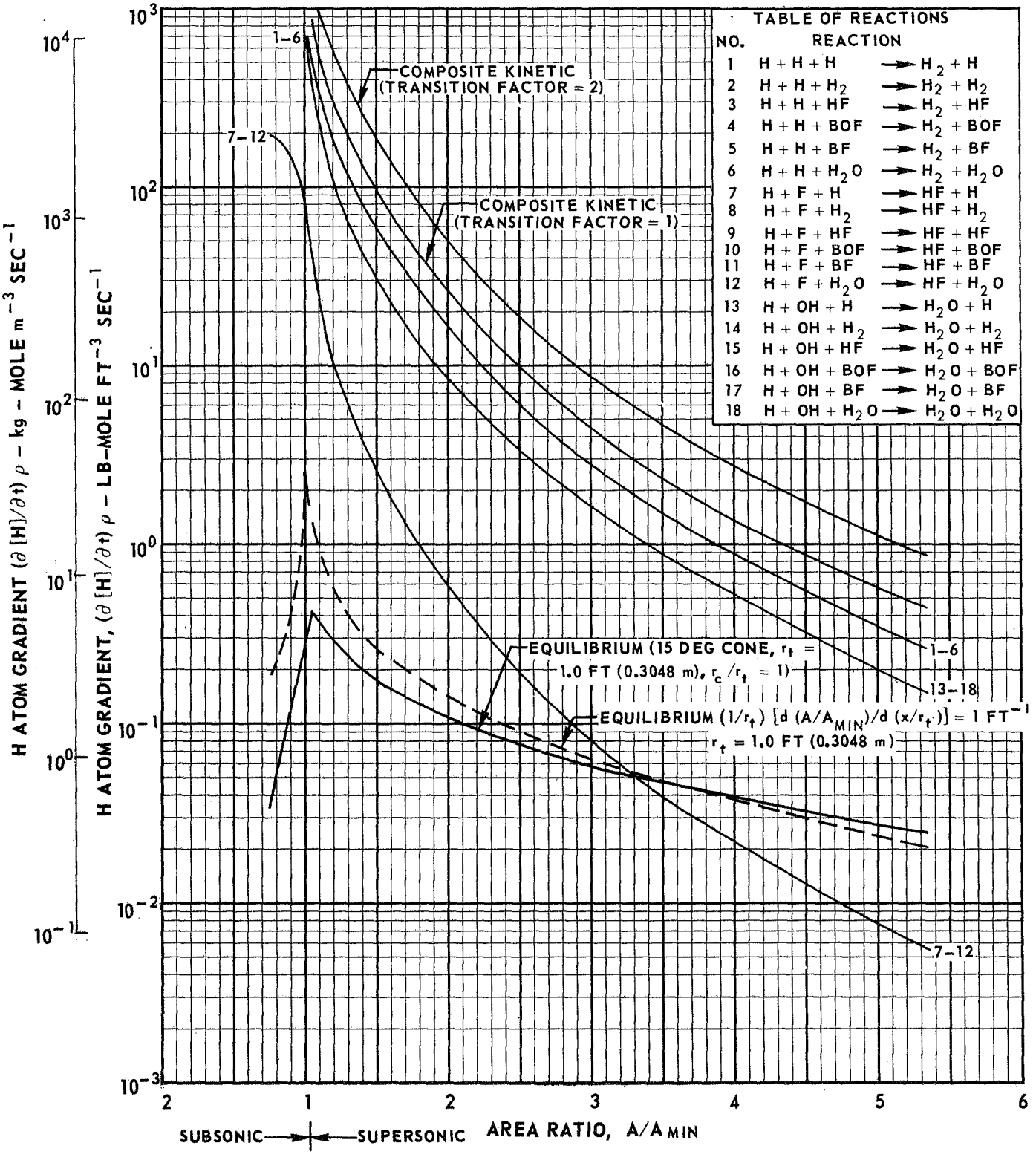

FIG. V-25

EFFECT OF FREEZING AREA RATIO ON NONEQUILIBRIUM PERFORMANCE FOR A DIBORANE – OF_2 PROPELLANT SYSTEM

B_2H_6 (ℓ) – OF_2 (ℓ)

P_C = 50 PSIA (3.448 X 10^5 N/m^2)

O/F = 3.0

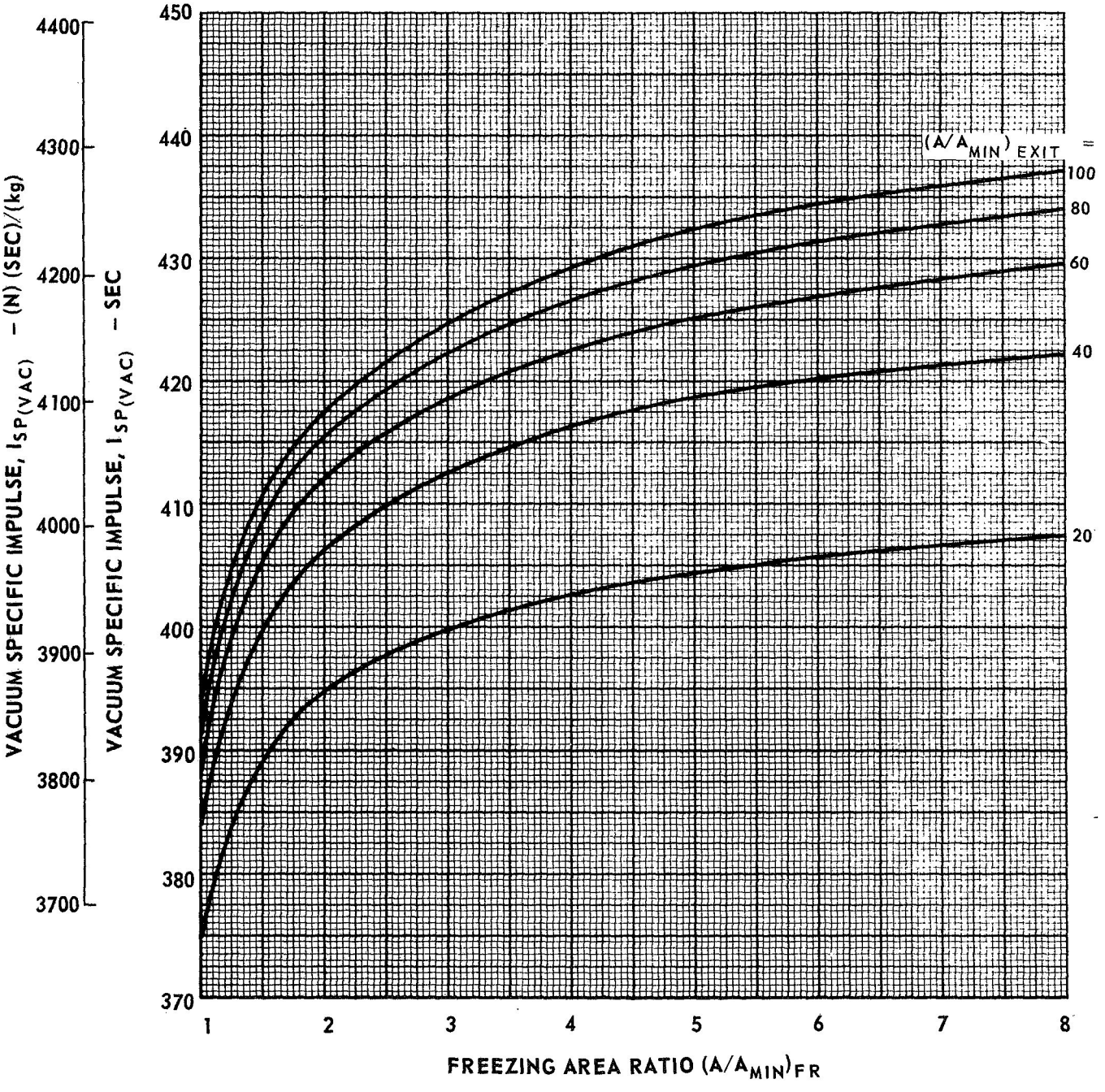

FIG. V-26

EFFECT OF FREEZING AREA RATIO ON NONEQUILIBRIUM PERFORMANCE FOR A DIBORANE – OF_2 PROPELLANT SYSTEM

B_2H_6 (ℓ) – OF_2 (ℓ)

P_C = 50 PSIA (3.448 X 10^5 N/m^2)

O/F = 3.5

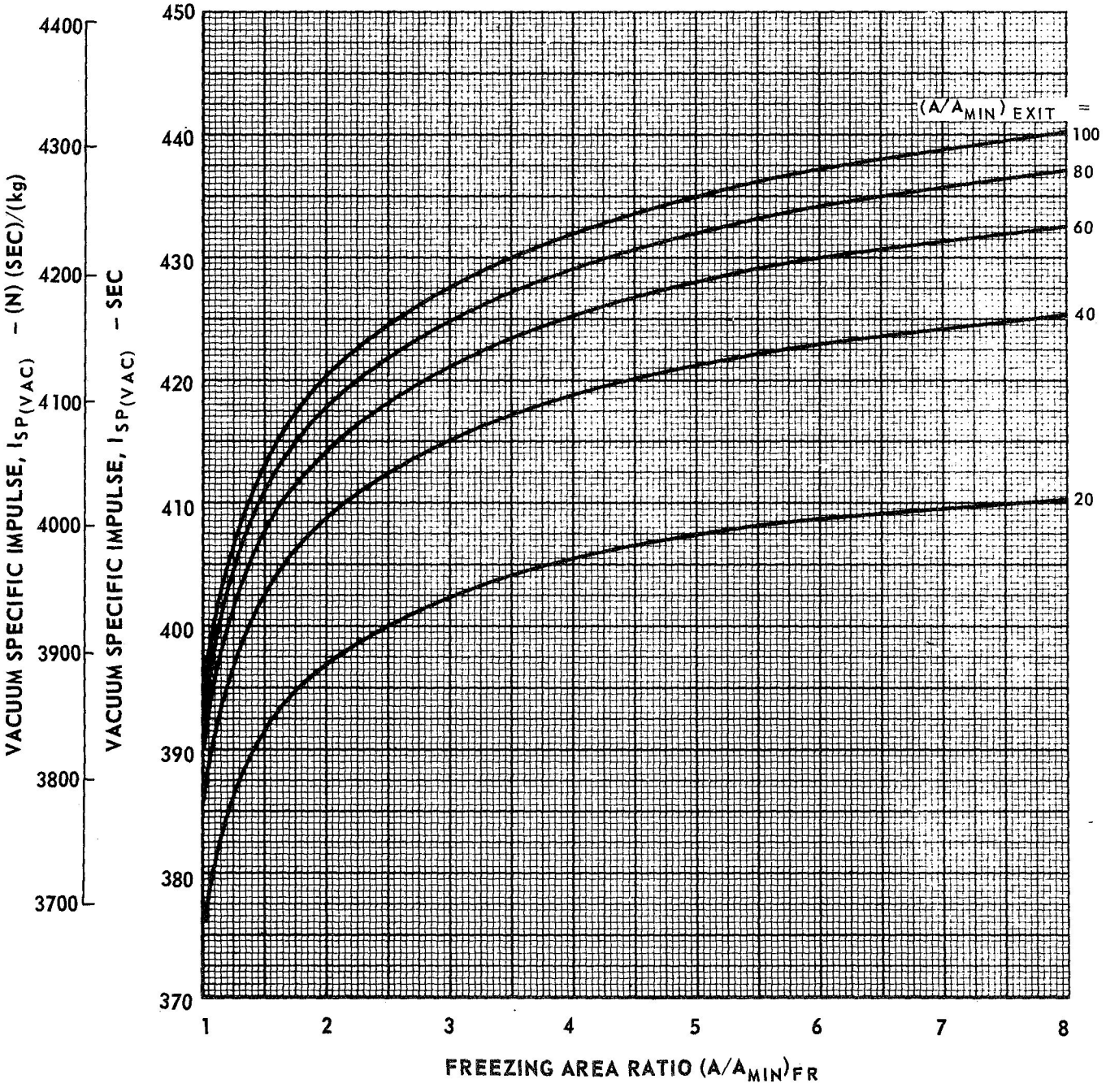

EFFECT OF FREEZING AREA RATIO ON NONEQUILIBRIUM PERFORMANCE FOR A DIBORANE – OF_2 PROPELLANT SYSTEM

B_2H_6 (ℓ) – OF_2 (ℓ)

P_C = 50 PSIA (3.448 X 10^5 N/m^2)

O/F = 4.0

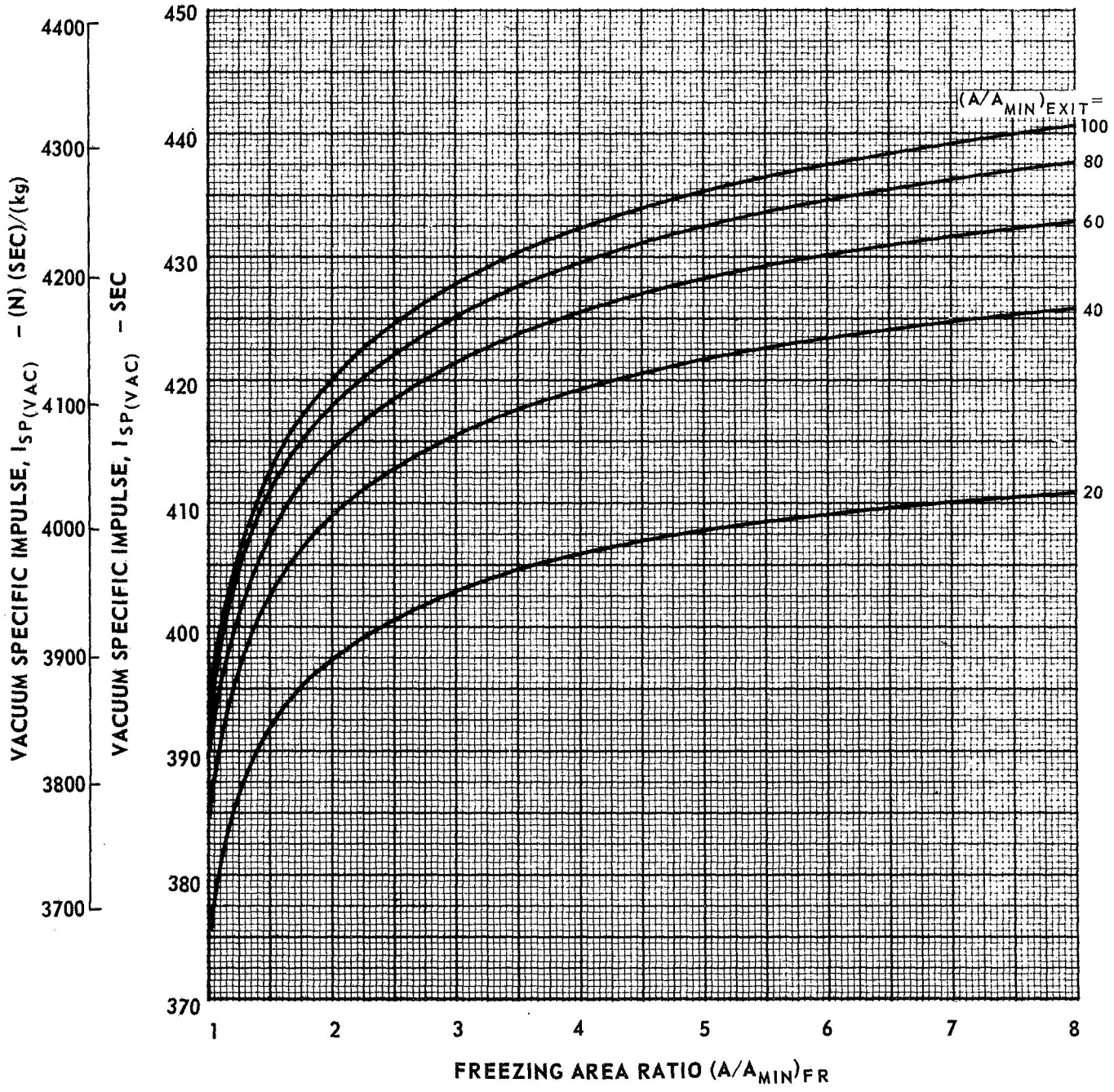

FIG. V-28

EFFECT OF FREEZING AREA RATIO ON NONEQUILIBRIUM PERFORMANCE FOR A DIBORANE – OF_2 PROPELLANT SYSTEM

B_2H_6 (ℓ) – OF_2 (ℓ)

P_C = 50 PSIA (3.448 X 10^5 N/m^2)

O/F = 4.5

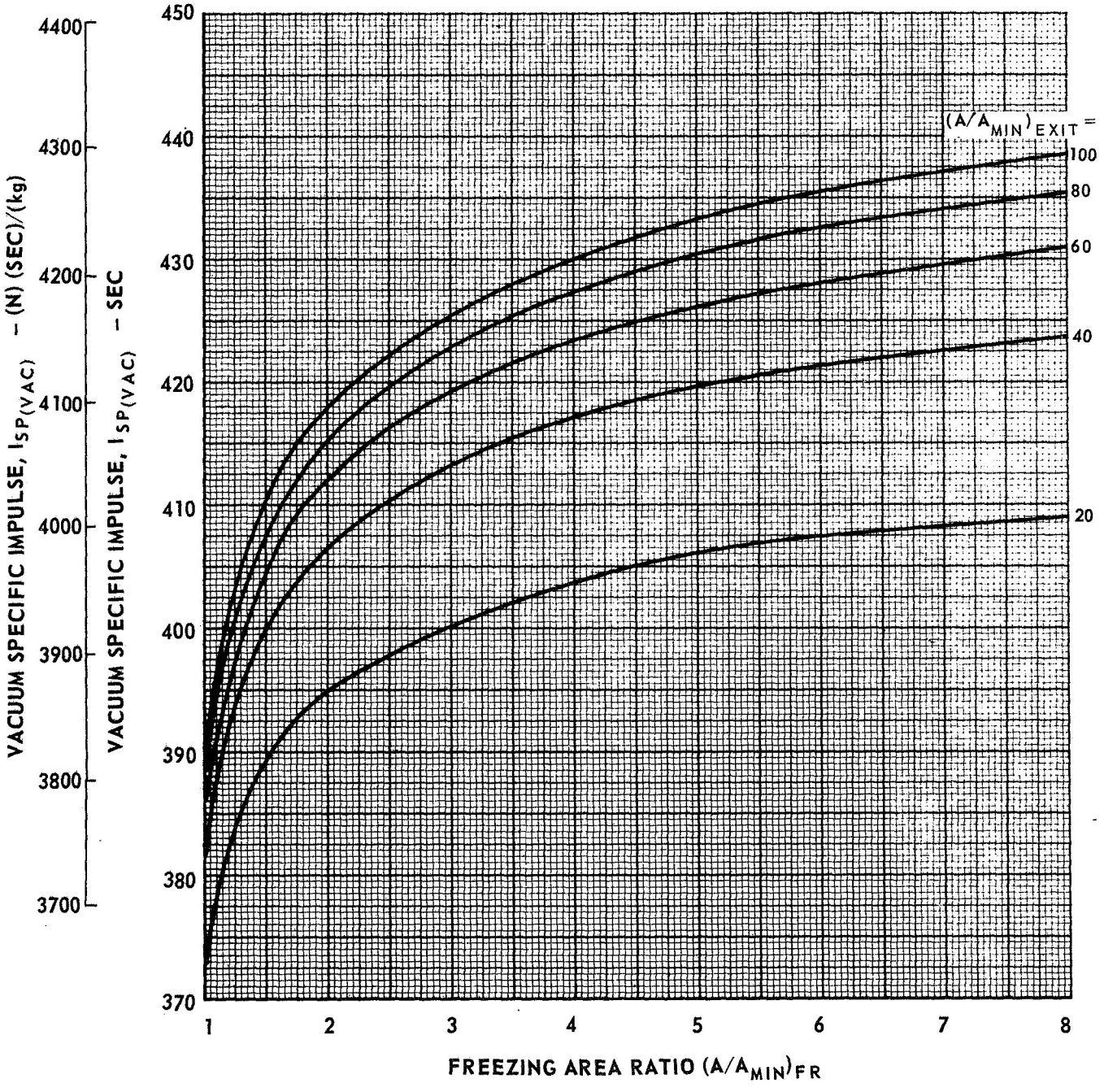

EFFECT OF FREEZING AREA RATIO ON NONEQUILIBRIUM PERFORMANCE FOR A DIBORANE – OF_2 PROPELLANT SYSTEM

B_2H_6 (ℓ) – OF_2 (ℓ)

P_C = 100 PSIA (6.985 X 10^5 N/m^2)

O/F = 3.0

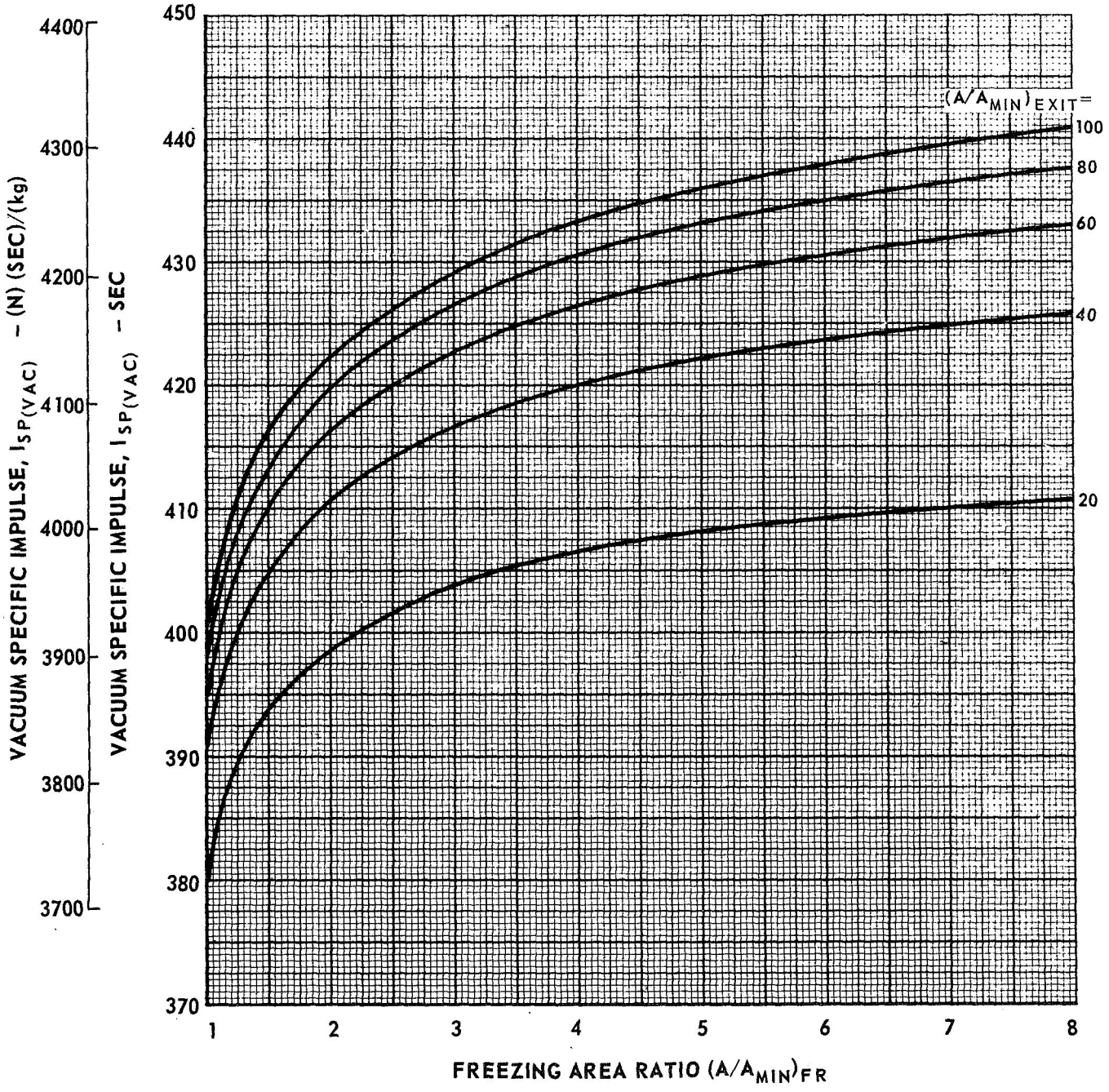

EFFECT OF FREEZING AREA RATIO ON NONEQUILIBRIUM PERFORMANCE FOR A DIBORANE – OF_2 PROPELLANT SYSTEM

B_2H_6 (ℓ) – OF_2 (ℓ)

P_C = 100 PSIA (6.985 X 10^5 N/m^2)

O/F = 3.5

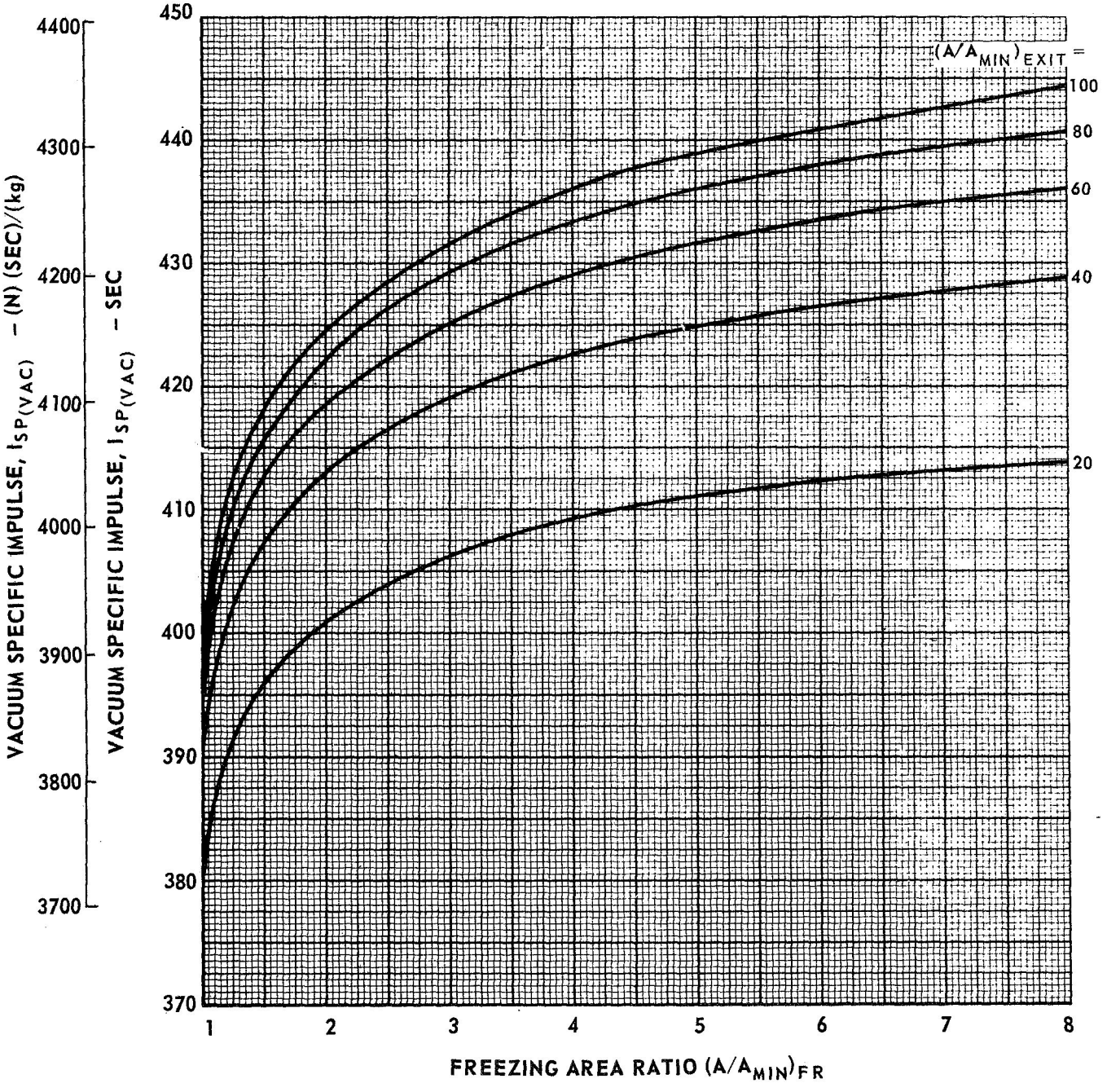

EFFECT OF FREEZING AREA RATIO ON NONEQUILIBRIUM PERFORMANCE FOR A DIBORANE – OF_2 PROPELLANT SYSTEM

B_2H_6 (ℓ) – OF_2 (ℓ)

P_C = 100 PSIA (6.985 X 10^5 N/m^2)

O/F = 4.0

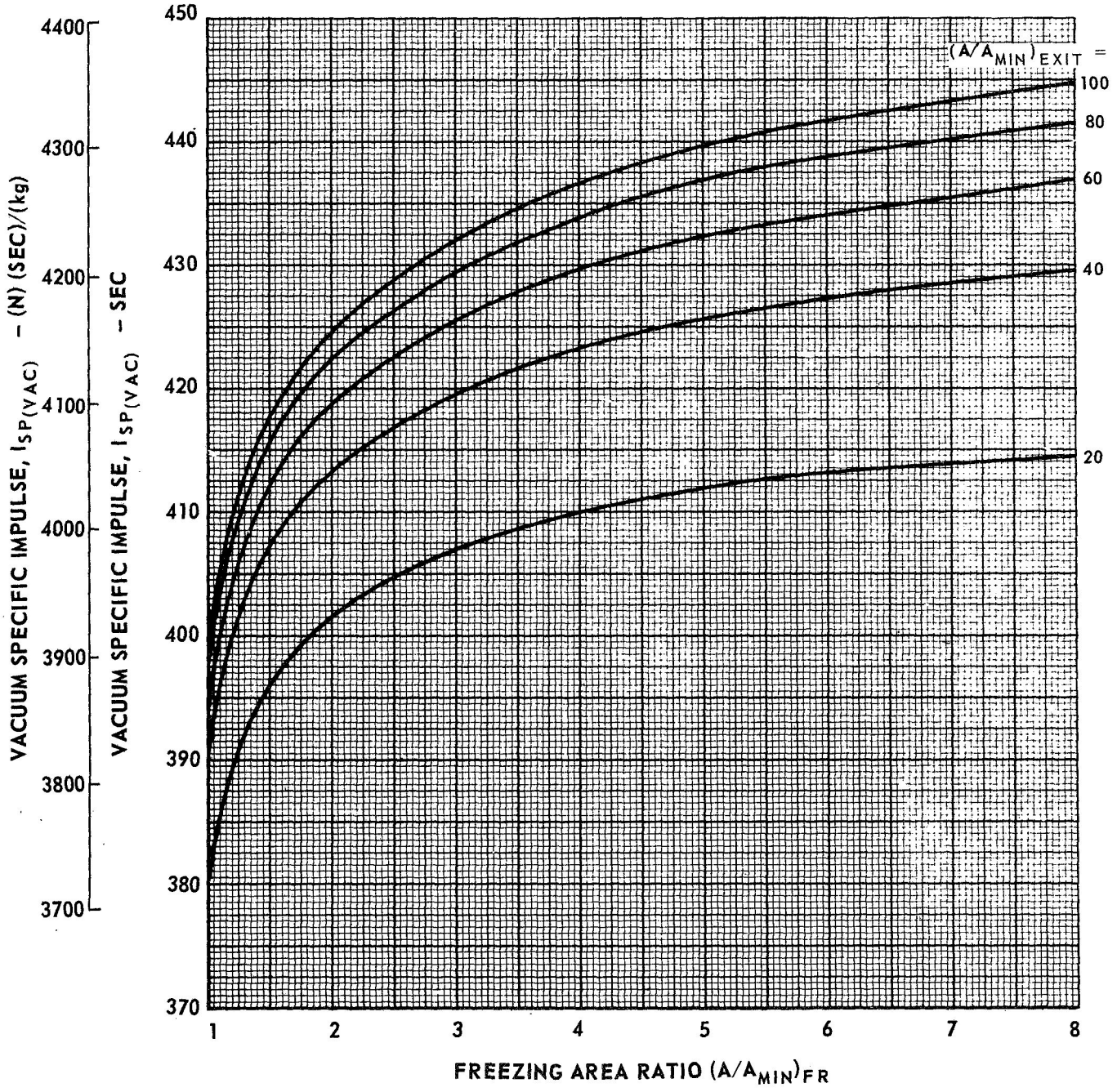

EFFECT OF FREEZING AREA RATIO ON NONEQUILIBRIUM PERFORMANCE FOR A DIBORANE - OF_2 PROPELLANT SYSTEM

$B_2 H_6$ (ℓ) - OF_2 (ℓ)

P_C = 100 PSIA (6.985 X 10^5 N/m^2)

O/F = 4.5

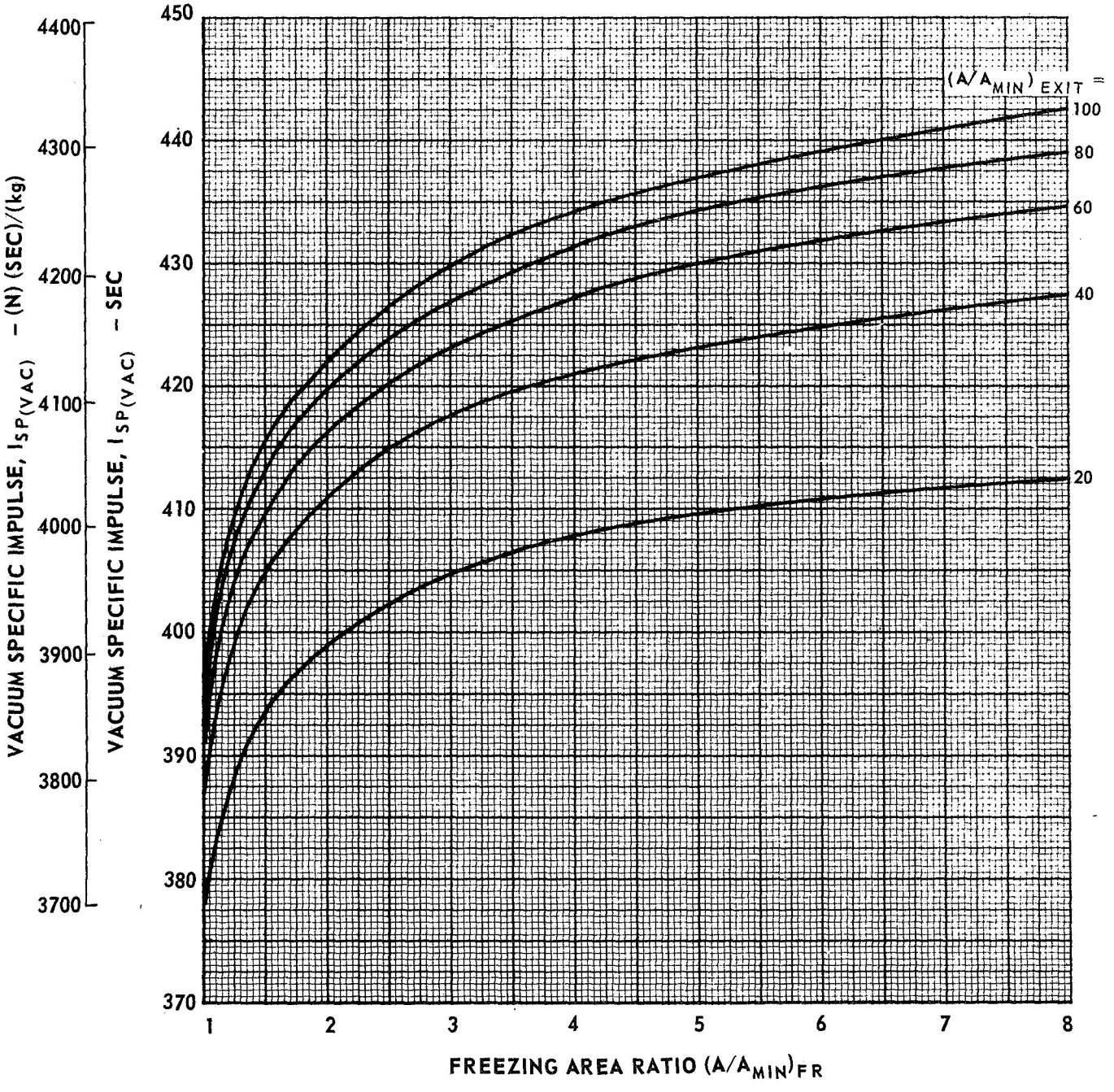

EFFECT OF FREEZING AREA RATIO ON NONEQUILIBRIUM PERFORMANCE FOR A DIBORANE – OF_2 PROPELLANT SYSTEM

$B_2 H_6$ (ℓ) – OF_2 (ℓ)

P_C = 250 PSIA (1.742 X 10^6 N/m^2)

O/F = 3.0

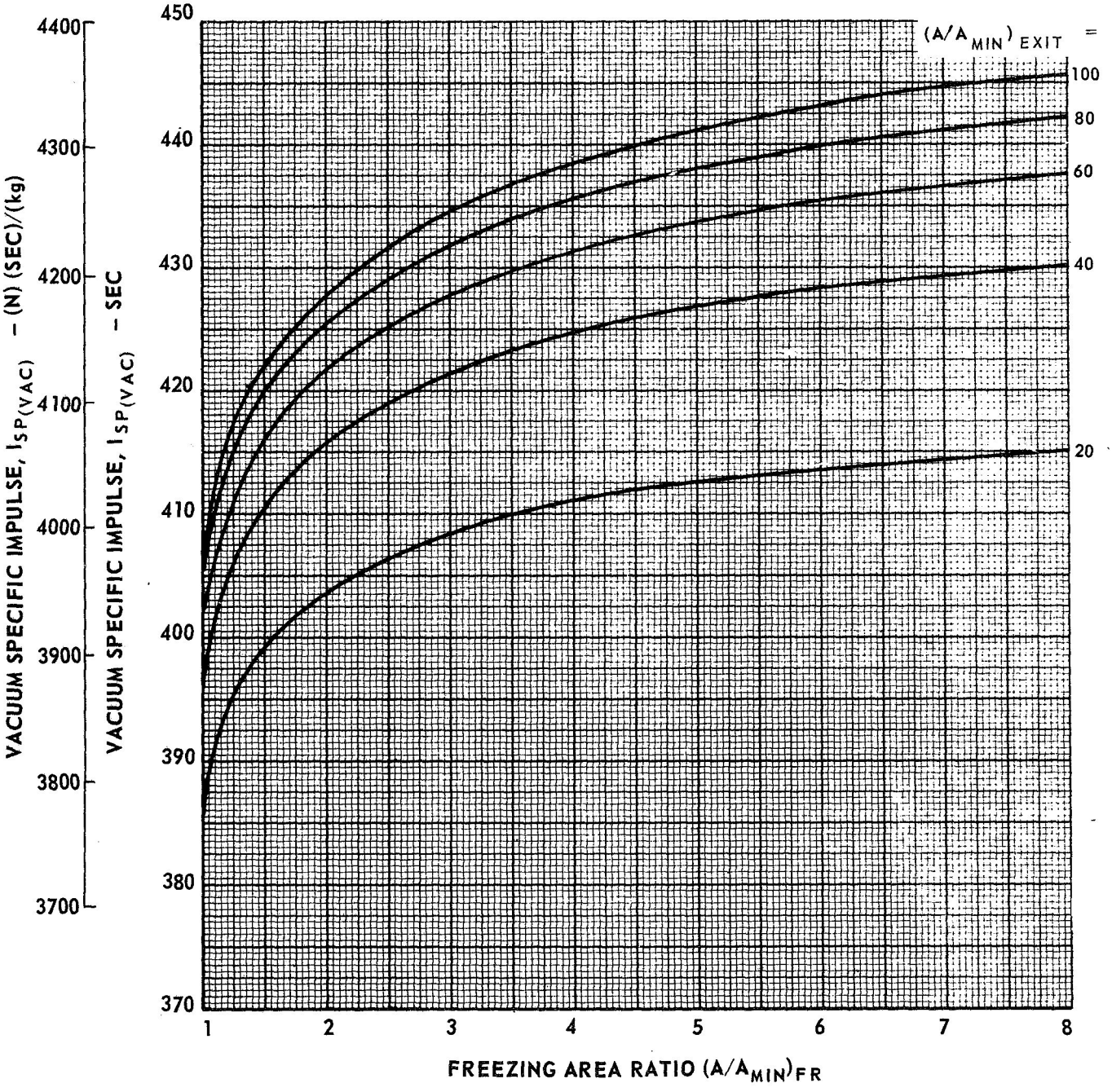

FIG. V-34

EFFECT OF FREEZING AREA RATIO ON NONEQUILIBRIUM PERFORMANCE FOR A DIBORANE – OF_2 PROPELLANT SYSTEM

B_2H_6 (ℓ) – OF_2 (ℓ)

P_C = 250 PSIA (1.742 X 10^6 N/m^2)

O/F = 3.5

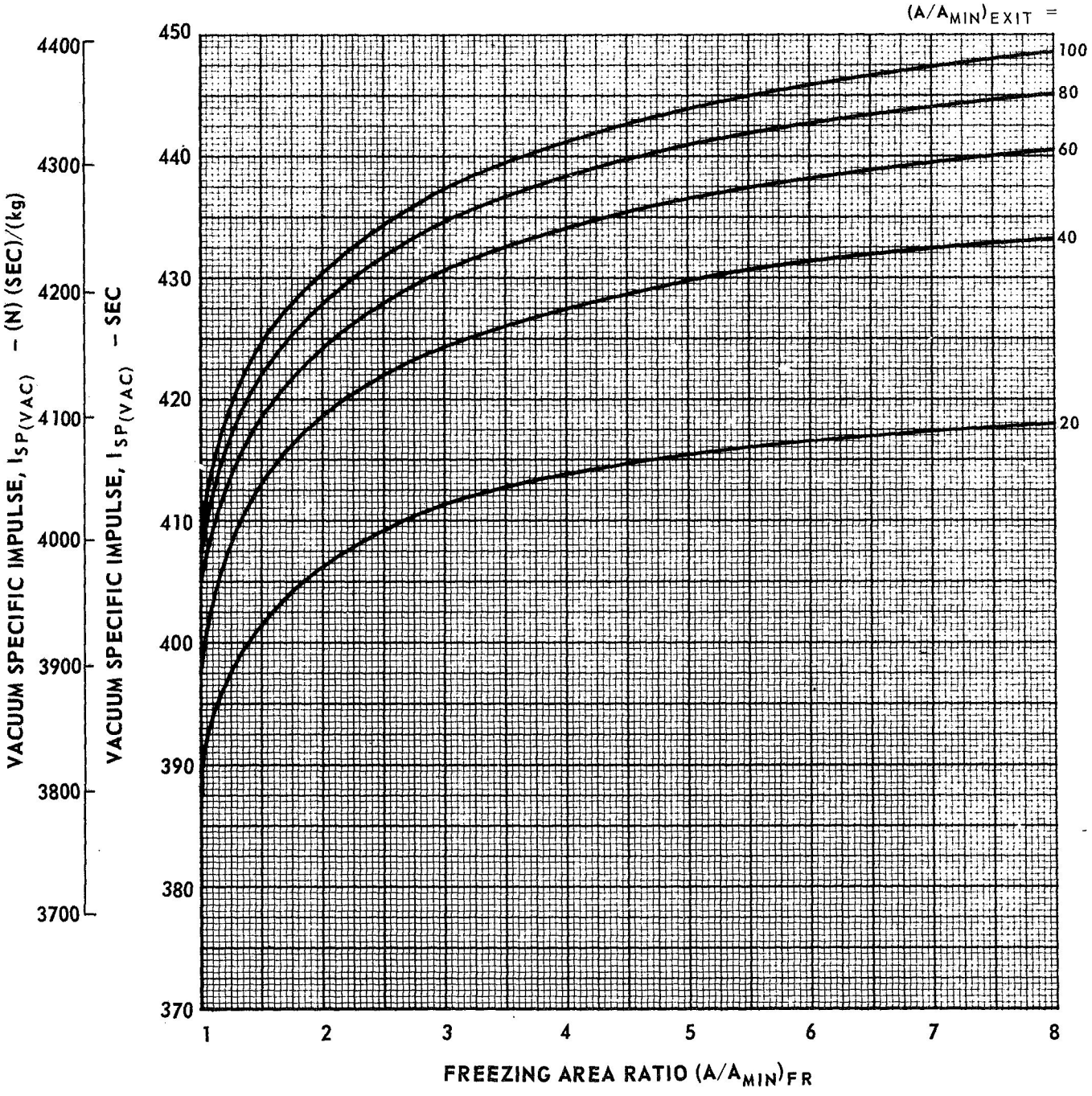

FIG. V-35

EFFECT OF FREEZING AREA RATIO ON NONEQUILIBRIUM PERFORMANCE FOR A DIBORANE - OF_2 PROPELLANT SYSTEM

B_2H_6 (ℓ) - OF_2 (ℓ)

P_C = 250 PSIA (1.742 X 10^6 N/m^2)

O/F = 4.0

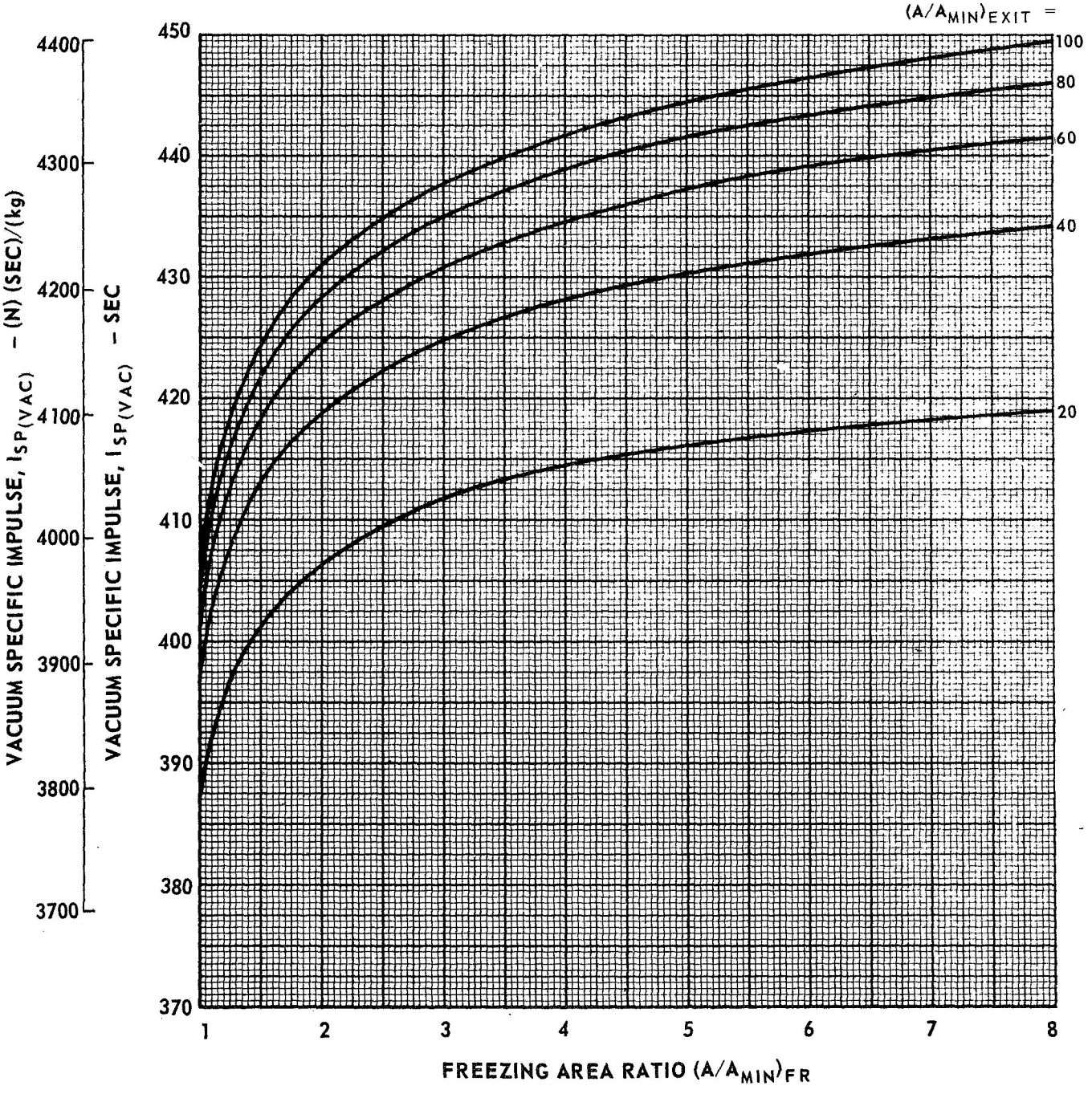

EFFECT OF FREEZING AREA RATIO ON NONEQUILIBRIUM PERFORMANCE FOR A DIBORANE – OF_2 PROPELLANT SYSTEM

$B_2 H_6$ (ℓ) – OF_2 (ℓ)

P_C = 250 PSIA (1.742 X 10^6 N/m^2)

O/F = 4.5

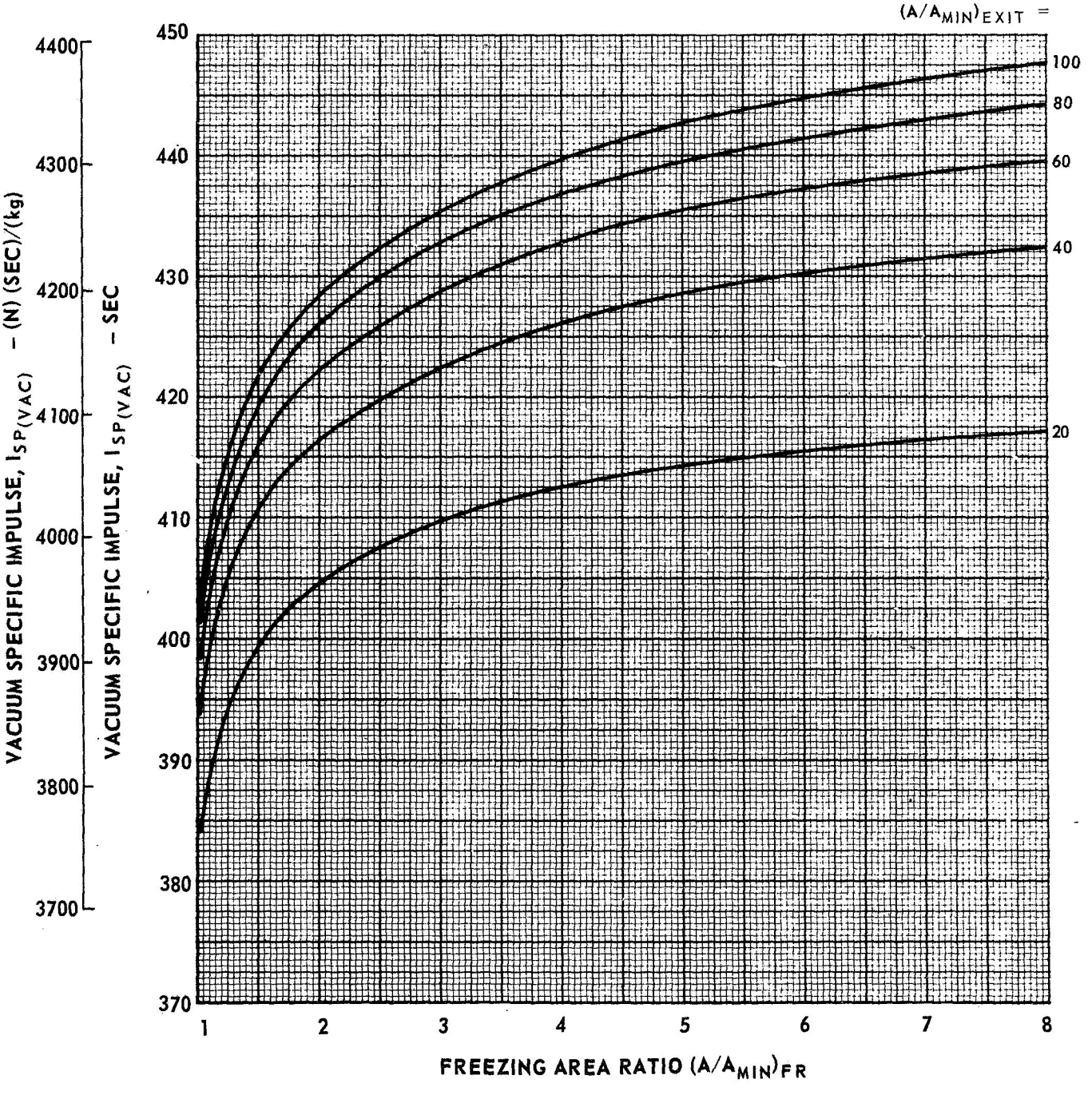

EFFECT OF FREEZING AREA RATIO ON NONEQUILIBRIUM PERFORMANCE FOR A DIBORANE – OF_2 PROPELLANT SYSTEM

B_2H_6 (ℓ) – OF_2 (ℓ)

P_C = 500 PSIA (3.4475 X 10^6 N/m^2)

O/F = 3.0

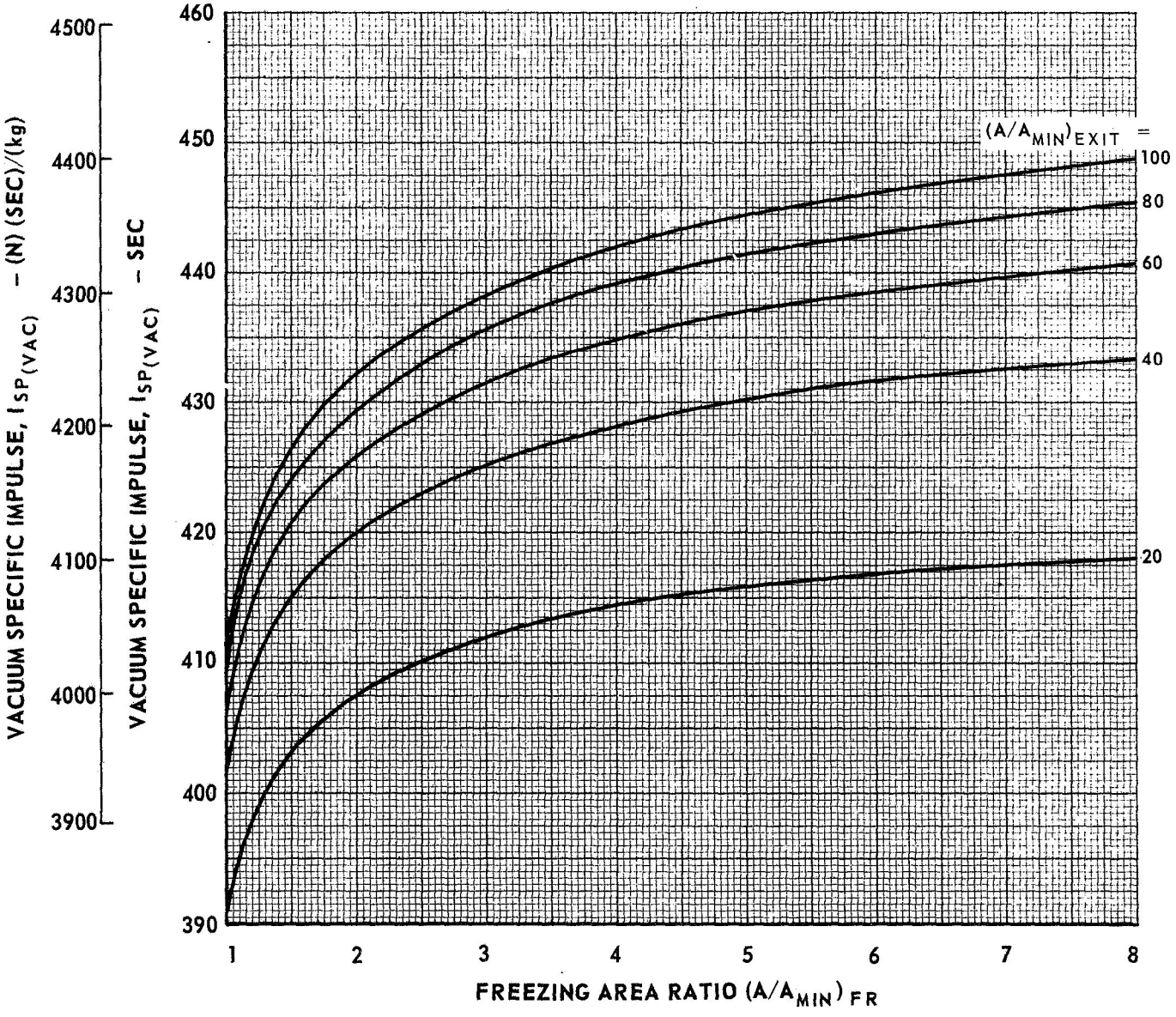

FIG. V-38

EFFECT OF FREEZING AREA RATIO ON NONEQUILIBRIUM PERFORMANCE FOR A DIBORANE – OF_2 PROPELLANT SYSTEM

B_2H_6 (ℓ) – OF_2 (ℓ)

P_C = 500 PSIA (3.4475 X 10^6 N/m^2)

O/F = 3.5

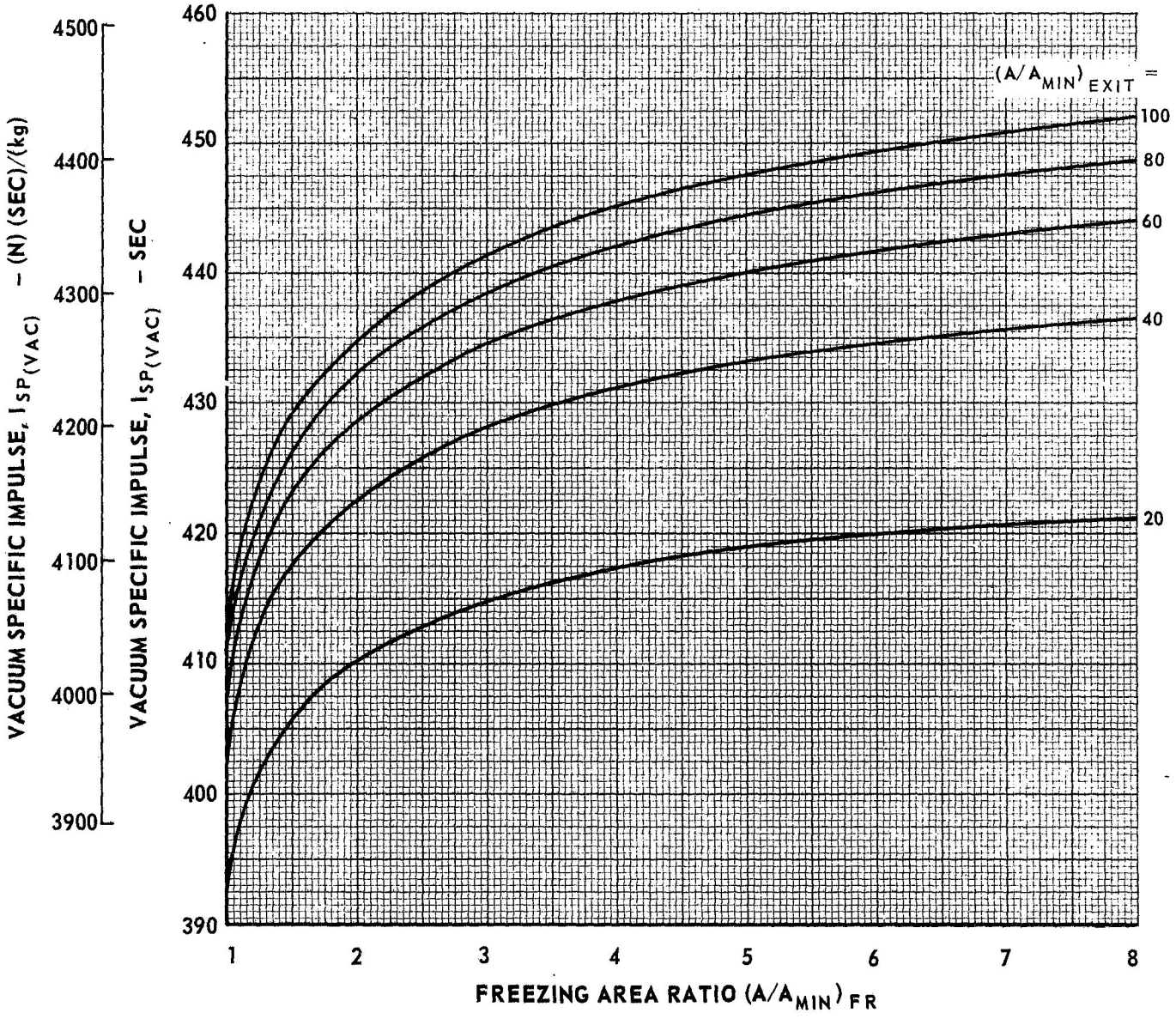

FIG. V-39

EFFECT OF FREEZING AREA RATIO ON NONEQUILIBRIUM PERFORMANCE FOR A DIBORANE – OF_2 PROPELLANT SYSTEM

B_2H_6 (ℓ) – OF_2 (ℓ)

P_C = 500 PSIA (3.4475 X 10^6 N/m^2)

O/F = 4.0

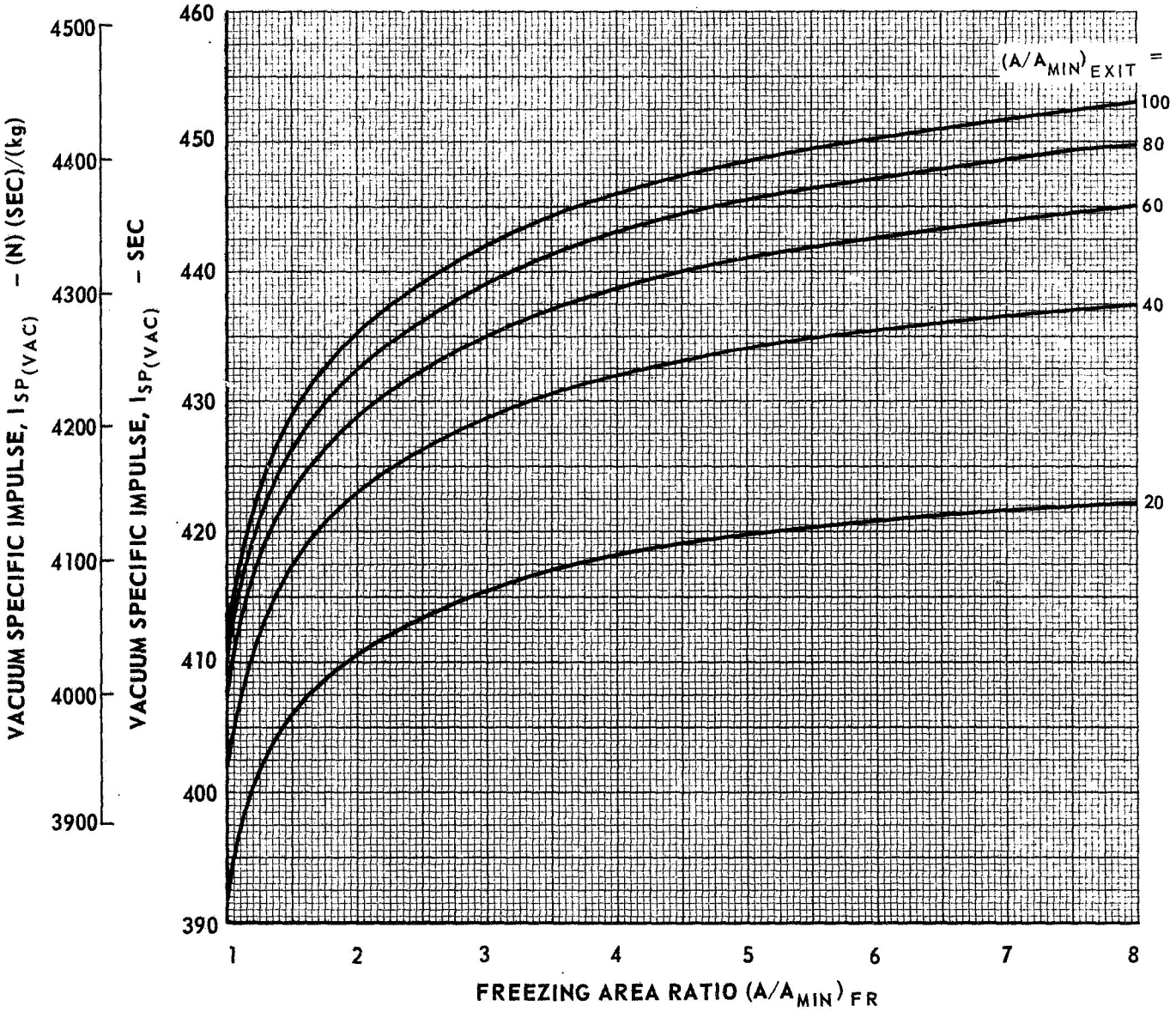

FIG. V-40

EFFECT OF FREEZING AREA RATIO ON NONEQUILIBRIUM PERFORMANCE FOR A DIBORANE – OF_2 PROPELLANT SYSTEM

B_2H_6 (ℓ) – OF_2 (ℓ)

P_C = 500 PSIA (3.4475 X 10^6 N/m^2)

O/F = 4.5

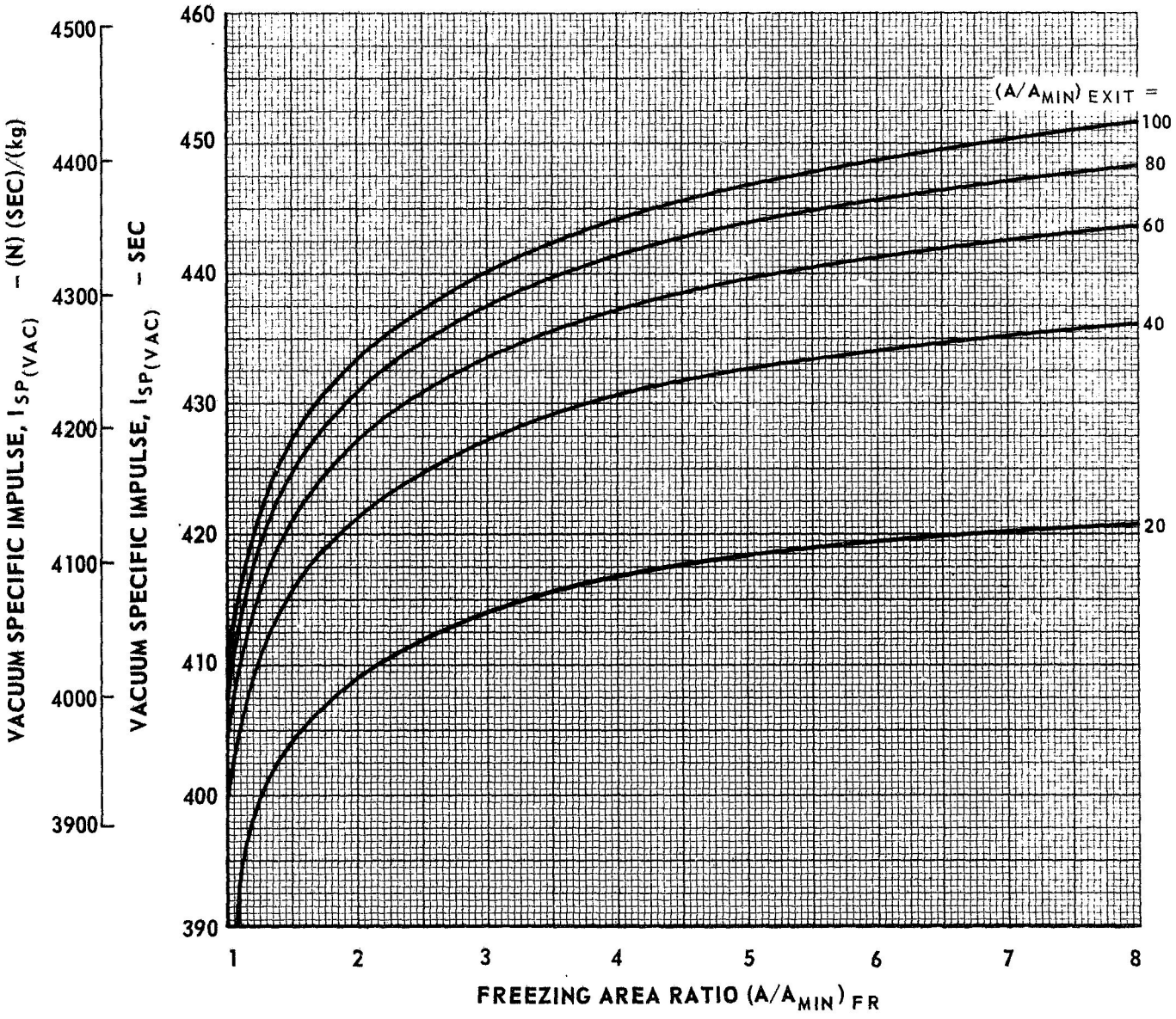

FIG. AL-1

AXISYMMETRIC PERFECT NOZZLE DIVERGENCE LOSS

SPECIFIC HEAT RATIO = 1.25

NOTE: DIVERGENCE LOSS = $\frac{\text{1D THRUST} - \text{2D THRUST}}{\text{1D THRUST}}$

$\frac{(A/A_{MIN})_{EXIT}}{(A/A_{MIN})_{DESIGN}} = \frac{\text{TRUNCATED NOZZLE RATIO}}{\text{PERFECT NOZZLE EXIT AREA RATIO}}$

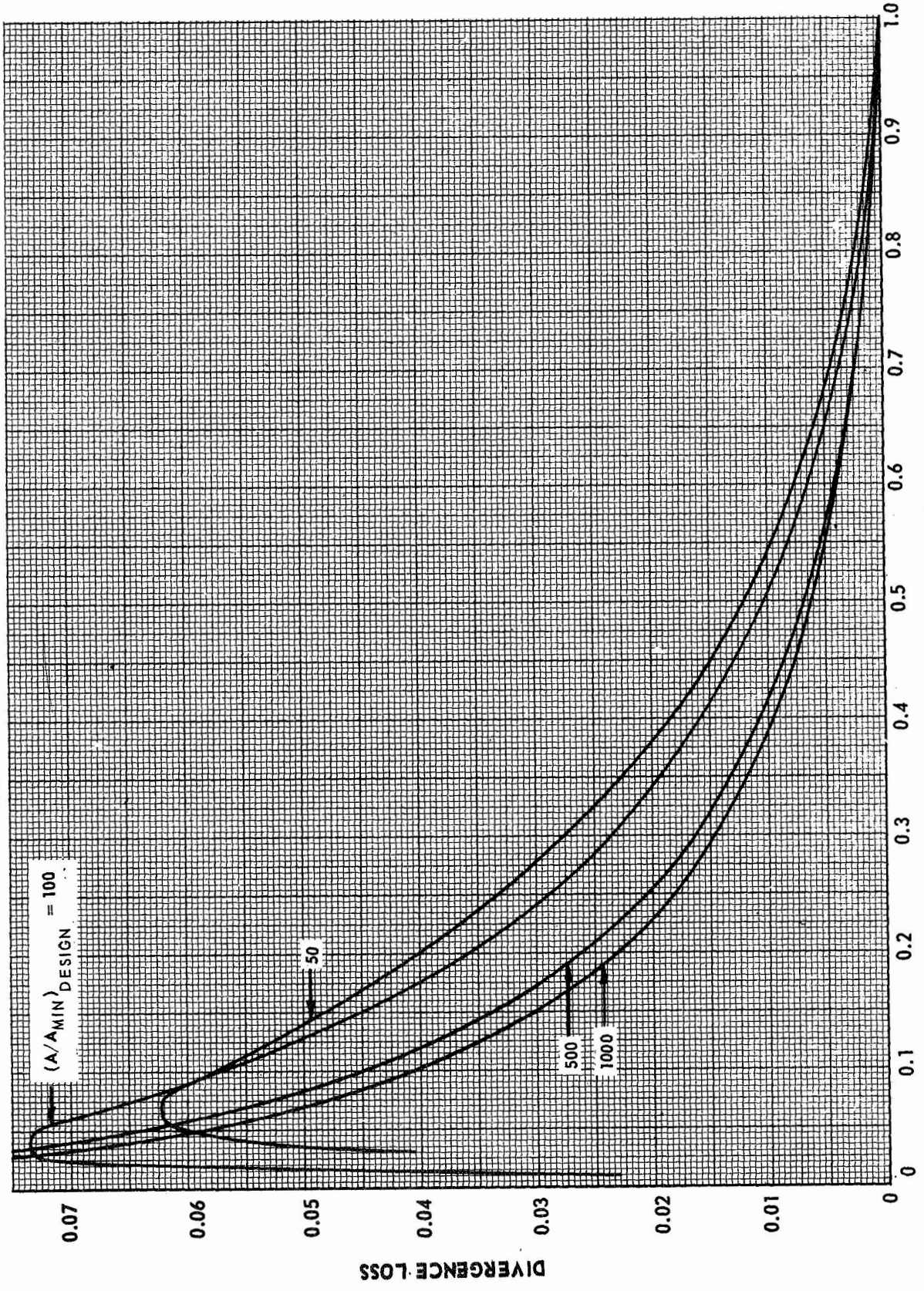

FIG. AL-2

AXISYMMETRIC PERFECT NOZZLE DIVERGENCE LOSS

SPECIFIC HEAT RATIO = 1.30

NOTE: DIVERGENCE LOSS = $\frac{\text{1D THRUST} - \text{2D THRUST}}{\text{1D THRUST}}$

$$\frac{(A/A_{MIN})_{EXIT}}{(A/A_{MIN})_{DESIGN}} = \frac{\text{TRUNCATED NOZZLE RATIO}}{\text{PERFECT NOZZLE EXIT AREA RATIO}}$$

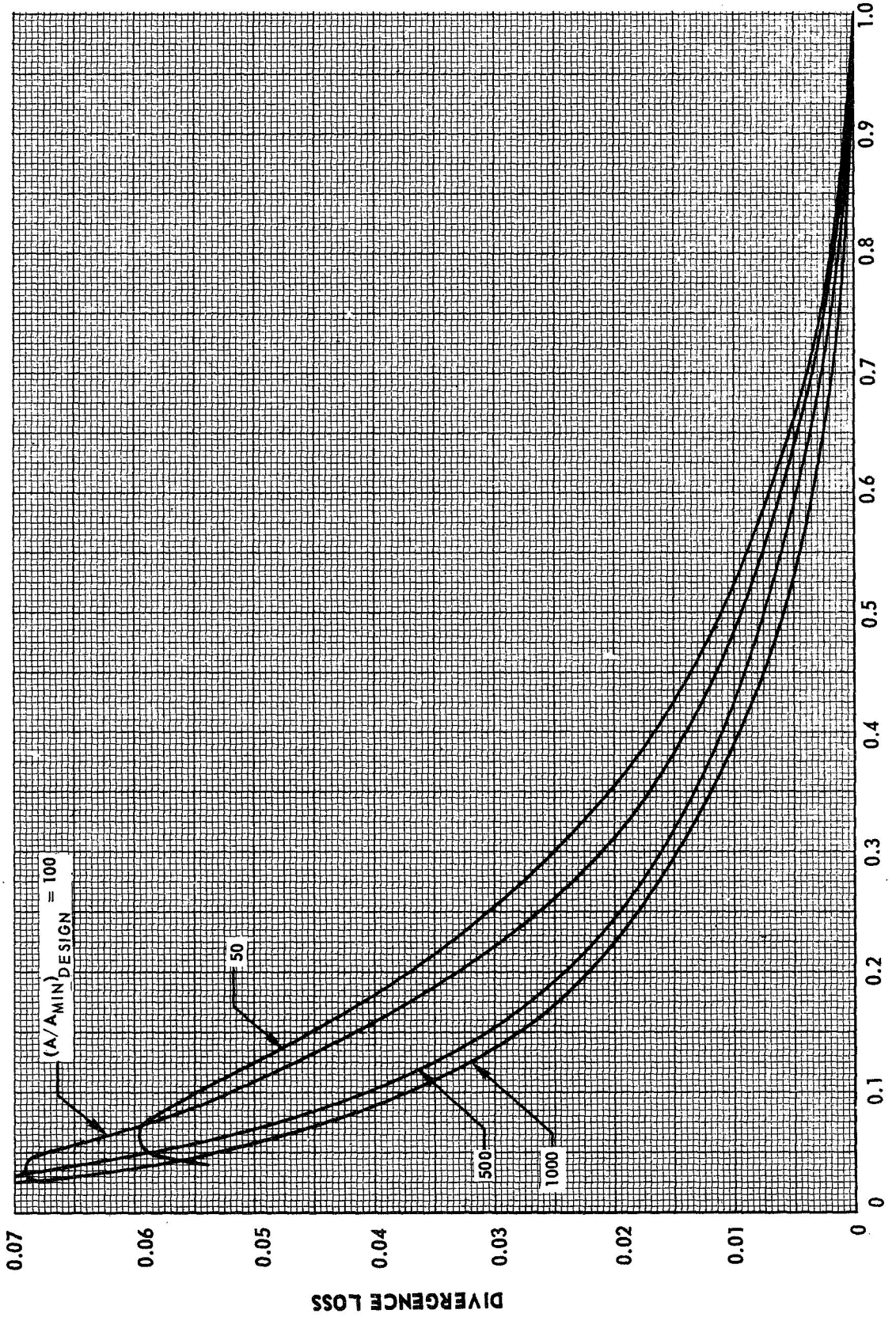

FIG. AL-3

AXISYMMETRIC PERFECT NOZZLE DIVERGENCE LOSS

SPECIFIC HEAT RATIO = 1.35

NOTE: DIVERGENCE LOSS = $\frac{\text{1D THRUST} - \text{2D THRUST}}{\text{1D THRUST}}$

$\frac{(A/A_{MIN})_{EXIT}}{(A/A_{MIN})_{DESIGN}}$ = $\frac{\text{TRUNCATED NOZZLE RATIO}}{\text{PERFECT NOZZLE EXIT AREA RATIO}}$

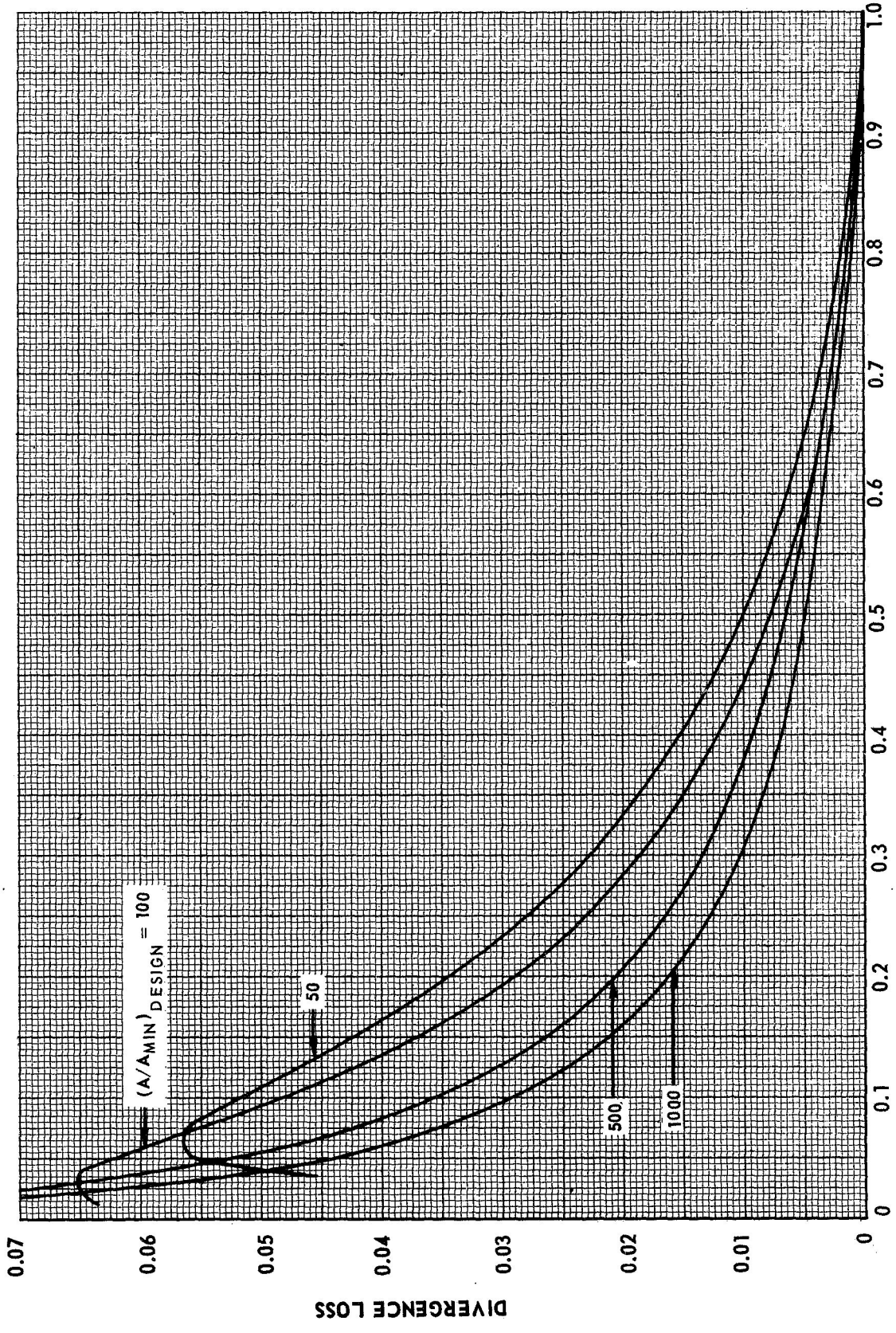

FIG. AL-4

VARIATION OF DIVERGENCE LOSS AS PERCENT OF FROZEN VACUUM SPECIFIC IMPULSE FOR 15 DEG CONICAL NOZZLE

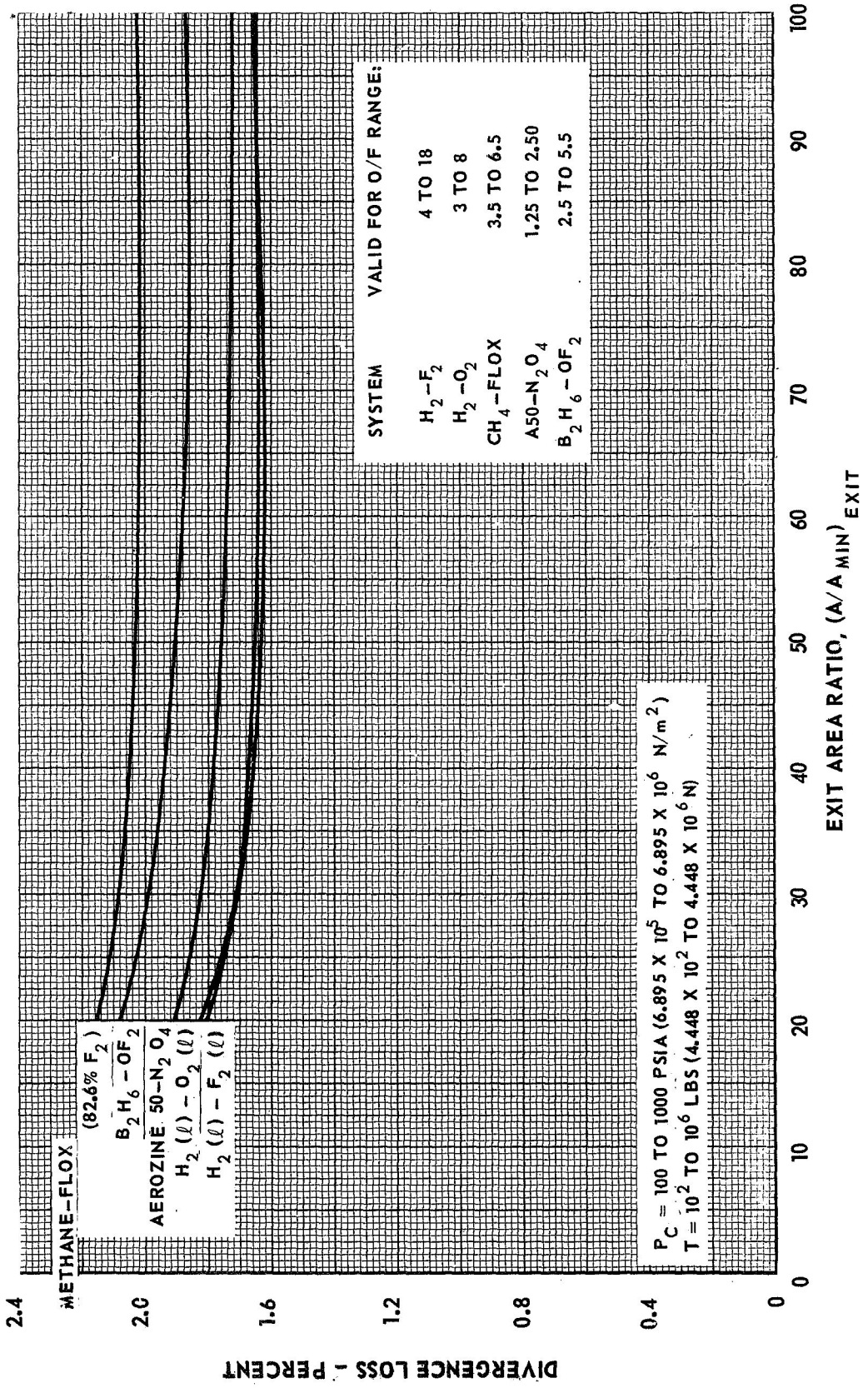

FIG. AL-5

VARIATION OF DIVERGENCE LOSS AS PERCENT OF FROZEN VACUUM SPECIFIC IMPULSE FOR 70% BELL NOZZLE

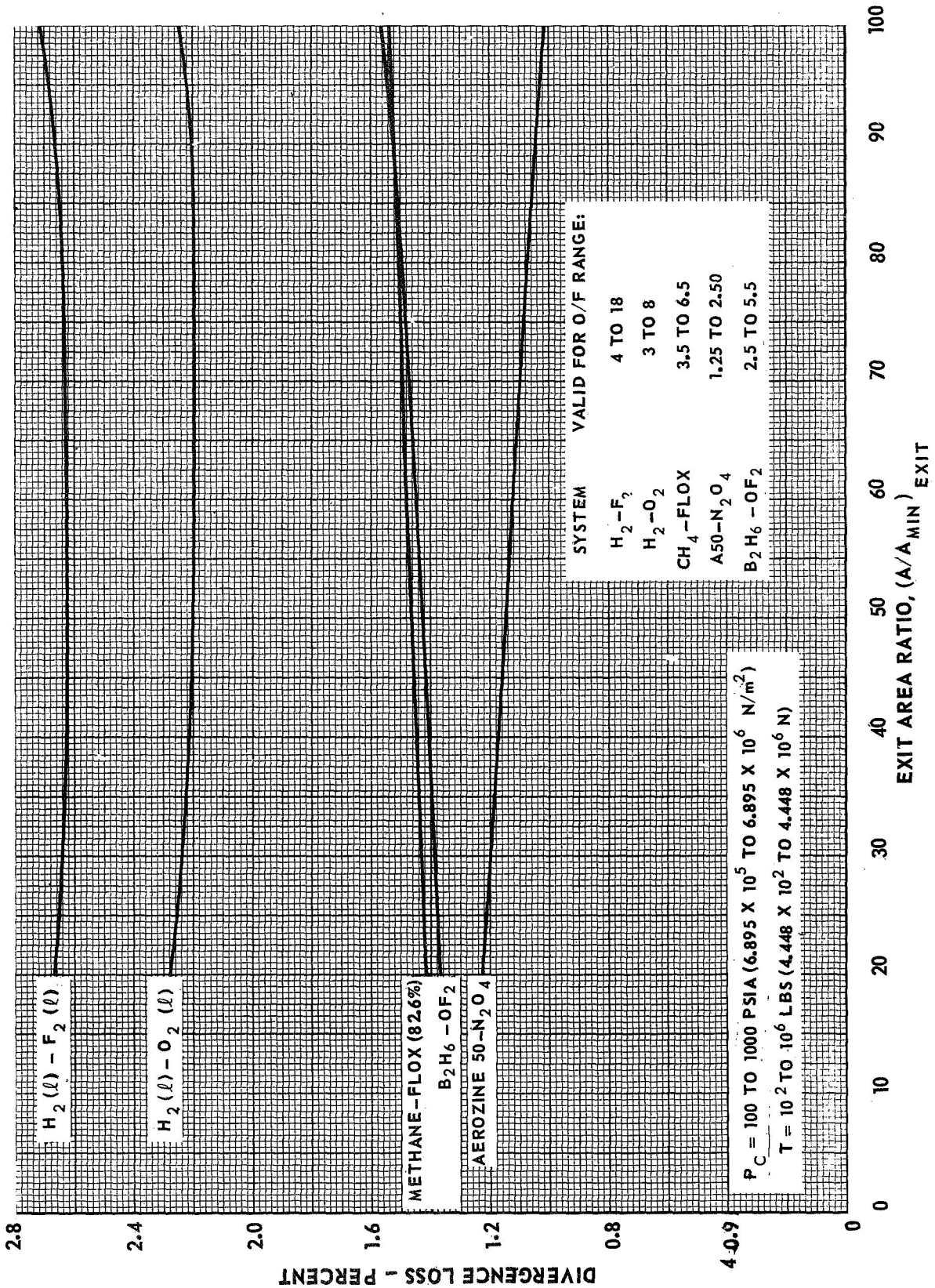

FIG. AL-6

VARIATION OF VISCOUS DRAG AS PERCENT OF FROZEN VACUUM SPECIFIC IMPULSE FOR 15° CONICAL NOZZLE

H_2 (ℓ) – F_2 (ℓ) $(4 \leq O/F \leq 18)$

METHANE-FLOX $(3.5 \leq O/F \leq 6.5)$
$(82.6\%\ F_2)$

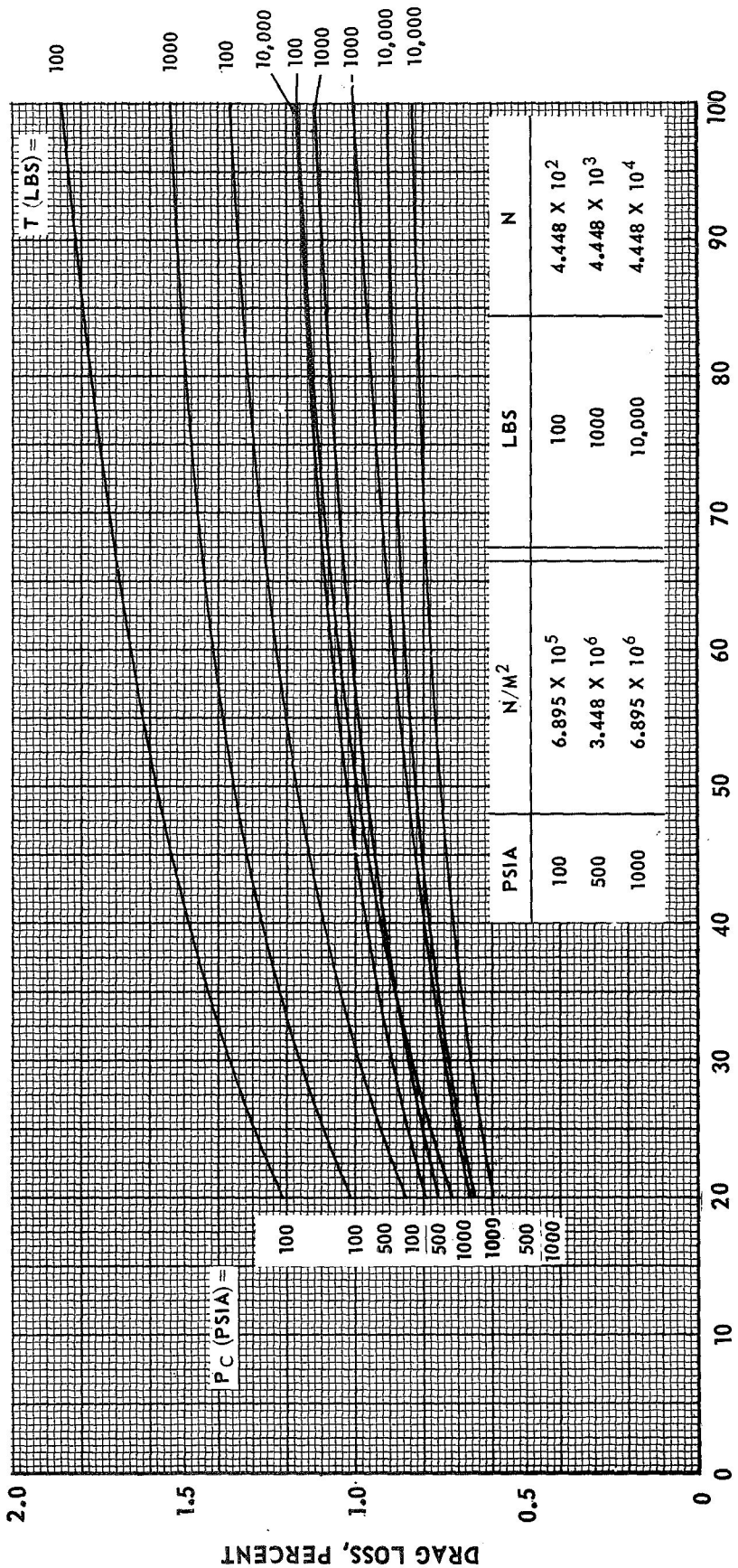

FIG. AL-7

VARIATION OF VISCOUS DRAG AS PERCENT OF FROZEN VACUUM SPECIFIC IMPULSE FOR 15° CONICAL NOZZLE

$H_2(\ell) - O_2(\ell)$ $(3 \leq O/F \leq 8)$

AEROZINE 50 - N_2O_4 $(1.25 \leq O/F \leq 2.5)$

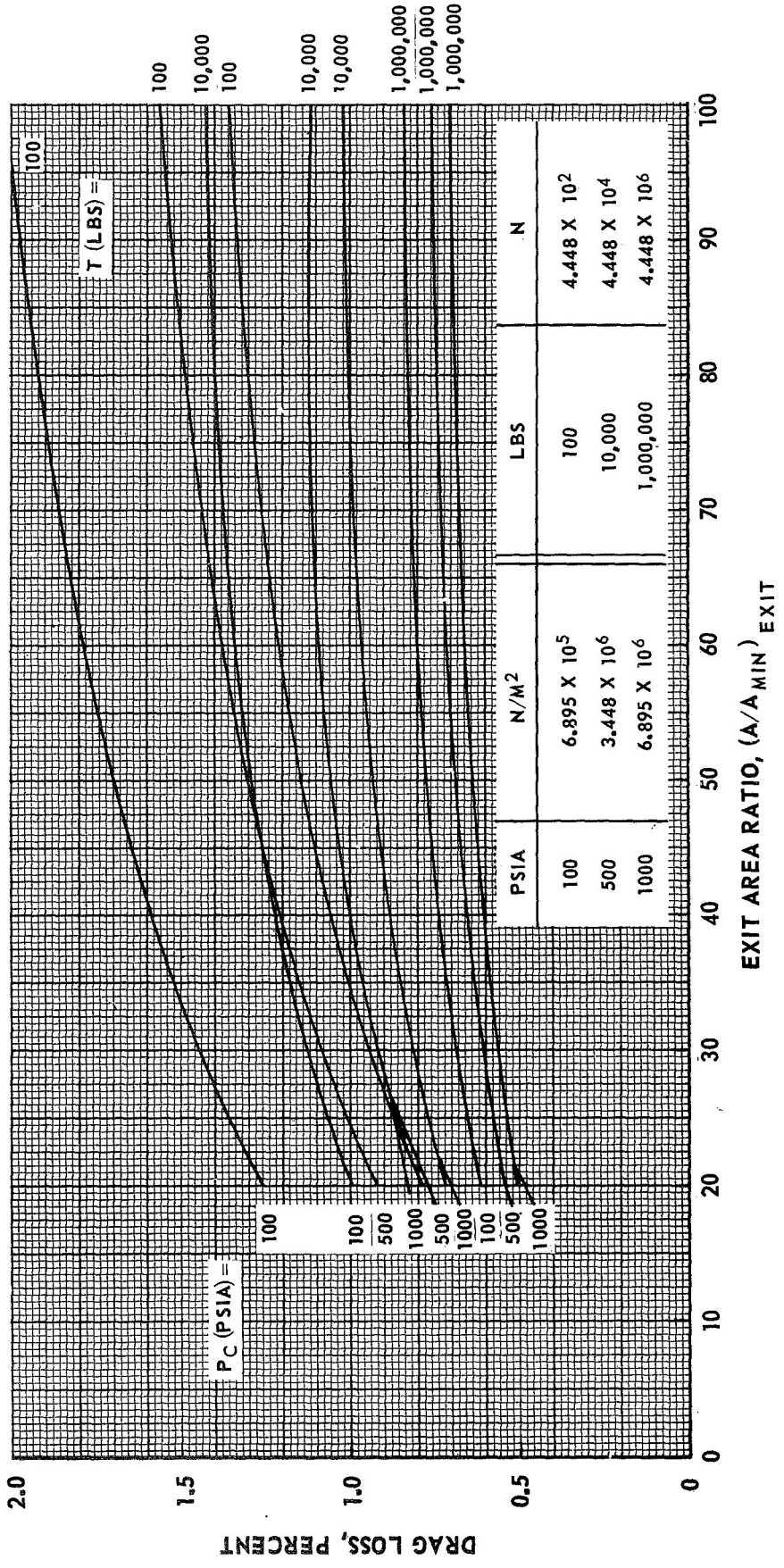

FIG. AL-8

VARIATION OF VISCOUS DRAG AS PERCENT OF FROZEN VACUUM SPECIFIC IMPULSE FOR 15 DEG CONICAL NOZZLE

$B_2H_6 - OF_2$ $(2.5 \leq O/F \leq 5.5)$

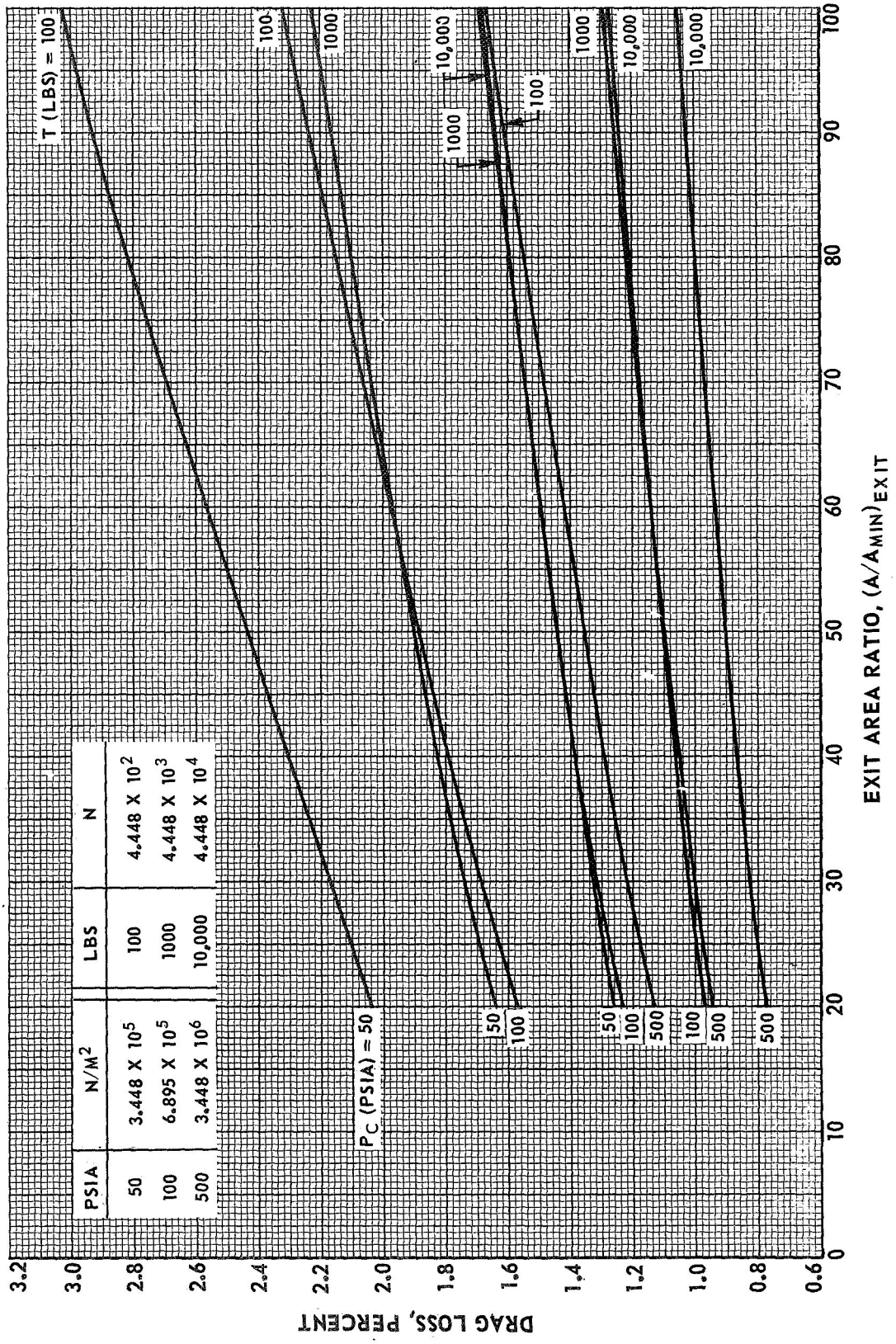

PSIA	N/M^2	LBS	N
50	3.448×10^5	100	4.448×10^2
100	6.895×10^5	1000	4.448×10^3
500	3.448×10^6	10,000	4.448×10^4

FIG. AL-9

VARIATION OF VISCOUS DRAG AS PERCENT OF FROZEN VACUUM SPECIFIC IMPULSE FOR 70% BELL NOZZLE

$H_2(\ell) - F_2(\ell)$

$4 \leq O/F \leq 18$

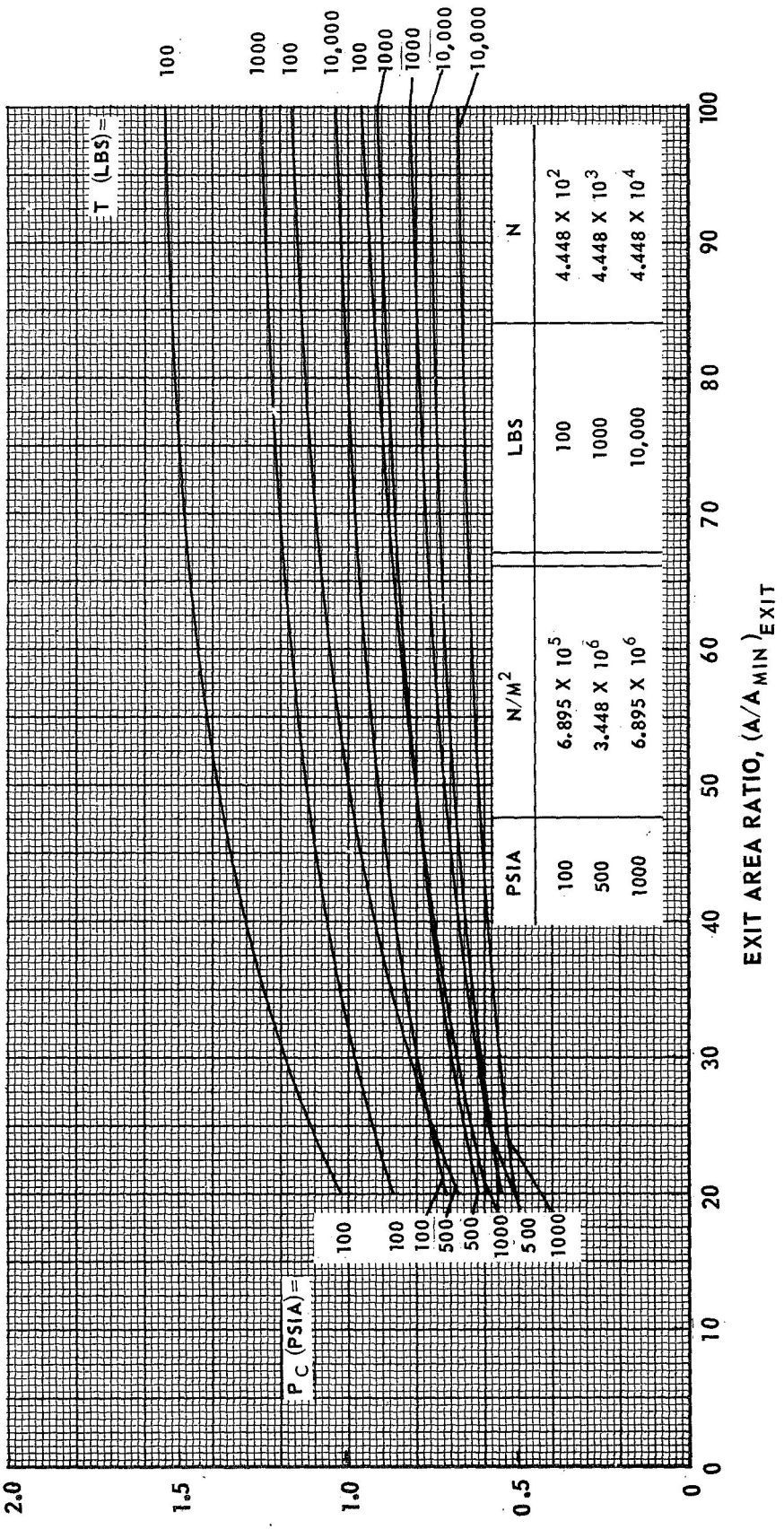

FIG. AL-10

VARIATION OF VISCOUS DRAG AS PERCENT OF FROZEN VACUUM SPECIFIC IMPULSE FOR 70% BELL NOZZLE

$H_2(\ell) - O_2(\ell)$

$3 \leq O/F \leq 8$

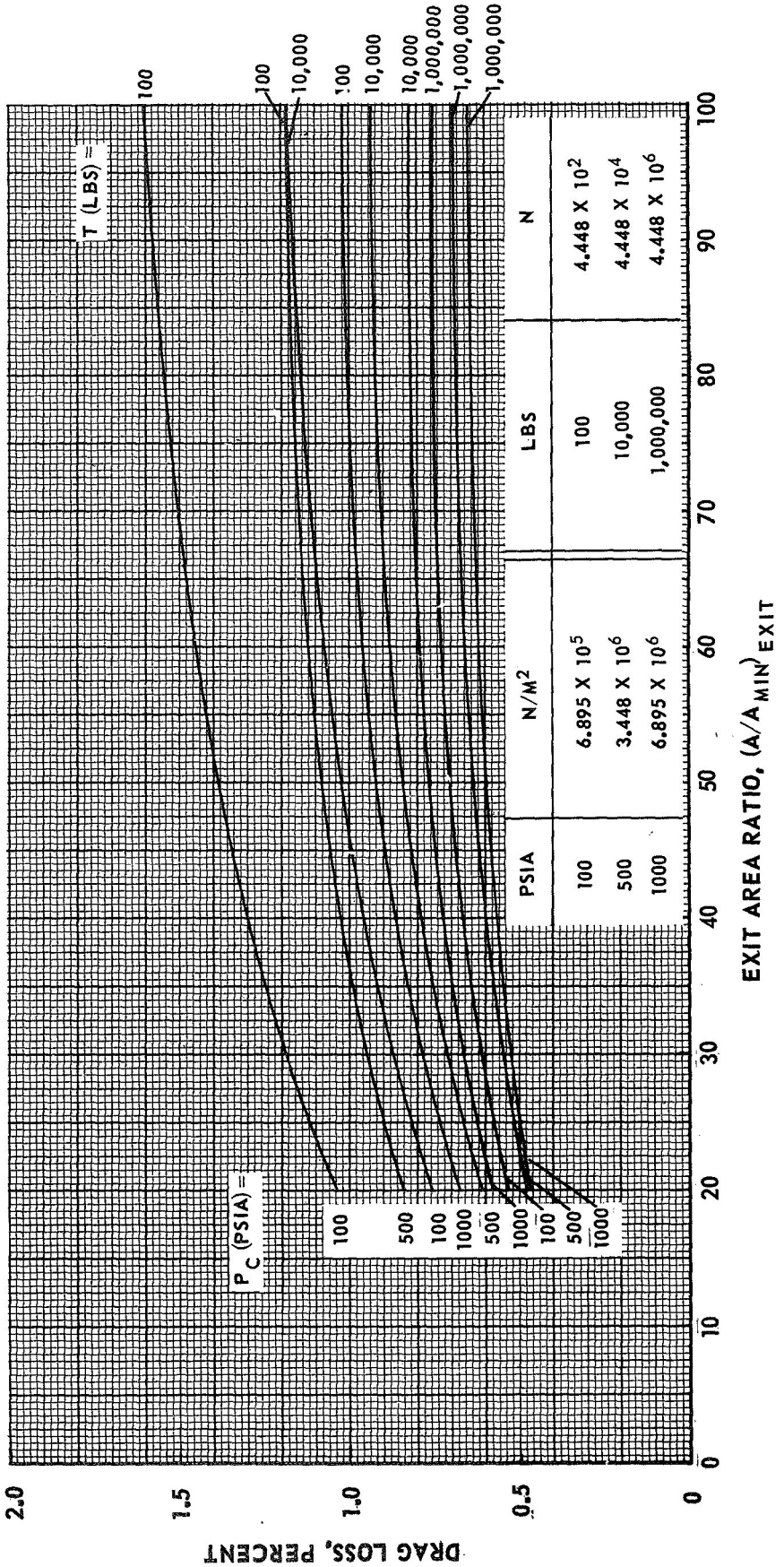

FIG. AL-11

VARIATION OF VISCOUS DRAG AS PERCENT OF FROZEN VACUUM SPECIFIC IMPULSE FOR 70% BELL NOZZLE

METHANE - FLOX (82.6% F_2)

$3.5 \leq O/F \leq 6.5$

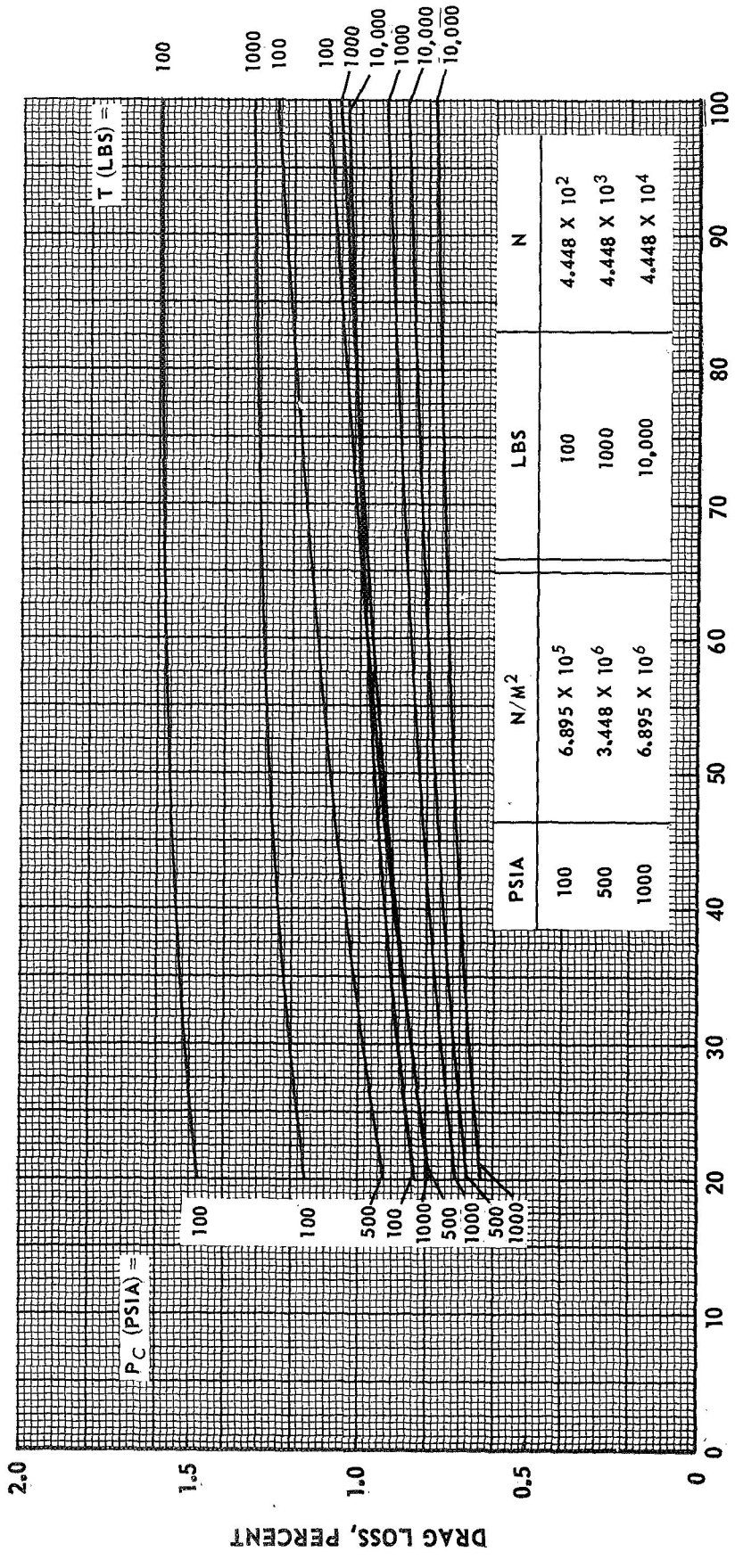

FIG. AL-12

VARIATION OF VISCOUS DRAG AS PERCENT OF FROZEN VACUUM SPECIFIC IMPULSE FOR 70% BELL NOZZLE

AEROZINE 50 – N_2O_4

$1.25 \leq O/F \leq 2.50$

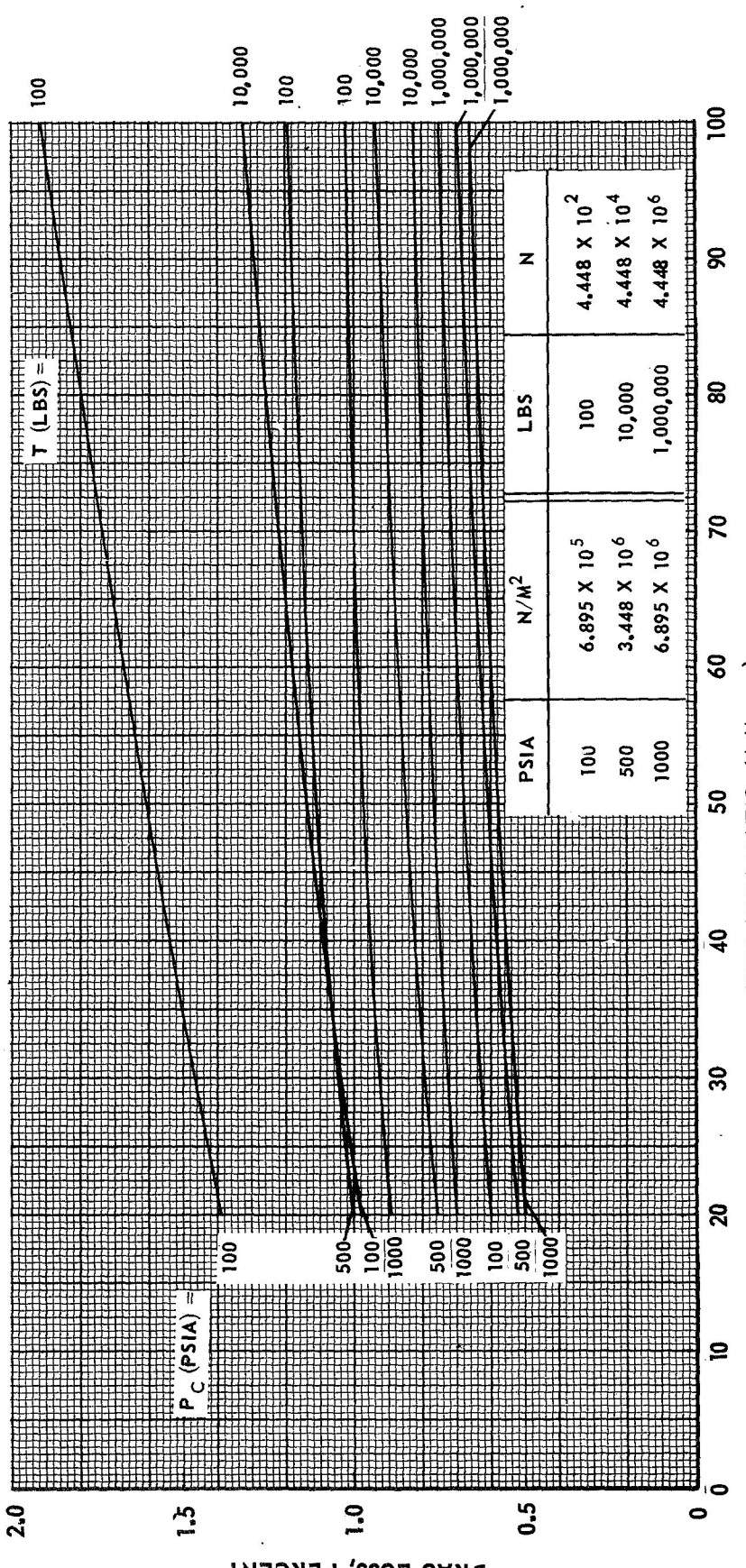

FIG. AL-13

VARIATION OF VISCOUS DRAG AS PERCENT OF FROZEN VACUUM SPECIFIC IMPULSE FOR 70% BELL NOZZLE
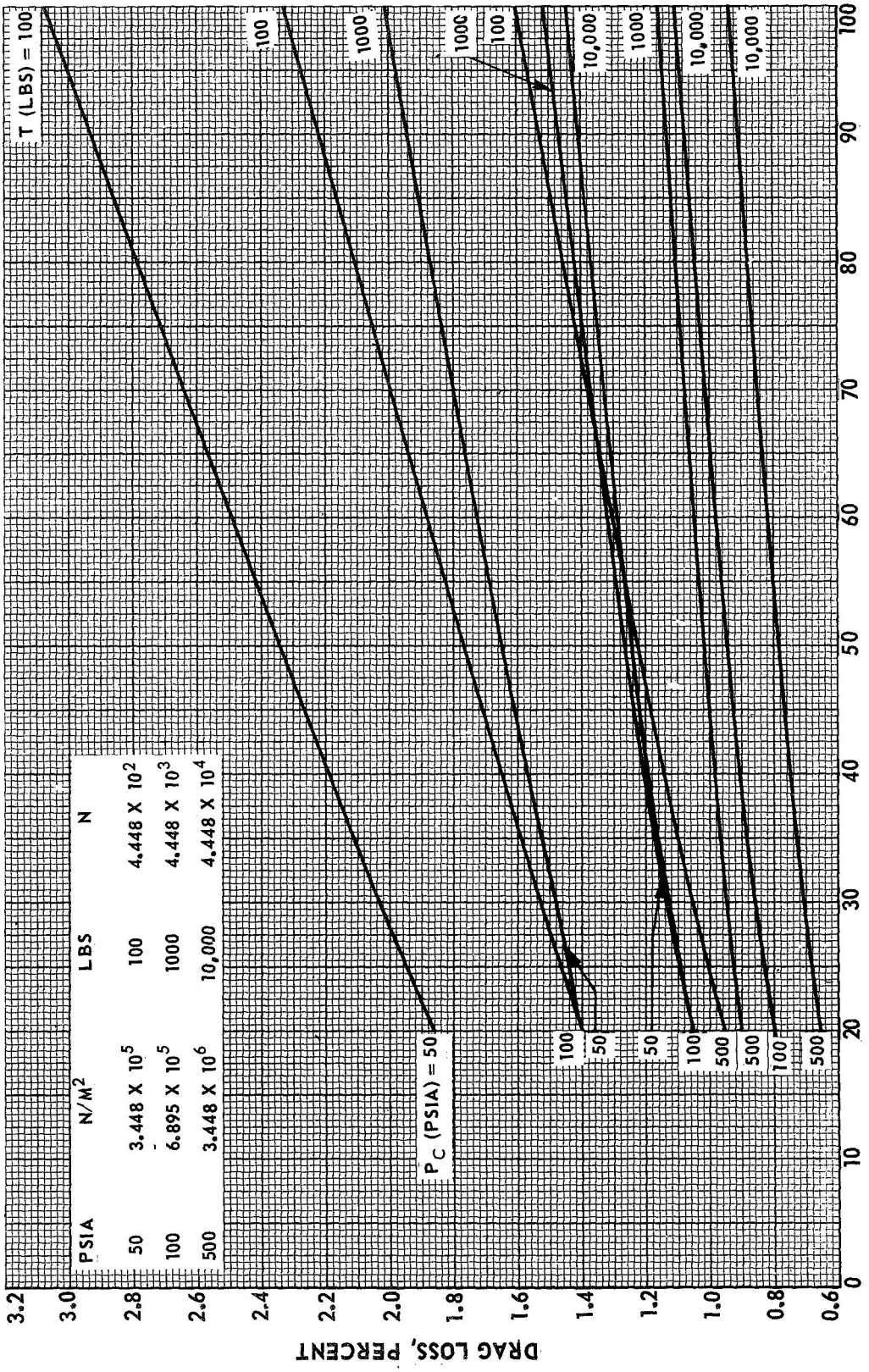
$B_2H_6 - OF_2$ $(2.5 \leq O/F \leq 5.5)$